Exploring novel approaches to metastatic heterogeneity and clonal evolution

Dr Lavinia Spain (MBBS(Hons) BMedSci FRACP)
MD(Res) Candidate
Institute of Cancer Research, London

Declaration

I declare that the work presented in this thesis is my own, except where contributions from others (for example, bioinformaticians) are acknowledged.

Dr Lavinia Spain

Funding and acknowledgments

This work has been funded by generous donations made to the Skin & Renal Unit Fund of the Royal Marsden Charity (including donations made by Melanoma UK and private individuals) as well as the McAlpine Foundation. The Melanoma TRACERx study receives additional funding from the Biomedical Research Council (BRC).

I sincerely thank my inspirational primary supervisor Dr Samra Turajlic, without whose vision and drive this work would not have eventuated. I also thank Professor Martin Gore and Professor James Larkin for all their mentoring, advocacy and advice. Professor Gore will always be greatly missed. What a privilege and a pleasure it has been to work with members of the PEACE and Lung TRACERx teams, in particular Professor Charlie Swanton, Dr Mariam Jamal-Hanjani, Dr David Moore, Dr Maise Al-Bakir, Ariana Huebner, Sophie Ward, Raju Veeriah, Joanna Laycock, Maryam Razaq and the PEACE CTC Team, and I thank them wholeheartedly for the opportunity to be involved in the PEACE study and their kind assistance with the Melanoma cohort.

I am incredibly grateful for the training in wet lab skills provided by Andrew Rowan, as well as his infinite patience and guidance. Desiree Schnidrig, Kevin Litchfield, Irene Lobon and Hang Xu have provided invaluable assistance with bioinformatic analyses, as well as nuanced data analysis and representation. I am lucky to have had enthusiastic support from Fiona Byrne as well as Tim Chambers in the advanced sequencing facility at the Crick. A big thank you to Lewis Au and Scott Shepherd for all the lab camaraderie, inter-continental support and Scott's expertise with FISH. I am also extremely grateful for the assistance of the Biological Specimen Collectors at the Royal Marsden (Somya, Nahid, Aida and Justine), research nurses (Kim, Sarah S and Sarah V), melanoma nurses (Nikki, Peta and Jaime) and trial coordinators (Dil, Lyra, Ellie and Sanjay), as well as the other clinical fellows with whom I have worked (Rob, Zayd, Jo, Karolina and Ben). It has been a pleasure to work with Nelson Alexander, Lisa Gallegos and the rest of their team from Roche Tissue Diagnostics on the HoLST-F study, as well as Ashley Gilchrist, Vanessa Primus and Glenn Noel-Storr from the Royal Marsden Histopathology Department.

Most importantly, none of these translational projects would be possible without the willing participation of patients and their families. I have been humbled by the enthusiastic

engagement of patients and their families in the PEACE project in particular, making a most generous contribution at a very emotional time.

Finally, to my husband Jonathan, and children Ella and Oliver, thank you for sparing me for many, many weekends over four years and for all your belief, love and support. To my family, in particular my mother, father, stepfather and sister, I would not have completed this thesis without your faith in me and your infinite help.

I also acknowledge the services of Sarah Endacott, of edit or die, who performed copy-editing and formatting on this document, according to the principles and standards of the Australian Institute of Professional Editors (IPEd).

Abstract

Background

Alternative methods are required to optimise the clinical insights that may be derived from studies of cancer evolution and heterogeneity. Profiling a single biopsy of tumour tissue underestimates potential genomic diversity. In melanoma, studies in this field have been limited by poor access to primary tumours, small cohorts and a bias to locoregional metastases. Through the use of extensive sampling at post-mortem and an analysis of homogenization of 'leftover' surgically resected tumour, I aimed to explore the potential utility of two novel strategies.

Research plan

An in-depth exploration of modes of metastatic seeding as well as inter-metastatic heterogeneity was facilitated by sampling multiple metastatic sites from a cohort of advanced melanoma patients undergoing a research post-mortem, coupled with analysis of primary tumours where possible. I also designed and implemented a pan-cancer study where non-embedded, leftover surgically resected tumours were 'homogenised' (blended) with a view to determine the feasibility of this approach as a potential tool to inform treatment decisions.

Conclusion

Polyclonal seeding dominates primary to metastatic evolution in melanoma. This leads to greater inter-metastatic heterogeneity than previously appreciated, which may underlie the clinical behaviour of certain sites of disease in response to treatment. Genomic mechanisms of treatment resistance may be heterogeneous and are insufficient to explain the majority of progression events on targeted and immune checkpoint treatment. Homogenisation of leftover tumour samples appears to be a feasible approach in primary breast, renal and tubo-ovarian cancers, as well as sarcomas and melanoma lymph node dissections. Through its inclusion of a greater volume of tissue, it is likely to yield greater depth of genomic information than routine molecular profiling of small samples, although further work is required to confirm this.

Contents

Tables

Figures

Acronyms and abbreviations

AD	adrenal
AE	adverse event
APOBEC	apolipoprotein B mRNA editing enzyme, catalytic polypeptide
APs	advanced practitioners
BDT	big dye terminator
BM	brain metastases
BT	Breslow thickness
CCF	cancer cell fraction
CIN	chromosomal instability
CMV	cytomegalovirus
COSMIC	Catalogue of Somatic Mutations in Cancer
CR	complete response
CT	computed tomography
CTC	circulating tumour cell
CTLA4	cytotoxic T-lymphocyte-associated protein 4
DI	diaphragm
DIN	DNA integrity score
DNA	deoxyribonucleic acid
ECM	extracranial metastases
FFPE	formalin-fixed for embedding in paraffin
FISH	fluorescent in situ hybridisation
FS	frameshift
GEL	Genomics England
GFP	green fluorescent probe
GI	gastrointestinal
GISTIC	Genomic Identification of Significant Targets in Cancer
GL	germline
GSST	Guys and St Thomas' NHS Foundation Trust
GTEX	genotype-tissue expression
Gy	Gray
H&E	haematoxylin and eosin
HLA	human leucocyte antigen
I&N	ipilimumab and nivolumab
ICC	interclass coefficient
ICI	immune checkpoint inhibitor
IHC	immunohistochemistry
indel	insertion or deletion mutation
ir-AE	immune-related adverse event
ITH	intratumour heterogeneity
iTME	immune tumour microenvironment
IV	intravenous
JAK	Janus kinase
JAK/STAT	Janus kinase / signal transducers and activators of transcription
LI	liver
LN	lymph node
LND	lymph node dissection
LOH	loss of heterozygosity
LU	lung
MAPK	mitogen-activated protein-kinase
Mb	megabase
MHC	major histocompatibility complex
MRI	magnetic resonance imaging
MRS	multi-region sampling
MUP	melanoma of unknown primary

NGS	next generation (genomic) sequencing
nsSNV	non-synonymous single nucleotide variant
ORR	overall response rate
PA	pancreas
PCR	polymerase chain reaction
PD	progressive disease
PD-1	programmed cell death receptor 1
PEACE	Posthumous Evaluation of Advanced Cancer Environment
PFS	progression-free survival
PM	post-mortem
PMI	post-mortem interval
PR	partial response
PV	paravertebral
QC	quality control
RECIST	response evaluation criteria in solid tumours
RFP	red fluorescent probe
RIN	RNA integrity score
RMH	Royal Marsden Hospital
RNA	ribonucleic acid
RTD	Roche Tissue Diagnostics
RT-PCR	reverse transcriptase polymerase chain reaction
SBRT	stereotactic body radiotherapy
SC	subcutaneous
SCNA	somatic copy number aberration
SD	stable disease
SLN	sentinel lymph node
SLNB	sentinel lymph node biopsy
SNP	single nucleotide polymorphism
SNV	single nucleotide variant
SNVs	single-nucleotide variants
SP	spleen
SRS	stereotactic radiosurgery
ST	soft tissue
SWI/SNF	switch/sucrose non-fermentable
TCGA	The Cancer Genome Atlas Program
TCR	T cell receptor
TH	tissue harvest
TIL	tumour infiltrating lymphocyte
TMB	tumour mutational burden
TTR	time to refrigeration
UCLH	University College London Hospital
UV	ultra-violet
UVR	ultraviolet radiation
VAF	variant allele frequency
WBRT	whole brain radiotherapy
WES	whole exome sequencing
WGD	whole genome doubling
WGII	weighted genome instability index
WGS	whole genome sequencing
WLE	wide local excision

Section 1 Introduction

Contents

Tables

Figures

1.1 Background

1.1.1 Importance of cancer evolution and tumour heterogeneity

The concept that the growth and spread of malignant cells follows an evolutionary path similar to that proposed by Charles Darwin in the *Origin of the Species* was proposed by Peter Nowell in 1976–; that is, that the fittest cells will survive and reproduce, under various selective pressures.[1] Recent cancer genomic studies have confirmed than many cancer types follow this framework.[2,3] Genomic instability can give rise to distinct lineages within a tumour – referred to as 'intra-tumour heterogeneity' (ITH) – and this provides a substrate for selection, which in turn drives evolution. Genomic instability is a hallmark of cancer, and refers to its propensity to generate random genetic changes.[4] Small-scale events such as mutations, for example, single nucleotide variants (SNVs) and insertions and deletions (indels) may occur. Larger-scale genomic alterations may also arise from chromosomal instability (CIN), where chromosome segregation errors occur during mitosis, resulting in structural and numerical chromosome abnormalities.[5] These range from gains or losses of a chromosome segment or arm, to chromothripsis (a complex rearrangement involving a single chromosome) and chromoplexy (a complex rearrangement involving more than one chromosome).[6]

Intra-tumour heterogeneity can occur at numerous levels; that is, genomic, transcriptomic, proteomic and within the immune tumour microenvironment (iTME) (Figure 1).

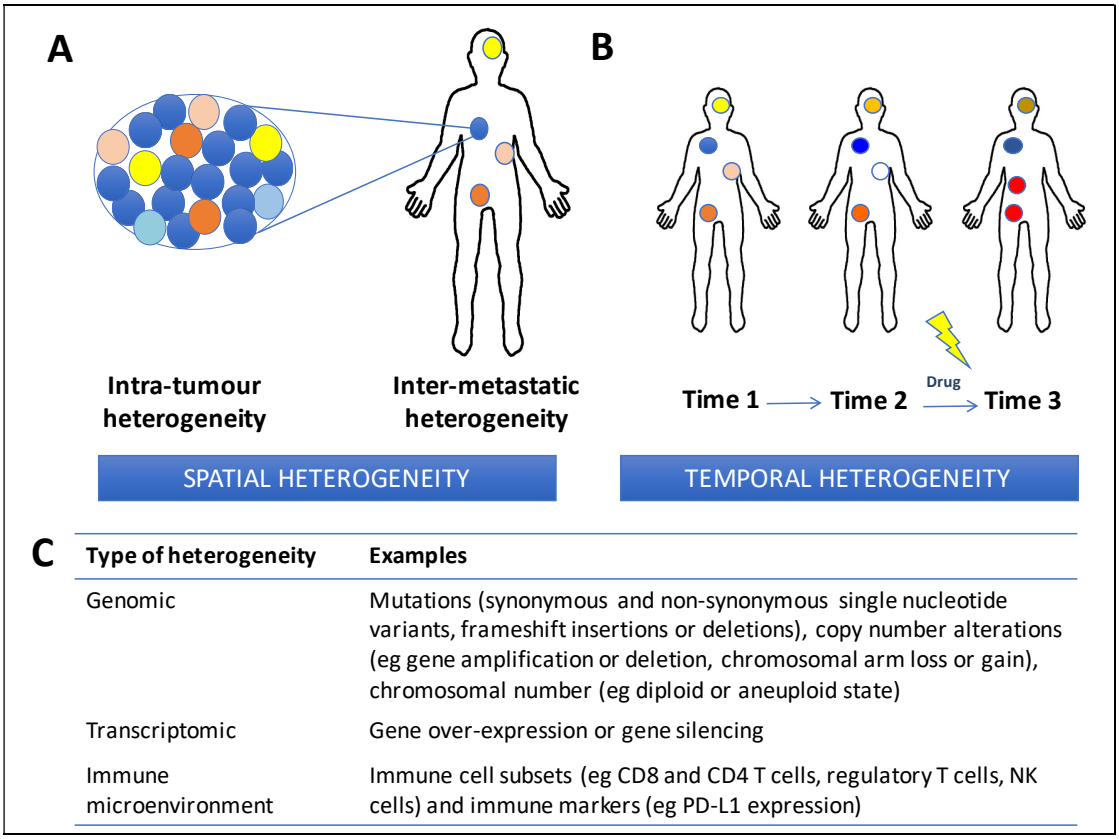

C

Type of heterogeneity	Examples
Genomic	Mutations (synonymous and non-synonymous single nucleotide variants, frameshift insertions or deletions), copy number alterations (eg gene amplification or deletion, chromosomal arm loss or gain), chromosomal number (eg diploid or aneuploid state)
Transcriptomic	Gene over-expression or gene silencing
Immune microenvironment	Immune cell subsets (eg CD8 and CD4 T cells, regulatory T cells, NK cells) and immune markers (eg PD-L1 expression)

Figure 1 Spatial and temporal tumour heterogeneity

A) Intra-tumour heterogeneity (left): primary tumour is made up of distinct subpopulations of cells (indicated by different coloured circles) which share a common clonal origin. Inter-metastatic heterogeneity (right): emerges because different subpopulations may seed different organ sites.
B) Both primary and metastatic tumours evolve over time as a result of changes in selective pressures, especially those posed by therapy.
C) Table describing the types of intra-tumour and inter-metastatic heterogeneity that may be measured through next generation sequencing (genomic and transcriptomic) and, for example, immunohistochemistry to evaluate the immune microenvironment.

The term ITH generally refers to heterogeneity within primary tumours. Three other types of tumour heterogeneity have been described:[7] intermetastatic heterogeneity, intrametastatic heterogeneity and inter-patient heterogeneity. Intermetastatic heterogeneity is influenced by the mode of dissemination from the primary tumour. Genomic heterogeneity is defined by clonal relationships: groups of cells that share genetic features; for example, mutations are termed ‘clones’ and different clones within the same tumour are referred to as ‘subclones’ (Figure 2). Clonal mutations are present in every cell in the tumour; whereas subclonal mutations are present in subsets of cells. The extent of primary tumour ITH is generally greater than intrametastatic heterogeneity.[8,9] Amongst the primary tumour clones only a few will have the metastatic competence to go on and seed other sites – a bottleneck event.

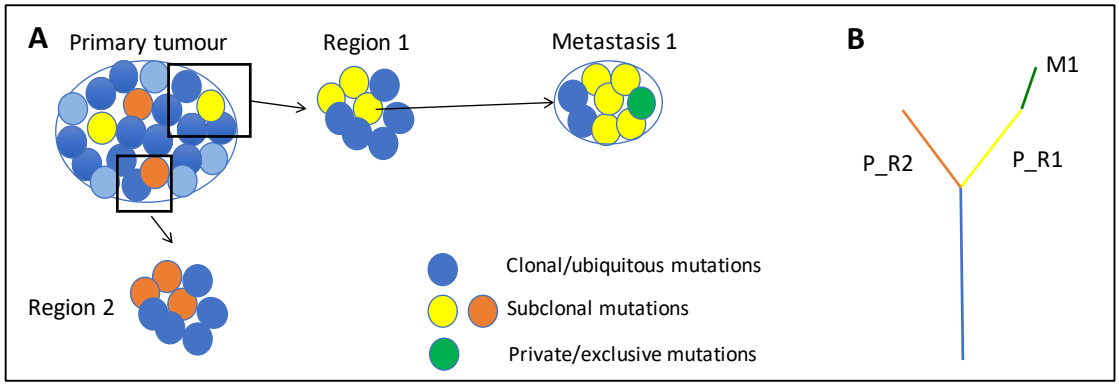

Figure 2 Representation of 'clonal' relationships within primary tumours and between matched primary and metastatic tumours

Black boxes indicate regions sampled.
A) Mutations that are ubiquitous – that is, shared between all sampled sites- are termed 'clonal' (represented in blue). Mutations that are present only in certain cells and may not be shared across all sites are termed 'subclonal' (represented in yellow and orange). Subclones that are only present in one sample or site are called 'private'. Single biopsies may not represent all the subclones, or they may infer that a mutation is clonal when it is subclonal.
B) These clonal relationships may also be represented in the form of a 'tree'. P_R1: primary tumour region 1; P_R2: primary tumour region 2; M1: metastasis 1.

The nature of clonal evolution in cancer influences patient outcomes,[2,3] and may help determine patient prognosis and inform therapeutic strategies.[9] Increasing tumour heterogeneity has been noted to be a poor prognostic factor.[10,11] In the largest study of ITH in lung cancer the extent of ITH was linked with outcomes.[3] In renal cancer, both ITH and genome instability are associated with prognosis.[2] ITH can underlie treatment resistance, thereby presenting a major hurdle to the elimination or control of cancer.[11] For example, in colorectal cancer initially responsive to EGFR-targeted antibodies such as cetuximab, selection of pre-existing subclones harbouring *KRAS* mutations (under the pressure of therapy) can lead to secondary resistance.[12] In *EGFR*-mutant lung cancer, coexistence of *T790M* and *T790* wild-type resistant subclones can drive mixed responses to EGFR inhibitors.[13] Thus, evaluation of ITH and the mechanisms that underpin it is highly relevant in the era of personalised medicine where treatment decisions are increasingly guided by tumour molecular profiling.

1.1.2 Modes of evolution

Cancer evolution is distinct from species' evolution in a number of critical ways. First, tumours comprise billions of cells that replicate in an asexual manner over much shorter timescales; that is, years rather than millions of years. Second, CIN is prevalent and facilitates major changes in genomic structure. Third, cancer cells may change their phenotype.[6]

Three key modes of evolution in the primary tumour have been described: linear, branched and punctuated. In the *linear* model, first described in the context of colorectal cancer, a step-wise acquisition of deleterious mutations is proposed, leading to progressively invasive cancer.[14] As each new driver mutation is acquired, a selective sweep occurs, with this new clone outcompeting the others to be the dominant one.[15] Therefore, analysis of distinct samples from the primary tumour are all very similar, and ITH is low. Any inferences regarding linear evolution are limited by sampling, in that a single sample, or even multiple samples, may fail to capture the presence of greater diversity within a tumour. In *branched* evolution, the clones diverge early from a common ancestor and continue to evolve in parallel, resulting in ITH.[15] There is a relatively greater proportion of subclonal to clonal mutations than is seen in the linear model, based upon the degree of divergence that occurs. However, the ratio depends on the length of the trunk (number of clonal mutations) versus the branches (subclonal mutations).

The presence of a driver mutation on one of the branches (that is, within a subclone) indicates a cell of superior fitness, and suggests that selection has occurred.[6] Treatment of cancer imposes a strong selective pressure and through elimination of susceptible clones it can influence the number of mutations present.[16,17] While some divergence (branching) occurs in all evolutionary modes, if there are no advantageous alterations characterising a branch, this is referred to as *neutral evolution*.[6] Another feature of branching evolution is *convergence*. This occurs when two independent clones (or branches of the tree) have a mutation in the same gene.[15] In *punctuated* evolution a 'big bang' event[4] –that is, a significant genomic event often involving somatic copy number changes or large-scale chromosomal rearrangements such as chromothripsis – occurs early in a tumour's life, followed by a period of relative stasis. As a result, there is limited heterogeneity within the tumour and it can be difficult to decipher from a linear pattern on the basis of mutation analyses alone.

The inference of evolutionary trajectory is made by distinguishing between clonal and subclonal mutations in tumour samples through analysis of next generation (genomic) sequencing (NGS) data with computational tools.[7,18] The variant allele frequency (VAF) is the frequency of a mutation in a particular tumour sample, and may be affected by both tumour purity (that is, the estimated percentage of tumour relative to non-tumour cells) and the copy number of the mutation. When this value is corrected for ploidy (that is, chromosomal number) and purity (that is, the percentage of tumour cells in a sample), the

proportion of cancer cells that harbour the mutation – the 'cancer cell fraction' (CCF) – may be derived.[19] With the aid of additional computational algorithms such as PyClone[20], the CCFs are used to decipher clonal (for example, CCF 100%) from subclonal (for example, CCF <100%) mutations, cluster mutations together and construct phylogenetic 'trees' that illustrate the pattern of evolution. Phylogenetic trees differ from the regional tree outlined in Figure 2 in the construction of branches, which proportionately demonstrate the size of subclones and rely on application of evolutionary principles in their construction.

Progression from a primary tumour to metastatic sites may follow a linear or parallel pattern (Figure 3, A and B).[21,22] The linear progression model posits that the clone that gives rise to metastases occurs late in tumour progression, and disseminates just prior to clinical detection of the primary tumour with limited ongoing evolution in the metastases. Relatively little divergence exists between the primary and metastatic sites. In contrast, in the parallel progression model, there is earlier dissemination of metastasis-forming clones from the primary tumour that continue to evolve in parallel with the primary. In this model, there is greater genetic divergence between the primary tumour and the metastases.[21] These two patterns are not mutually exclusive; rather, they represent two ends of a spectrum, and the ability to confidently discern which pattern dominates increases with more extensive profiling of the primary tumour and/or metastases (this is discussed further below).[21]

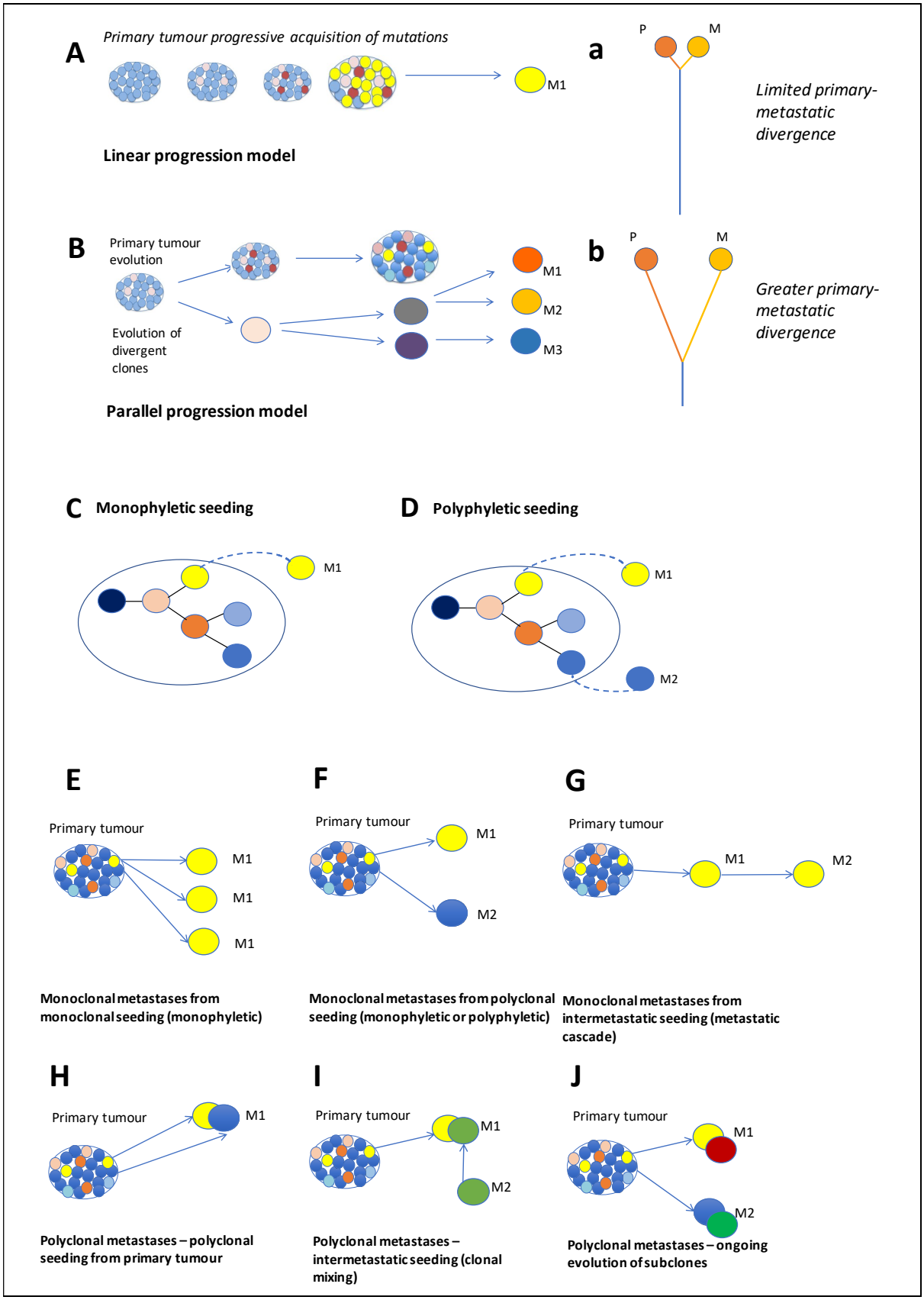

Figure 3 Patterns of primary to metastatic progression and seeding and clonal composition of metastases

A) In the linear progression model, the primary tumour progressively acquires mutations and then the 'fittest' clone is thought to leave the primary tumour late in development and seed metastases. The primary tumour and

metastases are therefore similar, sharing the vast majority of their mutations (as represented in the 'tree' shown in a, where the long trunk represents shared mutations).
B) In the parallel progression model, clones tend to diverge earlier from the primary tumour and acquire metastatic potential outside the primary. The metastasising clones and the primary tumour may then follow their own evolutionary path in parallel, leading to greater primary-metastatic divergence (as seen in b, where the 'tree' has a relatively shorter trunk and longer branches, the latter representing mutations that are distinct to each).
C) In monophyletic seeding, a single clone from one branch of the primary tumour's phylogenetic tree seeds all metastases.
D) In polyphyletic seeding, multiple clones from different branches of the primary tumour's phylogenetic tree seed metastases.
E, F, G: Monoclonal metastases may arise from monoclonal seeding where one clone from the primary seeds all metastatic sites (E) or polyclonal seeding (F), where different primary tumour clones individually seed different metastatic sites, or as a result of seeding by a clone from one metastasis to another (intermetastatic seeding; G).
H, I, J: Polyclonal metastases may arise from >1 primary tumour clone seeding a single metastatic site together (H), different clones from different sites co-seeding a metastasis (I) or from ongoing evolution of subclones with individual metastases.

Seeding of metastases from the primary tumour can be monophyletic or polyphyletic[21,23] (Figure 3, C and D). In monophyletic seeding, the clone(s) seeding all metastases are derived from a single branch of the primary tumour's phylogenetic tree. In polyphyletic seeding, these seeding clones are derived from different branches. If one clone seeds metastases, this is known as 'monoclonal' seeding; whereas if more than one clone seeds metastases, this is referred to as 'polyclonal' seeding. All polyphyletic seeding patterns are polyclonal by definition. Individual metastases can be established and/or characterised by multiple clones (polyclonal), or a single clone (monoclonal; Figure 3, E–J)).[21] A monoclonal metastasis will contain clusters of mutations all with a CCF around 100% whereas a polyclonal metastasis will contain clusters of mutations with CCFs <100%.

In the absence of comprehensive primary tumour profiling, inferences of modes of metastatic seeding can be made by assessing the clonal composition of various metastatic sites of disease. It is reasonable to assume that the mutations which are present at all sites (that is, clonal mutations) have all originated at some stage from the same clone in the primary tumour. The seeding clone from the primary may have been a dominant clone or a minor subclone. While it is not possible to determine the phyletic pattern of seeding without reference to the phylogenetic tree of the primary tumour itself, one may hypothesise whether one or more clones from the primary tumour seeded metastatic sites – that is, monoclonal or polyclonal seeding. Complicating the primary to metastatic seeding interpretation is the existence of other seeding possibilities, for example intermetastatic seeding (Figure 3) and re-seeding of the primary tumour by metastatic clones.[21] The extent of intermetastatic divergence can also give clues as to whether a more linear or parallel pattern of progression has occurred.

All evolutionary inferences are subject to a sampling bias. Analysis of a single sample may give the illusion of clonality, where the CCF in that sample supports a clonal mutation (that is, CCF close to 100%), but that mutation is actually absent from the rest of the tumour. More accurate description of patterns of evolution comes from studies involving multi-region sampling (MRS) of tumours, such as the large renal and lung TRACERx programs.[2,3,9] The greater the number of samples profiled, the more reliable the inference. For example, in the renal TRACERx study of primary tumours, the gain in driver detection per additional biopsy began to decline after eight biopsies, however in some cases driver events would still have been missed if only eight were taken.[2]

While heterogeneity within a primary tumour is well recognised,[2,3,24] heterogeneity between metastases and within individual metastases is not as thoroughly explored.[25,26] Evidence of polyclonal seeding was first demonstrated in mouse models,[27] and for the first time in humans in prostate cancer.[28] In their study of 10 autopsy cases subjected to MRS, Gundem and colleagues[28] found clusters of mutations present subclonally across multiple metastases in five out of 10 of cases, leading to greater intermetastatic heterogeneity. This would not have been possible to decipher from a single biopsy of one metastatic site.

Why is an understanding of tumour evolution relevant in the clinic? Precision medicine need not rest solely on genomic biomarkers, but in theory could involve the ability to understand an individual tumour's future behaviour (that is, its evolutionary trajectory). In renal cancer, different evolutionary subtypes (derived from multi-region sequencing of primary tumours) are associated with different clinical behaviour.[2] Metrics such as the degree of ITH (ITH index) and extent of the genome impacted by copy number aberrations (whole genome instability index (WGII), discussed further below in **Section 1.1.3**) correlated with certain subtypes and were associated with survival. For example, a low ITH index and high WGII – a characteristic of the 'multiple clonal driver' evolutionary subtype – had the most aggressive disease course and worst survival. In contrast, tumours with low ITH and low WGII – a common pattern in the '*VHL* monodriver subtype' – were enriched in earlier stages of disease. In colorectal cancer, an analysis of 118 primary and metastatic (liver and brain) samples from 23 patients demonstrated that in 90% of primary tumours in the metastasised cohort subclonal selection was evident, in comparison with 33% of primary tumours in earlier-stage disease.[29] This suggests that subclonal selection may be a marker of more aggressive disease. In addition to improving prognostication, understanding the path of

tumour evolution may alter the choice and timing of therapeutic intervention. It may also provide insight into a cancer's 'Achilles heel';[30] that is, its point of ultimate weakness which, if targeted, may eradicate all sites of disease.

1.1.3 Chromosomal instability and aneuploidy

Chromosomal instability (CIN) is a dynamic process in which chromosome mis-segregation happens at an increased frequency,[31] resulting in genetic variation between cells in a tumour (ITH, as discussed above) as well as aneuploidy (an unequal chromosome number of the haploid set due to an accumulation of gains and/or losses). Not all aneuploid states are inherently unstable. For example, in Trisomy 13 and some blood disorders, such as acute myeloid leukaemia,[32] aneuploid cells can replicate in a stable manner provided key replication machinery remains intact.[5] Aneuploidy may be defined by an abnormal quantity of chromosomes in a cell (either greater than or less than 2N) or by abnormal chromosomal structure, often due to gains/losses of whole chromosomes or chromosomal arms.[33]

Chromosomal instability is generally considered to be an early event in cancer evolution.[34,35] As discussed previously, these genomic changes may provide a major selective advantage and even lead to punctuated evolution and clonal sweeps.[6] CIN can also play an ongoing role in cancer evolution, enabling selection of somatic copy number aberrations (SCNAs) favourable for tumour progression.[36,37] Single chromosome gains can also function as promoters of metastasis (as well as suppressors).[38] CIN and the resulting aneuploid state may be tolerated in cancer cells through whole genome doubling (WGD), that is, duplication of the chromosomes in a cell due to segregation errors at mitosis.[39,40] Tetraploid cells, facilitated by WGD, are better able to tolerate mis-segregation errors, and therefore CIN, than diploid cells[39] and WGD has been associated with metastatic competence in large pan-tumour analyses.[41,42]

There are several methods that may be employed to evaluate SCNAs and aneuploidy in cancer These include next-generation sequencing techniques (whole exome or whole genome sequencing) and fluorescence in situ hybridisation (FISH). DNA quantification for overall ploidy may be performed using flow assisted cell sorting (FACS). Measures such as the weighted genome instability index (WGII) can be used to describe the proportion of the genome impacted by SCNAs.[43] Because CIN is a dynamic process, this is more challenging to demonstrate than aneuploidy, which is a fixed state, and can be inferred from the extent of SCNAs across the genome. Ultimately, cell to cell variation in chromosomal number is also

required to provide evidence of CIN. FISH can be used to demonstrate this, as can single-cell sequencing techniques.

1.1.4 Role of the immune system in shaping genomic tumour evolution

The interplay between the genomic characteristics of a tumour and the immune system is a focus of much research. Neoantigen formation, neoantigen clonality and disruption of antigen presentation machinery consequent to genomic alterations, can all affect clonal evolution.[44-47] This can occur through immune-mediated eradication of sensitive tumour clones ('immune-editing') or helping to avoid immune-mediated destruction ('immune escape'). The presence of cytosolic DNA consequent to CIN and aneuploidy may also trigger an immune response through the cGAS-STING pathway.[48]

Tumour mutations may encode novel peptides – 'neoantigens' – that incite an immune response when neoantigen-reactive T cells proliferate. Mutations present in all cancer cells (clonal mutations), rather than in subsets of cells (subclonal mutations) are associated with improved responses to immunotherapy in melanoma and lung cancer.[45,49,50] The quality, not quantity, of the neoantigen-T cell engagement is also important. Work done in melanoma for example has shown that only two neoantigen-reactive T cell clones are required to eradicate the majority of tumours *in vitro* and *in vivo*.[51]

Cells with excess DNA due to an aneuploid state (usually due to mis-segregation errors that occur as a consequence of CIN) are vulnerable to elimination by the innate immune system via the cGAS-STING pathway. The excess cytosolic DNA is sensed by cyclic GMP AMP synthase (cGAS) which then triggers a cascade of events resulting in the activation of STING. This stimulates an IFN-gamma mediated innate immune response (cGAS-STING pathway).[48,52,53] Cancer cells have ways of subverting this pathway to be pro-tumourigenic; however, therefore enabling CIN to drive metastasis formation.[5,31] Aneuploidy and CIN have also been associated with lower cytotoxic T cell immune infiltration, consistent with immune evasion.[47,54,55]

Mutations or SCNAs impacting important aspects of immune system machinery can also lead to impaired antigen presentation. In lung cancer, loss of heterozygosity in HLA is noted in 40% of early lung cancers and is postulated to be a mechanism of immune escape that drives tumour growth.[46] In the case of antigen presentation machinery disruption, it appears that this is selected for, with immune editing of more vulnerable clones.[47] In their pan-cancer study,

Tripathi et al.[47] note that epigenetic silencing is more likely than gene deletion in facilitating this process. Genomic mechanisms of resistance to immune checkpoint therapy involving disruption of antigen presentation machinery such as mutations in *B2M* and components of the JAK/STAT pathway are discussed in **Section 1.1.4**, below.

The immune system exerts a powerful influence on clonal evolution in cancer, and genomic factors such as CIN and aneuploidy can either manipulate this for survival, or be vulnerable to it. This immunogenomic interplay is particularly important in the context of response and resistance to immune checkpoint inhibitor therapy, discussed below in **Section 1.2.7**.

1.2 Melanoma

1.2.1 Histologic/genomic subtypes

Melanoma is a malignancy derived from cells that form the pigment melanin (melanocytes). There are three major subtypes of melanoma, reflecting the diverse locations of melanocytes within the body: 1) cutaneous melanoma, comprising over 90% of cases and with UV light recognised as a key carcinogen;[56] 2) mucosal melanoma; and 3) uveal melanoma. Cutaneous melanoma contains an 'acral' subgroup of melanomas arising on non-glabrous skin (for example, palms, soles and nail beds). Although derived from the same cell of origin, the melanocyte, cutaneous, mucosal and uveal melanomas are genomically distinct diseases (discussed below). In up to 15% of metastatic melanoma cases no primary tumour is identified, likely due to regression of the primary which occurred after disseminaton.[57] A small subset of patients have an inherited predisposition to melanoma development, most commonly due to mutations in *CDKN2A*, a key tumour suppressor gene.[58]

1.2.2 Driver mutations and tumour mutational burden

A number of studies have defined the genomic landscape of these melanoma subtypes. Sun-exposed cutaneous melanomas are characterised by *BRAF (40%)*, *NRAS (20%)* and *NF1* mutations (14%) which are usually mutually exclusive.[59,60] These genes encode proteins in the mitogen-activated protein-kinase (MAPK) pathway which is upregulated in melanomas, driving cell proliferation and tumour growth.[61] Where oncogenic mutations in *BRAF* and *NRAS* are typically missense mutations, the nature of *NF1* mutations are more varied and include indels. Sun-exposed cutaneous melanomas have a high mutation burden (16.8 mutations/Mb,[60] median 135 nsSNV[7] and tend to display C>T nucleotide transitions consistent with ultraviolet radiation (UVR) driven mutagenesis.[62] Many cases of unknown

primary melanoma also bear this UVR signature, suggesting they arise from a regressed sun exposed cutaneous primary tumour.[60] Acral cutaneous melanomas have a lower frequency of *BRAF* mutations (18%)[63] but around 10% may contain *KIT* mutations.[63] They tend to exhibit a greater number of SCNAs but have a lower mutational burden than sun-exposed sites (2.1mutations/Mb (range 0.68–34.9).[59,63-65] Subungual acral melanomas have a higher burden than palmar/plantar ones, and those on the soles of feet have the lowest tumour mutational burden (TMB).[63] Numerous other driver genes have been recognised in cutaneous melanoma, including *GRIN2A, CDKN2A, TERT, CCND1, PREX2, RAC1,* ARID2A.[59,60,65,66]

Mucosal and uveal melanomas have poorer survival outcomes than cutaneous melanomas.[67] Mucosal melanomas typically arise in the anorectum, female genital tract or in the sino-nasal passages.[68,69] SCNAs and structural variants are more frequent in these subtypes, and mutational burden is lower (2.7mutations/Mb (range 0.54–7.1).[63,69,70] *KIT* mutations are present in 4–25% of mucosal melanomas,[59,68,70-72] usually in vaginal and anorectal subtypes. *NRAS* mutations may also occur and appear to be enriched in sino-nasal melanomas, reported in up to 30%.[73] Recent landscape studies of mucosal melanoma have identified new candidate driver genes: *POM121* mutations in 15.4%[72] and *SPRED1* (loss of function) in 19%.[70] Uveal melanomas are characterised by *GNAQ* and *GNA11* mutations[74-76] and the metastasis-associated mutations *BAP1, SF3B1* and EIF1AX.[77-79] They have the lowest mutational burden of all melanoma subtypes.[80]

1.2.3 Somatic copy number aberrations in melanoma

In addition to gene mutations, gains or losses in the copy number of individuals genes, as well as chromosomes (focal segments, whole arms or even whole chromosomes) are features of melanoma. SCNAs are a feature in all subtypes of melanoma, but as mentioned above are more common in acral, mucosal and uveal subtypes. Driver SCNAs for cutaneous, acral and mucosal subtypes (relevant to this project) are summarised in Table 1.

Table 1 Chromosome (whole and arm) and cytoband somatic copy number aberrations across cutaneous, acral and mucosal melanoma subtypes[59,60,63,65,70,72]

	Cutaneous*		**Acral**		**Mucosal**	
	Gain	**Loss**	**Gain**	**Loss**	**Gain**	**Loss**
Arm-level/whole chrom	1q 6p 7 8 13q 20 22q	5q 6 9 10 11 13q 14q 16q 17p 18	7 8 6p 17q 20q	9 10 6q 11q 21q	1q 6p 7 8q 17q 20q	3q 4q 6q 8p 9p 10 11 21q
Cytoband-level	1p12 1q21.3 1q44 3p13 4q12 5p15.33 5q35.3 6p24.3 6q12 7p22.1 7q34 8q24.21 11q13.3 12q14.1 12q15 13q31.3 15q26.2 17q25.3 20q13.33 22q13.2	1p22.1 1p36.31 2q37.3 3p25.1 3q13.31 4p16.3 4q34.3 5p15.31 5q12.1 5q31.3 6q21 6q26 8p23.3 9p21.3 9p23 10p15.3 10q21.1 10q23.31 10q26.3 11p15.5 11q23.3 12q23.3 13q34 14q23.3 14q32.31 15q13.3 15q21.1 16p13.3 16q12.1 16q23.1 16q24.3 17p13.3 19p13.3 Xp21.1	5p13 5p15 6p22.3 6q12 7p21.3 11q13 12q14 15q26.3 17q23.2 17q24.3	1q21.1 6q13 9p21.3 11q22.3 15q15.1 17q11.2 21p11.2	1p12 1q31 4q12 5p15 11q13 12q13–15	9p21 17q15

**Based on Broad Institute GISTIC2 (Genomic Identification of Significant Targets in Cancer version 2) analysis of TCGA data,*[81] *contains a minority of acral cases.*

Through copy number gains, individual genes may be amplified, thereby increasing the 'dosage' of an oncogenic mutation (for example, *BRAF* chr 7q, NRAS),[61] or a non-mutated

pro-growth gene (for example, *CCND1* on chr 11q, *CDK4, MDM2* and *TERT* chr 5 – all significantly amplified in 'triple WT' tumours).[59,60] In uveal melanoma, metastases are also enriched with gains in 1q and 8q (the latter harbouring the *MYC* oncogene).[76] Conversely, tumour suppressor genes may be deleted, resulting in loss of heterozygosity, which in the context of a mutation on one allele, can provide the 'second-hit' required for loss of regulation of an abnormal growth state.[82] Key tumour suppressor genes in melanoma include *CDKN2A* (chr 9p) and *PTEN* (chr 10).[59,65] Genes with significant amplifications and deletions are summarised in Table 2.

Table 2 Cutaneous and mucosal melanoma driver gene amplifications and deletions[59,60,63,70,72]

Amplifications	Deletions
BRAF* (chr7)	ARID1B
CCND1 (chr11)	ARID2
CDK4	CDKN2A*
EGFR	NF1*
HRAS	PTEN*
KDR	RB1
KIT*	TERT promoter*
KRAS	TP53*
MDM2	
MET	
MITF	
NOTCH2	
NRAS*	
PDGFRA	
Additional in mucosal & acral subtypes:	Additional in mucosal subtype:
TERT*	ATM
MYC	
GAB2	
PAK1	
YAP1	
EP300	

** May also contain driver mutations.*
Underline – also noted in mucosal melanoma.[70]
***Bold** – also in acral.[63]*

Whole genome doubling (WGD) is noted in around 30–40% of melanoma metastases.[41,59,83] In a pan-cancer analysis, the median ploidy of WGD tumours was 3.3,[41] consistent with the observation that somatic copy number losses appear more prevalent than gains in genome-doubled tumours.[55] Although WGD tumours have a greater number of mutations, mutation load when corrected for ploidy across WGD and non-WGD tumours tends to be constant.[41] On a more focal level, however, the presence of WGD has been associated with greater amplification in driver genes – despite correction for ploidy.[42] WGD does not appear to be enriched in cutaneous melanoma metastases versus primary tumours, suggesting it is usually

a clonal event (~28% in both melanoma primary tumours and metastases).[41,83] In a large cohort of acral melanomas (n = 87), the majority were found to have undergone WGD (71%), with significantly higher rates of aneuploidy in this group.[63] In melanoma the majority of copy number events facilitated by CIN have been noted to occur after WGD.[83] In contrast, most mutations in melanoma occur prior to WGD.[83]

While mutations and loss of heterozygosity (LOH) through copy number changes may be detected with genomic sequencing, loss of gene function may also occur through epigenetic means such as methylation, and this requires additional techniques to decipher. In melanoma, methylation of promotor regions of key TSGs such as *CDKN2A* and *PTEN* has been described.[84] Patterns of methylation, including in driver genes such as PTEN, can also be heterogeneous across metastatic sites.[85]

1.2.4 Melanoma evolution and genomic heterogeneity

Trees representing clonal relationships in sun-exposed cutaneous melanoma typically have a very long trunk and relatively short branches, reflecting the dominant burden of shared UV-induced mutations.[86] Consistent with this, recent large pan-cancer single-biopsy studies (predominantly from metastases) looking at subclonal reconstruction have revealed relatively little intra-tumour heterogeneity in melanoma.[42,87] Accurately identifying subclones from single samples is challenging however.

Due to the small nature of primary tumours, which are usually entirely embedded in paraffin for diagnostic and medicolegal purposes, more in-depth melanoma-specific studies looking at cancer evolution and heterogeneity are challenging to undertake. Nonetheless, work to date has revealed a number of insights, summarised in Figure 4. The discussion hereon focuses on sun-exposed cutaneous melanoma as the majority of work has been done in this subtype.

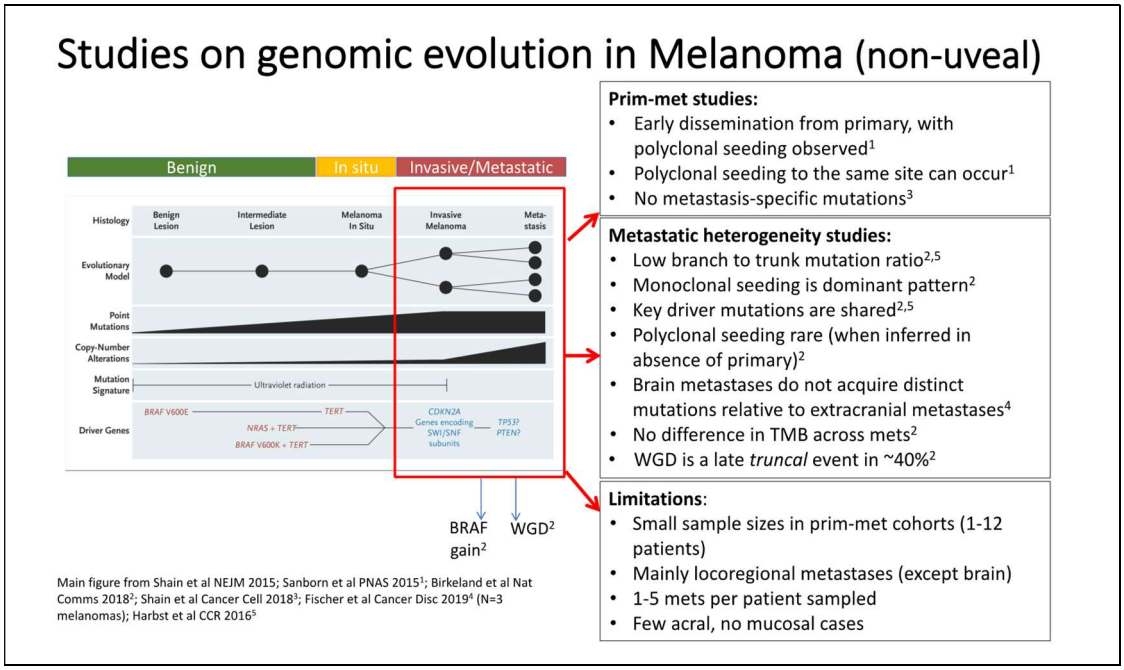

Figure 4 Summary of key findings from the studies on evolution in melanoma and their limitations
Adapted from figure in Shain et al.[88]

1.2.5 Genomic evolution of cutaneous melanoma

The most comprehensive study of melanoma evolution described the transition from benign naevi to invasive cutaneous lesions,[88] revealing that *BRAF* and *NRAS* mutations are present in pre-invasive cells and require additional mutations (for example, in tumour suppressors such as *CDKN2A* or *PTEN*) to develop into invasive lesions. Acquisition of SCNAs was also associated with invasion. They also described a transition from linear to branched evolution at later stages of primary tumour progression, with increasing ITH. In keeping with this, a separate cohort of benign naevi were shown to have increased MAPK signalling, but no mutations in *CDKN2A* or other cell cycle checkpoint genes,[89] reinforcing that loss of cell cycle checkpoint control is an essential transition phase from common naevi to invasive neoplasms.

Activation of the MAPK pathway is ubiquitous in all cutaneous melanomas, regardless of whether they harbor a specific *BRAF*, *NRAS* or *NF1* mutation.[90] Gene dosage appears to play a role as well; for example, with amplification of *BRAF* or *NRAS* mutations, or extent of *CDKN2A* loss.[61] Other pathways involved in the transition from benign to invasive lesions include SWI/SNF chromatin remodelling (encoded by genes such as *ARID 1 and ARID 2*, *SMARCA* etc), p53 (also impacted by loss of p14), as well as lineage-specific transcription

factors; for example, *MITF* & *SOX10* – known regulators of melanoma. Upregulation of telomerase also occurs.[61]

Heterogeneity was explored in seven acral primary melanomas with adjacent naevi, focusing on SCNA analysis as well as SNVs.[91] SCNA diversity was present between patients, as well as between individual tumour regions that had differing histological phenotypes within the same lesion. Some amplifications had copy numbers as high as 10. In one of the seven acral primaries, a phylogenetic tree was constructed demonstrating branched evolution.

At the time the projects for this thesis were undertaken, studies that looked at the evolution from cutaneous primary tumours to metastasis using next generation sequencing assays[88,92-94] were limited by their sample size (range: 1–12 patients) and biased to the study of locoregional and soft-tissue metastases. Table 3 summarises these studies.

Table 3 Summary of evolutionary and tumour heterogeneity studies in cutaneous melanoma using next generation sequencing (NGS) methods

Primary tumours			
Study	**Patient number**	**Regions sampled**	**NGS analysis**
Shain et al.[88]	n = 37 primaries (MRS)	Primary tumours & adjacent naevi	Panel seq
Shain et al.[90]	n = 85 primaries (MRS) (n = 37 from NEJM cohort + 48 others)	Primary tumours	Panel seq + RNAseq
Zhang et al.[91]	n = 7 primary acral melanomas	Primary tumours & adjacent naevi	WES (after WGA) + SCNA analysis
Harbst et al. 2016[95]	n = 2 (of cohort of 8)	Primary tumours	WES + RNAseq

Table 3 cont.			
Primary-metastasis pairs			
Study	**Patient number**	**Distant vs Regional Metastases**	**NGS analysis**
Shain et al.[90]	n = 12 pts	Regional mets only	Panel seq +Transcriptome
Sanborn et al.[92]	n = 8 pts	LN/locoregional Distant mets in n = 2	WES
Brastianos et al.[93]	n = 3 pts (with melanoma)	Primary+brain	WES
Turajlic et al.[94]	n = 1 pt (acral)	Primary + LN	WGS
Davidson et al.[96]	n = 1 pt	Primary plus locoregional mets, clonal evolution through treatment	WES
Rabbie et al.[97]	n = 1 pt	Primary and 13 distant metastases	WGS
Harbst et al.[98]	n = 1 pt (of cohort of 22)	Primary + locoregional LN	Panel seq + RNA microarray
Paired and individual metastases			
Study	**Patient number**	**Distant vs regional metastases**	**NGS analysis**
Birkeland et al.[83]	n = 53 pts (86 mets); n = 23 pts with ≥2 mets	n = 9 mets from visceral sites, n = 79 from soft tissue	WES
Fischer et al.[99]	n = 17 pts with matched BM (n = 21) & ECMs (n = 23)	Brain/extracranial	WES + RNAseq *NB: larger numbers of mets underwent RNAseq*
Reuben et al.[100]	n = 15 pts (n = 33 metastases)	Not specified	WES, neoantigen profiling, TCRseq
Rabbie et al.[97]	n = 7 pts (n = 19 metastases) – 1/7 acral, 6/7 cutaneous	Not specified for all; mix of locoregional and distant	WES
Harbst et al.[95]	n = 6 (of cohort of 8)	Not specified for all; mix of locoregional and distant	WES + RNAseq
Harbst et al.[98]	n = 21 (of cohort of 22), 49 metastases	Majority locoregional	Panel seq + RNA microarray; shallow WGS in n = 2 for SCNA analysis

Seq: sequencing; WES: whole exome sequencing; WGA: whole genome amplification; WGS: whole genome sequencing; RNA: ribonucleic acid; TCR: T cell receptor; MRS: multi-region sequencing; BM: brain metastases; ECM: extracellular metastases; SCNA: somatic copy number aberration.

Sanborn et al. describes evidence of polyclonal seeding and polyclonal metastases in their cohort of eight treatment-naïve patients, two of whom had visceral metastases.[92] In another group of 12 patients whose primary tumours and paired locoregional lymph nodes were profiled, there were no mutation-specific features of metastases compared with primary tumours.[90]

Other cutaneous melanoma studies have inferred evolutionary patterns from individual or paired metastases[83,95,100,101] (Table 3). The largest of these studies involved 86 metastases from 53 patients. The cohort was dominated by sun-exposed cutaneous melanoma and melanoma of unknown primary (87%); however, seven out of 53 were mucosal (n = 2), uveal (n = 2) and acral (n = 3) melanomas. Using WES profiling, they found that most metastases were monoclonal in origin, except for one case where polyclonality was demonstrated. WGD was noted in 40% and thought to pre-date metastatic divergence due to its clonal nature. Using whole exome sequencing, ITH in melanoma was explored by Harbst et al. in 41 regions of eight tumours (two primary lesions and six metastases).[95] Key driver mutations such as *BRAF* were ubiquitous with similar variant allele frequencies across regions. The proportion of heterogeneous somatic non-synonymous mutations in individual tumours ranged from 3–38%.[95] The majority of these were noted to be passenger mutations. Of the 129 mutations found in cancer genes (as per Catalogue of Somatic Mutations in Cancer – COSMIC – annotation),[179] 88% were clonal and 12% were subclonal. In one case, three different activating mutations in *PIK3CA* were noted in different tumour regions within the one metastasis, suggesting convergence on the PI3K pathway as a driver of metastatic growth.

Two studies have focused on brain metastases.[93,99] Differences in mutational profile between brain and primary tumours were evaluated in a pan-cancer cohort of patients, revealing 53% to have clinically relevant mutations exclusive to the brain.[93] Alterations in *CDKN2A* were the most frequent overall; however, this cohort only contained three melanoma cases. Analysis of 17 patients with paired brain and extracranial melanoma metastases did not reveal any difference in mutation profile; however, transcriptomic profiling suggested upregulation of oxidative phosphorylation in the brain relative to other sites.[99]

Work on pathways of evolution has also been undertaken in uveal melanoma. Field and colleagues looked at 151 primary uveal tumours and noted a dominant pattern of punctuated evolution. In a series of 35 patients with metastatic uveal melanoma to the liver,[102] a link between prognosis and evolutionary patterns was observed. Patients in whom a larger number of mutations specific to metastases as opposed to the primary tumour (that is, those with longer branches and shorter trunks on phylogenetic trees) had a superior disease free survival. No studies to date have focused on mucosal melanoma evolution. In the acral subtype, primary-metastatic comparative studies are limited to one case[94] (Table 3).

1.2.6 Non-genomic heterogeneity

Non-genomic heterogeneity is also recognised in melanoma. Morphological heterogeneity can be appreciated on histology within and between both primary and metastatic lesions[91,97] and transcriptional heterogeneity has been demonstrated using bulk as well as single-cell RNA sequencing.[103,104] Tumour microenvironment heterogeneity has also been shown with differing HLA-1 expression on IHC.[105]

1.2.7 Systemic treatment of melanoma and genomic mechanisms of treatment resistance

The systemic treatment of melanoma is broadly classified into: 1) Targeted therapy; and 2) immune checkpoint inhibitors (ICIs). Evidence supports a survival benefit of BRAF+/-MEK inhibition as well as ICIs in both the adjuvant and metastatic settings.[106-111]

1.2.8 Targeted therapy

The genomic profile of melanoma determines the efficacy of targeted therapies. Most common are somatic *BRAF V600* mutations, found in 40% of cutaneous melanomas.[112] The BRAF kinase is a component of the MAPK pathway, a key driver of cell proliferation. Mutations in *BRAF V600* (located in the kinase domain) lead to constitutive activation of this pathway,[112] driving tumour proliferation and growth.

In patients with a *BRAF V600* mutation, the seminal Phase III study of dabrafenib and trametinib[109] revealed an overall response rate (ORR) of 67%. The response rate of patients with *BRAF V600E* melanoma is superior to those with *BRAF V600K* alterations.[113] Progression free survival is around 11 months, and overall survival rates at four and five years are 37% and 34% respectively.[114] Mutations in *BRAF* outside of codon 600, which are much less common, do not respond in the same manner to targeted therapy.[115]

Despite initial high response rates, the majority of patients' tumours eventually become resistant to BRAF/MEK targeted therapies. Both acquired and intrinsic genomic resistance mechanisms to BRAF/MEK inhibitors have been reported, with the majority involving reactivation of MAPK signalling through other means.[116,117] In a study evaluating metastases progressing on dabrafenib and trametinib in 10 patients, resistance mechanisms were identified in 9/11 metastases. Acquired mutations in *MEK2* and *NRAS* were noted in five progressing tumours, and *BRAF* amplification was seen in 4. Interestingly in this study, while *MEK2* mutations were associated with progression, *MEK1* mutations were not.[118] Mutations

in genes involved in the PI3K pathway (*PIK3CA, PIK3R1, AKT1, AKT3* and *PTEN*) have also been associated with resistance.[119,120]

Targeted therapy to *KIT* mutations with agents such as imatinib is not as effective as BRAF/MEK inhibition, with response rates of ~20%, depending on the nature of the mutation.[121]

1.2.9 Immune checkpoint inhibitors

When the immune system is activated, inhibitory signals are also upregulated on immune cells to ensure the response is contained. Immune checkpoint inhibitors (ICIs) are monoclonal antibodies directed to inhibitory cell surface receptors, such as PD-1, expressed on T cells, B cells, dendritic cells and monocytes[122] and CTLA-4, expressed on activated CD4 and CD8 effector T cells and regulatory T cells.[123] By blocking negative inhibition, ICIs can enhance the anti-tumour immune response.

There are three main regimens of immune checkpoint inhibition: 1) single agent anti-PD-1 antibodies with agents such as nivolumab and pembrolizumab; 2) single agent anti-CTLA4 antibodies such as ipilimumab; and 3) a combination of anti-PD-1 and anti-CTLA4, most commonly as ipilimumab with nivolumab for four cycles, followed by nivolumab monotherapy maintenance (ipi+nivo). Combination ipi+nivo has the highest response rate (56%) and longest median PFS (11 months) relative to nivolumab (40%; six months) and ipilimumab (20%, three months) monotherapies.[110] It has a much higher rate of severe toxicity however (50% versus 15% for nivolumab monotherapy, or 28% for ipilimumab monotherapy).[110]

Thus far, studies looking at predictors of response and resistance to immune checkpoint therapy have evaluated cohorts treated with either ipilimumab monotherapy,[54,124,125] anti-PD-1 therapy[16,126] or sequential anti-CTLA4 and anti-PD1 treatments.[127] There has not yet been a systematic study of mechanisms of response and resistance to the combination of ipilimumab+nivolumab.

In melanoma, predictors of response to ICIs include a high TMB,[124,125] a higher proportion of clonal tumour-associated neoantigens,[45,49] an inflamed T cell gene expression signature (especially in conjunction with a high TMB)[128] and low scores on predictive tools designed to evaluate T cell dysfunction and exclusion.[129] Treatment resistance to ICIs may be due to a

combination of genomic and immune microenvironment factors.[100] Processes such as antigen presentation and antigen recognition as well as T cell engagement, signalling, proliferation and tumour infiltration are fundamental to efficacy. Potential causes of treatment resistance are broad-ranging; the focus herein is on genomically-mediated mechanisms of resistance.

A number of alterations in genes crucial to antigen presentation have been shown to influence responses to immune checkpoint therapy, including leading to resistance. There are several components to effective antigen presentation, including diversity of HLA genotypes encoding MHC Class I and II proteins[130] as well as optimal function of beta-2-microglobulin, a protein encoded by *B2M*, integral to MHC Class I protein folding and transport to the cell surface.[131] Where efficacy of anti-CTLA4 antibodies appears dependent on MHC Class I expression, response to anti-PD-1 antibodies appears more reliant on MHC Class II expression.[132] Mutations, deletions and associated loss of heterozygosity in *B2M* has been described as a mechanism of resistance to anti-PD-1 therapy in melanoma,[133,134] as well as lung cancer[135] and tumours with deficiency in DNA mismatch repair.[136]

The Janus kinase-signal transducer and activator of transcription (JAK-STAT) pathway is important in many immune regulatory processes, including driving anti-tumour immune responses through interferon gamma (IFN-γ) signalling.[137] This results in priming of dendritic cells to facilitate T cell activation, upregulation of MHC molecules on antigen-presenting cells (including tumour cells), PD-L1 upregulation on surface of T cells and immune cell migration, stimulation and differentiation.[137] Janus kinases 1 and 2 are encoded by *JAK1* and *JAK2* respectively. Inactivating mutations in these proteins have been noted in cases of primary[138] and acquired[133] resistance to anti-PD-1 therapy. In their work on cell lines derived from melanoma metastases, Sucker and colleagues revealed that loss of heterozygosity (LOH) at the *JAK1* and *JAK2* locus was present in 25% and 76%, respectively.[139] Analysing independent datasets as well as their own, SNVs/indels in *JAK1* and *JAK2* were noted in 5%–22%.[139] Copy number aberrations in genes involved in the IFN-γ pathway (including deletions of key mediators such as *JAK2* as well as gains in pathway inhibitors) have also been associated with poor responses to anti-CTLA4 therapies.[140]

Loss of PTEN has been linked to both primary and acquired resistance to anti-PD-1 therapy in melanoma, and acquired resistance in uterine leiomyosarcoma,[141-143] with loss of function mutations as well gene deletion of *PTEN* both described.[141,142] The absence of PTEN expression leads to an immune resistance phenotype, characterised by a tumour-supportive

cytokine milieu, reduction in immune cell infiltration and impaired autophagy, and may be present in 20–25% of tumours.[142]

CTNNB1 encodes the protein subunit beta-catenin which acts as an intracellular signal transducer in the canonical Wnt signalling pathway.[144] Alterations leading to activation of this pathway, both in *CTNNB1* and negative pathway regulators such as *APC, AXIN1* and *TCF1* have been associated with both innate and acquired resistance to immune checkpoint inhibition through immune exclusion.[143,145-148]

Greater numbers of SCNAs have been associated with resistance to ICIs.[54,127] Higher levels of SCNAs have been linked to poorer survival in melanoma patients treated with anti-CTLA4 antibodies. Where focal SCNAs were correlated with cell proliferation, arm- and chromosome-level alterations were linked to immune evasion.[54] However, in patients treated with anti-PD-1 therapies, higher ploidy (which may arise from accumulation of SCNAs) was evident in *responders*.[126] It is challenging to reconcile these divergent conclusions. In a cohort of patients treated with sequential anti-CTLA4 and anti-PD-1 antibodies, somatic copy number loss was most prevalent in patients who did not respond to either therapy, along with reduced immune gene expression.[127] Loss of chromosomes 6, 10 and 11q were frequently noted. Open questions remain about the significance of various SCNAs and ploidy across these cohorts, with differing methodologies to the SCNA analysis complicating interpretation.

To date, studies investigating resistance mechanisms rely on a single site biopsy, despite genomic heterogeneity within and between tumours as well as evidence that immune microenvironments can differ across metastases.[149] Inter-metastatic heterogeneity in mechanisms of targeted therapy resistance are also described.[150,151] Greater spatial profiling is needed to clarify the extent of heterogeneity in resistance pathways.

1.3 Novel approaches to the study of evolution and heterogeneity

With the increasing recognition of tumour heterogeneity and the role that it plays in treatment resistance in particular, novel approaches to tumour profiling are being pursued that may overcome the limitations imposed by a single biopsy. One that has gained popularity in recent years is that of ‘liquid biopsy’; that is, the potential of a blood sample to characterise the overall tumour profile, especially in the context of metastatic disease. Circulating tumour

cells and cell-free tumour nucleic acids may be extracted from blood samples and submitted for genomic, transcriptomic and cellular analyses.[152]

Other approaches include wide tumour sampling at post-mortem where access to multiple visceral sites is enabled. While this does not provide real-time information that may benefit the individual involved, post-mortem studies offer an opportunity to comprehensively research heterogeneity within and between cases in a particular tumour type. This multi-site evaluation lends itself to the more reliable reconstruction of a tumour's evolutionary pathway, especially in combination with primary, and if feasible longitudinal, tumour analysis.

There is also room for novel approaches, such as the proposed homogenisation (blending) of tumour samples to enable 'representative sequencing'.[153] This involves utilising a much greater proportion of tumour tissue from which a sample for profiling is derived, relative to standard of care approaches. The merits of post-mortem sampling and homogenisation are discussed in more detail below.

1.3.1 Post-mortem sampling

Post-mortem tumour sampling provides an opportunity to collect samples from a range of sites, especially those that are seldom available through diagnostic or research biopsies, including brain, liver and bone. The widespread sampling possible in the post-mortem setting enables a more rigorous reconstruction of tumour phylogeny from which to comprehensively evaluate evolutionary dynamics. The precedent for the utility of post-mortem tissue and its suitability for genomic analyses has now been well established, with research groups advocating its enormous potential.[154] A number of studies to date have evaluated aspects of heterogeneity and cancer evolution using this approach, in prostate,[28] pancreatic,[26,155,156] breast[150,157-159] and colorectal cancers.[160] Analyses of samples obtained at post-mortem have also complemented evolutionary studies in renal,[9] lung[161] and biliary cancer.[162] The quality of nucleic acids derived from studies with post-mortem intervals mostly <24 hours has been sufficient to yield reliable insights,[163] but the impact of longer post-mortem intervals is not established. More detail on this aspect is covered in the **Introduction to Section 3**.

Gundem and colleagues analysed samples from 10 patients with prostate cancer at post-mortem with whole genome sequencing (WGS), establishing complex patterns of seeding, including metastasis-to-metastasis spread and polyclonal seeding.[28] Dissemination patterns in

oesophageal adenocarcinoma have also been characterised using a WGS approach, involving 10 cases sampled at autopsy and a further eight cases with profiling of surgical resections.[164] The authors use the term 'clonal diaspora' to describe the dissemination of multiple primary tumour clones to different metastatic sites, which is essentially a polyclonal pattern of spread, and which they distinguish from parallel evolution by dissemination of the metastasising clones late in evolution of the primary tumour, and from linear in absence of step-wise progression from primary to lymph node to distant metastasis. Differences between individual metastases within the same organ were observed, suggesting multiple waves of seeding and an absence of tropism. In contrast to the prostate cancer autopsy series, polyclonal seeding and metastasis to metastasis spread were not noted, highlighting how different tumour types may favour particular pathways of metastatic spread. The small numbers in these studies, however, limit the ability to generalise any conclusions.

A number of post-mortem studies have shed insights into breast cancer. In one case, at least six different genomic alterations in *PTEN* were noted that led to loss of protein expression in 10 different metastases, five of which were progressing sites on treatment with a novel PI3K inhibitor – an example of convergent evolution.[150] The extent of heterogeneity in breast cancer metastases and the diverse relationships between primary and metastatic tumours was highlighted in four cases.[157] The intermetastatic heterogeneity in these was such that no single lesion represented the breadth of diversity, metastasis-metastasis seeding occurred and various treatment resistance mechanisms were noted. In one case, the authors describe how the seeding clone acquired its metastatic potential *after* divergence from the primary tumour. In the most comprehensive breast cancer study of this nature, De Mattos-Arruda and colleagues profiled the metastases of 10 breast cancer patients of various molecular subtypes, with matched (archival) primary tumours in six.[158] Similar to the aforementioned study by Savas et al.,[157] they noted metastatic heterogeneity and polyclonal seeding patterns, as well as subclonal LOH.

In pancreatic cancer, development of the metastatic clone was estimated to occur a decade after the primary tumour from analysis of seven autopsy cases, challenging the assumption that metastatic spread is an early event in pancreatic cancer and highlighting the opportunity for early detection to mitigate advanced disease.[155] Makohon-Moore et al.[26] looked at inter-metastatic heterogeneity in four cases of pancreatic cancer. They used WGS as well as targeted deep sequencing to evaluate the similarity between metastases, analysed 'genetic

distance' and the Jaccard similarity coefficient to determine extent of heterogeneity. Most metastases were extremely similar, with variation attributed to neutral evolution in the absence of any subclonal driver genes noted. This study suggests a more linear pattern of evolution in pancreatic cancer, with limited metastatic divergence.

Autopsy-based series show how even a limited number of cases sampled after death can profoundly inform our understanding of tumour clone dynamics across space and time. During the time dedicated to the projects in this thesis, only one case had been published in melanoma,[97] and this is discussed in more detail in the **Introduction to Section 3**.

1.3.2 Representative sequencing through tumour homogenisation

Within a single tumour both genetic and phenotypic variation are observed. ITH is recognised in multiple cancer types[10,64,165-167] and, as already discussed, is largely driven by genomic instability.[168] This limits the ability of a single sample of tumour to be representative of the whole. Intra-tumour heterogeneity is recognised as an important driver of tumour progression, drug resistance and treatment failure in solid tumours.[169] This has important implications for diagnosis and also for biomarkers guiding treatment decisions and prognosis.

When patients have cancer surgery, a portion of formalin fixed tumour is embedded in paraffin. In many tumour types, and especially in large tumours (which are noted to have a worse prognosis)[170-172] excess tumour tissue will not be embedded and will be discarded. This presents an opportunity to use this 'wasted' tissue to undertake more comprehensive molecular profiling.

Working with a team of collaborators at Roche Tissue Diagnostics, our group have developed a protocol that enables formalin-fixed tumour tissue (that is, before it becomes paraffin-embedded) to be blended, or 'homogenised'. With this method, a more representative sample than is otherwise provided by a limited number of biopsies may be sent for molecular (for example, genetic sequencing for mutations) and cellular (for example, flow cytometry for cell markers) analysis. In a pilot study conducted as part of the renal TRACERx protocol (CCR3723; unpublished data) surgical waste from a case of renal cell carcinoma was processed in this manner (see Figure 5, below). DNA was successfully isolated from the homogenised samples and subjected to library capture and sequencing. Analysis of the sequencing data revealed robust mutational calling (compared with fresh frozen tissue collected at the time of surgery) and a large number of additional variants were detected.

Importantly, all the clonal variants (ubiquitous in all cancer cells) were detected, enabling distinction between clonal and subclonal variants, and thus avoiding the risk of clonal illusion that is associated with single biopsy molecular assessments.

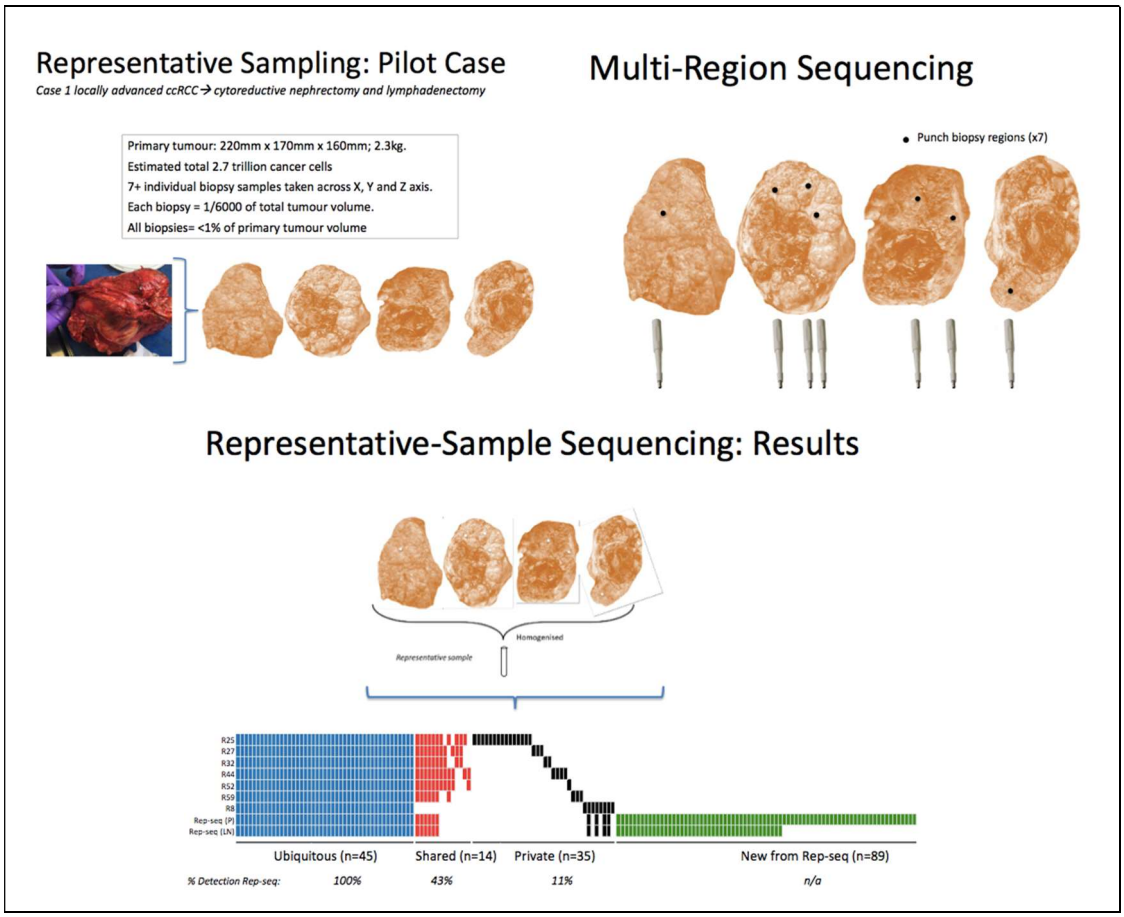

Figure 5 Kidney cancer pilot homogenisation case
A) dimensions of a primary kidney tumour that underwent homogenisation.
B) biopsies were taken at multiple sites within the tumour.
C) an additional number of mutations were identified in the homogenised sample (in green) compared to those identified by multi-region sampling (blue, red and black). Images and heatmap thanks to Kevin Litchfield.

The theoretical benefit of the homogenisation approach is supported in studies demonstrating the clinical limitations of ITH in various assays. For example, reports in prostate cancer strongly suggest that more thorough sampling of standard pathology samples yields more accurate information related to prognosis.[173,174] More specifically, in Cyll et al., the authors were able to link aneuploidy to shorter time to recurrence only when they improved their sampling methodology.[174] In comparing different PD-L1 assays in melanoma samples, it was found that geographic heterogeneity of the tumour accounted for most of the variance between these.[175] The ability to understand a greater spectrum of mutations within a tumour

may also enable identification of mechanisms of primary resistance to proposed therapies, influencing clinical decision making.

Patients with large primary tumours are the ones least served by a diagnostic approach reliant on a single or limited number of biopsies. The relationship between a larger primary tumour and a worse prognosis is documented across multiple tumour types,[170-172,176-178] and one explanation for this is likely to be the greater heterogeneity within a larger tumour volume. The ability to homogenise residual tissue in these cases and provide a representative sample may be particularly useful.

1.4 Rationale for proposed research

During the evolution of cancer within an individual, current methods used in the clinic are insufficient to reliably represent heterogeneity and track evolution as they utilise only a small proportion of tumour for molecular testing. Furthermore, extensive sampling of metastases requires multiple invasive biopsies. While multi-region sampling efforts have yielded important insights,[2,3] they are labour- and cost-intensive, and there is room for novel approaches to facilitate further research in this area. As our understanding of biomarkers becomes more nuanced, the amount of information we will need to integrate in our clinical decision making will grow, and accounting for heterogeneity will be a key part of treatment decisions that best serve all tumour features within a patient.

Through the analysis of: 1) extensive metastatic sampling at post-mortem; and 2) feasibility of tumour homogenisation, my research explores novel approaches to the study of cancer evolution and heterogeneity, with a focus on evolutionary patterns in advanced melanoma.

Aims

1. Undertake an in-depth analysis of cancer evolution, tumour heterogeneity and potential treatment resistance mechanisms in a cohort of patients with metastatic melanoma sampled at post-mortem.
2. Explore the utility of homogenisation of residual surgical tumour tissue in the assessment of tumour heterogeneity through design and implementation of a pan-cancer translational study

Hypotheses

Novel approaches to the study of evolution and heterogeneity – through post-mortem tumour sampling and homogenisation – will reveal clinically relevant insights into cancer biology.

- If comprehensive sampling of melanoma primary tumours and metastases is undertaken, then the dominant pattern of seeding from the primary tumour to metastases will appear polyclonal.
- If the post-mortem interval impacts nucleic acid quality, then there will be a negative correlation between an increasing post-mortem interval and measures of DNA and RNA integrity.
- Homogenisation of excess (non-embedded) tumour tissue will prove feasible across a number of tumour types.
- If a tumour homogenate is analysed using next-generation sequencing (NGS) techniques, then a greater number of variants will be evident than through routine clinical profiling.

References for Introduction

1. Nowell PC: The clonal evolution of tumor cell populations. *Science* 194: 23–8, 1976.
2. Turajlic S, Xu H, Litchfield K, et al. Deterministic Evolutionary Trajectories Influence Primary Tumor Growth: TRACERx Renal. *Cell* 173: 595–610 e11, 2018.
3. Jamal-Hanjani M, Wilson GA, McGranahan N, et al. Tracking the Evolution of Non-Small-Cell Lung Cancer. *N Engl J Med* 376: 2109–2121, 2017.
4. Hanahan D, Weinberg RA: Hallmarks of cancer: the next generation. *Cell* 144: 646–74, 2011.
5. Bakhoum SF, Cantley LC: The Multifaceted Role of Chromosomal Instability in Cancer and Its Microenvironment. *Cell* 174: 1347–1360, 2018.
6. Turajlic S, Sottoriva A, Graham T, et al. Resolving genetic heterogeneity in cancer. *Nat Rev Genet* 20: 404–416, 2019.
7. Vogelstein B, Papadopoulos N, Velculescu VE, et al. Cancer genome landscapes. *Science* 339: 1546–58, 2013.
8. Reiter JG, Makohon-Moore AP, Gerold JM, et al. Minimal functional driver gene heterogeneity among untreated metastases. *Science* 361: 1033–1037, 2018.
9. Turajlic S, Xu H, Litchfield K, et al. Tracking Cancer Evolution Reveals Constrained Routes to Metastases: TRACERx Renal. *Cell* 173: 581–594 e12, 2018.
10. Andor N, Graham TA, Jansen M, et al. Pan-cancer analysis of the extent and consequences of intratumor heterogeneity. *Nat Med* 22: 105–13, 2016.
11. Morris LG, Riaz N, Desrichard A, et al. Pan-cancer analysis of intratumor heterogeneity as a prognostic determinant of survival. *Oncotarget* 7: 10051–63, 2016.
12. Misale S, Di Nicolantonio F, Sartore-Bianchi A, et al. Resistance to anti-EGFR therapy in colorectal cancer: from heterogeneity to convergent evolution. *Cancer Discov* 4: 1269–80, 2014.
13. Piotrowska Z, Hazar-Rethinam M, Rizzo C, et al. Heterogeneity and Coexistence of T790M and T790 Wild-Type Resistant Subclones Drive Mixed Response to Third-Generation Epidermal Growth Factor Receptor Inhibitors in Lung Cancer. *JCO Precis Oncol* 2018, 2018.
14. Fearon ER, Vogelstein B: A genetic model for colorectal tumorigenesis. *Cell* 61: 759–67, 1990.
15. Davis A, Gao R, Navin N: Tumor evolution: Linear, branching, neutral or punctuated? *Biochim Biophys Acta Rev Cancer* 1867: 151–161, 2017.

16. Riaz N, Havel JJ, Makarov V, et al. Tumor and Microenvironment Evolution during Immunotherapy with Nivolumab. *Cell* 171: 934–949 e16, 2017.
17. Angelova M, Mlecnik B, Vasaturo A, et al. Evolution of Metastases in Space and Time under Immune Selection. *Cell* 175: 751–765 e16, 2018.
18. Turajlic S, McGranahan N, Swanton C: Inferring mutational timing and reconstructing tumour evolutionary histories. *Biochim Biophys Acta* 1855: 264–75, 2015.
19. Jolly C, Van Loo P: Timing somatic events in the evolution of cancer. *Genome Biol* 19: 95, 2018.
20. Roth A, Khattra J, Yap D, et al. PyClone: statistical inference of clonal population structure in cancer. *Nat Methods* 11: 396–8, 2014.
21. Turajlic S, Swanton C: Metastasis as an evolutionary process. *Science* 352: 169–75, 2016.
22. Caswell DR, Swanton C: The role of tumour heterogeneity and clonal cooperativity in metastasis, immune evasion and clinical outcome. *BMC Med* 15: 133, 2017.
23. Birkbak NJ, McGranahan N: Cancer Genome Evolutionary Trajectories in Metastasis. *Cancer Cell* 37: 8–19, 2020.
24. Qazi MA, Vora P, Venugopal C, et al. Intratumoral heterogeneity: pathways to treatment resistance and relapse in human glioblastoma. *Ann Oncol* 28: 1448–1456, 2017.
25. Reiter JG, Baretti M, Gerold JM, et al. An analysis of genetic heterogeneity in untreated cancers. *Nat Rev Cancer* 19: 639–650, 2019.
26. Makohon-Moore AP, Zhang M, Reiter JG, et al. Limited heterogeneity of known driver gene mutations among the metastases of individual patients with pancreatic cancer. *Nat Genet* 49: 358–366, 2017.
27. McFadden DG, Papagiannakopoulos T, Taylor-Weiner A, et al. Genetic and clonal dissection of murine small cell lung carcinoma progression by genome sequencing. *Cell* 156: 1298–1311, 2014.
28. Gundem G, Van Loo P, Kremeyer B, et al. The evolutionary history of lethal metastatic prostate cancer. *Nature* 520: 353–357, 2015.
29. Hu Z, Ding J, Ma Z, et al. Quantitative evidence for early metastatic seeding in colorectal cancer. *Nat Genet* 51: 1113–1122, 2019.
30. Greaves M, Maley CC: Clonal evolution in cancer. *Nature* 481: 306–13, 2012.
31. Hong C, Tijhuis AE, Foijer F: The cGAS Paradox: Contrasting Roles for cGAS-STING Pathway in Chromosomal Instability. *Cells* 8, 2019.
32. Paulsson K, Johansson B: Trisomy 8 as the sole chromosomal aberration in acute myeloid leukemia and myelodysplastic syndromes. *Pathol Biol* (Paris) 55: 37–48, 2007.
33. Ben-David U, Amon A: Context is everything: aneuploidy in cancer. *Nat Rev Genet* 21: 44–62, 2020.
34. Gao R, Davis A, McDonald TO, et al. Punctuated copy number evolution and clonal stasis in triple-negative breast cancer. *Nat Genet* 48: 1119–30, 2016.
35. Cross W, Kovac M, Mustonen V, et al. The evolutionary landscape of colorectal tumorigenesis. *Nat Ecol Evol* 2: 1661–1672, 2018.
36. Pavelka N, Rancati G, Zhu J, et al. Aneuploidy confers quantitative proteome changes and phenotypic variation in budding yeast. *Nature* 468: 321–5, 2010.
37. Watkins TBK, Lim EL, Petkovic M, et al. Pervasive chromosomal instability and karyotype order in tumour evolution. *Nature* 587: 126–132, 2020.

38. Vasudevan A, Baruah PS, Smith JC, et al. Single-Chromosomal Gains Can Function as Metastasis Suppressors and Promoters in Colon Cancer. *Dev Cell* 52: 413–428 e6, 2020.
39. Dewhurst SM, McGranahan N, Burrell RA, et al. Tolerance of whole-genome doubling propagates chromosomal instability and accelerates cancer genome evolution. *Cancer Discov* 4: 175–185, 2014.
40. Kuznetsova AY, Seget K, Moeller GK, et al. Chromosomal instability, tolerance of mitotic errors and multidrug resistance are promoted by tetraploidization in human cells. *Cell Cycle* 14: 2810–20, 2015.
41. Bielski CM, Zehir A, Penson AV, et al. Genome doubling shapes the evolution and prognosis of advanced cancers. *Nat Genet* 50: 1189–1195, 2018.
42. Priestley P, Baber J, Lolkema MP, et al. Pan-cancer whole-genome analyses of metastatic solid tumours. *Nature* 575: 210–216, 2019.
43. Endesfelder D, McGranahan N, Birkbak NJ, et al. A breast cancer meta-analysis of two expression measures of chromosomal instability reveals a relationship with younger age at diagnosis and high risk histopathological variables. *Oncotarget* 2: 529–37, 2011.
44. Anagnostou V, Smith KN, Forde PM, et al. Evolution of Neoantigen Landscape during Immune Checkpoint Blockade in Non-Small Cell Lung Cancer. *Cancer Discov* 7: 264–276, 2017.
45. McGranahan N, Furness AJ, Rosenthal R, et al. Clonal neoantigens elicit T cell immunoreactivity and sensitivity to immune checkpoint blockade. *Science* 351: 1463–9, 2016.
46. McGranahan N, Rosenthal R, Hiley CT, et al. Allele-Specific HLA Loss and Immune Escape in Lung Cancer Evolution. *Cell* 171: 1259–1271 e11, 2017.
47. Tripathi R, Modur V, Senovilla L, et al. Suppression of tumor antigen presentation during aneuploid tumor evolution contributes to immune evasion. *Oncoimmunology* 8: 1657374, 2019.
48. Tijhuis AE, Johnson SC, McClelland SE: The emerging links between chromosomal instability (CIN), metastasis, inflammation and tumour immunity. *Mol Cytogenet* 12: 17, 2019.
49. Wolf Y, Bartok O, Patkar S, et al. UVB-Induced Tumor Heterogeneity Diminishes Immune Response in Melanoma. *Cell* 179: 219–235 e21, 2019.
50. Miao D, Margolis CA, Vokes NI, et al. Genomic correlates of response to immune checkpoint blockade in microsatellite-stable solid tumors. *Nat Genet* 50: 1271–1281, 2018.
51. Kalaora S, Wolf Y, Feferman T, et al. Combined Analysis of Antigen Presentation and T-cell Recognition Reveals Restricted Immune Responses in Melanoma. *Cancer Discov* 8: 1366–1375, 2018.
52. Sun L, Wu J, Du F, et al. Cyclic GMP-AMP synthase is a cytosolic DNA sensor that activates the type I interferon pathway. *Science* 339: 786–91, 2013.
53. Mackenzie KJ, Carroll P, Martin CA, et al. cGAS surveillance of micronuclei links genome instability to innate immunity. *Nature* 548: 461–465, 2017.
54. Davoli T, Uno H, Wooten EC, et al. Tumor aneuploidy correlates with markers of immune evasion and with reduced response to immunotherapy. *Science* 355, 2017.
55. Taylor AM, Shih J, Ha G, et al. Genomic and Functional Approaches to Understanding Cancer Aneuploidy. *Cancer Cell* 33: 676–689 e3, 2018.
56. D'Orazio J, Jarrett S, Amaro-Ortiz A, et al. UV radiation and the skin. *Int J Mol Sci* 14: 12222–48, 2013.

57. Kuk D, Shoushtari AN, Barker CA, et al. Prognosis of Mucosal, Uveal, Acral, Nonacral Cutaneous, and Unknown Primary Melanoma From the Time of First Metastasis. *Oncologist* 21: 848–54, 2016.
58. Read J, Wadt KA, Hayward NK: Melanoma genetics. J Med Genet 53: 1–14, 2016.
59. Hayward NK, Wilmott JS, Waddell N, et al. Whole-genome landscapes of major melanoma subtypes. *Nature* 545: 175–180, 2017.
60. Cancer Genome Atlas N: Genomic Classification of Cutaneous Melanoma. *Cell* 161: 1681–96, 2015.
61. Zeng H, Judson-Torres RL, Shain AH: The Evolution of Melanoma – Moving beyond Binary Models of Genetic Progression. *J Invest Dermatol* 140: 291–297, 2020.
62. Alexandrov LB, Nik-Zainal S, Wedge DC, et al. Signatures of mutational processes in human cancer. *Nature* 500: 415–21, 2013.
63. Newell F, Wilmott JS, Johansson PA, et al. Whole-genome sequencing of acral melanoma reveals genomic complexity and diversity. Nat Commun 11: 5259, 2020.
64. Szerlip NJ, Pedraza A, Chakravarty D, et al. Intratumoral heterogeneity of receptor tyrosine kinases EGFR and PDGFRA amplification in glioblastoma defines subpopulations with distinct growth factor response. *Proc Natl Acad Sci USA* 109: 3041–6, 2012.
65. Curtin JA, Fridlyand J, Kageshita T, et al. Distinct sets of genetic alterations in melanoma. *N Engl J Med* 353: 2135–47, 2005.
66. Hodis E, Watson IR, Kryukov GV, et al. A landscape of driver mutations in melanoma. *Cell* 150: 251–63, 2012.
67. Bishop KD, Olszewski AJ: Epidemiology and survival outcomes of ocular and mucosal melanomas: a population-based analysis. *Int J Cancer* 134: 2961–71, 2014.
68. Heppt MV, Roesch A, Weide B, et al. Prognostic factors and treatment outcomes in 444 patients with mucosal melanoma. *Eur J Cancer* 81: 36–44, 2017.
69. Furney SJ, Turajlic S, Stamp G, et al. Genome sequencing of mucosal melanomas reveals that they are driven by distinct mechanisms from cutaneous melanoma. *J Pathol* 230: 261–9, 2013.
70. Newell F, Kong Y, Wilmott JS, et al. Whole-genome landscape of mucosal melanoma reveals diverse drivers and therapeutic targets. *Nat Commun* 10: 3163, 2019.
71. Johnson DB, Carlson JA, Elvin JA, et al. Landscape of genomic alterations (GA) and tumor mutational burden (TMB) in different metastatic melanoma (MM) subtypes. *Journal of Clinical Oncology* 35: 9536–9536, 2017.
72. Zhou R, Shi C, Tao W, et al. Analysis of Mucosal Melanoma Whole-Genome Landscapes Reveals Clinically Relevant Genomic Aberrations. *Clin Cancer Res* 25: 3548–3560, 2019.
73. Amit M, Tam S, Abdelmeguid AS, et al. Mutation status among patients with sinonasal mucosal melanoma and its impact on survival. *Br J Cancer* 116: 1564–1571, 2017.
74. Van Raamsdonk CD, Griewank KG, Crosby MB, et al. Mutations in GNA11 in uveal melanoma. *N Engl J Med* 363: 2191–9, 2010.
75. Van Raamsdonk CD, Bezrookove V, Green G, et al. Frequent somatic mutations of GNAQ in uveal melanoma and blue naevi. *Nature* 457: 599–602, 2009.
76. Field MG, Durante MA, Anbunathan H, et al. Punctuated evolution of canonical genomic aberrations in uveal melanoma. *Nat Commun* 9: 116, 2018.
77. Harbour JW, Roberson ED, Anbunathan H, et al. Recurrent mutations at codon 625 of the splicing factor SF3B1 in uveal melanoma. *Nat Genet* 45: 133–5, 2013.

78. Harbour JW, Onken MD, Roberson ED, et al. Frequent mutation of BAP1 in metastasizing uveal melanomas. *Science* 330: 1410–3, 2010.
79. Martin M, Masshofer L, Temming P, et al. Exome sequencing identifies recurrent somatic mutations in EIF1AX and SF3B1 in uveal melanoma with disomy 3. *Nat Genet* 45: 933–6, 2013.
80. Furney SJ, Pedersen M, Gentien D, et al. SF3B1 mutations are associated with alternative splicing in uveal melanoma. *Cancer Discov* 3: 1122–1129, 2013.
81. Institute B: SNP6 Copy number analysis (GISTIC2), 2016.
82. Knudson AG, Jr., Meadows AT, Nichols WW, et al. Chromosomal deletion and retinoblastoma. *N Engl J Med* 295: 1120–3, 1976.
83. Birkeland E, Zhang S, Poduval D, et al. Patterns of genomic evolution in advanced melanoma. *Nat Commun* 9: 2665, 2018.
84. Micevic G, Theodosakis N, Bosenberg M: Aberrant DNA methylation in melanoma: biomarker and therapeutic opportunities. *Clin Epigenetics* 9: 34, 2017.
85. Harbst K, Staaf J, Masback A, et al. Multiple metastases from cutaneous malignant melanoma patients may display heterogeneous genomic and epigenomic patterns. *Melanoma Res* 20: 381–91, 2010.
86. McGranahan N, Swanton C: Clonal Heterogeneity and Tumor Evolution: Past, Present, and the Future. *Cell* 168: 613–628, 2017.
87. Dentro SC, Leshchiner I, Haase K, et al. Characterizing genetic intra-tumor heterogeneity across 2,658 human cancer genomes. *Cell* 184: 2239–2254 e39, 2021.
88. Shain AH, Yeh I, Kovalyshyn I, et al. The Genetic Evolution of Melanoma from Precursor Lesions. *N Engl J Med* 373: 1926–36, 2015.
89. Colebatch AJ, Ferguson P, Newell F, et al. Molecular Genomic Profiling of Melanocytic Nevi. *J Invest Dermatol* 139: 1762–1768, 2019.
90. Shain AH, Joseph NM, Yu R, et al. Genomic and Transcriptomic Analysis Reveals Incremental Disruption of Key Signaling Pathways during Melanoma Evolution. *Cancer Cell* 34: 45–55 e4, 2018.
91. Zhang X, Peng Y, Li C, et al. Genomic Heterogeneity and Branched Evolution of Early Stage Primary Acral Melanoma Shown by Multiregional Microdissection Sequencing. *J Invest Dermatol* 139: 1526–1534, 2019.
92. Sanborn JZ, Chung J, Purdom E, et al. Phylogenetic analyses of melanoma reveal complex patterns of metastatic dissemination. *Proc Natl Acad Sci USA* 112: 10995–1000, 2015.
93. Brastianos PK, Carter SL, Santagata S, et al. Genomic Characterization of Brain Metastases Reveals Branched Evolution and Potential Therapeutic Targets. *Cancer Discov* 5: 1164–1177, 2015.
94. Turajlic S, Furney SJ, Lambros MB, et al. Whole genome sequencing of matched primary and metastatic acral melanomas. *Genome Res* 22: 196–207, 2012.
95. Harbst K, Lauss M, Cirenajwis H, et al. Multiregion Whole-Exome Sequencing Uncovers the Genetic Evolution and Mutational Heterogeneity of Early-Stage Metastatic Melanoma. *Cancer Res* 76: 4765–74, 2016.
96. Davidson G, Coassolo S, Kieny A, et al. Dynamic Evolution of Clonal Composition and Neoantigen Landscape in Recurrent Metastatic Melanoma with a Rare Combination of Driver Mutations. *J Invest Dermatol* 139: 1769–1778 e2, 2019.
97. Rabbie R, Ansari-Pour N, Cast O, et al. Multi-site clonality analysis uncovers pervasive heterogeneity across melanoma metastases. Nat Commun 11: 4306, 2020.
98. Harbst K, Lauss M, Cirenajwis H, et al. Molecular and genetic diversity in the metastatic process of melanoma. *J Pathol* 233: 39–50, 2014.

99. Fischer GM, Jalali A, Kircher DA, et al. Molecular Profiling Reveals Unique Immune and Metabolic Features of Melanoma Brain Metastases. *Cancer Discov* 9: 628–645, 2019.
100. Reuben A, Spencer CN, Prieto PA, et al. Genomic and immune heterogeneity are associated with differential responses to therapy in melanoma. *NPJ Genom Med* 2, 2017.
101. Ding L, Kim M, Kanchi KL, et al. Clonal architectures and driver mutations in metastatic melanomas. *PLoS One* 9: e111153, 2014.
102. Shain AH, Bagger MM, Yu R, et al. The genetic evolution of metastatic uveal melanoma. *Nat Genet* 51: 1123–1130, 2019.
103. Jerby-Arnon L, Shah P, Cuoco MS, et al. A Cancer Cell Program Promotes T Cell Exclusion and Resistance to Checkpoint Blockade. *Cell* 175: 984–997 e24, 2018.
104. Smalley I, Kim E, Li J, et al. Leveraging transcriptional dynamics to improve BRAF inhibitor responses in melanoma. *EBioMedicine* 48: 178–190, 2019.
105. Yan Y, Leontovich AA, Gerdes MJ, et al. Understanding heterogeneous tumor microenvironment in metastatic melanoma. *PLoS One* 14: e0216485, 2019.
106. Eggermont AMM, Blank CU, Mandala M, et al. Adjuvant Pembrolizumab versus Placebo in Resected Stage III Melanoma. *N Engl J Med* 378: 1789–1801, 2018.
107. Long GV, Hauschild A, Santinami M, et al. Adjuvant Dabrafenib plus Trametinib in Stage III BRAF-Mutated Melanoma. *N Engl J Med*, 2017.
108. Weber J, Mandala M, Del Vecchio M, et al. Adjuvant Nivolumab versus Ipilimumab in Resected Stage III or IV Melanoma. *N Engl J Med*, 2017.
109. Long GV, Stroyakovskiy D, Gogas H, et al. Dabrafenib and trametinib versus dabrafenib and placebo for Val600 BRAF-mutant melanoma: a multicentre, double-blind, phase 3 randomised controlled trial. *Lancet* 386: 444–51, 2015.
110. Larkin J, Chiarion-Sileni V, Gonzalez R, et al. Combined Nivolumab and Ipilimumab or Monotherapy in Untreated Melanoma. *N Engl J Med* 373: 23–34, 2015.
111. Robert C, Thomas L, Bondarenko I, et al. Ipilimumab plus dacarbazine for previously untreated metastatic melanoma. *N Engl J Med* 364: 2517–26, 2011.
112. Davies H, Bignell GR, Cox C, et al. Mutations of the BRAF gene in human cancer. *Nature* 417: 949–54, 2002.
113. Menzies AM, Haydu LE, Visintin L, et al. Distinguishing clinicopathologic features of patients with V600E and V600K BRAF-mutant metastatic melanoma. *Clin Cancer Res* 18: 3242–9, 2012.
114. Robert C, Grob JJ, Stroyakovskiy D, et al. Five-Year Outcomes with Dabrafenib plus Trametinib in Metastatic Melanoma. *N Engl J Med* 381: 626–636, 2019.
115. Menzer C, Menzies AM, Carlino MS, et al. Targeted Therapy in Advanced Melanoma With Rare BRAF Mutations. *J Clin Oncol* 37: 3142–3151, 2019.
116. Holderfield M, Deuker MM, McCormick F, et al. Targeting RAF kinases for cancer therapy: BRAF-mutated melanoma and beyond. *Nat Rev Cancer* 14: 455–67, 2014.
117. Turajlic S, Furney SJ, Stamp G, et al. Whole-genome sequencing reveals complex mechanisms of intrinsic resistance to BRAF inhibition. *Ann Oncol* 25: 959–67, 2014.
118. Long GV, Fung C, Menzies AM, et al. Increased MAPK reactivation in early resistance to dabrafenib/trametinib combination therapy of BRAF-mutant metastatic melanoma. *Nat Commun* 5: 5694, 2014.
119. Van Allen EM, Wagle N, Sucker A, et al. The genetic landscape of clinical resistance to RAF inhibition in metastatic melanoma. *Cancer Discov* 4: 94–109, 2014.
120. Shi H, Hugo W, Kong X, et al. Acquired resistance and clonal evolution in melanoma during BRAF inhibitor therapy. *Cancer Discov* 4: 80–93, 2014.

121. Carvajal RD, Antonescu CR, Wolchok JD, et al. KIT as a therapeutic target in metastatic melanoma. *JAMA* 305: 2327–34, 2011.
122. Freeman GJ, Long AJ, Iwai Y, et al. Engagement of the PD-1 immunoinhibitory receptor by a novel B7 family member leads to negative regulation of lymphocyte activation. *J Exp Med* 192: 1027–34, 2000.
123. Rudd CE, Taylor A, Schneider H: CD28 and CTLA-4 coreceptor expression and signal transduction. *Immunol Rev* 229: 12–26, 2009.
124. Snyder A, Wolchok JD, Chan TA: Genetic basis for clinical response to CTLA-4 blockade. *N Engl J Med* 372: 783, 2015.
125. Van Allen EM, Miao D, Schilling B, et al. Genomic correlates of response to CTLA-4 blockade in metastatic melanoma. *Science* 350: 207–11, 2015.
126. Liu D, Schilling B, Liu D, et al. Integrative molecular and clinical modeling of clinical outcomes to PD1 blockade in patients with metastatic melanoma. *Nat Med* 25: 1916–1927, 2019.
127. Roh W, Chen PL, Reuben A, et al. Integrated molecular analysis of tumor biopsies on sequential CTLA-4 and PD-1 blockade reveals markers of response and resistance. *Sci Transl Med* 9, 2017.
128. Cristescu R, Mogg R, Ayers M, et al. Pan-tumor genomic biomarkers for PD-1 checkpoint blockade-based immunotherapy. *Science* 362, 2018.
129. Jiang P, Gu S, Pan D, et al. Signatures of T cell dysfunction and exclusion predict cancer immunotherapy response. *Nat Med* 24: 1550–1558, 2018.
130. Neefjes J, Jongsma ML, Paul P, et al. Towards a systems understanding of MHC class I and MHC class II antigen presentation. Nat Rev Immunol 11: 823–36, 2011.
131. Perarnau B, Siegrist CA, Gillet A, et al. Beta 2-microglobulin restriction of antigen presentation. *Nature* 346: 751–4, 1990.
132. Rodig SJ, Gusenleitner D, Jackson DG, et al. MHC proteins confer differential sensitivity to CTLA-4 and PD-1 blockade in untreated metastatic melanoma. *Sci Transl Med* 10, 2018.
133. Zaretsky JM, Garcia-Diaz A, Shin DS, et al. Mutations Associated with Acquired Resistance to PD-1 Blockade in Melanoma. *N Engl J Med* 375: 819–29, 2016.
134. Sade-Feldman M, Jiao YJ, Chen JH, et al. Resistance to checkpoint blockade therapy through inactivation of antigen presentation. *Nat Commun* 8: 1136, 2017.
135. Gettinger S, Choi J, Hastings K, et al. Impaired HLA Class I Antigen Processing and Presentation as a Mechanism of Acquired Resistance to Immune Checkpoint Inhibitors in Lung Cancer. *Cancer Discov* 7: 1420–1435, 2017.
136. Le DT, Durham JN, Smith KN, et al. Mismatch repair deficiency predicts response of solid tumors to PD-1 blockade. *Science* 357: 409–413, 2017.
137. Owen KL, Brockwell NK, Parker BS: JAK-STAT Signaling: A Double-Edged Sword of Immune Regulation and Cancer Progression. *Cancers (Basel)* 11, 2019.
138. Shin DS, Zaretsky JM, Escuin-Ordinas H, et al. Primary Resistance to PD-1 Blockade Mediated by JAK1/2 Mutations. *Cancer Discov* 7: 188–201, 2017.
139. Sucker A, Zhao F, Pieper N, et al. Acquired IFNgamma resistance impairs anti-tumor immunity and gives rise to T-cell-resistant melanoma lesions. *Nat Commun* 8: 15440, 2017.
140. Gao J, Shi LZ, Zhao H, et al. Loss of IFN-gamma Pathway Genes in Tumor Cells as a Mechanism of Resistance to Anti-CTLA-4 Therapy. *Cell* 167: 397–404 e9, 2016.
141. George S, Miao D, Demetri GD, et al. Loss of PTEN Is Associated with Resistance to Anti-PD-1 Checkpoint Blockade Therapy in Metastatic Uterine Leiomyosarcoma. *Immunity* 46: 197–204, 2017.

142. Peng W, Chen JQ, Liu C, et al. Loss of PTEN Promotes Resistance to T Cell-Mediated Immunotherapy. *Cancer Discov* 6: 202–16, 2016.
143. Trujillo JA, Luke JJ, Zha Y, et al. Secondary resistance to immunotherapy associated with beta-catenin pathway activation or PTEN loss in metastatic melanoma. *J Immunother Cancer* 7: 295, 2019.
144. Zhan T, Rindtorff N, Boutros M: Wnt signaling in cancer. *Oncogene* 36: 1461–1473, 2017.
145. Spranger S, Bao R, Gajewski TF: Melanoma-intrinsic beta-catenin signalling prevents anti-tumour immunity. *Nature* 523: 231–5, 2015.
146. Harding JJ, Nandakumar S, Armenia J, et al. Prospective Genotyping of Hepatocellular Carcinoma: Clinical Implications of Next-Generation Sequencing for Matching Patients to Targeted and Immune Therapies. *Clin Cancer* Res 25: 2116–2126, 2019.
147. Pinyol R, Sia D, Llovet JM: Immune Exclusion-Wnt/CTNNB1 Class Predicts Resistance to Immunotherapies in HCC. *Clin Cancer Res* 25: 2021–2023, 2019.
148. Luke JJ, Bao R, Sweis RF, et al. WNT/beta-catenin Pathway Activation Correlates with Immune Exclusion across Human Cancers. *Clin Cancer Res* 25: 3074–3083, 2019.
149. Jimenez-Sanchez A, Memon D, Pourpe S, et al. Heterogeneous Tumor-Immune Microenvironments among Differentially Growing Metastases in an Ovarian Cancer Patient. *Cell* 170: 927–938 e20, 2017.
150. Juric D, Castel P, Griffith M, et al. Convergent loss of PTEN leads to clinical resistance to a PI(3)Kalpha inhibitor. *Nature* 518: 240–4, 2015.
151. Kemper K, Krijgsman O, Cornelissen-Steijger P, et al. Intra- and inter-tumor heterogeneity in a vemurafenib-resistant melanoma patient and derived xenografts. *EMBO Mol Med* 7: 1104–18, 2015.
152. Wan JC, Massie C, Garcia-Corbacho J, et al. Liquid biopsies come of age: towards implementation of circulating tumour DNA. *Nat Rev Cancer* 17: 223–238, 2017.
153. Litchfield K, Stanislaw S, Spain L, et al. Representative Sequencing: Unbiased Sampling of Solid Tumor Tissue. *Cell* Rep 31: 107550, 2020.
154. Iacobuzio-Donahue CA, Michael C, Baez P, et al. Cancer biology as revealed by the research autopsy. *Nat Rev Cancer* 19: 686–697, 2019.
155. Yachida S, Jones S, Bozic I, et al. Distant metastasis occurs late during the genetic evolution of pancreatic cancer. *Nature* 467: 1114–7, 2010.
156. Sakamoto H, Attiyeh MA, Gerold JM, et al. The Evolutionary Origins of Recurrent Pancreatic Cancer. *Cancer Discov* 10: 792–805, 2020.
157. Savas P, Teo ZL, Lefevre C, et al. The Subclonal Architecture of Metastatic Breast Cancer: Results from a Prospective Community-Based Rapid Autopsy Program 'CASCADE'. *PLoS Med* 13: e1002204, 2016.
158. De Mattos-Arruda L, Sammut SJ, Ross EM, et al. The Genomic and Immune Landscapes of Lethal Metastatic Breast Cancer. *Cell Rep* 27: 2690–2708 e10, 2019.
159. Brown D, Smeets D, Szekely B, et al. Phylogenetic analysis of metastatic progression in breast cancer using somatic mutations and copy number aberrations. *Nat Commun* 8: 14944, 2017.
160. Siravegna G, Lazzari L, Crisafulli G, et al. Radiologic and Genomic Evolution of Individual Metastases during HER2 Blockade in Colorectal Cancer. *Cancer Cell* 34: 148–162 e7, 2018.
161. Abbosh C, Birkbak NJ, Wilson GA, et al. Phylogenetic ctDNA analysis depicts early-stage lung cancer evolution. *Nature* 545: 446–451, 2017.

162. Goyal L, Saha SK, Liu LY, et al. Polyclonal Secondary FGFR2 Mutations Drive Acquired Resistance to FGFR Inhibition in Patients with FGFR2 Fusion-Positive Cholangiocarcinoma. *Cancer Discov* 7: 252–263, 2017.
163. Fan J, Khanin R, Sakamoto H, et al. Quantification of nucleic acid quality in postmortem tissues from a cancer research autopsy program. *Oncotarget* 7: 66906–66921, 2016.
164. Frankell AM, Jammula S, Li X, et al. The landscape of selection in 551 esophageal adenocarcinomas defines genomic biomarkers for the clinic. *Nat Genet* 51: 506–516, 2019.
165. Gerlinger M, Rowan AJ, Horswell S, et al. Intratumor heterogeneity and branched evolution revealed by multiregion sequencing. *N Engl J Med* 366: 883–892, 2012.
166. Torres L, Ribeiro FR, Pandis N, et al. Intratumor genomic heterogeneity in breast cancer with clonal divergence between primary carcinomas and lymph node metastases. *Breast Cancer Res Treat* 102: 143–55, 2007.
167. Campbell PJ, Pleasance ED, Stephens PJ, et al. Subclonal phylogenetic structures in cancer revealed by ultra-deep sequencing. *Proc Natl Acad Sci USA* 105: 13081–6, 2008.
168. Burrell RA, McGranahan N, Bartek J, et al. The causes and consequences of genetic heterogeneity in cancer evolution. Nature 501: 338–45, 2013.
169. Fisher R, Pusztai L, Swanton C: Cancer heterogeneity: implications for targeted therapeutics. *Br J Cancer* 108: 479–85, 2013.
170. Narod SA: Tumour size predicts long-term survival among women with lymph node-positive breast cancer. *Curr Oncol* 19: 249–53, 2012.
171. Kornprat P, Pollheimer MJ, Lindtner RA, et al. Value of tumor size as a prognostic variable in colorectal cancer: a critical reappraisal. *Am J Clin Oncol* 34: 43–9, 2011.
172. Jiang N, Deng JY, Ding XW, et al. Tumor volume as a prognostic factor was superior to the seventh edition of the pT classification in resectable gastric cancer. *Eur J Surg Oncol* 41: 315–22, 2015.
173. Haffner MC, Mosbruger T, Esopi DM, et al. Tracking the clonal origin of lethal prostate cancer. *J Clin Invest* 123: 4918–22, 2013.
174. Cyll K, Ersvaer E, Vlatkovic L, et al. Tumour heterogeneity poses a significant challenge to cancer biomarker research. *Br J Cancer* 117: 367–375, 2017.
175. Sunshine JC, Nguyen PL, Kaunitz GJ, et al. PD-L1 Expression in Melanoma: A Quantitative Immunohistochemical Antibody Comparison. *Clin Cancer Res* 23: 4938–4944, 2017.
176. Bilimoria MM, Holtz DJ, Mirza NQ, et al. Tumor volume as a prognostic factor for sarcomatosis. *Cancer* 94: 2441–6, 2002.
177. Lee JW, Cho A, Lee JH, et al. The role of metabolic tumor volume and total lesion glycolysis on (1)(8)F-FDG PET/CT in the prognosis of epithelial ovarian cancer. Eur *J Nucl Med Mol Imaging* 41: 1898–906, 2014.
178. Singer S, Baldini EH, Demetri GD, et al. Synovial sarcoma: prognostic significance of tumor size, margin of resection, and mitotic activity for survival. *J Clin Oncol* 14: 1201–8, 1996.
179. Tate JG, Bamford S, Jubb HC, et al: COSMIC: the Catalogue Of Somatic Mutations In Cancer. Nucleic Acids Res 47: D941–D947, 2019.

Section 2 Materials and methods

Contents

Figures

Tables

PEACE (Post-mortem) cohort

The Posthumous Evaluation of Advanced Cancer Environment (PEACE) study is a UK-wide, pan-tumour translational project (NIHR 18422) designed to comprehensively evaluate metastatic disease after death. Inclusion criteria include: 1) patients with advanced cancer, 2) consent provided by patient during life or by next of kin after death. Post-mortems are referred to as 'tissue harvests' (TH) within this study. These were conducted as soon as possible after death (within 24 hours up to a week, influenced by whether patients died in hospital or in a hospice, or at home) at either the University College London Hospital (UCLH) or Guys and St Thomas' NHS Foundation Trust (GSST) mortuaries. The post-mortem interval (PMI) and time to refrigeration (TTR) were noted for each case.

2.1 Logistics and sampling

I was closely involved in the running of the study within the Renal and Melanoma Unit at the Royal Marsden NHS Foundation Trust, actively recruiting and consenting patients in clinics from 2016 to 2018, and then with ongoing study logistics in 2019. Upon the death of a patient who consented to the study, I assisted in the logistics of arranging the post-mortem and I have attended multiple post-mortems to provide clinical direction for macroscopic tumour sampling (see Figure 6 for study processes and sampling). Data from the first 14 cases from the Royal Marsden Melanoma cohort has been included for analysis in my thesis.

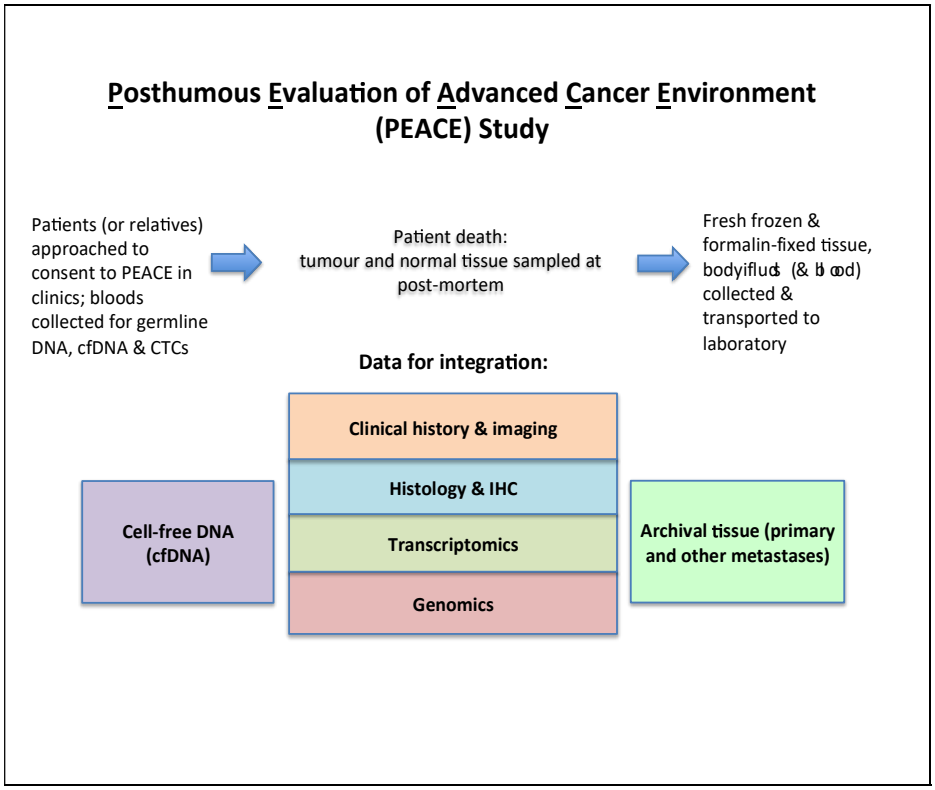

Figure 6 PEACE study sampling overview
Prior to death consented patients are asked to provide blood for germline analyses as well as for processing of plasma. At the post-mortem, cores of macroscopically evident metastatic tissue (identified by an attending histopathologist) are taken, with mirrored halves being both snap frozen and embedded in paraffin in the majority of cases. Body cavity fluids are also sampled, for example, ascitic or pleural. Normal tissue is also sampled, with particular emphasis on paired normal tissue from metastatic sites and any organ that may be subject to immune-related toxicity. Archival FFPE blocks from prior surgical resections, including primary melanomas, are sourced

2.2 DNA and RNA extraction from tissue & blood

Three-mm^3 sections are dissected from fresh frozen tumour samples and homogenised using the tissue raptor. They are then processed through a Qiagen QIAshredder and DNA and RNA is purified using the Qiagen All Prep DNA/RNA mini kit according to manufacturer's instructions. Qubit technology (ThermoFisher Scientific) was used for nucleic acid quantification (ng/uL). I extracted >10% of the samples across the 14 cases included in my thesis, in addition to re-extraction of one case (PEA005). I also extracted all of the RNA & DNA from the normal tissue samples (matched tissue sites for paired RNAseq analysis).

For archival FFPE tissue specimens, H&E slides were cut and tumour rich areas were identified by a qualified histopathologist. Punch biopsy, macrodissection and laser-capture microdissection methods have each been employed for the acquisition of tissue, depending on

the specimen size. The Qiagen GeneRead FFPE DNA extraction kit was used for DNA purification. I purified DNA from 64% of the archival samples included in the dataset for my thesis.

Germline DNA for each case was preferably extracted from whole blood (collected prior to death or at the tissue harvest) or a buffy coat (collected prior to death) using the Qiagen DNeasy blood and tissue kit, according to manufacturer's instructions. In the absence of germline DNA from blood, an area of normal tissue collected at the TH was used. These extractions were undertaken by one of the scientists involved in the PEACE study.

2.3 Quality control of DNA & RNA from post-mortem cases

For each post-mortem case, a selection of samples of DNA and RNA (from fresh-frozen tissues) were run on 1.2% agarose gels to review their quality. For DNA samples, routine tapestation analysis was performed for DNA integrity assessment (DIN score) for 11 of the 14 cases. For the other cases, library preparation was undertaken at a different institution (UCLH) for PEA004 and for PEA005 and PEA016, these were prepped prior to this operating procedure being in place. RNA samples selected for sequencing were also assessed for integrity on the agilent bioanalyser to give an integrity score (RIN).

Spearman's correlation coefficients were calculated between the DIN and RIN scores and the post-mortem interval (PMI) and time to refrigeration (TTR).

2.4 Estimation of tumour presence and purity using Sanger sequencing

I performed Sanger sequencing on tissue samples to confirm the presence of a known driver mutation (for example, in *BRAF*, *NRAS* or *KIT*) in eight cases (PEA005, PEA017, PEA020, PEA023, PEA025, PEA026, PEA036, PEA038) as a surrogate for tumour presence (approximately 20% purity is required to find mutation on Sanger sequencing). This had already been completed for PEA016. In brief, a PCR product using dedicated forward and reverse primers (for example, for *BRAF V600E)* is generated using DNA purified from each tumour region. Exopase is then added to the PCR product to prepare for the sequencing reaction. A mastermix of big dye terminator (BDT), water and each primer separately is prepared and DNA is added to this in a 96 well plate for the sequencing reaction. Traces were generated by the team at the Equipment Park at the Francis Crick Institute.

The Sanger traces were assessed as a surrogate for tumour purity, based on the height of the variant nucleotide peak relative to the normal nucleotide. Scores of 0 did not suggest tumour presence (that is, control values expected to be 0), scores of 4–5 reflected high purity and scores of 3 reflected moderate purity. Examples are shown in Figure 7 below.

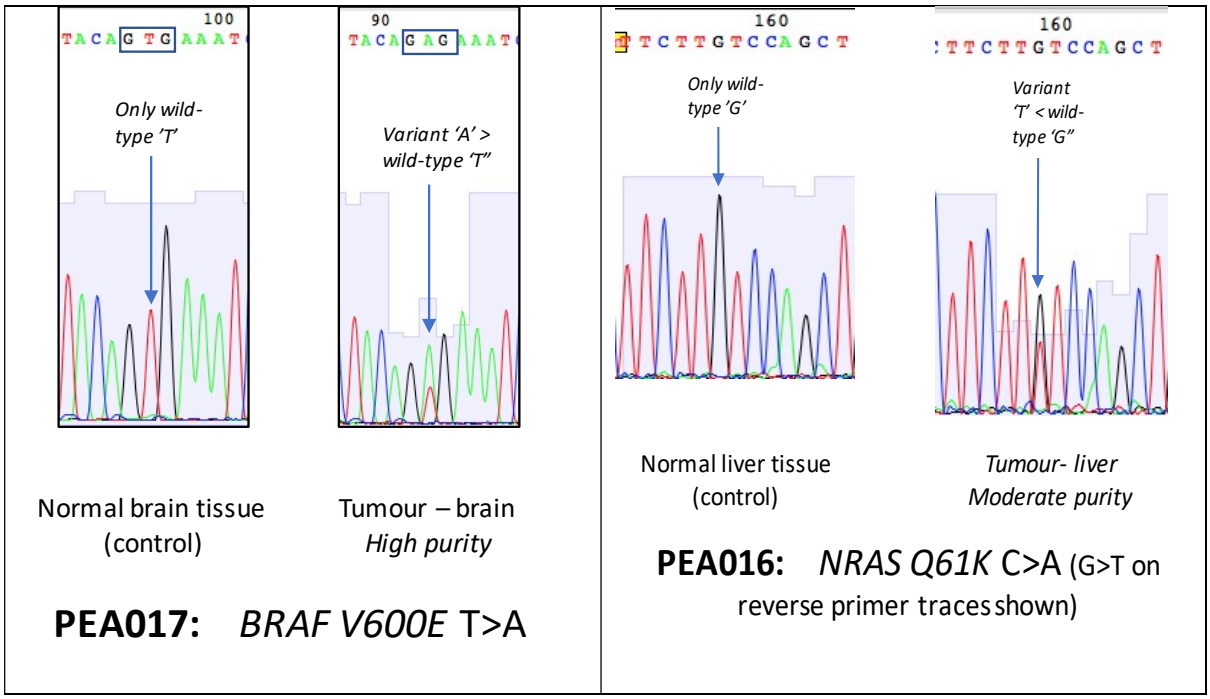

Figure 7 Examples of Sanger sequencing traces for samples in PEA017 and PEA016

The Sanger sequencing information was then used to select samples for submission for WES – only those with a score of >2 were deemed to be of sufficient purity.

For the other five cases, PEA004 had sites selected and submitted for WES as part of another project and preliminary panel sequencing data was used to select sites for WES for PEA009 (see **Section 2.7**), PEA012, PEA060 and PEA080. PEA009, PEA060 and PEA080 did not have a known driver mutation from clinical molecular profiling to enable Sanger sequencing, and the TH for PEA012 was undertaken after panel availability, unlike the prior cases. Selection of sites was also informed by histology H&E reviews (see **Section 2.6**, below) where available.

2.5 Melanin removal

In DNA purified from fresh frozen tumour regions belonging to PEA036 and for selected PEA005 archival FFPE tissue blocks, samples were heavily pigmented with melanin and did not yield a primer PCR product. Given melanin's ability to inhibit DNA polymerase and potentially interfere with polymerase chain reaction cycles involved in library preparation

and sequencing, I processed these samples with a Qiagen DNAeasy Powerclean silica spin column to remove excess melanin, as per the manufacturer's instructions.

2.6 Histopathologist review of H&E slides from post-mortem sampled tumour regions

For the majority of fresh frozen tumour samples taken at post-mortem, a paired sample is paraffin-embedded and slides are cut from this for haematoxylin and eosin (H&E) staining. I reviewed each slide (n = 487) with a consultant histopathologist to denote the viable tumour content (categories: a) no tumour; b) up to 25% tumour; c) 25–50% tumour; d) 50–75% tumour; e) 75–100% tumour), extent of any necrosis (categories a) necrotic; b) mostly necrotic; c) 50% viable; d) mostly viable; e) near 100% viable); post-mortem tissue changes such as autolysis and an estimated degree of tumour infiltrating lymphocyte (TIL) invasion (categories a) none; b) mild; c) moderate; d) heavy). Any marked changes in morphology were noted within cases, although detailed morphology was not systematically documented. Other aberrations such as heavy melanin pigmentation were also recorded.

2.7 Melanoma gene panel development

To facilitate more efficient sequencing of large numbers of samples, I developed a melanoma gene panel. First, I performed a comprehensive review of the literature for melanoma driver genes,[1-7] for genes involved in treatment resistance (for both BRAF/MEK targeted therapy and immune checkpoint therapies)[8-17] as well as DNA repair genes.[18] A list of the most common genes mutated in melanoma according to COSMIC[19] (top 20) and MutSig as well as a pre-existing list of immune genes included in a renal panel,[20] and variants of germline interest that may be involved in immune-related toxicity were all incorporated (Table 4). A single nucleotide polymorphism (SNP) backbone was included to improve the accuracy of copy number calling. The total size of the panel was 1.9Mb.

Table 4 Genes included in the melanoma panel (n = 308)

Gene	Codelen	Gene	Codelen	Gene	Codelen
NRAS	941	UGT2B15	3232	HLA-DPA1	890
TP53	1890	RB1	3700	POLQ	7889
CDKN2A	1002	STK31	3156	H2AFX	983
NF1	12120	PTPRB	6840	RAD50	4035
PTEN	1244	B2M	374	TP53BP1	6042
RAC1	660	ROS1	7212	FCGR2B	963
ARID2	5588	AHNAK	17797	BRCA1	5750
C15orf23	1024	RASA2	2644	HLA-DQB1	804
NUDT11	500	HLA-DOB	844	REV3L	9517
ZFX	2505	MYH7	5960	MITF	1836
SLC38A4	1700	MECOM	3797	BBS1	1987
FAM58A	762	HYDIN	15717	TACC1	2466
PPP6C	1057	HHLA2	1277	EFNB3	1592
C7orf58	3209	KIT	3013	NOTCH2	7548
COL3A1	4601	GNA11	1104	HFE	1067
CDK4	940	FANCM	6320	PDIA3	1566
DSG3	3060	ABCB5	3919	AXIN1	2629
MLL	12052	MAP2K2	1243	PTPRD	5944
DDX3X	2053	CD86	1014	MAP3K9	3405
HSD11B1	905	HLA-DRA	783	PRKDC	12728
ALPK2	6561	LAMA3	10475	BTBD12	5557
ATP5F1	1201	RP1	6483	LAG3	1635
RPTN	2363	PREX2	5208	JAK2	3491
KRTAP5-10	611	GRM3	2656	HLA-DQA2	786
GML	489	MAGEC1	3434	TSC1	3579
MAP2K1	1224	NRK	4861	MRPS31	1216
IDH1	1277	MSH6	4123	IL1A	840
KEL	2271	TET2	6134	HLA-DOA	771
RQCD1	927	STAB1	7990	MLL2	16826
NGF	730	DIDO1	6905	CALR	1288
DMC1	1075	COL4A5	5269	PVR	1309
TRERF1	3655	TAP2	2294	CWH43	2160
CYP3A5	1559	TRRAP	11773	HLA-C	1131
BRAF	2371	FGFR2	2782	FCGR2A	980
NBPF1	3519	ARID1B	6826	CHEK1	1606

ZNF780B	2518	SETD2	7777	CENPE	8300
STK19	3764	SMARCA4	5189	HLA-F	1360
KYNU	1478	BRCA2	10361	POLE	7082
ANO4	2863	HSPA5	1993	HLA-E	1107
SLC27A5	2111	TAP1	2471	TAPBP	3255
POTEG	1568	PPARG	1544	CEACAM1	1710
TPTE	1740	ERBB4	4037	GRIN2A	4443
USH2A	15901	PIK3R1	2361	DEFB134	204
XIRP2	12234	APC	8592	MDC1	6385
THSD7B	4837	FGFR3	2642	CSF1R	3007
USP17L2	1593	TNFSF18	609	ADORA2A	1243
S100A8	292	ASXL3	6793	MDM2	1534
CTNNB1	2406	PALB2	3726	MICA	1178
USP9X	7885	SNX31	1375	MRE11A	2379
C10orf28	2361	MAGEC3	2328	NDST3	2670
MAN1A1	2006	COL17A1	4714	CCL2	310
OXA1L	1524	PDCD11	5756	CHCHD2	470
NAP1L2	1383	HLA-DRB1	823	CD58	775
MPP7	1791	HLA-DMB	812	TNFSF4	560
BTK	2052	HLA-A	1128	ULBP1	753
SLC9A11	3483	RAD52	1301	DDC	1499
EMG1	1360	AXIN2	2568	AKT3	1662
SELP	2558	TNFSF14	739	RAET1E	808
PARM1	945	ATM	9439	SOX2	954
ACSBG1	2229	PIK3CA	3287	CD274	897
CCK	356	HRAS	659	HS6ST2	1524
C1QTNF9	1014	MYC	1373	RBPMS2	658
UBE2V2	452	GNAQ	1106	BAP1	2254
BOLA1	418	IRF1	1014	TNFRSF4	860
IFNGR2	1038	ERCC6	6344	VTCN1	871
KRAS	709	HLA-DQA1	786	MLH1	4162
ZNF595	1956	ERBB2	3887	CANX	1835
PRKAA2	1693	TSC2	5590	CREBBP	7449
MMP27	1582	PDCD1LG2	846	APLNR	1143
POLR2B	4560	FANCD2	4667	CCND1	904
CSN3	565	KDR	4187	CTLA4	684
CASP8	1749	SOX10	1413	RPA2	845

PPFIA1	3721	HLA-DMA	804	HNF1A	1934
ZNF490	1611	PDGFRA	3358	LGALS9	1108
IL5RA	1327	CD40	868	NBN	2325
LILRB5	1824	MICB	1172	PES1	1825
C10orf72	1114	TCF12	2278	STAT1	2346
C3orf71	873	HAVCR2	930	CHEK2	2071
ZNF589	1109	APC2	6968	IDO1	1248
DSP	8708	NOS2	3566	BCL2A1	592
ZZZ3	2756	PTPRK	4461	MSH2	2867
MCART2	896	EP300	7365	SOX11	1328
CD2	1074	MAPK1	1115	ATR	8119
CD209	1241	TNFRSF9	796	FAT4	15010
C2orf16	5957	CDK12	4525	EGFR	3999
GLRB	1530	IDH2	1401	JAK1	3561
PKDREJ	6762	HDAC9	3442	POLD1	3430
PTPRT	4507	TNFRSF18	997	HLA-G	1041
FAM55C	1696	KNTC1	6882	HLA-DPB1	884
NUDT4	562	EZH2	2332	SHPRH	5210
MYPOP	1208	MTOR	8871	TERT	3461
MLL4	8293	RPA1	1930	LRP1B	14160
MMP1	1450	AKT1	1495	CD70	590
THEMIS	2067	HLA-B	1119	FCGR3B	718
ACO1	2750	ARID1A	6934	LGALS3	860
MUC7	1142	CD80	887	MLANA	373
TP63	2258	IL1B	834	RAD51	1181
APCS	678	MET	4307	RPA3	380
MAP3K5	4241	HOXD8	877	RPL23	443
COL21A1	2990	MAPK3	1229	RPS14	474
MLL3	14968	TNFSF9	775	TAPBPL	1856
SF3B1	4035	VEGFA	1291		
DPYD	3207	WNT7B	1062		
		CD276	1641		

2.8 DNA sequencing

I normalised samples of purified DNA in preparation for library preparation and sequencing. The actual library preparation was undertaken by one of the scientists in the laboratory.

Whole exome sequencing (WES)

Approximately 10 tumour regions from each case were selected for whole exome sequencing (WES). At least one sample representative of each metastatic area was selected. For DNA purified from fresh frozen samples, 1700–3000 ng was submitted for library preparation. First, DNA was sheared into fragments using covaris sonication. SureSelectXT library preparation kits were utilized as per the manufacturer's instructions. A total of six pre-capture PCR cycles and 12 post-capture PCR cycles were used for each batch.

The Kapa HyperPrep kit was used for archival FFPE-derived DNA samples, according to the manufacturer's instructions, with the following variations: After a failed library preparation for our first batch of samples prepped with the Kapa kit, we extended the adapter ligation period from 60 minutes to three hours. We then adopted this approach for every subsequent batch. Given the variable inputs (50–200ng of DNA), the number of pre-capture PCR cycles varied from six to 12.

Agilent Human Exome v5 baits were used and samples were sequenced on the Hiseq 4000, with paired end (PE) 100 read length. We aimed for 300× coverage for samples derived from fresh frozen tissue and 150× coverage for FFPE-derived samples. Coverage detailed in Table 5, below.

Table 5 Median de-duplication coverage and duplication rate for samples submitted for whole exome sequencing (WES) across the cohort

	De-dup coverage		Duplication rate (%)	
	Median TH	***Median FFPE***	***Median TH***	***Median FFPE***
PEA004	195	191	19	58
PEA005	312	na*	25	na*
PEA009	225	na	25	na
PEA012	227	na*	24	na*
PEA016	330	151	23	66
PEA017	227	232	25	67
PEA020	305	329	29	52
PEA023	224	257	22	59
PEA025	247	348	21	43
PEA026	234	na	24	na
PEA036	227	357	23	40
PEA038	215	333	23	52
PEA060	195	256	27	60
PEA080	194	352	25	41
COHORT median	***227***	***293***	***24***	***55***

na= sample not available; na = sample(s) available, but quality not sufficient for analysis*

Targeted panel sequencing

All samples were prepared using the SureSelectXT library preparation kit. The custom-designed melanoma gene panel was used for capture. Sequencing was undertaken on the NextSeq (Illumina), PE 150 read length, aim for minimum 300× coverage. The panel sequencing data has not been included in my results as processing and analysis were not completed.

2.9 RNA sequencing

Matched RNA from tumour samples submitted for WES for each case were profiled, in addition to any sampled paired normal tissue. KAPA kit library preparation (including ribodepletion) was utilised, with sequencing specifications of 100 PE reads and 50 million reads. RNAseq was performed on all samples that underwent WES, as well on matched normal tissues. The RNAseq data has not been included in my results as processing and analysis is not yet completed.

The Bioanalyser 2000 was used to determine RNA integrity values – measured by the RIN score.

2.10 Fluorescence in situ hybridisation (FISH)

To assist in the selection of solutions for estimation of tumour ploidy using ABSOLUTE[21] (see Appendix A Bioinformatic analyses), an orthogonal approach to the determination of tumour ploidy was undertaken using fluorescence in situ hybridisation (FISH). Slides from corresponding FFPE tissue blocks of at least two samples per case that were submitted for WES (two samples from the tissue harvest and any available archival specimens) were submitted for FISH (4–5 micron thickness). Soft tissue and lymph node samples were preferentially selected based on anecdotal experience within the lab suggesting other sites were more vulnerable to background artefact.

Probe selection

Two centromeric probes were selected by the Bioinformaticians involved in this project – for chromosomes 2 and 15 – and used across all cases. These chromosomes do not contain key driver genes for melanoma and were deemed less likely to be impacted by selected losses and/or gains.

FISH staining protocol

The wet lab and image acquisition components of the FISH workflow were undertaken by another member of the lab.

Table 6 Details of reagents used for preparation of slides for FISH

	Stock	Final concentration	Volume
Wash buffer*	20×	1×	500 mL (25 mL stock in 475 mL PBS)
Pre-treatment solution*	20×	1×	50 mL (2.5 mL stock made up with 47.5 mL PBS)
Stringent wash buffer*	20×	1×	100 mL (5 mL stock made up with 95 mL PBS)
Ethanol	100%	100%, 80% & 70%	
Xylene	1×	1×	
Agilent stock pepsin*	1×		

**Dako FISH accessory kit.*
Probe mastermix for FFPE slide: 1.5ul probe 1, 1.5ul probe 2 and 12ul buffer.

Method

Day 1

3. Turn on water bath to 96–98° Celsius.
4. Make up pre-treatment solution. Place sealed Coplin jar with 50 mL of pre-treatment solution in water bath to heat to 96° Celsius.
5. Take 4uM FFPE tissue sections and dewax in Xylene for 3–5 minutes then repeat in second xylene bath.
6. Serial rehydration of sections in 100%, 80% and 70% ethanol (two minutes each).
7. Wash twice in Agilent technologies wash buffer at normal room temperature (two minutes each).
8. Incubate at 95–99° Celsius in pre-treatment solution in sealed Colpin jar for 10 minutes.
9. Remove from water bath and allow to slowly cool for an additional 15 minutes. Turn off the water bath.
10. Turn on heat block at 37º Celsius.
11. Wash slides twice in room temperature wash buffer (two minutes each).
12. Stock pepsin is applied to the slide for 10 minutes at 37º Celsius on heat block.
13. Wash slides twice with agilent wash buffer (two minutes each) and set heat block to 90º Celsius.
14. Serial dehydration of slides using 70, 80, 100% ethanol prior to probe hybridisation.

15. After last wash allow ethanol to evaporate.
16. Chromosome enumeration probes (Abbott molecular/vysis), labelled with both SpectrumGreen and SpectrumOrange fluorophores, are mixed with Abbott molecular hybridisation buffer prior to being applied to the tissue section.
17. First thaw on ice and vortex for 15 seconds, and spin in microfuge.
18. Apply coverslip and use glue to secure coverslip and prevent specimen drying out.
19. Denaturation of CEP probes and tissue by placing slide on heatblock at 90º Celsius for five minutes.
20. Incubate slide overnight in a humidified chamber at 37º Celsius for 16 hours.

Day 2

1. Heat agilent stringent wash buffer to 63º Celsius in a Coplin jar in wash bath.
2. Remove slides from incubator and remove coverslip, place into RT stringent wash buffer.
3. Wash for 10 minutes in stringent wash buffer at 63º Celsius.
4. Wash twice in RT wash buffer (two minutes each).
5. Dehydrate in 70%, 80% and 100% ethanol, and allow to air dry.
6. Counter stain with DAPI (ThermoFisher) and mount coverslip.
7. Seal slide.
8. Capture positive nuclei using the applied precision DeltaVision microscope (can store in dark at 4º Celsius).

FISH Images

Acquired images (1–5 tiles per slide) were visualised and stacked using ImageJ software. The 'reset' mode for brightness/contrast of probes (minimizing probe fluorescence) was used for probe enumeration.

Probe enumeration

A manual approach to probe enumeration was selected. At least three tiles per slide were counted with >100 single nuclei (with demarcated borders) counted per slide. Diploid controls (normal tissue from spleen) were stained and enumerated in the same manner. I undertook the primary enumeration (n = 7238 nuclei), with another lab member counting 10 nuclei per tile for an inter-rater assessment. The inter-class coefficient was then used to

determine inter-observer reliability. The enumeration data representation was undertaken by the bioinformaticians with data I supplied.

Main interphase FISH correction

There are a number of issues inherent in the use of interphase – as opposed to metaphase – FISH. Cells may overlap on tissue slices, confounding the interpretation of probes and ploidy. Nuclei can also be segmented when slides are cut from formalin-fixed paraffin-embedded (FFPE) tissue blocks and this may impact probe enumeration. Cells with a higher ploidy may have a larger nucleus and be more susceptible to under-enumeration. In order to account for this potential bias, two normal spleen tissue samples from two independent patients were formalin-fixated with the same method as the tumour samples and analysed with FISH. A total of 947 nuclei with two chromosome stains per nucleus were counted across the two samples. 1146/1894 (61%) chromosome counts in these known diploid samples were below two, while 59/1894 (3%) were above. This range of true-positive values was used to correct the ploidy estimates in the tumour samples by removing the lowest 61% and the highest 3% of the counts per slide.

2.11 Bioinformatic analyses of sequencing data

Bioinformatic analyses have been performed by Dr Turajlic's team at the Francis Crick Institute (Desiree Schnidrig and Kevin Litchfield). While I understand the purpose of and output from each specific tool, can navigate spreadsheets of processed bioinformatic data and can assess individual variant calls in integrated genomic viewer (IGV), I have not been directly involved in the processing or analysis of raw sequencing data. I have not constructed the phylogenetic trees; however, I have assisted in the definition of putative driver mutations for annotation and the definition of cluster subclonality (see below) and undertaken the evolutionary interpretation of the phylogenetic trees. For reference, detailed bioinformatic methods employed in these analyses are outlined in Appendix A (as compiled by Desiree Schnidrig).

Driver mutation annotation and definition of cluster subclonality

I defined driver mutations according to the parameters in Table 7, below, and annotated these on the relevant branches of the phylogenetic trees.

Table 7 Driver mutation definition for PEACE melanoma cohort

Driver mutation	Melanoma or cancer gene: • oncogene (from The Cancer Gene Census[19]) – mutation in ≥3 reports in COSMIC • tumour suppressor gene (TSG; from The Cancer Gene Census[19]) – stop gain or predicted deleterious by 2/3 in silico callers* • (*SIFT, Polyphen2-HDIV, MutationTaster). Frameshift insertion or deletion mutation in a melanoma TSG (based on list curated for Melanoma Panel, see **Section 2.7**, above).

Clusters represented on the phylogenetic trees with a CCF >15% from the CCF of the clonal cluster were deemed subclonal for the purpose of this analysis. Therefore, a tumour region was deemed polyclonal if it contained clusters with CCFs >15% from the clonal cluster. If all clusters had a CCF ≤15% from the clonal cluster CCF, then the region was deemed monoclonal. For example, if the CCF of the clonal cluster for Region A was 97% and the CCF of cluster x was 70%, Region A would be deemed polyclonal in its composition. If the CCF of cluster x was 90%, Region A would be deemed monoclonal in its composition. A region was also deemed polyclonal if it contained two clusters that were exclusive to each other – that is, represented on different branches of the phylogenetic tree.

References for Materials and Methods

1. Cancer Genome Atlas N: Genomic Classification of Cutaneous Melanoma. *Cell* 161: 1681–96, 2015
2. Ding L, Kim M, Kanchi KL, et al: Clonal architectures and driver mutations in metastatic melanomas. *PLoS One* 9: e111153, 2014
3. Hayward NK, Wilmott JS, Waddell N, et al: Whole-genome landscapes of major melanoma subtypes. *Nature* 545: 175–180, 2017
4. Hodis E, Watson IR, Kryukov GV, et al: A landscape of driver mutations in melanoma. *Cell* 150: 251–63, 2012
5. Krauthammer M, Kong Y, Ha BH, et al: Exome sequencing identifies recurrent somatic RAC1 mutations in melanoma. *Nat Genet* 44: 1006–14, 2012
6. Krauthammer M, Kong Y, Bacchiocchi A, et al: Exome sequencing identifies recurrent mutations in NF1 and RASopathy genes in sun-exposed melanomas. *Nat Genet* 47: 996–1002, 2015
7. Stark MS, Woods SL, Gartside MG, et al: Frequent somatic mutations in MAP3K5 and MAP3K9 in metastatic melanoma identified by exome sequencing. *Nat Genet* 44: 165–9, 2011

8. Long GV, Fung C, Menzies AM, et al: Increased MAPK reactivation in early resistance to dabrafenib/trametinib combination therapy of BRAF-mutant metastatic melanoma. *Nat Commun* 5: 5694, 2014
9. Shi H, Hugo W, Kong X, et al: Acquired resistance and clonal evolution in melanoma during BRAF inhibitor therapy. Cancer Discov 4:80–93, 2014
10. Smalley I, Kim E, Li J, et al: Leveraging transcriptional dynamics to improve BRAF inhibitor responses in melanoma. EBioMedicine 48:178–190, 2019
11. Van Allen EM, Wagle N, Sucker A, et al: The genetic landscape of clinical resistance to RAF inhibition in metastatic melanoma. Cancer Discov 4:94–109, 2014
12. Wagle N, Van Allen EM, Treacy DJ, et al: MAP kinase pathway alterations in BRAF-mutant melanoma patients with acquired resistance to combined RAF/MEK inhibition. Cancer Discov 4:61–8, 2014
13. Sweis RF, Spranger S, Bao R, et al: Molecular Drivers of the Non-T-cell-Inflamed Tumor Microenvironment in Urothelial Bladder Cancer. Cancer Immunol Res 4:563–8, 2016
14. Zaretsky JM, Garcia-Diaz A, Shin DS, et al: Mutations Associated with Acquired Resistance to PD-1 Blockade in Melanoma. N Engl J Med 375:819–29, 2016
15. Patel SJ, Sanjana NE, Kishton RJ, et al: Identification of essential genes for cancer immunotherapy. Nature 548:537–542, 2017
16. Spranger S, Bao R, Gajewski TF: Melanoma-intrinsic beta-catenin signalling prevents anti-tumour immunity. Nature 523:231–5, 2015
17. Hugo W, Zaretsky JM, Sun L, et al: Genomic and Transcriptomic Features of Response to Anti-PD-1 Therapy in Metastatic Melanoma. Cell 165:35–44, 2016
18. Chae YK, Anker JF, Carneiro BA, et al: Genomic landscape of DNA repair genes in cancer. Oncotarget 7:23312–21, 2016
19. Tate JG, Bamford S, Jubb HC, et al: COSMIC: the Catalogue Of Somatic Mutations In Cancer. Nucleic Acids Res 47:D941–D947, 2019
20. Turajlic S, Xu H, Litchfield K, et al: Deterministic Evolutionary Trajectories Influence Primary Tumor Growth: TRACERx Renal. Cell 173:595–610 e11, 2018
21. Carter SL, Cibulskis K, Helman E, et al: Absolute quantification of somatic DNA alterations in human cancer. Nat Biotechnol 30:413–21, 2012

Section 3 Evolutionary dynamics of metastatic melanoma in a post-mortem cohort

Contents

Tables

Figures

3.1 Introduction

As discussed in **Section 1.3.1 Post-mortem sampling** in the **Main Introduction**, research post-mortem (PM) studies have provided valuable insights into cancer evolution, even with limited subject numbers. The opportunity to evaluate metastatic heterogeneity after failure of multiple lines of therapy may also help inform potential treatment options for progressive, late-stage cancers. This is a space yet to be thoroughly explored in advanced melanoma.

3.1.1 Post-mortem research samples and quality control

To date, a number of different nucleic acid and tissue analyses have been conducted from PM-derived samples, including DNA sequencing, RNA sequencing, TCR sequencing and immunohistochemistry.[1-4]

Tissue samples collected at post-mortem are subject to more variables that impact on quality relative to samples collected fresh at the time of surgery or biopsy. This may have an impact on downstream data outputs. Once death has occurred, stasis of blood flow and resulting hypoxia lead to loss of cell integrity, and eventually autolysis. This may in turn affect nucleic acids that are input for next-generation sequencing analyses. Suboptimal storage conditions are more likely to impact RNA than DNA.[5] The post-mortem interval (PMI), mode of death and time to refrigeration (TTR) may all affect tissue and nucleic acid quality. Downstream from sampling, nucleic acid extraction and library preparation methods may also introduce artefacts into the data. These variables are summarised in Table 8.

Table 8 Variables that may impact DNA quality (adapted from[6-9])

Process	Variable
Sample collection	Cause of death, for example, sepsis/acidosis = worse quality Post-mortem interval Time to refrigeration Duration of post-mortem (exposure/oxidation) Type of tumour and contaminants Organ sampled
Extraction & storage	Extraction process (that is, concurrent DNA and RNA extraction or individual) and reagents Duration of time in freezer, or FFPE
Library Preparation	Amount of DNA used (for example, 200 ng vs 1 μg) Method and extent of shearing – (that is, Covaris vs enzymatic, fragment size 150 bp vs 500 bp)
Sequencing	Less likely to be a factor – Illumina error rates are low and well described

The post-mortem interval (PMI) is an important consideration in the tissue and nucleic acid quality because the longer the interval, the greater the chance of degradation. The majority of studies in this space have analysed non-tumour tissues, and malignant tissues may present additional challenges such as necrosis. Integrity scores, such as the DIN (DNA integrity number), providing a numerical representation of DNA integrity from one (strongly degraded DNA) to 10 (highly intact DNA),[10] and RIN (RNA integrity number),[11] an electrophoretic basic method for evaluating 28S to 18S ribosomal subunit ratio, reflecting RNA integrity as a whole[11] are commonly used to represent nucleic acid quality.

DNA

The influence of PMI on deoxyribose nucleic acid (DNA) quality has been evaluated in normal and tumour tissue. Hansen and colleagues used a polymerase chain reaction (PCR)-based approach to evaluate DNA and RNA integrity from skeletal muscle samples taken at PMIs of one to 14 days. DNA integrity was assessed by scoring the longest PCR fragment (up to 1000 bp) that could be amplified from each DNA sample. PMI groups from one to three days showed PCR amplification of a 1000bp *PYGM* gene product in all frozen samples. In samples with a PMI of 3–14 days the range of fragment sizes able to be amplified

increased, but the median remained 1000 bp. In samples with PMIs >14 days the median fragment length amplified was shorter (600 bp), reflecting a reduction in DNA integrity with prolonged PMIs.[9]

One of the only studies looking at post-mortem nucleic acid quality in cancer tissues was undertaken by Fan and colleagues,[8] who evaluated 371 frozen tissue samples from 80 autopsy cases and studied a range of tumour and normal tissue variables. They also assessed DNA integrity by quantitative PCR across five different loci, in 36 samples from five patients in two categories: PMIs of 1–5 hours and PMIs >21 hours. Of these, only four (11%) were deemed to be damaged, with three of the four coming from the longer PMI group. All four samples were from the liver, suggesting tissue type may be important as well.

RNA

RNA is degraded by ribonucleases already present in the cell. Ribonuclease-rich organs, such as pancreas and liver have more rapid RNA fragmentation, as opposed to the brain, which is more stable.[5] A number of studies have evaluated the quality of ribodeoxynucleic acid (RNA) over varying PMIs, with the vast majority analysing normal (non-tumour) tissues within the genotype-tissue expression (GTEX) project. Most of the samples within these studies have been within a PMI range <24 hours,[8,12-14] with only a few consistently examining samples with greater intervals[9,15,16] (summarised in Figure 8). Most studies use the RIN score as their method of quality assessment;[11] however, alternative approaches, including quantifying gene expression with reverse transcriptase PCR (RT-PCR) , as well as analysis of array-based hybridisation and gene expression based on RNAseq data are also utilised.

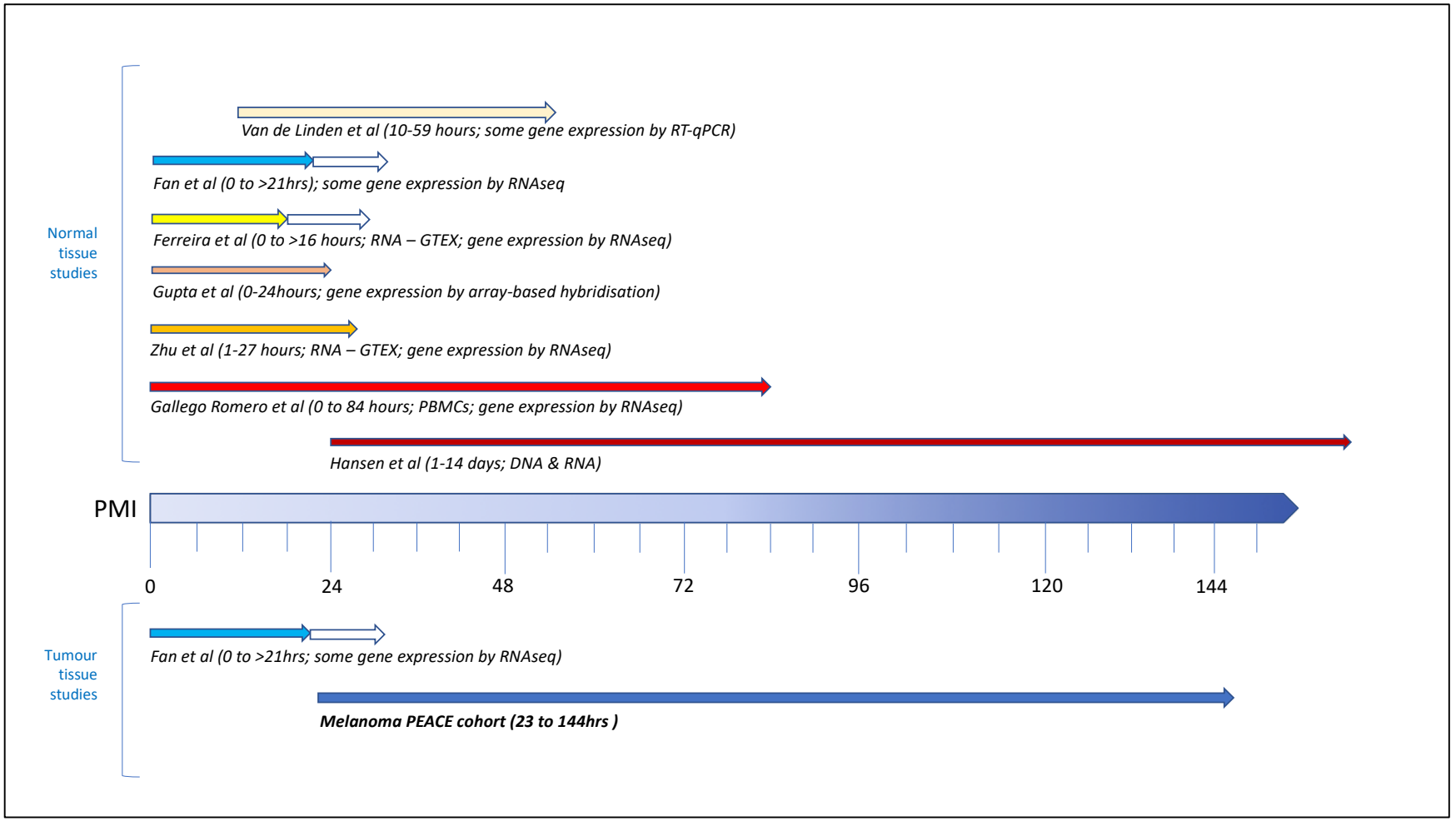

Figure 8 Summary of studies of RNA quality in post-mortem tissue mapped according to the post-mortem interval evaluated
Solid coloured arrows represent the majority of the analysed cohort, with outliers represented by outlined arrows only. Methods by which ribonucleic acid (RNA) quality was analysed included; RTqPCR: reverse transcriptase quantitative PCR, RNAseq: RNA sequencing, GTEX: Genotype Tissue Expression (Project). Figure adapted from data in[8,12-16].

The GTEX project is a large study of normal tissue samples collected at post-mortem from individuals to analyse tissue-specific gene expression across human tissues, linking them to disease states and examining tissue-specific contexts. Analyses have consistently noted tissue-specific PMI-related mRNA degradation,[12,14,17] with the GI tract being more vulnerable to degradation than the brain, for example. Average RIN values decline from >7 for PMs within eight hours to <6 when PMs are performed more than eight hours from the time of death.[17]

Fan et al.[8] found that RNA integrity in *normal* tissues changed with increasing PMIs in a tissue-specific manner (kidney worst, skeletal muscle best), and that generally, a longer PMI led to poorer RNA quality. On the contrary, *tumour* sample quality (majority were pancreatic cancer samples; 52 primary tumour and 35 metastases) was inconsistently related to the PMI and varied between metastases in the same patient, suggesting tumour-specific impact on RNA quality.

In a study comparing RNA quality between heart, liver and kidney specimens surgically resected during life vs sampled at 'minimally invasive' autopsy (CT-guided core needle biopsies) versus 'conventional' autopsy (PMIs were from 10 to 59 hours), both cohorts of samples had notably lower RIN values and *GAPDH* expression as measured by RT-PCR.[16] While generally the 'minimally invasive' autopsy yielded a higher quality sample than the 'conventional' autopsy, there were significant differences in the timing and sample processing that confound these results.

While the PMI has been a focus of several studies, its relative importance remains unclear. A study of 18 sites of normal tissue sampling in 389 samples from elderly patients determined that RIN and RNA yield did not depend solely on PMI.[18] Age was not a factor in RNA quality, but consistent with the aforementioned studies, integrity and yield varied between tissue types.

While assessment of gene expression through RT-PCR or RNAseq can be performed on samples with low RIN or at long PMIs, degradation may impact transcript length and quality, and therefore the interpretation and validity of findings. Studies have also demonstrated evidence of active and ongoing regulation of transcription after death, with down regulation of immune genes.[12] A notable exception is in interferon gamma which shows a greater range

of expression with longer PMIs, with a trend towards increased expression that may be indicative of ongoing activity after death.[14]

Given DNA and eventually RNA sequencing provide the foundation for our PEACE study cohort analysis, it was important to understand the limitations of tissue quality according to relevant integrity measures. In the PEACE study, PMIs tend to be longer than in other 'rapid' autopsy studies. Tumour sampling is guided by a histopathologist, but the samples are not microscopically assessed at the time of tissue harvest. As such, I sought to assess both macroscopic sampling accuracy and standard measures of DNA and RNA integrity from this cohort, and relate them to the PMI and TTR. Other factors such as acidosis from sepsis or hypoxia[5,8] were not routinely documented or measured in this cohort, so their impact cannot be evaluated.

3.1.2 Fluorescent in situ hybridisation (FISH) in the analysis of aneuploidy in melanoma

Somatic copy number aberrations are a hallmark of invasive melanoma, often used to distinguish borderline invasive primary tumours from benign naevi, using fluorescent in situ hybridisation (FISH).[19] FISH involves the hybridisation (binding) of fluorescent probes to specified regions of chromosomes (focal segments or whole arms) or their centromeres, enabling these to be enumerated (counted). Through use of centromeric probes to enumerate overall chromosomal number, FISH may also serve as a method to estimate ploidy. FISH may also be used to infer CIN, because it is capable of demonstrating cell to cell variation in ploidy.[20-22] While bioinformatic estimates of ploidy are typically generated from NGS data, large studies have engaged FISH to orthogonally validate bioinformatics results in subsets of patients.[23,24]

The accuracy and interpretation of FISH varies with the nature of tissue used and at which point in the cell cycle the analysed cells sit. Chromosome number is most accurately represented by performing FISH during metaphase, ideally on single cells in a suspension. However, this is often impractical in the context of tumour samples embedded in paraffin. On such samples, interphase FISH may be undertaken. Limitations of interphase FISH include cells overlapping or clumping and impairing the definition of nuclear borders, inconsistent sectioning of nuclei compromising reliable probe enumeration and non-tumour cell 'contamination'. Some of these limitations may be overcome by scoring greater numbers of nuclei, and ensuring tumour-rich regions are analysed.

3.1.3 Insights from post-mortem evaluation of melanoma to date

As discussed in **Section 1.2.4 Melanoma evolution and genomic heterogeneity** in the **Main Introduction**, studies of melanoma evolution are limited by small cohorts and a focus on primary tumours alone or on soft-tissue metastatic sites that are predominantly locoregional. Despite the increasing number of post-mortem studies in breast, pancreatic and other cancer types, only one melanoma post-mortem case had been published at the time of results analysis for this project.

In this case,[4] the post-mortem was undertaken 48 hours after death. The patient had widespread metastases including to the brain, and was naïve to systemic therapy. Thirteen metastatic sites (including the brain and lung) were profiled with immunohistochemistry, whole genome sequencing (WGS) and RNA sequencing. DNA from one sample of the primary tumour was sequenced using a custom panel. The authors described a branched evolutionary pattern, with inter-metastatic mutational heterogeneity across sites. Two distinct metastatic clones were identified: one seeded all the lung metastases and both clones seeded different sites within the brain. Despite the clonal diversity across brain metastases, the gene expression profiles and immune microenvironment features were similar, suggestive of an organ-specific influence on protein expression and the immune system. Where a mutational signature consistent with UV damage dominated the clonal mutations, there was evidence of apolipoprotein B mRNA editing enzyme, catalytic polypeptide (APOBEC) associated mutagenesis in subclonal mutations at different metastatic sites, suggesting a potential role of APOBEC-enzyme induced damage in the selection of clones with metastatic competence.

This case, in addition to the primary-metastasis analysis by Sanborn et al[25] (discussed in the **Section 1.2.5 Genomic evolution of cutaneous melanoma** in the **Main Introduction**) highlights the importance of multi-region sampling in melanoma in order to capture branching evolutionary patterns and metastatic heterogeneity. Heterogeneity and subclonality are much harder to capture accurately in single biopsy studies (for example, in a large pan-tumour cohort, only a 9% subclonal fraction was reported in melanoma)[26] and underestimate diversity in melanoma leading to incorrect inferences of a linear/monoclonal metastatic model.

3.2 Aims

1. Evaluate the quality of samples in the first 14 cases from the PEACE melanoma cohort

- tumour yield from macroscopic sampling
- post-mortem tissue quality – DNA and RNA

2. Undertake a comprehensive analysis of primary to metastatic evolution and inter-tumour heterogeneity in a cohort of patients with metastatic melanoma, sampled at post-mortem

    - explore and validate the range of ploidy noted in a preliminary analysis of WES samples using FISH (this aim became apparent after the project was underway – explained in **Section 3.3.3 Analysis of ploidy by fluorescent in situ hybridisation**, below)
    - describe for each case patterns of metastatic seeding, evolutionary inferences and inter-metastatic heterogeneity
    - identify putative genomic treatment resistance mechanisms in each case.

3.3 Results

3.3.1 Cohort clinical summary

An overview of the clinical characteristics for the 14 autopsy cases for analysis is detailed in Table 8. These included six sun-exposed cutaneous, three acral, one peri-anal cutaneous and one sino-nasal mucosal primary melanoma(s), as well as three cases of melanoma of unknown primary (MUP). All cases with the exception of PEA060 and PEA080 had a recognised oncogenic driver alteration in *BRAF* (*V600* in six cases, non-*V600* in two)*, NRAS* (three cases) or *KIT* (one case). Archival primary tumour material was available in eight cases and non-primary archival tumour tissue was available in 10 cases.

Table 9 Clinical characteristics of the Melanoma PEACE cohort

Melanoma subtype, driver alterations established from clinical/routine molecular profiling, archival tumour availability and features, treatment history. SLN: sentinel lymph node; BT: Breslow thickness; ipi+nivo: combination ipilimumab & nivolumab; nivo: nivolumab (monotherapy); pembro: pembrolizumab; met: metastasis; subcut: subcutaneous; CT: computed tomograph.

	Subtype	Key oncogenic driver alteration	Primary Tumour (archival)	Other tissue (archival)	Treatment received
PEA004	Peri-anal cutaneous	***BRAF K601E***	11mm BT, 2014	Resected inguinal lymph nodes	Adjuvant nivo; ipi; pembro; dabrafenib
PEA005	cutaneous	***BRAF V600E***	1. 1mm BT, 2005 2. 4mm BT, 2003	Liver biopsy cores	Dabrafenib; pembro; ipi+nivo
PEA009	cutaneous	***NRAS***	1996 – not available	Sternal core biopsy (insufficient tumour)	Pembro
PEA012	Unknown primary	***BRAF V600E***	Not applicable	Pre-Rx Pleural fluid cell block	Ipi+nivo x2; dabrafenib+trametinib; vemurafenib+cobiemtinib; cisplatin/DTIC; pembro
PEA016	Mucosal (sinonasal)	***NRAS***	1. Polyp fragments, Nov 2016 2. Debulking 'T4' on op notes, not on path report, Dec 2016	No	Ipi+nivo; carboplatin/DTIC
PEA017	cutaneous	***BRAF V600E***	2.1mm BT, 2013	Pleural fluid cell block	Ipi+nivo; dabrafenib+trametinib
PEA020	Unknown primary	***BRAF V600E***	Not applicable	Brain met resection	Nivo; dabrafenib+trametinib
PEA023	Acral	***KIT exon 13***	3.3mm BT, 2014	No	Pembro; KIT inhibitor x2 (imatinib & novel KIT inhibitor)
PEA025	cutaneous	***BRAF V600E***	2014- not available	LND	Ipi+nivo; dabrafenib+trametinib; pembro
PEA026	Acral	***BRAF V600E***	1997 - not available	LND – not available	Ipi+nivo; dabrafenib+trametinib
PEA036	cutaneous	***BRAF K601E***	10mm BT, 2016	No	Pembro; dabrafenib+trametinib
PEA038	cutaneous	***NRAS***	3mm BT, 2015	SLN- not available	Ipi+nivo; temozolamide
PEA060	Unknown primary	**Not identified**	Not applicable	Pre-Rx Subcut met & LND (2 timepoints)	Ipi+nivo
PEA080	Acral (subungual)	**Not identified**	8.5mm BT, 2017	SLN- insufficient tumour	Ipi+nivo; pembro

The median time from diagnosis to Stage IV was 13.5 months (Figure 8). The median overall survival from diagnosis of Stage IV disease for the entire cohort was 15.4 months (Figure 8); 8.75 months for the acral/mucosal/peri-anal cases (5/14) and 23.1 months for the cutaneous/MUP cases (9/14).

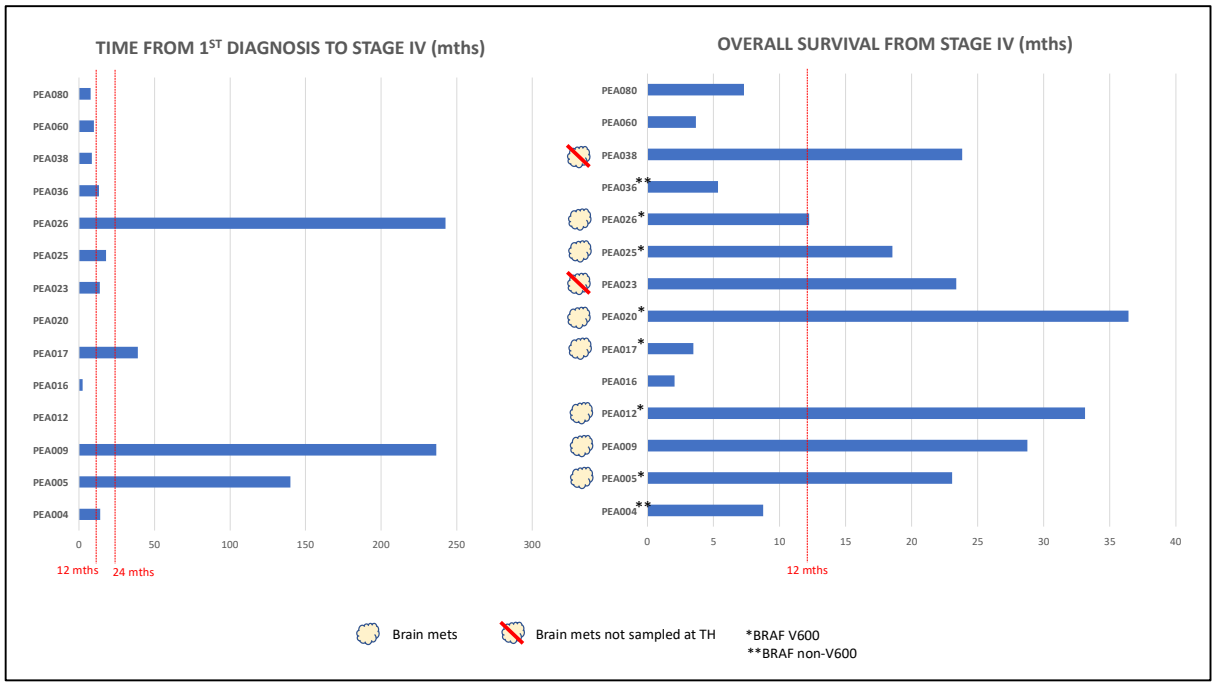

Figure 9 Survival for the Melanoma PEACE cohort
Left-hand side: overall survival from first diagnosis of melanoma; right-hand side: overall survival from Stage IV disease. Variables such as presence of brain metastases and BRAF mutation are annotated. Numbers along x axes denote months.

All patients received immune-checkpoint therapy with 9/14 receiving combination ipilimumab+nivolumab, 8/14 in the first-line setting (Table 9) and the remaining 5/14 receiving monotherapy. The eight patients with a *BRAF* mutation (including the two with a non-V600 mutation) received a BRAF inhibitor, with the majority receiving combined BRAF/MEK inhibition. Combined BRAF/MEK inhibition was not yet available in 2015 when PEA004 and PEA005 started their treatment. As indicated in Table 10, only three patients had a response to BRAF +/- MEK inhibition and only 3/14 demonstrated a response to immune checkpoint inhibition.

Table 10 Treatment responses across the cohort for MAPK inhibitor targeted treatment and immune checkpoint inhibitor regimens

Overall cohort biased towards a treatment refractory phenotype, in keeping with poor overall survival as detailed in Figure 9.

Treatment responses: MAPK & Immune checkpoint inhibitors

	MAPKi – PR/CR	MAPKi - SD	MAPKi - PD	*BRAF-WT*
ICI – response	PEA005 (I+N response)[3] PEA012[4]	PEA020 (PR nivo)[6]		
ICI – SD only				PEA038 (ECM)[10]
ICI – progression	PEA017 (ECM) (PEA005 – pembro PD)	PEA020 (PD-Ipi)[6] PEA025[7] PEA026[8] PEA036[9] PEA017 (brain)	PEA004[1]	PEA009[2] PEA016 PEA038 (brain)[10] PEA080 PEA060 **PEA023**[5]

ECM = extracranial mets
Received chemo
Received KIT inhibitors
Received ipi+nivo
Received only anti-PD-1
Sequential ipi & PD-1

[1]PEA004 - BRAF K601E mutation; PD on adj nivo, 1L ipi, then D&T SD in liver only with rest PD, then pembro PD
[2]PEA009 – durable responses with PD-1 & RTx despite PD
[3]PEA005 – D&T PR, pembro – PD, I+N – PR when first had it, then RIP after C1 of 2nd round I+N
[4]PEA012 - I+N1 – PR, D+T – PR, I+N2 – PR, C+V- PR, pembro PD/(EOL)
[5]PEA023 - KIT-mutant; PD on pembro (given RTx); PD on imatinib & PLX
[6]PEA020 – BRAF mutant, PR on nivo (after ipi- PD) but non-evaluable for D+T
[7]PEA025- I+N (?pneumonitis) then PD, D&T PR, pembro PD
[8]PEA026 – I+N – PD, D&T- SD
[9]PEA036 – pembro PD, D&T SD (K601E) – but only 1 cycle, had intra-abdo infection
[10]PEA038 – SD extracranial on I+N, PD intracranial; then PR to TMZ

Across the cohort a total of 522 samples (range 9–75 per patient) were acquired at tissue harvest (TH) from 365 individual metastases (range 5–54 per patient; Table 10). In total, 153 samples were submitted for WES, 137 of which (90%) were successfully profiled (see Methods 1.10.1). Of the 46 archival FFPE tumour samples submitted for WES (including primary tumour regions), 34 were successfully profiled by WES (74%).

Table 11 Summary of sampling at tissue harvest (TH)

Number (No.) of metastatic sites and samples collected, as well as the number submitted for whole exome sequencing (WES) and the proportion of these that passed quality control (QC) for WES based on purity and suitability for copy number profiling.

	No. metastases sampled at Tissue Harvest	No. tumour samples taken at Tissue Harvest	No. tumour TH samples submitted for WES	No. passed WES QC	*% passed WES QC*	No. archival FFPE tissue specimens submitted for WES	No. archival FFPE tissue specimens passed QC WES
PEA004	24	45	22	19	86	2	2
PEA005	19	30	15	8	53	4	0
PEA009	8	9	5	5	100	na	na
PEA012	27	51	13	13	100	1	0
PEA016	5	9	9	8	89	6	5
PEA017	18	41	10	10	100	3	3
PEA020	17	36	10	9	90	2	2
PEA023	34	35	10	9	90	3	3
PEA025	32	36	10	10	100	1	0
PEA026	25	32	9	9	100	na	na
PEA036	54	75	10	10	100	2	2
PEA038	14	26	10	10	100	9	6
PEA060	38	38	10	7	70	8	7
PEA080	50	59	10	10	100	5	4
Total	***365***	***522***	***153***	***137***	***median=100%***	***46***	***34***

Tumour mutational burden (TMB) varied widely across the cohort, with the mucosal/acral/perianal cases demonstrating a lower TMB (median 2.52 SNVs/Mb) than the cutaneous/MUP cases (median 13.26 SNVs/Mb), as expected (Table 12 and Figure 10). The number of exonic insertions and deletions (indels) ranged from 4–48 across the cases. In 11/14 cases, the majority of mutations were clonal (Figure 11). These metrics are further discussed within the individual case descriptions (**Section 3.3.4 Case descriptions of the genomic evolution of melanoma and inter-metastatic heterogeneity**, below).

Table 12 Summary of tumour mutational burden (TMB) metrics

Summary of different measures of mutational burden. TMB clonality is derived from SNVs within the valid clusters of the phylogenetic trees, hence clonal+subclonal values are less than the total SNV number due to some mutations being contained within excluded clusters. SNV: single nucleotide variant, nsSNV: non-synonymous SNV, Mb: megabase, indel: insertion or deletion mutation, FS: frameshift.

	Subtype	TMB - SNVs & Indels							TMB clonality			
		Total SNVs	exonic SNVs	exonic nsSNVs	mutations/Mb (SNVs only)	Total indels	indels (exonic)	indels (exonic, FS only)	Clonal Mutations	Subclonal Mutations	Clonal %	Subclonal %
PEA004	perianal	128	77	46	2.6	23	6	6	63	51	55	45
PEA005	cutaneous	268	171	112	5.4	17	4	3	140	102	58	42
PEA009	cutaneous	3236	2006	1222	64.7	32	13	11	2747	20	99	1
PEA012	MUP	6144	3794	2375	122.9	55	21	15	2404	3117	44	56
PEA016	mucosal	112	71	51	2.2	24	7	6	75	31	71	29
PEA017	cutaneous	475	311	188	9.5	24	5	3	211	163	56	44
PEA020	MUP	450	294	191	9.0	14	9	6	327	82	80	20
PEA023	acral	51	32	23	1.02	24	10	8	41	5	89	11
PEA025	cutaneous	663	410	262	13.26	36	15	10	304	138	69	31
PEA026	acral	371	232	159	7.42	30	11	9	65	297	18	82
PEA036	cutaneous	2586	1562	927	51.72	31	12	8	1864	89	95	5
PEA038	cutaneous	37510	21843	13476	750.2	256	48	41	52	8206	1	99
PEA060	MUP	493	321	187	9.86	18	5	4	426	29	94	6
PEA080	acral	126	88	59	2.52	20	6	4	61	15	80	20

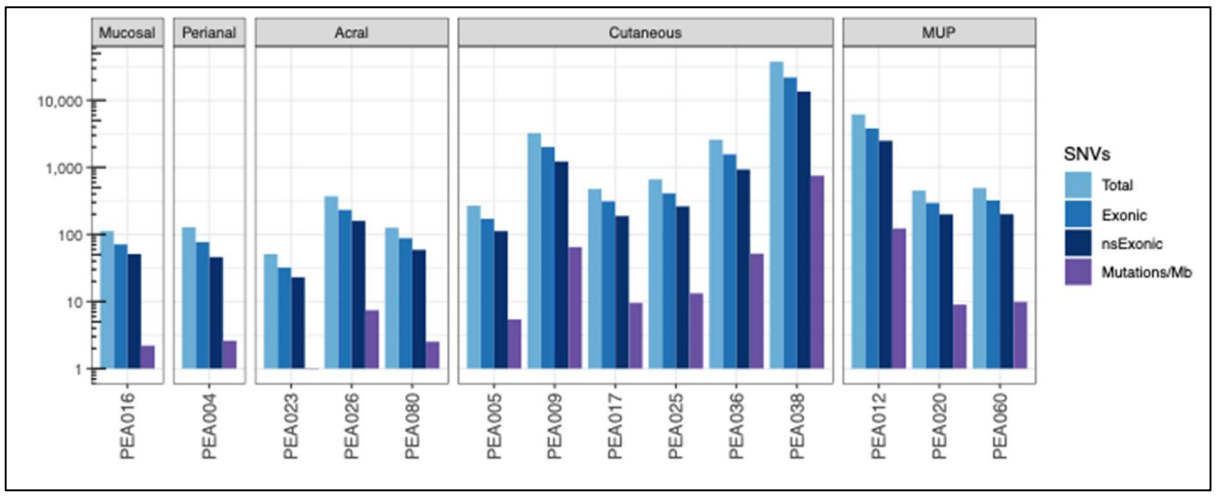

Figure 10 Tumour mutational burden across all cases
Number of mutations on y axis (log10 scale), individual cases highlighted on x axis. Data represented from Table 11. Log figure courtesy of Irene Lobon with data I supplied.

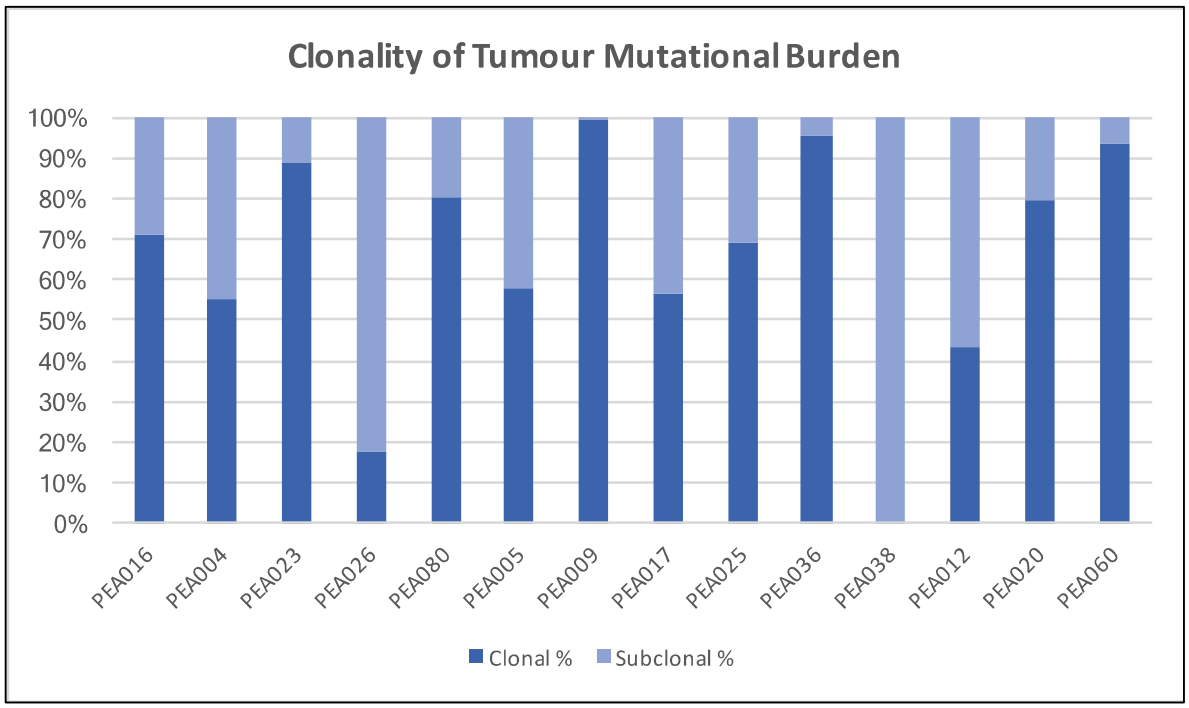

Figure 11 Tumour mutational burden: clonal vs subclonal fractions
Data represented from Table 12 'TMB clonality' and represents both SNVs and indels included in the clusters of the phylogenetic trees for each case (discussed in ***Section 3.3.4****).*

3.3.2 Quality of post mortem sampling

The post-mortem intervals (PMI) of the 14 cases ranged from 23 to 144 hours (median of 52 hours). Time to refrigeration (TTR) data was available for 11/14 cases and ranged from one to 22 hours (median seven hours). See Figure 12.

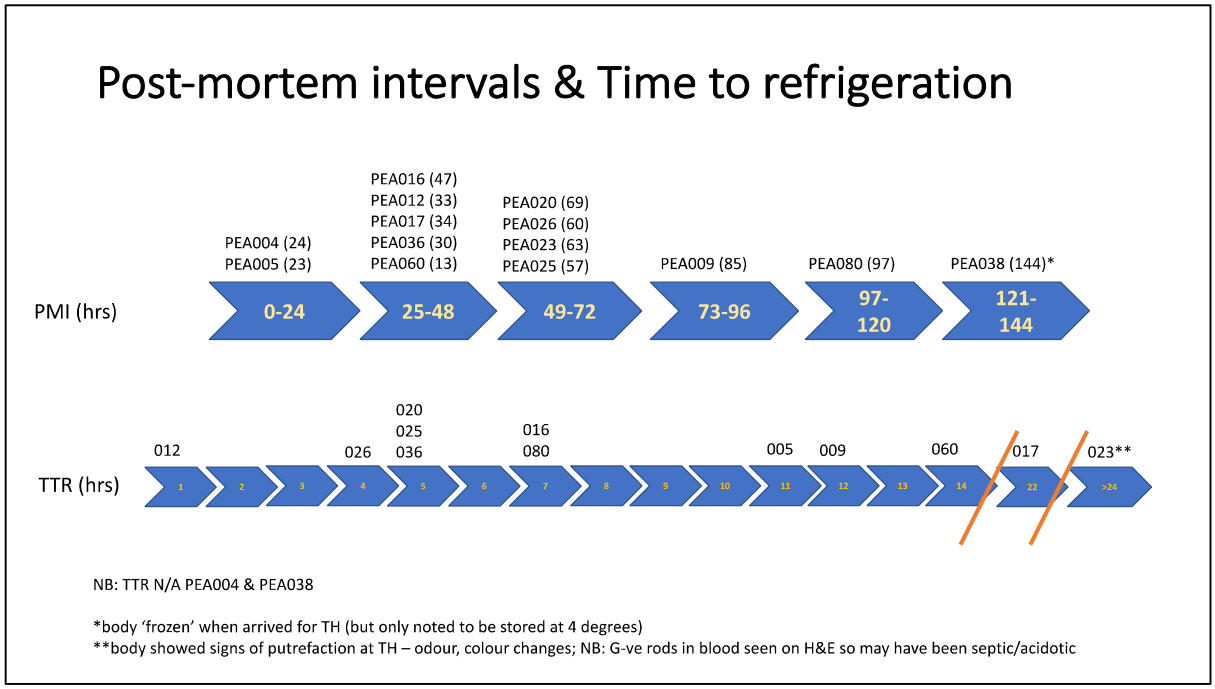

Figure 12 Cohort breakdown by post-mortem interval (PMI) and time to refrigeration (TTR)
Summary diagram representing PMIs and TTR for patients in the cohort.

Of the 522 snap frozen samples from the THs, n = 487 (93%) had a paired sample formalin-fixed for embedding in paraffin (FFPE). Haematoxylin and eosin (H&E) slides were cut from each of the FFPE tissue blocks and reviewed (see **Materials and Methods Section 2.10 Fluorescence in situ hybridisation (FISH)**). The accuracy of macroscopic sampling for tumour was excellent, with only 37/487 (8%) samples demonstrating an absence of tumour (Figure 13), with a further 19/487 (4%) unable to be reliably assessed on H&E due to substantial necrosis or heavy melanin pigmentation. Of 487 only 393 (80%) had >50% tumour purity. Tumour viability (defined as lack of necrosis) was >50% in 386/487 (73%). Changes consistent with autolysis were noted in only 15 of 431 (3%) of confirmed tumour specimens.

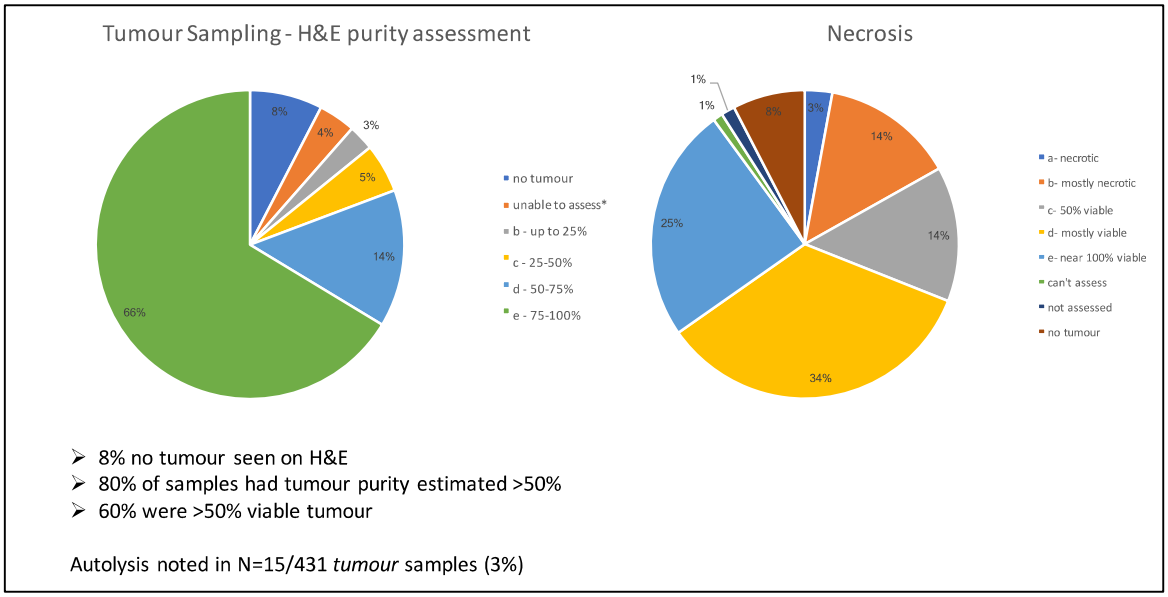

Figure 13 Macroscopic sampling accuracy and purity by haematoxylin and eosin (H&E) assessment of tumour samples from tissue harvests
Pie graph on the left denotes the proportion of samples across five categories of purity (including no tumour seen) and the proportion that were unable to be assessed. The pie graph on the right denotes the proportion of samples across five categories describing a range of necrosis.

DNA integrity as measured by the DIN score was collated for 125/153 samples that were subjected to WES (82%) and correlated with both the PMI and TTR where data was available (see Figure 14). The 28 missing samples (18%), were derived from the first three tissue harvests conducted at the start of the study (PEA004, PEA005, PEA016) before DINs were routinely recorded and DNA stock was exhausted. Overall, the majority of samples had a DIN greater than 6 (107/125, 86%). I observed no trend between the DIN score and increasing PMI (Figure 14, left). A weak but significant positive correlation was noted with TTR (Spearman r 0.20, p 0.04) suggesting that DNA quality improves with increasing TTR, however this is counterintuitive and unlikely to be meaningful.

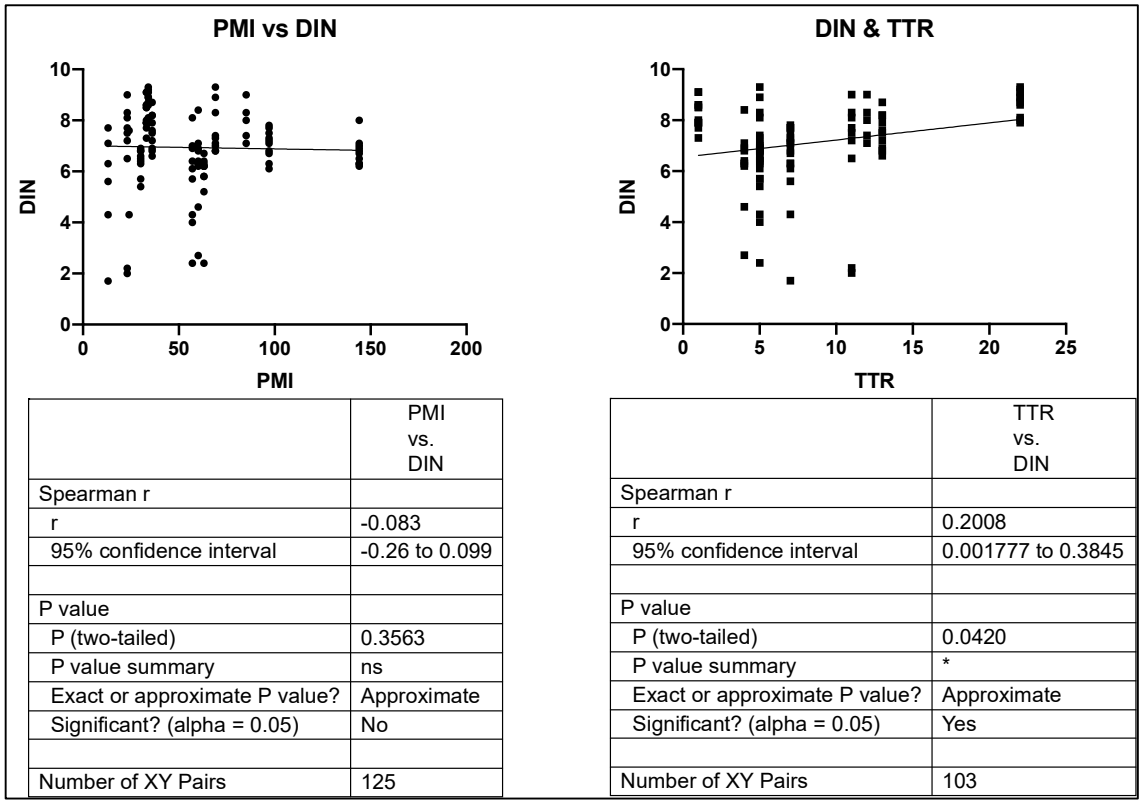

	PMI vs. DIN
Spearman r	
r	-0.083
95% confidence interval	-0.26 to 0.099
P value	
P (two-tailed)	0.3563
P value summary	ns
Exact or approximate P value?	Approximate
Significant? (alpha = 0.05)	No
Number of XY Pairs	125

	TTR vs. DIN
Spearman r	
r	0.2008
95% confidence interval	0.001777 to 0.3845
P value	
P (two-tailed)	0.0420
P value summary	*
Exact or approximate P value?	Approximate
Significant? (alpha = 0.05)	Yes
Number of XY Pairs	103

Figure 14 Correlations between DIN scores and Post-mortem interval (PMI; left) and time to refrigeration (TTR; right)

I further evaluated the time to TH using a cut-off of 48 hours after death. There was a moderate positive correlation between increasing PMI and DNA integrity in cases where the TH was within 48 hours that reached statistical significance (Spearman r 0.50, p <0.0001). This did not appear to be moderated by the TTR (Figure 15). There was no significant trend however between the PMI and DIN score for cases after 48 hours (Spearman r 0.22, p 0.08; Figure 15).

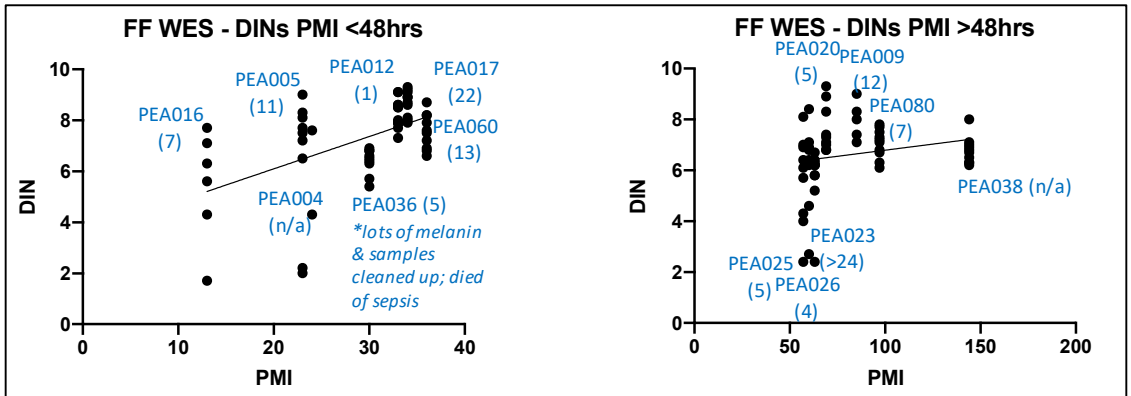

	X vs. Column A
Spearman r	
r	0.4952
95% confidence interval	0.2688 to 0.6697
P value	
P (two-tailed)	<0.0001
P value summary	****
Exact or approximate P value?	Approximate
Significant? (alpha = 0.05)	Yes
Number of XY Pairs	60

	X vs. Column A
Pearson r	
r	0.2162
95% confidence interval	-0.02927 to 0.4370
R squared	0.04673
P value	
P (two-tailed)	0.0837
P value summary	ns
Significant? (alpha = 0.05)	No
Number of XY Pairs	65

Figure 15 Correlations between DINs and post-mortem interval <48 hours (left) and >48 hours (right). *Time to refrigeration for each case annotated in blue text (hours).*
Time to refrigeration (hours)

Evaluation of RNA integrity as measured by the RIN score was undertaken for tumour samples included in the RNAseq analysis (n = 111 with available information). I observed a wide range of RIN scores from 0.0 to 8.2, with a median of 4.3. A RIN ≥6 was noted in 12%. There was a significant but weak negative correlation with the PMI (r=-0.23, p 0.02). No trend was observed between the RIN and TTR (Figure 16).

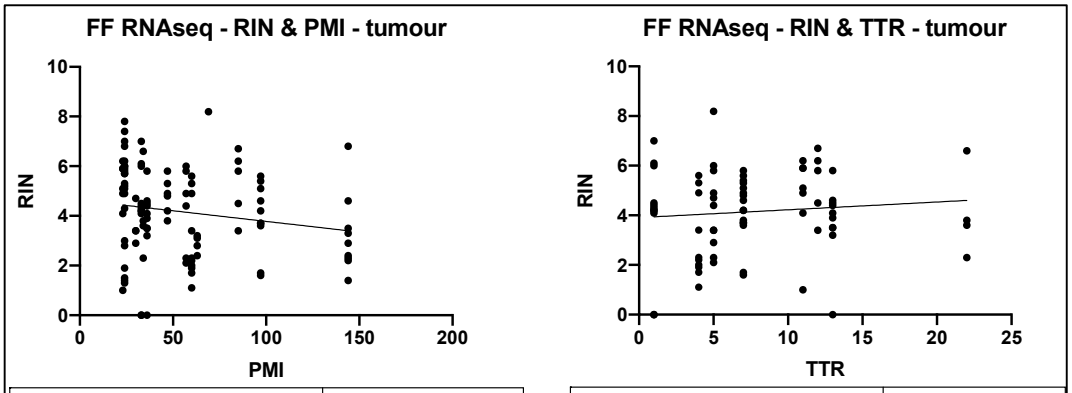

	PMI vs. RIN
Spearman r	
r	-0.2291
95% confidence interval	-0.4032 to -0.03909
P value	
P (two-tailed)	0.0156
P value summary	*
Exact or approximate P value?	Approximate
Significant? (alpha = 0.05)	Yes
Number of XY Pairs	111

	TTR vs. RIN
Spearman r	
r	0.09639
95% confidence interval	-0.1402 to 0.3226
P value	
P (two-tailed)	0.4107
P value summary	ns
Exact or approximate P value?	Approximate
Significant? (alpha = 0.05)	No
Number of XY Pairs	75

Figure 16 Correlation between RIN scores with post-mortem interval (PMI) and time to refrigeration (TTR)

DNA and RNA was extracted from 30 normal tissue samples obtained at TH (for paired tumour/normal RNAseq analyses) across the cohort. There was a much greater variation in DIN between samples within each case for normal tissue samples (cohort median 6.3, range 1.1–9.1), relative to tumour samples (cohort median 7.0, range 1.7–9.3). The variation between normal samples is further illustrated in Figure 18 by the DNA fragment ranges (from which the DIN score is derived) overlayed for each case. For DNA samples, there was a weak negative correlation overall with PMI which did not reach statistical significance possibly due to limited numbers (Spearman r -0.21, p 0.27; see Figure 17). For normal tissue RNA samples, there was no correlation with the RIN score for either PMI or TTR (Figure 19). The cohort median RIN was 3.8 (range 0–6.9), similar to tumour samples (median RIN 4.3, range 0–8.2).

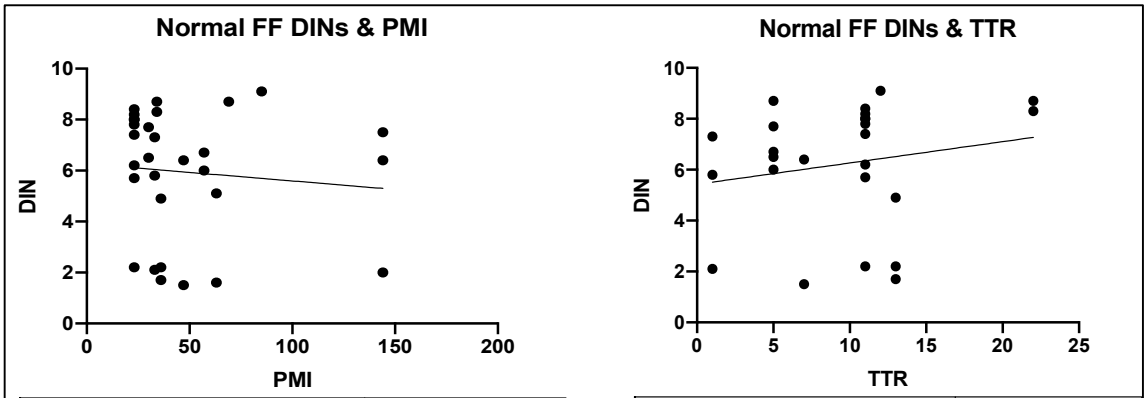

	PMI vs. DIN
Spearman r	
r	-0.2091
95% confidence interval	-0.5374 to 0.1743
P value	
P (two-tailed)	0.2675
P value summary	ns
Exact or approximate P value?	Approximate
Significant? (alpha = 0.05)	No
Number of XY Pairs	30

	TTR vs. DIN
Spearman r	
r	0.1845
95% confidence interval	-0.2388 to 0.5490
P value	
P (two-tailed)	0.3772
P value summary	ns
Exact or approximate P value?	Approximate
Significant? (alpha = 0.05)	No
Number of XY Pairs	25

Figure 17 Normal tissue sample DIN scores correlated with post-mortem interval (PMI, left) and time to refrigeration (TTR, right)

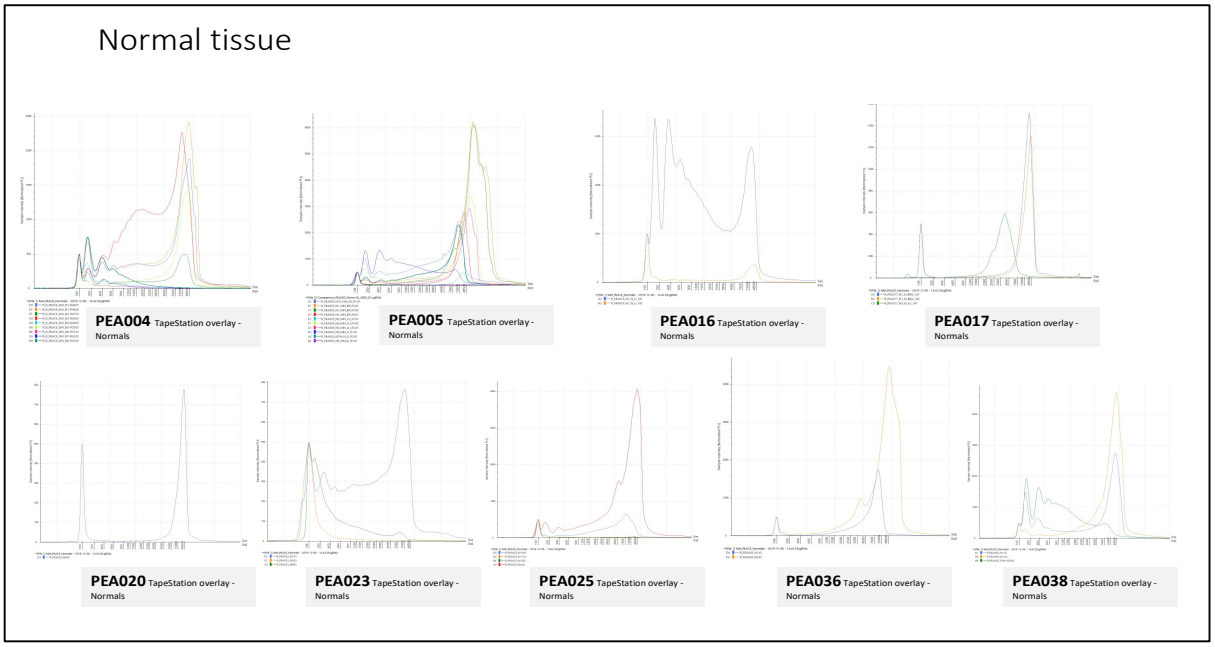

Figure 18 Normal tissue DNA fragment profiles
The fragment profiles of DNA extracted from normal tissue samples grouped by case are displayed below. These were generated by TapeStation analysis of the size (x axis: markers from 100 base pairs to 48,500 base pairs) and quantity (y axis: as measured by sample intensity (normalised fluorescent units)) of DNA strands of various sizes.

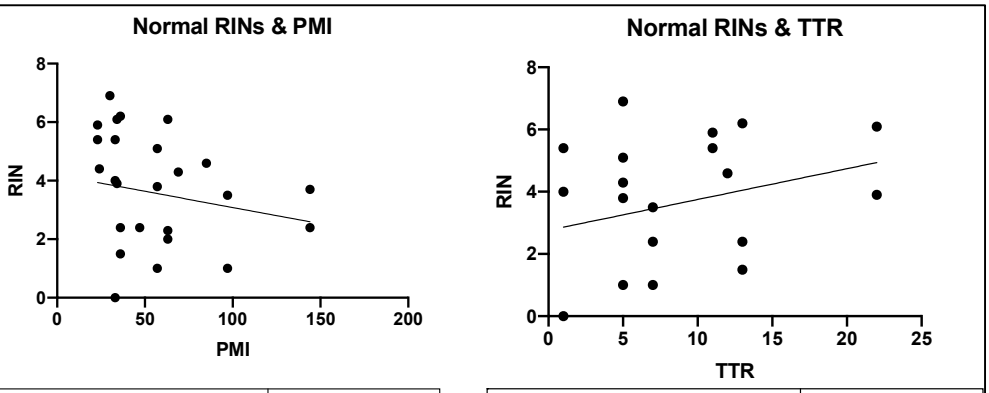

	PMI vs. RIN
Spearman r	
r	-0.2968
95% confidence interval	-0.6156 to 0.1055
P value	
P (two-tailed)	0.1327
P value summary	ns
Exact or approximate P value?	Approximate
Significant? (alpha = 0.05)	No
Number of XY Pairs	27

	TTR vs. RIN
Spearman r	
r	0.2154
95% confidence interval	-0.2513 to 0.6008
P value	
P (two-tailed)	0.3484
P value summary	ns
Exact or approximate P value?	Approximate
Significant? (alpha = 0.05)	No
Number of XY Pairs	21

Figure 19 Normal tissue sample RIN scores correlated with post-mortem interval (PMI, left) and time to refrigeration (TTR, right)

3.3.3 Analysis of ploidy by fluorescent in situ hybridisation

A preliminary bioinformatic analysis of ploidy across the first eight PEACE cases submitted for WES revealed a greater range of ploidy than noted in a previously published cohort of primary and metastatic melanomas (Figure 20).[27] PEACE samples ranged from diploid (2 copies of each chromosome) to septaploid (seven chromosomal copies), suggesting multiple rounds of genome doubling had occurred.

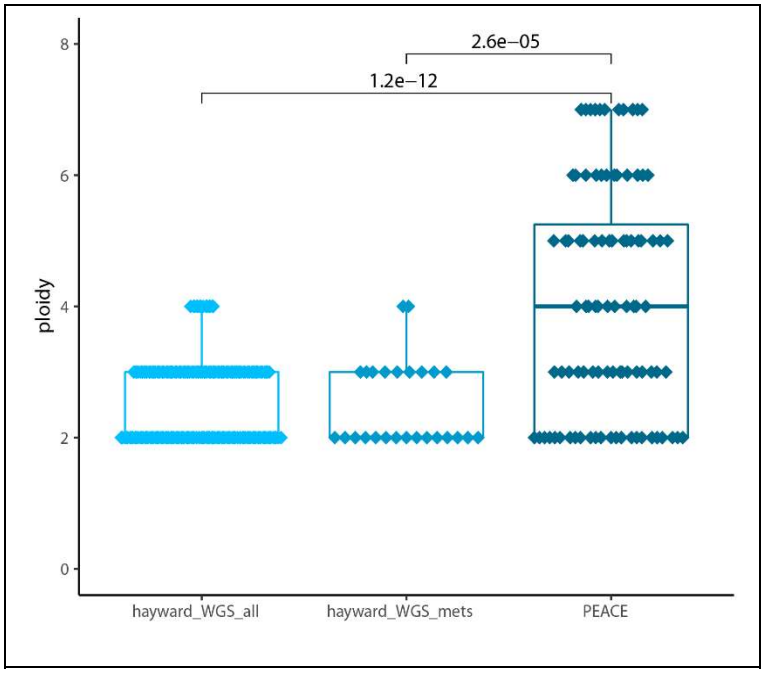

Figure 20 Preliminary analysis of ploidy across PEACE cases
Preliminary ploidy assessment of PEA004, PEA005, PEA016, PEA020, PEA023, PEA025, PEA026 & PEA036 using ABSOLUTE. The three categories compared include data from all tumour samples in the Hayward dataset[27] (left); metastatic tumours from the Hayward dataset (middle) and PEACE samples (right). Y axis represents ploidy (where 2 is diploid).

In order to calculate the CCF of various mutations – an important value to assist in the construction of phylogenetic trees – a copy number solution must be determined. Various bioinformatics algorithms exist to help with this (for example, ABSOLUTE[28]), and purity and ploidy estimates are central to finding the 'best-fit' solution. Given the higher than anticipated ploidy in this preliminary analysis of the PEACE samples (Figure 20), an orthogonal method of ploidy estimation was required to assist in the selection of solutions for bioinformatic processing. Interphase FISH was therefore undertaken. Two metastatic samples from the tissue harvest per case (that were also submitted for WES), as well as archival FFPE tumour blocks (primary tumours and metastases) were selected (see **Materials and Methods Section 2.10 Fluorescence in situ hybridisation (FISH)**). Centromeric probes for chromosomes two and 15 were used across all cases. These chromosomes are not typically subject to SCNAs in melanoma.[29,30] Samples subjected to FISH along with their estimated tumour purity on H&E assessment, are detailed in Appendix B. The majority of samples from the TH were successfully profiled (26/28, 93%). From archival FFPE tissue blocks (including primary tumours), only 6/29 (21%) yielded images that could be reliably analysed, including primary tumour regions from both PEA017 and PEA023.

Evaluation of interphase FISH is challenging, and options for probe enumeration include the use of an automated tool which requires training, optimisation and validation, or a manual approach. In the absence of a suitable ready-made tool, manual enumeration was selected for this cohort. In total, 7238 individual nuclei from 33 tumour samples and two normal tissue samples were scored across the cohort, giving an average of 207 nuclei scored per sample.

3.3.3.1 Bioinformatic-derived ploidy and WGII

The bioinformatic-derived median ploidy for primary tumours and metastases from each case across the cohort is outlined in Table 13, below. The median ploidy across sun-exposed cutaneous/MUP cases is 2.53 (range 1.67–4.37), and for acral cases it is 2.25 (range 1.99–6.20). PEA017 is the only case with a notable difference between the median ploidy of the primary tumour regions in comparison to metastatic sites (2.15 and 3.37 respectively). In all other cases the ploidy is similar. Whole genome doubling is evident in 9/14 cases, with 6/9 displaying a subclonal pattern of genome doubling. Comparisons between the computationally-derived and FISH-estimated ploidy for each case are discussed in **Section 3.3.4 Case descriptions of the genomic evolution of melanoma and inter-metastatic heterogeneity**.

The weighted genome instability index (WGII) is a measure of the proportion of the genome altered by copy number.[31] The median WGII of primary and metastatic regions for each case, along with the range of values, are also summarised in Table 13. The median WGII for the nine sun-exposed cutaneous/MUP cases is 0.44 (range 0.14–0.79) and for the four acral/non-sun-exposed cutaneous cases it is 0.40 (range 0.26–0.70).

Table 13 Median computationally-derived ploidy and WGII of metastases sampled at tissue harvest across cases

Median ploidy values (and the range for each case) derived from primary and metastatic ('Mets') tumour samples using ABSOLUTE. Presence of whole genome doubling (WGD) and its clonality per case. Median whole genome weighted instability index (WGII) for primary and metastatic ('Mets') tumour samples and range for each case.

	Subtype	Median Ploidy				WGD		Median WGII			
		Primary	*range*	*Mets*	*range*	*Present*	*Clonal/ subclonal*	*Primary*	*range*	*Mets*	*range*
PEA004	perianal	2.26	na	2.22	(2.08-3.89)	yes	subclonal	0.27	na	0.31	(0.26-0.59)
PEA005	cutaneous	na*	na*	2.56	(1.73-4.06)	yes	subclonal	na*	na*	0.49	(0.41-0.69)
PEA009	cutaneous	na	na	2.08	(2.05-2.09)	no	none	na	na	0.17	(0.16-0.23)
PEA012	MUP	na	na	2.29	(2.15-2.39)	no	none	na	na	0.24	(0.20-0.32)
PEA016	mucosal	3.27	(3.17-3.63)	3.72	(2.93-4.24)	yes	subclonal	0.67	(0.49-0.68)	0.65	(0.56-0.68)
PEA017	cutaneous	2.15	(2.05-2.24)	3.37	(2.1-3.89)	yes	subclonal	0.3	(0.16-0.44)	0.44	(0.14-0.62)
PEA020	MUP	na	na	2.44	(2.29-2.49)	no	none	na	na	0.45	(0.40-0.50)
PEA023	acral	5.14	(4.90-6.2)	5.3	(5.21-5.40)	yes	clonal	0.7	(0.59-0.70)	0.61	(0.59-0.69)
PEA025	cutaneous	na	na	2.04	(1.71-2.1)	no	none	na	na	0.3	(0.24-0.36)
PEA026	acral	na	na	2.33	(2.13-4.32)	yes	subclonal	na	na	0.42	(0.28-0.66)
PEA036	cutaneous	3.23	(3.15-3.31)	3.1	(2.85-3.14)	yes	clonal	0.52	(0.45-0.66)	0.52	(0.45-0.56)
PEA038	cutaneous	na*	na*	3.46	(1.70-4.22)	yes	subclonal	na*	na*	0.54	(0.22-0.77)
PEA060	MUP	na	na	4.15	(3.54-4.37)	yes	clonal	na	na	0.7	(0.65-0.79)
PEA080	acral	2.11	(2.02-2.12)	2.1	(1.99-2.16)	no	none	0.4	(0.37-0.47)	0.41	(0.37-0.51)

na= sample not available; na = sample available, but quality not sufficient for analysis.*

3.3.3.2 Inter-rater reliability for FISH enumeration

In order to assess the robustness of probe enumeration, an inter-rater assessment was undertaken on >1000 scored nuclei. Inter-rater reliability was very high, with an interclass coefficient of >0.96 (where 1.0 is perfect agreement) across all probe counts, as well as for each centromeric probe considered on its own (Figure 21, below).

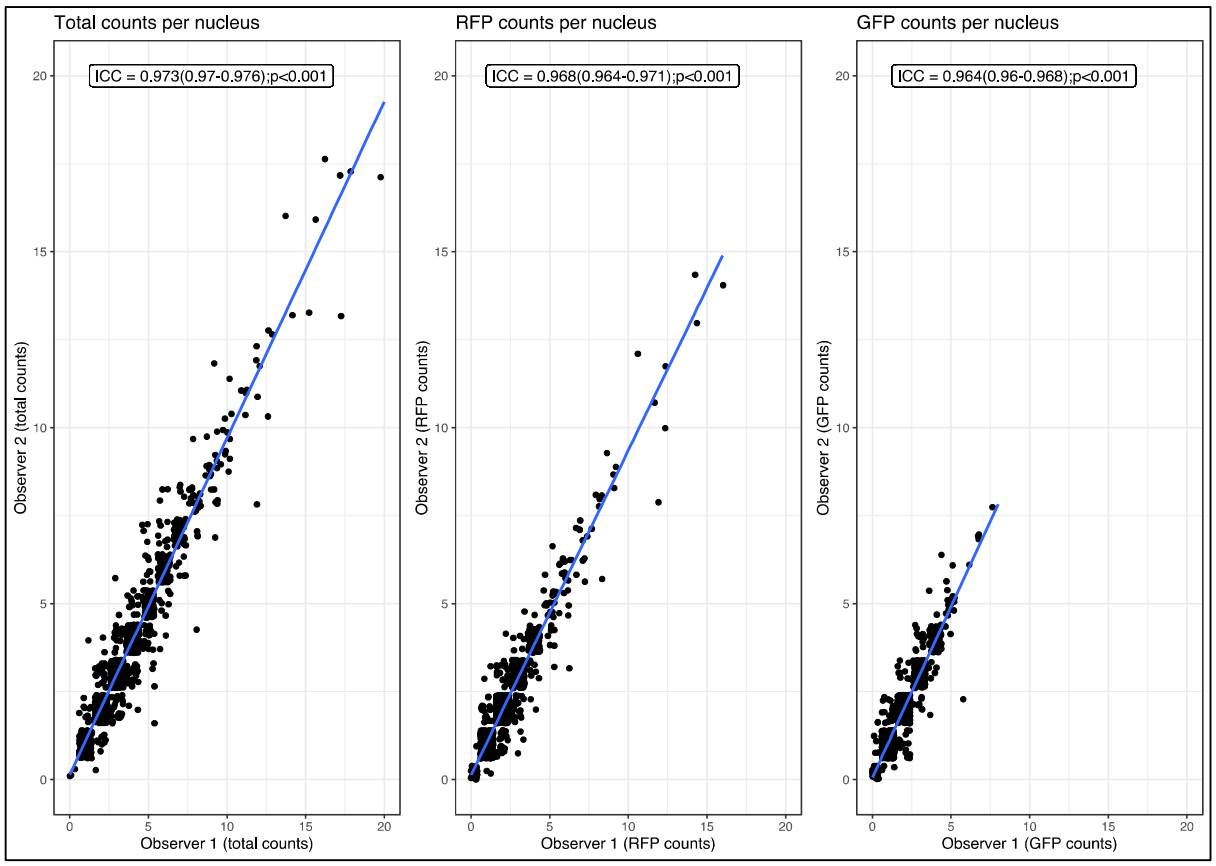

Figure 21 Inter-rater reliability for fluorescent in situ hybridisation (FISH) enumeration
The plots below demonstrate the concordance between Observer 1 and Observer 2 regarding total counts per nucleus (left), red fluorescent probe (RFP) counts per nucleus (middle), and green fluorescent probe (GFP) counts per nucleus (right). The interclass coefficient (ICC) for each plot is noted in the box at the top.

3.3.3.3 Probe concordance

There were fewer Chr 15 (green) probes noted at scores suggestive of higher ploidy, perhaps due to Chr 15 being smaller and therefore more subject to nuclear segmentation or potentially copy number loss. Concordance between the Chr 2 (red) and green probes overall was excellent (Figure 22), especially where the chromosome copy number ranged from 1 to 4.

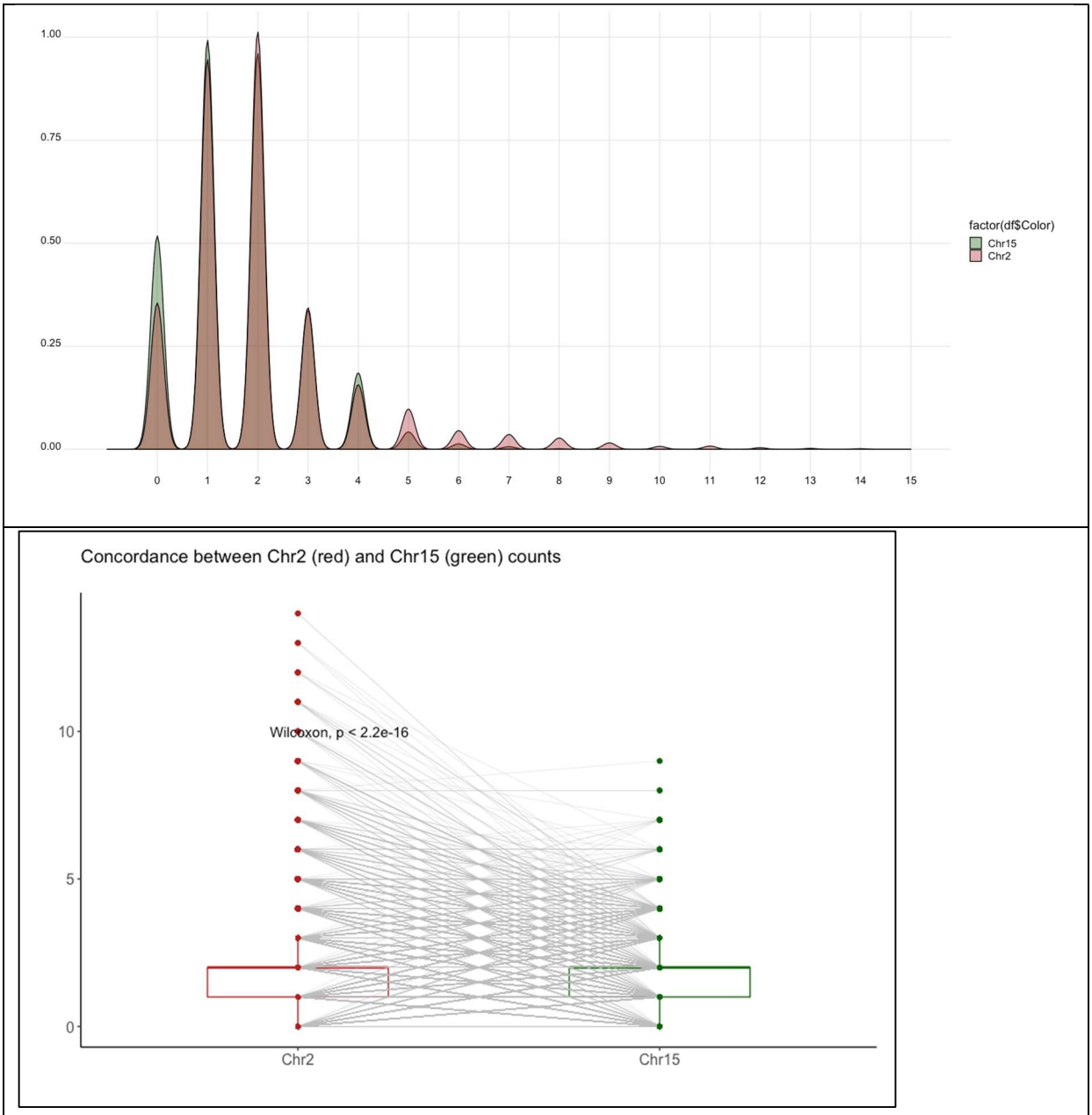

Figure 22 Concordance between Chr 2 (red) and Chr 15 (green) probes
Top: The x axis indicates the probe enumeration score and the y axis indicates the relative proportions of each score. The green (Chromosome 15) and red (Chromosome 2) probe data is overlayed; Bottom: Wilcoxon matched-pairs signed-ranks test, demonstrating that there is no difference in the median enumeration for red and green probes.

3.3.3.4 Probe enumeration and correction

On initial review of FISH images, cell to cell heterogeneity in ploidy was noted in most cases (examples provided in Figure 23), suggesting subclonal variation in ploidy within individual samples.

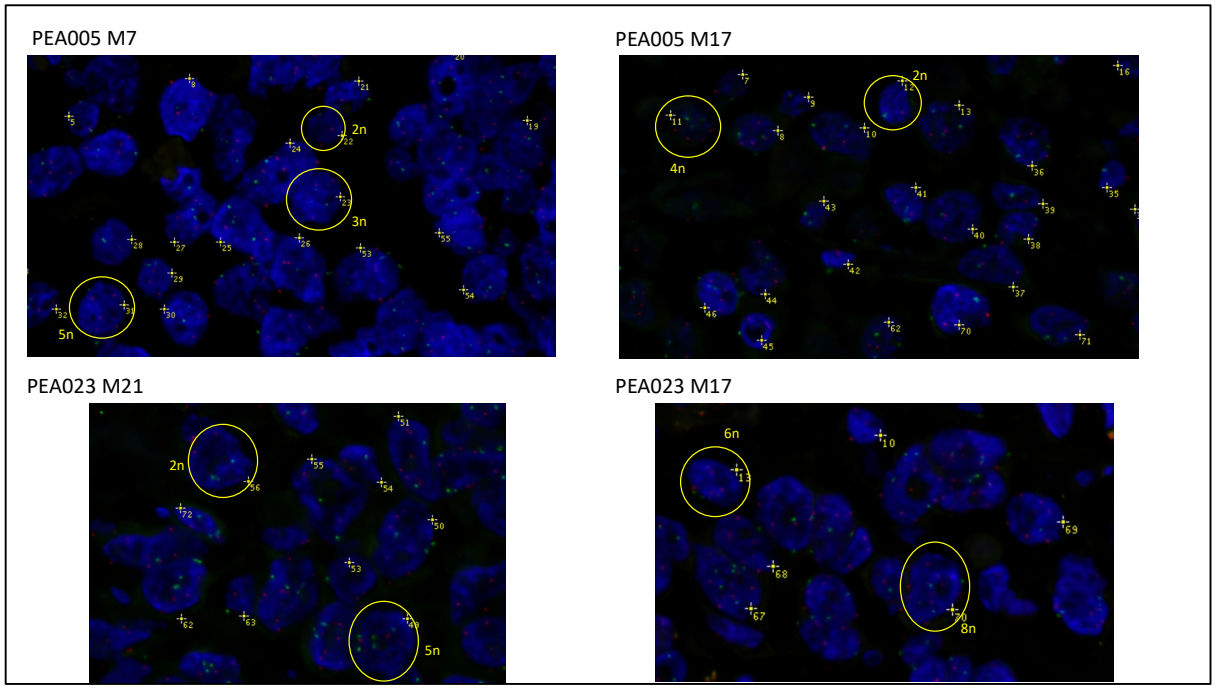

Figure 23 Examples of cell-to-cell heterogeneity in ploidy illustrated by FISH
Each tile below represents a different sample from patients PEA005 and PEA023. The top left tile (M7) is a sample from a brain metastases and the top right (M17) is from a lung metastasis. Bottom left (M21) is a from a liver metastasis and bottom right (M17) is from a lymph node. The yellow circles highlight individual cells in these samples where probe enumeration suggests differing ploidy. For example, 2n = diploid, 3n = triploid, 4n = quadraploid. The possible confounder of overlapping cells is highlighted in the PEA023 M17 sample. The numbers attached to each cell with a '+' identifies the cells for enumeration.

The total number of nuclei counted is outlined in Table 14. As outlined in **Materials and Methods Section 2.10 Fluorescence in situ hybridisation (FISH)**, in order to correct for the impact of nuclear segmentation as a consequence of interphase FISH (that is, nuclear segmentation and overlapping nuclei impacting true probe counts), we used a correction factor derived from two diploid control samples (that is, normal tissue – sourced from normal spleen in PEA038 and PEA080 – see Figure 24). By eliminating the lowest 61% and top 3% of scores for these diploid controls the estimated ploidy was 2, with very few counts outside of this (Table 14).

Table 14 Raw data on total counts from FISH probe enumeration

Number of probes scored (total counts), final number of probe enumerations included in corrected plots (counts included), minimum and maximum probe number (corrected values), nature of tissue.

Slide	TotalCounts	CountsIncluded	Min	Max	Tissue type
PEA038_N_S_1	738	266	2	3	normal
PEA080_N_S_1	1156	417	1	2	normal
PEA004_M16	284	104	2	4	tumour
PEA004_M20	372	135	2	4	tumour
PEA005_M17_LU1	462	168	2	4	tumour
PEA005_M7	446	161	4	6	tumour
PEA009_M1	986	356	2	3	tumour
PEA009_M2	274	100	2	4	tumour
PEA012_M20	720	260	2	3	tumour
PEA012_M42	460	167	2	3	tumour
PEA016_M4	208	76	3	4	tumour
PEA016_M5	134	50	3	5	tumour
PEA016_PI	158	58	2	5	tumour
PEA017_M15	708	256	2	4	tumour
PEA017_TB54	372	135	2	4	tumour-archival
PEA017_TB55	498	180	1	3	tumour-archival
PEA020_M26	324	118	2	4	tumour
PEA023_A1	178	65	2	5	tumour-archival
PEA023_B1	108	40	3	7	tumour-archival
PEA023_M17	424	154	4	11	tumour
PEA023_M21	284	104	4	8	tumour
PEA025_M1	452	164	2	3	tumour
PEA025_M16	304	111	2	3	tumour
PEA025_TB49	308	112	1	2	tumour-archival
PEA026_M18	322	117	1	2	tumour
PEA026_M5	370	134	2	4	tumour
PEA036_M54	574	208	2	3	tumour
PEA036_M69	564	204	2	4	tumour
PEA038_M11	366	132	3	4	tumour
PEA038_M26	440	159	3	5	tumour
PEA038_TB40	262	96	2	4	tumour-archival
PEA060_M13	324	118	2	4	tumour
PEA060_M19	306	111	2	3	tumour
PEA080_M1	208	76	2	4	tumour
PEA080_M14	382	139	2	4	tumour
TOTAL	14476	5251			

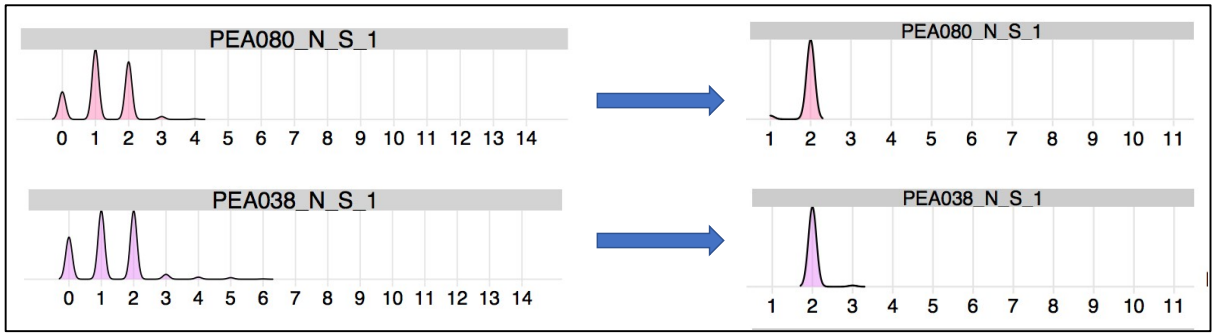

Figure 24 Example of FISH-estimated ploidy correction based on normal splenic tissue values
Left: raw enumeration values for normal spleen samples from patients PEA080 and PEA038 assumed to be diploid; right: corrected values.

Tumour samples displayed a much greater distribution of scores than the normal tissue controls, ranging from 0 to 14 in the uncorrected data and 1 to 11 in the corrected data (Figure 25 and Figure 26 below). This is suggestive of ploidy ranging from monoploid (1n) to decaploid (10n) and beyond at a cellular level.

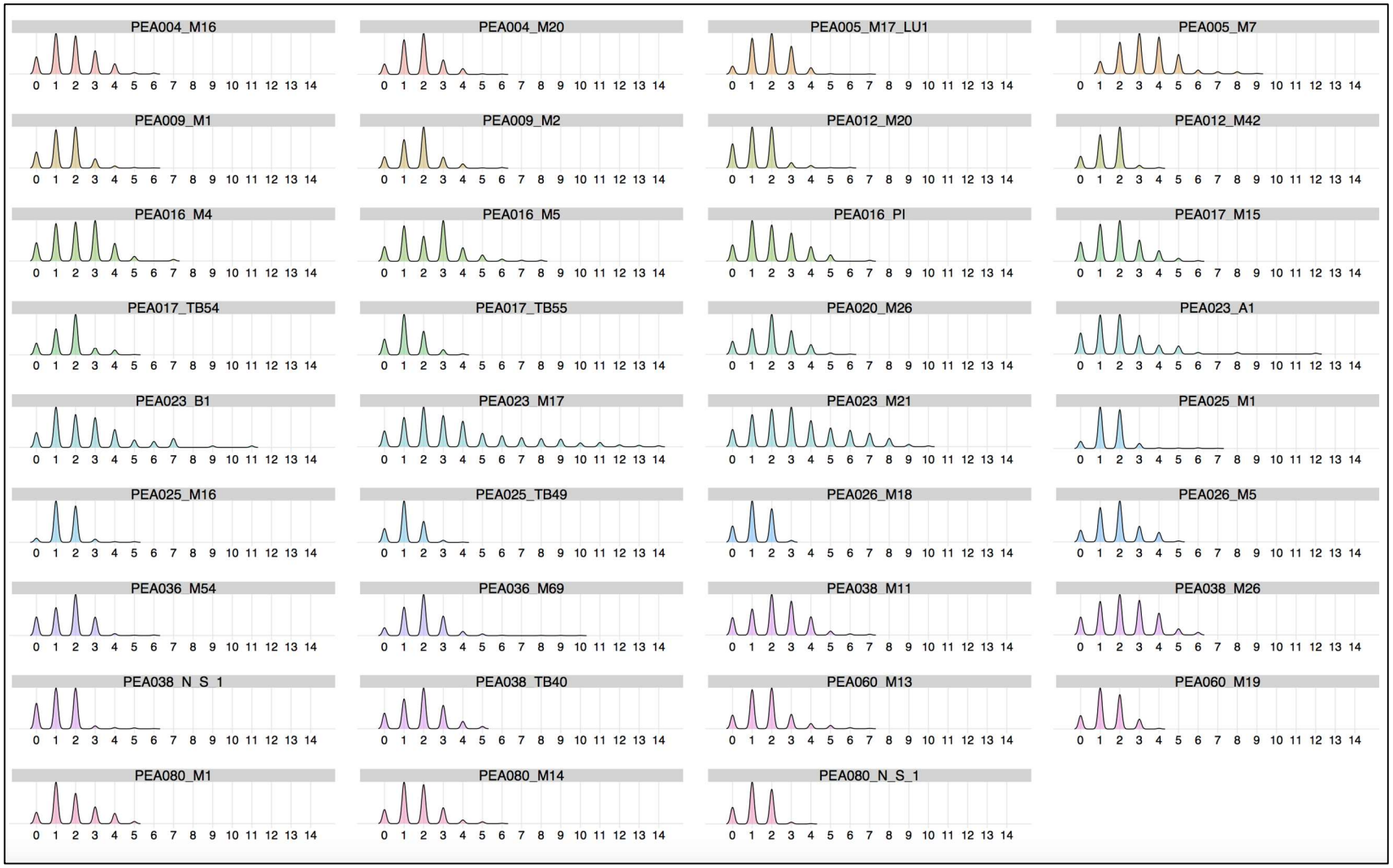

Figure 25 FISH-estimated ploidy enumeration – raw counts (prior to correction)
PEA038_N_S_1 and PEA080_N_S_1 are the diploid controls. X axis shows probe enumeration score and y axis indicates relative proportions of each score.

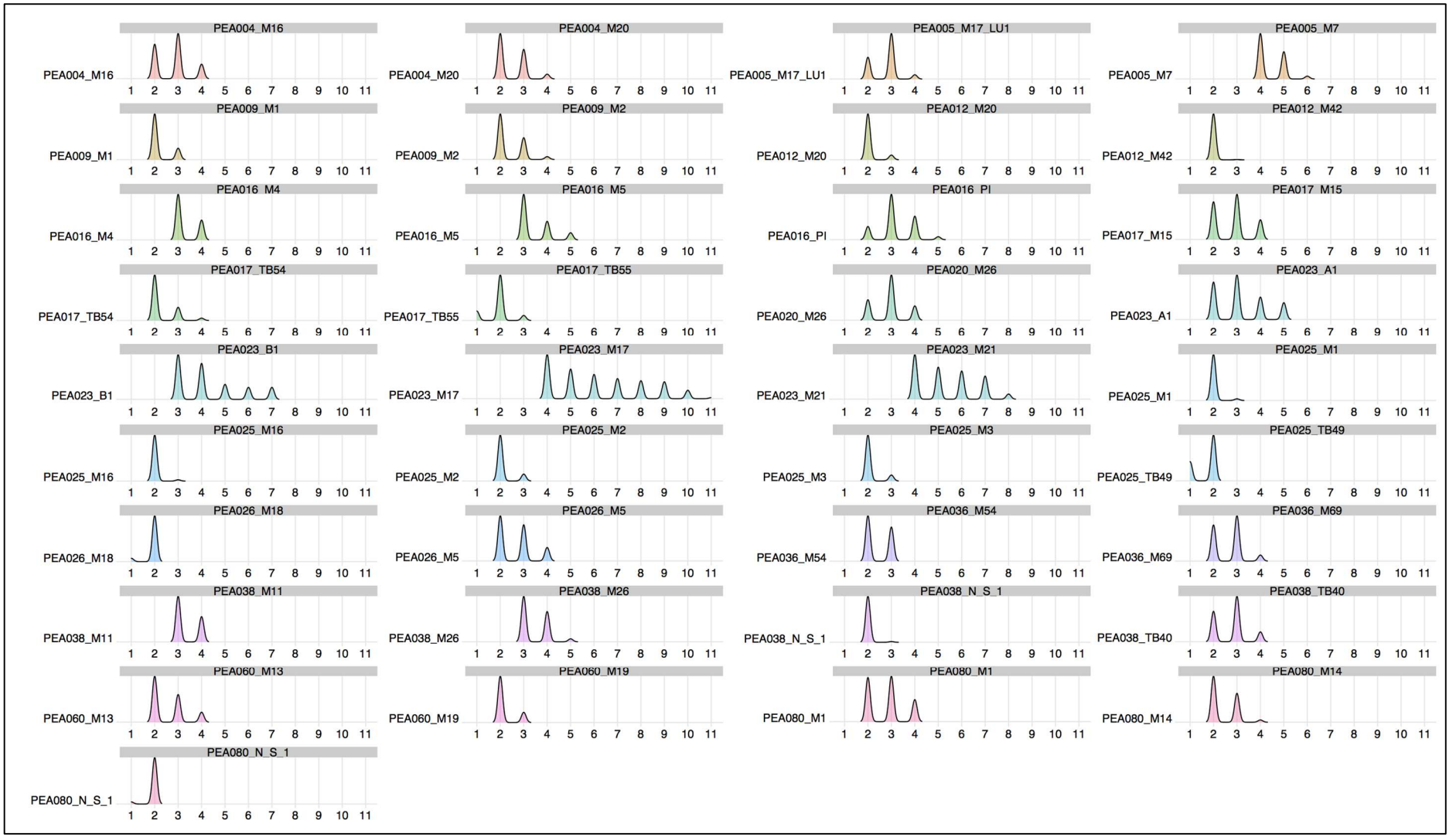

Figure 26 FISH-estimated ploidy enumeration – corrected values
PEA038_N_S_1 and PEA080_N_S_1 are the diploid controls. X axis shows probe enumeration score and y axis indicates relative proportions of each score. NB: PEA025 M2 & M3 – not included in main analysis (training data).

While some cases appear predominantly diploid (PEA009, PEA012, PEA025, PEA026), others appear to harbor a range of cells of different ploidy states (for example, PEA005, PEA023). Intermetastatic heterogeneity in ploidy is also apparent. For example, PEA005 M17 has a dominant triploid population whereas in PEA005 M7 the dominant population is quadraploid (Figure 26). In a further example, for PEA017 the diploid population is most prevalent in the primary tumour samples (TB54 & TB55); however, the metastasis (M15) is characterised by a triploid population, with some cells also showing tetraploid status (Figure 26).

3.3.4 Case descriptions of the genomic evolution of melanoma and inter-metastatic heterogeneity

To facilitate interpretation of the 14 case studies in the following section, I have recapped the definition of the following terms (also see **Section 1.1.2 Modes of evolution** in the **Main Introduction** and Figure 3):

Evolutionary modes from primary tumour to metastatic sites:

Monoclonal seeding: one clone from the primary tumour is responsible for seeding metastatic sites (note that this clone may evolve outside of the primary, prior to seeding).

Polyclonal seeding: more than one clone from the primary tumour seeds metastatic sites (noting these clones may further evolve outside of the primary, prior to seeding).

The term '**polyclonal seeding**' may also refer to the situation where more than one clone seeds a particular metastatic site, whether or not both come from the primary tumour. For example, additional clones may seed metastatic sites as a result of intermetastatic seeding.

Clonal composition of metastatic regions (based on cancer cell fraction (CCF) values):

Monoclonal region: The CCF value of all mutation clusters within a region are within 15% of the CCF of the clonal cluster. This implies that all clusters are clonal (within the limitations of our analysis).

Polyclonal region: The CCF value of at least one mutation cluster within a region is more than 15% lower than the CCF of the clonal cluster. For example, if the CCF of the clonal cluster (Cluster 1) is 100%, and Cluster 2 has a CCF of 70% it would be considered subclonal. The existence of the two subclonal populations (that is, cells with clusters one only and cells with Clusters 1+2) may arise from ongoing (neutral) evolution in a group of cells at

that site, polyclonal seeding from the primary tumour to that site or from intermetastatic seeding.

The nomenclature for the sampled sites indicated on the phylogenetic trees in the following 14 case descriptions is as follows.

- Anatomical site_metastasis number_sampled region number; for example, **LN_1_R2** represents lymph node metastasis 2, Region 2 (implying >1 region sampled from this individual site).
- The primary tumour sites have prefix 'PR'.
- The additional profiled archival FFPE samples have an 'a' (archival).
- For example, **LNa_1_R1** represents archival lymph node 1, Region 1.
- The anatomical location prefixes (for example, Ln = lymph node, LI=liver) are detailed in the figure legend for each case.

Please note: references pertaining to each case study are listed at the end of each case; whereas the remainder of the referencing for this section is listed after the **Discussion** section.

Case study 1: PEA004

Clinical summary

Patient PEA004 was a 75 year old woman initially diagnosed with an 11 mm Breslow thickness cutaneous perianal *BRAF K601E* mutant melanoma in 2014. In January 2015 she developed a locoregional recurrence for which she underwent a right ilioinguinal lymph node dissection, with 4/8 inguinal nodes involved by melanoma. In April 2015 she commenced adjuvant nivolumab within the Checkmate-238 study.[1] Symptomatic recurrent disease in the peri-anal and pelvic regions was diagnosed on imaging after three cycles of nivolumab. In May 2015 she commenced ipilimumab but progressed after two cycles in her pelvis and lungs. In July 2015 dabrafenib was initiated with stable disease in the liver, but progression at all other sites. Pembrolizumab was started in November 2015, in conjunction with a course of palliative radiotherapy to bulky pelvic disease. Despite this, her disease continued to progress and she died in February 2016. The clinical course is summarised in Figure 27.

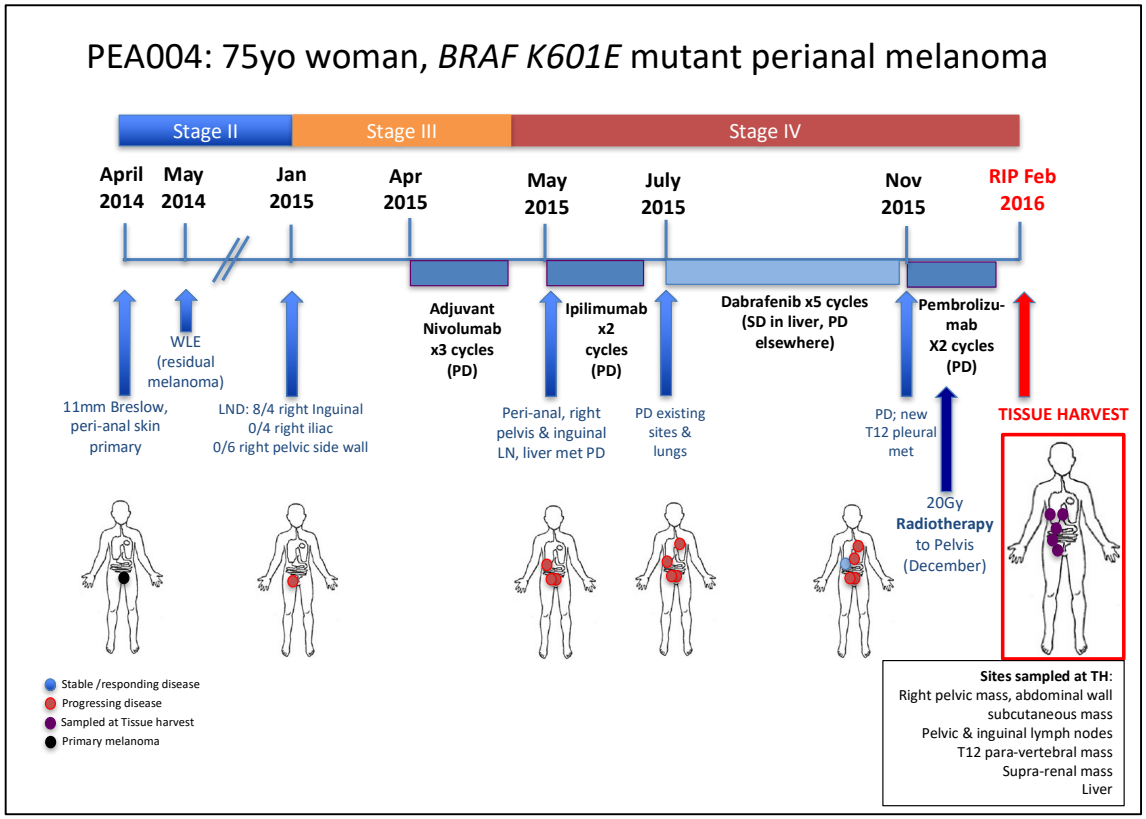

Figure 27 Timeline of clinical events, treatment and disease response in PEA004
Best overall RECIST response is included in brackets for each line of treatment (CR: complete response; PR: partial response; SD: stable disease; PD: progressive disease). WLE: wide local excision. Adj: adjuvant; nivo: nivolumab; ipi: ipilimumab; pembro: pembrolizumab; Gy: Gray (radiation unit); LN: lymph node; LND: lymph node dissection

.

Tissue harvest (TH) sampling and quality control considerations

Forty-five tumour regions were sampled at the TH from 24 individual metastases involving lymph nodes, subcutaneous, pelvic, suprarenal and paravertebral tissues, liver and bone. Of these 45 samples, 22 were submitted for WES as part of another project.[2] The archival FFPE samples from both the primary melanoma and the resected locoregional (Stage III) inguinal lymph node disease were dissected and 'homogenised' (blended) as part of the other study,[2] and the DNA extracted from these homogenates was submitted for sequencing. Nineteen of the 22 TH samples were successfully profiled using WES, as well as both homogenised archival FFPE specimens.

Genomic features

The overall TMB is low for this case (2.6/Mb, 46 nsSNVs), which was closer to that of an acral/sun-protected melanoma (acral melanoma 2.1 mutations/Mb)[3] than a UV-exposed cutaneous melanoma (16.8 mutations/Mb[4] or median 135 nsSNVs).[5] The clonal SNV burden

was 55% (Table 12 in **Section 3.3.1)**. The dominant clonal mutational signature is age-related (Signature 1A),[6] and no UV signature is evident (Figure 28).

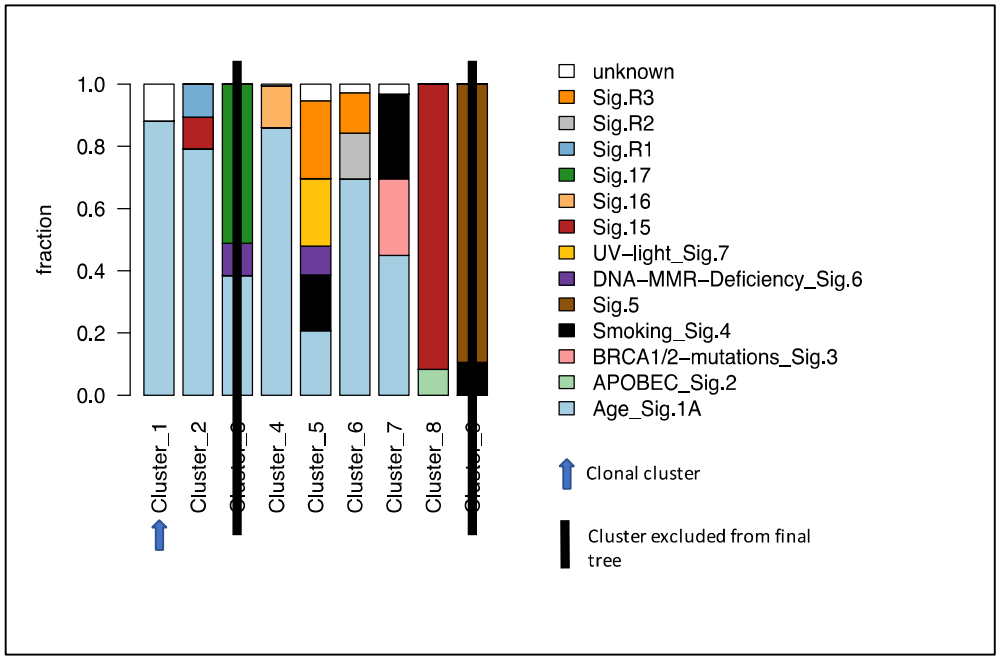

Figure 28 Mutational signature analysis of PEA004
Mutational signatures are based on Pyclone clustering of mutations for creation of phylogenetic trees, with the clonal cluster representing the ubiquitous mutations. Cluster 1 is the clonal cluster and is the only cluster with enough SNVs for reliable signature analysis. Clusters 3 and 9 were removed from the final tree.

The median computationally derived ploidy is 2.2, with the majority of samples being diploid (Table 13 in **Section 3.3.3**). However, one of two regions from a right internal iliac lymph node (LN_1_R1) appears to have undergone whole genome doubling with a ploidy of 3.89. The two samples profiled using FISH each capture a different mode ploidy (that is, LN_1_R1 mode 3 versus ST_2_R2 (right groin soft tissue tumour) mode 2) (Figure 29), consistent with the bioinformatics estimate. Median WGII was 0.30 across metastases, with the exception of the genome-doubled right internal iliac lymph node Region 1 (LN_1_R1), which had a higher WGII score of 0.59.

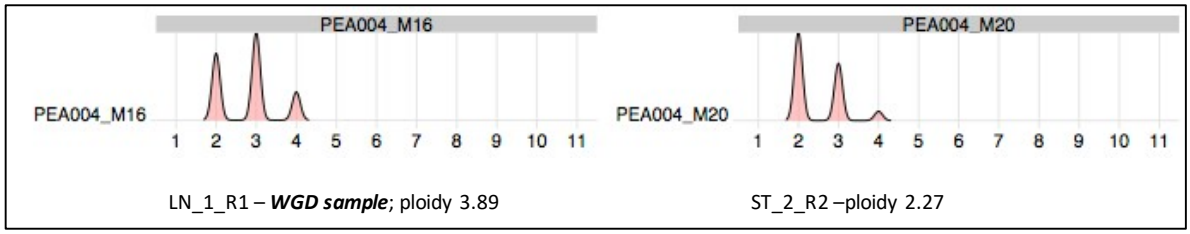

Figure 29 Corrected ploidy estimates of PEA004 samples analysed by FISH
*The x axis denotes the total probe count for each chromosome (see **Section 3.3.3**) and the y axis denotes the relative frequency.*

Driver alterations

The key clonal driver mutation in this case is *BRAF K601E* (Figure 30). Putative subclonal driver alterations are noted in *PIK3CA H1047L* (discussed further in the **Genomic mechanisms of treatment resistance** section below) and *GNAS R186C*. Both mutations are reported in Catalogue of Somatic Mutations in Cancer (COSMIC). Figure 34 summarises the clinical course.

The majority of somatic copy number aberrations (SCNAs) are subclonal. Clonal arm-level gains are noted in 7p and 8q, with clonal loss in 10q (harbouring *PTEN*), all common in non-sun-exposed and acral subtypes (Figure 31).[3,7] Clonal putative driver cytoband SCNAs relevant to acral tumours[3,7] included gains in 1q21, 6q12, 11q13 (harbouring *CCND1*) and 15q26. Additional potential driver SCNAs (as per GISTIC analysis of TCGA data) included gains in 7q34 (harbouring *BRAF*) and 17q25 and losses in 2q37, 6q26, 15q21 (Figure 32). Clonal driver gene amplifications and deletions were mainly attributable to the arm- and cytoband-level copy number changes described, with the exception of a more focal clonal copy number loss of *ARID1B* (Figure 33).

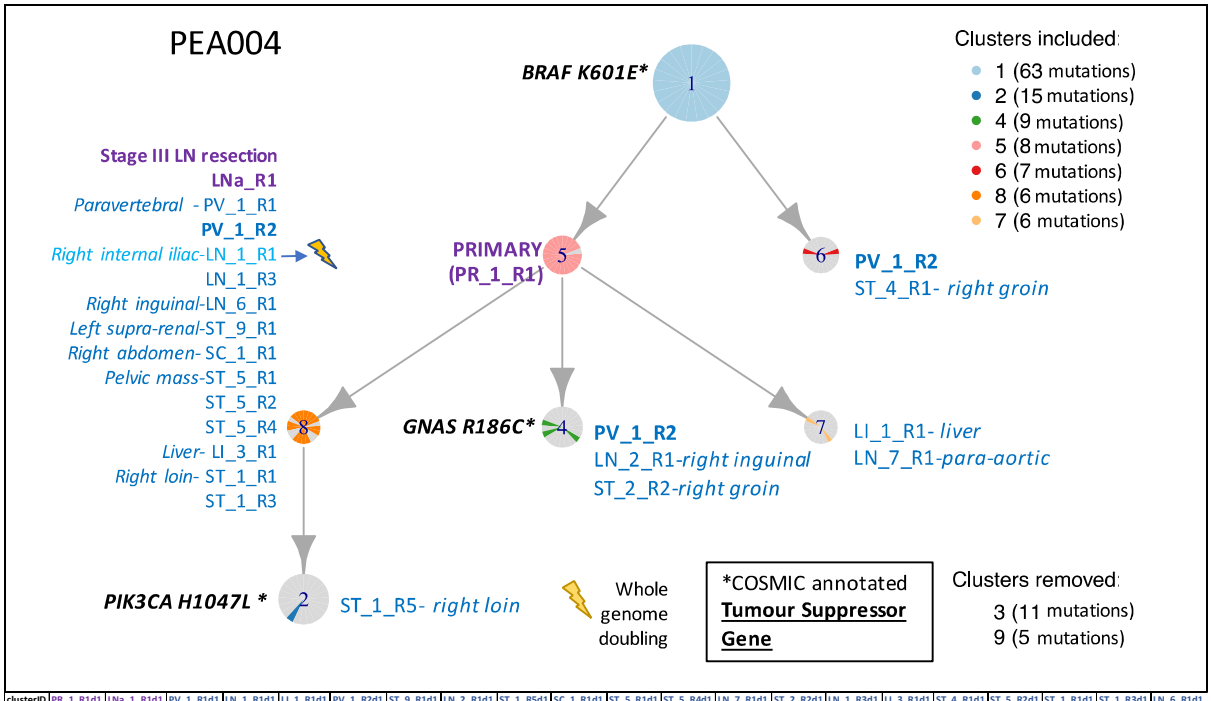

clusterID	PR_1_R1d1	LNa_1_R1d1	PV_1_R1d1	LN_1_R1d1	LI_1_R1d1	PV_1_R2d1	ST_9_R1d1	LN_2_R1d1	ST_1_R5d1	SC_1_R1d1	ST_5_R1d1	ST_5_R4d1	LN_7_R1d1	ST_2_R2d1	LN_1_R3d1	LI_3_R1d1	ST_4_R1d1	ST_5_R2d1	ST_1_R1d1	ST_1_R3d1	LN_6_R1d1
1	93	92	99	98	97	99	99	98	95	98	98	95	97	97	99	97	95	98	93	96	98
5	68	93	94	95	90	92	92	89	92	91	94	83	94	93	94	95	0	94	93	93	93
8	0	36	85	91	0	47	54	0	89	89	90	82	0	0	78	86	0	91	84	82	77
6	0	0	0	0	0	20	0	0	0	0	0	0	0	0	0	0	95	0	0	0	0
4	0	0	0	0	0	35	0	60	0	0	0	0	0	89	0	0	0	0	0	0	0
7	0	0	0	0	50	0	0	0	0	0	0	0	92	0	0	0	0	0	0	0	0
2	0	0	0	0	0	0	0	0	10	0	0	0	0	0	0	0	0	0	0	0	0

Figure 30 Phylogenetic tree for PEA004
The clonal cluster of shared mutations sits at the trunk of the tree. Driver mutations belonging to each cluster are annotated.
The cancer cell fraction (CCF) of each cluster per metastatic site is detailed in the table beneath the tree.
LN = lymph node; PV = paravertebral; ST = soft tissue; SC = subcutaneous; LI = liver.

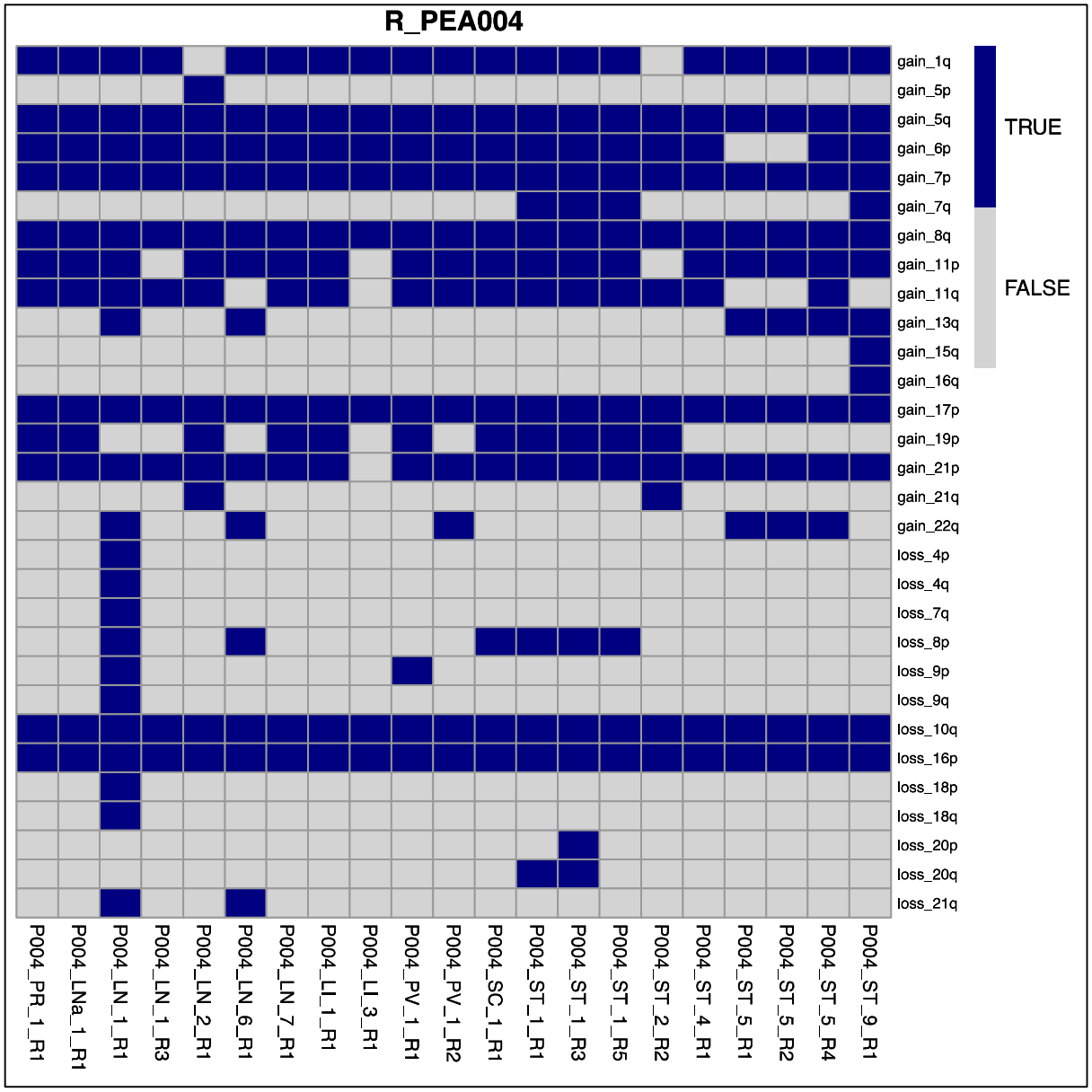

Figure 31 Chromosomal arm-level losses and gains
Blue squares indicate whether there was loss or gain of at least one copy of the chromosome arm relative to the mean ploidy of all samples.

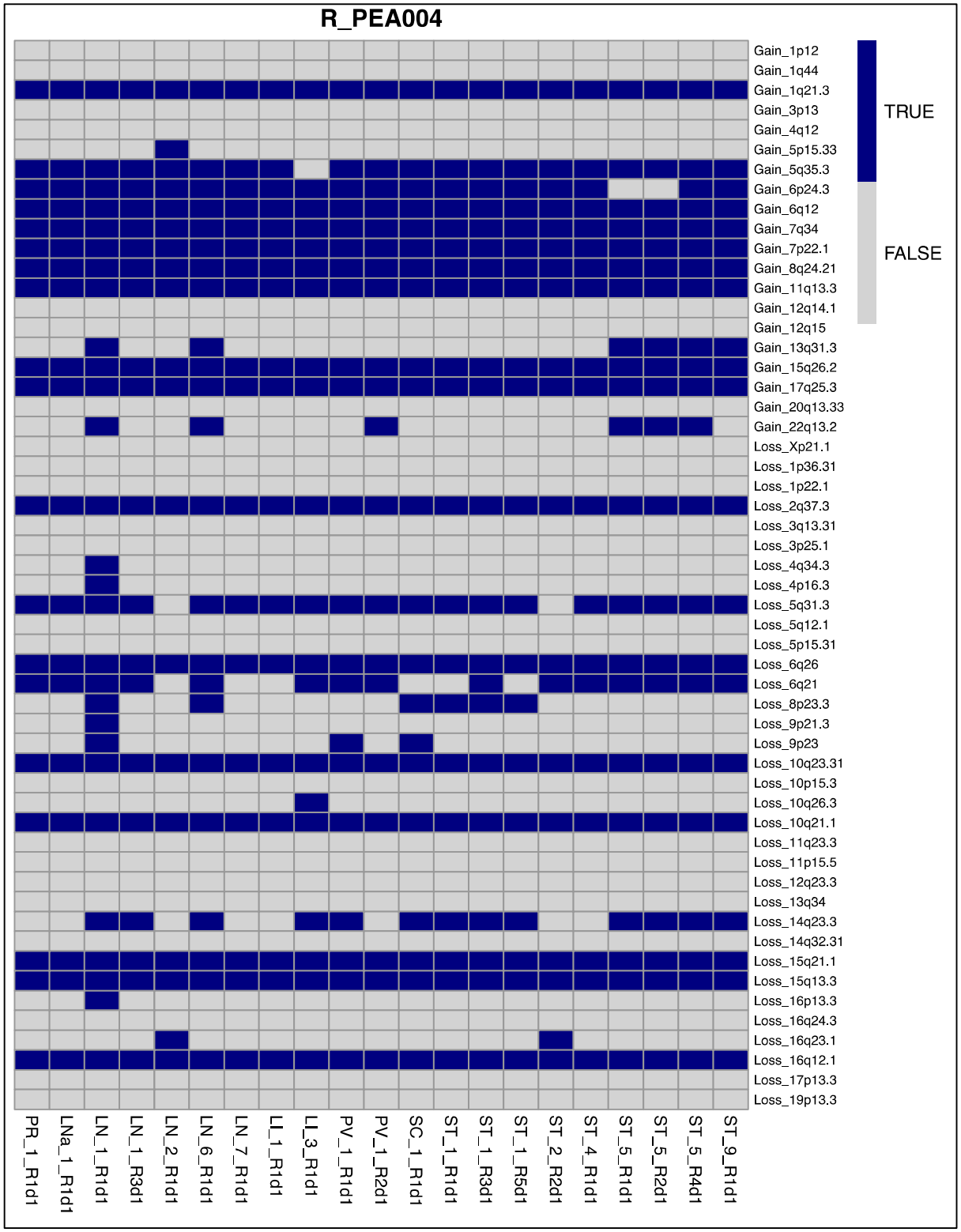

Figure 32 Cutaneous melanoma driver cytoband gains and losses

Annotated cytobands are melanoma driver regions determined by a GISTIC analysis of TCGA data.[4] Blue squares indicate whether there was loss or gain of at least one copy of the cytoband relative to the mean ploidy of all samples.

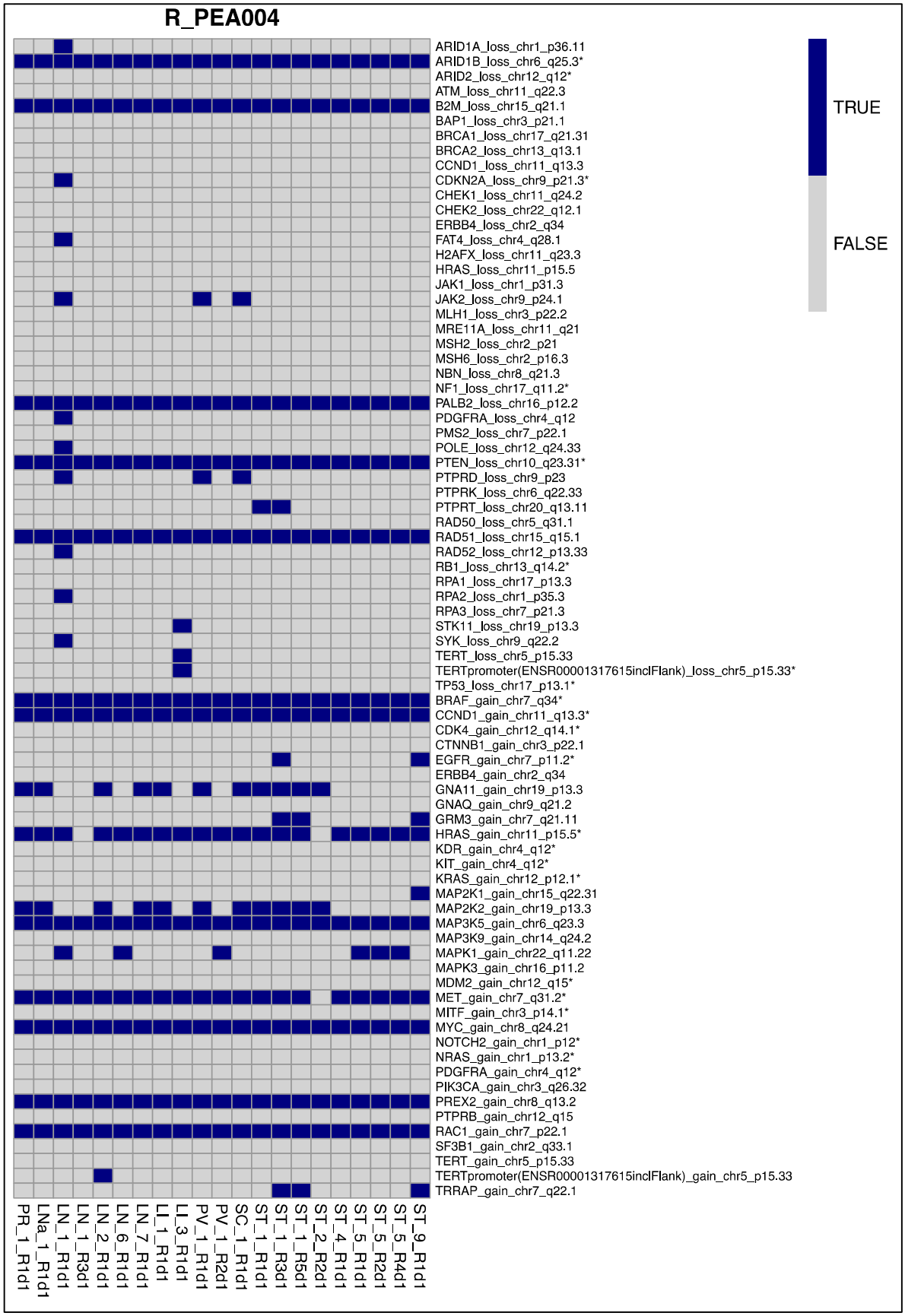

Figure 33 Driver gene gains and losses

Genes with an asterisk (*) are noted driver genes in the TCGA and Hayward data sets.[4]. Blue squares indicate whether there was loss or gain of at least one copy of the gene relative to the mean ploidy of all samples.

Evolution and metastatic seeding patterns

The phylogenetic tree for PEA004 is shown in Figure 30. A clone harbouring Clusters 1 and 5 characterises the primary tumour which appears polyclonal as the CCF of Cluster 5 in the primary is 68%, suggesting it is not present in all the cells of the primary tumour. All metastatic regions except one (right groin Region 1 (ST_4_R1)) contain Cluster 5 at CCFs >90%, suggestive that they are seeded from this primary tumour clone. Right groin Region 1 is seeded by a clone harbouring Clusters 1 and 6, the latter being an exclusive set of seven SNVs, not evident with the primary tumour sample. This may have been a minor primary tumour clone which has not been captured within the limitations of the current sampling.

Overall, the primary to metastatic seeding pattern appears polyclonal, with evidence of >1 distinct clone seeding spatially separate metastatic sites that have a different recent common ancestor. For example, the recent common ancestor for paravertebral metastasis 1 Region 2 (PV_1_R2) and right groin soft tissue metastasis Region 1 (ST_4_R1) is characterised by Cluster 6; whereas for all other metastatic sites (including lymph nodes, liver and subcutaneous metastases), the recent ancestor is characterised by Cluster 5. The fact that the Cluster 5 mutations are detected in the primary tumour discounts a scenario where there was one seeding event with acquisition of this cluster outside of the primary tumour.

While 12/19 metastases appear monoclonal in their composition (that is, CCFs >15% lower than the CCF of the clonal cluster), 7/19 are polyclonal (that is, CCFs $\leq$15% from the CCF of the clonal cluster). Paravertebral Region 2 (PV_1_R2) is a polyclonal metastasis that contains three clones from exclusive branches of the phylogenetic tree (that is, clone 1 = Clusters 1+6, clone 2 = Clusters 1+5+4, clone 3 = Clusters 1+5+8). Because this was a late-emerging metastasis noted in November 2015, it may be an example of metastasis-to-metastasis seeding creating this mixture of clones, or it may have been seeded by $\geq$1 clone from the primary tumour and remained clinically dormant.

In this case, the resected Stage III right ilioinguinal lymph node sample (LNa_R1) harbours the same clone as the majority of metastases (containing Clusters 1+5+8). It is likely that distant metastatic dissemination occurred concurrently with Stage III disease. Supporting this is the fact that LNa_R1 sits on one branch of the tree and most of the other metastases seeded by this clone have not acquired private mutations (which they may have done if they were

seeded via the lymph node). Also, there was a short, four-month interval between Stage III diagnosis and clinical progression to Stage IV, in keeping with this hypothesis.

Intra-lesional heterogeneity in SCNAs is apparent in this case. As mentioned above, one of the two sampled regions of the right internal iliac lymph node metastasis (LN_1) has undergone WGD (LN_1_R1); whereas the other region (LN_1_R3) appears diploid. LN_1_R1 has the greatest number of SCNAs, visible across all three somatic copy number heatmaps (Figure 31, Figure 32 and Figure 33).

Genomic mechanisms of treatment resistance

The *BRAF K601E* mutation is not generally considered responsive to BRAF targeted therapy, although data are limited.[9] In this case, stable disease was noted in the liver, with progression elsewhere, during the five cycles of dabrafenib. One region of the right loin soft tissue mass (ST_1_R5) harbours a *PIK3CA H1047L* mutation. PI3K pathway mutations have been implicated in resistance to dabrafenib,[10] and this was a progressive site during dabrafenib. However, it was not the sole site of progression, suggesting multiple resistance mechanisms were at play. These have not been elucidated in this analysis and may involve non-genetic mechanisms.

The clonal SNV burden was 55%, suggesting a relatively high proportion of subclonal mutations, and therefore relatively fewer clonal neoantigens, a pattern enriched in non-responders to ICIs.[11] Within the limitations of our analysis, there are no identifiable mutations that would confer resistance to ICIs in this case. There was clonal somatic copy number loss of both *B2M* and *PTEN*, which, in the majority of metastases, will lead to loss of heterozygosity (LOH) due to their diploid nature (except in LN_1_R1, which underwent WGD). In the presence of a remaining wild type allele, however, the significance of these alterations is unclear. The DECIPHER tool[12] does suggest that *PTEN* is likely to be haploinsufficient (that is, where one wild-type allele is not adequate for normal gene expression) with a score of 0.07% (1–10% being the rank in which HI is likely); whereas this is much less likely for *B2M* with a score of 77.92% (rank 90–100% suggests a gene is not likely to be susceptible to HI).

Case summary

This case demonstrates tumour heterogeneity on several levels, with 19 profiled sites in soft tissues and viscera providing a comprehensive representation of metastatic disease. The

heterogeneity is a function of the polyclonal seeding pattern from the primary tumour and possibly cross-metastatic seeding. Overall, this melanoma was refractory to several lines of treatment and despite adjuvant immune checkpoint therapy, survival from resected Stage III disease was only 13 months.

One of two sequenced regions from a right internal iliac lymph node (LN_1_R1) appears to have undergone WGD, which may be a clue to progressive genomic instability, and signify that copy number changes are a key survival strategy by this tumour. This particular sample had the most gains/losses of all, likely due to the improved tolerance of SCNAs in WGD samples.[13] To date, WGD in melanoma is reported as an earlier, clonal event, rather than a subclonal phenomenon.[8,14] In this case, the computational WGD result was orthogonally confirmed by FISH.

References for PEA004

1. Weber J, Mandala M, Del Vecchio M, et al. Adjuvant Nivolumab versus Ipilimumab in Resected Stage III or IV Melanoma. *N Engl J Med*, 2017.
2. Litchfield K, Stanislaw S, Spain L, et al. Representative Sequencing: Unbiased Sampling of Solid Tumor Tissue. *Cell Rep* 31: 107550, 2020.
3. Newell F, Wilmott JS, Johansson PA, et al. Whole-genome sequencing of acral melanoma reveals genomic complexity and diversity. *Nat Commun* 11: 5259, 2020.
4. Cancer Genome Atlas N: Genomic Classification of Cutaneous Melanoma. *Cell* 161: 1681–96, 2015.
5. Vogelstein B, Papadopoulos N, Velculescu VE, et al. Cancer genome landscapes. *Science* 339: 1546–58, 2013.
6. Alexandrov LB, Nik-Zainal S, Wedge DC, et al. Signatures of mutational processes in human cancer. *Nature* 500: 415–21, 2013.
7. Curtin JA, Fridlyand J, Kageshita T, et al. Distinct sets of genetic alterations in melanoma. *N Engl J Med* 353: 2135–47, 2005.
8. Hayward NK, Wilmott JS, Waddell N, et al. Whole-genome landscapes of major melanoma subtypes. *Nature* 545: 175–180, 2017.
9. Menzer C, Menzies AM, Carlino MS, et al. Targeted Therapy in Advanced Melanoma With Rare BRAF Mutations. *J Clin Oncol* 37: 3142–3151, 2019.
10. Van Allen EM, Wagle N, Sucker A, et al. The genetic landscape of clinical resistance to RAF inhibition in metastatic melanoma. *Cancer Discov* 4: 94–109, 2014.
11. McGranahan N, Furness AJ, Rosenthal R, et al. Clonal neoantigens elicit T cell immunoreactivity and sensitivity to immune checkpoint blockade. *Science* 351: 1463–9, 2016.
12. Firth HV, Richards SM, Bevan AP, et al. DECIPHER: Database of Chromosomal Imbalance and Phenotype in Humans Using Ensembl Resources. *Am J Hum Genet* 84: 524–33, 2009.
13. Lopez S, Lim EL, Horswell S, et al. Interplay between whole-genome doubling and the accumulation of deleterious alterations in cancer evolution. *Nat Genet* 52: 283–293, 2020.

14. Birkeland E, Zhang S, Poduval D, et al. Patterns of genomic evolution in advanced melanoma. *Nat Commun* 9: 2665, 2018.

Case study 2: PEA017

Clinical summary

Patient PEA017 was a 40 year old woman first diagnosed with a 2.1 mm Breslow thickness primary melanoma on the chest in 2013. No sentinel lymph node biopsy was performed. In January 2017 she relapsed with a high burden of intra-thoracic disease. A pleural effusion was drained, and cytology from this confirmed recurrent melanoma, with a *BRAF V600E* mutation. A solitary asymptomatic brain metastasis was also noted at this time. She commenced dual MAPK inhibition with dabrafenib and trametinib, with a complete response evident in the intrathoracic disease after two cycles of treatment; the solitary brain metastasis was unchanged. In April 2017 she progressed substantially in the lungs, pleura and mediastinal lymph nodes, with the brain lesion remaining stable. One salvage cycle of ipilimumab and nivolumab was given, but she died three weeks later.

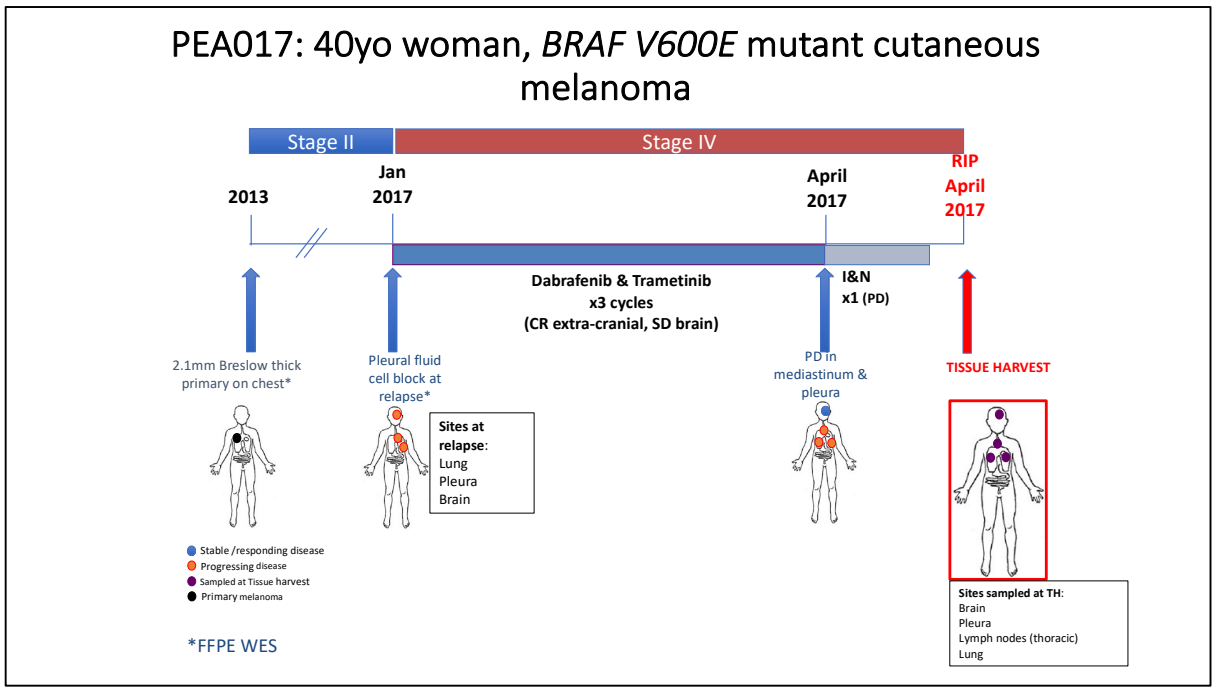

Figure 34 Timeline of clinical events and treatment in PEA017
Best overall RECIST response is included in brackets for each line of treatment (CR: complete response; PR: partial response; SD: stable disease; PD: progressive disease). I&N: ipilimumab and nivolumab; FFPE WES: formalin-fixed paraffin-embedded tissue underwent whole exome sequencing.

Tissue harvest (TH) sampling and quality control considerations

Forty-one tumour samples from 18 metastases involving the brain, mediastinal and paraaortic lymph nodes, pleura and diaphragm were taken at the TH. All samples had viable tumour, as evidenced by the presence of a *BRAF V600E* mutation on Sanger sequencing. Ten sites from

the tissue harvest encompassing the range of metastatic sites were selected for WES. Two primary tumour regions from archival FFPE tissue, as well as DNA purified from the pleural fluid cell block obtained at relapse (also archival FFPE) were also submitted for WES. All samples were successfully profiled.

Genomic features

The tumour mutational burden in this case is 188 nsSNVs or 9.5 mutations/Mb. The clonal TMB proportion is 56% (see Table 12 in **Section 3.3.1**). The clonal mutations (Cluster 1; Figure 35) were characterised by a dominant UV-light signature (Signature 7). Cluster 2, which was exclusive to the brain metastasis (BR_1_R1) also had a dominant UV-damage signature (Figure 35).

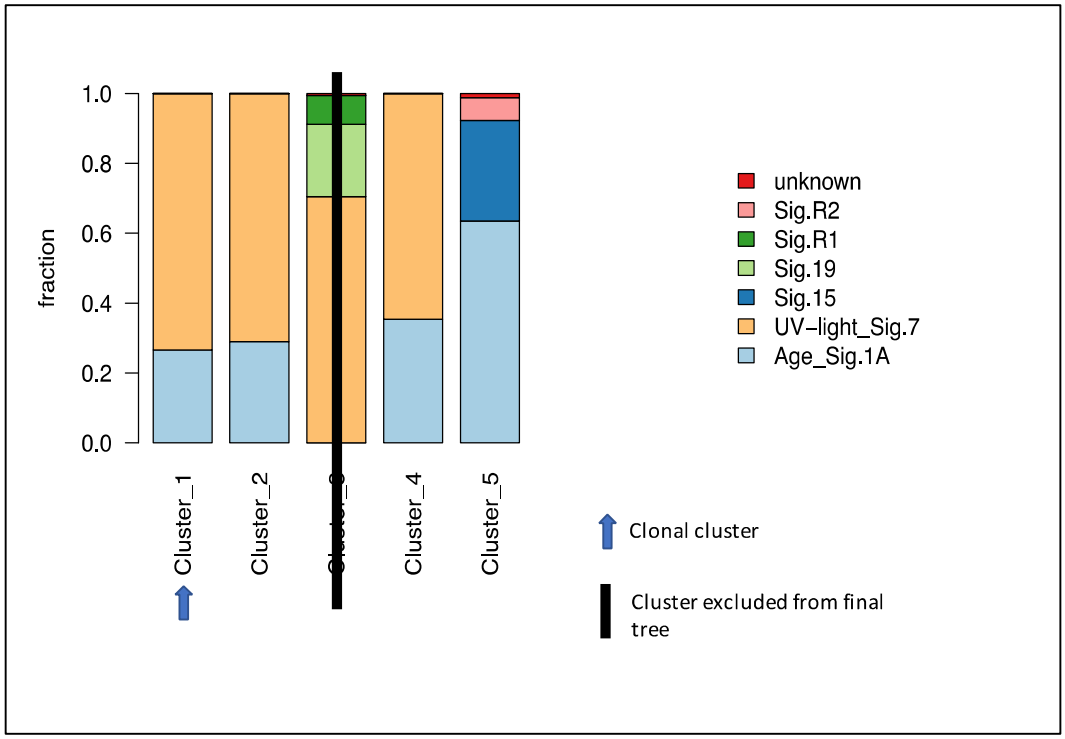

Figure 35 Mutational signature analysis for PEA017
Mutational signatures are based on Pyclone clustering of mutations for creation of phylogenetic trees, with the clonal cluster representing the ubiquitous mutations. Cluster 1 is the clonal cluster; Cluster 2 suitable for signature analysis (>50 SNVs), but Clusters 4 and 5 are not (<50 SNVs). Cluster 3 was excluded from the final phylogenetic tree.

Median computationally derived ploidy is 3.05 overall; however, there are two distinct sample groups: 1) those with a diploid status (the two primary tumour regions and the brain metastasis; median ploidy 2.1); and 2) those which were WGD (all other metastatic sites; median ploidy 3.38). In this case, the mode ploidy as determined by FISH is consistent with the bioinformatic ploidy estimate – a mode of 2 in the primary tumour regions (TB54 =

PR_1_R1, TB55 = PR_1_R2), but mode of 3 in the mediastinal lymph node region (LN_2_R1; Figure 36).

The median WGII is 0.44. The majority of samples have a WGII score >0.40, except for the brain and one primary region (PR_1_R1) where the score was <0.20 (Table 13 in **Section 3.3.3**).

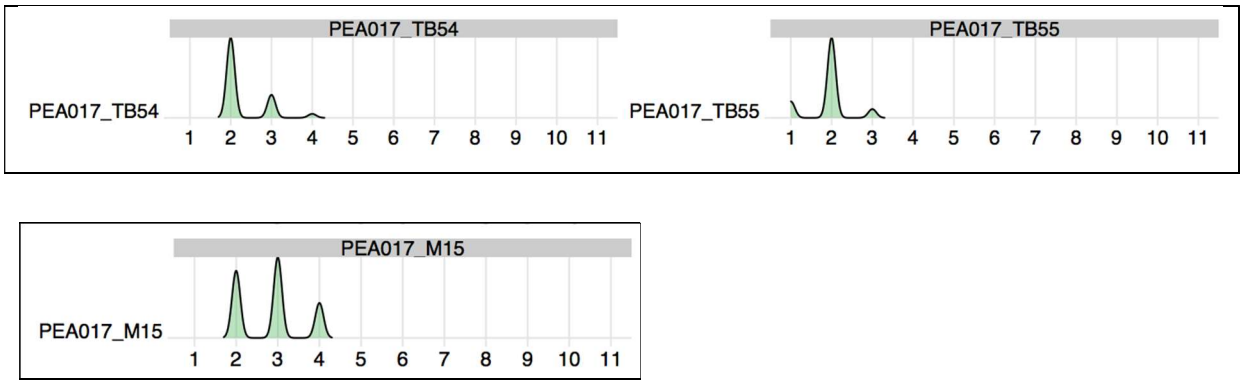

Figure 36 Corrected ploidy estimates of PEA017 samples analysed by FISH
*The x axis denotes the total probe count for each chromosome (see **Section 3.3.3**) and the y axis denotes the relative frequency.*
NB: TB54 = PR_1_R1, TB55 = PR_1_R2, M15 = LN_2_R1.

Driver alterations

The key oncogenic driver in PEA017 is the clonal *BRAF V600E* mutation (Figure 37). Other clonal drivers include tumour suppressor genes. The *TET2* alteration was a stopgain mutation and *TET2* has been noted to be mutated in 13% melanomas.[1] It resides at 4q and copy number loss of this arm was noted at the majority of sites (Figure 38). The others (*LEF1* (4q25), *CSMD3* (8q23) and *CIITA* (16p13)) met driver mutation criteria, but are not frequently reported in melanoma. There was no corresponding copy number loss of 8q, and loss of 16p was noted at two sites only. No putative subclonal driver mutations were noted.

While there are numerous SCNAs in this case, the vast majority are subclonal (Figure 38, Figure 39 and Figure 40). 12p loss was the only clonal arm-length event (and is not a recognised driver event per TCGA; Figure 38). At the cytoband level[2] there is a clonal gain of 8q24 and clonal losses in 9p21, 9p23 and 16q24 (Figure 39), all of these being putative driver SCNAs. Clonal copy number loss is noted at the *JAK2* locus (Figure 40).

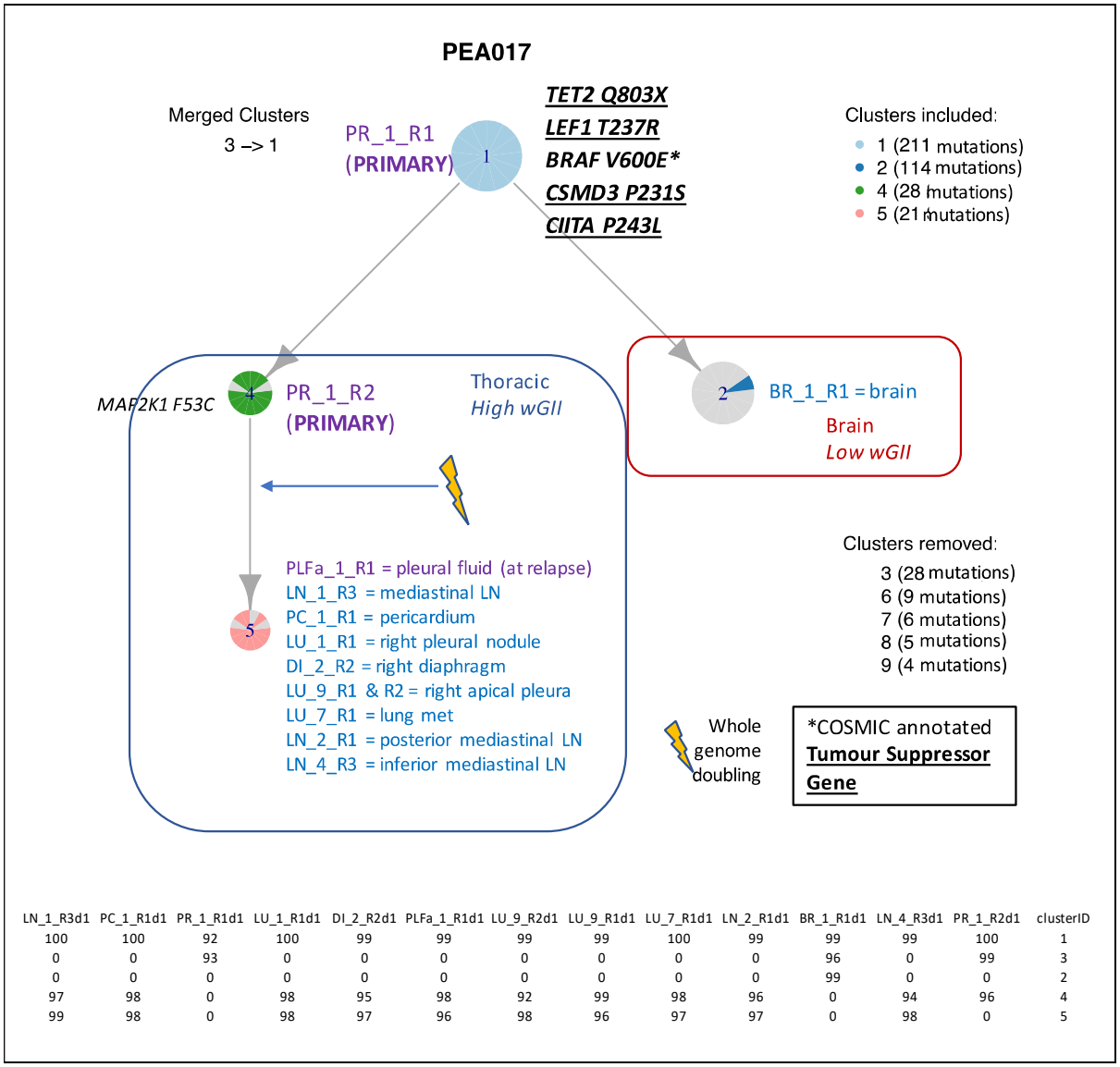

LN_1_R3d1	PC_1_R1d1	PR_1_R1d1	LU_1_R1d1	DI_2_R2d1	PLFa_1_R1d1	LU_9_R2d1	LU_9_R1d1	LU_7_R1d1	LN_2_R1d1	BR_1_R1d1	LN_4_R3d1	PR_1_R2d1	clusterID
100	100	92	100	99	99	99	99	100	99	99	99	100	1
0	0	93	0	0	0	0	0	0	0	96	0	99	3
0	0	0	0	0	0	0	0	0	0	99	0	0	2
97	98	0	98	95	98	92	99	98	96	0	94	96	4
99	98	0	98	97	96	98	96	97	97	0	98	0	5

Figure 37 Phylogenetic tree for PEA017
The clonal cluster of shared mutations (Cluster 1) sits at the trunk of the tree. Driver mutations belonging to each cluster are annotated. The CCFs for each cluster are shown in the table below. LN = lymph node; PC = pericardium; Lung = lung; DI = diaphragm; BR = brain
.

Evolution and metastatic seeding patterns

The phylogenetic tree for PEA017 is shown in Figure 37. In this case, two regions from the primary tumour were sampled, with two clones evident: one harbouring Cluster 1 only, and the other harbouring Clusters 1 and 4. Overall, the seeding pattern appears polyclonal, with the brain and intra-thoracic sites each seeded by a different clone from the primary tumour. The thoracic metastases (indicated by the blue square outline in Figure 37) are likely seeded from a clone in Region 2 of the primary tumour (PR_1_R2) because they share Clusters 1 and 4. This subclone appears to have further evolved outside the primary tumour, acquiring additional mutations (Cluster 5) and undergoing WGD. The brain metastasis (BR_1_R1), however, appears more closely related to Region 1 of the primary (PR_1_R1), and is on a

separate branch of the tree to the thoracic metastases. It also shares a similar SCNA profile with PR_1_R1, reinforcing a common origin. WGD is not noted in either of these regions.

Interestingly, both clusters contained in the clone seeding the brain metastasis (Clusters 1 and 2) show evidence of a UV-induced mutation profile. Cluster 2 also contains a large number of mutations (114 SNVs) relative to the other non-clonal clusters. These factors suggest that Cluster 2 may have originated in the primary tumour, but has not been detected within the limits of sampling. In addition to their genomic divergence, the clinical behaviour of the brain and intrathoracic metastases is distinct – the brain site was relatively quiescent in contrast to the fulminant intrathoracic progression.

All metastases appear monoclonal in their composition. In the case of the intrathoracic disease, metastasis-to-metastasis seeding may have occurred based on the widespread volume of disease in a close anatomical range.

Despite the similarity in the thoracic metastases on the basis of the clustering analysis, there was still evidence of intermetastatic heterogeneity in SCNA profiles, suggestive of ongoing CIN facilitated by WGD. In particular, lung metastasis 7 (LU_7_R1) and the pericardial metastasis (PC_1_R1) appear similar in that they are characterised by arm- and cytoband-level losses, rather than gains (Figure 38 and Figure 39), distinct from the other thoracic sites.

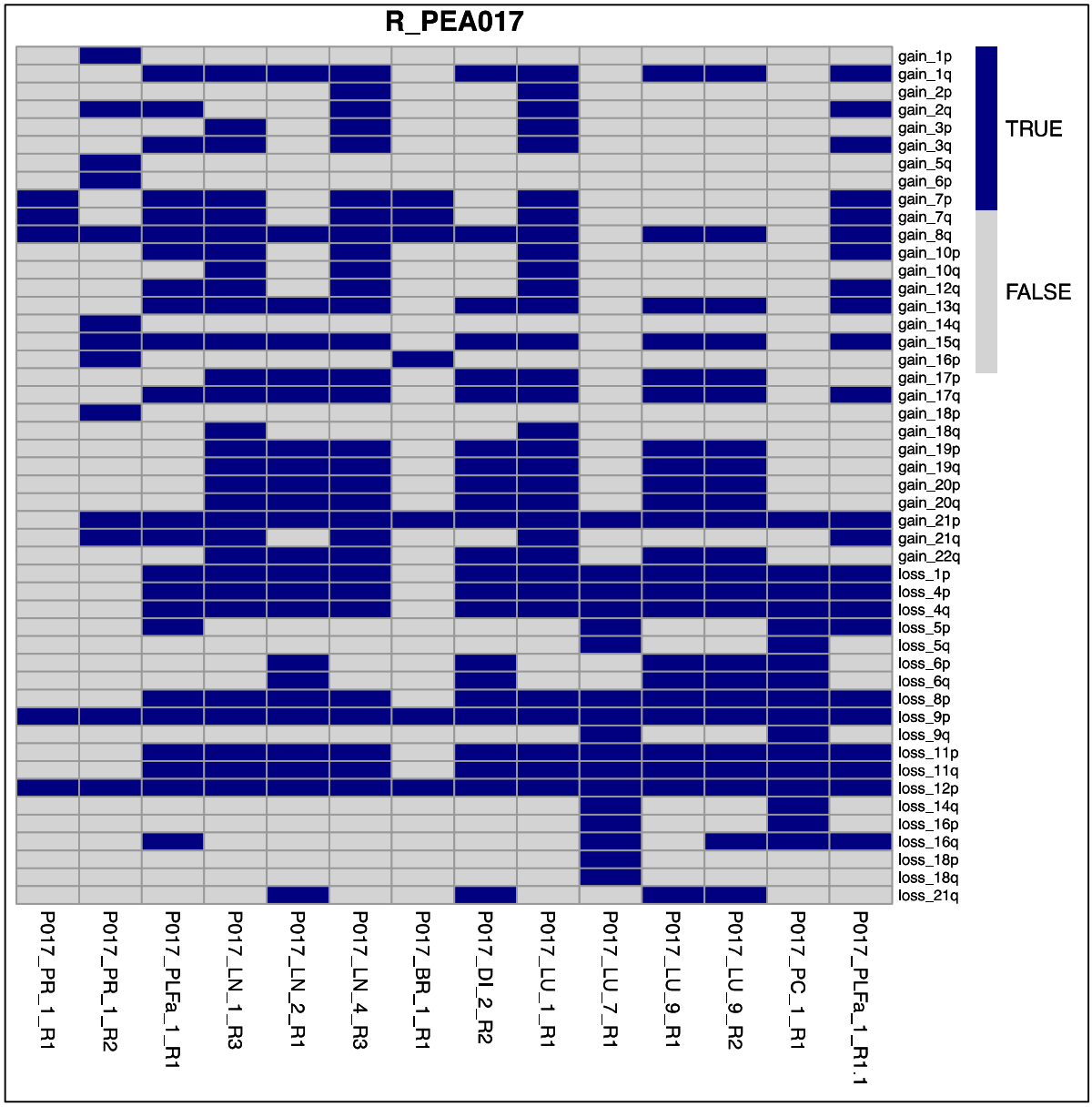

Figure 38 Chromosomal arm-level losses and gains
Blue squares indicate whether there was loss or gain of at least one copy of the chromosome arm relative to the mean ploidy of all samples.

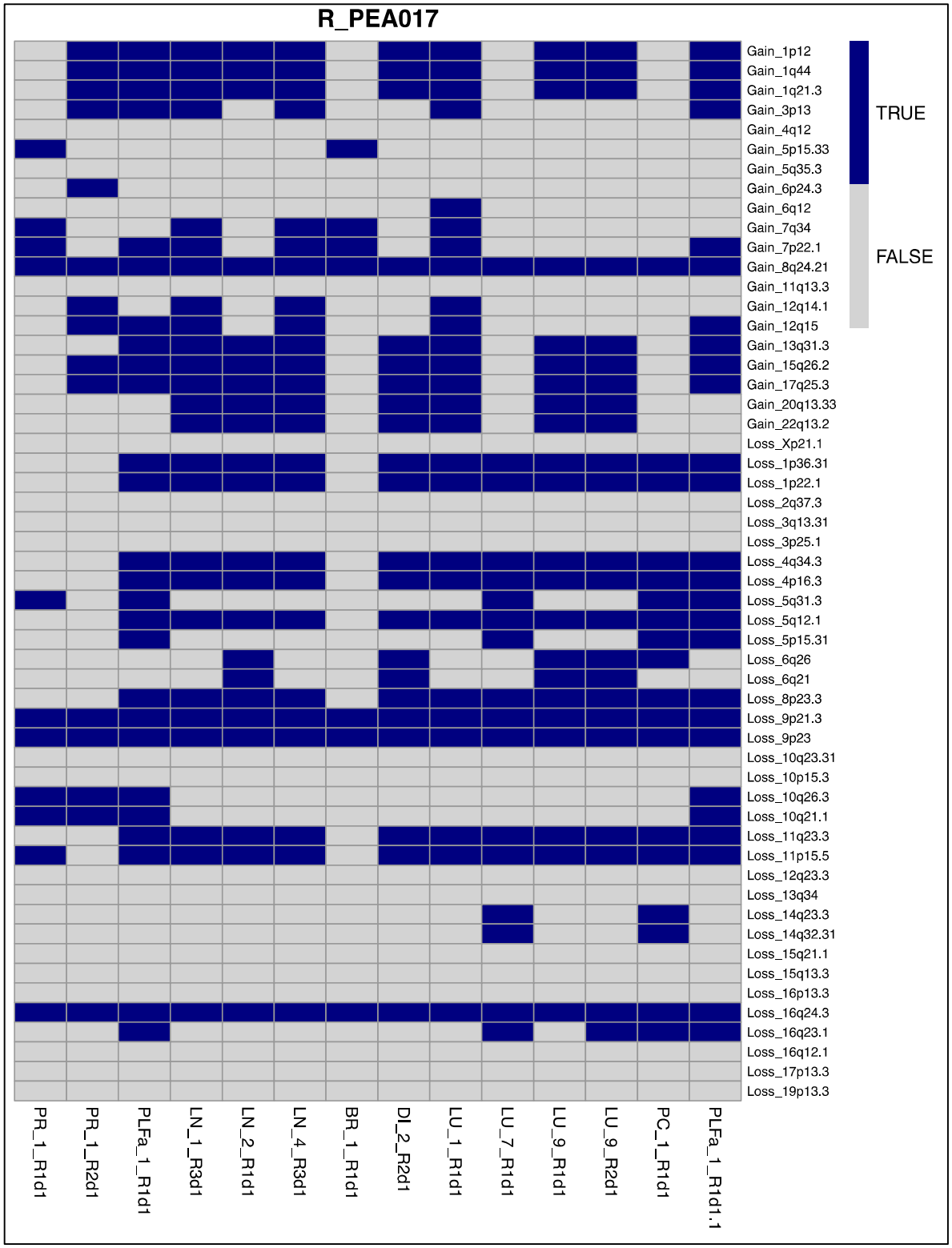

Figure 39 Cutaneous melanoma driver cytoband gains and losses
Annotated cytobands are melanoma driver regions determined by a GISTIC analysis of TCGA data.[2] Blue squares indicate whether there was loss or gain of at least one copy of the cytoband relative to the mean ploidy of all samples.

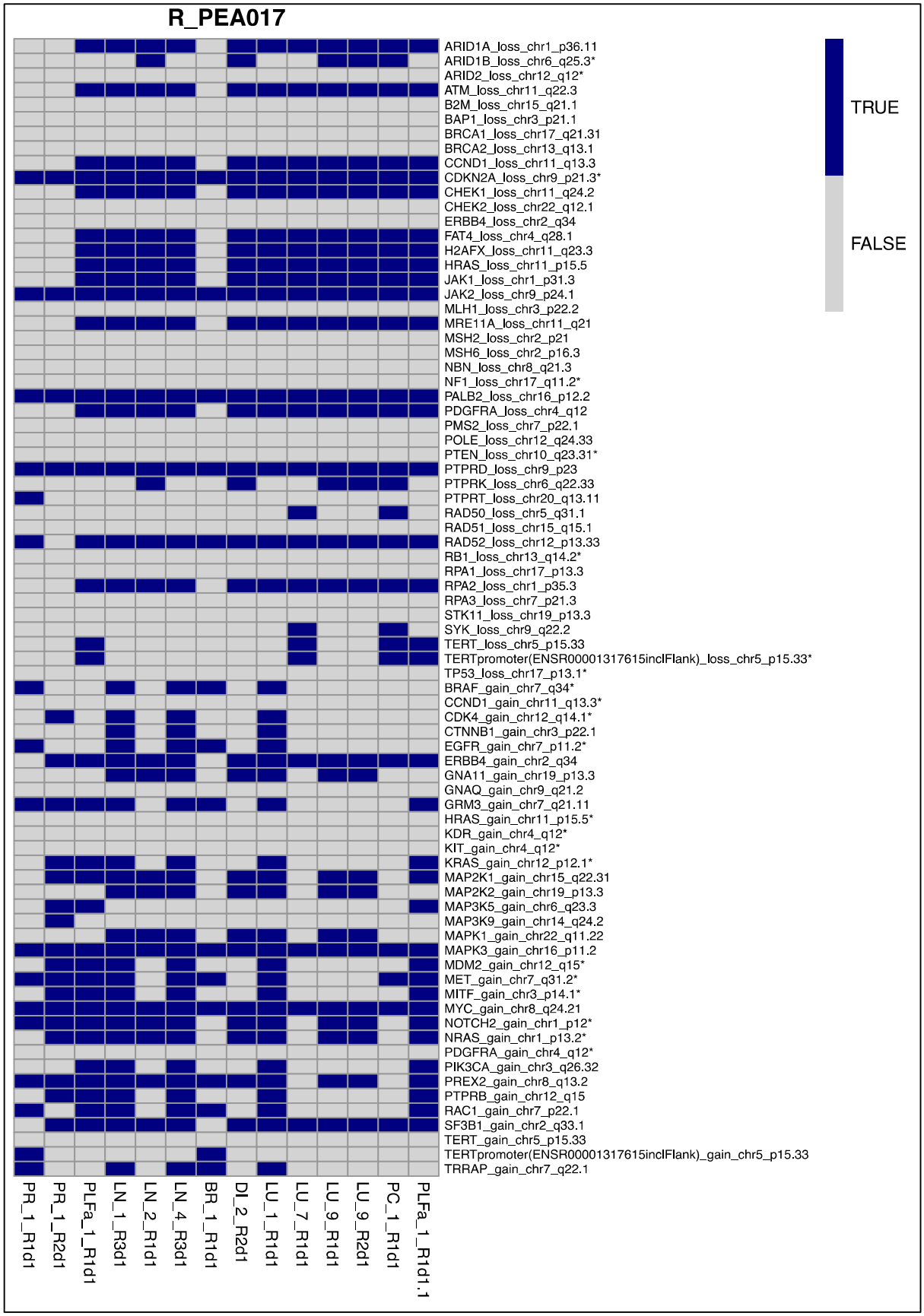

Figure 40 Driver gene gains and losses

Genes with an asterisk (*) are noted driver genes in the TCGA and Hayward data sets.[1,2] Blue squares indicate whether there was loss or gain of at least one copy of the gene relative to the mean ploidy of all samples.

Genomic mechanisms of treatment resistance

In this case, treatment resistance to dabrafenib and trametinib emerged early after an initial complete response in the intrathoracic disease and stability of the solitary brain lesion. *MAP2K1* mutations have been reported to mediate resistance to BRAF/MEK targeted therapy.[3] Although this specific variant (*p.F53C*) has not previously been described in the literature, it is located in the negative regulatory domain,[4] and is present in the intrathoracic metastases which progressed on dabrafenib and trametinib. Its presence in the pre-treatment pleural fluid sample, however, at comparable CCFs to the metastases, make it less likely to be an acquired phenomenon to account for the rapid progression on dabrafenib and trametinib after near-complete response.

In PEA017 clonal copy number loss of JAK2 is evident, with concurrent JAK1 copy number loss in the thoracic metastases. There are no corresponding mutations, however, in either gene, suggesting the other alleles are intact. Janus kinase 1 (JAK1) and Janus kinase 2 (JAK2) are proteins involved in the interferon gamma (IFN-γ) pathway, responsible for local immune infiltration (see **Section 1.2.9 Immune checkpoint inhibitors** in the **Main Introduction**). Both JAK1 and JAK2 are predicted to be susceptible to haploinsufficiency according to the DECIPHER tool.[5] JAK1 has a HI index of 14% (where genes ranked 0–10% are most likely to demonstrate haploinsufficiency (HI) and those ranked 90–100% are least likely). JAK2 appears more susceptible to haploinsufficiency with a HI index of 0.84%. Whether dual haploinsufficiency of these pathways could have contributed to treatment resistance is possible, but remains speculative. IHC and functional analyses would be required to demonstrate this.

Given the different behaviour of the WGD intrathoracic disease relative to the brain in response to treatment, WGD appears to have favoured tumour growth and treatment resistance.

Case summary

The case of PEA017 reveals how distinct genomic features can underpin different clinical behaviour. While the two sampled primary tumour regions both appeared diploid, Region 2 had more SCNAs and a higher WGII than Region 1 (0.44 versus 0.16), suggestive of CIN. It is likely that a clone from this region then underwent WGD and developed metastatic competence before seeding intrathoracic sites (that is, evolving in parallel), with CIN as the

driving force behind metastatic progression in the thorax, but not in the brain. As the treatment-naive pleural fluid sample also shares this WGD profile, it was not acquired under the selective pressure of treatment.

The key genomic driver in this case is the *BRAF V600E* mutation. Despite treatment with dual BRAF/MEK inhibition and an initial intrathoracic complete response, the duration of response was only two months, inferior to the median of 11 months reported in the COMBI-V trial.[6] The mechanism of resistance is not clear from this analysis, and may include upregulation of MAPK pathway signalling through mechanisms such as CRAF upregulation,[7] COT overexpression,[8] as well as variant splicing and dimerisation of BRAF[9] which could be revealed through transcriptomic profiling.

References for PEA017

1. Hayward NK, Wilmott JS, Waddell N, et al. Whole-genome landscapes of major melanoma subtypes. *Nature* 545: 175–180, 2017.
2. Cancer Genome Atlas N: Genomic Classification of Cutaneous Melanoma. *Cell* 161: 1681–96, 2015.
3. Long GV, Fung C, Menzies AM, et al. Increased MAPK reactivation in early resistance to dabrafenib/trametinib combination therapy of BRAF-mutant metastatic melanoma. *Nat Commun* 5: 5694, 2014.
4. Kang H, Jha S, Deng Z, et al. Somatic activating mutations in MAP2K1 cause melorheostosis. *Nat Commun* 9: 1390, 2018.
5. Firth HV, Richards SM, Bevan AP, et al. DECIPHER: Database of Chromosomal Imbalance and Phenotype in Humans Using Ensembl Resources. *Am J Hum Genet* 84: 524–33, 2009.
6. Robert C, Karaszewska B, Schachter J, et al. Two year estimate of overall survival in COMBI-v, a randomized, open-label, phase III study comparing the combination of dabrafenib (D) and trametinib (T) with vemurafenib (Vem) as first-line therapy in patients (pts) with unresectable or metastatic BRAF V600E/K mutation-positive cutaneous melanoma, European Cancer Congress (ECC). Vienna, *European Journal Cancer* (Supp 3), 2015.
7. Montagut C, Sharma SV, Shioda T, et al. Elevated CRAF as a potential mechanism of acquired resistance to BRAF inhibition in melanoma. *Cancer Res* 68: 4853–61, 2008
8. Johannessen CM, Boehm JS, Kim SY, et al. COT drives resistance to RAF inhibition through MAP kinase pathway reactivation. *Nature* 468: 968–72, 2010.
9. Poulikakos PI, Persaud Y, Janakiraman M, et al. RAF inhibitor resistance is mediated by dimerisation of aberrantly spliced BRAF(V600E). *Nature* 480: 387–90, 2011.

Case study 3: PEA023

Clinical summary

Patient PEA023 was a 74 year old man diagnosed with a primary acral melanoma of the heel (Breslow thickness 3.3 mm, ulcerated) in 2014, found to harbour an exon 13 *KIT V654A* mutation on routine molecular profiling. In February 2016, he relapsed with lung metastases and was commenced on pembrolizumab. He progressed by RECIST criteria with increasing size of one of the lung nodules and received stereotactic body radiotherapy (SBRT) to this site in September 2016. The pembrolizumab was stopped due to presumed immune-related hepatitis in October 2016 and he underwent imaging surveillance, with stable disease off treatment. Upon further progressive disease in May 2017, PEA023 was enrolled on a clinical trial of a novel KIT inhibitor, but he progressed soon after in the brain, requiring stereotactic radiosurgery (SRS) to a solitary brain metastasis, and had RECIST-defined extra-cranial progression after three cycles. Imatinib (another KIT inhibitor) was initiated in August 2017 but again he progressed after three cycles. He died in January 2018. Figure 41 summarises the clinical course of PEA023

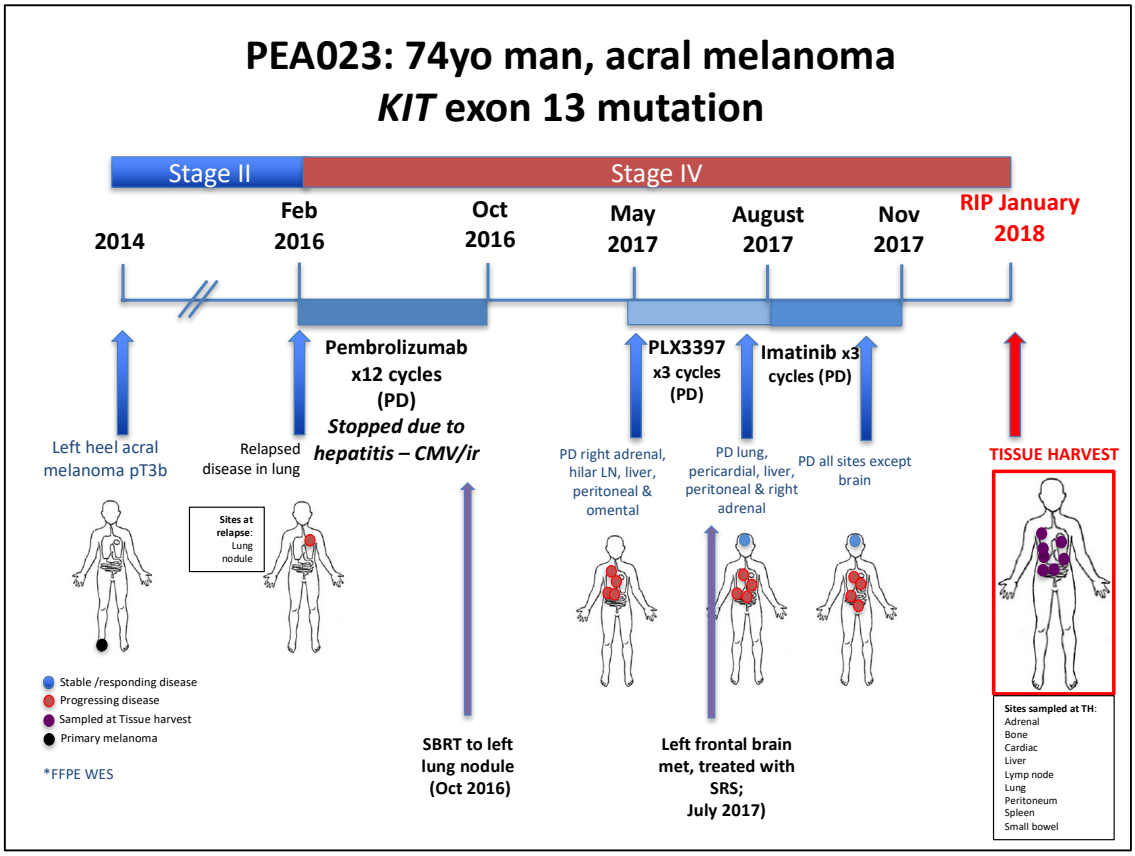

Figure 41 Timeline of clinical events, treatment and disease response in PEA023
Best overall RECIST response is included in brackets for each line of treatment (CR: complete response; PR: partial response; SD: stable disease; PD: progressive disease). CMV: cytomegalovirus; ir: immune-related; LN: lymph node; SBRT: stereotactic body radiotherapy; SRS: stereotactic radiosurgery.

Tissue harvest (TH) sampling and quality control considerations

Thirty-five tumour samples were taken at the TH from 34 individual metastases involving intra-abdominal sites such as the liver, spleen, pancreas, adrenal gland, peritoneum and mesentery, as well as the lung, mediastinal lymph nodes, pericardium and diaphragm. No brain metastases were evident at the TH. Of these 35 samples, 33 were sequenced by the Sanger method and 31/33 were shown to have the *KIT V654A* mutation (with amplification of the variant evident on Sanger traces), consistent with presence of tumour cells. Ten samples were submitted for WES, covering the spectrum of sampled metastatic sites. Of these 10, one sample failed due to poor purity. Although purity on Sanger sequencing appeared adequate for this sample, on paired H&E review the tumour content was <25%.

Genomic features

There is a relatively low tumour mutation burden (23 nsSNV, 1.0 mutations/Mb; (see Table 12 in **Section 3.3.1**) in this case, compared to the median for acral tumours (2.1 mutations/Mb).[1] The majority of mutations are clonal (89%). The dominant mutation

signature is age-related (Signature 1A; Figure 42). Both the low TMB and age-related signature are features consistent with the acral subtype.

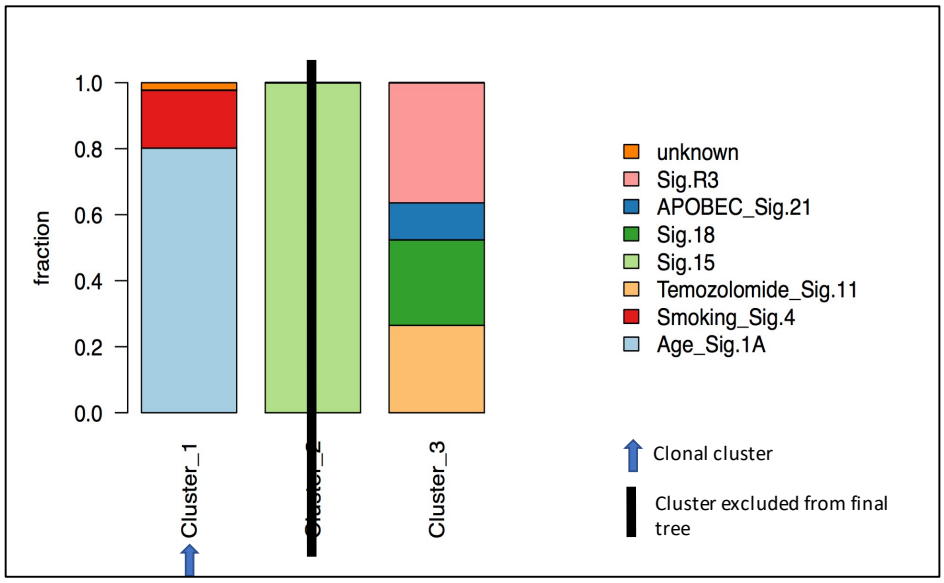

Figure 42 Mutational signature analysis of PEA023
Mutational signatures are based on Pyclone clustering of mutations for creation of phylogenetic trees, with the clonal cluster representing the ubiquitous mutations. Cluster 1 is the clonal cluster and the only one with sufficient SNVs for reliable signature analysis.

The median computationally derived ploidy in this case is 5.3 (see Table 13 in **Section 3.3.3**). This was consistent with two rounds of WGD, including in the primary tumour regions. The samples that underwent FISH analysis demonstrate a wide range of (aneu)ploidy (2N to 10N), suggestive of cell-to-cell heterogeneity in ploidy (see Figure 43). The median WGII is 0.61 (see Table 13 in **Section 3.3.3**), the third-highest overall in this cohort.

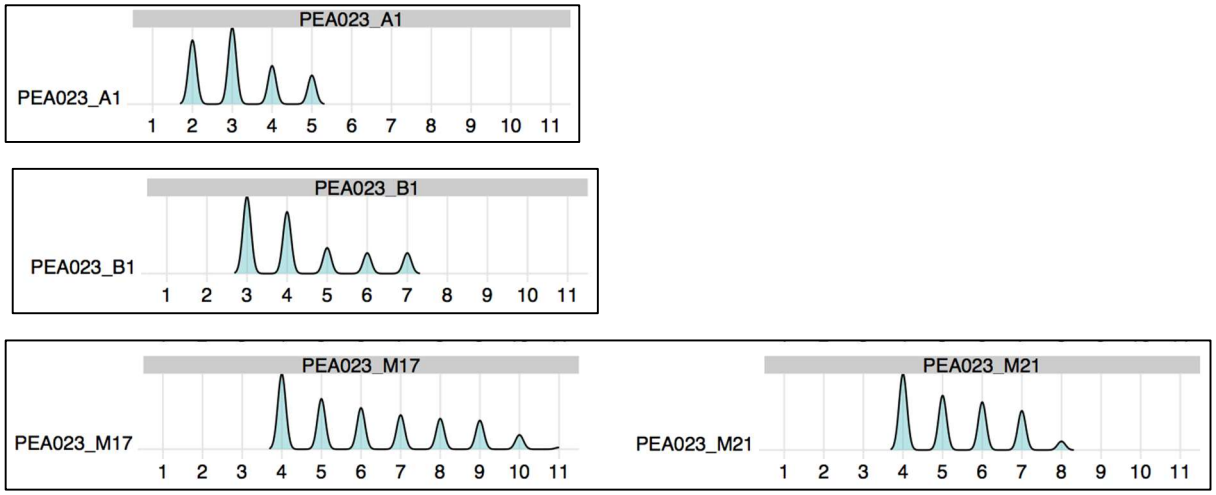

Figure 43 Corrected ploidy estimates of PEA023 samples analysed by FISH
*The x axis denotes the total probe count for each chromosome (see **Section 3.3.3**) and the y axis denotes the relative frequency.*
NB: A1 = PR_1_R1; B1= PR_1_R2; M17 = LI_3_R1; M21 = LN_1_R1.

Driver alterations

The *KIT p.V654A* exon 13 driver mutation is clonal in all samples (Figure 44). *V654A* is an uncommon but previously reported *KIT* mutation in melanoma.[2] It lies in the tyrosine kinase 1 domain of the gene.[3]

There are numerous somatic copy number aberrations (SCNA) in this case (Figure 45, Figure 46 and Figure 47), reflected in the relatively high WGII. Clonal gains of chromosome 7, 6p and 20q and clonal loss of chromosome 10, 6q, 9p and 11q (Figure 45) are seen, consistent with previously reported common acral SCNAs.[1,4] Other clonal chromosome arm-level gains (1q, 6p, 20p and 22q) and losses (6q, 9p, 11q, 14q and 17p) reported as cutaneous melanoma driver events[5] are evident (Figure 45). In addition, amplification of cytobands at 4q12 (harbouring *KIT*) as well as 11q13[1,4] are clonal (Figure 46). While the SCNA profile is largely shared across the metastases, there is evidence of heterogeneity within the primary tumour (Figure 45, Figure 46 and Figure 47)). For example, Region 1 of the primary tumour (PR_1_R1) has more arm-level losses and Region 2 has more arm-level gains.

Evolution and metastatic seeding patterns

The phylogenetic tree for PEA023 is shown in Figure 44. There were three regions from the primary tumour sampled in this case, with no heterogeneity demonstrated in mutations. The seeding pattern appears monoclonal, with a single clone comprised of Clusters 1+3 evident at all sites. Cluster 3 is subclonal in the primary regions (CCFs 11–36%) but appears clonal in

metastases, making this the likely subclone from the primary tumour that has seeded all metastatic sites.

The SCNA profiles of the three primary tumour regions appear distinct from each other, suggesting a degree of ITH not reflected in the clustering analysis which is mutation-based. By contrast, there is very little copy number heterogeneity across metastatic sites. Given the differences in the primary tumour region and metastatic copy number profiles, it is possible that the exact metastasis-seeding clone from the primary tumour may not have been sampled, or that further SCNAs were acquired after the clone left the primary tumour, prior to metastatic seeding.

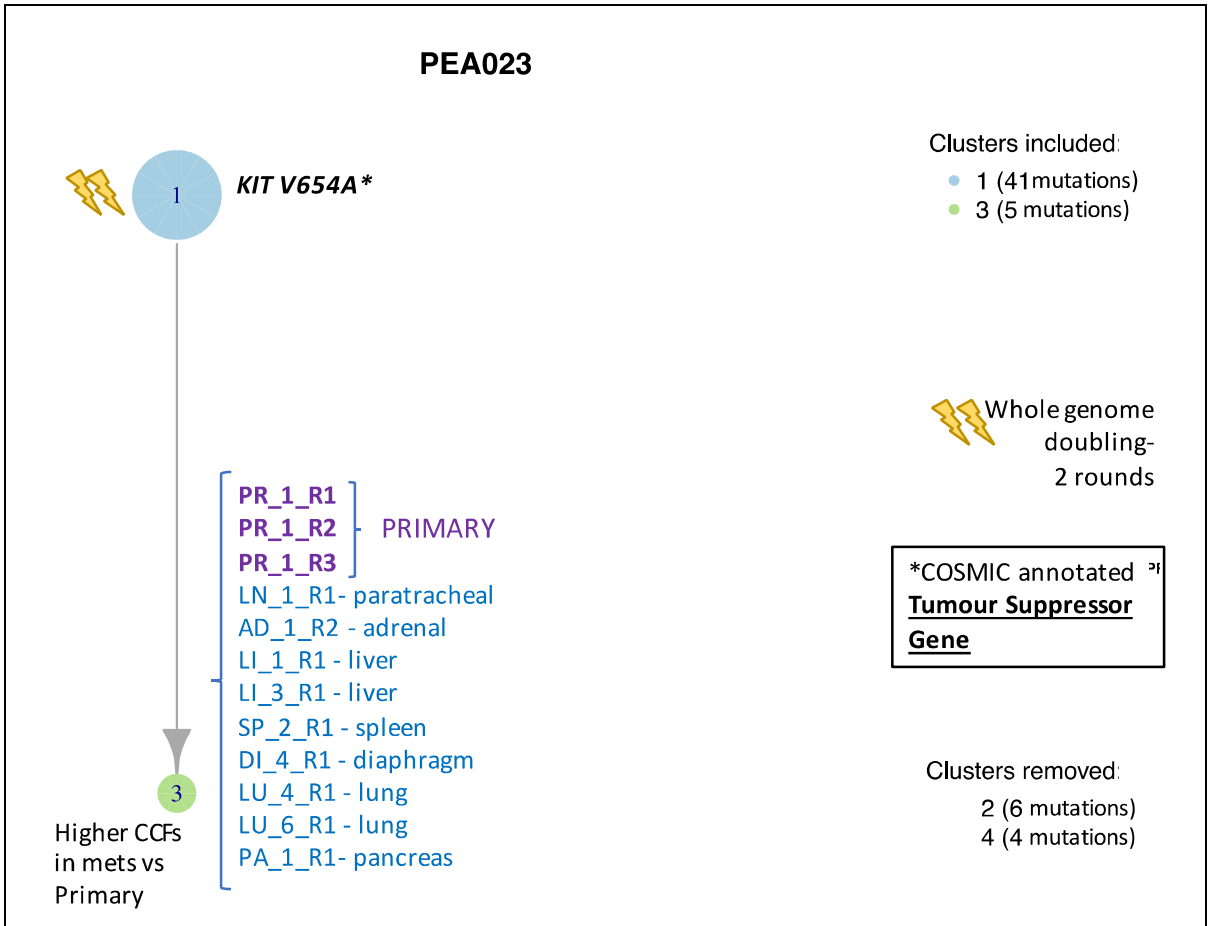

PR_1_R1d1	PR_1_R2d1	PR_1_R3d1	LN_1_R1d1	AD_1_R2d1	LI_1_R1d1	LI_3_R1d1	SP_2_R1d1	DI_4_R1d1	LU_4_R1d1	LU_6_R1d1	PA_1_R1d1	clusterID
96	96	97	97	96	97	96	98	95	95	96	95	1
0	0	0	0	0	0	0	0	0	0	0	0	2
36	33	11	83	88	89	86	86	84	83	84	91	3

Figure 44 Phylogenetic tree for PEA023
The clonal cluster of shared mutations sits at the trunk of the tree (Cluster 1). Driver mutations belonging to each cluster are annotated.
The cancer cell fraction (CCF) of each cluster per metastatic site is detailed in the table beneath the tree. LN = lymph node; AD = adrenal; LI = liver; SP = spleen; DI = diaphragm; LU = lung; PA = pancreas.

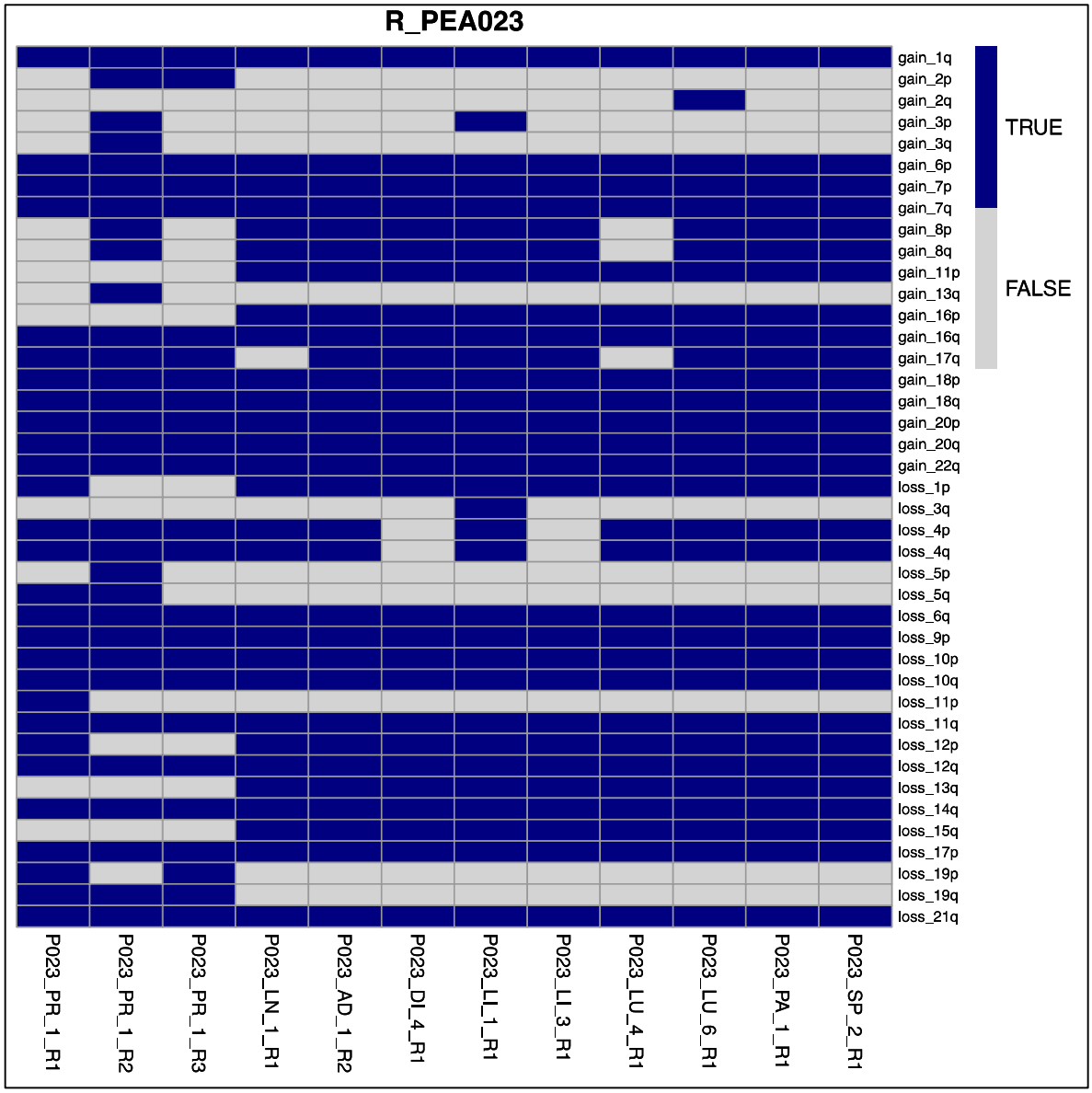

Figure 45 Chromosomal arm-level losses and gains
Blue squares indicate whether there was loss or gain of at least one copy of the chromosome arm relative to the mean ploidy of all samples.

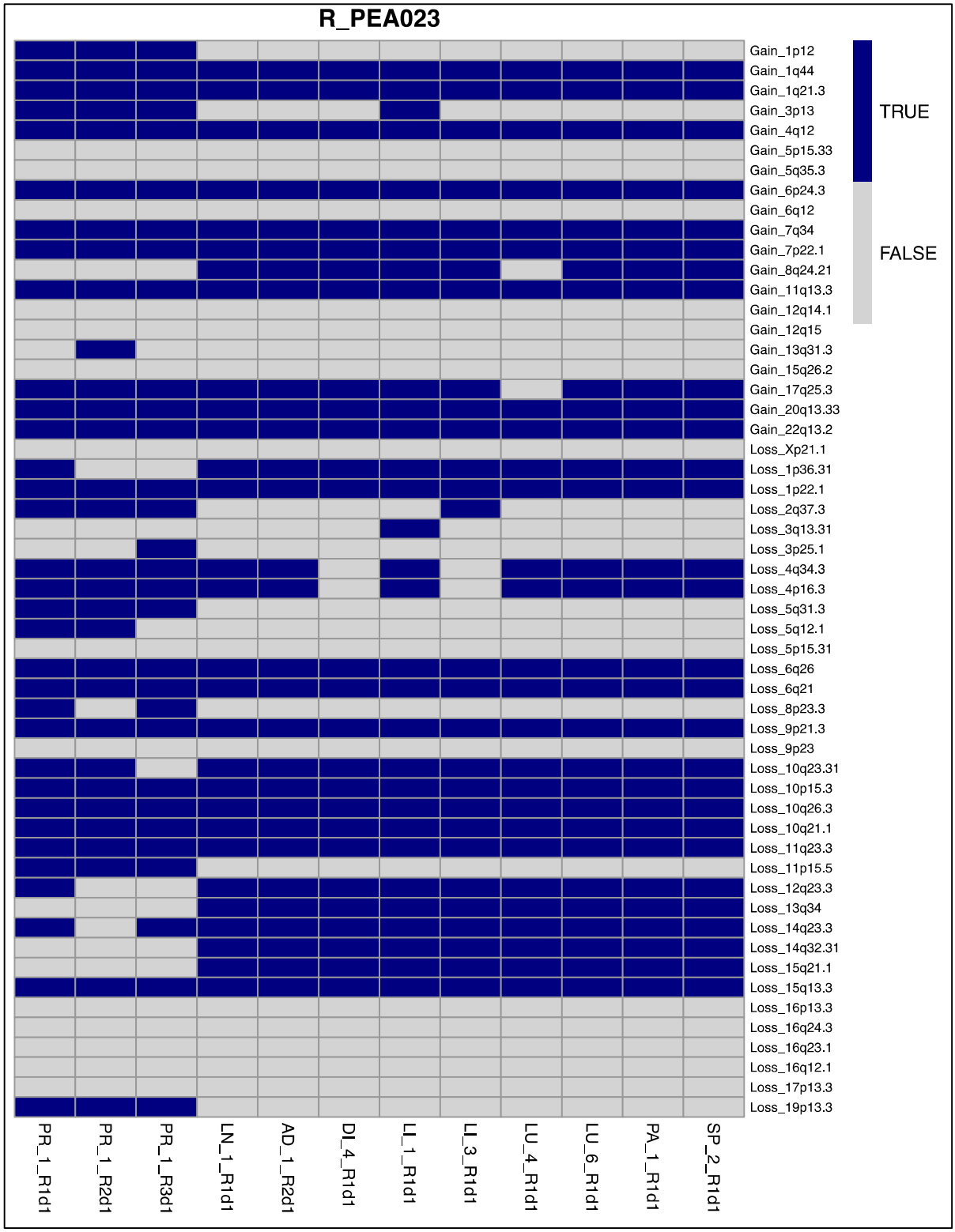

Figure 46 Cutaneous melanoma driver cytoband gains and losses
Annotated cytobands are melanoma driver regions determined by a GISTIC analysis of TCGA data.[5] Blue squares indicate whether there was loss or gain of at least one copy of the cytoband relative to the mean ploidy of all samples.

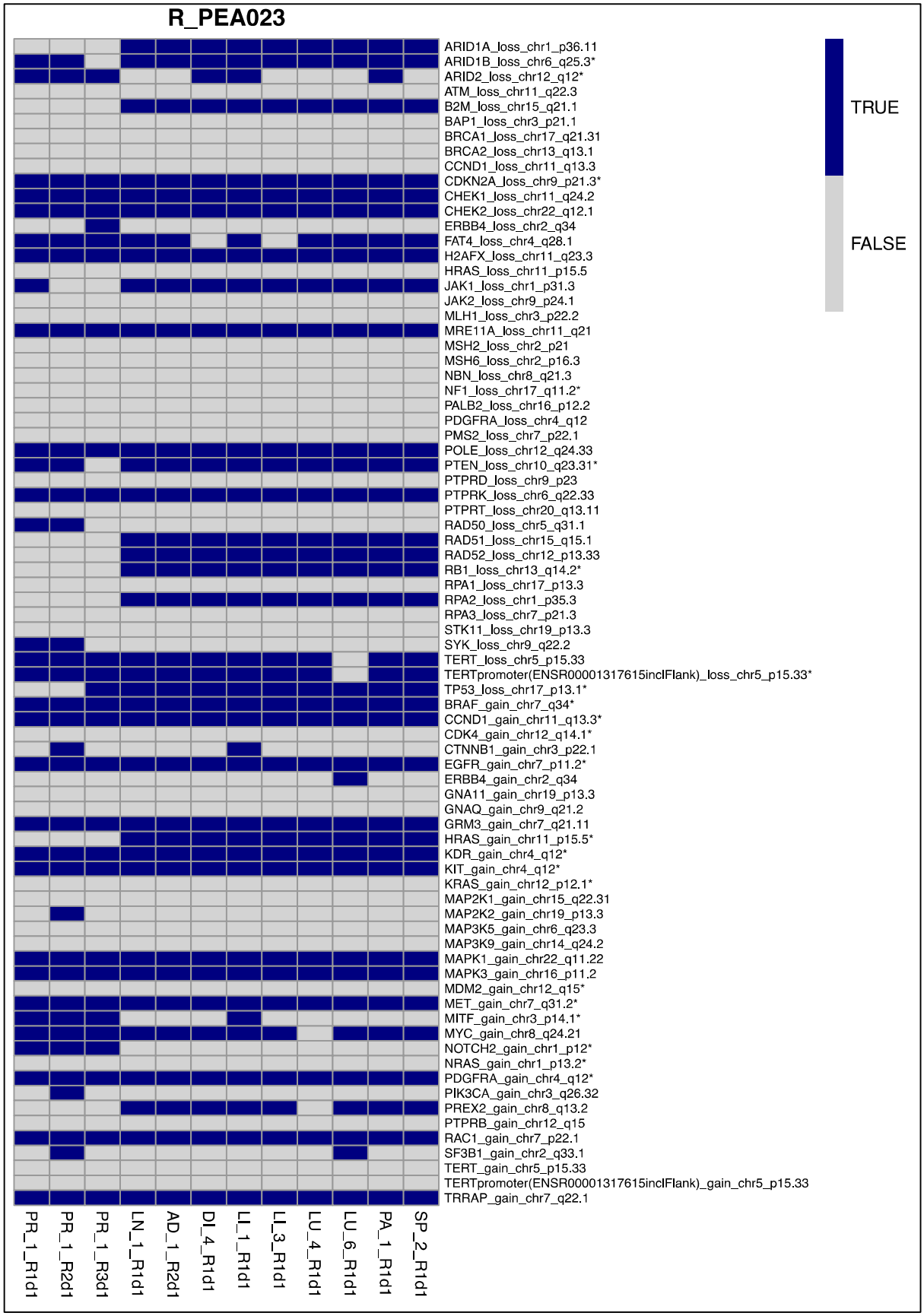

Figure 47 Driver gene gains and losses

Genes with an asterisk (*) are noted driver genes in the TCGA and Hayward data sets.[5,6] Blue squares indicate whether there was loss or gain of at least one copy of the gene relative to the mean ploidy of all samples.

Genomic mechanisms of treatment resistance

PEA023 received both pembrolizumab monotherapy and two different KIT inhibitors. There are no recognised mutations associated with ICI resistance in this case. There is clonal copy number loss of *JAK1*, as well as *B2M* in the metastases (not seen in the primary regions); however, in the absence of mutations in the other alleles, the significance of this is uncertain. According to the DECIPHER tool,[7] *B2M* is unlikely to exhibit haploinsufficiency; whereas *JAK1* might.

Aneuploidy itself has been postulated as a mechanism of immune evasion via induction of tolerance mechanisms to the cGAS-STING pathway (usually activated to destroy cells with excess cytosolic DNA).[8] In keeping with this aneuploidy has been reported to be associated with checkpoint inhibitor resistance in anti-CTLA4 treated cohorts,[9] but not in patients treated with anti-PD-1.[10]

The *KIT V654A* mutation is not a recurrent hotspot mutation in melanoma (as *KIT L576P* is noted to be),[2] and in this case *KIT* amplification was also present. No objective tumour responses were noted to two different KIT inhibitors. In one published case harbouring this same mutation there was no response to treatment with imatinib.[2] There is limited data on exon 13 mutations in gastrointestinal stromal tumours (GIST), another type of malignancy that is associated with *KIT* mutations, although responses to imatinib are noted.[3]

Case summary

The striking feature of the acral melanoma in patient PEA023 was the degree of overall aneuploidy, with two rounds of clonal WGD, potentially permissive for the extent of somatic driver copy number alterations noted. Because these features were also noted in the primary tumour, they may have resulted from a punctuated evolutionary event. In PEA023, SCNAs may be the primary drivers of growth and metastatic spread, rather than mutations. The range of ploidy values suggested by FISH also raises the possibility of cell-to-cell heterogeneity, consistent with CIN.

Although there was no ITH in the primary tumour at the level of mutations, due to the conservative method of only calling variants in FFPE samples that are present in the fresh frozen TH samples, the mutational ITH may be underestimated. There was, however,

evidence of somatic copy number ITH. The monoclonal nature of metastases and the lack of inter-metastatic heterogeneity suggest seeding by a dominant clone and are consistent with a more linear metastatic seeding mode due to the lack of genomic divergence.

Despite early progression in the lungs, PEA023 derived disease control for over 12 months at other sites from pembrolizumab monotherapy. The mechanism of eventual resistance is not evident from genomic analyses alone. No response was seen to two types of KIT inhibitors, which is not unexpected given the non-hotspot mutation.[2]

References for PEA023

1. Newell F, Wilmott JS, Johansson PA, et al. Whole-genome sequencing of acral melanoma reveals genomic complexity and diversity. *Nat Commun* 11: 5259, 2020
2. Carvajal RD, Antonescu CR, Wolchok JD, et al. KIT as a therapeutic target in metastatic melanoma. *JAMA* 305: 2327–34, 2011. *J Invest Dermatol*
3. Garrido MC, Bastian BC: KIT as a therapeutic target in melanoma. *J Invest Dermatol* 130: 20–7, 2010.
4. Curtin JA, Fridlyand J, Kageshita T, et al. Distinct sets of genetic alterations in melanoma. *N Engl J Med* 353: 2135–47, 2005.
5. Cancer Genome Atlas N: Genomic Classification of Cutaneous Melanoma. *Cell* 161: 1681–96, 2015.
6. Hayward NK, Wilmott JS, Waddell N, et al. Whole-genome landscapes of major melanoma subtypes. *Nature* 545: 175–180, 2017.
7. Firth HV, Richards SM, Bevan AP, et al. DECIPHER: Database of Chromosomal Imbalance and Phenotype in Humans Using Ensembl Resources. *Am J Hum Genet* 84: 524–33, 2009.
8. Bakhoum SF, Cantley LC: The Multifaceted Role of Chromosomal Instability in Cancer and Its Microenvironment. *Cell* 174: 1347–1360, 2018.
9. Davoli T, Uno H, Wooten EC, et al. Tumor aneuploidy correlates with markers of immune evasion and with reduced response to immunotherapy. *Science* 355, 2017.
10. Liu D, Schilling B, Liu D, et al. Integrative molecular and clinical modeling of clinical outcomes to PD1 blockade in patients with metastatic melanoma. *Nat Med* 25: 1916–1927, 2019.

Case study 4: PEA036

Clinical summary

Patient PEA036 was a 78 year old woman, first diagnosed with a primary cutaneous melanoma of the left lower limb (Breslow thickness 10 mm and ulcerated) in June 2016 (Figure 48). No sentinel lymph node biopsy was undertaken. A *BRAF K601E* mutation was noted on molecular profiling. In June 2017, metastatic disease was incidentally found in the lungs. In August 2017, due to evidence of progressive metastatic disease in the lungs, pleura and liver, single agent pembrolizumab was initiated. Symptomatic disease progression was noted in September 2017 (after two cycles of treatment), with imaging demonstrating extensive right-sided pleural disease, mediastinal lymphadenopathy and new liver metastases. Dabrafenib and trametinib were initiated but ceased after one cycle in the context of a diverticular abscess (unrelated to melanoma). Stable disease was noted on a CT scan in October. The patient died of complications of intra-abdominal infection in November 2017, five months after the diagnosis of Stage IV melanoma.

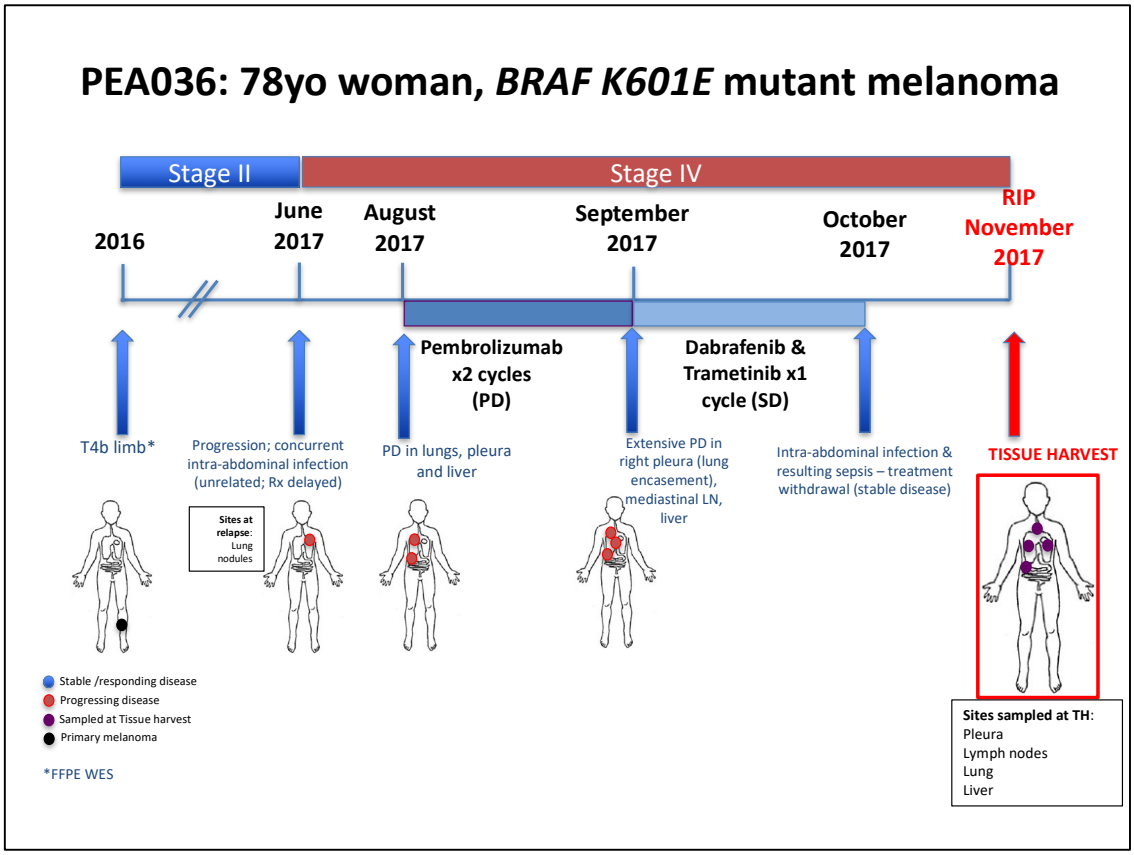

Figure 48 Timeline of clinical events, treatment and disease response in PEA036
Best overall RECIST response is included in brackets for each line of treatment (CR: complete response; PR: partial response; SD: stable disease; PD: progressive disease). FFPE: formalin fixed paraffin-embedded; WES: whole exome sequencing; LN: lymph node.

Tissue harvest (TH) sampling and quality control considerations

Seventy-five samples from 54 individual metastases encompassing liver, lung, lymph nodes and kidney were collected at the TH. Of these, 71/75 had evidence of a *BRAF K601E* mutation by Sanger sequencing. Ten of the 71 samples encompassing the range of metastatic sites sampled were submitted for WES, along with two regions of the archival primary melanoma, and all were successfully profiled.

Genomic features

A high tumour mutational burden is evident in this case, with 927 exonic nsSNVs (median 135 for cutaneous melanoma),[1] or 51.72 mutations per megabase (median 16.8mut/Mb for cutaneous melanoma;[2] Table 12 in **Section 3.3.1**). The clonal proportion of mutations is 95%. Consistent with the sun exposed origin of the primary melanoma, the dominant clonal mutational signature is that of UV-induced damage (Signature 7; Figure 49).

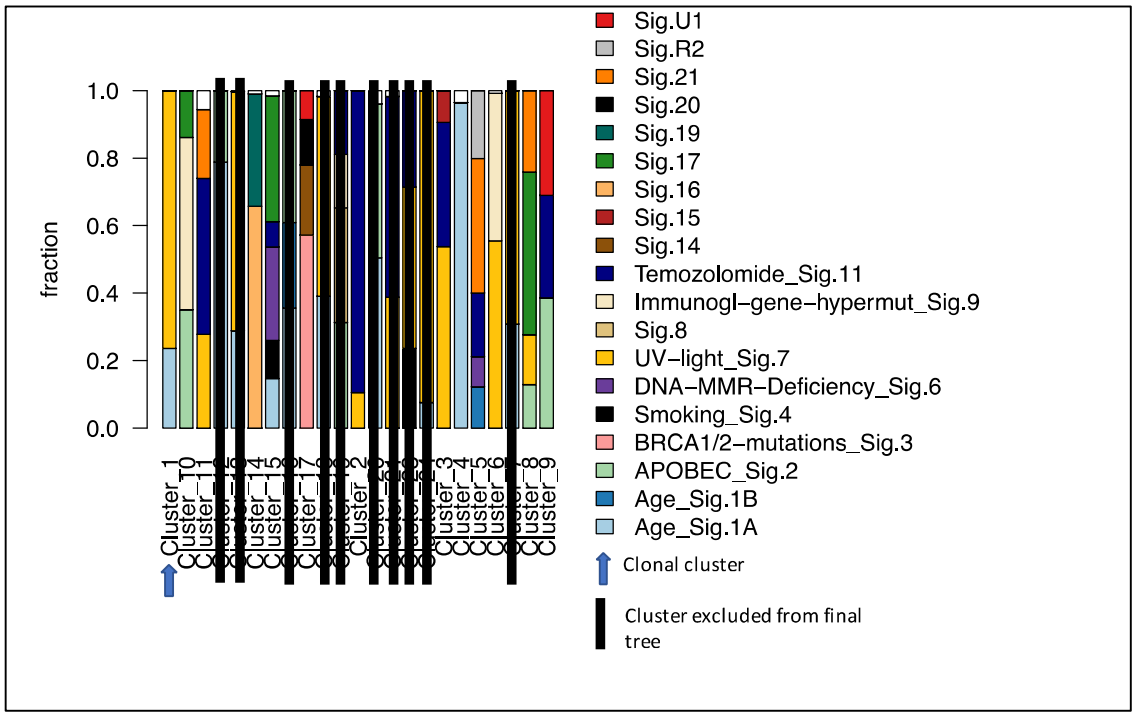

Figure 49 Mutational signature analysis of PEA036
Mutational signatures are based on Pyclone clustering of mutations for creation of phylogenetic trees, with the clonal cluster representing the ubiquitous mutations. Cluster 1 is the clonal cluster and is the only cluster with enough SNVs for reliable signature analysis; Clusters 2 and 3 were merged into Cluster 1; clusters were removed from the final tree.

There is evidence of whole genome doubling in all samples, including the primary tumour. Median computationally-derived ploidy in the primary tumour is 3.23, and in the metastases it is 3.10 (see Table 13 in **Section 3.3.3**). The two samples that underwent FISH analysis differed in their modal ploidy estimate (see Figure 50): the liver sample (LI_18_R1/M54) has a corrected modal ploidy of 2 (range of 2–3); whereas the peritoneal metastasis (PE_1_R1/M69) has a modal ploidy of 3 (range 2–4).

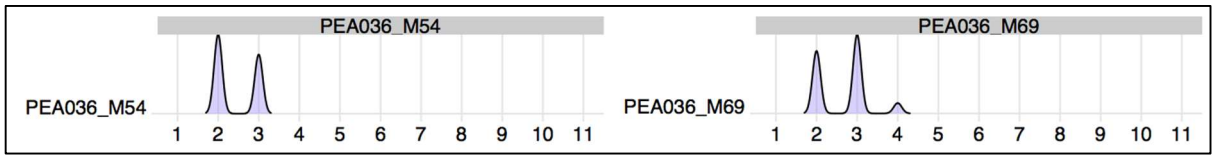

Figure 50 Corrected ploidy estimates of PEA036 samples analysed by FISH
*The x axis denotes the total probe count for each chromosome (see **Section 3.3.3**) and the y axis denotes the relative frequency.*
NB: M54 = LI_18_R1 (liver) and M69 = PE_1_R1 (peritoneum).

The median WGII is 0.52 in both primary tumour regions and metastases (see Table 13 in **Section 3.3.3**). This is above the median for cutaneous melanomas within our cohort (0.41 for primary tumours and 0.44 for TH metastases).

Driver alterations

There are 15 putative clonal driver mutations revealed by WES in this case (Figure 51), including two in oncogenic hotspots: *BRAF K601E* and *CTNNB1 p.S45F*. A clonal SNV in *TP53* was detected (p.G113D), with evidence of clonal somatic copy number loss at the *TP53* locus. Several other known melanoma tumour suppressor genes were mutated (*ARID1B, CREBBP, LRP1B, SMARCA4, GRIN2A, DDX3X* and *FAT4*). Only two putative driver mutations were subclonal, both in tumour suppressor genes not commonly associated with melanoma: *EPS15* (Cluster 15) and *EXT2* (Cluster 4). Neither variant is annotated in COSMIC and therefore their significance is uncertain.

Overall, most SCNAs were subclonal (Figure 52, Figure 53 and Figure 54). Clonal arm-level gains deemed driver events[2] are seen at 7q and 10q, with driver arm-level losses at 9p, 10, 11p and 14q. Clonal driver cytoband gains are noted at 12q14 and 12q15, with losses at 12q23, 15q21 and 15q13. While SCNA loss at 17p is noted in several metastatic sites, concordant losses are not noted at the level of the 17p13.3 cytoband, most likely due to methodological constraints. At the level of the gene, clonal copy number loss of *TP53* was evident, as mentioned.

There was considerable inter-metastatic SCNA heterogeneity, including between metastases present in the same organ (for example, liver metastases 2, 12 and 18 (LI_2_R1, LI_12_R1 and LI_18_R1)). There was also evidence of ITH in SCNAs between the two primary tumour regions sampled, most evident in the chromosome 3, 4, 11q and 13q gains of Region 2 (PR_1_R2) relative to Region 1 (PR_1_R1; Figure 52).

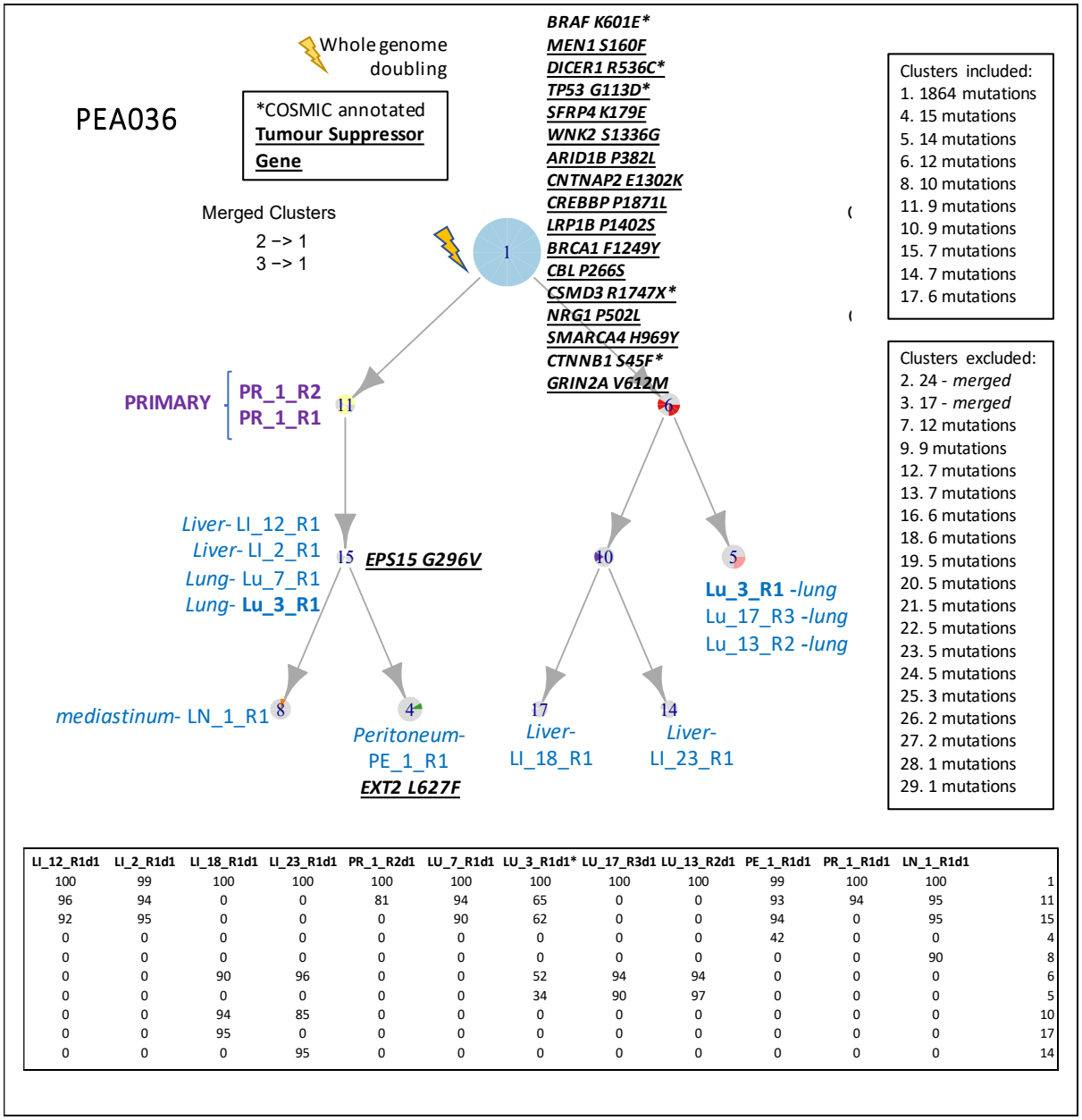

LI_12_R1d1	LI_2_R1d1	LI_18_R1d1	LI_23_R1d1	PR_1_R2d1	LU_7_R1d1	LU_3_R1d1*	LU_17_R3d1	LU_13_R2d1	PE_1_R1d1	PR_1_R1d1	LN_1_R1d1	
100	99	100	100	100	100	100	100	100	99	100	100	1
96	94	0	0	81	94	65	0	0	93	94	95	11
92	95	0	0	0	90	62	0	0	94	0	95	15
0	0	0	0	0	0	0	0	0	42	0	0	4
0	0	0	0	0	0	0	0	0	0	0	90	8
0	0	90	96	0	0	52	94	94	0	0	0	6
0	0	0	0	0	0	34	90	97	0	0	0	5
0	0	94	85	0	0	0	0	0	0	0	0	10
0	0	95	0	0	0	0	0	0	0	0	0	17
0	0	0	95	0	0	0	0	0	0	0	0	14

Figure 51 Phylogenetic tree for PEA036
The clonal cluster of shared mutations sits at the trunk of the tree. Driver mutations belonging to each cluster are annotated. The cancer cell fraction (CCF) of each cluster per metastatic site is detailed in the table beneath the tree. LN = lymph node.

Evolution and metastatic seeding patterns

The phylogenetic tree for PEA036 is shown in Figure 51. There is a very long trunk with the clonal cluster (Cluster 1) containing the vast majority of mutations (95%; Table 12 in **Section 3.3.1**). WGD was a clonal event in this case, and may be associated with the clonal *TP53* mutation.[3]

Two primary tumour regions were sampled, both containing Clusters 1+11. The seeding pattern from primary to metastases appears to be polyclonal, with two branches of the

phylogenetic tree containing mutually exclusive common ancestors for metastasis-bearing clones. The first, Cluster 11, is a recent ancestor to a group of metastases in the liver (LI_2, LI_12), lung (LU_3, LU_7), mediastinal lymph node (LN_1) and peritoneum (PE_1). Another group of metastases are seeded by a clone harbouring Clusters 1+6. This suggests that at least one additional metastasis-seeding clone descended from the primary tumour, but was missed within the limits of this analysis due to undersampling of the primary tumour. Metastases characterised by a clone bearing Clusters 1+6 include other liver (LI_18, LI_23) and lung (LU_3, LU_17 and LU_13) sites. The clone(s) bearing Clusters 1+11 as well as the clone(s) bearing Clusters 1+6 are both present in the liver and the lung, suggesting at least two waves of metastatic dissemination from the primary tumour.

Most metastases appear monoclonal in their composition and a metastasis-to-metastasis seeding trajectory is also a possible mechanism of spread (as opposed to all metastases being seeded from the primary tumour). Only two metastases were polyclonal: the right lung (LU_3_R1) and peritoneal (PE_1_R1) metastases. The right lung metastasis (LU_3_R1) contains clones which appear on exclusive branches (that is, Clusters 15 and 5) and are also evident at other metastatic sites – likely due to cross-metastatic seeding, or alternatively due to seeding from an undersampled primary tumour clone. The peritoneal metastasis contains a private cluster (Cluster 4) at a CCF of 42%, and also harbours a private driver mutation in *EXT2*. Ongoing evolution at this site, possibly with selection for *EXT2*, is the most parsimonious explanation as no other site shares this cluster.

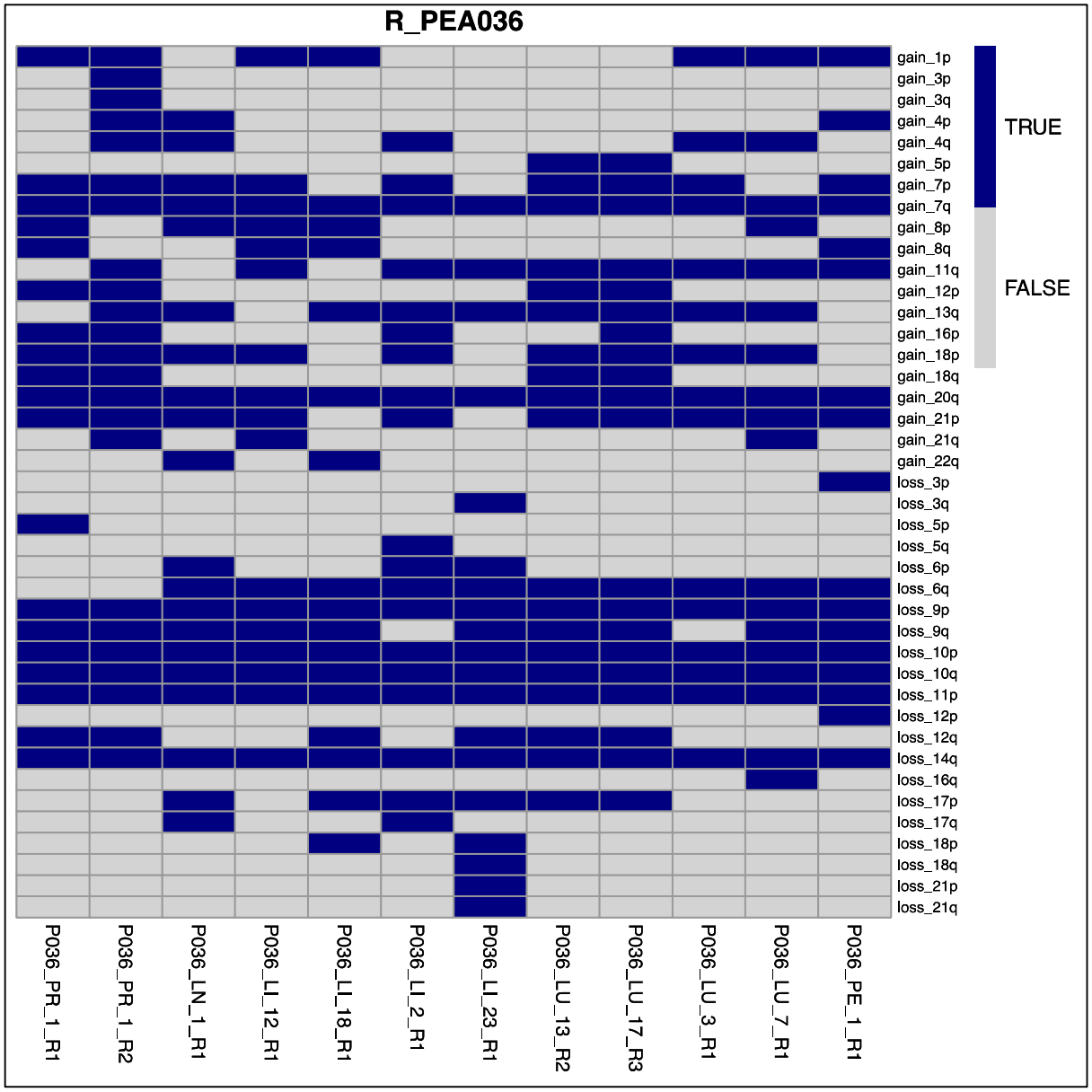

Figure 52 Chromosomal arm-level losses and gains
Blue squares indicate whether there was loss or gain of at least one copy of the chromosome arm relative to the mean ploidy of all samples.

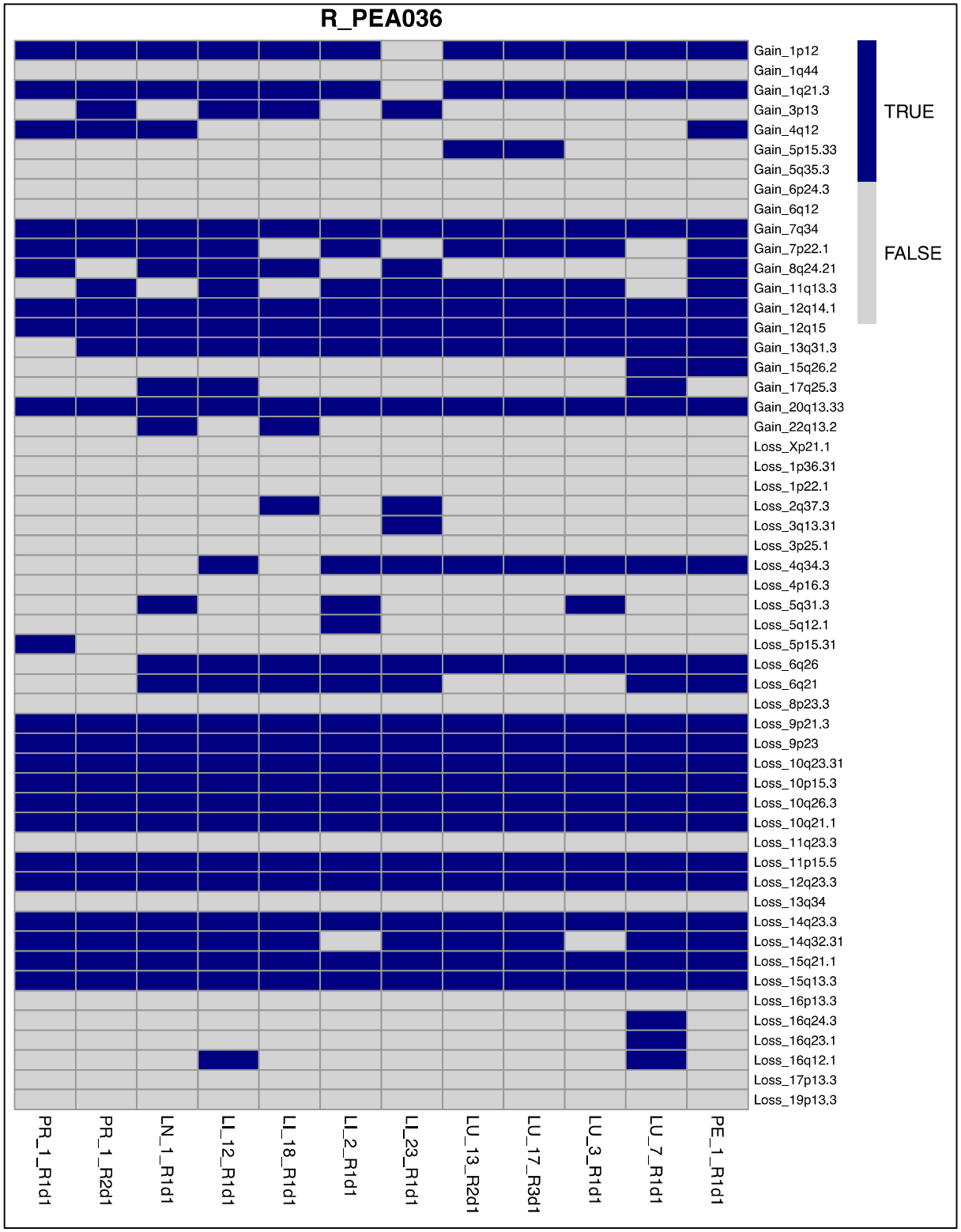

Figure 53 Cutaneous melanoma driver cytoband gains and losses
Annotated cytobands are melanoma driver regions determined by a GISTIC analysis of TCGA data.[2] Blue squares indicate whether there was loss or gain of at least one copy of the cytoband relative to the mean ploidy of all samples.

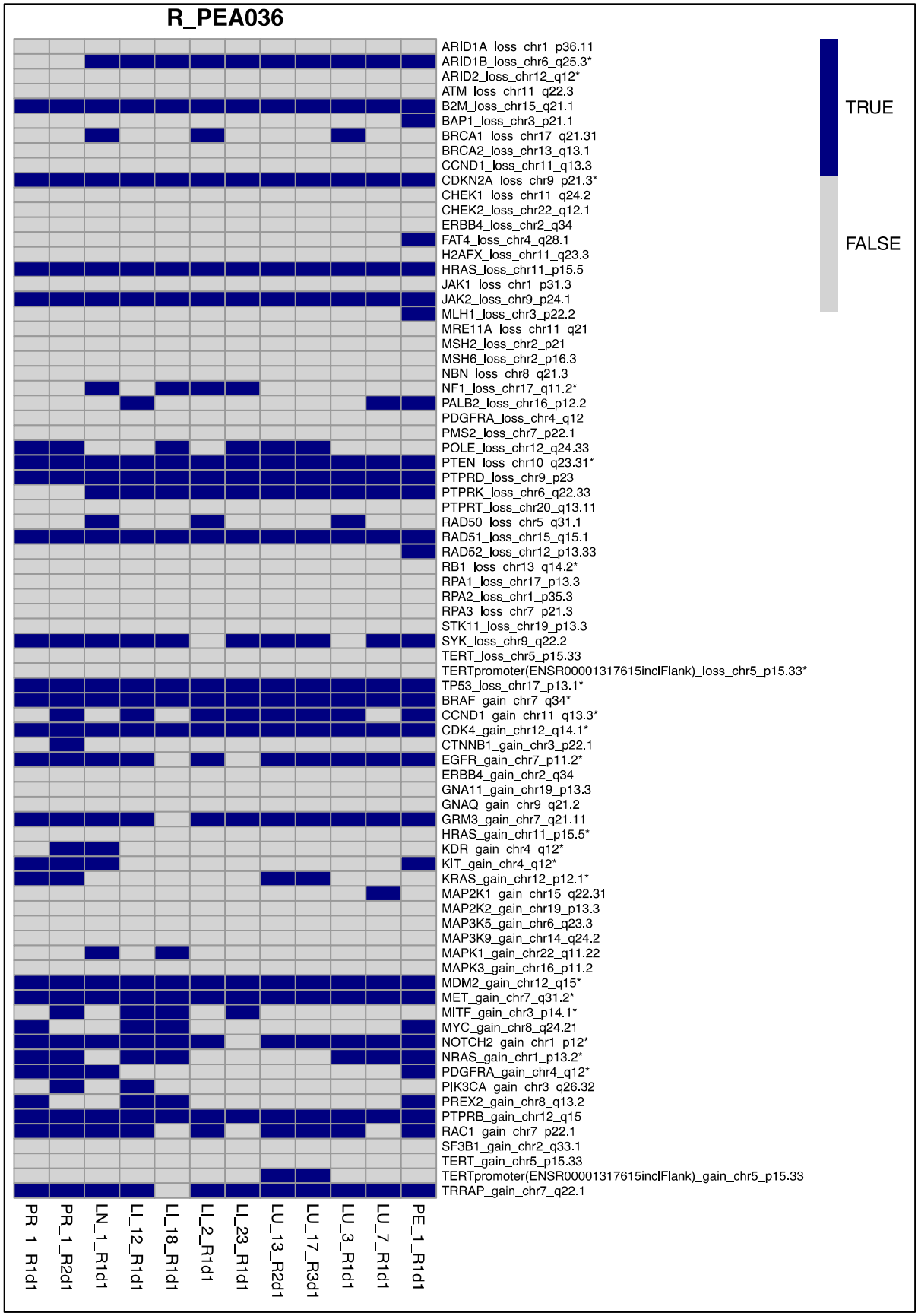

Figure 54 Driver gene gains and losses

Genes with an asterisk (*) are noted driver genes in the TCGA and Hayward data sets.[2,4] Blue squares indicate whether there was loss or gain of at least one copy of the gene relative to the mean ploidy of all samples.

Genomic mechanisms of treatment resistance

Patient PEA036 received both pembrolizumab, to which her disease was refractory, and dabrafenib+trametinib. As previously discussed in PEA004, the *BRAF K601E* mutation does not typically predict response to BRAF/MEK inhibition. In a cohort of 11 patients with a K601E mutation, only one (9%) had an objective response to MAPK inhibition.[5] In this case the response was not evaluable as BRAF/MEK inhibition was ceased early due to intercurrent critical illness.

Genomic factors that may have contributed to primary progression on pembrolizumab include a clonal mutation in *CTNNB1.* This gene encodes the protein subunit beta-catenin which acts as an intracellular signal transducer in the Wnt signalling pathway, which is involved in the production of IL-10, an immunosuppressive cytokine that impairs dendritic cell function.[6] Mutations in *CTNNB1* are prevalent in different cancer types, and are found in primary melanomas and their associated metastases.[7] Alterations in *CTNNB1* have been associated with both innate and acquired resistance to immune checkpoint inhibition through immune exclusion.[8,9] In this case, the *CTNNB1 p.S45F* alteration is a recognised hotspot (COSMIC) and may have impaired T cell infiltration in response to pembrolizumab, contributing to primary resistance.

Aneuploidy may have provided another means of immune evasion and resistance to anti-PD-1 therapy in this case, although as discussed in PEA023, this has only been suggested in cohorts of patients treated with anti-CTLA4 immune checkpoint inhibitors as opposed to anti-PD-1.

Case summary

PEA036 represents a case of melanoma where seeding from the primary tumour to metastatic sites involved at least two clones. The vast majority of mutations were clonal and most metastases were monoclonal in their composition. Metastatic divergence was therefore limited. A COSMIC-reported *TP53* mutation was clonal and may have facilitated early WGD.[3] A *BRCA1* mutation was clonal in this case, but the absence of a BRCA1/2 signature and the lack of COSMIC annotation of this variant make its contribution uncertain. The clonal *CTNNB1* mutation may have led to immune exclusion and primary resistance to pembrolizumab. These represent adverse factors that may have contributed to the five-month

overall survival from diagnosis of Stage IV disease, in addition to the intercurrent diverticular illness at the end of life.

Considerable heterogeneity in somatic copy number events across metastatic sites is apparent, and also within the primary tumour in this case, suggesting that this is the process that dominated subclonal diversifaction and disease evolution. While the primary tumour appears monoclonal within the constraints of our mutation clustering analysis, this is likely to be an underestimate as our methods restrict de novo mutations being called from FFPE. The extent of subclonal SCNAs across metastatic sites, reflected in the high WGII score relative to the other cutaneous melanoma cases in this cohort, is suggestive of ongoing CIN.

References for PEA036

1. Vogelstein B, Papadopoulos N, Velculescu VE, et al. Cancer genome landscapes. *Science* 339: 1546–58, 2013.
2. Cancer Genome Atlas N: Genomic Classification of Cutaneous Melanoma. *Cell* 161: 1681–96, 2015.
3. Bielski CM, Zehir A, Penson AV, et al. Genome doubling shapes the evolution and prognosis of advanced cancers. *Nat Genet* 50: 1189–1195, 2018.
4. Hayward NK, Wilmott JS, Waddell N, et al. Whole-genome landscapes of major melanoma subtypes. *Nature* 545: 175–180, 2017.
5. Menzer C, Menzies AM, Carlino MS, et al. Targeted Therapy in Advanced Melanoma With Rare BRAF Mutations. *J Clin Oncol* 37: 3142–3151, 2019.
6. Yaguchi T, Goto Y, Kido K, et al. Immune suppression and resistance mediated by constitutive activation of Wnt/beta-catenin signaling in human melanoma cells. *J Immunol* 189: 2110–7, 2012.
7. Sanborn JZ, Chung J, Purdom E, et al. Phylogenetic analyses of melanoma reveal complex patterns of metastatic dissemination. *Proc Natl Acad Sci USA* 112: 10995–1000, 2015.
8. Harding JJ, Nandakumar S, Armenia J, et al. Prospective Genotyping of Hepatocellular Carcinoma: Clinical Implications of Next-Generation Sequencing for Matching Patients to Targeted and Immune Therapies. *Clin Cancer Res* 25: 2116–2126, 2019.
9. Trujillo JA, Luke JJ, Zha Y, et al. Secondary resistance to immunotherapy associated with beta-catenin pathway activation or PTEN loss in metastatic melanoma. *J Immunother Cancer* 7: 295, 2019.

Case study 5: PEA080

Clinical summary

Patient PEA080 was a 69 year old woman diagnosed in March 2017 with a *BRAF/NRAS/KIT* wild-type subungual (acral) melanoma (Breslow thickness 8.5 mm, ulcerated), Stage III at diagnosis with one positive sentinel lymph node (of two sampled). A completion left ilio-inguinal lymph node dissection was undertaken in June 2017 without evidence of any additional melanoma lymph node metastases. In December 2017 she developed metastatic relapse with involvement of the left ilio-inguinal lymph nodes and liver. Combination ipi+nivo was started and was complicated by Grade 3 hepatitis after one cycle. In March 2018, after subsequent progression in both the left pelvic and hepatic metastases anti-PD-1 monotherapy was restarted, but without any evidence of treatment response. She died in July 2018, seven months from her Stage IV melanoma diagnosis. The clinical course is summarised in Figure 55.

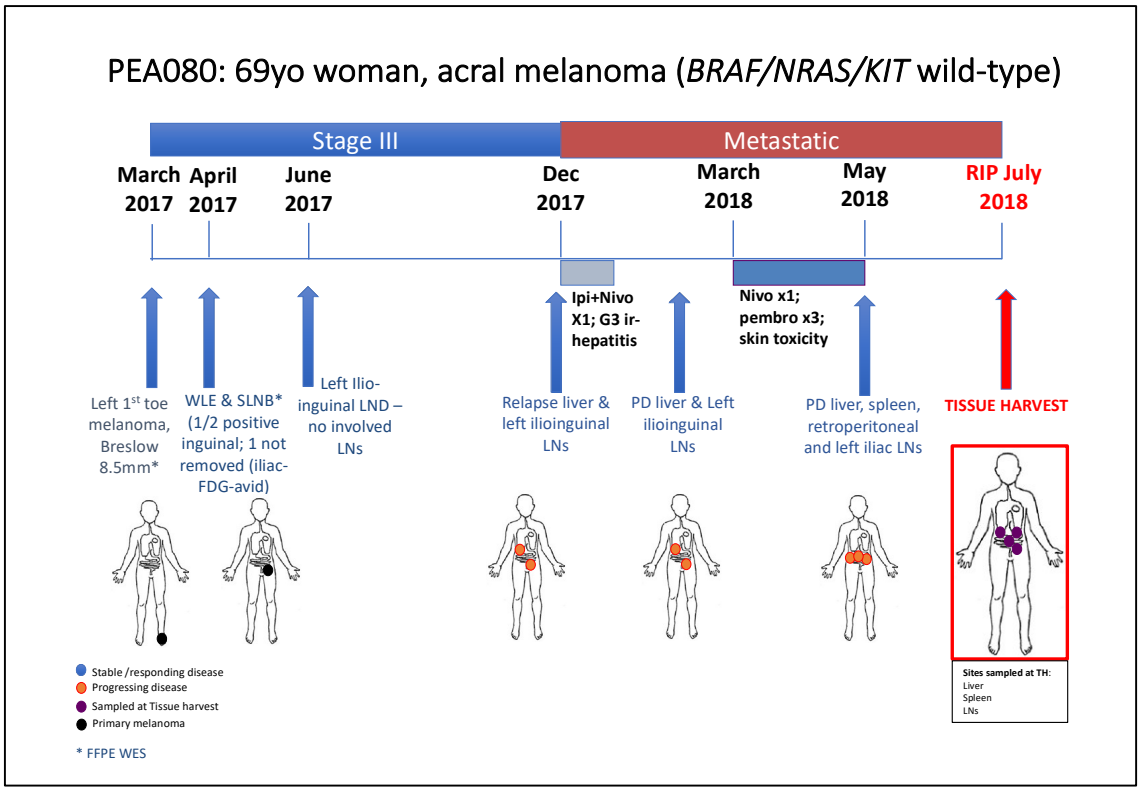

Figure 55 Timeline of clinical events, treatment and disease response in PEA080
Best overall RECIST response is included in brackets for each line of treatment (CR: complete response; PR: partial response; SD: stable disease; PD: progressive disease). WLE: wide local excision; SLNB: sentinel lymph node biopsy; FFPE: formalin-fixed paraffin-embedded; WES: whole exome sequencing; LN(s): lymph node(s); Ipi+nivo: ipilimumab and nivolumab combination therapy; pembro: pembrolizumab.

Tissue harvest (TH) sampling and quality control considerations

At the tissue harvest, 59 tumour samples were taken from 50 individual metastases, the vast majority from the liver (38/59 samples) as well as the lung and lymph nodes (para-aortic, left inguinal, porta hepatis). As no driver mutations could be leveraged for Sanger sequencing evaluation, broader melanoma gene panel sequencing was undertaken. On the basis of successful panel sequencing, 10 tumour samples were selected for WES and all were successfully profiled. In addition, four primary tumour regions obtained from archival tissue were submitted for sequencing and successfully profiled.

Genomic features

Tumour mutational burden is 59 nsSNVs or 2.52 mutations/Mb (Table 12 in **Section 3.3.1**), consistent with reports in acral melanoma (median 2.1 mutations/Mb).[1] The clonal mutation proportion is 80%. The dominant mutation signature in this case is age-related (Signature 1A), consistent with the acral histology (Figure 56).

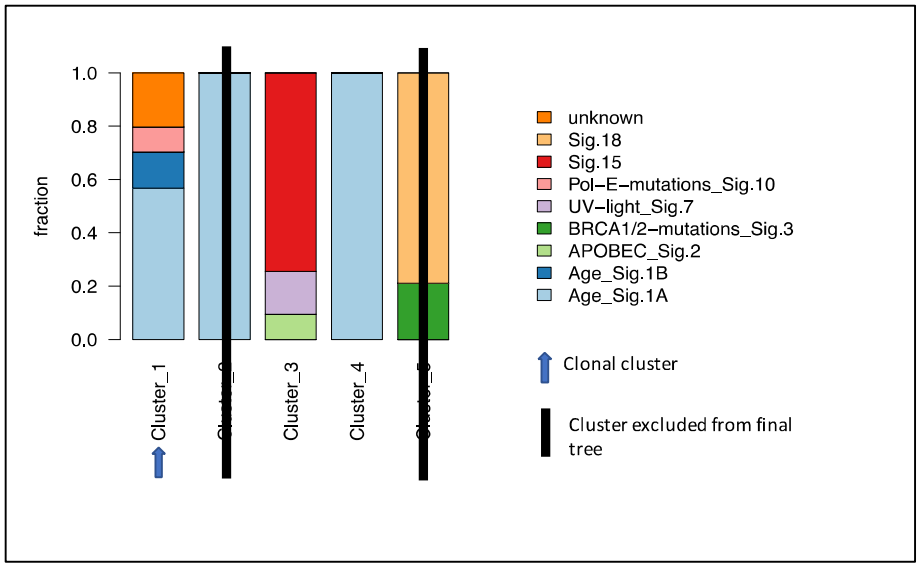

Figure 56 Mutational signature analysis for PEA080
Mutational signatures are based on Pyclone clustering of mutations for creation of phylogenetic trees, with the clonal cluster representing the ubiquitous mutations. Cluster 1 is the clonal cluster and is the only cluster with enough SNVs for reliable signature analysis. Clusters 2 and 5 were removed from the final tree.

The tumour samples appear diploid by computational methods (median ploidy 2.1). This is concordant with FISH undertaken on M14 (LN_6_R2) which had a mode ploidy of 2 (range 2–4), but is not concordant with M1 (LN_1_R1) which has a mode ploidy of 3 (Figure 57). The median WGII score is 0.41 (less than the median for the acral/mucosal cohort; Table 13 in **Section 3.3.3**).

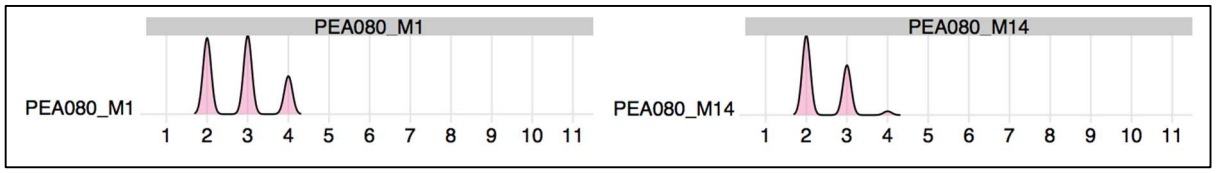

Figure 57 Corrected ploidy estimates of PEA080 samples analysed by FISH
*The x axis denotes the total probe count for each chromosome (see **Section 3.3.3**) and the y axis denotes the relative frequency.*
NB: M1 = LN_1_R1; M14 = LN_6_R2.

Driver alterations

The only putative clonal driver mutation is in *LZTR1 p.P226L* (Figure 58). This is a recognised tumour suppressor gene, germline mutations in which are known to lead to Noonan syndrome in an autosomal dominant manner.[2] This particular variant is not reported in COSMIC, however. An *LZTR1 p.Gly248Arg* mutation has been previously described in another subungual melanoma case.[3]

Both clonal and subclonal SCNAs are equally evident in PEA080. Clonal arm-level chromosomal aberrations common to acral melanoma include gains in 6p and 8q, as well as losses in 6q, 9p, 10 and 11q (Figure 59).[1,4] In addition, cutaneous melanoma clonal driver arm-level SCNAs[5] include gains in 1q and 22q, and losses in 16q and 17p. The driver cytobands 5p15 and 11q13, recognised in cutaneous melanoma as well as in acral melanoma, were gained. 19p13, a cutaneous melanoma driver cytoband[5] was lost (Figure 60). The gain of 11q13 despite evidence of an 11q arm-level loss highlights how a ≥50% approach to calling chromosome arm-level gains and losses can be imperfect (see **Appendix A Section 1.3**). There is also evidence of clonal copy number loss of the loci for *NF1* and *ARID1B* (Figure 61), without evidence of mutations in these genes.

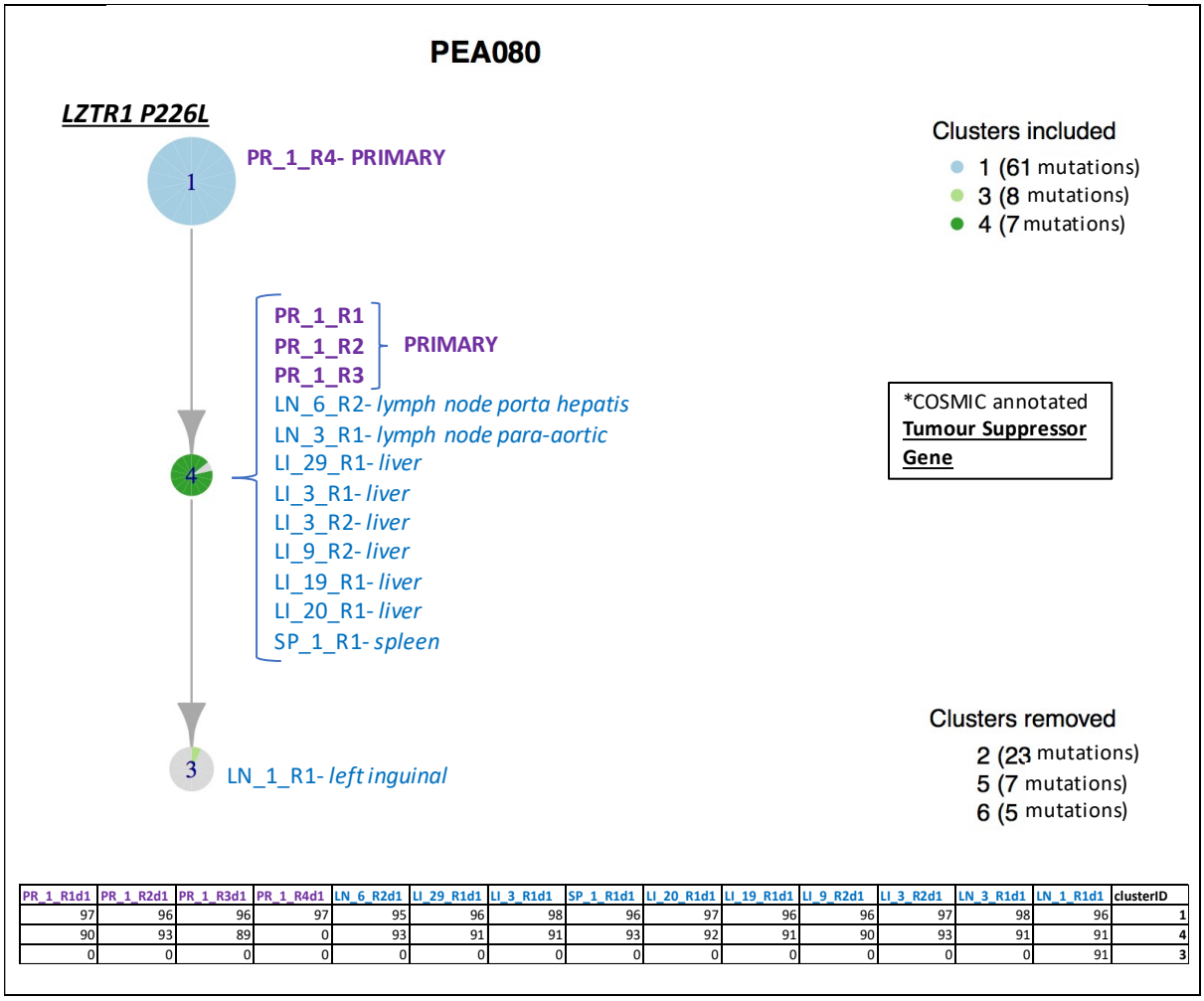

PR_1_R1d1	PR_1_R2d1	PR_1_R3d1	PR_1_R4d1	LN_6_R2d1	LI_29_R1d1	LI_3_R1d1	SP_1_R1d1	LI_20_R1d1	LI_19_R1d1	LI_9_R2d1	LI_3_R2d1	LN_3_R1d1	LN_1_R1d1	clusterID
97	96	96	97	95	96	98	96	97	96	96	97	98	96	1
90	93	89	0	93	91	91	93	92	91	90	93	91	91	4
0	0	0	0	0	0	0	0	0	0	0	0	0	91	3

Figure 58 Phylogenetic tree for PEA080
The clonal cluster of shared mutations sits at the trunk of the tree. Driver mutations belonging to each cluster are annotated. The cancer cell fraction (CCF) of each cluster per metastatic site is detailed in the table beneath the tree. LN = lymph node.

Evolution and metastatic seeding patterns

In this case, four regions from the primary tumour were sampled, revealing a polyclonal primary tumour with at least two clones – one containing Cluster 1 only, and the other Clusters 1+4 (Figure 58). Primary tumour Region 4 (PR_1_R4) – which only contains the clonal cluster – also has a different SCNA profile to the other primary regions, with some cytoband- and arm-level gains and losses private to that region (Figure 59 and Figure 60).

The dominant pattern of seeding from the primary tumour in PEA080 appears monoclonal. One of the primary tumour regions containing Cluster 4 (PR_1_R1, R2 or R3) is likely to have seeded the metastases. All metastases themselves appear monoclonal in their composition (CCFs all >90%), with little metastatic divergence in mutations evident overall. Only the left inguinal lymph node (LN_1_R1) sample contains a private cluster of mutations

(Cluster 3), which is clonal in this sample (CCF 91%). In keeping with a monoclonal primary-metastasis seeding pattern, it may have developed after the Cluster 1+4 clone departed the primary tumour (but prior to seeding this site). There is also the possibility that this cluster originated in the primary tumour, but has not been captured within the limitations of this analysis. This situation would render this case a polyclonal seeding scenario.

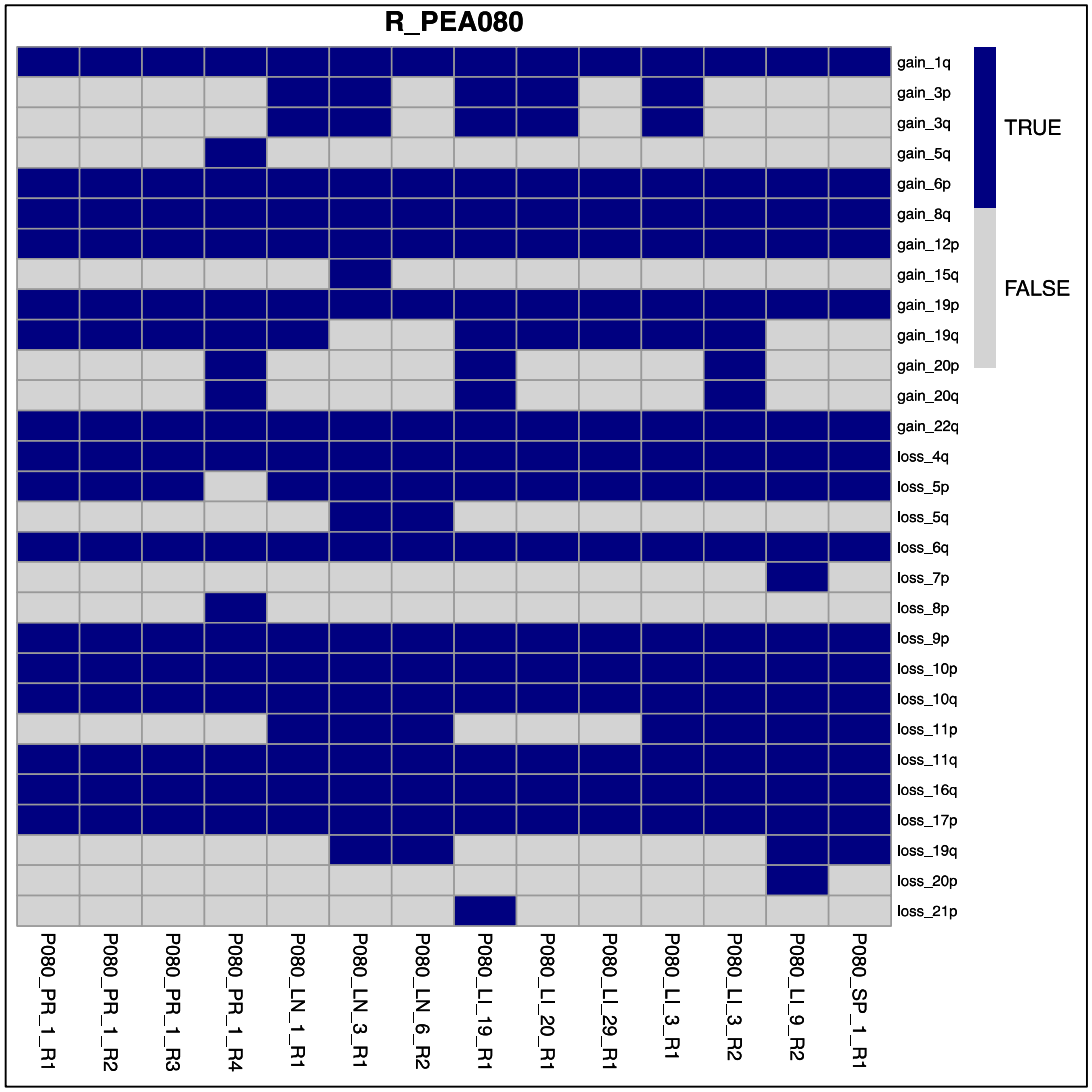

Figure 59 Chromosomal arm-level losses and gains
Blue squares indicate whether there was loss or gain of at least one copy of the chromosome arm relative to the mean ploidy of all samples.

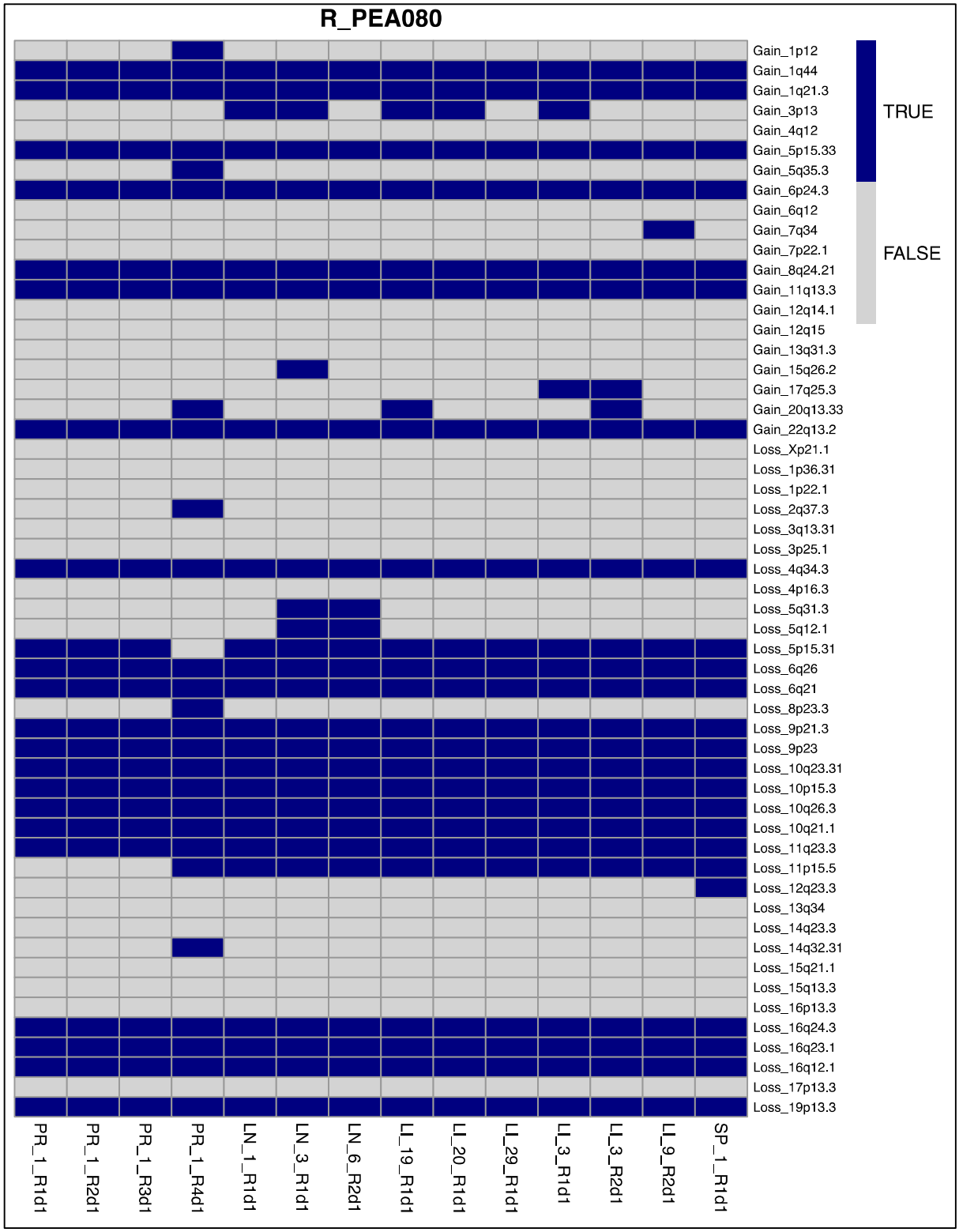

Figure 60 Cutaneous melanoma driver cytoband gains and losses
Annotated cytobands are melanoma driver regions determined by a GISTIC analysis of TCGA data.[5] Blue squares indicate whether there was loss or gain of at least one copy of the cytoband relative to the mean ploidy of all samples.

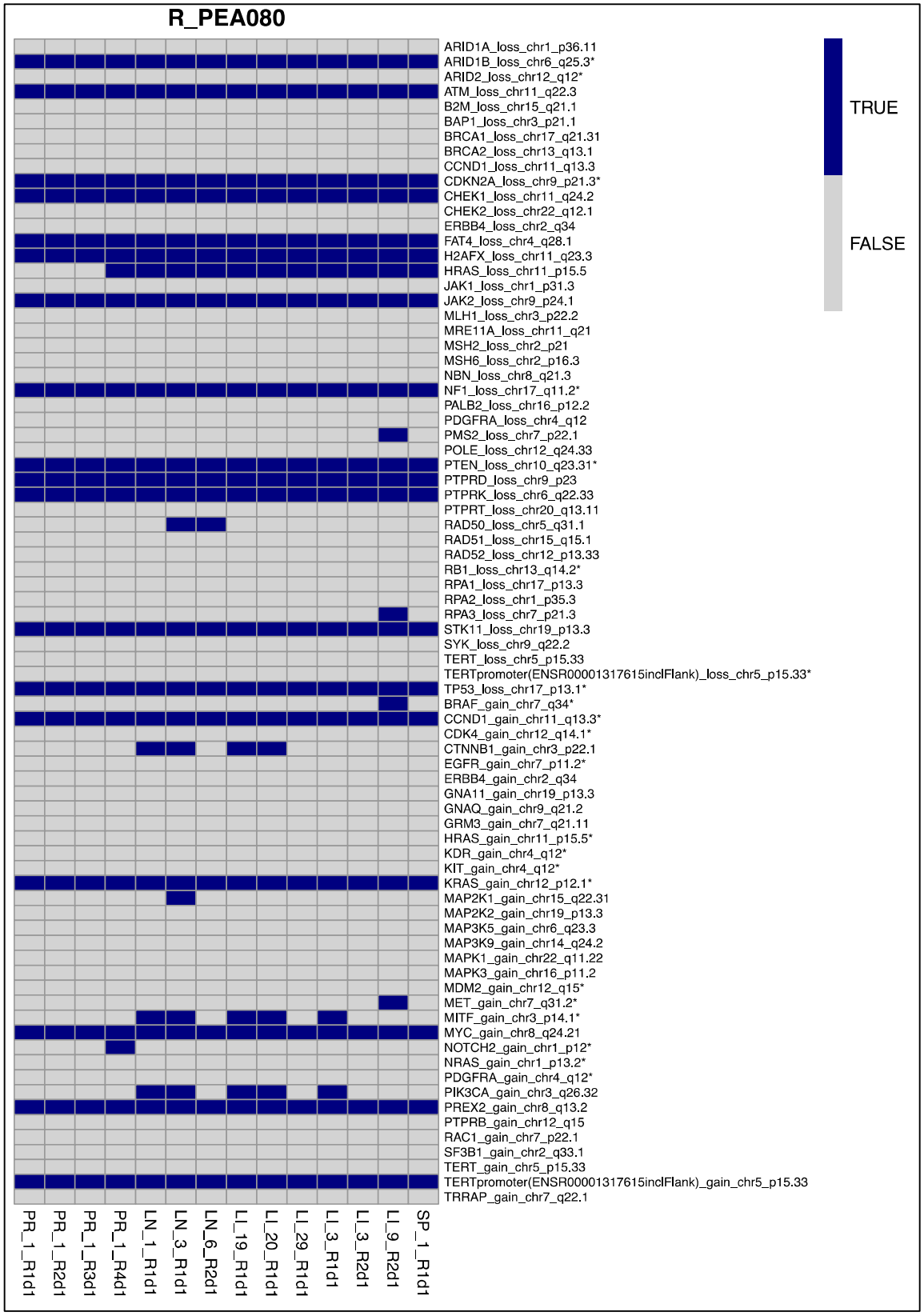

Figure 61 Driver gene gains and losses

Genes with an asterisk (*) are noted driver genes in the TCGA and Hayward data sets.[5,6] Blue squares indicate whether there was loss or gain of at least one copy of the gene relative to the mean ploidy of all samples.

Genomic mechanisms of treatment resistance

There are no recognised mutations associated with response/resistance to immune checkpoint inhibition in this case. Overall, it appears that the burden of SCNA loss is greater than gain (Figure 59 and Figure 60), a feature noted in double non-responders to sequential anti-CTLA4 and PD-1.[7]

The burden of disease was mainly in the liver, a site that generally demonstrates poorer responses to immune checkpoint blockade.[8] There may be a number of explanations for this, including the immuno-privileged status of the liver with greater presence of antigen-tolerant dendritic cells and cell-surface expression of molecules that regulate the immune response.[9] The presence of hepatic metastases has also been shown to reduce immunotherapy efficacy through sequestration of CD8 T cells from the circulation and induction of T cell apoptosis.[10]

Case summary

The case of patient PEA080 highlights the course of an aggressive melanoma phenotype, refractory to combination checkpoint blockade. The overall survival was only 16 months from first primary tumour diagnosis (albeit diagnosed at a late-stage given the Breslow thickness of 8.5 mm). There appears to be a dominant subclone in the primary tumour responsible for seeding the majority of metastases in a monoclonal manner.

Given there is only one putative driver mutation evident, copy number changes are likely to have played an important role in promotion of tumour growth, a recognised feature of acral melanomas.[1,4] The median computational ploidy of 2.1 suggests this is a diploid melanoma and the WGII was relatively low for our cohort. One of the FISH samples was not concordant with a diploid status, potentially highlighting a degree of cell-to-cell variation in ploidy status that evaded detection in our sampling and/or computational approach. In their landscape analysis of acral melanomas Newell et al. describe significantly higher rates of aneuploidy in subungual versus other acral tumours, but this is not reflected here.[1] Copy number loss of key TSGs for example, *CDKN2A* (9p), *PTEN* (10q) and *TP53* (17p) is evident through arm-level losses, but without any corresponding mutations. While haploinsufficiency may have played a role in enabling tumour growth, it is also possible that the other TSG alleles were methylated.[11] Evaluating methylation was beyond the scope of my role in this project.

The clonal mutation in *LZTR1* is notable in that germline mutations in this gene can predispose to a syndrome of multiple schwannomas, usually with LOH of the wild-type

allele.[2] However, in PEA080 there is gain of chr22q, and no evidence of somatic copy number loss within the extent of the analysis undertaken. Mutations in *LZTR1* are also noted in glioblastoma and colorectal cancers,[12] as well as in melanoma.[3] The protein impacted in this case does not match these other cases, and therefore its significance as a driver here requires further validation. Demonstration of protein loss may be pursued through immunohistochemistry, and analysis of matched RNAseq data may shed light on this as well.

References for PEA080

1. Newell F, Wilmott JS, Johansson PA, et al. Whole-genome sequencing of acral melanoma reveals genomic complexity and diversity. *Nat Commun* 11: 5259, 2020
2. Piotrowski A, Xie J, Liu YF, et al. Germline loss-of-function mutations in LZTR1 predispose to an inherited disorder of multiple schwannomas. *Nat Genet* 46: 182–7, 2014.
3. Oiso N, Sakai K, Narita T, et al. Lymph node metastatic melanoma from ungual melanoma: Identification of somatic mutations in KIT and LZTR1. *J Dermatol* 45: e5–e6, 2018.
4. Curtin JA, Fridlyand J, Kageshita T, et al. Distinct sets of genetic alterations in melanoma. *N Engl J Med* 353: 2135–47, 2005.
5. Cancer Genome Atlas N: Genomic Classification of Cutaneous Melanoma. *Cell* 161: 1681–96, 2015.
6. Hayward NK, Wilmott JS, Waddell N, et al. Whole-genome landscapes of major melanoma subtypes. *Nature* 545: 175–180, 2017.
7. Roh W, Chen PL, Reuben A, et al. Integrated molecular analysis of tumor biopsies on sequential CTLA-4 and PD-1 blockade reveals markers of response and resistance. *Sci Transl Med* 9, 2017.
8. Pires da Silva I, Lo S, Quek C, et al. Site-specific response patterns, pseudoprogression, and acquired resistance in patients with melanoma treated with ipilimumab combined with anti-PD-1 therapy. *Cancer* 126: 86–97, 2020.
9. Forrester JV, Xu H, Lambe T, et al. Immune privilege or privileged immunity? *Mucosal Immunol* 1: 372–81, 2008.
10. Yu J, Green MD, Li S, et al. Liver metastasis restrains immunotherapy efficacy via macrophage-mediated T cell elimination. *Nat Med* 27: 152–164, 2021.
11. Micevic G, Theodosakis N, Bosenberg M: Aberrant DNA methylation in melanoma: biomarker and therapeutic opportunities. *Clin Epigenetics* 9: 34, 2017.
12. Tate JG, Bamford S, Jubb HC, et al. COSMIC: the Catalogue Of Somatic Mutations In Cancer. *Nucleic Acids Res* 47: D941–D947, 2019.

Case study 6: PEA016

Clinical summary

Patient PEA016 was a 77 year old woman who presented with a symptomatic *NRAS Q61K* mutant sino-nasal melanoma in November 2016. The initial diagnosis was made on resection of a sinus polyp, but staging in December 2016 revealed locally extensive disease and palliative debulking surgery was then undertaken. Given the locally advanced tumour (into the orbit, cavernous sinus and clivus), as well as right cervical lymphadenopathy, systemic therapy with ipi+nivo was initiated post-operatively. Unfortunately, the disease progressed after two cycles with spread to visceral sites including the liver, lung and bone. In January 2017, two cycles of palliative chemotherapy with carboplatin/DTIC were administered with further progression of disease. The patient died soon after in March 2017. The clinical course is summarised in Figure 62.

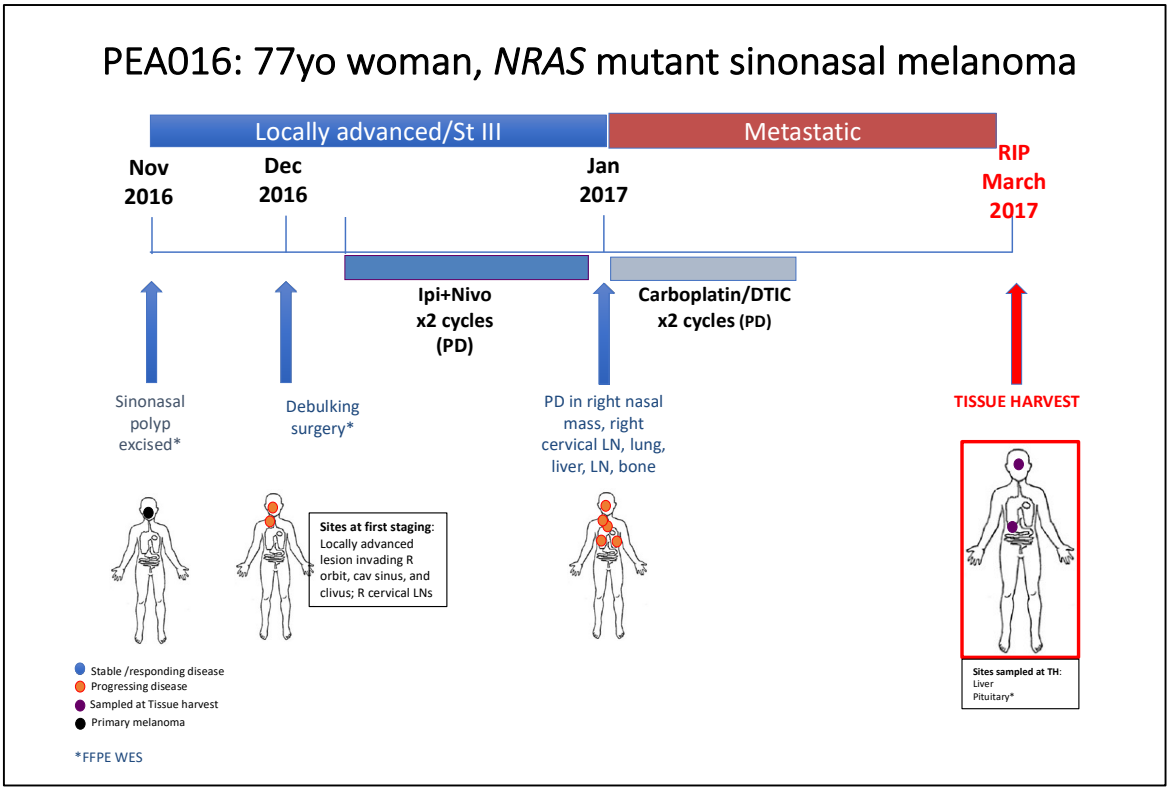

Figure 62 Timeline of clinical events, treatment and disease response in PEA016
Best overall RECIST response is included in brackets for each line of treatment (CR: complete response; PR: partial response; SD: stable disease; PD: progressive disease). Ipi+nivo: ipilimumab and nivolumab combination therapy. FFPE WES: formalin fixed paraffin embedded tissue underwent whole exome sequencing.

Tissue harvest (TH) sampling and quality control considerations

A total of nine regions from five metastatic sites (four liver lesions and the pituitary gland) were sampled at the tissue harvest (TH). Notably, the pituitary appeared macroscopically normal at the TH, but on histology review it was deemed to be involved with tumour and two regions were sampled for profiling. All nine were submitted for WES and eight were successfully profiled. One sample was omitted as a suitable copy number solution could not be found for incorporation in the final phylogenetic tree. In addition, six samples from archival FFPE were submitted for WES: one region from the November 2016 primary tumour biopsy and five regions from the December 2016 primary tumour debulking surgery. Five of the six were successfully profiled.

Genomic features

The TMB is relatively low in this case- 51 nsSNVs or 2.2 mutations/Mb (Table 12 in **Section 3.3.1**) – consistent with this being a mucosal melanoma (median 2.7 mutations/Mb (range 0.54–7.1)).[1,2] The majority of mutations are clonal (71%). The dominant clonal mutational signature was age-related (Signature 1a; Figure 63). There was no signature of UV damage noted.

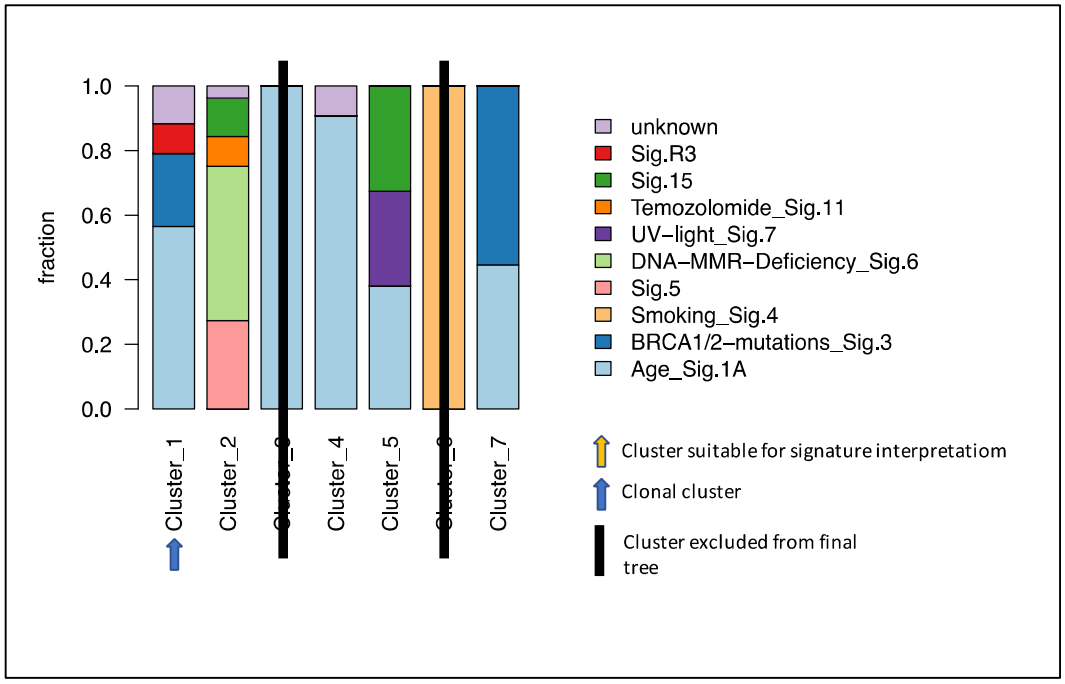

Figure 63 Mutational signature profile for PEA016
Mutational signatures are based on Pyclone clustering of mutations for creation of phylogenetic trees, with the clonal cluster representing the ubiquitous mutations. Cluster 1 is the clonal cluster and the only cluster containing enough SNVs for reliable mutational signature analysis. Clusters 3 and six were removed from the final tree.

The median computationally derived ploidy for both the archival primary tumour samples and the metastases sampled at TH is 3.48 (Table 13 in **Section 3.3.3**), consistent with clonal whole genome doubling. Two samples in the liver (LI_3_R2, LI_1_R1) as well both pituitary regions (PI_1_R1 and R2) and one primary region (PR_2_R1) appear to have undergone a further round of WGD. The FISH-estimated ploidy is consistent with the computationally derived ploidy (Figure 64).

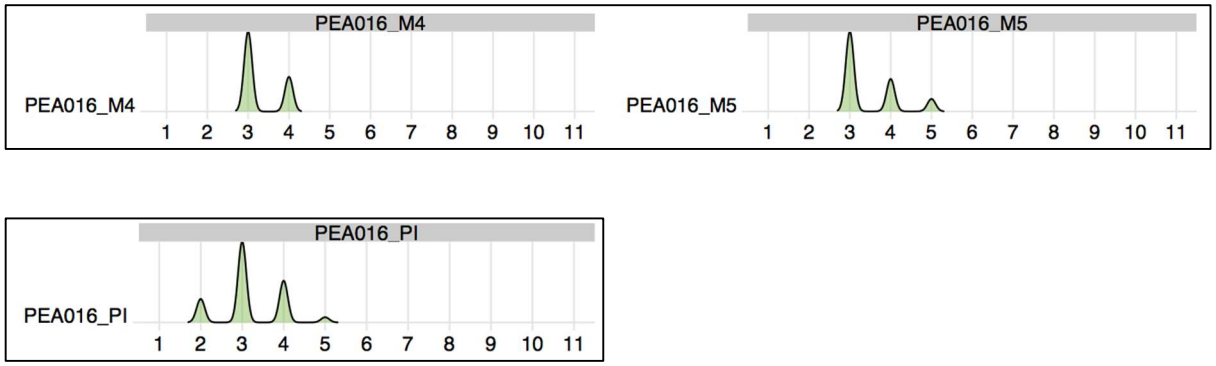

Figure 64 Corrected ploidy estimates of PEA016 samples analysed by FISH
*The x axis denotes the total probe count for each chromosome (see **Section 3.3.3**) and the y axis denotes the relative frequency.*
NB: M4 = LI_3_R1, M5 = LI_3_R2, PI = PI_1_R1.

The WGII for PEA016 is the second highest in the cohort, with a median of 0.65 in both the primary regions and the metastases (Table 13 in **Section 3.3.3**). This is consistent with the fact that mucosal melanomas tend to have higher numbers of SCNAs relative to cutaneous melanomas.[3,4]

Driver alterations

There are two clonal driver mutations in PEA016: a hotspot *NRAS Q61K* mutation and a *B2M R101P* (exon 2) mutation (Figure 65). One putative subclonal driver mutation is in *CAMTA1 R1134H*, private to liver metastasis 2 (LI_2_R1, one of the four profiled liver metastases). This gene encodes calmodulin-binding transcription activator 1, recognised as a tumour suppressor gene, although its biological relevance in melanoma has not been established.

Overall, the majority of SCNAs are subclonal. Clonal arm-level gains (Figure 66) in 1q and 8q, as well as arm-level losses in 6q, 8p, 9p, 10, 11 and 14q are all recognised as common aberrations in mucosal melanomas.[2,3,5] One clonal putative driver cytoband-level gain at 1p12 was also noted[1] (Figure 67).

ITH is also evident across regions of the primary tumour in terms of arm- and cytoband-level copy number events (Figure 66 and Figure 67). For example, primary tumour 1 (PR_1_R1), the original diagnostic sample from the sino-nasal tumour, has a distinct profile of fewer arm-level gains than most debulked primary tumour tissue (PR_2 regions). Region 1 of the debulked primary tumour specimen (PR_2_R1) looks distinct from the other debulked regions (PR_2_R2, R3 and R5) in that is has a greater number of arm-level copy number losses. Intermetastatic and intrametastatic heterogeneity are also evident. The SCNA profile of liver metastasis 2 (LI_2_R1) is distinct from the other liver metastases 1 and 3 (LI_1 and LI_3; Figure 66). Liver metastasis 4 (LI_4_R1) shares a similar profile to the first primary tumour sample (PR_1_R1; Figure 66). Region 1 of liver metastasis 3 (LI_3_R1) harbours more losses than regions 2 and 3.

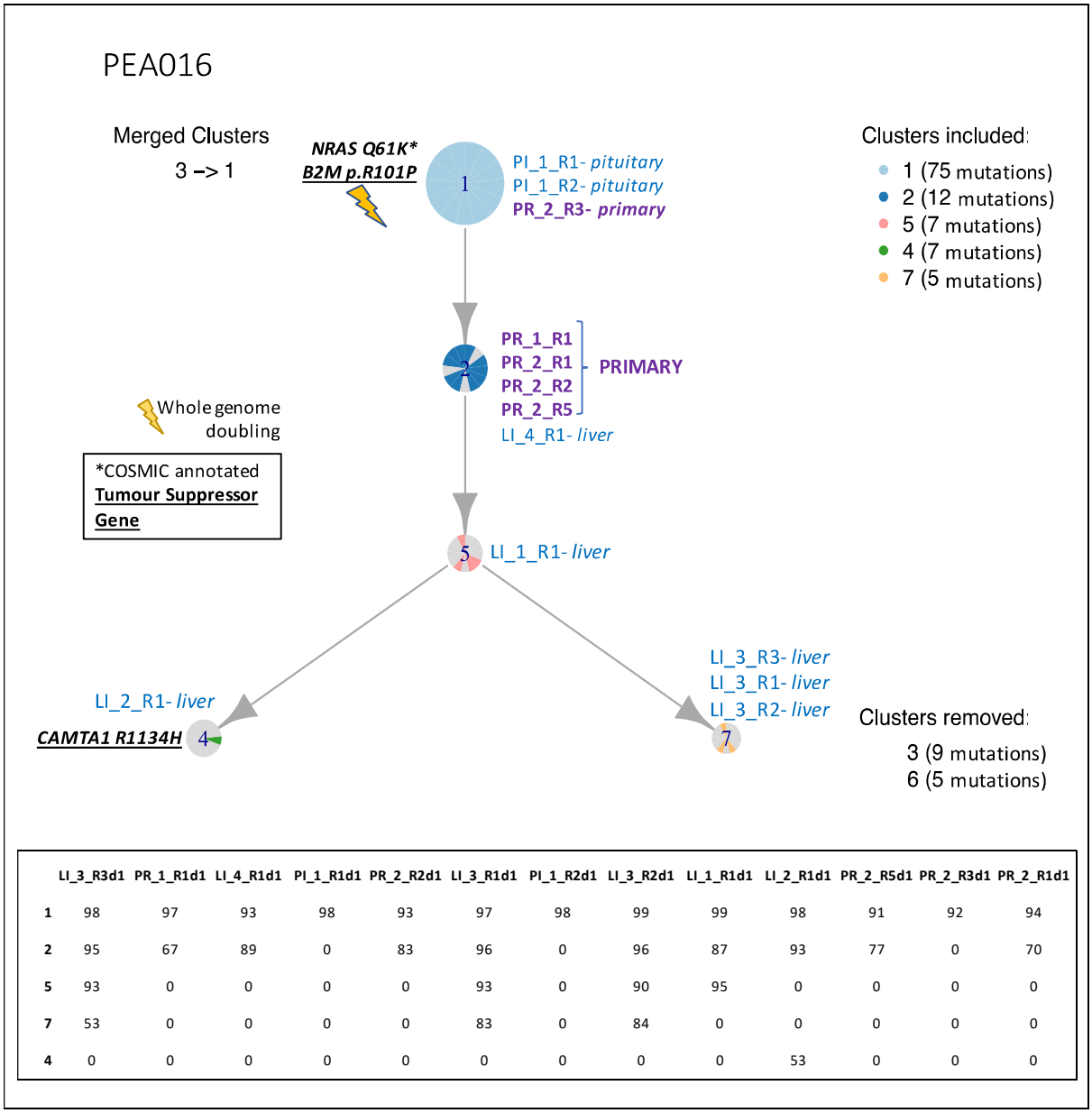

	LI_3_R3d1	PR_1_R1d1	LI_4_R1d1	PI_1_R1d1	PR_2_R2d1	LI_3_R1d1	PI_1_R2d1	LI_3_R2d1	LI_1_R1d1	LI_2_R1d1	PR_2_R5d1	PR_2_R3d1	PR_2_R1d1
1	98	97	93	98	93	97	98	99	99	98	91	92	94
2	95	67	89	0	83	96	0	96	87	93	77	0	70
5	93	0	0	0	0	93	0	90	95	0	0	0	0
7	53	0	0	0	0	83	0	84	0	0	0	0	0
4	0	0	0	0	0	0	0	0	0	53	0	0	0

Figure 65 Phylogenetic tree for PEA016
The clonal cluster of shared mutations (Cluster 1) sits at the trunk of the tree. Driver mutations belonging to each cluster are annotated. The CCFs for each cluster are shown in the table beneath the tree.

Evolution and metastatic seeding patterns

The phylogenetic tree for PEA016 is outlined in Figure 65. Five primary tumour regions were sampled, from two different timepoints (PR_1 in November 2016, PR_2 in December 2016 – See Figure 62, Clinical timeline, above) and two clones are evident within this primary tumour (one containing Cluster 1 only, and the other containing Clusters 1+2) making it polyclonal. The fact that 4/5 primary tumour regions derive from one clone (containing Clusters 1+2), however, suggests there is limited genomic diversity at the level of SNVs. The high WGII provides a clue that a punctuated evolutionary event may characterise this tumour. Given all sites of disease show evidence of WGD, this is likely to have been an early event.

The seeding pattern from the primary to metastatic sites appears polyclonal, as there are metastases seeded by >1 clone. All the liver metastases were seeded by a clone harbouring Clusters 1+5. The two pituitary metastatic regions (PI_1_R1 and R2) may have been seeded earlier than the liver metastases as they are derived from a clone that only contains Cluster 1.

Six of the eight metastatic regions are monoclonal in their composition. Two metastatic regions appear polyclonal in their composition by virtue of their CCFs being >15% lower than the CCF of the clonal cluster: Region 3 of liver metastasis 3 (LI_3_R3) and Region 1 of liver metastasis 2 (LI_2_R1). For LI_2_R1, ongoing evolution is the most parsimonious explanation for the development of the mutations within Cluster 4 (CCF 53%), exclusive to this site. As for LI_3_R3, Cluster 7 has a CCF of 53%, rendering the region polyclonal. The clone harbouring this cluster may have then expanded at Regions 1 and 2 of liver metastasis 3 as Cluster 7 is clonal in both of these.

Overall, the pattern of arm-level SCNAs reinforces the results of the clustering analysis (Figure 66), but is suggestive of more heterogeneity than can be appreciated at the level of the mutations in the primary tumour and metastatic regions, as discussed above. This is consistent with the significant driver role of SCNAs in non-UV driven melanomas.

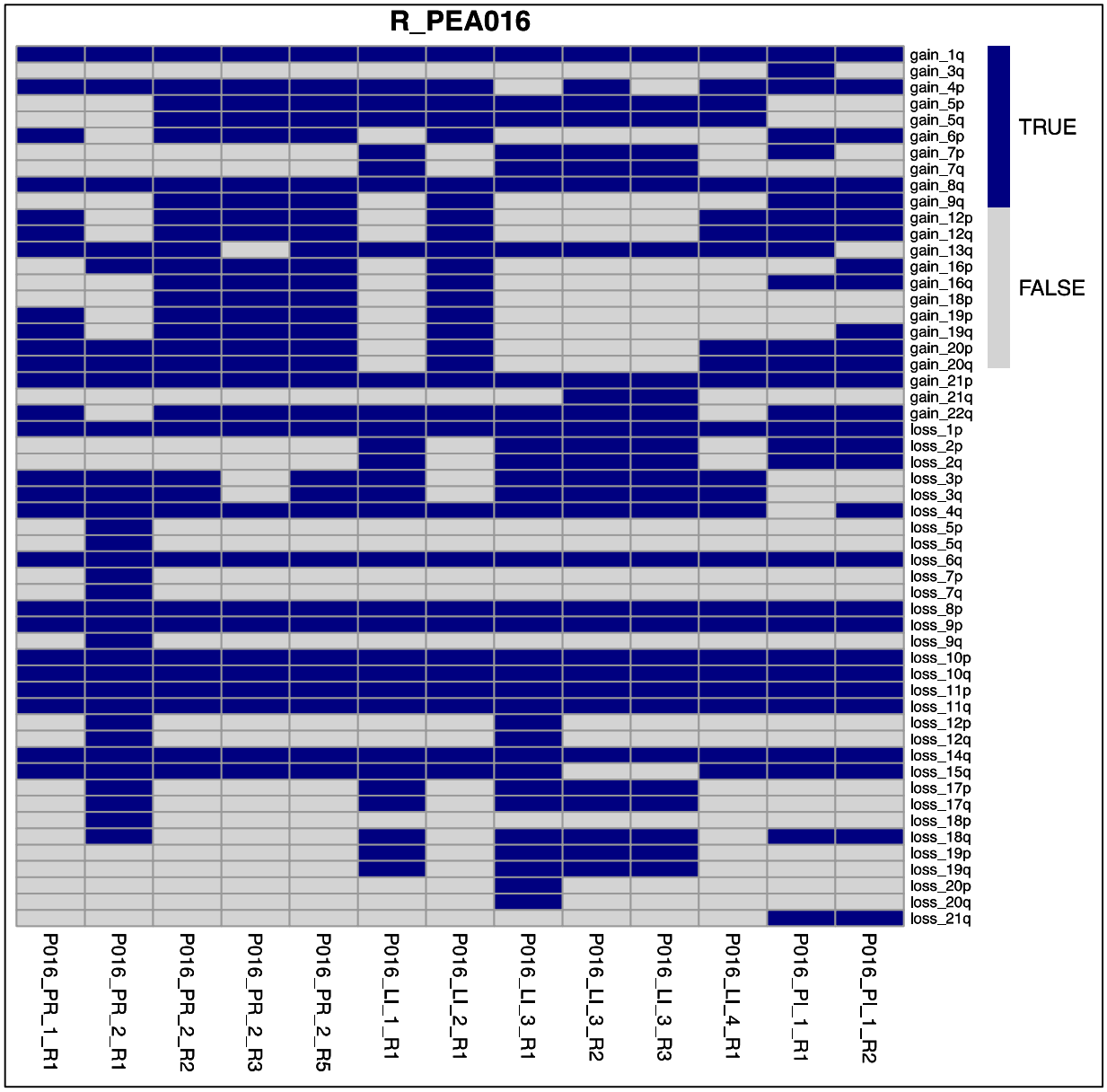

Figure 66 Chromosomal arm-level losses and gains
Blue squares indicate whether there was loss or gain of at least one copy of the chromosome arm relative to the mean ploidy of all samples.

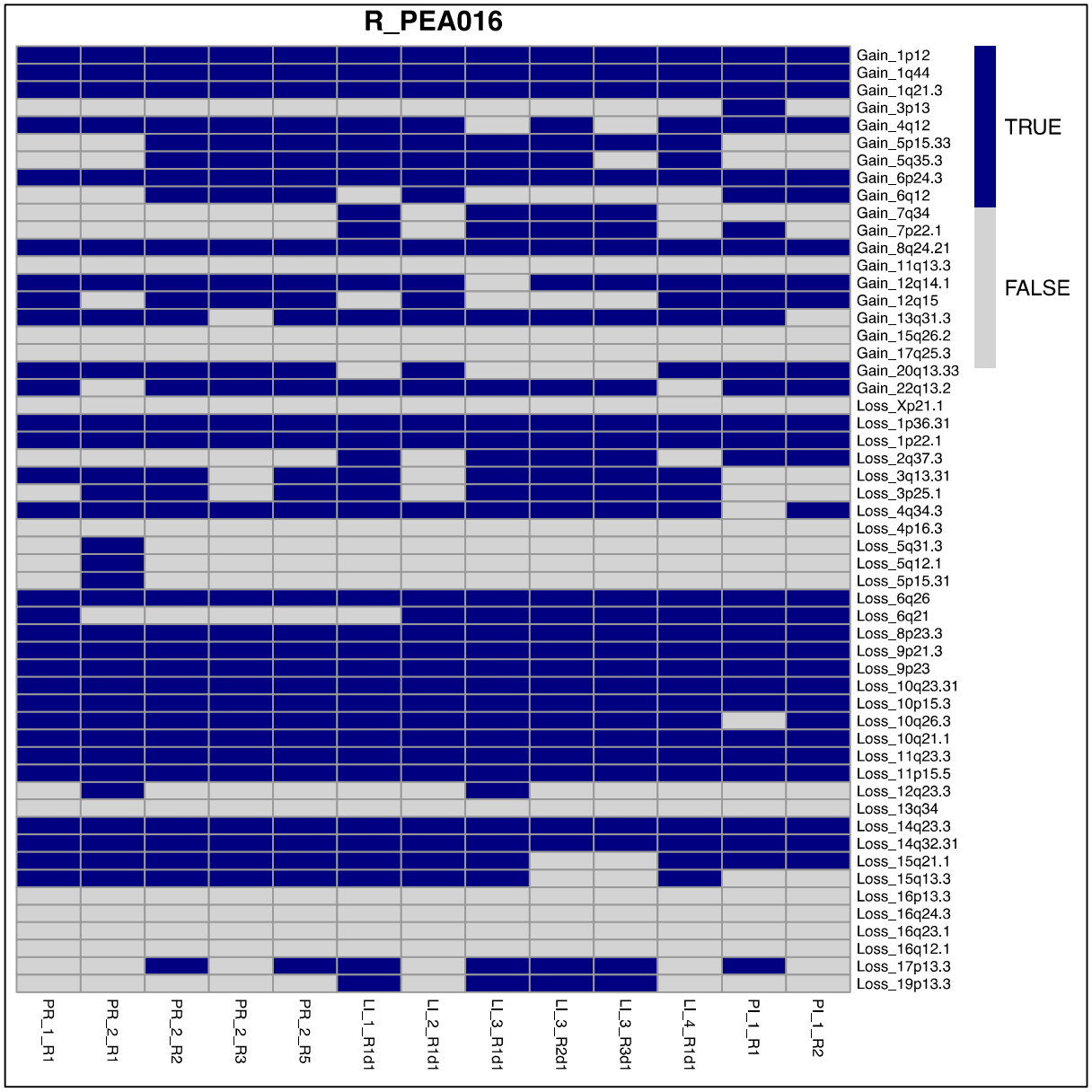

Figure 67 Cutaneous melanoma driver cytoband gains and losses
Annotated cytobands are melanoma driver regions determined by a GISTIC analysis of TCGA data.[6] Blue squares indicate whether there was loss or gain of at least one copy of the cytoband relative to the mean ploidy of all samples. For PEA016 being a mucosal case these SCNAs are to be interpreted with caution.

Figure 68 Driver gene gains and losses
Genes with an asterisk (*) are noted driver genes in the TCGA and Hayward data sets.[6,7] Blue squares indicate whether there was loss or gain of at least one copy of the gene relative to the mean ploidy of all samples.

Genomic mechanisms of treatment resistance

Mucosal melanomas generally have lower response rates to immune checkpoint blockade,[8] possibly due to a lower tumour mutation burden and therefore a lower probability of immunogenic mutations (neoantigens). In this case refractory to combination immune

checkpoint blockade, there is a clonal *B2M R101P* (exon 2) missense mutation with associated somatic copy number loss (at the level of the gene) in nearly all samples, with the exception of two regions in liver metastasis 3 (LI_3_R2 and LI_3_R3). In these two samples this could be a technical artefact as gene-level amplifications and deletions are detected by changes at the beginning or end of the gene only (see **Appendix A Section 1.3**). Although this particular mutation has not been previously reported in COSMIC, it appears that the protein impacted lies in the functional domain (Figure 69, below). Loss of function of B2M may have impaired antigen presentation[9] (assuming that some mutations resulted in neoantigens), thereby enabling the tumour cells to escape and proliferate despite ipi+nivo therapy. The aneuploid state of the tumour cells could have also contributed to immune evasion, as discussed in the case of PEA023.[10]

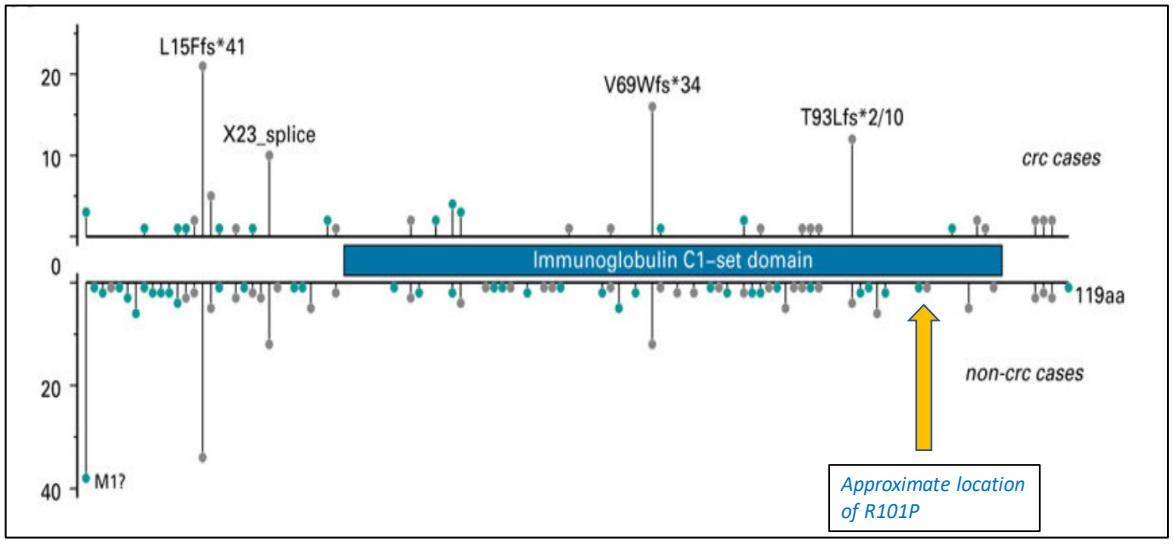

Figure 69 B2M gene functional map
(From Middha et al.).[11] The approximate location of the B2M R101P variant seen in this case is indicated by the yellow arrow.

Case summary

In PEA016 the spread from primary tumour to metastases in the liver and pituitary appears polyclonal. The rapid clinical progression of the primary tumour, clonal WGD and a high WGII suggestive of CIN could be explained by a punctuated evolutionary event. Metastatic competence may have also been acquired at this event as the progression to stage IV disease from diagnosis occurred within two months. The SCNA profiles suggest greater heterogeneity in the primary tumour regions, as well as in the liver metastases than is evident by clustering analysis of mutations alone. While the primary tumour and two metastatic

regions were polyclonal by definition, there was limited genomic divergence. The small numbers of mutations in clusters other than the clonal cluster perhaps decrease the sensitivity to detect significant metastatic divergence.

This patient progressed rapidly through ipi+nivo treatment, with two putative resistance mechanisms identified: a clonal *B2M* mutation that may have disabled antigen presentation and an aneuploid state possibly contributing to immune evasion.

In this case, only liver and pituitary metastases were sampled at the TH but other sites of disease were evident on the last set of scans; unfortunately the locally advancing primary tumour, cervical lymph nodes and bone metastases were not deemed accessible. The pituitary metastatic regions (PI_1) are restricted in the assessment of variants given they were subjected to the same treatment as other FFPE tissue samples (that is, no new variants are called). As such, the profiling of this case may underestimate its true complexity.

References for PEA016

1. Newell F, Kong Y, Wilmott JS, et al. Whole-genome landscape of mucosal melanoma reveals diverse drivers and therapeutic targets. *Nat Commun* 10: 3163, 2019
2. Zhou R, Shi C, Tao W, et al. Analysis of Mucosal Melanoma Whole-Genome Landscapes Reveals Clinically Relevant Genomic Aberrations. *Clin Cancer Res* 25: 3548–3560, 2019.
3. Curtin JA, Fridlyand J, Kageshita T, et al. Distinct sets of genetic alterations in melanoma. *N Engl J Med* 353: 2135–47, 2005.
4. Furney SJ, Turajlic S, Stamp G, et al. Genome sequencing of mucosal melanomas reveals that they are driven by distinct mechanisms from cutaneous melanoma. *J Pathol* 230: 261–9, 2013.
5. Newell F, Wilmott JS, Johansson PA, et al. Whole-genome sequencing of acral melanoma reveals genomic complexity and diversity. *Nat Commun* 11: 5259, 2020
6. Cancer Genome Atlas N: Genomic Classification of Cutaneous Melanoma. *Cell* 161: 1681–96, 2015.
7. Hayward NK, Wilmott JS, Waddell N, et al. Whole-genome landscapes of major melanoma subtypes. *Nature* 545: 175–180, 2017.
8. D'Angelo SP, Larkin J, Sosman JA, et al. Efficacy and Safety of Nivolumab Alone or in Combination With Ipilimumab in Patients With Mucosal Melanoma: A Pooled Analysis. *J Clin Oncol* 35: 226–235, 2017.
9. Zaretsky JM, Garcia-Diaz A, Shin DS, et al. Mutations Associated with Acquired Resistance to PD-1 Blockade in Melanoma. *N Engl J Med* 375: 819–29, 2016.
10. Davoli T, Uno H, Wooten EC, et al. Tumor aneuploidy correlates with markers of immune evasion and with reduced response to immunotherapy. *Science* 355, 2017.
11. Middha S, Yaeger R, Shia J, et al. Majority of B2M-Mutant and -Deficient Colorectal Carcinomas Achieve Clinical Benefit From Immune Checkpoint Inhibitor Therapy and Are Microsatellite Instability-High. *JCO Precis Oncol* 3, 2019.

Case study 7: PEA005

Clinical summary

Patient PEA005 was a 27 year old man with a recognised pathogenic germline *CDKN2A* intronic splice site mutation (IVS2-105A>G).[1] He developed his first primary melanoma of the scalp at age 13 in 2003 (4 mm Breslow thickness, non-ulcerated), and then in 2008 had another melanoma removed from the right shoulder (1 mm Breslow thickness, non-ulcerated). In February 2015 he presented with abdominal pain and imaging revealed metastatic disease in the liver, gallbladder, lung and spleen. A biopsy confirmed melanoma with a *BRAF V600E* mutation. Dabrafenib was initiated with response seen at all sites. Brain imaging had not been performed at initial diagnosis but asymptomatic brain metastases were detected on MRI in September 2015 during the course of dabrafenib. In December 2015, multi-site progression (brain, liver and spleen) occurred and pembrolizumab was initiated, in conjunction with whole brain radiotherapy. In March 2016, further progressive disease in the tonsils and cervical lymph nodes was seen and systemic therapy was changed to ipi+nivo. Two cycles of treatment were complicated by episodes of symptomatic cerebral oedema and then Grade 3 immune-related hepatitis, necessitating a treatment break. Despite immune modulation with steroids and mycofenolate mofetil, PEA005 experienced a progression-free interval of 10 months. In January 2017 he developed lung and intracranial progression with leptomeningeal disease, and died in February 2017 despite receiving one further cycle of ipi+nivo. The clinical course is summarised in Figure 70.

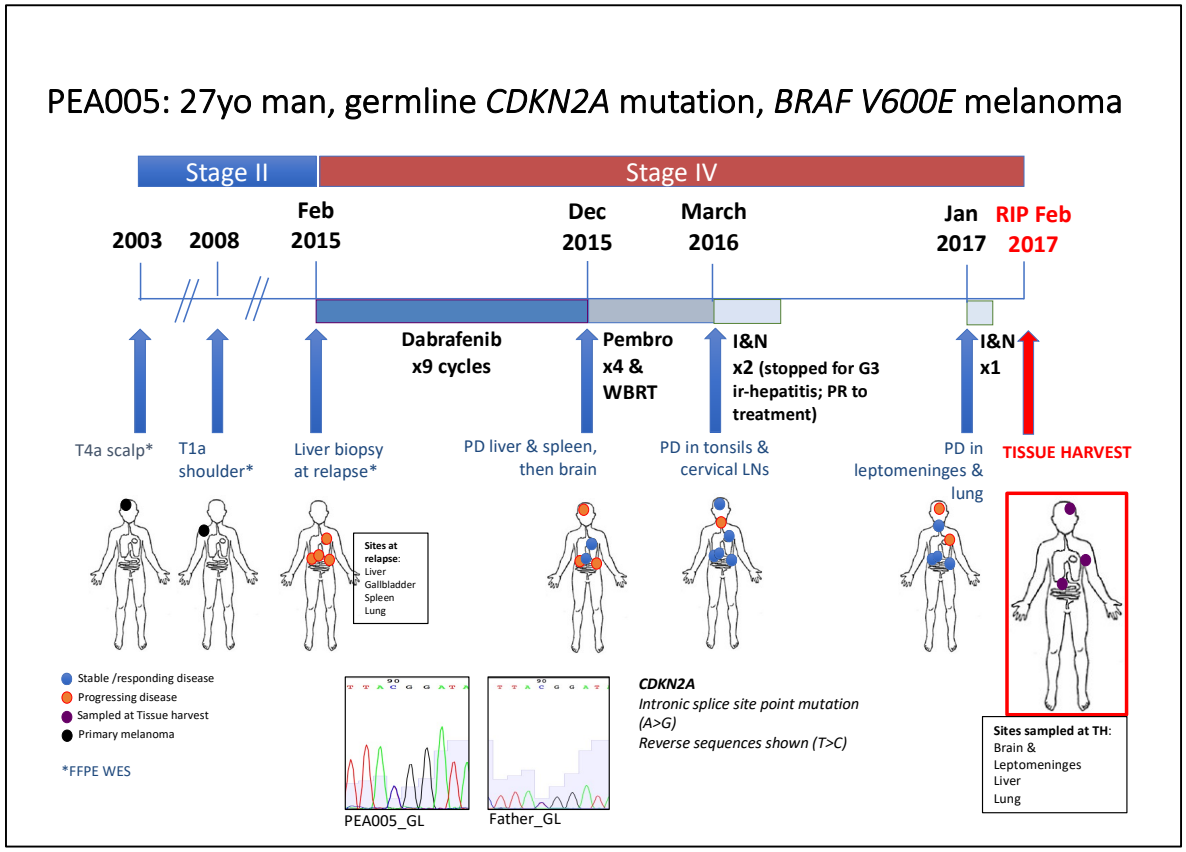

Figure 70 Timeline of clinical events, treatment and disease response in PEA005
Best overall RECIST response is included in brackets for each line of treatment (CR: complete response; PR: partial response; SD: stable disease; PD: progressive disease). WLE: wide local excision. Dab: dabrafenib; pembro: pembrolizumab; ipi+nivo, I+N: ipilimumab and nivolumab combination; WBRT: whole brain radiotherapy; LN: lymph node. Sanger sequencing traces for the germline CDKN2A mutation are included below, with the patient and his father's germline (GL) samples demonstrating heterozygosity with evidence of the pathogenic point mutation.

Tissue harvest (TH) sampling and quality control considerations

Thirty-one samples from 19 metastatic tumour sites were taken at the TH (brain and leptomeninges, liver, spleen, ureter and lung). Of these, 15 samples were submitted for WES (liver, brain and lung; prior to my involvement in the project) but only eight were successfully profiled (brain and lung). Sanger sequencing was repeated on all 31 samples and 11 samples were identified as containing evidence of a *BRAF V600E* mutation, including the eight samples that had passed WES QC. Review of H&E slides revealed an absence of viable tumour in the ureteric regions and the presence of melanin in all liver and some brain samples that completely obscured the ability to report on tumour presence/purity.

Archival FFPE tissue blocks were acquired for the two primary melanomas. From the 2003 scalp primary, two regions were sampled and submitted for WES. This primary tumour with higher risk features (that is, Breslow thickness of 4 mm) was deemed to be the likely source

of metastatic seeding and its *BRAF V600E* molecular profile was consistent with the diagnostic liver biopsy. Insufficient DNA was extracted from the 2008 primary tumour for WES. DNA from two core biopsy samples from the 2015 liver biopsy were also submitted for WES. Unfortunately, due to low purity, all these archival FFPE tissue samples were excluded from further analysis, including the primary tumour.

Genomic features

The tumour mutational burden in this case is 112nsSNVs, or 5.4 mutations/Mb (Table 12 in **3.3.1**), the latter being lower than the mean TMB reported for cutaneous melanomas in the TCGA cohort (16.8 mutations/Mb).[2] The clonal mutation proportion is 58%. The dominant clonal mutational signature is related to UV-induced damage (Signature 7; Figure 71 below), consistent with a sun-exposed primary cutaneous site.

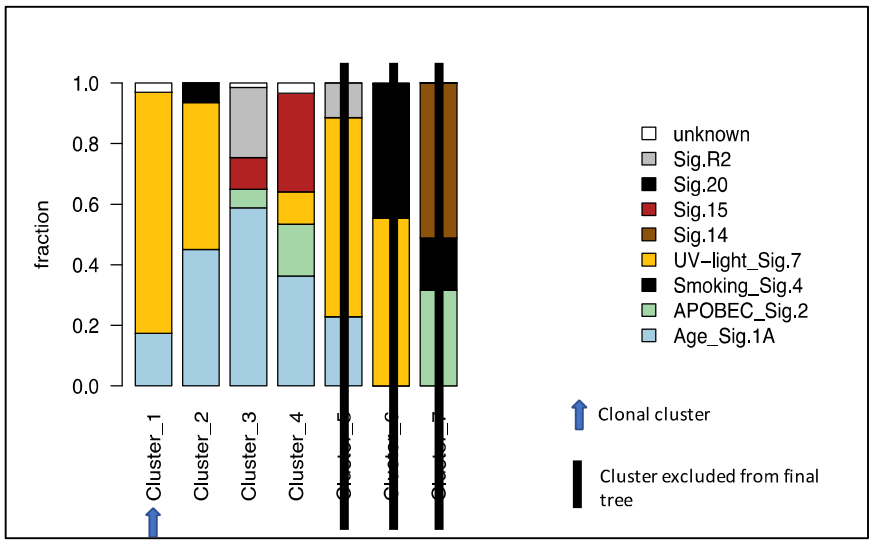

Figure 71 Mutational signature analysis for PEA005
Mutational signatures are based on Pyclone clustering of mutations for creation of phylogenetic trees, with the clonal cluster representing the ubiquitous mutations. Cluster 1 is the clonal cluster. Clusters 2, 3 and 4 had insufficient SNVs (that is, ≥50 mutations) for reliable signature analysis. Clusters 5, 6 and 7 were excluded from the final tree.

The median computationally derived ploidy across the metastatic sites in PEA005 is 2.58 (see Table 13 in **Section 3.3.3**). Six of the eight sites appear to have undergone whole genome doubling (brain: BR_4, BR_5, BR_7, BR_12, BR_13 and lung: LU_1_R1), with one region (LU_1_R1) characterised by two rounds of WGD. Region 2 of lung metastasis 1 (LU_1_R2) and brain metastasis 8 (BR_8) do not appear genome-doubled. The FISH-estimated ploidy does not entirely reflect the bioinformatic-estimated ploidy (Figure 72). For LU_1_R1 (M17),

the FISH-estimated modal ploidy estimate is 3 (range 2–4); whereas the bioinformatic estimate is 4.06. For BR_7 (M7) the modal ploidy estimate by FISH is 4; whereas the computationally derived estimate is 2.61.

The median WGII across metastases is 0.49 (see Table 13 in **Section 3.3.3**), close to the median for the cutaneous/MUP cases in this cohort (0.44). Region 1 of lung metastasis 1 (LU_1_R1), the sample that has undergone two rounds of WGD, has the highest WGII score at 0.69.

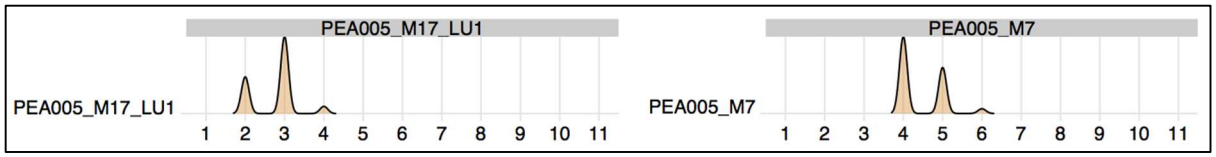

Figure 72 Corrected ploidy estimates of PEA005 samples analysed by FISH
*The x axis denotes the total probe count for each chromosome (see **Section 3.3.3**) and the y axis denotes the relative frequency.*
NB: M17 = LU_1_R1 and M7 = BR_7.

Driver alterations

In the context of the known pathogenic germline *CDKN2A* mutation,[1] clonal somatic copy number loss of chromosome 9 (harbouring *CDKN2A*) is evident across the profiled metastases in this case. This is consistent with the Knudsen two-hit hypothesis for tumour suppressor gene inactivation.[3]

Alterations in *CDKN2A*, located in the 9p21 locus, are the most common inherited melanoma predisposition, occurring in 20% of familial melanoma.[4] The gene encodes two proteins which have vital roles in regulating progress through the cell cycle: 1) p16INK4A which binds to and inhibits CDK4, activating the retinoblastoma protein (RB) family thereby promoting cell cycle arrest in G1, and 2) p14ARF which acts via the p53 pathway, facilitating cell cycle arrest and apoptosis.[5]

There is a clonal driver mutation in BRAF V600E, as well as a CIITA G10E mutation, a tumour suppressor gene encoding a protein involved in antigen presentation (Figure 73).[6] *CIITA* resides on chromosome 16p13 and copy number loss was noted here in one sample (BR_5_R1). No subclonal driver mutations are noted.

The majority of SCNAs are subclonal. Clonal arm-level driver SCNAs[2] include a gain in 7q, as well as losses of 5q, 6q, Chr 9, 11p, and Chr 18 (Figure 74). Clonal driver cytoband

SCNAs (according to GISTIC analysis of TCGA data) include amplifications in 1p12, 1q44, 1q21.3, 5p15.33 and losses in 1p36.31, 1p22.1, 4q34.3, 4p16.3, 8p23.3, 10q26.3 and 19p13.3 (Figure 75). At gene level, clonal loss is noted in *NF1* (Figure 76). Copy number alterations in relevant driver genes (for example, *CDKN2A* on 9p, *MET* on 7q and *NOTCH2* on 1p12)[2,7] occur as a result of cytoband- or arm-level changes.

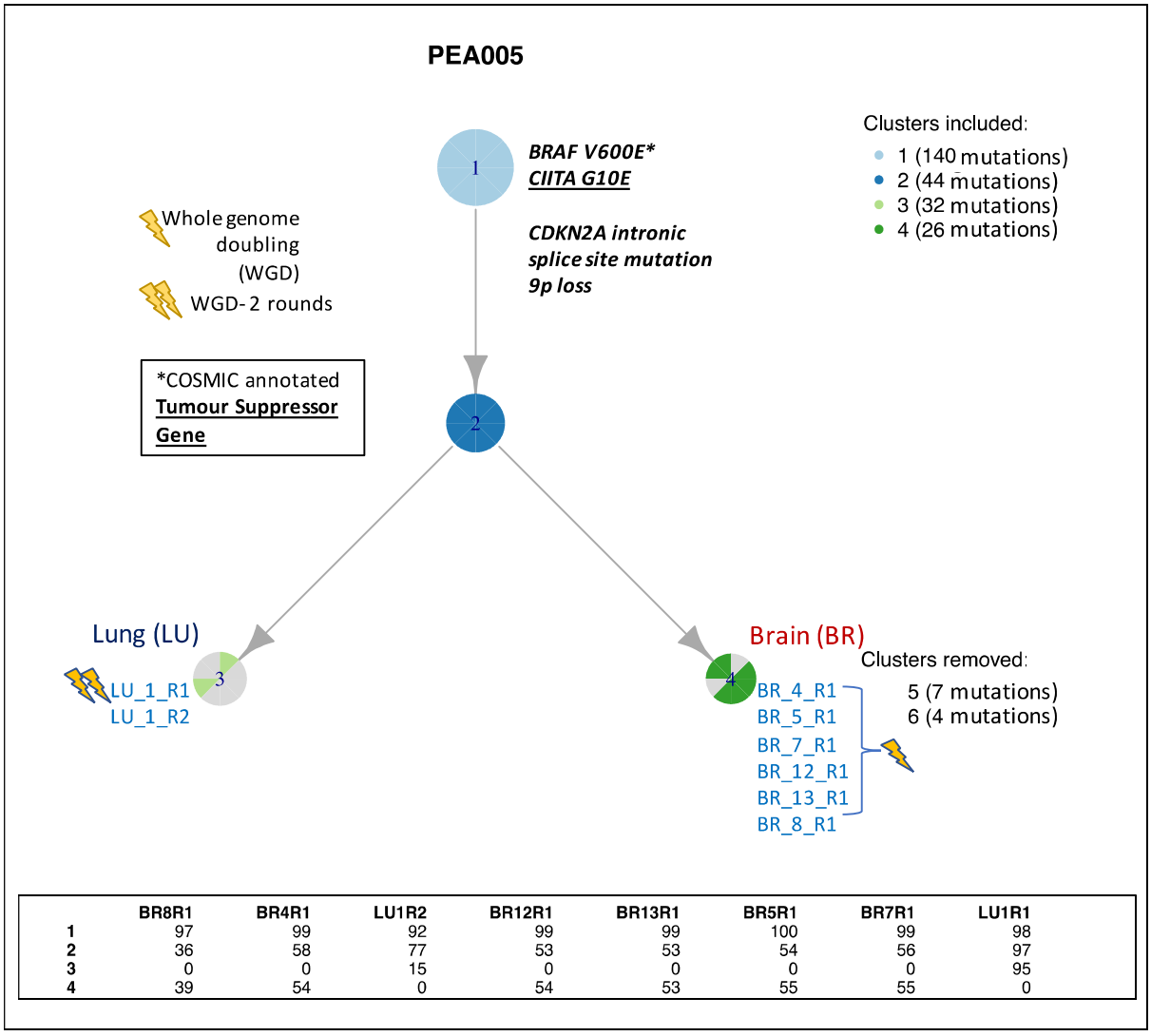

	BR8R1	BR4R1	LU1R2	BR12R1	BR13R1	BR5R1	BR7R1	LU1R1
1	97	99	92	99	99	100	99	98
2	36	58	77	53	53	54	56	97
3	0	0	15	0	0	0	0	95
4	39	54	0	54	53	55	55	0

Figure 73 Phylogenetic tree for PEA005
The clonal cluster of shared mutations (Cluster 1) sits at the trunk of the tree. Driver mutations belonging to each cluster are annotated. The cancer cell fraction (CCF) of each cluster per metastatic site is detailed in the table beneath the tree.

Evolution and metastatic seeding patterns

In this case inferring the mode of metastatic seeding is more challenging in the absence of primary tumour profiling, as one cannot directly reference the clonal composition of the primary in relation to the metastatic sites. Analysis of the clonal composition of metastatic

sites on its own, however, can provide insights into the seeding trajectories. In this case there are two clusters shared by all metastases – the first is clonal at all sites (Cluster 1) and the second (Cluster 2) is subclonal (that is, CCFs ≥15% from the CCF of the clonal cluster) in all regions except for lung metastasis 1 Region 1 (LU_1_R1) in which it is clonal. In addition, there are clusters private to each metastatic organ (but shared across samples in these organs) that lead to branching of the phylogenetic tree: Cluster 3 is seen only in the lung metastatic regions, and Cluster 4 only in the brain.

One may hypothesise that both Clusters 1 and 2 arose in the primary tumour given they both have a mutational signature consistent with UV damage (Signature 7), noting, however, that the mutational signature in Cluster 2 needs to be interpreted with caution as the cluster contains only 44 SNVs (≥50 required for confidence in mutational signature interpretation). There are two possible modes of primary to metastatic seeding: 1) monoclonal seeding from the primary tumour with a clone harbouring Clusters 1+2, with the development of Clusters 3 and four outside of the primary; and 2) polyclonal seeding from the primary tumour, with the assumption that Clusters 3 and/or 4 also developed as subclones in the primary tumour.

All metastatic regions except one (lung metastasis Region 1, LU_1_R1) in this case appear polyclonal by virtue of their CCFs, giving weight to the polyclonal seeding scenario. In the case of the lung metastasis (LU_1), which has two sampled regions, a clone containing Clusters 1+2+3 from Region 2 (which is polyclonal) may have clonally expanded at Region 1 (as Region 1 is monoclonal).

Whole genome doubling appears to have occurred as a subclonal event in this case in Region 1 of the lung metastasis (LU_1_R1), as well as in five of the six brain regions (BR_4, BR_5, BR_7, BR_12, BR_13). As these regions sit on different branches of the tree, this is an example of convergent evolution. In the case of lung metastasis Region 1, it is possible that WGD may have driven the clonal expansion mentioned above.

In keeping with the mutational clustering analysis, the copy number profiles of most brain metastases were shared (Figure 74, Figure 75 and Figure 76). Brain metastasis 8 (BR_8) was an outlier as the only brain metastasis *not* noted to have undergone WGD and had fewer arm-level gains and losses than the other brain samples. However, in the two regions of lung metastasis 1 (LU_1) there was intra-metastatic heterogeneity in SCNAs, suggestive of CIN. Region 1 (LU_1_R1) displayed more arm-level driver gains than Region 2 (LU_1_R2; that

is, at 1q, 7p, 13q and 20q; Figure 74), but Region 2 displayed more driver arm-level losses (that is, at Chr 10, 11q, 13q and 17p; Figure 74).

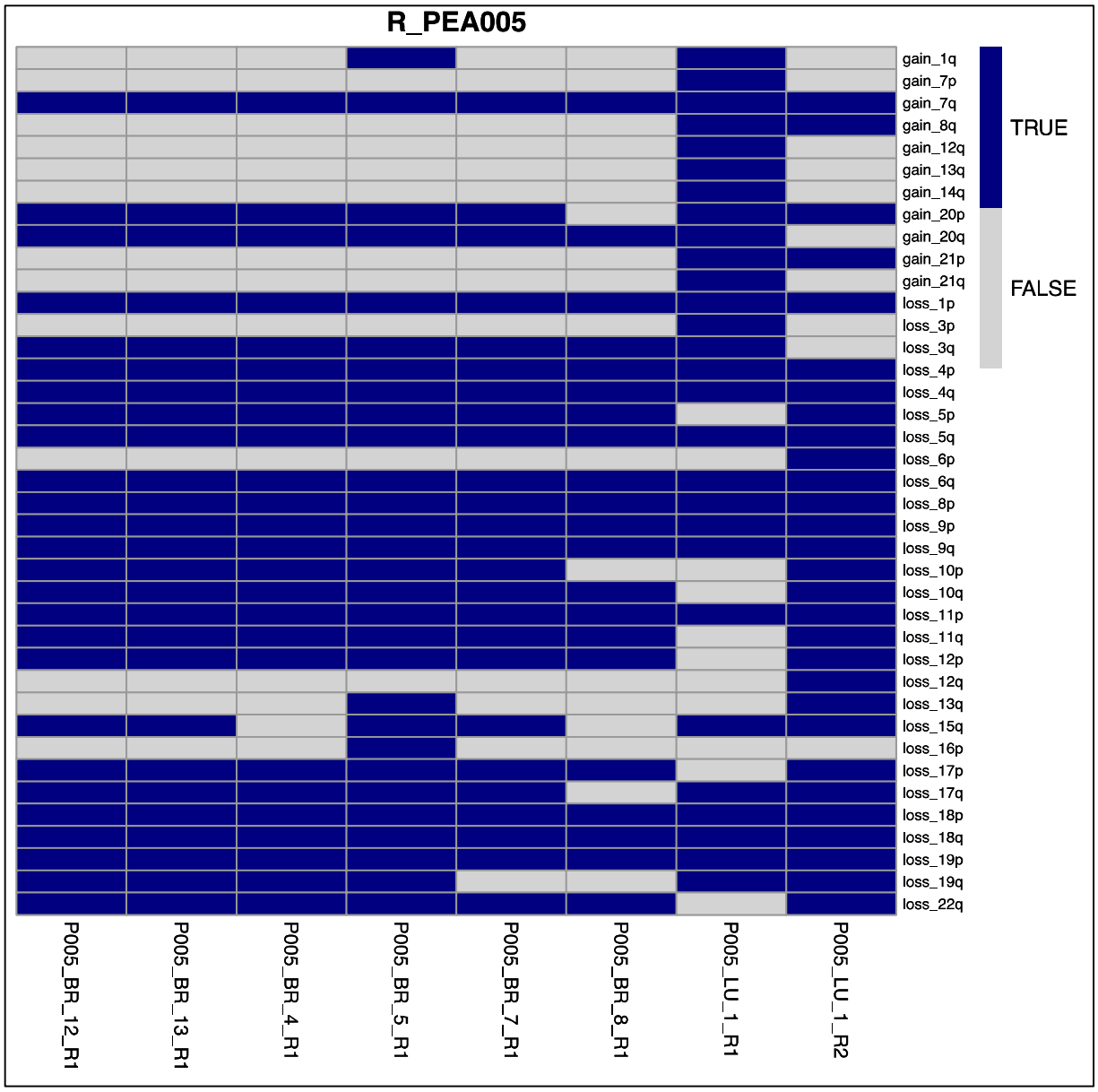

Figure 74 Chromosomal arm-level losses and gains
Blue squares indicate whether there was loss or gain of at least one copy of the chromosome arm relative to the mean ploidy of all samples.

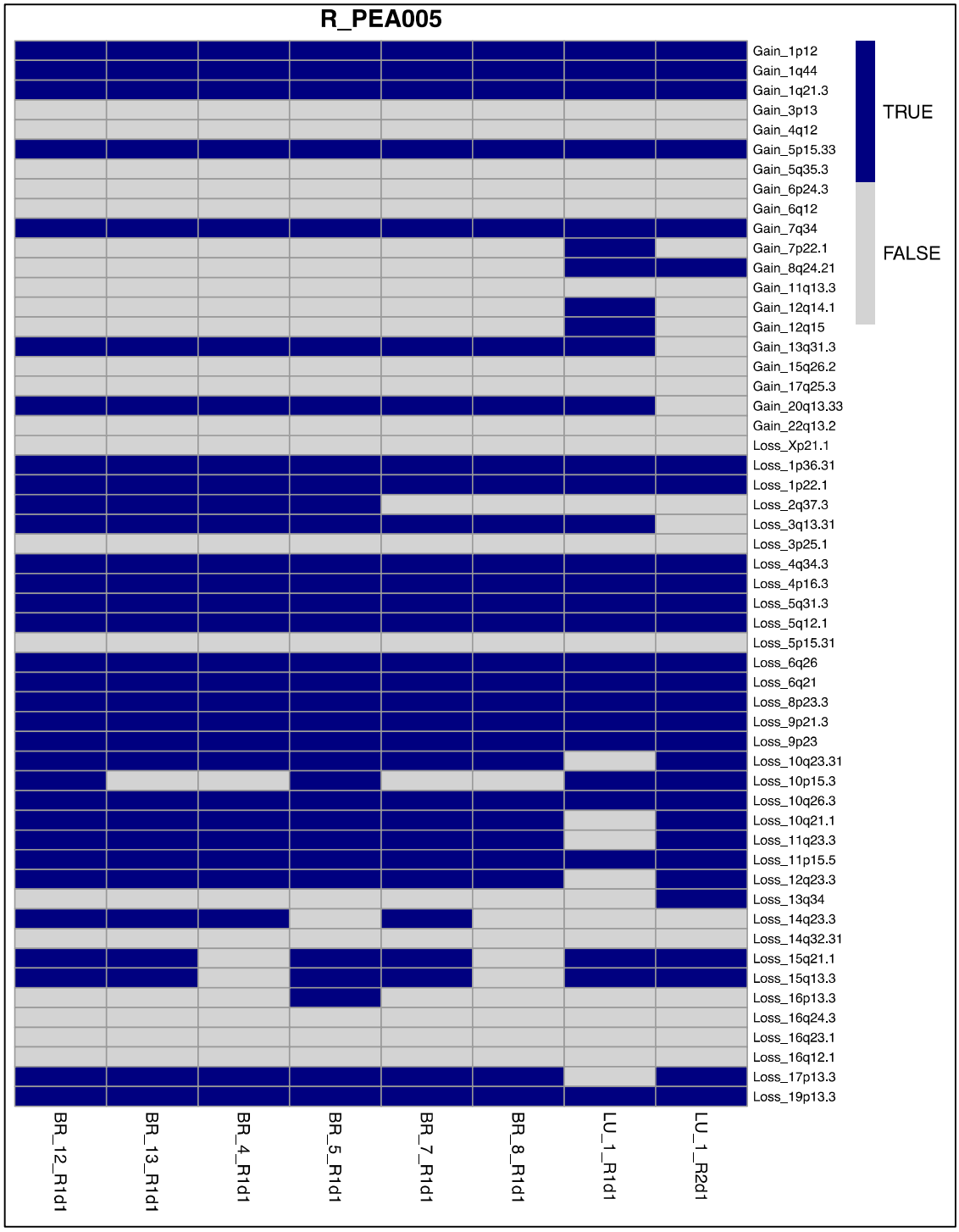

Figure 75 Cutaneous melanoma driver cytoband gains and losses
Annotated cytobands are melanoma driver regions determined by a GISTIC analysis of TCGA data.[2] Blue squares indicate whether there was loss or gain of at least one copy of the cytoband relative to the mean ploidy of all samples.

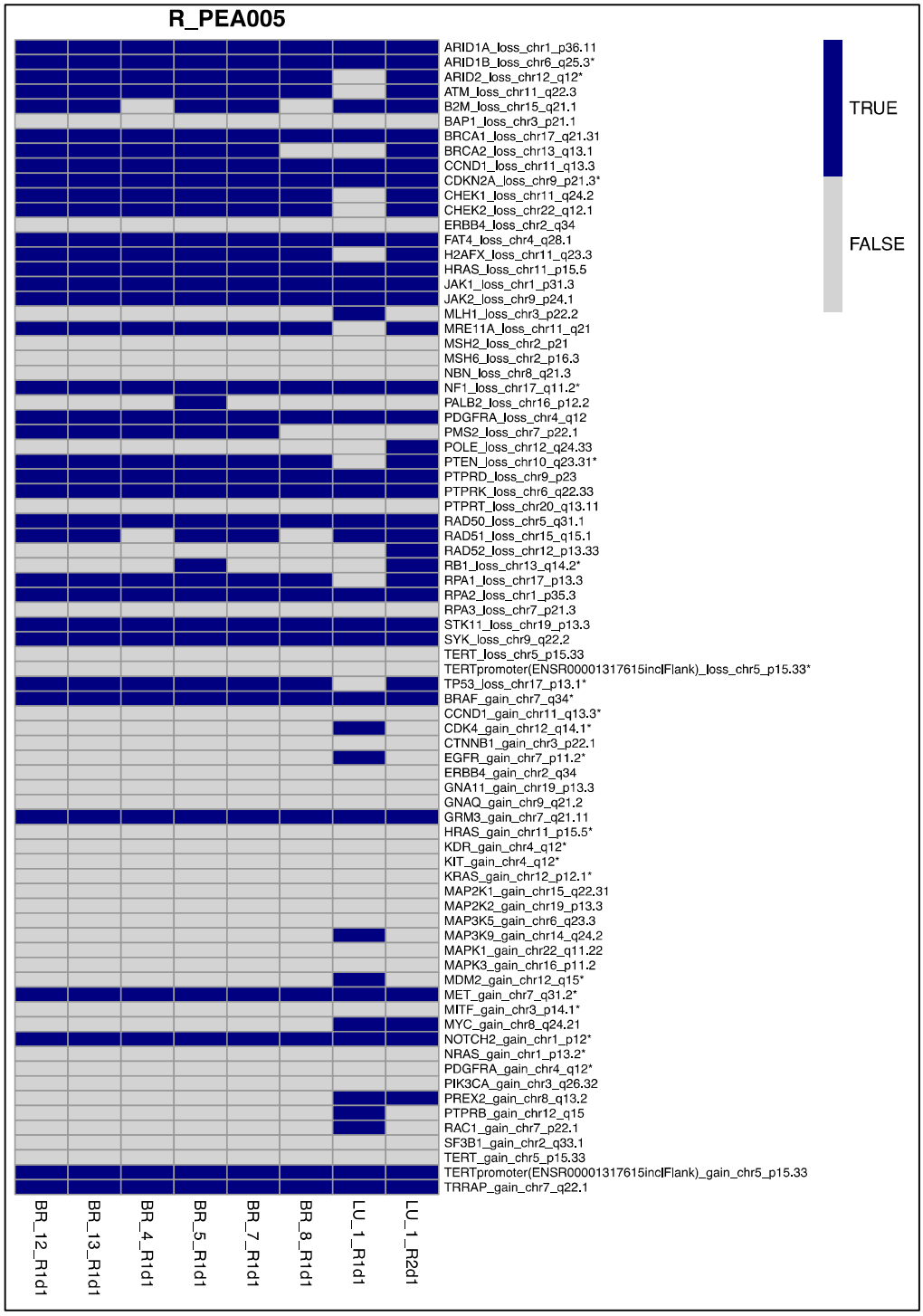

Figure 76 Driver gene gains and losses
Genes with an asterisk (*) are noted driver genes in the TCGA and Hayward et al. data sets.[2,7] *Blue squares indicate whether there was loss or gain of at least one copy of the gene relative to the mean ploidy of all samples.*

Genomic mechanisms of treatment resistance

In this case treatment resistance to dabrafenib emerged after nine months on therapy. Progression was noted on pembrolizumab after four cycles, suggesting refractory disease to anti-PD-1 monotherapy, but then a response was observed with combination ipi+nivo,

followed by a progression-free interval of 10 months. There are no mutations specifically associated with resistance to targeted or immune checkpoint therapies in the profiled tumour sites (lung and brain) in this case.

There is a clonal mutation in *CIITA*, a global regulator for expression of genes involved in antigen presentation.[6] Specifically, it encodes a transactivator of MHC Class II genes. However, it seems unlikely that this mutation would have had a functional impact on antigen presentation and immune checkpoint response in this case, given that there is no corresponding somatic copy number loss at 16p13, except in brain metastasis 5 (BR_5_R1). Also, the DECIPHER tool[9] suggests that it is unlikely to display haploinsufficiency (HI index 69.47%; 0–10% ranking supports haplosufficiency).

Although progressive disease occurred on pembrolizumab monotherapy, a partial response was seen with combination ipi+nivo. A retrospective analysis by Helgadottir et al. suggests a higher overall response rate to immune checkpoint therapy in *CDKN2A* germline carriers.[10] Of the 3/19 *CDKN2A* germline mutation carriers who received ipi+nivo, two had a CR and one had PD, although the small numbers of cases limit the ability to generalise. They also looked at melanoma samples in four publicly available datasets harbouring somatic *CDKN2A* mutations and found these to have a significantly higher number of total mutations in 1461 cancer genes relative to wild-type melanomas, postulating that the higher TMB may underlie improved ICI responses, as has been previously shown.[11] However, the TMB in PEA005 is lower than the median reported from analysis of the overall TCGA cohort (5.36 versus 16.8 mutations/Mb). The response to combination ipi+nivo after progression on pembrolizumab may arise from the distinct mechanism of action of combination anti-CTLA4 and anti-PD-1 relative to anti-PD-1 alone.[12]

Case summary

In patient PEA005 the most likely mode of primary tumour to metastatic dissemination is polyclonal, supported by the majority of metastases being polyclonal in their composition. The origin of the clones seeding the metastases is challenging to infer in the absence of primary tumour profiling. In this case, profiled metastatic regions only represent a small proportion of involved metastatic sites over the course of disease progression and are biased to treatment resistant sites. Subclonal WGD is noted as a parallel event in the lung and brain, suggestive of selection and convergent evolution.

In this case, the estimation of ploidy using FISH was not consistent with the bioinformatically-derived solutions. There is no clear explanation for this. Although somatic copy number loss of 15q was evident in both of the samples profiled by FISH (and a chromosome 15 centromeric probe was used), in theory this should have led to an underestimation of ploidy in both samples; whereas an underestimation was only noted in the lung metastasis. This highlights the challenges of using interphase FISH, particularly in the context of differing nuclear sizes that may arise with increasing ploidy (see **Materials and Methods Section 2.10** and **Section 3.3.3** on FISH analysis). Repeating FISH on these samples as well as including a greater range of samples for analysis from this case will be important to help reconcile this discrepancy.

References for PEA005

1. Harland M, Mistry S, Bishop DT, et al. A deep intronic mutation in CDKN2A is associated with disease in a subset of melanoma pedigrees. *Hum Mol Genet* 10: 2679–86, 2001.
2. Cancer Genome Atlas N: Genomic Classification of Cutaneous Melanoma. *Cell* 161: 1681–96, 2015.
3. Knudson AG, Jr., Meadows AT, Nichols WW, et al. Chromosomal deletion and retinoblastoma. *N Engl J Med* 295: 1120–3, 1976.
4. Aoude LG, Wadt KA, Pritchard AL, et al. Genetics of familial melanoma: 20 years after CDKN2A. Pigment *Cell Melanoma Res* 28: 148–60, 2015.
5. Potrony M, Badenas C, Aguilera P, et al. Update in genetic susceptibility in melanoma. *Ann Transl Med* 3: 210, 2015.
6. Chang CH, Flavell RA: Class II transactivator regulates the expression of multiple genes involved in antigen presentation. J Exp Med 181: 765–7, 1995.
7. Hayward NK, Wilmott JS, Waddell N, et al. Whole-genome landscapes of major melanoma subtypes. *Nature* 545: 175–180, 2017.
8. Long GV, Stroyakovskiy D, Gogas H, et al. Dabrafenib and trametinib versus dabrafenib and placebo for Val600 BRAF-mutant melanoma: a multicentre, double-blind, phase 3 randomised controlled trial. *Lancet* 386: 444–51, 2015.
9. Decipher. https://decipher.sanger.ac.uk/info/haploinsufficiency Sanger Institute, 2020.
10. Helgadottir H, Ghiorzo P, van Doorn R, et al. Efficacy of novel immunotherapy regimens in patients with metastatic melanoma with germline CDKN2A mutations. *J Med Genet*, 2018.
11. Snyder A, Wolchok JD, Chan TA: Genetic basis for clinical response to CTLA-4 blockade. *N Engl J Med* 372: 783, 2015.
12. Wei SC, Anang NAS, Sharma R, et al. Combination anti-CTLA-4 plus anti-PD-1 checkpoint blockade utilizes cellular mechanisms partially distinct from monotherapies. *Proc Natl Acad Sci USA* 116: 22699–22709, 2019.

Case study 8: PEA009

Clinical summary

Patient PEA009 was an 84 year old man diagnosed with a primary melanoma of the left ear in 1996. In March 2016 he relapsed with metastatic disease involving the sternum and spine. A sternal biopsy was molecularly profiled and was *BRAF* and *NRAS* wildtype. The melanoma relapse was preceded by R-CHOP biochemotherapy for diffuse large B cell lymphoma in 2010. He underwent palliative radiotherapy to the thoracic spine and then commenced on pembrolizumab monotherapy in June 2016. Unfortunately restaging after four cycles in August 2016 revealed progressive disease in the lumbar spine (treated with further radiotherapy), and an asymptomatic brain metastasis. Pembrolizumab was recommenced in December 2016 and on further progression with multiple brain metastases in March 2017, whole brain radiotherapy was administered and systemic treatment ceased. Despite the progressive disease in the brain (usually associated with a short survival) and cessation of systemic therapy, PEA009 lived for another 17 months. He died in August 2018. Figure 77 outlines the timeline of events.

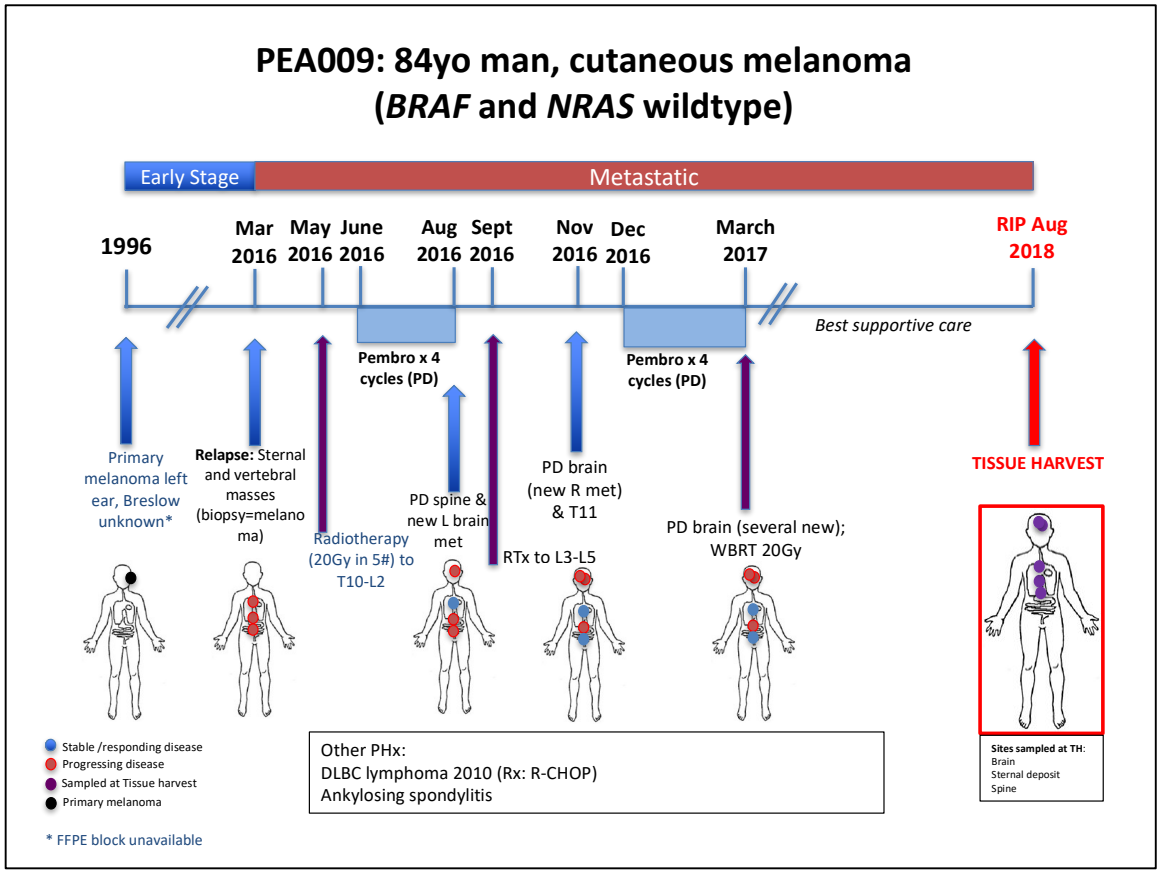

Figure 77 Timeline of treatment and disease response in PEA009
Best overall RECIST response is included in brackets for each line of treatment (CR: complete response; PR: partial response; SD: stable disease; PD: progressive disease). Pembro: pembrolizumab; Gy: Gray (unit of radiotherapy); #: fractions of radiotherapy; L: left; R: right.

Tissue harvest (TH) sampling and quality control considerations

There were nine metastatic regions sampled at the tissue harvest (from eight metastases in the brain, spine and sternal deposits) and all were submitted for panel sequencing (see **Materials and Methods Section 2.7 Melanoma gene panel development**). In 3/9 regions, panel sequencing failed due to low purity (two regions from a right occipital brain metastasis and a lumbar spine tumour sample) and in 1/9 insufficient DNA for sequencing was purified from the thoracic spine lesion. Subsequent review of the corresponding H&E slides did not reveal tumour in these samples. Five samples were submitted for WES on the basis of successful sequencing using the melanoma gene panel. No other visceral metastases or novel sites of disease were noted at the TH in this case, suggesting the disease had been relatively stable for the 18 months of life post end of treatment. Unfortunately, there was no available archival tumour for this case (the primary tumour from 1996 was not able to be sourced and there was insufficient remaining DNA extracted from the sternal biopsy performed at metastatic relapse to submit for sequencing).

Genomic features

The overall tumour mutational burden for this case is high (1222 nsSNVs, 64.7 mutations/Mb), but still within the realm of cutaneous melanoma as reported by the TCGA (median 16.8 mutations/Mb;[1] see Table 12 in **Section 3.3.1**). The clonal mutation proportion is 99%. There is a dominant signature of UV-induced damage (Signature 7; Figure 78) in the clonal cluster, consistent with a primary melanoma of the ear that had high sun exposure.

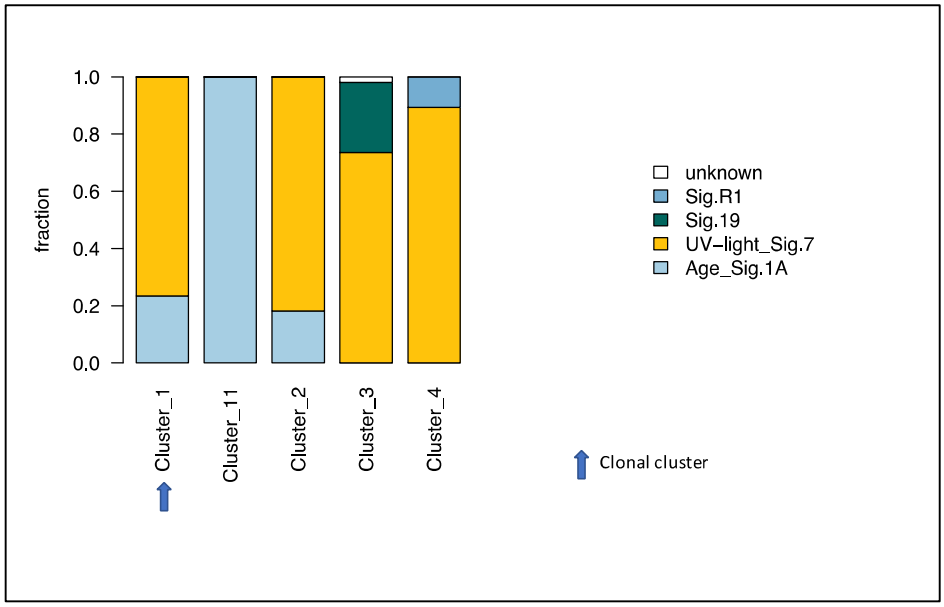

Figure 78 Mutational signature analysis in PEA009
Mutational signatures are based on Pyclone clustering of mutations for creation of phylogenetic trees, with the clonal cluster representing the ubiquitous mutations. Cluster 1 is the clonal cluster. Clusters 2, 3 & 4 were merged with Cluster 1 in final tree; Cluster 11 did not have sufficient SNVs for reliable signature analysis.

The samples all appear diploid by computational methods (median ploidy 2.08; see Table 13 in **Section 3.3.3**), and this is consistent with the FISH-derived mode ploidy (see Figure 79). The samples from this case have the lowest median WGII relative to the other cutaneous melanoma (and MUP) cases (PEA009 median 0.17; range 0.16–0.23 versus sun-exposed/MUP cohort median 0.44 (range 0.14–0.79)).

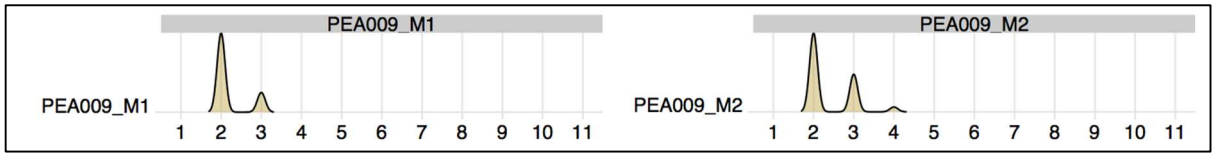

Figure 79 Corrected ploidy estimates of PEA009 samples analysed by FISH
*The x axis denotes the total probe count for each chromosome (see **Section 3.3.3**) and the y axis denotes the relative frequency.*

Driver alterations

Exome analysis of the five profiled regions reveals a clonal *NRAS Q61L* mutation. This is inconsistent with the diagnostic molecular profiling at Stage IV diagnosis, on which there was no *NRAS* mutation evident; however, this was likely a false negative result. In addition to the *NRAS* mutation, there are a number of clonal variants in putative driver genes meeting criteria for driver status, but these specific variants are not reported in COSMIC (see Figure 80): *ARID1A, PTPRC, PTPRD, XPC, IKZF1, ABL1, DDB2, GRIN2A and PALB2*. Given the high background mutation rate, the likelihood of passenger mutations in driver genes is higher than in other cases. There are two mutations in *XPC (p.V681L* and *p.H682Y*), located on chromosome 3p, the gene encoding the protein xeroderma pigmentosum complementation group C, a component of the nucleotide excision repair pathway. There was no corresponding arm-level somatic copy number loss of 3p, but whether smaller cytoband or gene-level losses could have led to LOH requires a more detailed SCNA analysis. *GRIN2A* is one of the 20 most commonly mutated genes in melanoma[2] and encodes a glutamate (N-methyl-(D)-aspartic acid (NMDA)) receptor subunit. In this case, the alteration is not one of the recurrent alterations previously described as putative drivers in melanoma.[3]

Relative to other cases, there are very few SCNAs in PEA009 (consistent with its low WGII) and the vast majority of SCNAs are clonal across the five metastases. There are clonal arm-level gains in 6p and 22q and losses in noted in 9p and 10q, all deemed putative driver events[1] (Figure 81). In addition, driver cytoband regions were gained at 8q24, and lost at 15q13 (Figure 82). There were no gene-level amplifications or deletions of note beyond those contained within the larger-scale alterations discussed (Figure 83).

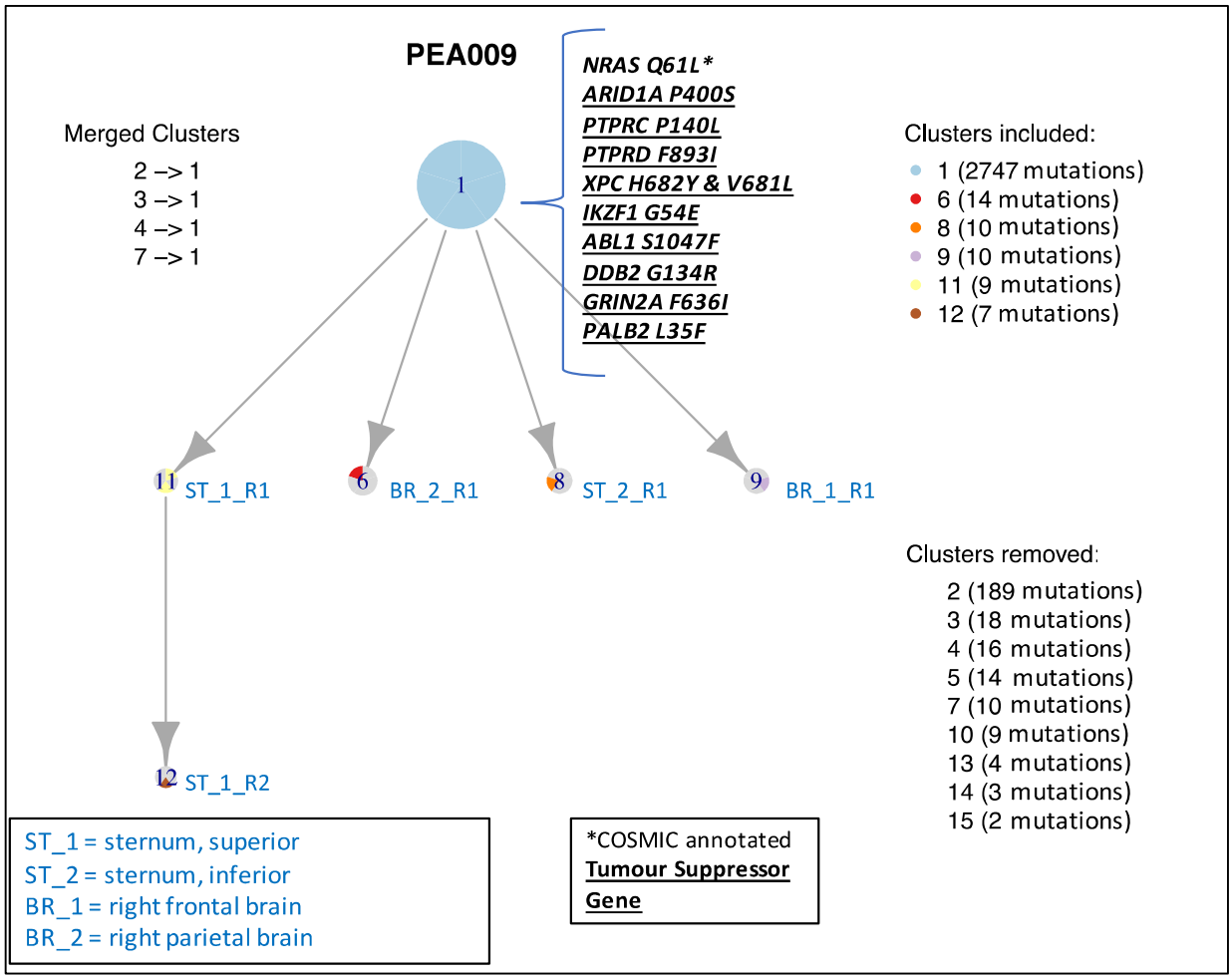

clusterID	BR_2_R1d1	ST_2_R1d1	ST_1_R2d1	BR_1_R1d1	ST_1_R1d1
1	99	98	99	98	99
6	86	0	0	0	0
8	0	94	0	0	0
9	0	0	0	96	0
11	0	0	98	0	97
12	0	0	98	0	0

Figure 80 Phylogenetic tree for PEA009
The clonal cluster of shared mutations (Cluster 1) sits at the trunk of the tree. Driver mutations belonging to each cluster are annotated.

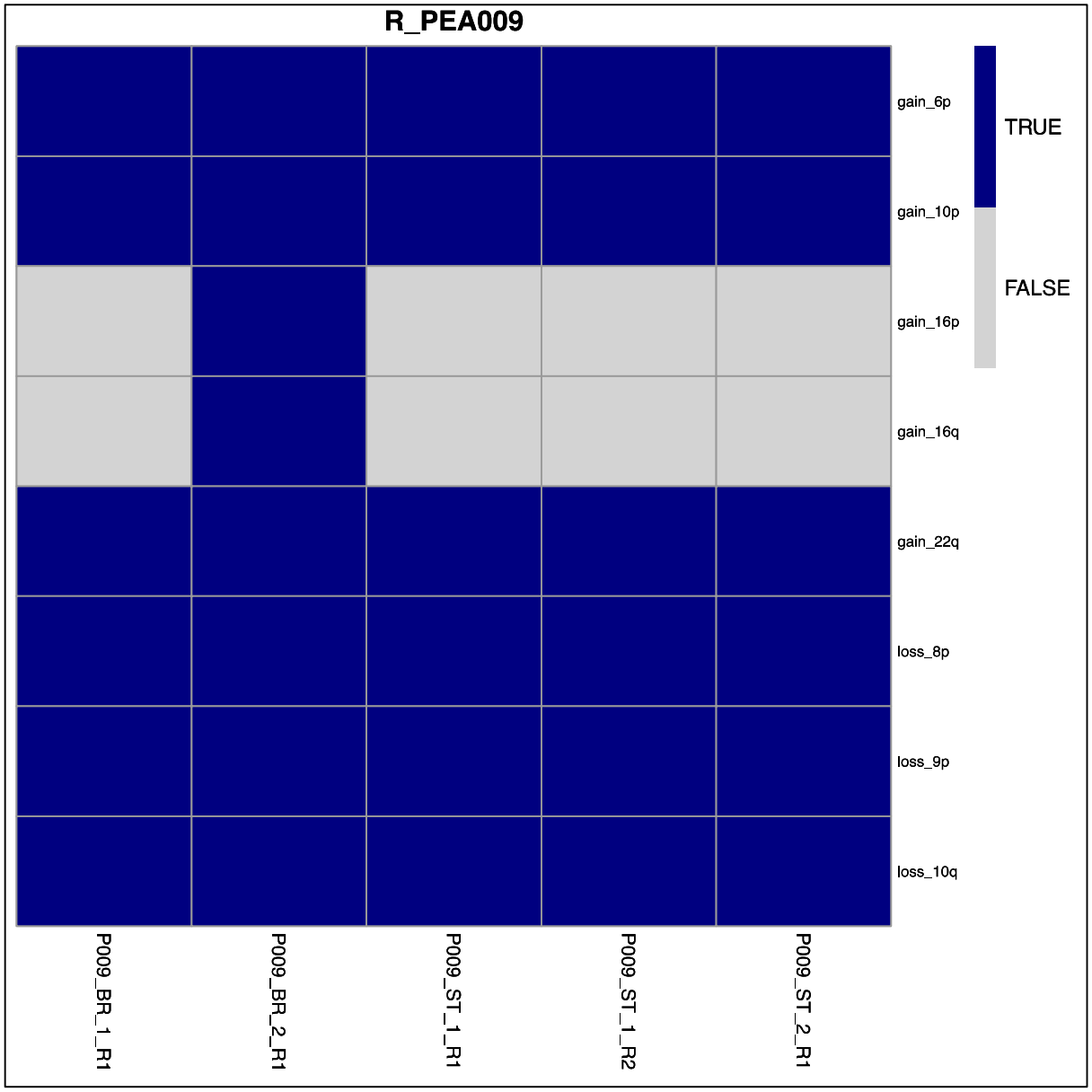

Figure 81 Chromosomal arm-level losses and gains
Blue squares indicate whether there was loss or gain of at least one copy of the chromosome arm relative to the mean ploidy of all samples.

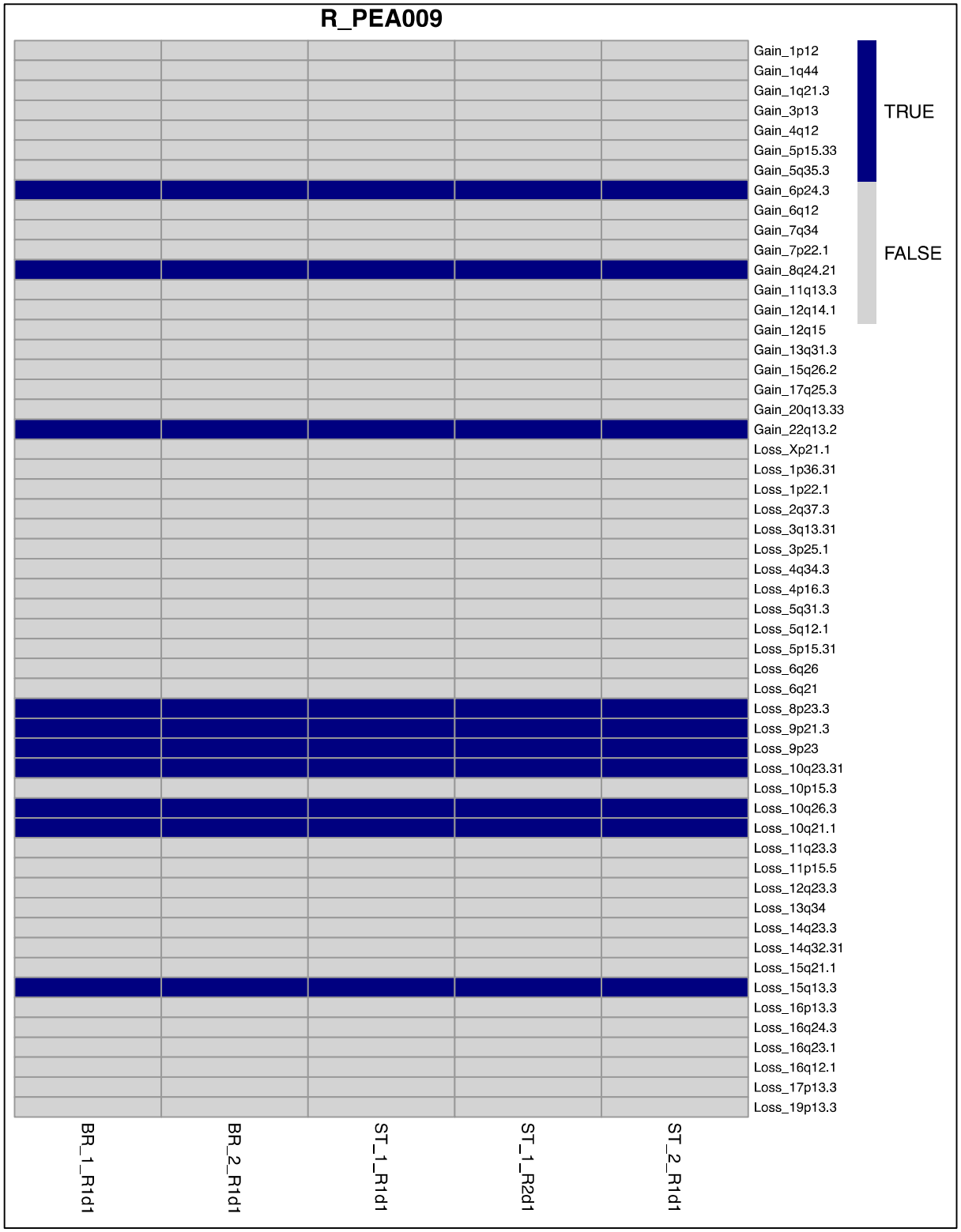

Figure 82 Cutaneous melanoma driver cytoband gains and losses
Annotated cytobands are melanoma driver regions determined by a GISTIC analysis of cutaneous melanoma TCGA data.[1] Blue squares indicate whether there was loss or gain of at least one copy of the cytoband relative to the mean ploidy of all samples.

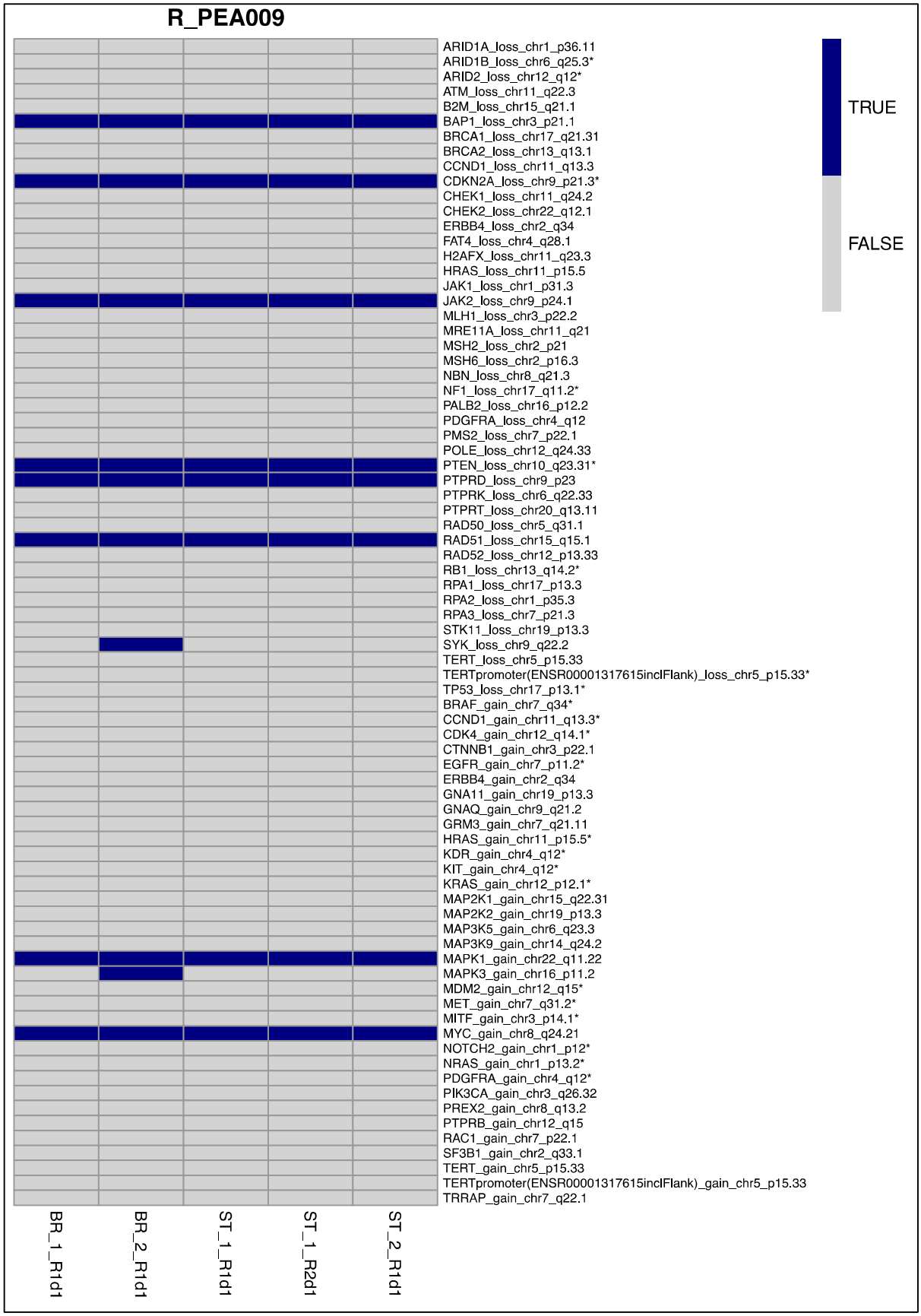

Figure 83 Driver gene gains and losses

Genes with an asterisk (*) are noted driver genes in the TCGA and Hayward data sets.[1,4] Blue squares indicate whether there was loss or gain of at least one copy of the gene relative to the mean ploidy of all samples.

Evolution and seeding patterns

The phylogenetic tree for PEA009 is represented in Figure 80. This case contains a very long trunk (2747 clonal mutations in Cluster 1) with relatively short branches (7–14 mutations across remaining clusters). Although there is no primary tumour available for reference, the dominant UV signature in this clonal cluster is consistent with the history of a sun-exposed primary tumour.

The metastases themselves appear monoclonal, with CCFs for each cluster approaching 100%. Ongoing neutral evolution in each metastatic site most likely accounts for the small number of private mutations (grouped in private clusters) in each region, in the absence of any notable driver mutations. While in general the absence of primary tumour profiling for comparative purposes makes inferencing of seeding patterns very challenging, in this case monoclonal seeding is most likely given the lack of intermetastatic heterogeneity (99% clonal mutations).

Genomic mechanisms of treatment resistance

PEA009 received pembrolizumab as their only line of systemic therapy and there are no definite genomic markers of resistance to anti-PD-1 therapy in this case. There is a clonal mutation in JAK1 p.S961L but the particular variant did not meet the criteria for a 'driver alteration' (see **Materials and Methods Section 2.11 Bioinformatic analyses of sequencing data**). This mutation is located in the protein kinase domain,[5] but there is no associated copy number loss of JAK1. There is also evidence of clonal copy number loss at the JAK2 locus. As discussed in PEA017 and PEA023, both JAK1 and JAK2 are predicted to be susceptible to haploinsufficiency according to the DECIPHER tool.[6] The functional relevance of these alterations in this case is unclear, and IHC and other functional analyses would be required to demonstrate this.

Case summary

The case of PEA009 is interesting in the dissonance between consistent progressive disease on pembrolizumab and the long latency from the third radiologically defined progression event (with multiple brain metastases) until death. There was also a long latency from diagnosis of the primary tumour to metastatic disease. The trigger for development of metastatic disease is unlikely to be genomic given that most mutations are clonal, consistent with acquisition in the primary tumour. The lack of additional sites of disease at tissue

harvest, and the fact that no somatic variants consistent with active tumour could be identified in the thoracic and lumbar spine samples, as well as one of the brain metastases, also highlight the effectiveness of pembrolizumab and radiotherapy at certain sites. An alternative, but less likely explanation, is inaccurate sampling at the tissue harvest. This case highlights how RECIST criteria for progressive disease can fail to correlate with overall survival benefit in the assessment of immune checkpoint inhibitor therapy.

Given the high number of clonal mutations in this case, there may be a large number of tumour associated neoantigens that prompted CD8 T cell recognition, inducing more effective immune surveillance than suggested by progression on scans, and benefiting survival. Whether or not XPC protein loss may have led to an impaired DNA-damage response to account for the high mutational load would require further validation with IHC and functional analyses.

The final anti-cancer treatment in PEA009 was whole brain radiotherapy (WBRT). There is a link between radiation and generation of indel mutations,[7] and indels have been associated with immunogenic neoantigens favouring ICI responses.[8] On closer review, however, there does not appear to be a specific enrichment in indels in the private mutations for BR_2 (3 FS indels) and BR_1 (no FS indels) compared with ST_1 and ST_2 (that is, the non-irradiated sites; 2 FS indels in ST_1; data not shown) that would suggest this as an explanation for a durable response to WBRT.

While genomically the metastases are all monoclonal, and there is very little inter-metastatic heterogeneity, one can see from Figure 77 that the sternal metastasis was stable after treatment with anti-PD-1; whereas the brain metastases were ongoing sites of progression, although likely responsive to WBRT in some way. This demonstrates the limitations of uni-dimensional analyses, and the need for transcriptomic and immune microenvironment profiling in addition to genomics, to understand different patterns of clinical behaviour.

References for PEA009

1. Cancer Genome Atlas N: Genomic Classification of Cutaneous Melanoma. *Cell* 161: 1681–96, 2015.
2. Tate JG, Bamford S, Jubb HC, et al. COSMIC: the Catalogue Of Somatic Mutations In Cancer. *Nucleic Acids Res* 47: D941–D947, 2019.
3. Wei X, Walia V, Lin JC, et al. Exome sequencing identifies GRIN2A as frequently mutated in melanoma. *Nat Genet* 43: 442–6, 2011.
4. Hayward NK, Wilmott JS, Waddell N, et al. Whole-genome landscapes of major melanoma subtypes. *Nature* 545: 175–180, 2017.

5. Eletto D, Burns SO, Angulo I, et al. Biallelic JAK1 mutations in immunodeficient patient with mycobacterial infection. *Nat Commun* 7: 13992, 2016.
6. Firth HV, Richards SM, Bevan AP, et al. DECIPHER: Database of Chromosomal Imbalance and Phenotype in Humans Using Ensembl Resources. *Am J Hum Genet* 84: 524–33, 2009.
7. Adewoye AB, Lindsay SJ, Dubrova YE, et al. The genome-wide effects of ionizing radiation on mutation induction in the mammalian germline. *Nat Commun* 6: 6684, 2015.
8. Turajlic S, Litchfield K, Xu H, et al. Insertion-and-deletion-derived tumour-specific neoantigens and the immunogenic phenotype: a pan-cancer analysis. *Lancet Oncol* 18: 1009–1021, 2017.

Case study 9: PEA012

Clinical summary

Patient PEA012 was a 69 year old man who presented with de novo Stage IV melanoma in June 2015, without any prior history of primary melanoma. Molecular profiling of a lung biopsy revealed a *BRAF V600K* mutation. He was initially treated with ipilimumab+nivolumab but developed significant neurological and hepatic toxicity after one cycle, necessitating high dose corticosteroids. Despite an initial partial response, he developed progressive disease in October 2015 and was commenced on dabrafenib+trametinib. He again experienced a partial response to treatment, however progressed in May 2016. Third-line therapy with another three cycles of combination ipi+nivo was initiated, complicated by colitis requiring further steroid therapy, but resulting in a partial response. Maintenance nivolumab was continued until further progression in January 2017. Vemurafenib + cobimetinib was commenced as fourth line therapy, with a short-lived partial response (three months disease control). He received six cycles of cisplatin and DTIC, resulting in stable disease for eight months, before progression in the brain, liver and left hilum. Sixth-line pembrolizumab, commenced in January 2018, was ceased after two cycles due to substantial multi-site progressive disease. PEA012 died from advanced melanoma in April 2018, 34 months from diagnosis of metastatic disease and after six lines of systemic treatment. The clinical course is summarised in Figure 84.

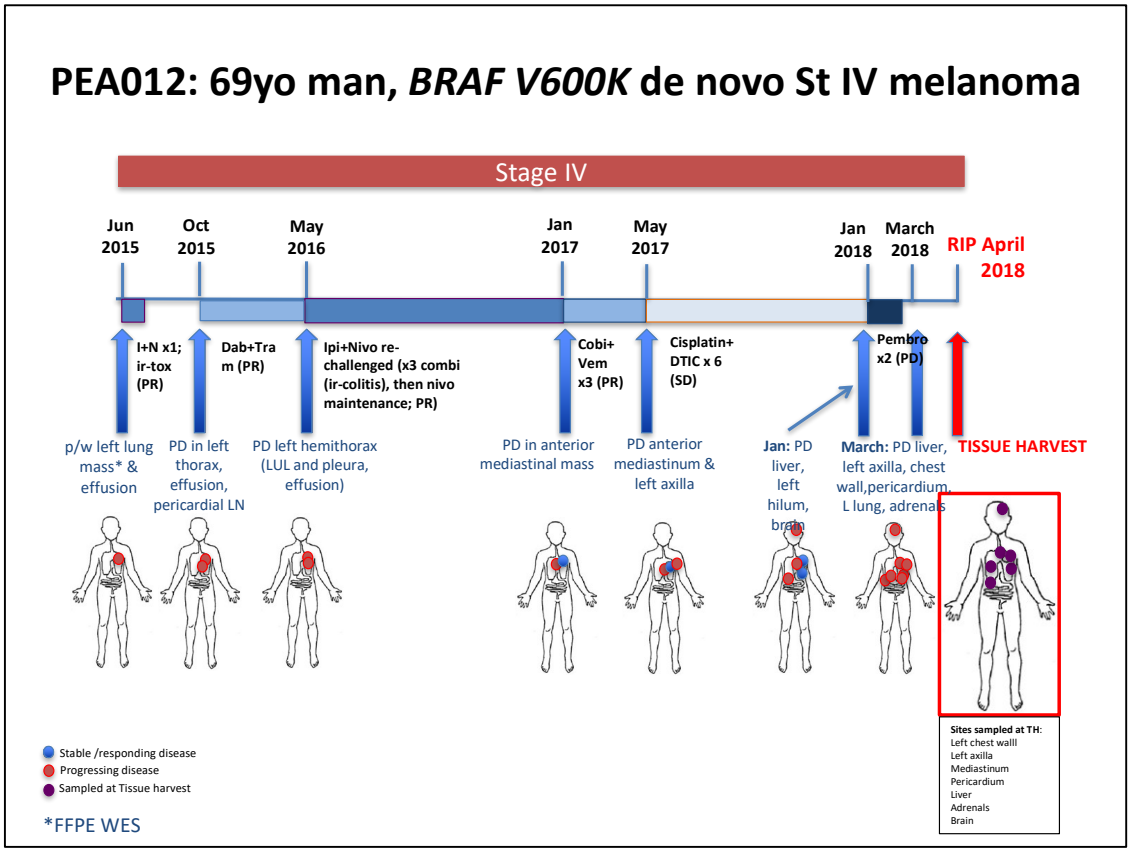

Figure 84 Timeline of clinical events, treatment and disease response in PEA012
Best overall RECIST response is included in brackets for each line of treatment (CR: complete response; PR: partial response; SD: stable disease; PD: progressive disease). p/w: presented with; I+N: ipilimumab and nivolumab; ir-tox: immune-related toxicity; FFPE WES: formalin fixed paraffin embedded sample underwent whole exome sequencing; dab+tram: dabrafenib with trametinib; cobi+vem: cbimetinib with vemurafenib; LN: lymph node; LUL: left upper lobe; combi: combination ipilimumab with nivolumab; nivo: nivolumab; L: left; pembro: pembrolizumab; TH: tissue harvest.

Tissue harvest (TH) sampling and quality control considerations

Fifty-one tumour regions were sampled from 27 metastatic sites at TH, involving the lungs, mediastinum, adrenal glands, liver, brain and chest wall/axilla. Panel sequencing was undertaken on 46 regions, with 41 successfully profiled. Of these, 13 were selected to represent the sites of metastatic disease and successfully profiled using WES. Archival FFPE-derived DNA from the pre-treatment diagnostic lung biopsy was obtained and also submitted for WES. While suitable for variant detection, this sample was of insufficient quality for determination of copy number calling and cancer cell fraction which precluded it from clustering analysis. Nonetheless, the variants from this sample were used to determine which mutations were present prior to and which were acquired after treatment.

Genomic features

A very high TMB is evident in this case, with a total of 2375 nsSNVs or 123 mutations/Mb (see Table 4 in **Section 1.3.1**), the second highest in our cohort according to both parameters. The clonal mutation proportion is 44%. The dominant clonal mutational signature reflects UV-induced damage (Signature 7; Figure 85). In addition a temozolomide-induced signature (Signature 11; consistent with DTIC chemotherapy) was seen in a number of clusters (Figure 85). This is discussed further in the **Evolution and metastatic seeding patterns** section below.

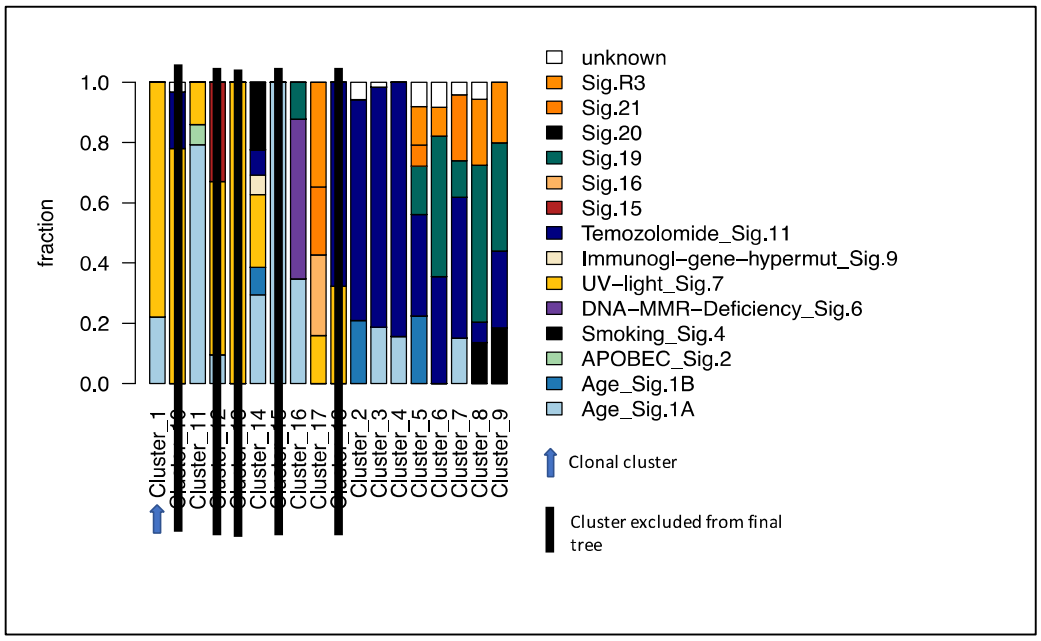

Figure 85 Mutational signature analysis in PEA012
Mutational signatures are based on Pyclone clustering of mutations for creation of phylogenetic trees, with the clonal cluster representing the ubiquitous mutations. Cluster 1 is the clonal cluster (blue arrow). Clusters 1, 2, 3, 4, 5, 6, 7, 8 and 9 contain sufficient SNVs for reliable signature analysis (that is, ≥50).

The median computationally derived ploidy across the metastases sampled at the TH is 2.29 (see Table 12 in **Section 3.3.1**). This is consistent with the FISH-estimated ploidy (see Figure 86). The median WGII score is the second lowest of the cohort at 0.24 (Table 13 in **Section 3.3.3**). No samples appear to have undergone whole genome doubling in this case.

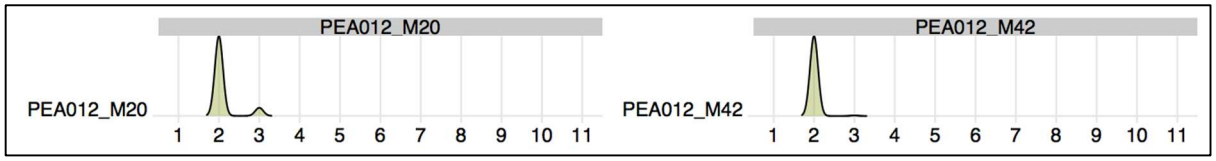

Figure 86 Corrected ploidy estimates of PEA012 samples analysed by FISH
The x axis denotes the total probe count for each chromosome (see ***Section 3.3.3****) and the y axis denotes the relative frequency.*
M20 = ST_4_R5 (soft tissue metastasis 4, Region 5); M42 = LI_10_R1 (liver metastasis 10, Region 1).

Driver alterations

A number of clonal driver mutations are evident in this case (see Figure 87). There are hotspot mutations in *BRAF (V600K*) and *RAC1 (P29S).* In addition, the specific variants in *TPR, ZFHX4 and PTPRT* have all been previously annotated in COSMIC.

Subclonal driver mutations include both *NRAS G13R* and *NRAS Q61H*. Mutations in key tumour suppressor genes such as *TP53 (C106Y)* and *CDKN2A (E149K)* are also evident in some regions (Figure 87). A frameshift deletion in *B2M D96fs* was noted in the brain metastasis (BR_1_R1), as well as the pericardium sample (PC_1_R1) and one of the anterior mediastinal regions (ST_4_R5). None of these subclonal mutations were noted in the treatment-naïve archival metastatic sample, suggesting acquisition in the context of progression on treatment.

Most SCNAs are subclonal in this case. Clonal arm-level driver events include gains in 1q, 6p and chromosome 7 (Figure 88), as well as loss of cytoband 1p22 (Figure 89). No focal driver gene amplifications or deletions are noted (Figure 90).

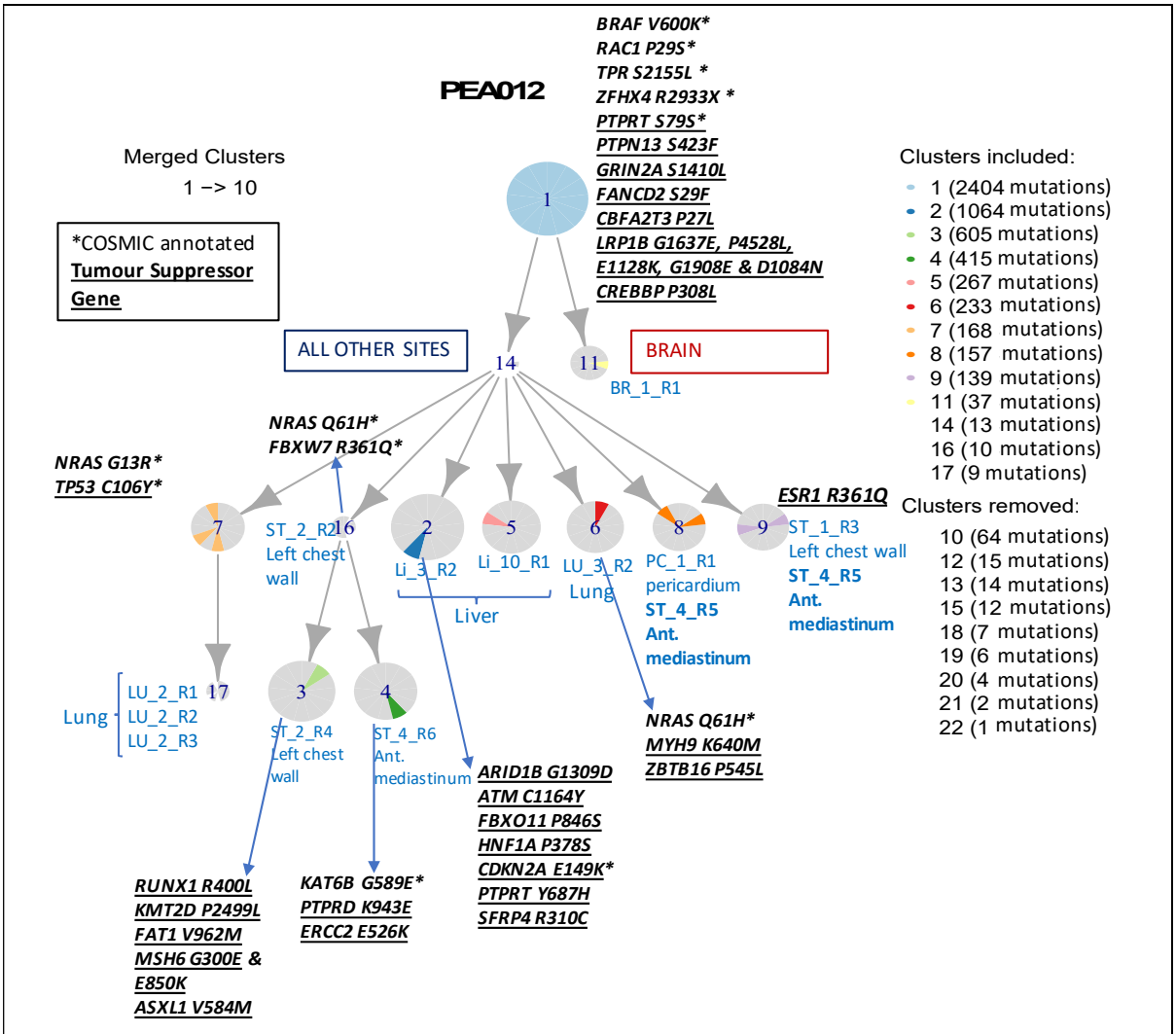

LU_2_R1d1	PC_1_R1d1	LI_10_R1d1	ST_1_R3d1	LU_2_R2d1	LI_3_R2d1	LU_2_R3d1	ST_4_R6d1	ST_2_R2d1	BR_1_R1d1	ST_4_R5d1	ST_2_R4d1	LU_3_R2d1	clusterID
100	100	99	98	100	99	100	100	100	98	100	99	100	**1**
0	0	0	0	0	0	0	0	0	95	0	0	0	**11**
97	94	98	98	99	98	99	99	99	0	99	97	97	**14**
88	0	0	0	94	0	87	0	0	0	0	0	0	**7**
39	0	0	0	16	0	15	0	0	0	0	0	0	**17**
0	0	0	0	0	0	0	94	97	0	0	98	0	**16**
0	0	0	0	0	0	0	0	0	0	0	100	0	**3**
0	0	0	0	0	0	0	100	0	0	0	0	0	**4**
0	0	0	0	0	99	0	0	0	0	0	0	0	**2**
0	0	98	0	0	0	0	0	0	0	0	0	0	**5**
0	0	0	0	0	0	0	0	0	0	0	0	78	**6**
0	83	0	0	0	0	0	0	0	0	53	0	0	**8**
0	0	0	89	0	0	0	0	0	0	15	0	0	**9**

Figure 87 Phylogenetic tree for PEA012
The clonal cluster of shared mutations sits at the trunk of the tree. Driver mutations belonging to each cluster are annotated. The cancer cell fraction (CCF) of each cluster per metastatic site is detailed in the table beneath the tree. ST = soft tissue; Ant. = anterior.

Evolution and seeding patterns

While no primary tumour is available as a point of reference for deciphering the mode of evolution in this case, one can appreciate significant branching of the phylogenetic tree

(Figure 87), with the large subclonal mutation fraction (56%) reflecting substantial intermetastatic heterogeneity.

Even in the absence of a primary tumour, the seeding pattern in this case appears polyclonal. The majority of metastases (liver, lung, soft tissue, pericardium) are seeded by a clone containing Clusters 1+14 as their recent common ancestor, with the exception of the brain metastasis (BR_1_R1), which is seeded by a clone containing Clusters 1+11. Clusters 14 and 11 are on separate branches of the phylogenetic tree, rendering them mutually exclusive.

Based on signature analysis, I hypothesise that two separate clones from a regressed sun-exposed primary tumour seeded distinct anatomical sites. There is a small proportion of Signature 7 (UV induced mutagenesis) in both Cluster 11 and Cluster 14. This supports the notion that the brain was directly seeded from the primary tumour by a clone containing Clusters 1+11, and that a separate primary tumour clone containing Clusters 1+14 went on to seed the other metastatic sites. Mutational signature analysis of Clusters 11 and 14 is not entirely reliable, however, because these clusters contain <50 mutations. An alternative explanation that disregards the interpretation of these signatures is that there was one metastasis-seeding clone that descended from the primary tumour (that is, a monoclonal seeding pattern), with further clonal evolution and branching occurring outside the primary tumour but prior to metastasis formation.

Eight of 13 sampled regions appear monoclonal in their composition; whereas 5/13 appear polyclonal and are further discussed here. In lung metastasis 2 (LU_2, left upper lobe), polyclonal by this definition (Cluster 17, private to this site, CCFs 15–39%) all three sampled regions appear similar. The absence of a driver mutation in Cluster 17 suggests ongoing (neutral) evolution in a group of cells within this metastasis as the most likely explanation. In lung metastasis 3 Region 2 (LU_3_R2), Cluster 6 is private to this site and noted at a CCF of 78%. It contains three putative driver mutations (*NRAS p.Q61H, MYH9* and *ZBTB16*), making selection the likely driver of the clonal expansion (*NRAS p.Q61H* is further discussed below). The third polyclonal region is one of the anterior mediastinal metastases (ST_4_R5), where polyclonal seeding is likely. This sample contains two exclusive clusters (Cluster 8 at 53% CCF and Cluster 9 at 15% CCF), each of which are also present at a different metastatic site on exclusive branches of the phylogenetic tree (Cluster 8 in pericardial metastasis 1 (PC_1_R1) and Cluster 9 in left chest wall metastasis 1 (ST_1_R3)), making inter-metastatic

seeding the probable explanation given that these metastatic sites were linked by confluent disease noted at the tissue harvest.

The presence of two different *NRAS* hot spot mutations at multiple different anatomical sites across different branches of the phylogenetic tree in this case (*NRAS p.G13R* at Cluster 7 and *p.Q61H* at Clusters 6 and 16) is an example of convergent evolution. Acquisition of *NRAS* mutations has been noted as a resistance mechanism to BRAF-targeted monotherapy,[1] as well as BRAF/MEK combinations.[2] In this case, there is clinical evidence of selection for the resistant clones at lung metastasis 2 (LU_2, left upper lobe), lung metastasis 3 (LU_3, left lower lobe), left chest wall/axilla metastasis 2 (ST_2), and in one of the anterior mediastinal soft tissue metastases (ST_4), as these were all sites of disease progression on BRAF/MEK inhibitor therapy.

A temozolomide mutational signature (Signature11) is noted within Clusters 2, 3, 4, 5, 6, 7, 8 and 9, encompassing all sites exposed to DTIC chemotherapy (that is, lung, liver and soft tissue regions). Cluster 11, private to the brain metastasis, did not contain evidence of temozolomide signature (Figure 85), consistent with the clinical picture as the brain was a site of progression after chemotherapy exposure (see Figure 84). As mentioned earlier, with only 37 SNVs in Cluster 11 the mutational signature analysis less reliable, however. The temozolomide-induced mutagenesis may account for the high numbers of subclonal driver alterations associated with these clusters, many of which are private to certain metastatic regions. Similar to reports in gliomas exposed to temozolomide chemotherapy, mutations in genes associated with DNA damage repair are seen, for example, *MSH6* in the left chest wall/axilla soft tissue mass (ST_2_R4, Cluster 3) and *ATM* in liver metastasis 3 (LI_3_R2, Cluster 2).[8]

COSMIC-reported subclonal mutations in the key tumour suppressor genes *TP53* and *CDKN2A* are evident in lung metastasis 2 (LU_2, Cluster 2) and liver metastasis 3 (LI_3_R2, Cluster 7), respectively. These events may have arisen due to DTIC-induced mutagenesis and then been selected for their fitness advantage.

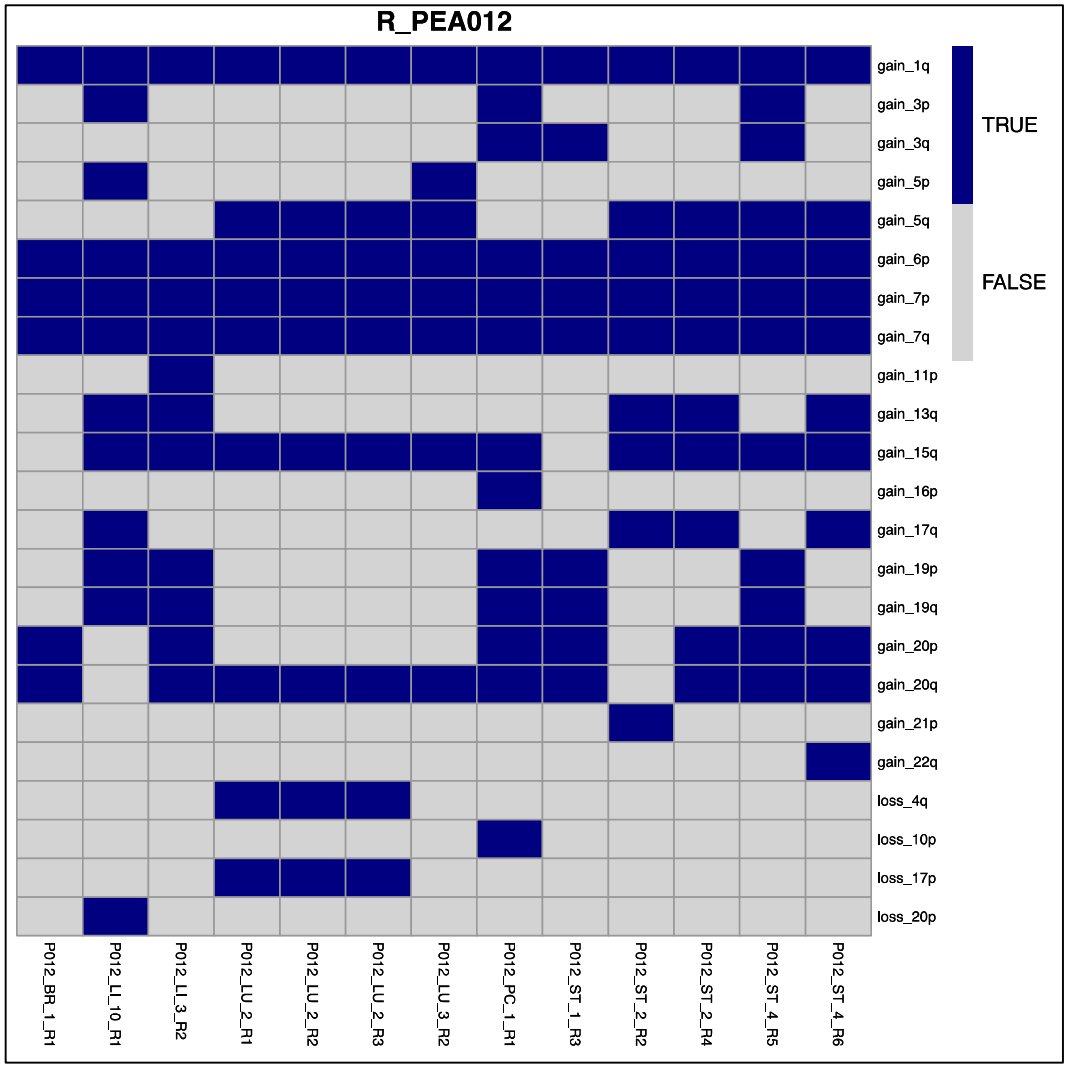

Figure 88 Chromosomal arm-level losses and gains
Blue squares indicate whether there was loss or gain of at least one copy of the chromosome arm relative to the mean ploidy of all samples.

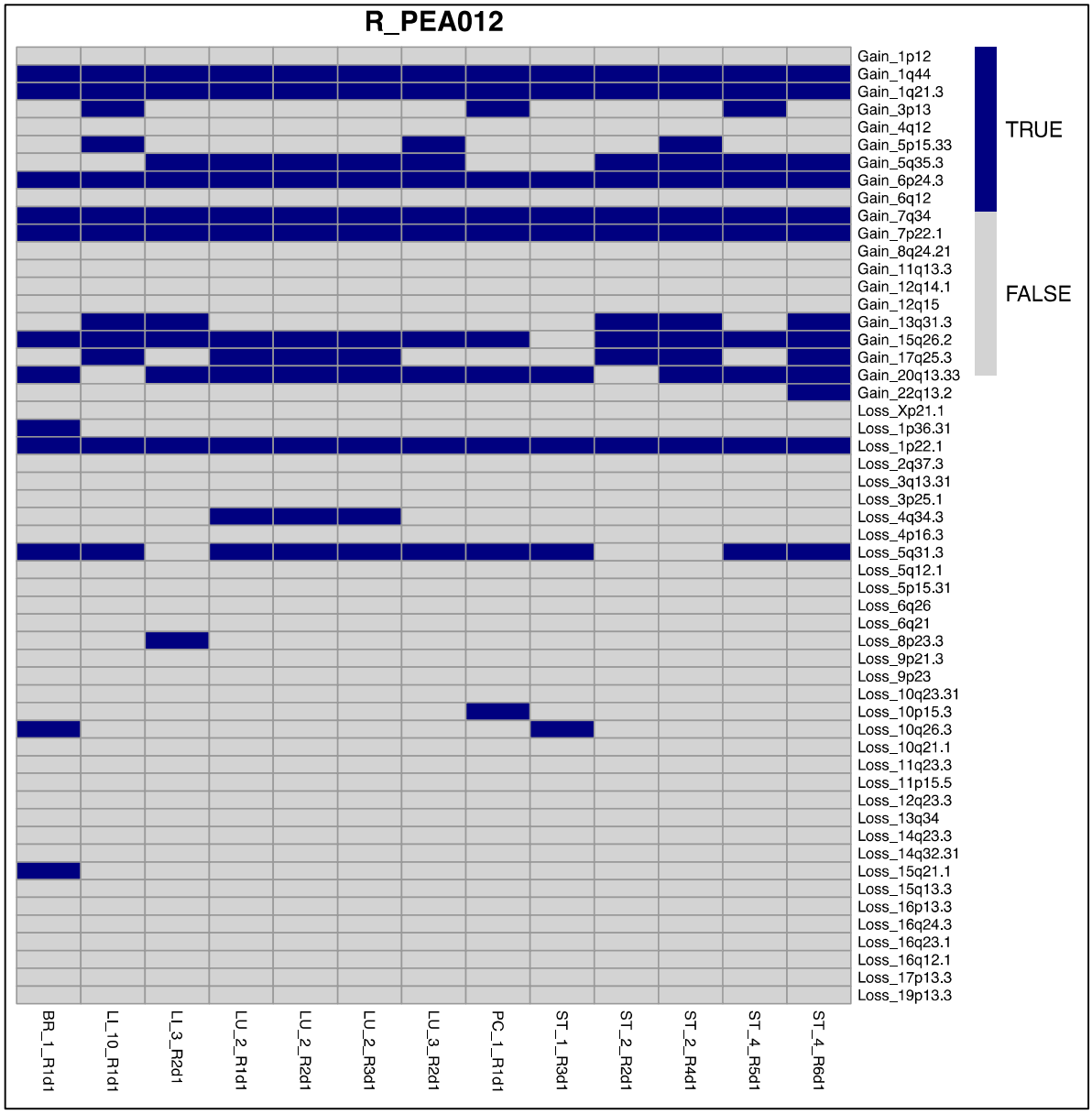

Figure 89 Cutaneous melanoma driver cytoband gains and losses

Annotated cytobands are melanoma driver regions determined by a GISTIC analysis of TCGA data.[3] Blue squares indicate whether there was loss or gain of at least one copy of the cytoband relative to the mean ploidy of all samples.

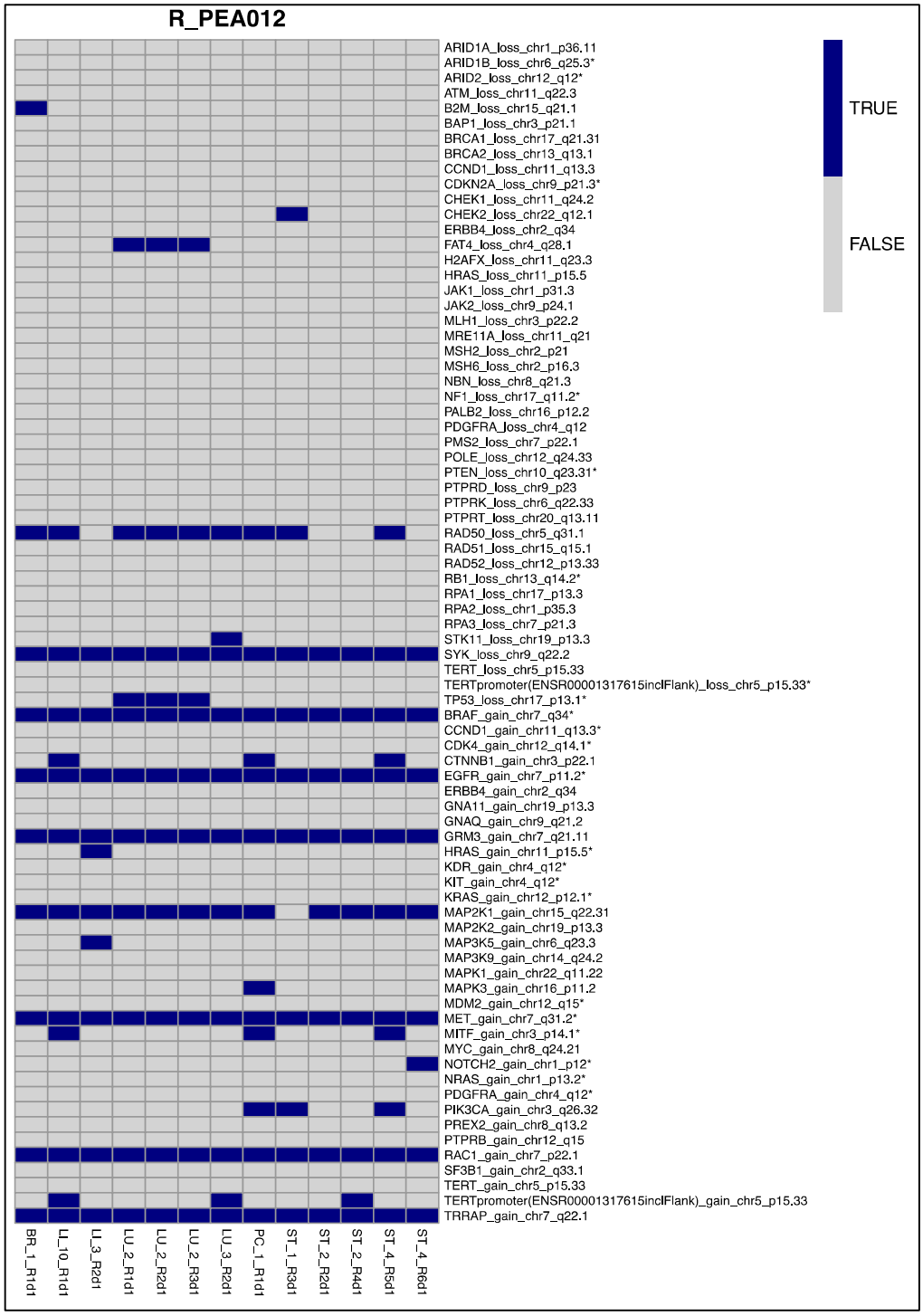

Figure 90 Driver gene gains and losses
Genes with an asterisk (*) are noted driver genes in the TCGA and Hayward data sets.[3,4] Blue squares indicate whether there was loss or gain of at least one copy of the gene relative to the mean ploidy of all samples.

Genomic mechanisms of treatment resistance

Patient PEA012 underwent three lines of immune checkpoint therapy – two rounds of combination ipi+nivo, and then pembrolizumab monotherapy. Although there was a response noted to ipi+nivo on both occasions, progression-free survival (four months and then eight

months) was shorter than the median of 11 months reported in the CM-067 study.[5] The high number of clonal mutations may have increased the probability of immunogenic neoantigens. Ultimately, however, the likely DTIC-induced subclonal mutation burden, and therefore predominance of subclonal neoantigens, may have negatively impacted the response to pembrolizumab as the sixth line of treatment.[6,7] The acquired *B2M D96fs* deletion noted in three regions that progressed late in the course of disease (brain, pericardium and anterior mediastinum) lies within the functional domain of the gene. There was corresponding copy number loss of the 15q21.1 cytoband that harbours *B2M* in the brain (probably leading to LOH given the diploid nature of this case) and this may represent a means of treatment resistance through loss of antigen presentation. Other genomic mechanisms of acquired resistance to immune checkpoint therapy are not evident within the limitations of our analysis.

As already discussed above in the section **Evolution and seeding patterns**, there were two acquired *NRAS* mutations in known hotspots (*G13R* and *Q61H*) across different metastatic sites, both possible mechanisms of resistance to BRAF/MEK inhibition.

Case summary

PEA012 represents a case of *BRAF V600K* mutant melanoma of likely regressed cutaneous primary tumour origin based on the presence of a dominant clonal UV-damage signature. Consistent with this there is a high clonal TMB, with further subclonal contributions to the overall TMB from temozolomide-induced mutagenesis. The profiled regions comprehensively represent the sites of known metastatic disease, including the brain.

The mode of seeding from the primary tumour is most likely polyclonal, contributing to further intermetastatic heterogeneity. Interestingly, the clone seeding the brain – a late clinical event – only shares the clonal cluster of mutations with other sites, raising the possibility of early tumour seeding from the primary with dormancy of the clone, or acquisition of metastatic competence outside the primary tumour akin to a parallel metastatic evolution model (see **Main Introduction Section 1.1.2 Modes of evolution**). Whether the brain TME may have somehow 'protected' this clone from the mutagenic impact of temozolomide is speculative but further exploration of the TME composition using RNAseq and IHC analysis could provide an insight. The majority of metastatic sites are monoclonal, with probable metastasis-to-metastasis seeding at one site in the anterior mediastinum.

As reported in glioblastoma, there appear to be subclonal alterations in genes associated with DNA damage repair, including *MSH6* as well as *ATM,* after exposure to DTIC.[8] If functional, these mutations could have contributed to a hypermutated state, although this has not been confirmed. While the temozolomide-induced mutagenesis in theory may have generated additional neoantigens, in this case there was no response seen to pembrolizumab subsequent to temozolomide treatment, possibly due to the greater proportion of subclonal neoantigens[6,7] and/or presence of non-genomic acquired resistance mechanisms.

References for PEA012

1. Van Allen EM, Wagle N, Sucker A, et al. The genetic landscape of clinical resistance to RAF inhibition in metastatic melanoma. *Cancer Discov* 4: 94–109, 2014.
2. Long GV, Fung C, Menzies AM, et al. Increased MAPK reactivation in early resistance to dabrafenib/trametinib combination therapy of BRAF-mutant metastatic melanoma. *Nat Commun* 5: 5694, 2014.
3. Cancer Genome Atlas N: Genomic Classification of Cutaneous Melanoma. *Cell* 161: 1681–96, 2015.
4. Hayward NK, Wilmott JS, Waddell N, et al. Whole-genome landscapes of major melanoma subtypes. *Nature* 545: 175–180, 2017.
5. Larkin J, Chiarion-Sileni V, Gonzalez R, et al. Combined Nivolumab and Ipilimumab or Monotherapy in Untreated Melanoma. *N Engl J Med* 373: 23–34, 2015.
6. McGranahan N, Furness AJ, Rosenthal R, et al. Clonal neoantigens elicit T cell immunoreactivity and sensitivity to immune checkpoint blockade. *Science* 351: 1463–9, 2016.
7. Wolf Y, Bartok O, Patkar S, et al. UVB-Induced Tumor Heterogeneity Diminishes Immune Response in Melanoma. *Cell* 179: 219–235 e21, 2019.
8. Johnson BE, Mazor T, Hong C, et al. Mutational analysis reveals the origin and therapy-driven evolution of recurrent glioma. *Science* 343: 189–193, 2014.

Case study 10: PEA020

Clinical summary

Patient PEA020 was a 70 year old man who was diagnosed with Stage IV melanoma after presenting with lung metastases and retroperitoneal lymphadenopathy in September 2014. There was no identified primary tumour, but there was a *BRAF V600E* mutation on molecular profiling of a retroperitoneal lymph node biopsy. First-line therapy was initiated with ipilimumab in March 2015 and was complicated by hypophysitis after three cycles, necessitating cortisone replacement. Upon progression in August 2015 second-line nivolumab was administered on the Checkmate-172 study, but in August 2016 this was ceased due to immune-related hepatitis, treated with corticosteroids. In February 2017, progressive disease was confirmed in the peritoneum and brain. The left frontal brain metastasis was resected, with consolidation stereotactic radiosurgery (SRS) given to the resection bed, and definitive SRS to a possible right occipital metastasis. Dabrafenib and trametinib were prescribed as third-line systemic treatment in April 2017, but only continued for one cycle. Despite this, PEA020 survived for another 12 months, dying in May 2018. Figure 91 below outlines the timeline of events.

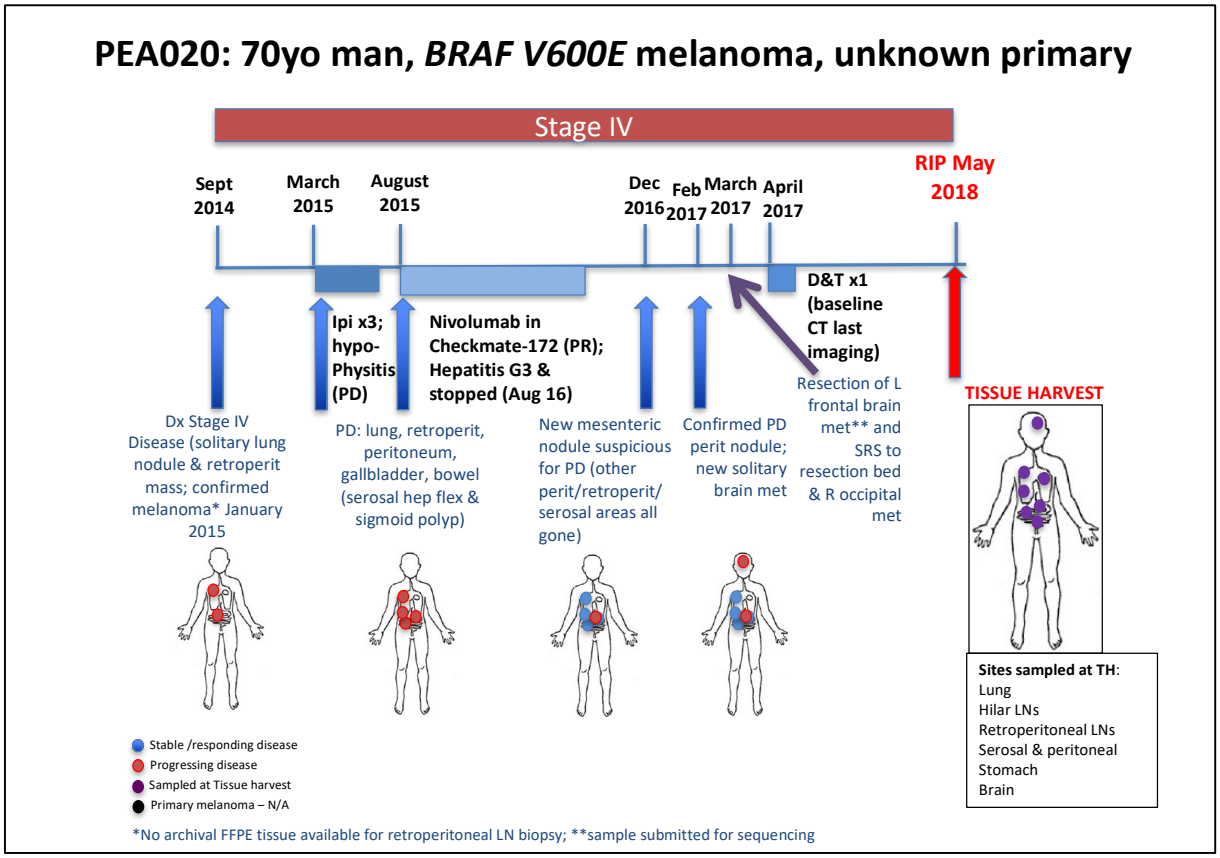

Figure 91 Timeline of clinical events, treatment and disease response in PEA020
Best overall RECIST response is included in brackets for each line of treatment (CR: complete response; PR: partial response; SD: stable disease; PD: progressive disease). Ipi: ipilimumab; D&T: dabrafenib and trametinib; FFPE: formalin fixed paraffin embedded; L: left; R:right; retroperit: retroperitoneal; hep flex: hepatic flexure; peri: peritoneal.

Tissue harvest (TH) sampling and quality control considerations

At the tissue harvest 36 samples were taken from 17 metastatic sites including the small bowel, mesentery, peritoneum, pylorus and lymph nodes, brain and optic nerve. Of these, only 25 were deemed to contain tumour on the basis of Sanger sequencing revealing a *BRAF V600E* mutation. This was concordant with H&E review of tumour content. Ten of these 25 sites were selected for WES to cover the anatomical range of metastases, with one failing QC due to poor tumour purity. DNA purified from archival tissue of the resected left frontal brain metastasis was also submitted for WES.

Genomic features

Tumour mutational burden is relatively high in this case (nine mutations/Mb, 191 nsSNVs; Table 12 in **Section 3.3.1**) with a dominant UV signature (Figure 92), as expected in a melanoma of unknown primary, with a suspected regressed cutaneous primary tumour origin. The clonal mutation proportion is 80%.

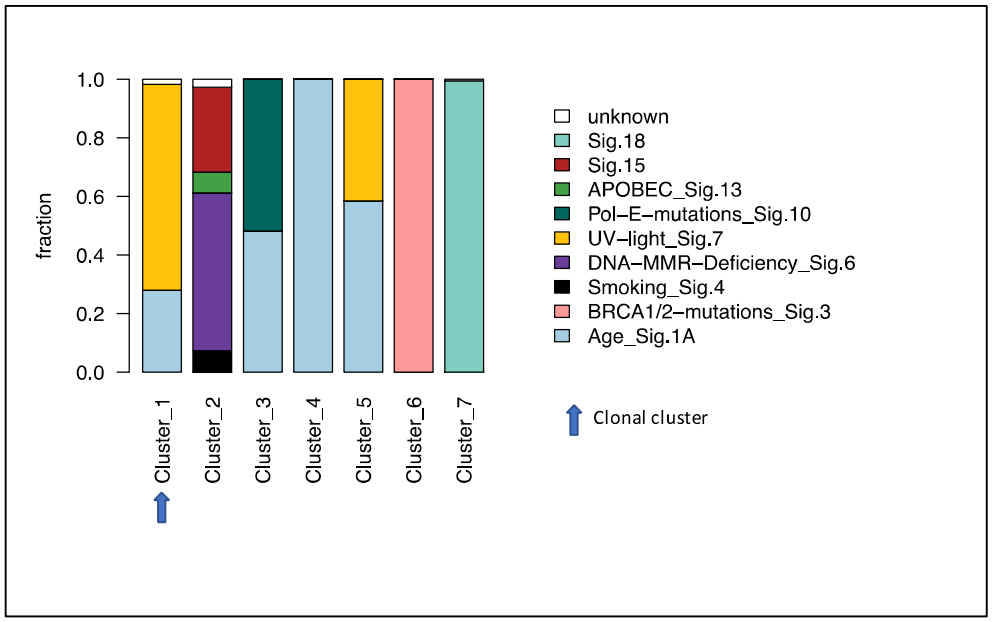

Figure 92 Mutational signature analysis of PEA020
Mutational signatures are based on Pyclone clustering of mutations for creation of phylogenetic trees, with the clonal cluster representing the ubiquitous mutations. Cluster 1 is the clonal cluster and is the only cluster with enough SNVs for reliable signature analysis.

Median computationally derived ploidy is 2.44, less than that estimated by FISH where the mode ploidy is 3 (see Figure 93 below). Only one FISH sample is available for this case, however. Median WGII was 0.45 across the TH metastases (Table 13 in **Section 3.3.3**).

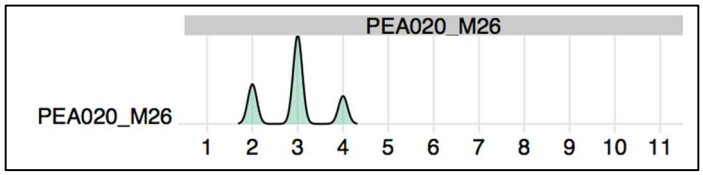

Figure 93 Corrected ploidy estimates of PEA020 samples analysed by FISH
*The x axis denotes the total probe count for each chromosome (see **Section 3.3.3**) and the y axis denotes the relative frequency.*
NB: M26 = ON_1_R1; one sample failed processing.

Melanoma driver alterations

In this case there is a clonal *BRAF V600E* mutation (Figure 94). Clonal copy number gains dominate this case, including whole chromosome gains in chr7 (*BRAF*) and Chr 8, both of which are melanoma driver events[1] (Figure 95). Driver arm-level gains occurred at 6p and 22q as well as loss at 16q (Figure 95). At the driver cytoband level (Figure 96) there was also

clonal loss at 3p25. No gains or losses in driver genes outside of these larger events were noted (Figure 97).

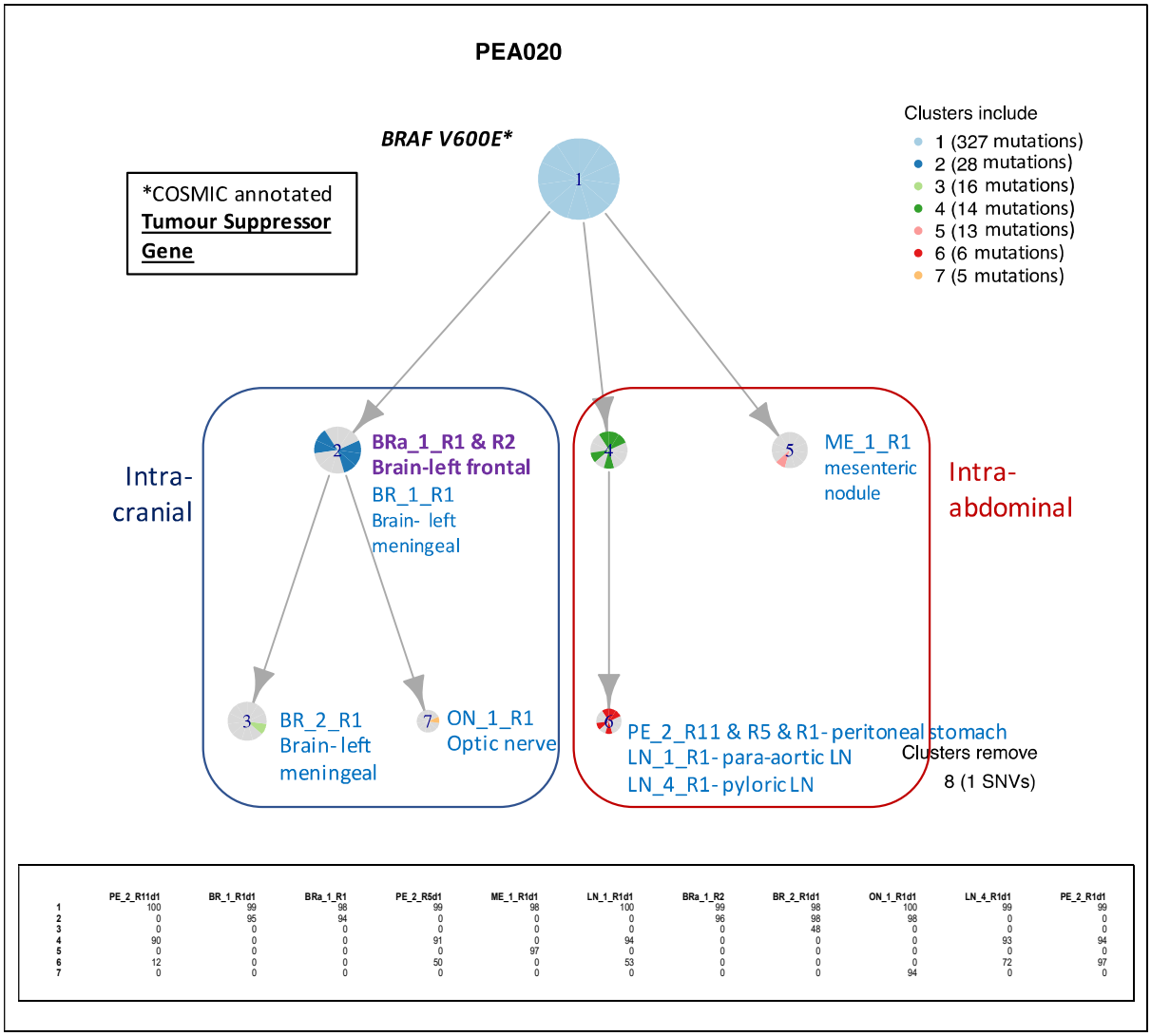

	PE_2_R11d1	BR_1_R1d1	BRa_1_R1	PE_2_R5d1	ME_1_R1d1	LN_1_R1d1	BRa_1_R2	BR_2_R1d1	ON_1_R1d1	LN_4_R1d1	PE_2_R1d1
1	100	99	98	99	98	100	99	98	100	99	99
2	0	95	94	0	0	0	96	98	98	0	0
3	0	0	0	0	0	0	0	48	0	0	0
4	90	0	0	91	0	94	0	0	0	93	94
5	0	0	0	0	97	0	0	0	0	0	0
6	12	0	0	50	0	53	0	0	0	72	97
7	0	0	0	0	0	0	0	0	94	0	0

Figure 94 Phylogenetic tree for PEA020
The clonal cluster of shared mutations sits at the trunk of the tree. Driver mutations belonging to each cluster are annotated. The cancer cell fraction (CCF) of each cluster per metastatic site is detailed in the table beneath the tree.

Evolution and metastatic seeding patterns

The absence of a primary tumour in this case presents a challenge in determining the pattern of seeding. Looking at the phylogenetic tree outlined in Figure 94 above, one may infer a polyclonal pattern of seeding given that clones seeding metastases at distinct anatomical sites have distinct recent common ancestors. For example, the intracranial disease sites seeded by a clone containing Clusters 1+2; whereas for the peritoneal metastasis, para-aortic and pyloric lymph node metastases the seeding clone contains Clusters 1+4+6.

Five of 11 metastatic regions appear polyclonal based on CCF values. In brain metastasis 2 (BR_2) there is a private subclonal cluster (Cluster 3, 48%), most likely due to ongoing evolution at this site in a subset of cells. In the case of Regions 5 and 11 of the peritoneal metastasis (PE_2_R5 & _R11), as well as the para-aortic (LN_1) and pyloric (LN_4) lymph nodes Cluster 6 is subclonal (CCFs 12–72%); whereas in Region 1 of the peritoneal metastasis (PE_2_R1) Cluster 6 is clonal (CCF 97%) making this a monoclonal region. We may infer that PE_2_R1 was seeded by a clone containing Clusters 1+4+6 from one of these other metastatic sites, for example, PE_2_R5 or PE_2_R11. As to why the other sites contain Cluster 6 at a lower (subclonal) CCF, there are several possible scenarios: 1) the cluster originated there; 2) polyclonal migration (seeding) occurred; and 3) a clone containing Cluster 6 migrated there, but did not replace the existing clone.

The SCNA patterns support the clustering analysis in that the intracranial sites appear to share similar gains and losses distinct from the peritoneal, para-aortic and pyloric lymph node metastases (Figure 95 and Figure 96). However, the mesenteric nodule (ME_1_R1) shares some features with the intra-cranial sites, including a gain in Chr 11, suggesting there may have been an early common ancestor in the primary tumour that seeded these sites.

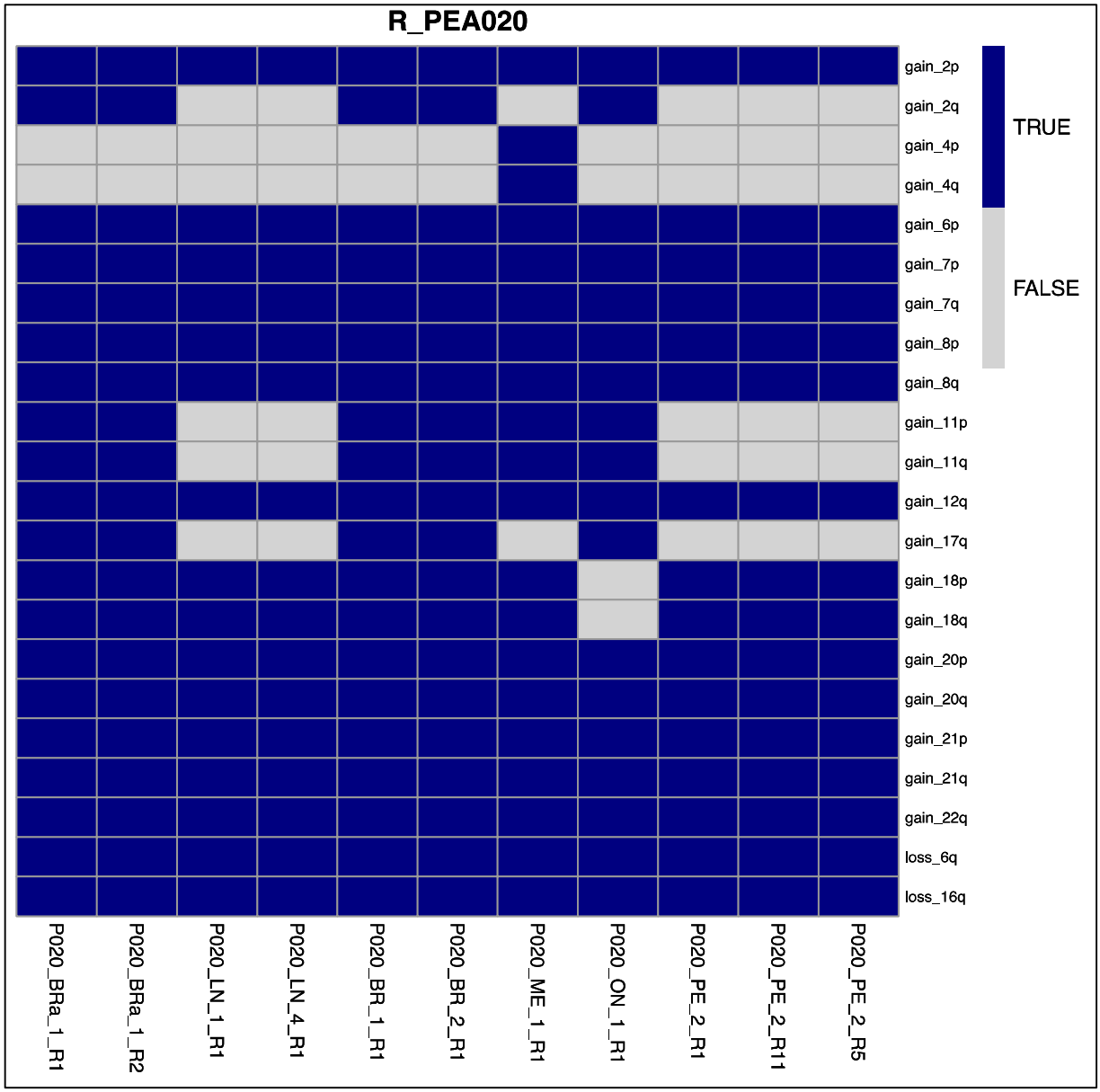

Figure 95 Chromosomal arm-level losses and gains
Blue squares indicate whether there was loss or gain of at least one copy of the chromosome arm relative to the mean ploidy of all samples.

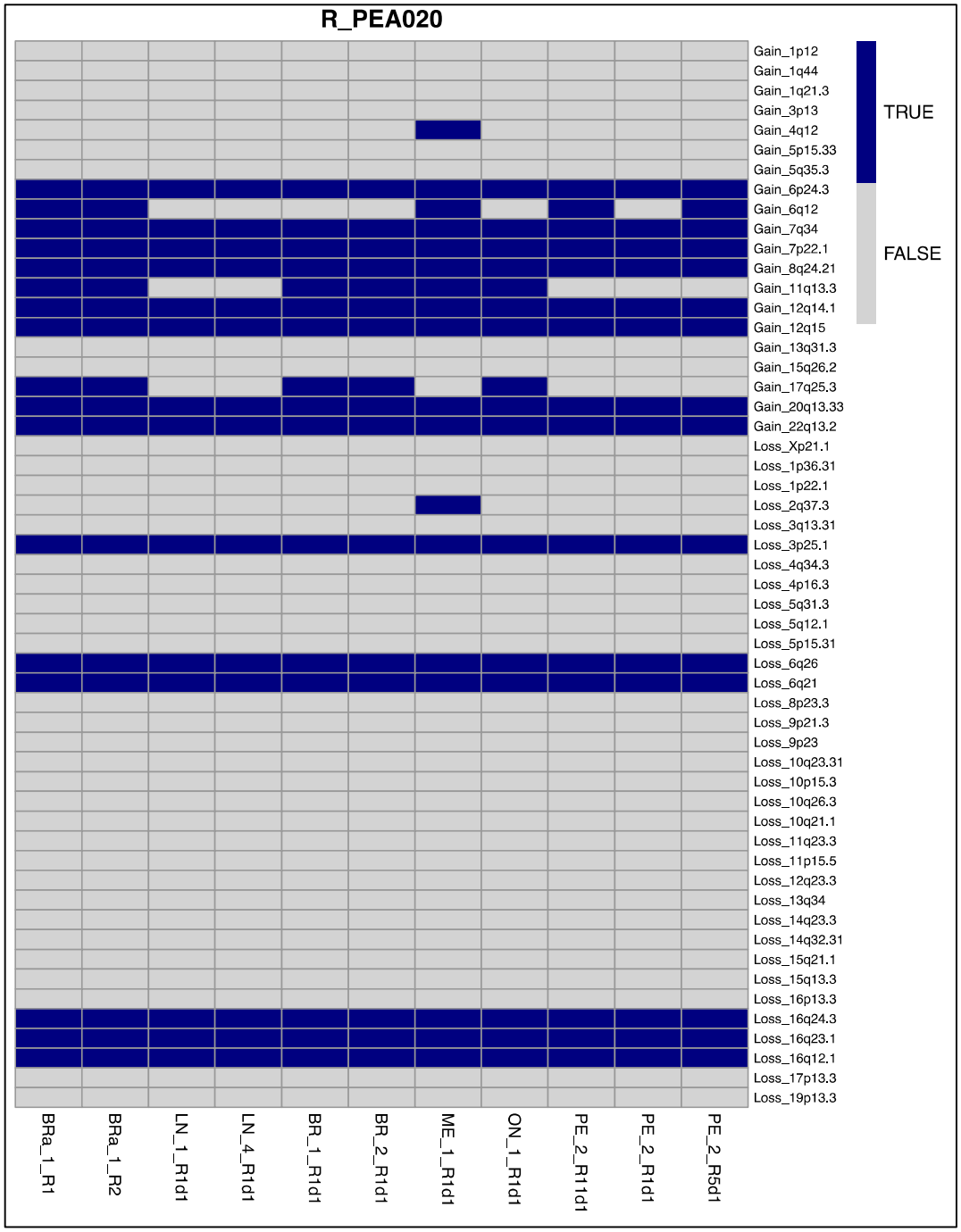

Figure 96 Cutaneous melanoma driver cytoband gains and losses
Annotated cytobands are melanoma driver regions determined by a GISTIC analysis of TCGA data.[1] Blue squares indicate whether there was loss or gain of at least one copy of the cytoband relative to the mean ploidy of all samples.

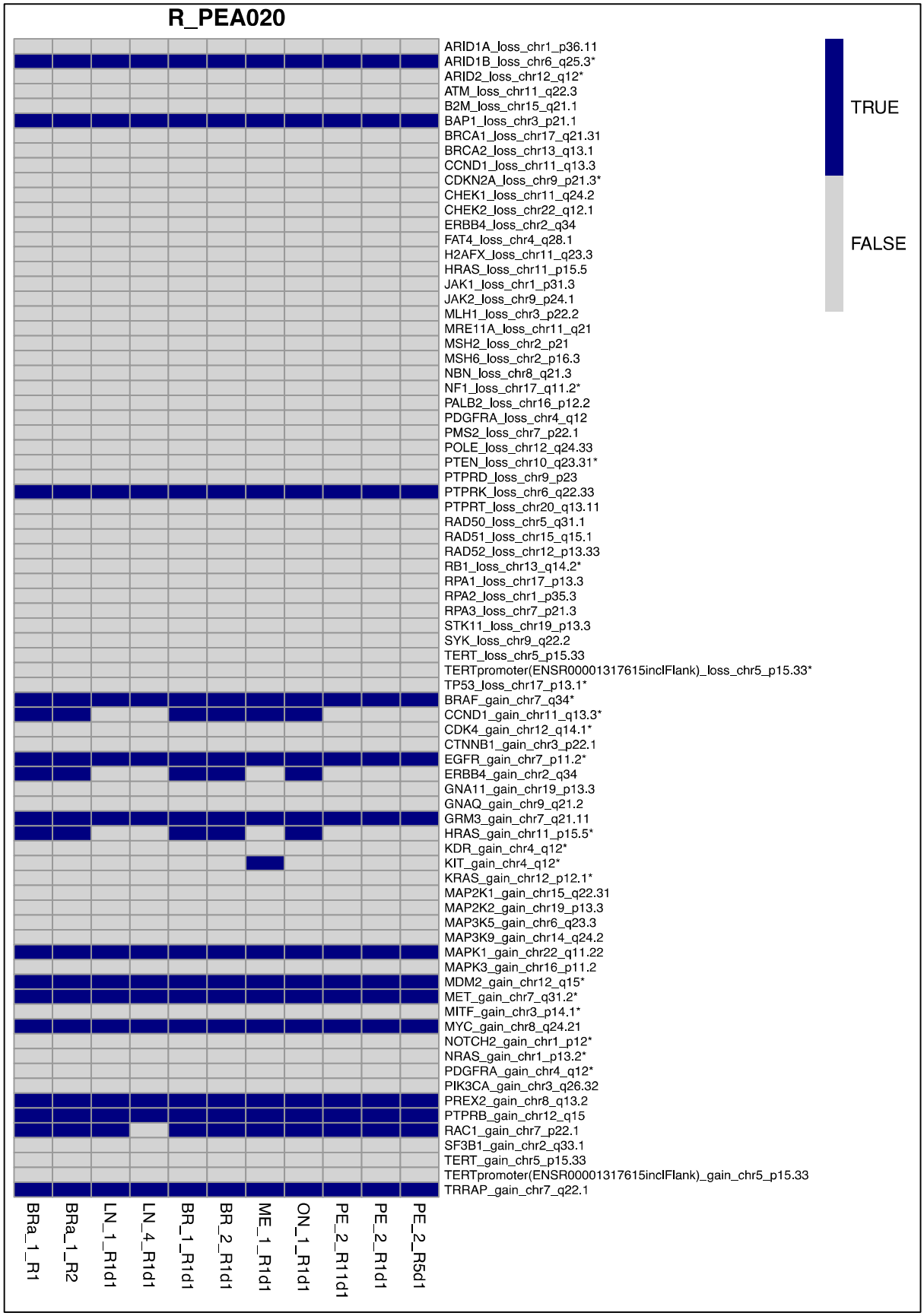

Figure 97 Driver gene gains and losses

Genes with an asterisk (*) are noted driver genes in the TCGA and Hayward data sets.[1,2] Blue squares indicate whether there was loss or gain of at least one copy of the gene relative to the mean ploidy of all samples.

Genomic mechanisms of treatment resistance

Patient PEA020 developed resistance to both ipilimumab and then nivolumab therapy, but no known genomic mechanisms of resistance to ICIs were identified, within the limits of our analysis. The patient self-ceased dabrafenib and trametinib after a month of therapy and therefore was not evaluable for response.

Case summary

Although there is no known primary tumour in PEA020, genomic features such as the relatively high TMB, evidence of a UV-induced damage mutational signature and presence of a *BRAF V600E* mutation all support a sun-exposed cutaneous primary tumour origin. The inferred primary to metastatic seeding pattern in this case appears polyclonal. The composition of metastases varies, with some appearing monoclonal and others polyclonal. Based on the clustering analysis there appeared to be one clone responsible for seeding intracranial sites, distinct from clone(s) seeding the intra-abdominal metastases. Nonetheless, some copy number changes were shared between the mesenteric nodal metastasis and the intracranial sites, highlighting the complexity of evolutionary patterns and raising the possibility of clonal mixing between these sites.

The overall survival of 3.5 years from diagnosis, with sequential exposure to anti-CTLA4 (ipilimumab) then anti-PD-1 (nivolumab) monotherapy, and the latency between end of systemic treatment and death suggest ongoing efficacy of immune checkpoint therapy in PEA020, similar to PEA009. The lung metastases, present from diagnosis, completely responded to nivolumab. At the tissue harvest, two lung nodules and three mediastinal lymph nodes were sampled, but did not contain tumour. This heterogeneity in treatment response is clinically important, but unable to be thoroughly explored in our genomic analyses, given sequenced tissues are biased to sites of treatment resistance.

References for PEA020

1. Cancer Genome Atlas N: Genomic Classification of Cutaneous Melanoma. *Cell* 161: 1681–96, 2015.
2. Hayward NK, Wilmott JS, Waddell N, et al. Whole-genome landscapes of major melanoma subtypes. *Nature* 545: 175–180, 2017.

Case study 11: PEA025

Clinical summary

Patient PEA025 was a 31 year old woman first diagnosed at age 28 in November 2014 with a primary melanoma on the back (13.5 mm Breslow thickness; Figure 98). There was no relevant family history to suggest a germline predisposition to melanoma. In May 2015, she underwent a right axillary lymph node dissection with one of 16 lymph nodes involved. Stage IV disease was confirmed in April 2016, with lung and multiple brain metastases. A *BRAF V600E* mutation was evident on molecular profiling. After whole-brain radiotherapy in May 2016, she commenced on ipi+nivo in June 2016. The first cycle was complicated by possible grade four pneumonitis warranting intensive care admission. On further progression in September 2016, dabrafenib and trametinib were started; disease control was achieved for nine months. In June 2017 pembrolizumab was commenced but symptomatic intra-cranial progression with leptomeningeal disease led to cessation of treatment after three cycles. She died three years from initial primary tumour diagnosis in November 2017, 19 months from the diagnosis of metastatic melanoma.

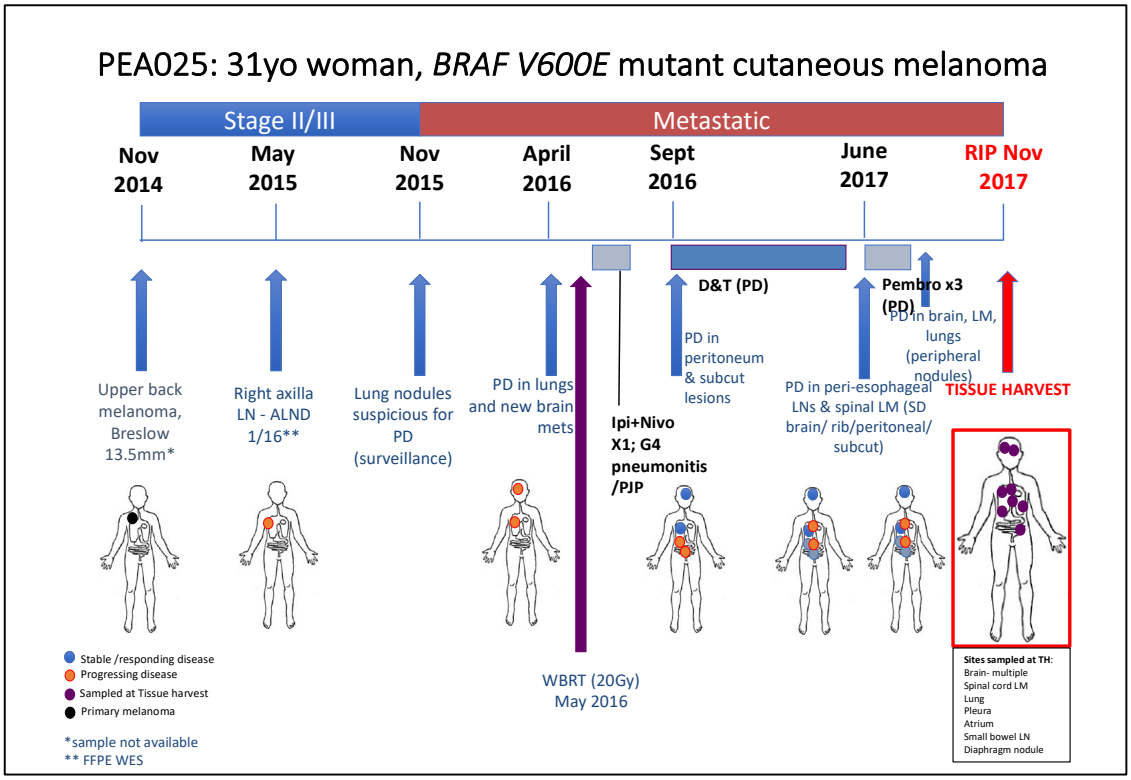

Figure 98 Timeline of clinical events, treatment and disease response in PEA025
Best overall RECIST response is included in brackets for each line of treatment (CR: complete response; PR: partial response; SD: stable disease; PD: progressive disease). FFPE: formalin fixed paraffin embedded; WES: whole exome sequencing; LN: lymph node; ALND: axillary lymph node dissection; WBRT: whole brain radiotherapy; Gy: Gray (radiation unit); Ipi+NIvo: ipilimumab and nivolumab combination therapy; D&T: dabrafenib & trametinib; subcut: subcutaneous; LM: leptomeningeal/leptomeninges; G4: CTCAE Grade 4; PJP: pneumocystis pneumonia.

Tissue harvest (TH) sampling and quality control considerations

A total of 36 tumour samples were collected at the TH from 32 metastases involving the brain, spinal cord leptomeninges, lung, pericardium and subcutaneous tissues. Thirty out of 36 had evidence of a *BRAF V600E* mutation on Sanger sequencing confirming adequate tumour content. Ten out of the 30 were selected as a broad representation of sites of metastatic disease and successfully underwent whole exome sequencing (WES). The primary tumour FFPE block(s) were unavailable in this case. FFPE tissue from the right axillary lymph node dissection was submitted for sequencing but failed due to low purity.

Genomic features

The overall mutational burden in this case is 262 nsSNVs, or 13.26 mutations/Mb (Table 12, **Section 3.3.1**), around the median for cutaneous melanoma (16.8 mutations/Mb).[1] The clonal mutation proportion is 69%. The dominant clonal mutational signature was UV-induced (Signature 7; Figure 99), consistent with a primary tumour on a sun-exposed site.

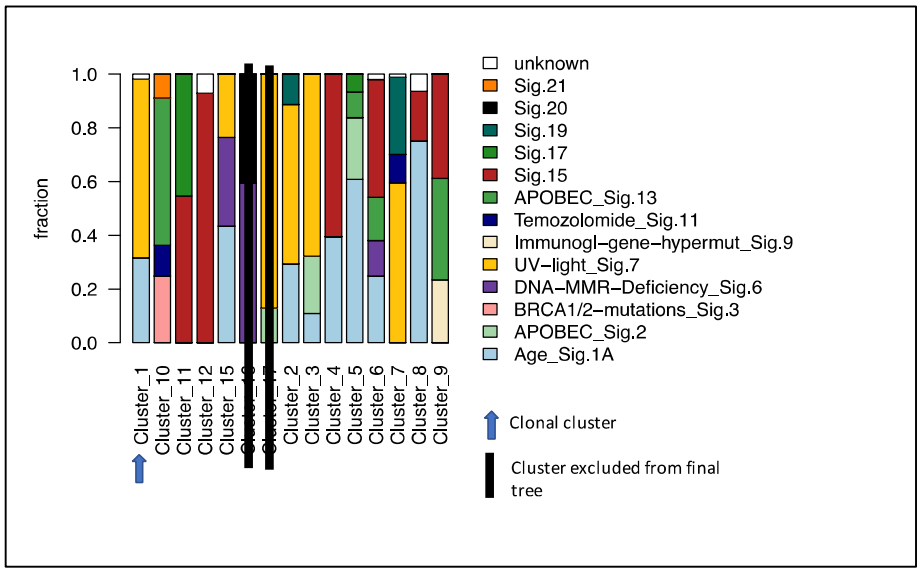

Figure 99 Mutational signature analysis of PEA025
Mutational signatures are based on Pyclone clustering of mutations for creation of phylogenetic trees, with the clonal cluster representing the ubiquitous mutations. Cluster 1 is the clonal cluster and is the only cluster with enough SNVs for reliable signature analysis (that is, ≥50); Clusters 2, 3, 7 were merged into Cluster 1 in the final tree (and all contain evidence of a dominant UV signature, consistent with Cluster 1) and Clusters 16 and 17 were removed from the final tree.

The median computationally derived ploidy is 2.04. This is consistent with FISH-estimated ploidy (Figure 100). The median WGII is 0.30 (Table 13 in **Section 3.3.3**), less than the median for cutaneous/MUP cases in this cohort (0.44). There is no evidence of whole genome doubling in any sample.

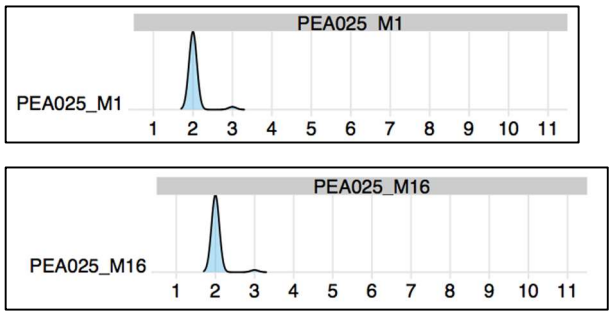

Figure 100 Corrected ploidy estimates of PEA025 samples analysed by FISH
*The x axis denotes the total probe count for each chromosome (see **Section 3.3.3**) and the y axis denotes the relative frequency.*
NB: M1 = SC_1_R1; M16 = PC_1_R1.

Driver alterations

The only clonal driver mutation is in BRAF V600E (Figure 101). A subclonal driver mutation in BRCA2 was identified (on Cluster 4, brain metastasis 3 (BR_3_R2), Figure 101). This *BRCA2* variant has not been previously reported in COSMIC and there is no corresponding loss of heterozygosity, therefore it is most likely a passenger event.

Most SCNAs in PEA025 are subclonal. Clonal arm-level driver SCNAs include gains in 6p and 8q as well as losses in 6q and 11q (Figure 102).[1] Clonal cytoband-level driver copy number losses included 8p23, 9p23, 16q23.1 and 16q24.3 (Figure 103).[1] There are no copy number gains or losses in driver genes separate from these larger-scale changes (Figure 104).

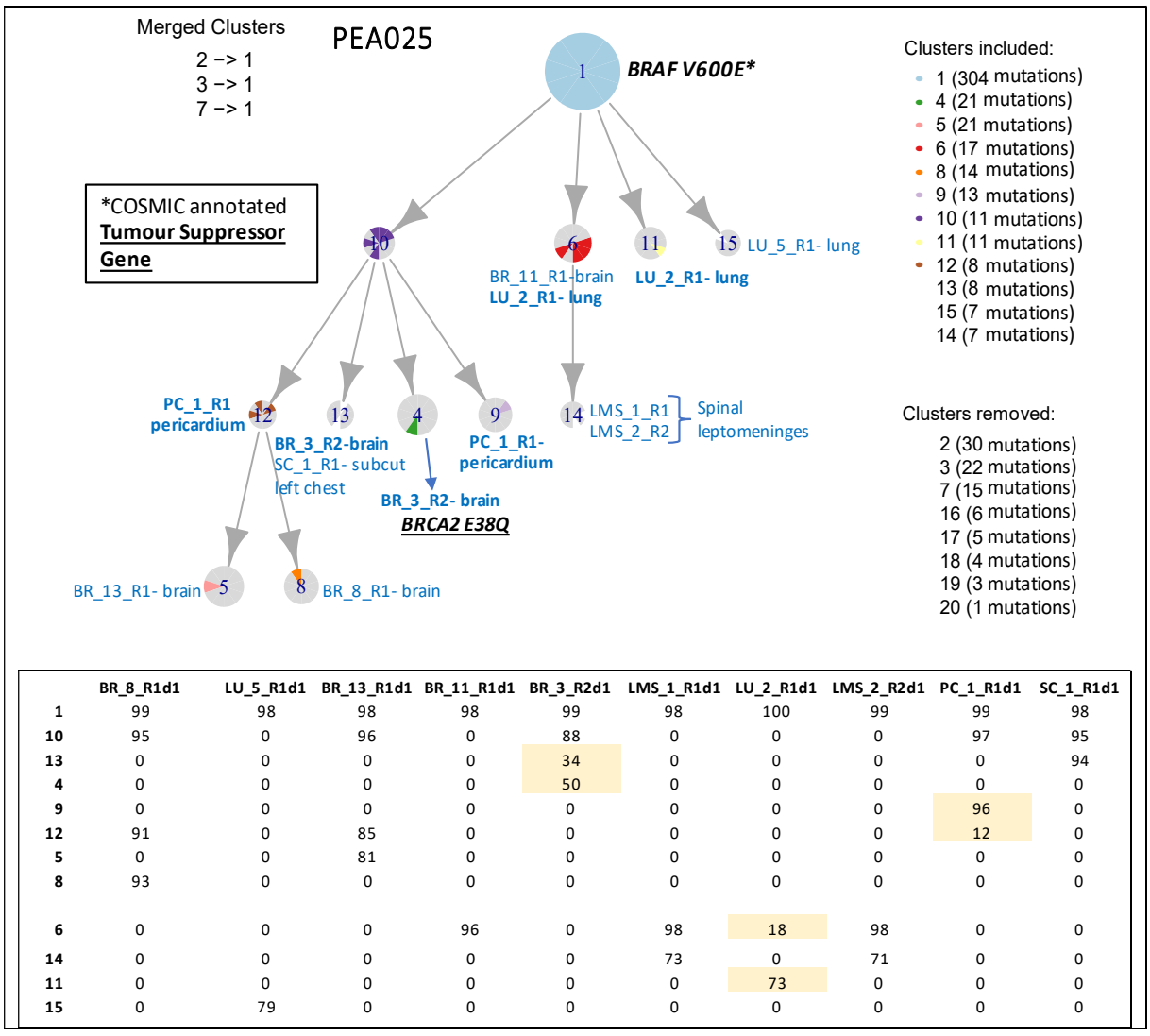

	BR_8_R1d1	LU_5_R1d1	BR_13_R1d1	BR_11_R1d1	BR_3_R2d1	LMS_1_R1d1	LU_2_R1d1	LMS_2_R2d1	PC_1_R1d1	SC_1_R1d1
1	99	98	98	98	99	98	100	99	99	98
10	95	0	96	0	88	0	0	0	97	95
13	0	0	0	0	34	0	0	0	0	94
4	0	0	0	0	50	0	0	0	0	0
9	0	0	0	0	0	0	0	0	96	0
12	91	0	85	0	0	0	0	0	12	0
5	0	0	81	0	0	0	0	0	0	0
8	93	0	0	0	0	0	0	0	0	0
6	0	0	0	96	0	98	18	98	0	0
14	0	0	0	0	0	73	0	71	0	0
11	0	0	0	0	0	0	73	0	0	0
15	0	79	0	0	0	0	0	0	0	0

Figure 101 Phylogenetic tree for PEA25
The clonal cluster of shared mutations (Cluster 1) sits at the trunk of the tree. Driver mutations belonging to each cluster are annotated. The cancer cell fraction (CCF) of each cluster per metastatic site is detailed in the table beneath the tree.

Evolution and metastatic seeding patterns

As previously discussed, a lack of primary tumour profiling limits the possible inferences of seeding patterns. Nonetheless, there is evidence of multiple seeding events in this case, consistent with polyclonal seeding from the primary tumour to metastatic sites. Tumour regions at different anatomical sites are clonally related but have distinct recent ancestors, suggesting they have originated from distinct subclones within the primary tumour. For example, on one branch of the tree (represented at the left of Figure 101) a number of metastatic regions were seeded by a clone harbouring Clusters 1+10 (for example, pericardium, brain metastases 3, 8 and 13). Other sites were seeded by a clone harbouring Clusters 1+6 (for example, brain metastasis 11, leptomeningeal metastases). Clusters 6 and 10 are mutually exclusive, supporting a distinct origin in the primary tumour. An alternative explanation is that one metastasis-competent clone left the primary tumour and evolved into separate clones before seeding metastatic sites (that is, a monoclonal seeding pattern from the primary tumour).

Seven out of the 10 metastatic regions appeared polyclonal in their composition by virtue of subclonal clusters. In 3/7 polyclonal metastatic regions >1 clone from exclusive branches of the phylogenetic tree were present. The first is the pericardial sample (PC_1_R1) which contains a clone harbouring Clusters 1+10+12 in addition to one harbouring Clusters 1+10+9. Cluster 9 is exclusive to the pericardial sample and may be the result of ongoing evolution at this site alone. However, Cluster 12 is on an exclusive branch of the phylogenetic tree to Cluster 9, and is shared with brain metastases 8 and 13. The second polyclonal region is brain metastasis 3 (BR_3_R2), which harbours one clone with Clusters 1+10+4, and another clone with Clusters 1+10+13, the latter also being shared with the subcutaneous chest wall metastasis (SC_1_R1). The third is lung metastasis 2 (LU_2_R1), which contains 1+6 and 1+11. These polyclonal metastases most likely arise from clonal mixing and may have arisen from cross-metastatic seeding, or by virtue of polyclonal seeding from the primary tumour. In the absence of primary tumour sampling this is not possible to discern.

In the other 4/7 metastatic regions with polyclonal compositions, the clusters are private to each metastasis, raising the possibility of ongoing evolution at these sites. Examples include the spinal leptomeningeal metastases 1 and 2 (LMS_1 and LMS_2) which both contain Cluster 14 at CCFs of 73% and 71% respectively, lung metastasis 5 (LU_5_R1) containing

Cluster 15 at a CCF of 79% and brain metastasis 13 (BR_13_R1) which contains Cluster 5 at a CCF of 81%.

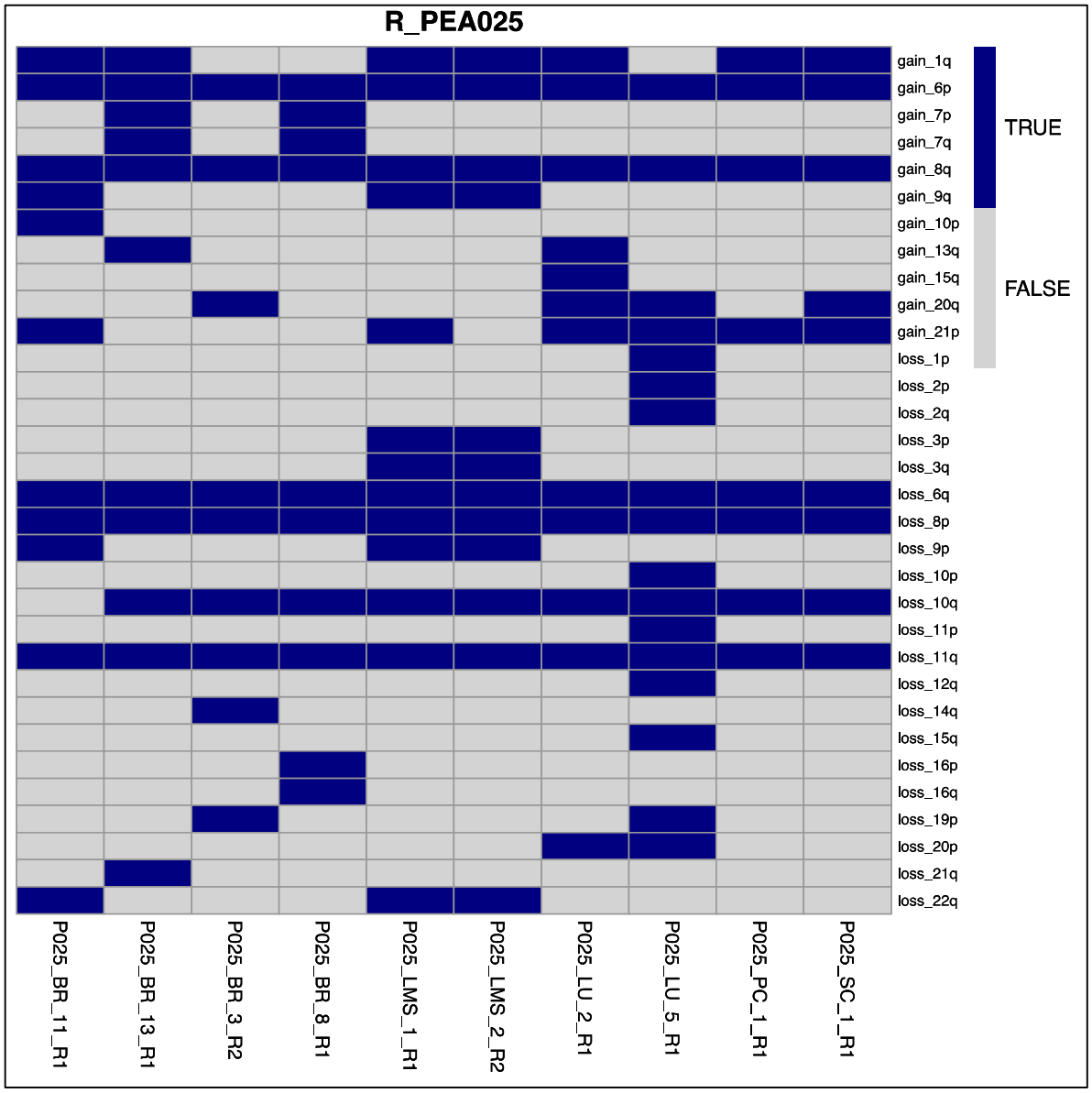

Figure 102 Chromosomal arm-level losses and gains
Blue squares indicate whether there was loss or gain of at least one copy of the chromosome arm relative to the mean ploidy of all samples.

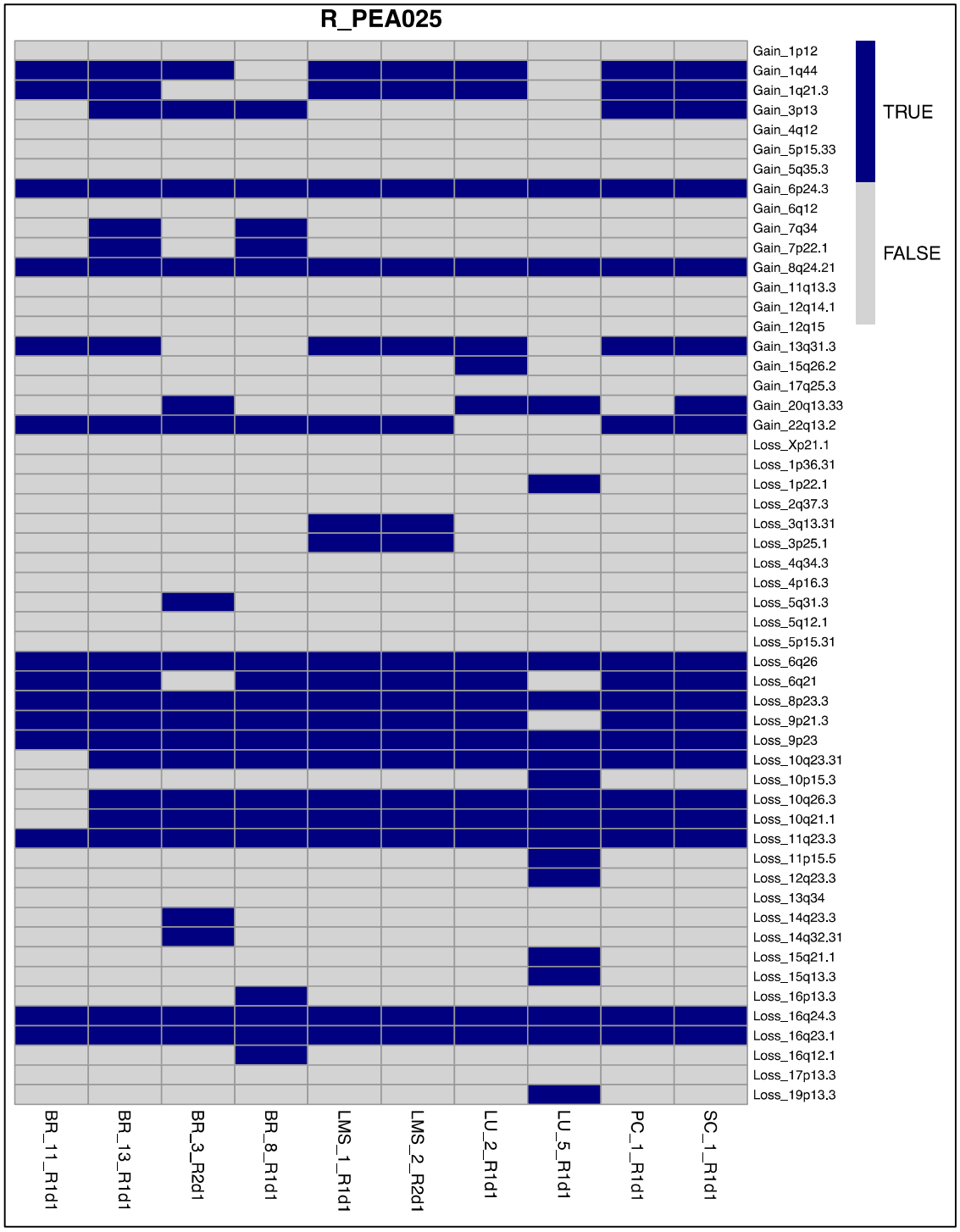

Figure 103 Cutaneous melanoma driver cytoband gains and losses
Annotated cytobands are melanoma driver regions determined by a GISTIC analysis of TCGA data.1 Blue squares indicate whether there was loss or gain of at least one copy of the cytoband relative to the mean ploidy of all samples.

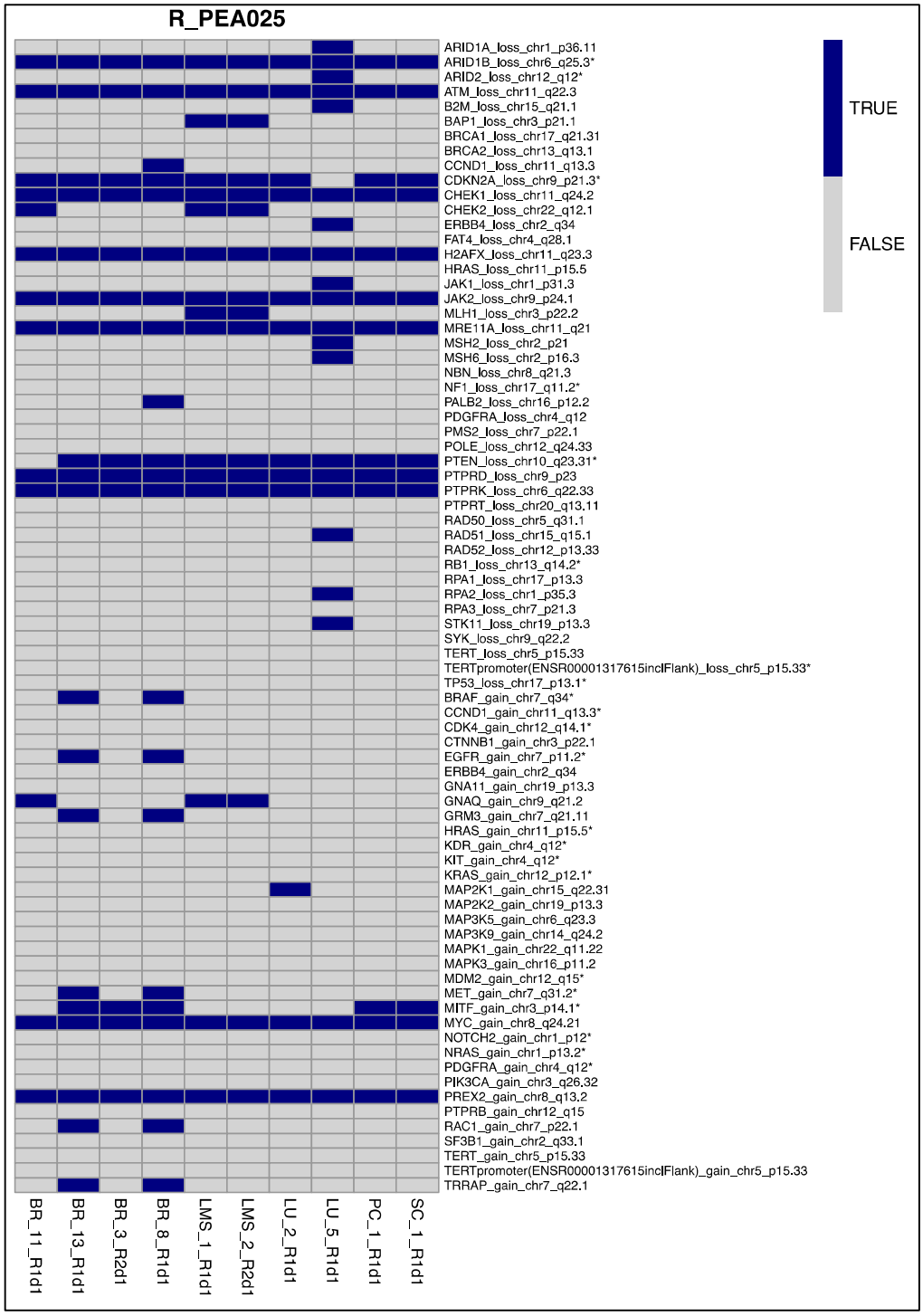

Figure 104 Driver gene gains and losses
Genes with an asterisk (*) are noted driver genes in the TCGA and Hayward data sets.[1,2] Blue squares indicate whether there was loss or gain of at least one copy of the gene relative to the mean ploidy of all samples.

Genomic mechanisms of treatment resistance

No alterations associated with either targeted therapy or immune checkpoint inhibitor treatment resistance have been identified in this case. Speculatively, clonal copy number loss of *JAK2* (9p24.1) may be relevant (as discussed in other cases and the section **Immune**

checkpoint inhibitors in the **Main Introduction Section 1.1.3**), but there was no evidence of a homozygous deletion nor a corresponding mutation.

Case summary

PEA025 represents a case of melanoma with a sun-exposed cutaneous primary and a *BRAF V600E* mutation. The early presence of brain metastases was a clinical adverse prognostic marker, but there was no distinct clone that appeared to seed the brain metastases, as observed in other cases in the cohort. Progression-free survival on first line ipi+nivo was only four months, but with the complicating factors of severe immune-related pneumonitis and preceding steroid therapy for management of brain metastases which is likely to have reduced immunotherapy efficacy.[3] No specific genomic markers of treatment resistance were identified to explain these outcomes. *JAK2* may be susceptible to haploinsufficiency, but this remains speculative as a possible mechanism of ICI resistance on its own.

Polyclonal seeding is inferred in this case, with presence of polyclonal metastases containing clones from different branches of the phylogenetic tree. Plausible mechanisms include polyclonal seeding from the primary tumour and/or metastasis-to-metastasis seeding. The resulting metastatic inter-tumour heterogeneity may have been a barrier to broad tumour control through neoantigen and possible immune microenvironment diversity, both of which will be explored in future analyses.

References for PEA025

1. Cancer Genome Atlas N: Genomic Classification of Cutaneous Melanoma. *Cell* 161: 681–96, 2015.
2. Hayward NK, Wilmott JS, Waddell N, et al. Whole-genome landscapes of major melanoma subtypes. *Nature* 545: 175–180, 2017.
3. Long GV, Atkinson V, Lo S, et al. Combination nivolumab and ipilimumab or nivolumab alone in melanoma brain metastases: a multicentre randomised phase 2 study. *Lancet Oncol* 19: 72–681, 2018.

Case study 12: PEA026

Clinical summary

Patient PEA026 was a 65 year old woman, with an interval of eight years between first diagnosis of a right heel primary melanoma and an ipsilateral right inguinal lymph node relapse, both managed surgically. Approximately 11 years later she presented with high-volume Stage IV disease and a *BRAF V600* mutation was noted on biopsy. She was commenced on ipilimumab+nivolumab, but due to ongoing clinical progression as well as immune-related colitis, she was switched to dabrafenib and trametinib after one cycle, and also received palliative radiotherapy to vertebral metastases. After a period of six months of disease stability, progressive disease was noted in the right retroperitoneum and a second cycle of ipilumumab+nivolumab was given, with recurrence of colitis. Further progression ensued, with clinically problematic pain and presumed tumour thrombus of the pelvic veins. She died from advanced melanoma 12 months from the detected Stage IV relapse. The clinical course is summarised in Figure 105.

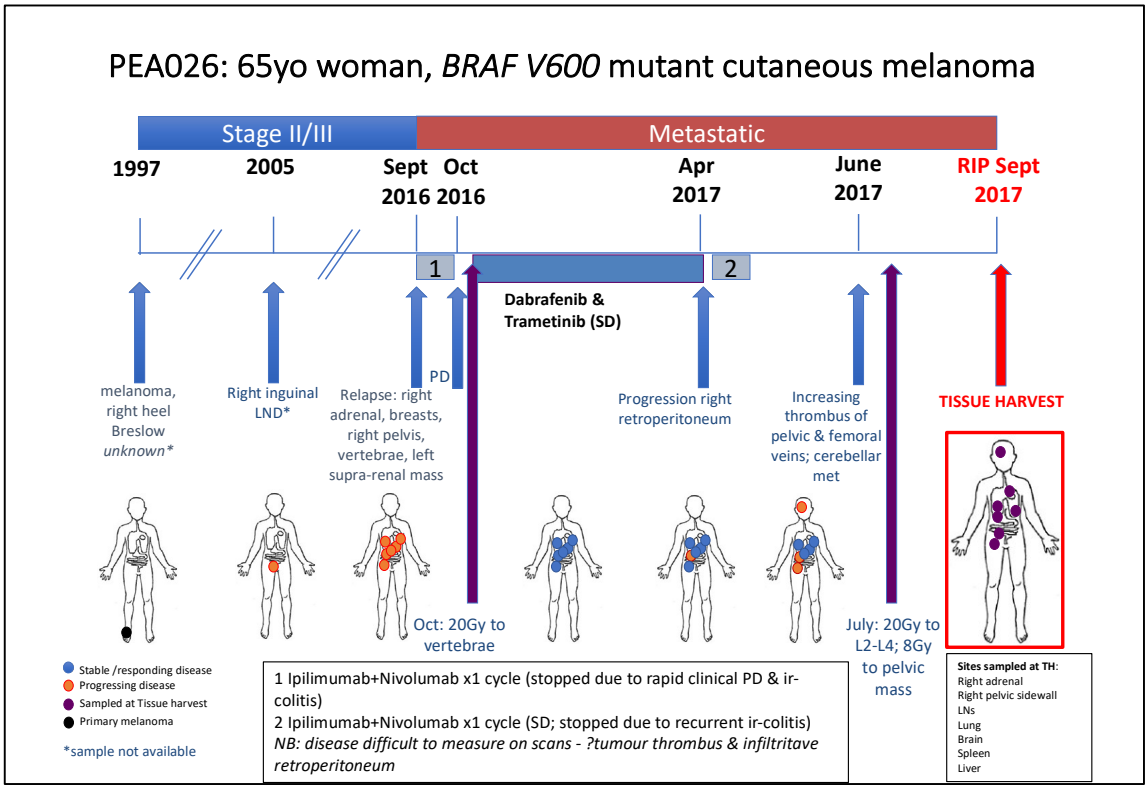

Figure 105 Timeline of clinical events, treatment and disease response in PEA026
Best overall RECIST response is included in brackets for each line of treatment (CR: complete response; PR: partial response; SD: stable disease; PD: progressive disease). WES: whole exome sequencing; LN: lymph node; LND: lymph node dissection; Gy: Grey (radiation unit).

Tissue harvest (TH) sampling and quality control considerations

Thirty-two tumour regions were sampled from 25 metastases involving adrenal glands, bone, pelvic soft tissue, lymph nodes, lung and brain. All of these showed evidence of a *BRAF V600E* mutation by Sanger sequencing, thus confirming tumour content. Of the 10 sites selected for WES, only nine were of sufficient purity for downstream analysis. The sample that failed, while demonstrating evidence of a BRAF mutation via Sanger sequencing, did not contain any tumour on paired H&E review. No archival primary tumour or pre-treatment tissue samples were available in this case.

Genomic features

The tumour mutation burden of 159 nsSNVs, or 7.4 mutations/Mb appears higher than usual for an acral primary (median 2.1 mutations/Mb).[1] The clonal mutation proportion is 18%. The dominant clonal signature – Signature 1A/Age – is in keeping with a non-sun-exposed primary (Figure 106). It remains possible that a second primary tumour could have arisen in a sun-exposed site and regressed (that is, that the metastatic disease be the result of a melanoma of unknown primary, accounting for the relatively high tumour mutational burden); however, I would have expected evidence of a UV signature, which is not appreciated (Figure 106). Clusters 1, 3 and 4, present at different metastatic sites (splenic hilar lymph node, right pelvis and left adrenal gland respectively), also displayed evidence of BRCA 1/2 (Signature 3) and APOBEC (Signature 13) signatures.

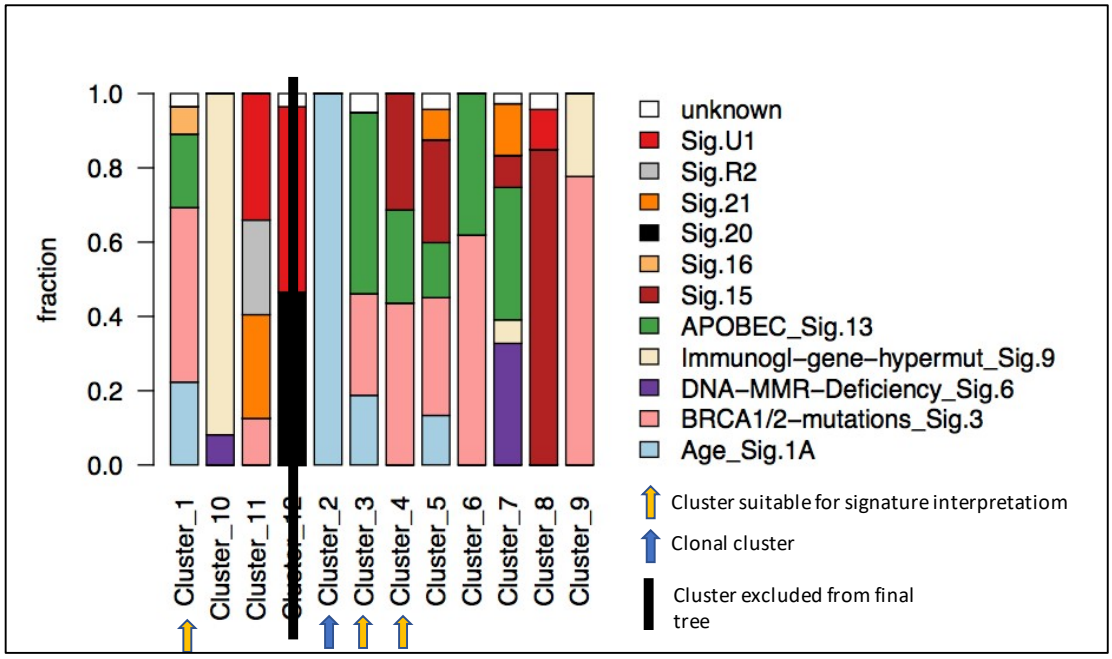

Figure 106 Mutational signature analysis of PEA026
Mutational signatures are based on Pyclone clustering of mutations for creation of phylogenetic trees, with the clonal cluster representing the ubiquitous mutations. Cluster 2 is the clonal cluster. Clusters 1, 2, 3 and 4 contain >50SNVs for reliable signature analysis.

Four of the nine samples appear to have undergone whole-genome doubling (ploidy ~4; brain (BR_2_R1), bone (BO_1_R1), liver (LI_4_R1) and left adrenal (AD_3_R2)), while the remaining 5/9 samples appear diploid (ploidy ~2, Table 13 in **Section 3.3.3**). FISH undertaken on the right adrenal metastasis (AD_1_R3; M5) and splenic hilar lymph node (LN_2_R1; M18) is consistent with a diploid state (Figure 107). While the inferred ploidy range of 2–4 in AD_1_R3 is suggestive of cell-to-cell heterogeneity, the mode was 2, consistent with the computationally derived ploidy. The WGD samples demonstrate a higher WGII than the diploid samples (median 0.64 versus 0.36).

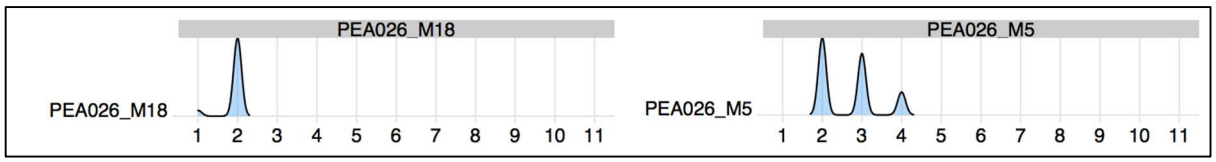

Figure 107 Corrected ploidy estimates of PEA026 samples analysed by FISH.
*The x axis denotes the total probe count for each chromosome (see **Section 3.3.3**) and the y axis denotes the relative frequency.*

Driver alterations

The only clonal driver mutation in this case is BRAF V600E (Figure 108). Subclonal driver mutations include *NRAS Q61R* and *B2M*, and are discussed in the **Evolution and metastatic seeding** section below.

In terms of SCNAs, subclonal events were more common than clonal events. Considerable heterogeneity between metastatic regions is evident (Figure 109, Figure 110 and Figure 111), with the highest number of copy number changes seen in the four genome-doubled samples (BR_2, BO_1, AD_3 & LI_4). This is reflected in the elevated WGII score as discussed above. Arm-level clonal SCNAs recognised as common events in acral tumours include gain of 6p, 7p and 8q and loss of 6q.[2] In addition, gain in 1q is recognised as a driver event in cutaneous melanoma.[3] Clonal driver events at the cytoband level for cutaneous melanomas include a copy number gain in 20q13, and losses in 15q21 (harbouring *B2M*) and 15q13. Copy number changes in relevant driver genes (*EGFR, ARID1B)* were consequent to the larger-scale alterations.

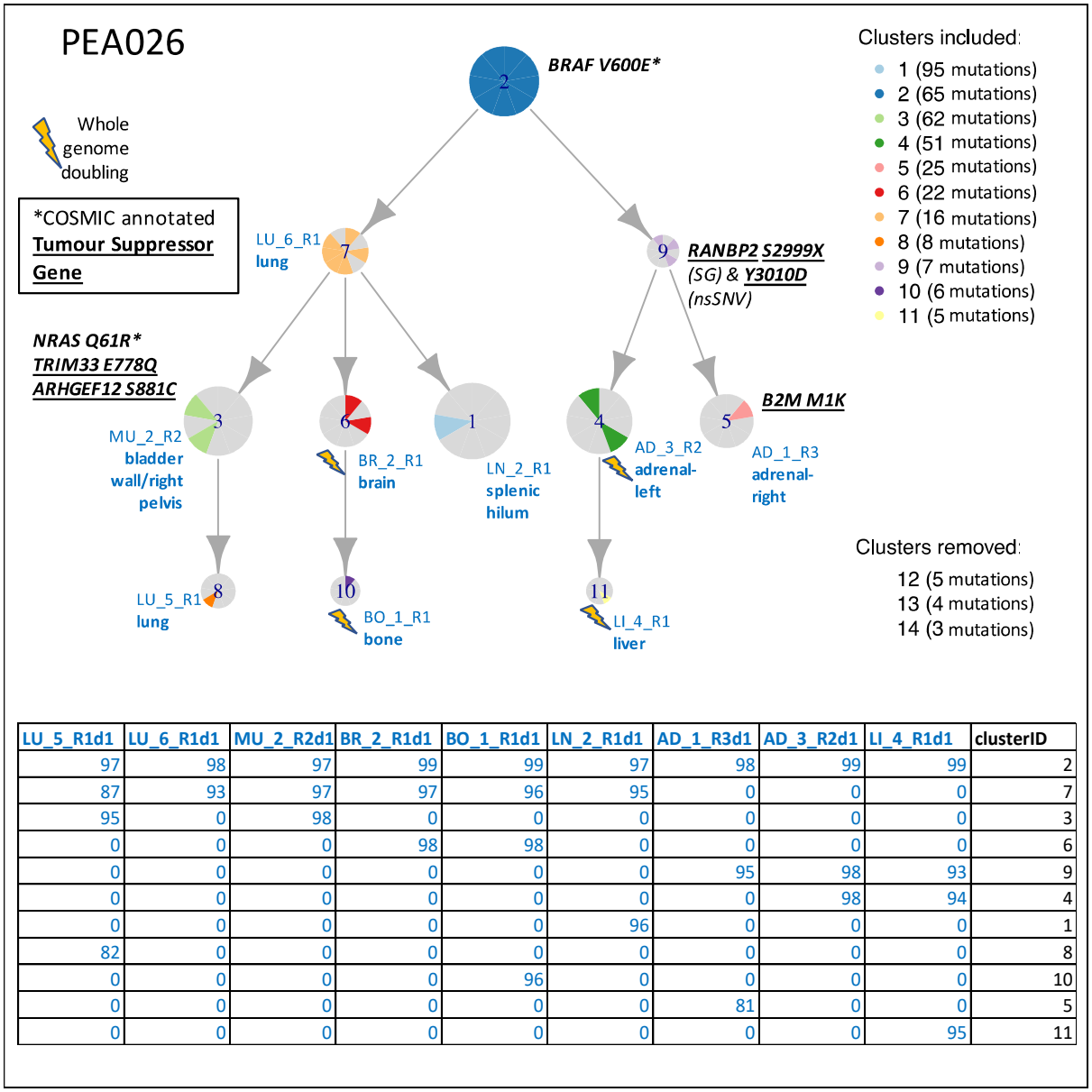

LU_5_R1d1	LU_6_R1d1	MU_2_R2d1	BR_2_R1d1	BO_1_R1d1	LN_2_R1d1	AD_1_R3d1	AD_3_R2d1	LI_4_R1d1	clusterID
97	98	97	99	99	97	98	99	99	2
87	93	97	97	96	95	0	0	0	7
95	0	98	0	0	0	0	0	0	3
0	0	0	98	98	0	0	0	0	6
0	0	0	0	0	0	95	98	93	9
0	0	0	0	0	0	0	98	94	4
0	0	0	0	0	96	0	0	0	1
82	0	0	0	0	0	0	0	0	8
0	0	0	0	96	0	0	0	0	10
0	0	0	0	0	0	81	0	0	5
0	0	0	0	0	0	0	0	95	11

Figure 108 Phylogenetic tree for PEA26
The clonal cluster of shared mutations sits at the trunk of the tree. Driver mutations belonging to each cluster are annotated. The cancer cell fraction (CCF) of each cluster per metastatic site is detailed in the table beneath the tree.

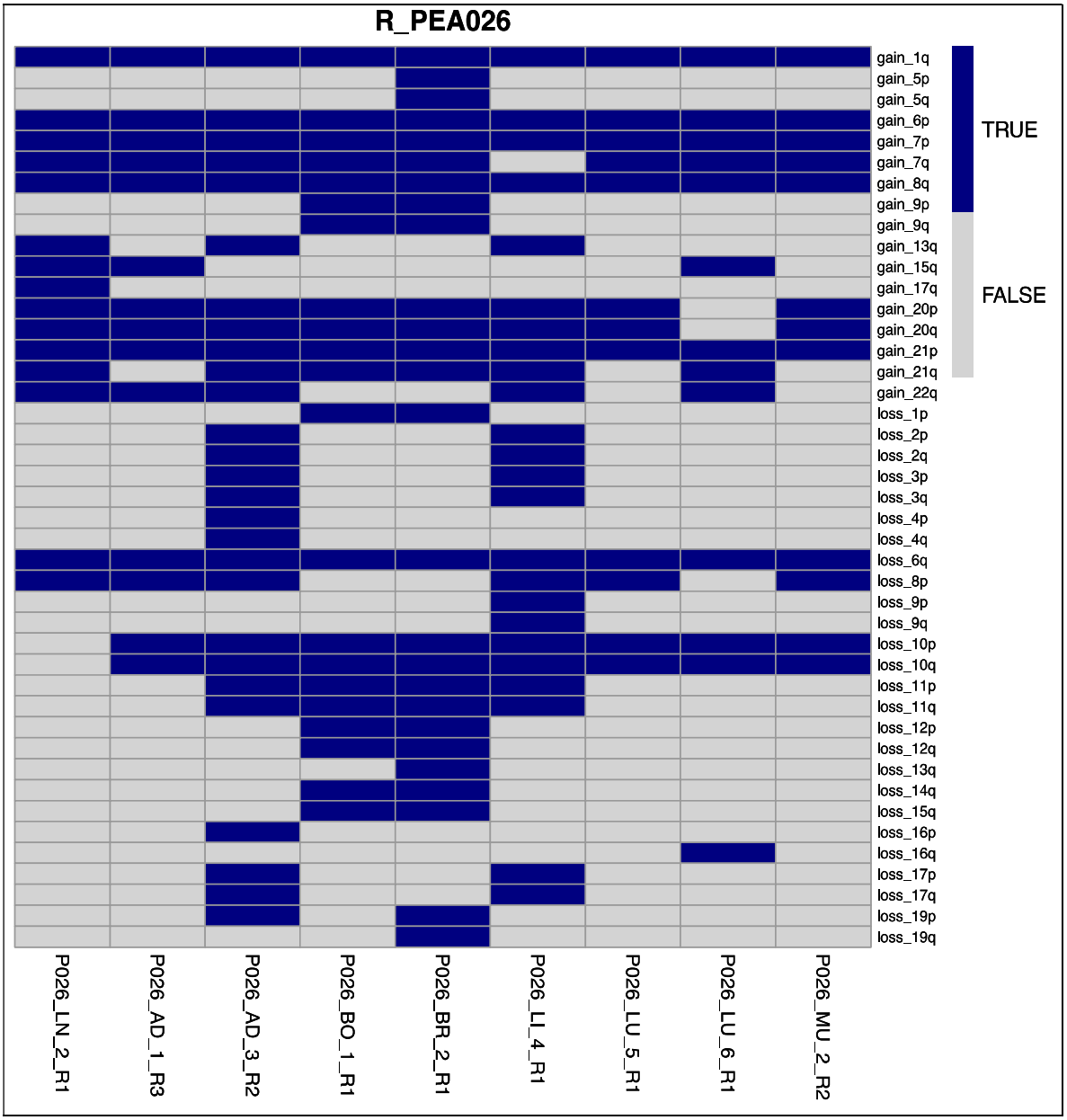

Figure 109 Chromosomal arm-level losses and gains
Blue squares indicate whether there was loss or gain of at least one copy of the chromosome arm relative to the mean ploidy of all samples.

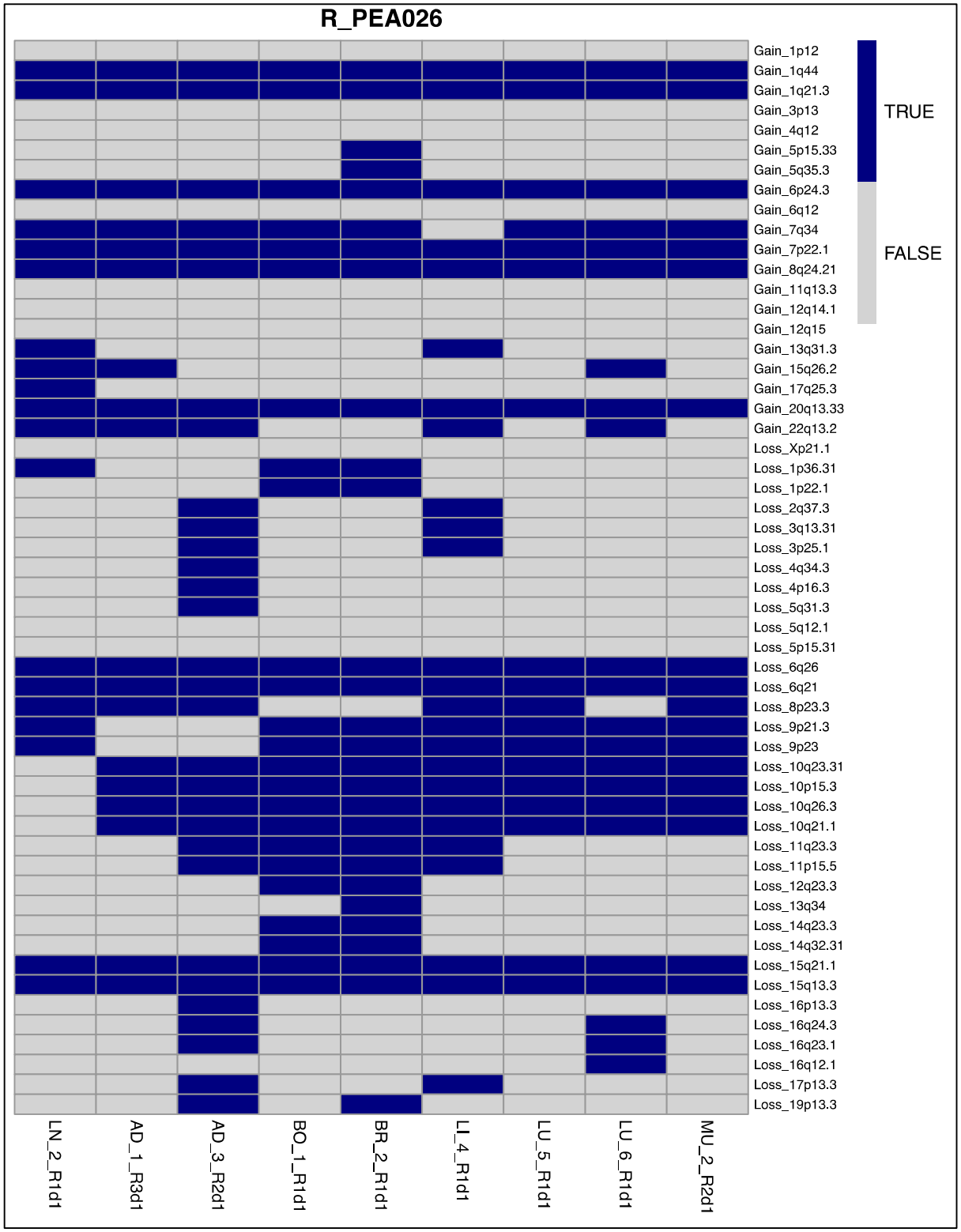

Figure 110 Cutaneous melanoma driver cytoband gains and losses
Annotated cytobands are melanoma driver regions determined by a GISTIC analysis of cutaneous melanoma TCGA data.[3] Blue squares indicate whether there was loss or gain of at least one copy of the cytoband relative to the mean ploidy of all samples.

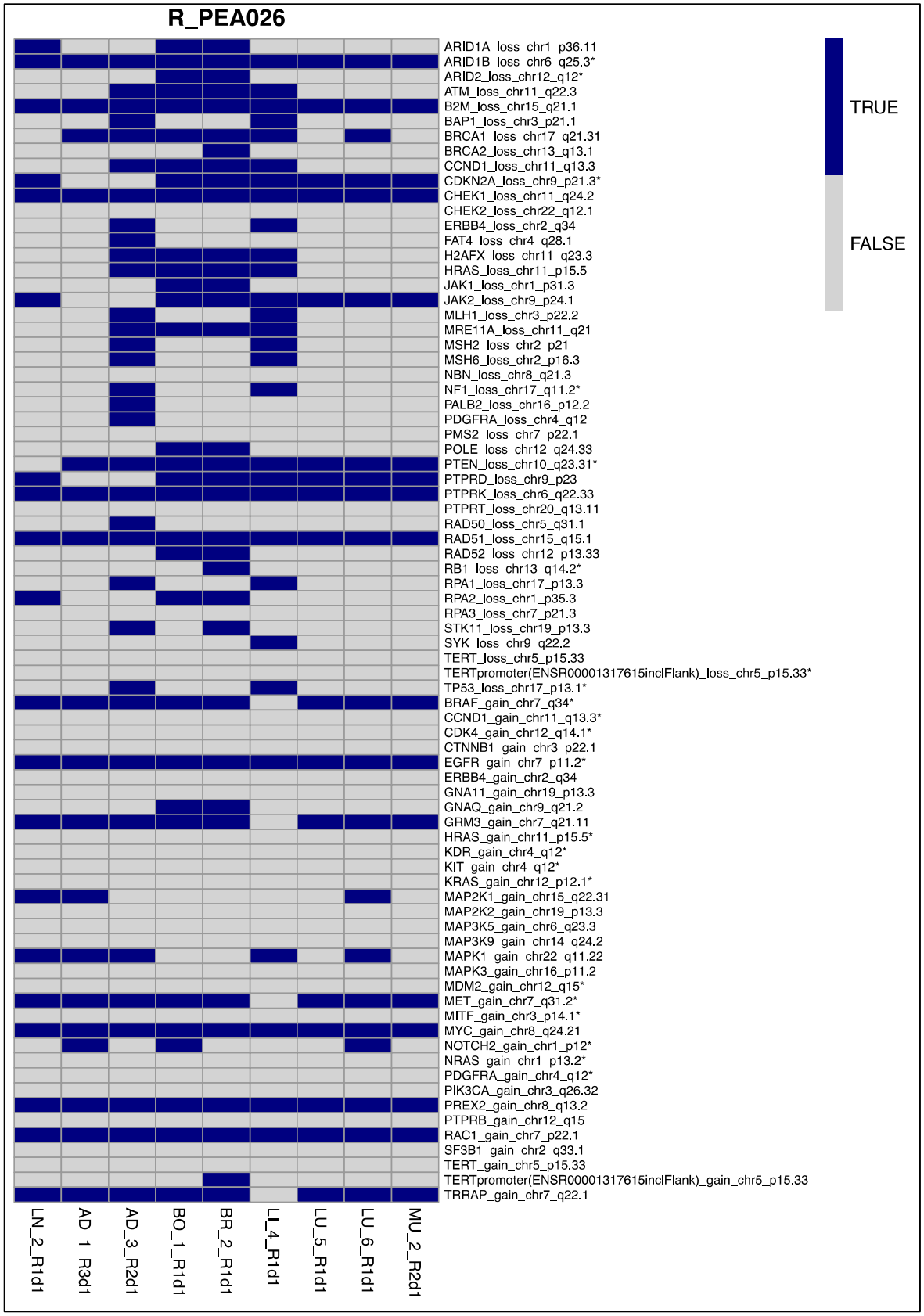

Figure 111 Driver gene gains and losses

Genes with an asterisk (*) are noted driver genes in the TCGA and Hayward data sets.[3,4] Blue squares indicate whether there was loss or gain of at least one copy of the gene relative to the mean ploidy of all samples.

Evolution and metastatic seeding patterns

In this case, despite the limitations imposed by the absence of primary tumour profiling, the seeding pattern appears polyclonal. There appear to be two main branches of the phylogenetic tree (Figure 108), each with a different recent common ancestor for metastasis-seeding clones: Cluster 9 and Cluster 7. Where one group of metastases are seeded by a clone containing Clusters 2+7, another is seeded by a clone containing Clusters 2+9.

The metastases themselves all appear monoclonal in their composition (that is, CCFs are within 15% from the CCF value in the clonal cluster), suggestive of a single founding clone for each metastasis. Clusters 1, 3 and 4 display evidence of APOBEC and BRCA1/2 signatures (with >50 mutations per cluster). These signature profiles are not evident in the clonal Cluster 2, meaning these mutations were most likely acquired after the clone(s) left the primary tumour. No alterations were detected in the genes encoding the APOBEC family of enzymes, nor is there evidence of a *BRCA* mutation in this case, to account for these signatures.

Subclonal driver mutations are evident. *NRAS Q61R* is a driver hot-spot mutation in melanoma and a recognised mechanism of treatment resistance to MAPK inhibition. The *B2M* mutation associated with the AD_1 clone (right adrenal) may also have been selected for as a potential resistance mechanism to immune checkpoint therapy. These are further discussed in the **Genomic mechanisms of treatment resistance** section below.

Whole genome doubling is a subclonal event in this case. Although the exact timing of WGD is not possible to decipher from the analysis, it appears that the left temporoparietal brain (BR_2) and bone (BO_1) metastases descend from the same seeding clone (Clusters 2+7+6), as do the liver (LI_4) and left adrenal (AD_3; Clusters 2+9+4). The two ‘pairs’ are, however, exclusive from each other, belonging to different branches of the tree. These WGD events occurred in parallel, providing evidence of selection and convergent evolution for the WGD clones. The left adrenal metastasis (AD_3) may have seeded liver metastasis 4 (LI_4), and this is consistent with the clinical picture as liver metastases were a late event seen at TH, but not on prior imaging. Brain metastases (for example, BR_2) were also late clinical events only evident at TH and therefore BR_2 seems unlikely to have seeded the L2/3 vertebral bone metastasis (BO_1) as L3 vertebral disease was evident at first relapse. Th copy number pattern appears similar for these brain and bone metastases (BR_2 and BO_1 respectively), as well as for the left adrenal and liver metastases (AD_3 and LI_4; see

Figure 109, Figure 110 and Figure 111), supporting the algorithmic clustering approach.

Genomic mechanisms of treatment resistance

There are three potential genomic mechanisms of resistance to treatment evident in PEA026, all noted in different sites of disease (that is, a subclonal pattern): two mechanisms of ICI resistance (relevant to the ipi+nivo therapy) and one to MAPKi therapy (relevant to dabrafenib/trametinib). The first related to ICI resistance is a *B2M p.M1K* mutation (Chr 15, exon 1) evident in the right adrenal metastasis (AD_1_R3). *B2M* encodes the beta-2 microglobulin (B2M) protein, a key component of MHC Class 1 molecules, and therefore it is a critical component of antigen presentation. Loss of function of the B2M protein (through a frameshift inactivating mutation with LOH) has been associated with acquired resistance to anti-PD-1 therapy.[7] The *B2M* missense mutation seen in PEA026 has been previously reported[8] with unclear functional significance because it lies outside of the functional domain. Clinically, this right adrenal metastasis was present at first diagnosis of metastatic disease and did not grow in a disproportionate manner through treatment. Nonetheless, in the context of clonal somatic copy number loss at 15q21 which encompasses *B2M*, this may have led to loss of antigen presentation at this site, and an ineffective local tumour immune response.

The second putative mechanism of ICI treatment resistance is more speculative. Both BO_1 (bone - L2/3 vertebra) & BR_2 (brain) have lost one copy of both *JAK1 & JAK2*, in addition to *B2M* (through clonal loss of 15q21, as discussed). *JAK1* and *JAK2* encode the proteins Janus kinase 1 (JAK1) and Janus kinase 2 (JAK2), both involved in sensitivity to interferon gamma signalling. Loss of function can lead to poor T cell recruitment and reduced activity in the tumour microenvironment, as already discussed in other cases (PEA009, PEA017 and PEA023).[9] Copy number loss of *JAK2* in particular, which is likely to demonstrate haploinsufficiency according to the DECIPHER tool (score 0.82% (0–10% likely to display haploinsufficiency)), may have had some impact on this pathway. The brain metastasis was a late event in this case, and although the L2/3 vertebral site was present early on, there was a suggestion of progression on the last staging CT in June 2017, three months before death.

The third potential resistance mechanism is the *NRAS Q61R* mutation seen in the bladder wall/right pelvic sidewall metastasis (MU2_R2). *NRAS* encodes a key signalling protein in the MAPK pathway and mutations are described as a mechanism of acquired resistance to *BRAF* inhibition.[10,11] The right pelvic sidewall infiltrative disease, from which this region is

sampled, initially shrunk after eight weeks on dabrafenib+trametinib. Four months later it appeared to progress.

In addition to these specific genomic alterations, the high percentage of subclonal mutations (82%) may not have been favourable for ICI response,[12,13] as discussed in PEA004 and PEA012.

Case summary

In this case, despite eight years between primary tumour diagnosis and Stage III recurrence and then another 11 years before development of Stage IV disease, survival from detection of metastatic disease was only 12 months. This was despite treatment with both combination ipi+nivo and BRAF/MEK inhibition for which Phase 3 studies show a median PFS of ~11 months for each when administered in the first-line setting.[14,15]

The acquisition of APOBEC (Signature 13) and BRCA (Signature 3) mutational signatures in some metastases raises the possibility of disruption of these pathways in clones with metastatic competence, outside of the primary tumour. Acquisition of APOBEC mutational signatures in metastatic tumours has been previously described in melanoma.[16] In PEA026 there are no recognised mutations in genes involved in these pathways, but other mechanisms such as increased expression of enzymes or silencing of pathway regulators by methylation may play a role.

There is evidence of subclonal WGD in metastatic sites harbouring exclusive clones (that is, brain and bone, left adrenal and liver). This is an example of convergent evolution on a trait (WGD in this case), which is likely to confer a selection advantage.

There are a number of putative treatment resistance mechanisms in this case (mutation in *B2M,* copy number loss of *JAK2*, an acquired *NRAS* mutation) with heterogeneity demonstrated between sites of disease. Further validation with immunohistochemistry for protein loss in the case of *B2M* and *JAK2* is warranted. Analysis of RNAseq data may show differential MAPK pathway regulation between the right pelvic sidewall/bladder wall region and other sites in the context of the acquired *NRAS* mutation.

The dominance of subclonal mutations in this case is interesting. A single biopsy of a tumour in PEA026 may misrepresent both tumour mutational burden (which varies across samples due to extensive branching) as well as potential mechanisms of treatment resistance.

References for PEA026

1. Newell F, Wilmott JS, Johansson PA, et al. Whole-genome sequencing of acral melanoma reveals genomic complexity and diversity. *Nat Commun* 11: 5259, 2020
2. Curtin JA, Fridlyand J, Kageshita T, et al. Distinct sets of genetic alterations in melanoma. *N Engl J Med* 353: 2135–47, 2005.
3. Cancer Genome Atlas N: Genomic Classification of Cutaneous Melanoma. *Cell* 161: 1681–96, 2015.
4. Hayward NK, Wilmott JS, Waddell N, et al. Whole-genome landscapes of major melanoma subtypes. *Nature* 545: 175–180, 2017.
5. Andre S, S PN, Silva F, et al. Analysis of Epigenetic Alterations in Homologous Recombination DNA Repair Genes in Male Breast Cancer. *Int J Mol Sci* 21, 2020.
6. Bielski CM, Zehir A, Penson AV, et al. Genome doubling shapes the evolution and prognosis of advanced cancers. *Nat Genet* 50: 1189–1195, 2018.
7. Zaretsky JM, Garcia-Diaz A, Shin DS, et al. Mutations Associated with Acquired Resistance to PD-1 Blockade in Melanoma. *N Engl J Med* 375: 819–29, 2016.
8. Middha S, Yaeger R, Shia J, et al. Majority of B2M-Mutant and -Deficient Colorectal Carcinomas Achieve Clinical Benefit From Immune Checkpoint Inhibitor Therapy and Are Microsatellite Instability-High. *JCO Precis Oncol* 3, 2019.
9. Gide TN, Wilmott JS, Scolyer RA, et al. Primary and Acquired Resistance to Immune Checkpoint Inhibitors in Metastatic Melanoma. *Clin Cancer Res* 24: 1260-1270, 2018.
10. Long GV, Fung C, Menzies AM, et al. Increased MAPK reactivation in early resistance to dabrafenib/trametinib combination therapy of BRAF-mutant metastatic melanoma. *Nat Commun* 5: 5694, 2014.
11. Van Allen EM, Wagle N, Sucker A, et al. The genetic landscape of clinical resistance to RAF inhibition in metastatic melanoma. *Cancer Discov* 4: 94–109, 2014.
12. McGranahan N, Furness AJ, Rosenthal R, et al. Clonal neoantigens elicit T cell immunoreactivity and sensitivity to immune checkpoint blockade. *Science* 351: 1463–9, 2016.
13. Wolf Y, Bartok O, Patkar S, et al. UVB-Induced Tumor Heterogeneity Diminishes Immune Response in Melanoma. *Cell* 179: 219–235 e21, 2019.
14. Larkin J, Chiarion-Sileni V, Gonzalez R, et al. Combined Nivolumab and Ipilimumab or Monotherapy in Untreated Melanoma. *N Engl J Med* 373: 23–34, 2015.
15. Long GV, Stroyakovskiy D, Gogas H, et al. Combined BRAF and MEK inhibition versus BRAF inhibition alone in melanoma. *N Engl J Med* 371: 1877–88, 2014,
16. Rabbie R, Ansari-Pour N, Cast O, et al. Multi-site clonality analysis uncovers pervasive heterogeneity across melanoma metastases. *Nat Commun* 11: 4306, 2020,

Case study 13: PEA038

Clinical summary

Patient PEA038 was a 75 year old woman diagnosed with a 4 mm thick primary melanoma on the right lower leg in March 2015. Four sentinel lymph nodes were sampled, two of which contained melanoma. In February 2016 a locoregional relapse was detected clinically and was resected (pelvic side wall and external iliac lymph nodes scar recurrence). An *NRAS Q61K* mutation was detected on molecular profiling. Two months later she developed metastatic disease in the lung, liver, spleen and mediastinal lymph nodes. She was treated with ipilimumab and nivolumab in April 2016 for four cycles, followed by maintenance nivolumab. After one month of maintenance nivolumab two new brain lesions were detected, one of which was resected and the other received stereotactic radiotherapy, while nivolumab was continued. The extracranial disease remained stable. In February 2017, progressive disease was noted in the spleen, left axilla and the brain. Temozolomide chemotherapy was commenced, with a partial response in extracranial sites, but emergence of a further two brain lesions. These were treated with stereotactic radiotherapy. In August 2017, temozolomide was ceased due to further intracranial progression, with maintained disease control extracranially at that time. In December 2017, the patient died from metastatic melanoma. The clinical course is summarised in Figure 112.

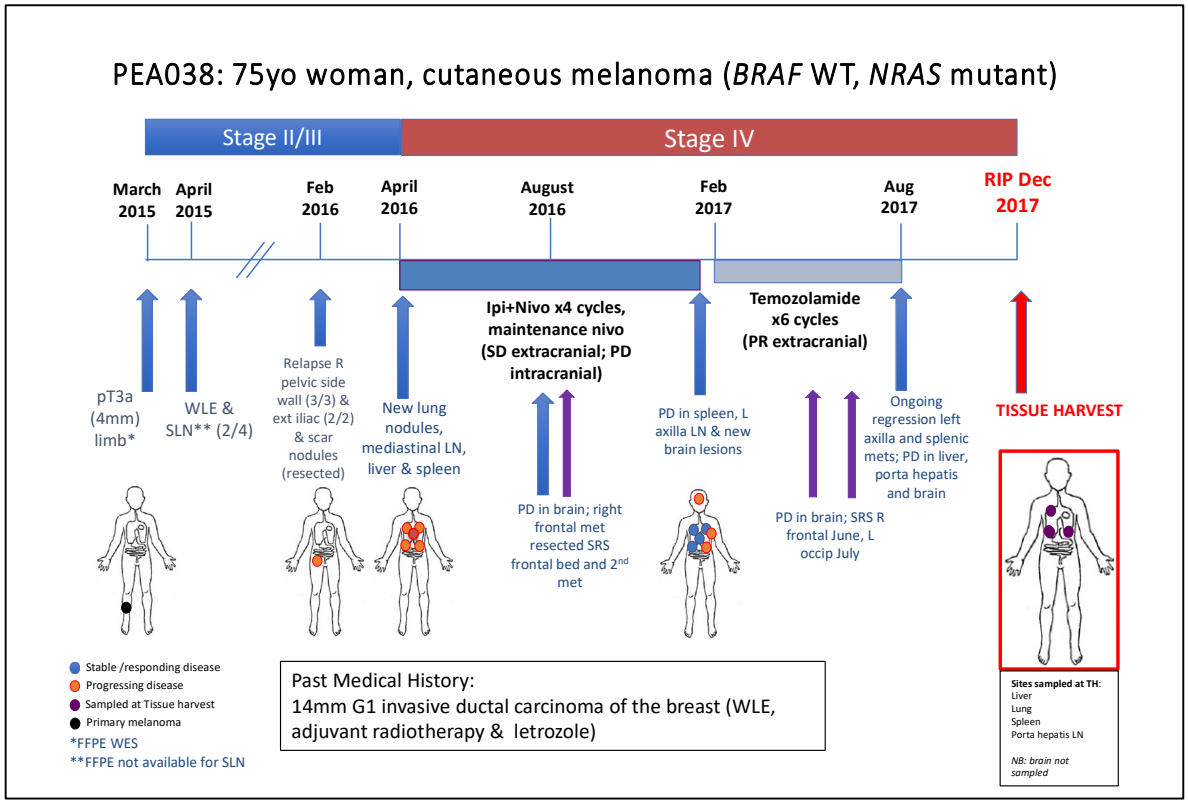

Figure 112 Timeline of clinical events, treatment and disease response in PEA038
Best overall RECIST response is included in brackets for each line of treatment (CR: complete response; PR: partial response; SD: stable disease; PD: progressive disease). WLE: wide local excision; SLN: sentinel lymph node; FFPE: formalin-fixed paraffin-embedded; WES: whole exome sequencing; R: right; L: left; ext: external; met: metastasis; occip: occipital; LN: lymph node; ipi+nivo: ipilimumab and nivolumab; SRS: stereotactic radiodurgery; TH: tissue harvest.

Tissue harvest (TH) sampling and quality control considerations

Twenty-six tumour samples were obtained at the TH from 14 individual metastases in the right lung, liver, porta hepatis lymph node, right pelvic wall and spleen. The brain was not sampled due to time constraints. 15/26 samples had evidence of an *NRAS Q61K* mutation by Sanger sequencing. The sampled spleen and right pelvic wall metastases did not have evidence of a *NRAS Q61K* mutation*;* accordingly, there was no evidence of tumour on H&E review.

Ten samples were successfully profiled using WES. WES was attempted in nine regions from five archival samples (resected brain lesion, resected lymph nodes, two scar recurrence samples and the original primary tumour). Samples from the primary tumour and two lymph node samples failed WES.

Genomic features

The TMB is 13476 nsSNVs, or 750.2 mutations/Mb (see Table 11**, Section 3.3.1**). The clonal mutation proportion is 1%. While these overall TMB metrics are at the extremely high end for sun-exposed cutaneous melanomas, they have been influenced by chemotherapy exposure in the metastatic sites, as evidenced by the dominance of subclonal versus clonal mutations. Consistent with this, mutational signatures reveal UV-induced mutagenesis (Signature 7) in the clonal cluster as well as in Clusters 8 and 11. These clusters are present in clones at resected disease sites prior to chemotherapy exposure (locoregional lymph nodes and soft tissue as well as brain – discussed in **Evolution and metastatic seeding patterns** section below). There is a dominant temozolomide-induced signature (Signature 11) in most metastatic sites (Figure 113). The exception to this is in Cluster 9, which is found in two regions from a lung metastasis, in which a UV-induced signature was evident and there was no suggestion of temozolomide impact. This is also further discussed below.

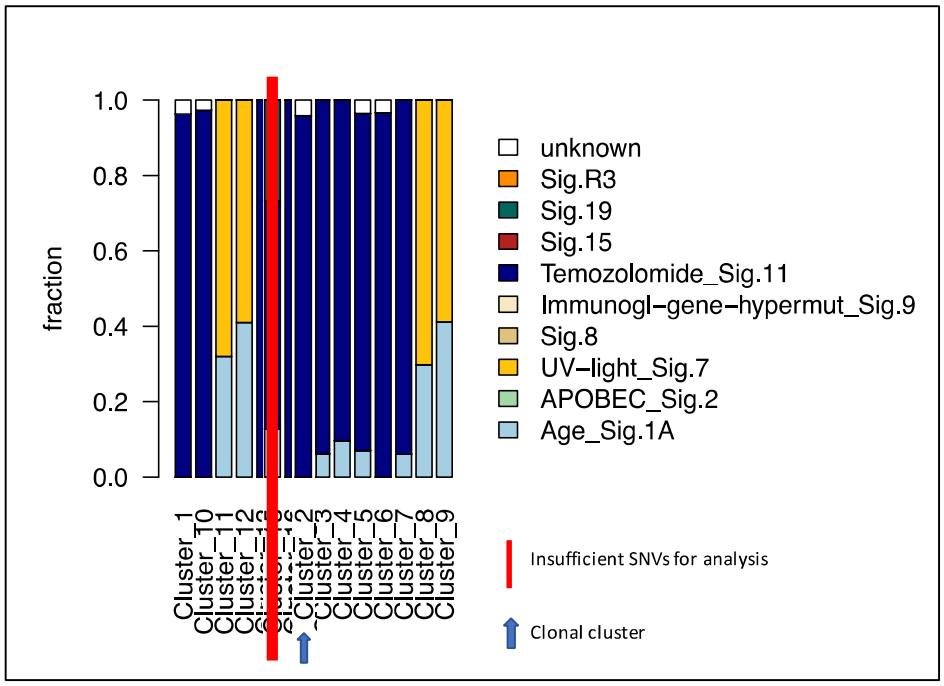

Figure 113 Mutational signature analysis in PEA038
Mutational signatures are based on Pyclone clustering of mutations for creation of phylogenetic trees, with the clonal cluster representing the ubiquitous mutations. Cluster 12 is the clonal cluster. Clusters 1, 2, 3, 4, 5, 6, 7, 8, 9, 11 and 12 contain sufficient SNVs for reliable signature analysis (that is, ≥50).

The median computationally derived ploidy is 3.46 (range 1.70–4.22) across all metastatic sites (including archival; see Table 13 in **Section 3.3.3**). This is in keeping with the FISH analysis (see Figure 114 below), where a modal ploidy of 3 is observed in the two samples

analysed. The median computationally derived ploidy of the archival samples, however, is 1.72 (range 1.67–1.96). The FISH analysis performed on TB40 (archival resected lymph node) is suggestive of a higher estimated ploidy (mode of 3) than the computationally derived ploidy of 1.96 for this sample.

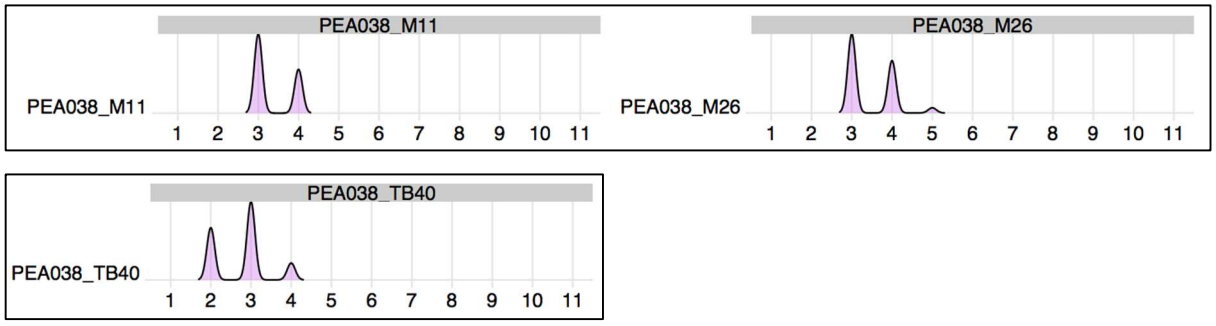

Figure 114 Corrected ploidy estimates of PEA038 samples analysed by FISH.
*The x axis denotes the total probe count for each chromosome (see **Section 3.3.3**) and the y axis denotes the relative frequency.*
NB: TB40 = LNa_2_R2 (archival resected locoregional lymph node); M11 = LN_1_R3 (porta hepatis lymph node); M26 = LI_8_R1 (right lobe liver).

WGD was observed in all the metastatic samples collected at the TH with the exception of one lung region (LU_1_R3). The other sampled region of this lung metastasis (LU_1_R1) did show evidence of WGD. None of the archival samples, including the resected brain lesion, had evidence of WGD. This suggests that WGD was either a subclonal event in the primary tumour, or had emerged outside the primary tumour in different clones in parallel.

The median WGII is 0.54 (range of 0.22 to 0.77) in this case (see Table 13 in **Section 3.3.3**), higher than the median for cutaneous/MUP cases in the cohort (0.44). This was driven by a higher WGII in the nine samples that had undergone WGD (median 0.68) versus the seven that were not WGD (median 0.33).

Driver alterations

The only clonal driver mutation detected by WES was *NRAS Q61K.* A large number of subclonal driver mutations were noted, all in TSGs. Those reported in COSMIC included variants in *TP53, PTEN, CSMD3, MSH6, GATA3* and *ATM*.

The vast majority of SCNAs were subclonal. Clonal arm-level driver SCNAs[1] that were detected included loss of 9p and loss of 17p.

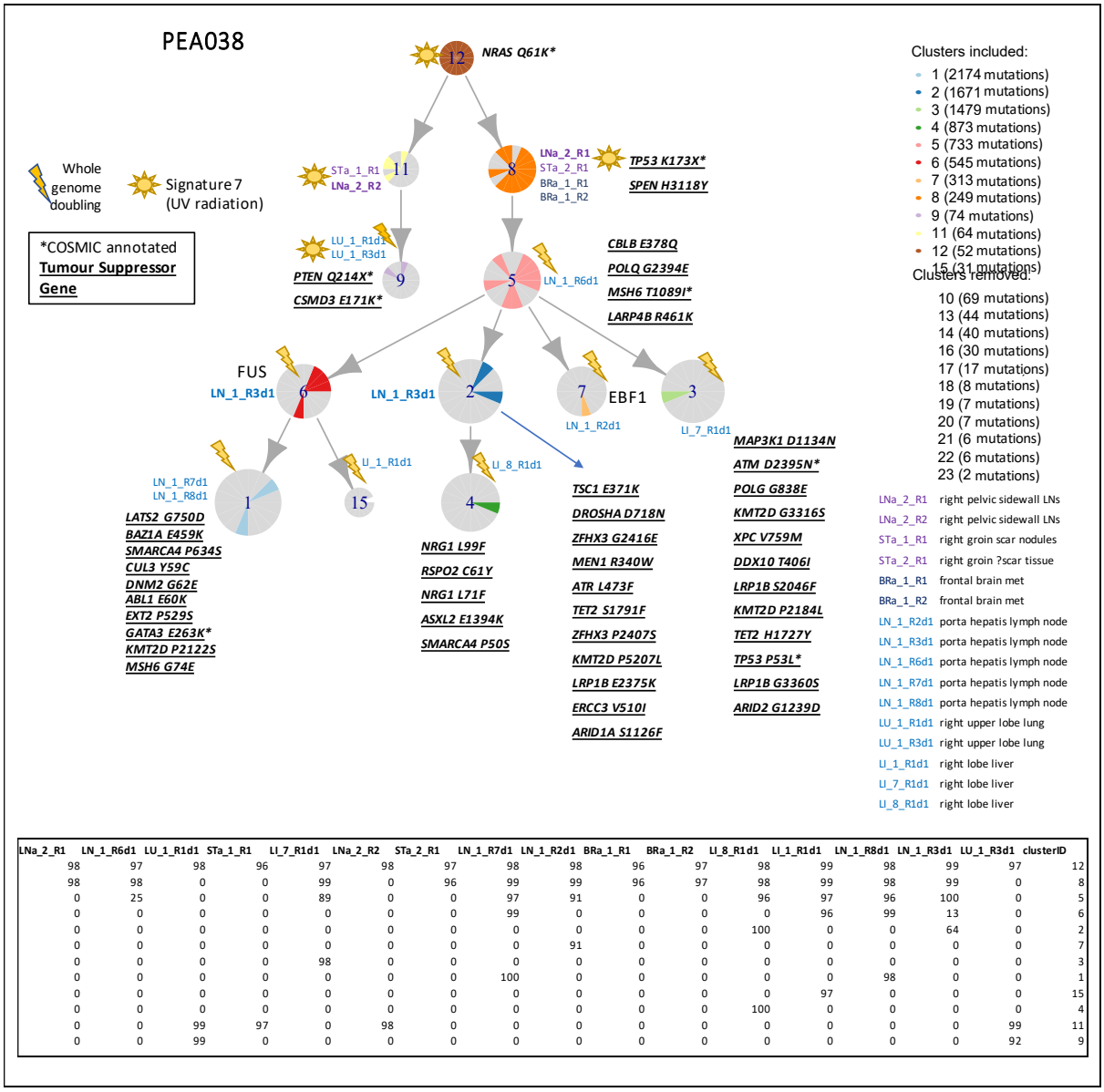

LNa_2_R1	LN_1_R6d1	LU_1_R1d1	STa_1_R1	LI_7_R1d1	LNa_2_R2	STa_2_R1	LN_1_R7d1	LN_1_R2d1	BRa_1_R1	BRa_1_R2	LI_8_R1d1	LI_1_R1d1	LN_1_R8d1	LN_1_R3d1	LU_1_R3d1	clusterID
98	97	98	96	97	98	97	98	98	96	97	98	99	98	99	97	12
98	98	0	0	99	0	96	99	99	96	97	98	99	98	99	0	8
0	25	0	0	89	0	0	97	91	0	0	96	97	96	100	0	5
0	0	0	0	0	0	0	99	0	0	0	0	96	99	13	0	6
0	0	0	0	0	0	0	0	0	0	0	100	0	0	64	0	2
0	0	0	0	0	0	0	0	91	0	0	0	0	0	0	0	7
0	0	0	0	98	0	0	0	0	0	0	0	0	0	0	0	3
0	0	0	0	0	0	0	100	0	0	0	0	0	98	0	0	1
0	0	0	0	0	0	0	0	0	0	0	0	97	0	0	0	15
0	0	0	0	0	0	0	0	0	0	0	100	0	0	0	0	4
0	0	99	97	0	98	0	0	0	0	0	0	0	0	0	99	11
0	0	99	0	0	0	0	0	0	0	0	0	0	0	0	92	9

Figure 115 Phylogenetic tree for PEA038
The clonal cluster of shared mutations sits at the trunk of the tree. Driver mutations belonging to each cluster are annotated. The cancer cell fraction (CCF) of each cluster per metastatic site is detailed in the table beneath the tree.

Evolution and metastatic seeding patterns

The phylogenetic tree for PEA038 (Figure 115) is characterised by a clonal cluster of mutations (Cluster 12) which is much smaller than the majority of the subclonal clusters (52 SNVs versus >500 SNVs in Clusters 1, 2, 3, 4, 5 and 6). In this case, the large number of subclonal mutations (99% subclonal, see Table 12 in **Section 3.3.1**) are most likely driven by DTIC-induced mutagenesis, supported by the temozolomide signature occurring in all clusters except 12, 11, 8 and 9.

As discussed in the previous cases, the absence of paired primary tumour profiling makes it more challenging to decipher evolutionary patterns. Nonetheless, the pattern of primary to metastatic seeding appears polyclonal, with metastatic dissemination a result of at least two separate clones from the primary tumour seeding distant sites. Metastatic sites are seeded either by: 1) a clone harbouring Clusters 12+8 (for example, the brain metastasis (BRa_1), porta hepatis lymph node (LN_1) and liver metastases (LI_1, LI_7 and LI_8) or 2) a clone harbouring Clusters 12+11 (for example, lung metastasis (LU_1)). Supporting this theory is the fact that in addition to Cluster 12, Clusters 8, 9 and 11 show convincing evidence of a UV signature, consistent with an origin in the primary tumour.

The majority of metastatic regions (14/16) are monoclonal based on their CCF values. However, there is evidence of polyclonal seeding. There are two polyclonal metastases that contain clusters from exclusive branches of the phylogenetic tree, suggestive of polyclonal seeding. First, in the resected Stage III right pelvic side wall metastasis (LNa_2), which occurred prior to distant metastatic dissemination evident on imaging, two separate clones from the primary tumour may have seeded this site (12+11 and 12+8), in that both regions sampled (LNa_2_R1 and LNa_2_R2) each contain an exclusive cluster (that is, Cluster 8 in LNa_2_R1 and Cluster 11 in LNa_2_R2). The CCFs of clusters in these two regions suggest they are all clonal, making it likely that the seeding clone already harboured Clusters 8 and 11. Alternatively, it may have developed later, but undertaken a clonal sweep of this region. Second, Region 3 of a large porta hepatis lymph node (LN_1_R3) contains both a clone harbouring Clusters 12+8+5+6 and one harbouring 12+8+5+2, with Clusters 6 and 2 being on exclusive branches of the tree. Other regions of this porta hepatis lymph node contain Cluster 6 at a clonal fraction, suggesting this region (where Cluster 6 is subclonal) could have seeded the metastasis and then clonally expanded. The only other site that shares Cluster 2 is a liver metastasis in which the cluster is clonal, suggesting that it may have been seeded by LN_1_R3.

Whole genome doubling occurred in all distant metastatic sites with the exception of the resected brain metastases and one region of the sampled lung metastasis (LU_1_R3). All of the metastatic regions sampled from the porta hepatis lymph node (LN_1) and the three liver metastases (LI_1, LI_7 and LI_8) were genome doubled and share Cluster 5. While Cluster 5 appears subclonal in Region 6 of the porta hepatis lymph node (LN_1_R6) with a CCF of 25%, it is clonal in all the other regions and in the liver metastases. As such, this may be the

subclone that expanded in the porta hepatis lymph node and seeded the liver metastases. In keeping with a shared clonal origin, the arm-level SCNA profile of the porta hepatis lymph node and the liver metastases appears distinct from the archival metastatic sites (LNa_2, STa_1, STa_2 and BRa_1) and those of the lung metastasis (LU_1), with a much greater number of arm-level gains (Figure 116). These sites also share a temozolomide mutational signature. The porta hepatis lymph node and right liver metastases were noted to be progressing sites of disease after temozolomide therapy and a genome doubling event may have driven this. Region 1 of the lung metastasis (LU_1_R1) was also noted to have undergone whole genome doubling. This appears to be a parallel, independent event from the genome doubling in the porta hepatis and liver metastases, and its differing SCNA profile also supports this (Figure 116 and Figure 117). It shares the same pattern of arm and cytoband copy number losses as Region 3 of the lung metastasis, distinct from the porta hepatis and liver metastatic sites.

A temozolomide signature was not evident in the resected metastatic sites – pelvic sidewall lymph node (LNa_2), scar recurrence (STa_1 and STa_2) or brain metastasis (BRa_1) – consistent with a lack of exposure to this treatment. All metastases exposed to temozolomide had evidence of a temozolomide signature other than the right lung metastasis (LU_1_R1 and R3). The histology from these lung regions was reviewed and a spindle-cell, rather than an epithelioid cell morphology was noted.

The arm-level copy number profiles of the metastases support the mutational clustering and provide additional support for both intrametastatic heterogeneity (for example, within LNa and LN_1) and intermetastatic heterogeneity (Figure 116 and Figure 117).

A large number of subclonal driver alterations were detected (Figure 115). Notably, a *PTEN* mutation in the lung metastasis, with concurrent copy number loss of *PTEN* (see Figure 118). There are two *TP53* mutations, one found in the resected locoregional relapse, as well as the resected brain metastasis, and another in liver metastasis 7. Clonal arm-level loss at 17p (harbouring *TP53*) was evident. An *MSH6* mutation, belonging to the mismatch-repair family of genes, and also reported in COSMIC in two CNS and one skin tumour, was found in the porta hepatis and liver metastases (Cluster 5). In addition, a number of other DNA damage repair genes are subclonal drivers in these metastatic sites impacted by temozolomide-induced DNA damage, including a second *MSH6* mutation (Cluster 1), an *ATR* mutation (Cluster 2) and an *ATM* mutation (Cluster 3). Hypermutation as a consequence of

temozolomide-induced DNA damage repair mutations may have occurred as Clusters 1, 2 and 3 have the highest number of SNVs. This phenomenon has been described in glioblastoma.[2]

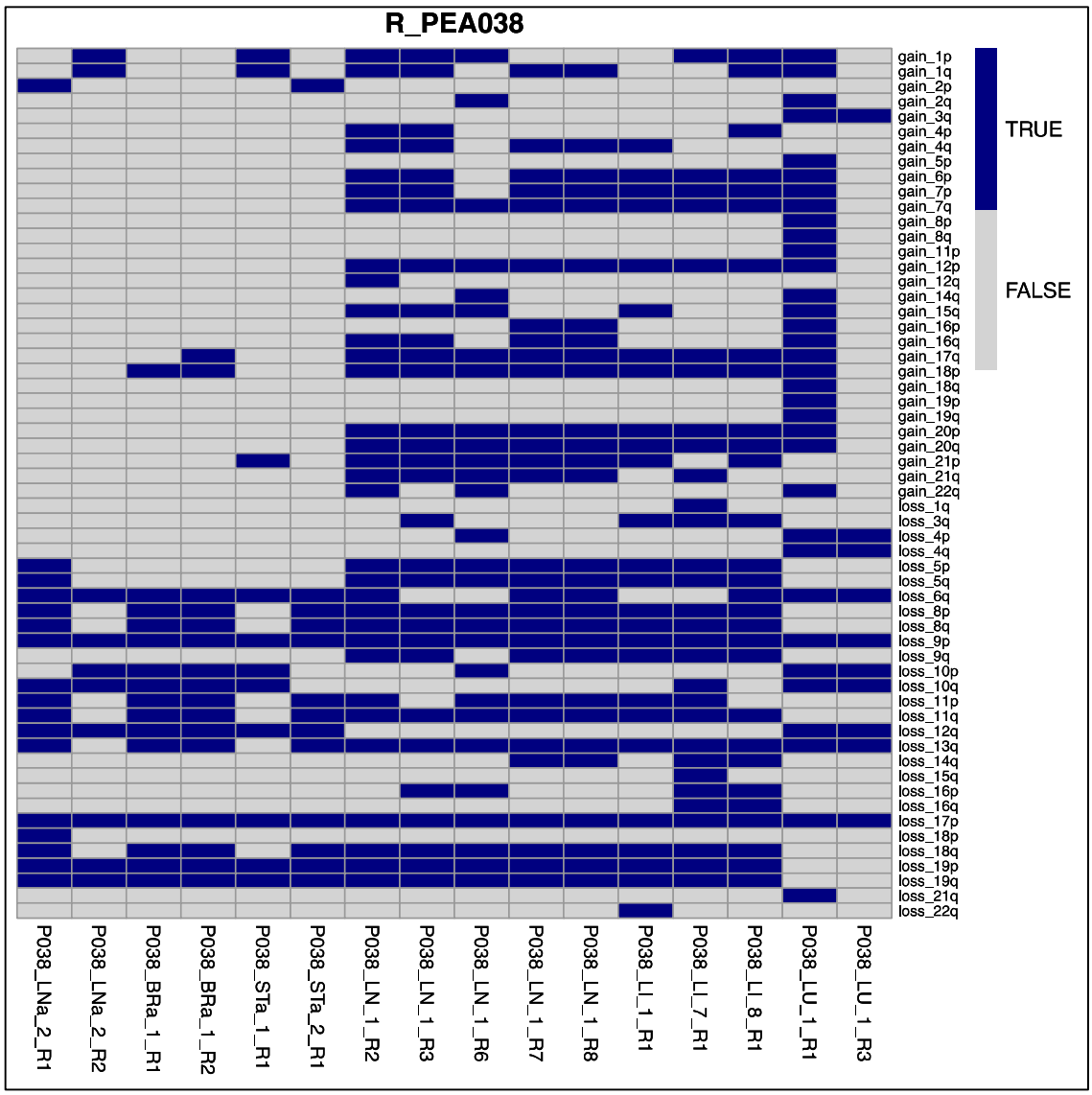

Figure 116 Chromosomal arm-level losses and gains
Blue squares indicate whether there was loss or gain of at least one copy of the chromosome arm relative to the mean ploidy of all samples.

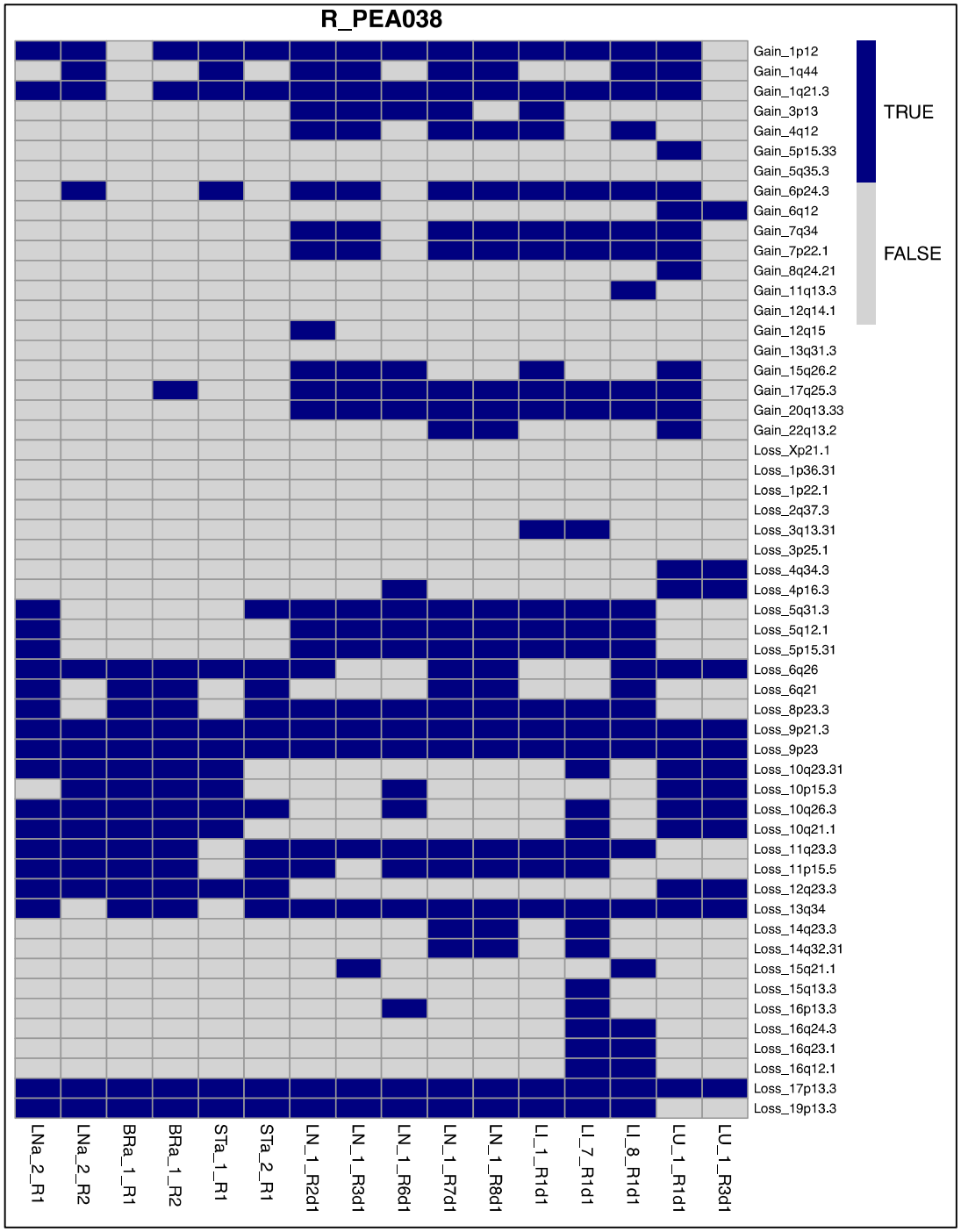

Figure 117 Cutaneous melanoma driver cytoband gains and losses
Annotated cytobands are melanoma driver regions determined by a GISTIC analysis of TCGA data.[1] Blue squares indicate whether there was loss or gain of at least one copy of the cytoband relative to the mean ploidy of all samples.

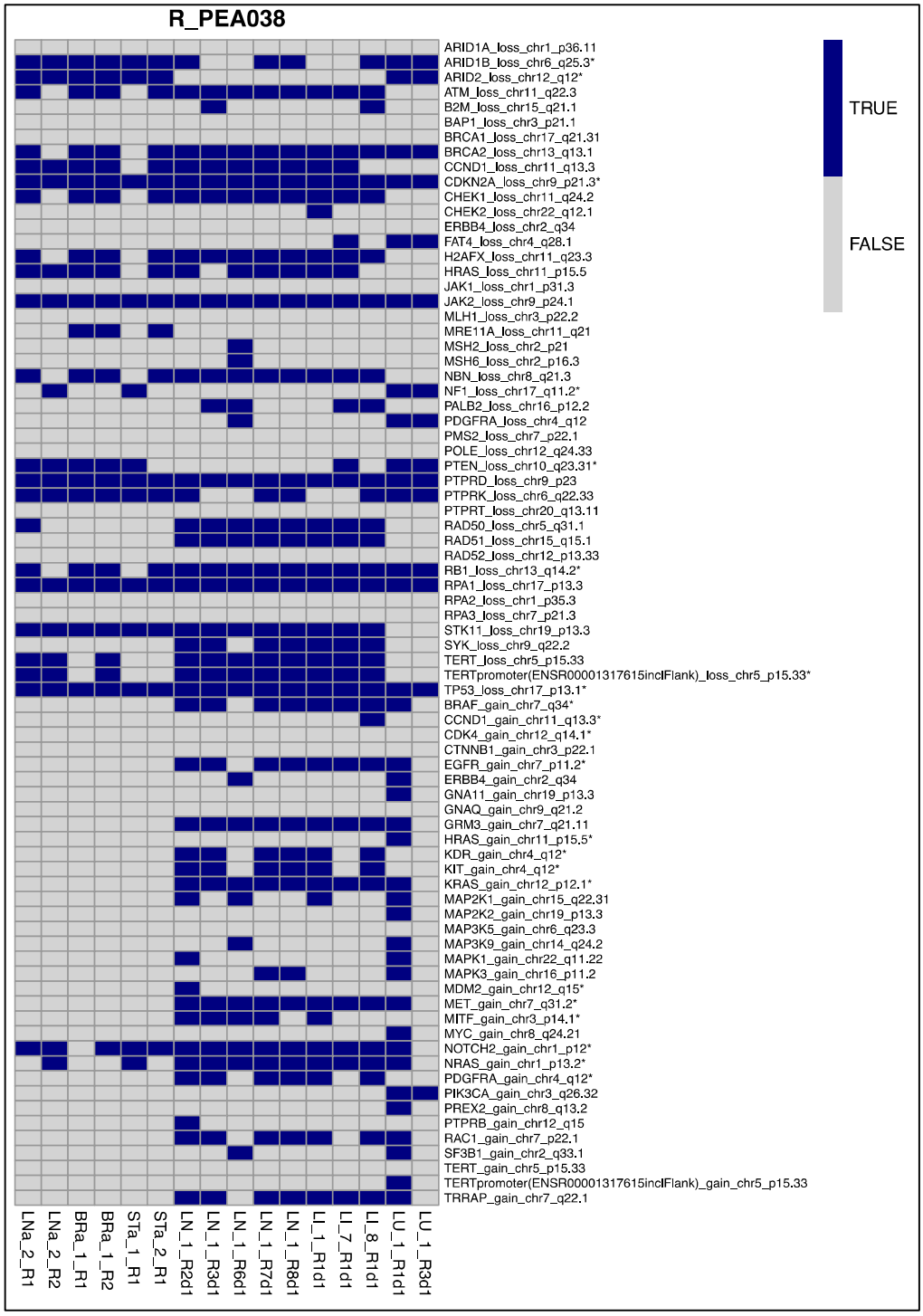

Figure 118 Driver gene gains and losses
Genes with an asterisk (*) are noted driver genes in the TCGA and Hayward data sets.[1,3] Blue squares indicate whether there was loss or gain of at least one copy of the gene relative to the mean ploidy of all samples.

Genomic mechanisms of treatment resistance

In terms of possible treatment resistance mechanisms, the right lung metastatic regions (LU_1) contain a *PTEN* mutation with evidence of copy number loss (see Figure 118), and were noted to develop and progress during the course of ipi+nivo. *PTEN* loss has been

associated with immune escape, as discussed in the **Main Introduction Section 1.2.7 Systemic treatment of melanoma and genomic mechanisms of treatment resistance**.[4] In the resected brain metastasis which progressed during the course of ipi+nivo, SCNAs were dominated by losses, rather than gains at the arm and cytoband levels (Figure 116 and Figure 117)|, a phenomenon described in non-responders to sequential anti-CTLA4 and anti-PD1.[5] Relative to the high overall mutational burden in this case (13476 nsSNVs), only a very small proportion of mutations were clonal (1%), with the high burden of subclonal mutations likely induced from temozolomide treatment.

Mutations in genes involved in DNA damage repair pathways emerged on temozolomide therapy: *MSH6, ATM* and *ATR*. The high resultant mutation burden may have provided the substrate for resistance to temozolomide, as has been described in glioblastoma.[6,7]

Case summary

In PEA038, the pattern of metastatic dissemination from the primary tumour appears polyclonal, with at least two separate clones seeding different metastatic sites. With the exception of the resected brain metastasis, the profiled distant metastatic sites were those progressing on temozolomide. The samples taken from the spleen and right pelvis did not yield any tumour, likely due to treatment response. The progressive intracranial disease evident at the end of life unfortunately was not accessible due to time constraints at the TH.

Although the overall TMB was very high, this was largely driven by the temozolomide treatment, as evidenced by the temozolomide signature in the majority of metastases. The clonal mutation burden was low for a sun-exposed cutaneous melanoma.

There are several points of interest in this case. First, there may have been a WGD event that occurred in the porta hepatis lymph node driving progression and metastatic spread, on the background of a *TP53* mutation. Second, it appears that WGD has occurred as a parallel event in one of two regions of the right lung metastasis. Third, the right lung metastasis appears to have been spared the mutagenic effects of temozolomide. Two hypotheses may be considered to explain this phenomenon. A phenotypic switch may have occurred, resulting in a non-proliferating, drug-tolerant state.[8] Phenotypic plasticity is described in melanoma[9] and the altered, spindle cell morphology supports a morphological change. Alternatively, there may have been a particular characteristic of the TME that helped reduce temozolomide

exposure. Characterisation of the TME will be undertaken as part of further work in this cohort.

References for PEA038

1. Cancer Genome Atlas N: Genomic Classification of Cutaneous Melanoma. *Cell* 161: 1681–96, 2015.
2. Johnson BE, Mazor T, Hong C, et al. Mutational analysis reveals the origin and therapy-driven evolution of recurrent glioma. *Science* 343: 189–193, 2014.
3. Hayward NK, Wilmott JS, Waddell N, et al. Whole-genome landscapes of major melanoma subtypes. *Nature* 545: 175–180, 2017.
4. Peng W, Chen JQ, Liu C, et al. Loss of PTEN Promotes Resistance to T Cell-Mediated Immunotherapy. *Cancer Discov* 6: 202–16, 2016.
5. Roh W, Chen PL, Reuben A, et al. Integrated molecular analysis of tumor biopsies on sequential CTLA-4 and PD-1 blockade reveals markers of response and resistance. *Sci Transl Med* 9, 2017.
6. Yip S, Miao J, Cahill DP, et al. MSH6 mutations arise in glioblastomas during temozolomide therapy and mediate temozolomide resistance. *Clin Cancer Res* 15: 4622–9, 2009.
7. Hunter C, Smith R, Cahill DP, et al. A hypermutation phenotype and somatic MSH6 mutations in recurrent human malignant gliomas after alkylator chemotherapy. *Cancer Res* 66: 3987–91, 2006.
8. Mani SA, Guo W, Liao MJ, et al. The epithelial-mesenchymal transition generates cells with properties of stem cells. *Cell* 133: 704–15, 2008.
9. Arozarena I, Wellbrock C: Phenotype plasticity as enabler of melanoma progression and therapy resistance. *Nat Rev Cancer* 19: 377–391, 2019.

Case study 14: PEA060

Clinical summary

Patient PEA060 was a 53 year old man who presented in March 2017 with palpable right inguinal lymphadenopathy confirmed on biopsy to be *BRAF* wild-type melanoma. He had no prior history of a primary melanoma; hence, his first presentation was with Stage III disease. Following right inguinal lymph node dissection, he developed another two episodes of local recurrence in the right groin in August and October 2017, both resected. In December 2017 he was diagnosed with widespread metastatic disease involving the liver, lungs, bones and pelvic lymph nodes and commenced systemic treatment in January 2018, with combination ipilimumab and nivolumab. After two cycles of therapy he was admitted to hospital with acute delirium. There was no definitive evidence of brain metastases on MRI and his presentation may have been a neurological immune-related adverse event secondary to immune checkpoint blockade. Treatment was discontinued in February 2018, and weeks later he had multi-site progression, dying in April 2018 (Figure 119).

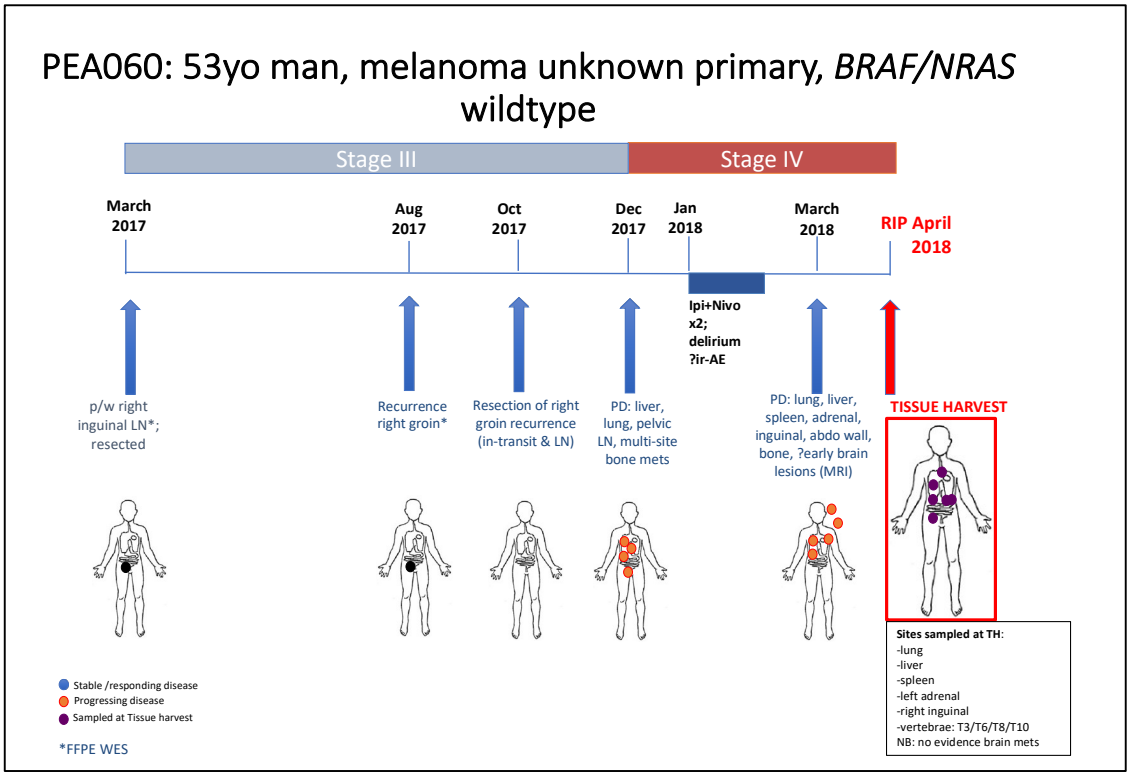

Figure 119 Timeline of clinical events, treatment and disease response in PEA060
Best overall RECIST response is included in brackets for each line of treatment (CR: complete response; PR: partial response; SD: stable disease; PD: progressive disease). LN: lymph node(s); FFPE: formalin-fixed paraffin-embedded; WES: whole exome sequencing; mets: metastases; ipi+nivo: ipilimumab and nivolumab; ir-AE: immune-related adverse event; MRI: magnetic resonance imaging.

Tissue harvest (TH) sampling and quality control considerations

At the TH, 38 tumour regions were sampled from 38 individual metastases. Given the absence of a known driver mutation, and availability of the melanoma panel at the time of this case, 36 out of the 38 samples were submitted for panel sequencing (in 2/38 there was an inadequate concentration of extracted DNA). Ten of these were selected for WES to cover the spectrum of metastatic sites. In addition, eight regions from the locoregional lymph node and soft tissue resections (archival FFPE tissue blocks) were submitted. Three out of the 10 samples from the TH and 1/8 FFPE tissue samples failed QC for low tumour purity. Of the three TH samples (from lung and bone metastases), one had poor purity on retrospective H&E review (0–25% tumour), but another had high purity (>75%). This discrepancy could be explained by variable tumour content in this sample. There was no matched slide for the third sample.

Genomic features

The TMB is 187 nsSNVs or 9.86 mutations/Mb. The clonal proportion of mutations is 94%. A dominant UV signature is evident (Figure 120), consistent with a regressed cutaneous primary tumour (see Table 12 in **Section 3.3.1**).[1]

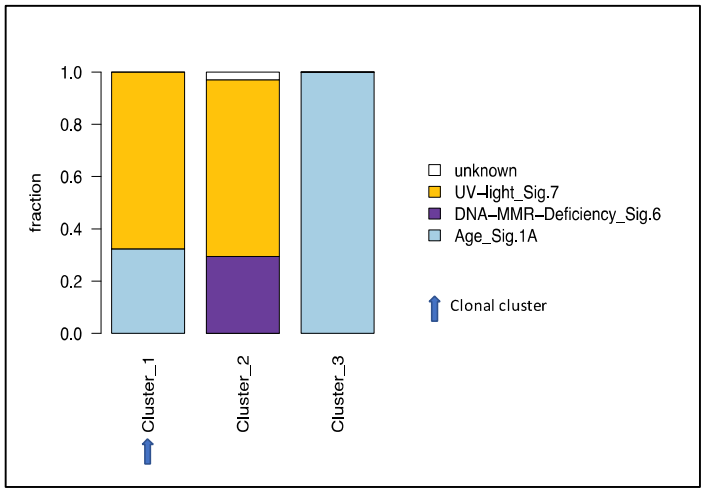

Figure 120 Mutational signature analysis of PEA060
Mutational signatures are based on Pyclone clustering of mutations for creation of phylogenetic trees, with the clonal cluster representing the ubiquitous mutations. Cluster 1 is the clonal cluster and is the only cluster with enough SNVs for reliable signature analysis.

The median computationally derived ploidy for PEA060 is 4.15, with evidence of two rounds of WGD in all samples. The FISH analyses of two metastases reveals a mode ploidy of 2 in each sample (range 2–4) suggestive of a dominant diploid population. (Figure 121). The median WGII is 0.70 (see Table 13 in **Section 3.3.3**).

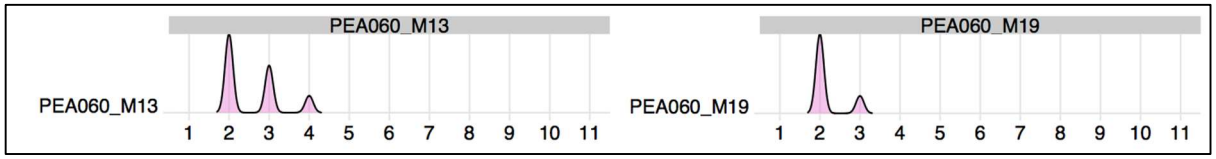

Figure 121 Corrected ploidy estimates of PEA060 samples analysed by FISH
*The x axis denotes the total probe count for each chromosome (see **Section 3.3.3**) and the y axis denotes the relative frequency.*
NB: M13 = AD_1_R1; M19 = LI_4_R1.

Driver alterations

Clonal mutations previously annotated in COSMIC[2] are noted in the key TSGs *CDKN2A*, *PTEN* & *TP53* (Figure 122). There is associated copy number loss of these gene loci in all samples, with the exception of two regions from the resected right inguinal lymph nodes (at the first presentation of melanoma, Figure 119) where no loss of the *TP53* gene locus is noted

(LNa_1_R1 and R4). Given the median ploidy of this case is >2, 'loss' does not imply loss of heterozygosity as there may be additional copies gained of the wild-type allele (see **Appendix A Bioinformatic methods**).

There are also clonal mutations in other TSGs predicted to be deleterious (see **Materials and Methods Section 2.11**): *MAP2K4, SMARCA4* and *RUNX1*.

There are multiple SCNAs across the samples in this case, the majority being subclonal. Clonal driver arm-level gains are seen in Chr 7, 8q, Chr 20 and 22q, with driver arm-level losses at 5q, 6q, Chr 9, 10q, 11p and 18q (Figure 123).[1] The clonal SCNAs at the cytoband and gene level are all consequent to arm-level changes (Figure 124 and Figure 125.

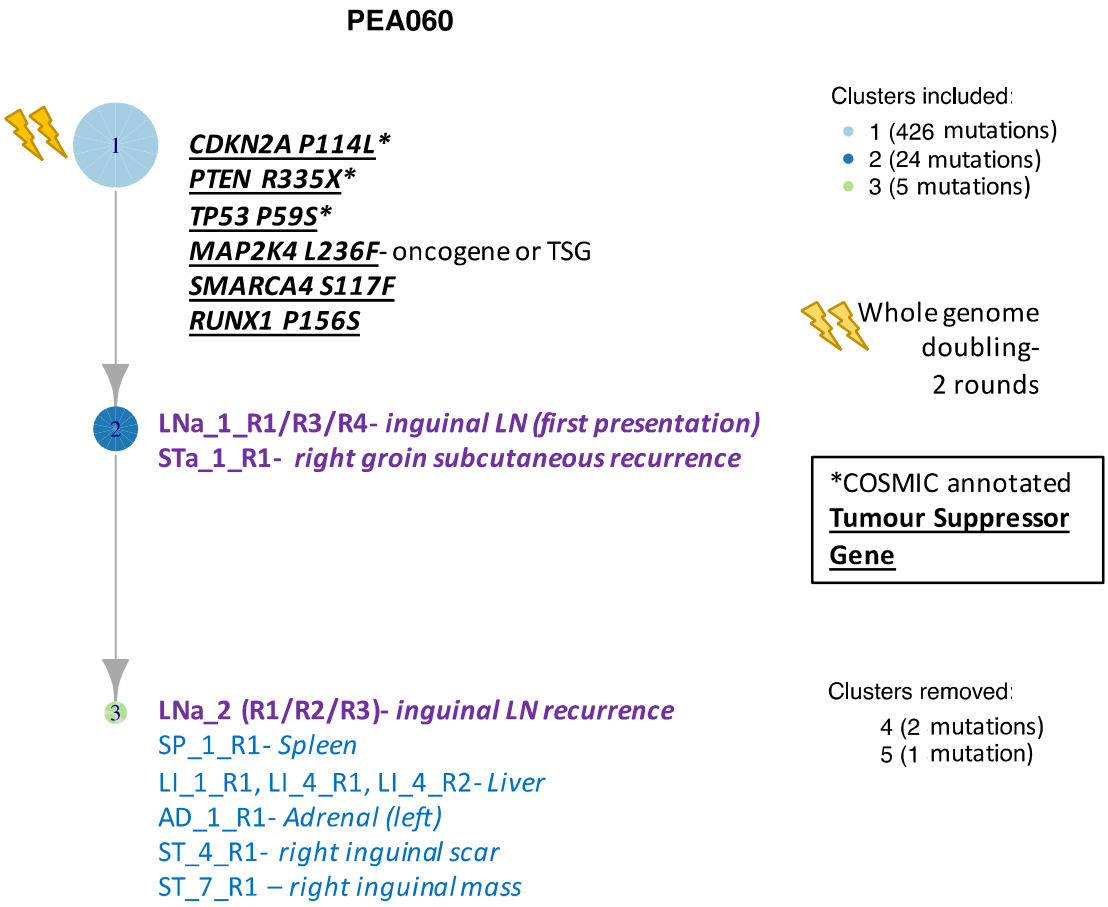

LNa_2_R1d1	LNa_2_R2d1	LNa_2_R3d1	LNa_1_R1d1	LNa_1_R3d1	LNa_1_R4d1	STa_1_R1d1	SP_1_R1d1	LI_1_R1d1	LI_4_R1d1	LI_4_R2d1	AD_1_R1d1	ST_4_R1d1	ST_7_R1d1	clusterID
100	99	100	97	98	99	100	99	99	99	100	99	100	99	1
86	84	87	72	65	77	87	90	95	94	93	93	95	97	2
93	87	87	0	0	0	0	93	90	88	88	92	96	89	3

Figure 122 Phylogenetic tree for PEA060
The clonal cluster of shared mutations sits at the trunk of the tree (Cluster 1). Driver mutations belonging to each cluster are annotated. The cancer cell fraction (CCF) of each cluster per metastatic site is detailed in the table beneath the tree.

Evolution and metastatic seeding patterns

As discussed in previous cases, the absence of comprehensive primary tumour profiling limits the inferences that can be made regarding the pattern of metastatic seeding. In this case, there are two clones that appear to have seeded metastatic sites (Figure 122): the first, containing Clusters 1+2, appears responsible for the first presentation of disease in the right inguinal lymph nodes (March 2017; Figure 119). The second clone, containing Clusters 1+2+3, is likely a descendant clone from the first that further evolved and is responsible for seeding the right inguinal lymph node disease at the first recurrence (LNa_2_R1/2/3; August

2017), as well as the distant metastatic sites at Stage IV relapse (that is, spleen, liver and adrenal gland). It is probable that this second clone evolved after the first seeded the right inguinal lymph node metastases, because Cluster 3 only contains five mutations and appears later (that is, at the recurrence). Assuming this is the case, the primary to metastatic seeding pattern is monoclonal.

All three regions of the right inguinal lymph node specimen from the first presentation (LNa_1_R1/R3/R4) are polyclonal in their composition as the CCFs for Cluster 2 vary between 65–77% across the three sampled regions. All distant metastases sampled at tissue harvest are monoclonal in their composition, as is the inguinal lymph node recurrence.

The chromosome arm-level SCNA profile of the original right inguinal lymph node (LNa_1) suggests heterogeneity between the regions sampled (Figure 123). Region 1 (LNa_1_R1) appears most similar to the recurrent inguinal lymph node disease (LNa_2) as well as the distant metastases, suggesting it may represent the clone responsible for metastatic seeding.

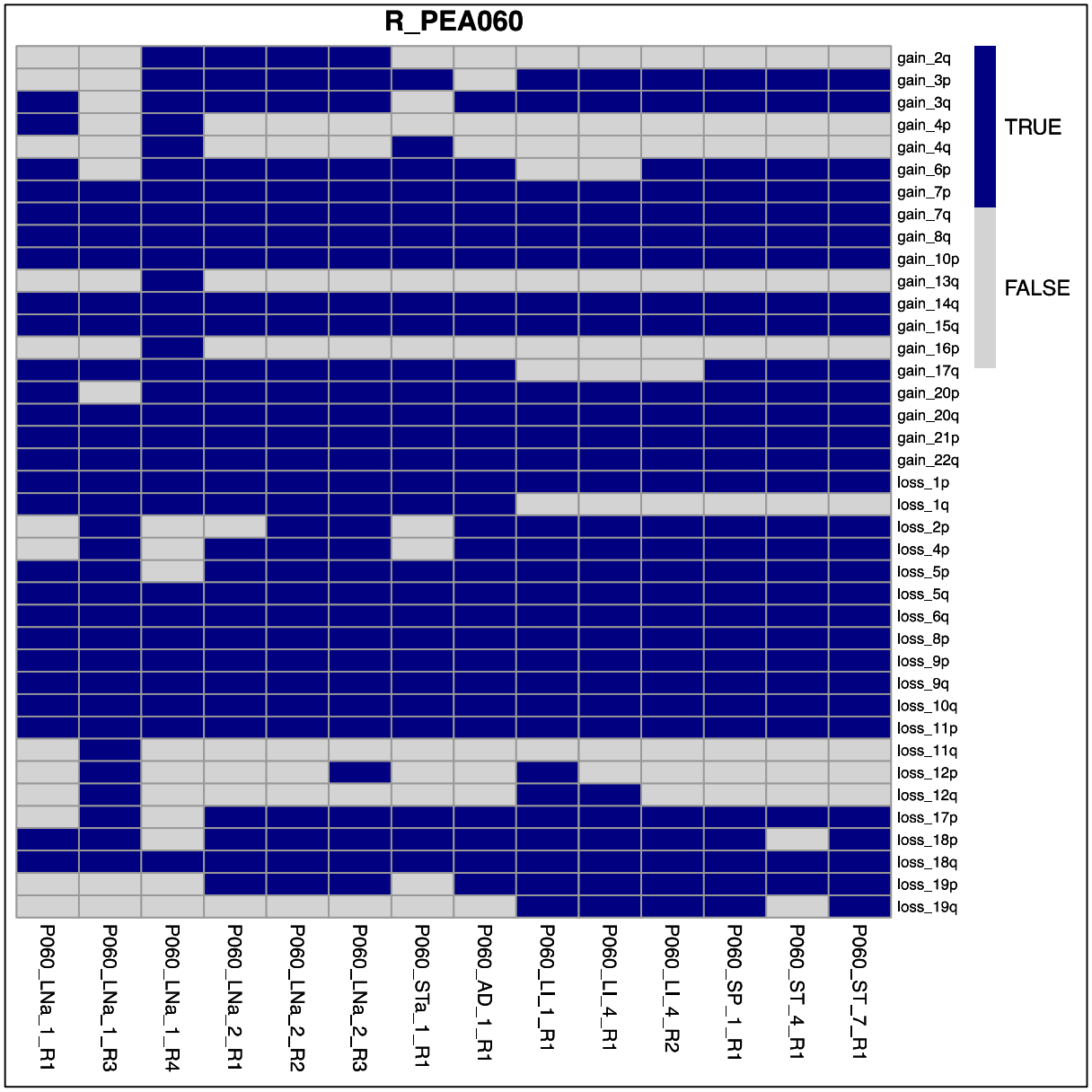

Figure 123 Chromosomal arm-level losses and gains
Blue squares indicate whether there was loss or gain of at least one copy of the chromosome arm relative to the mean ploidy of all samples.

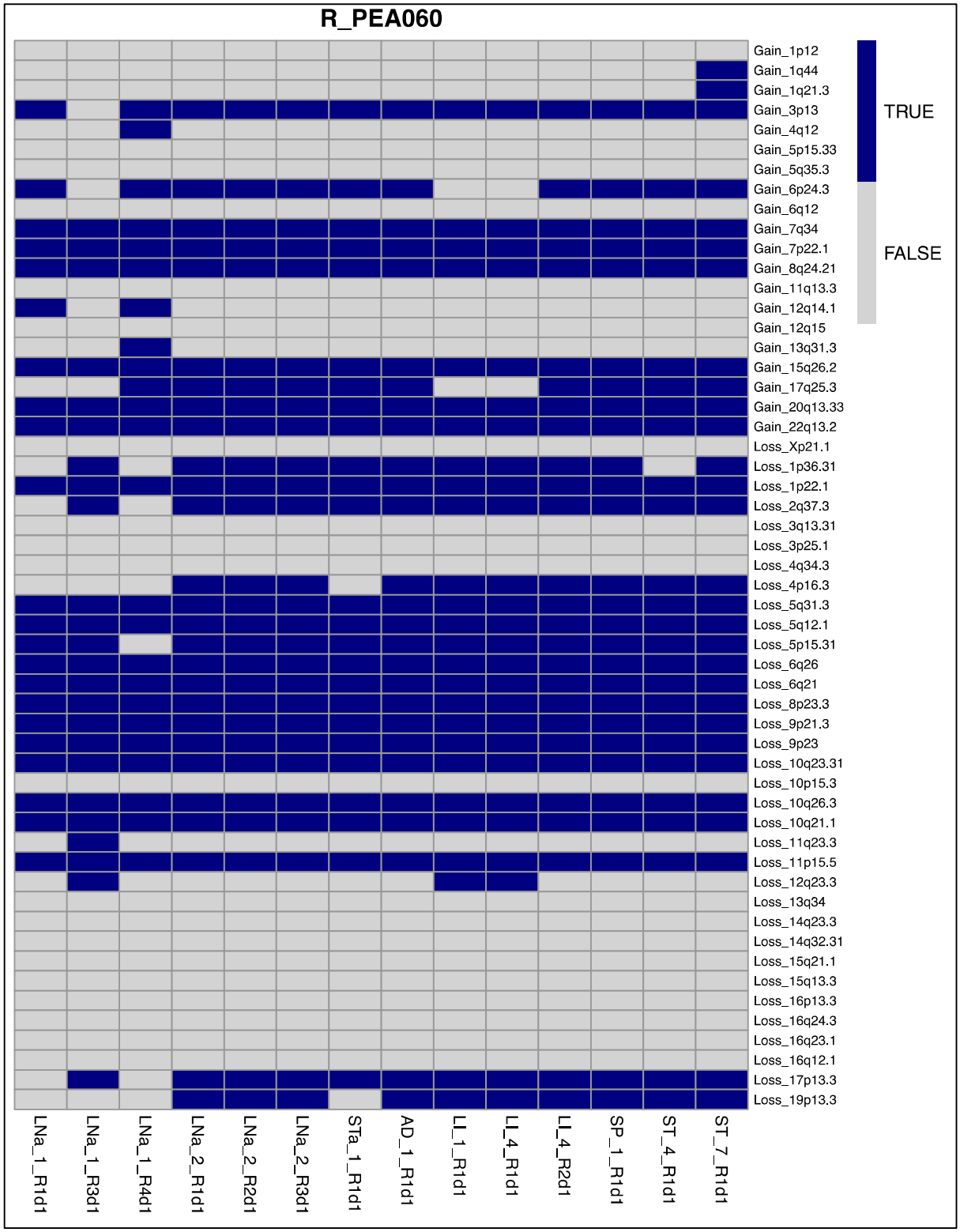

Figure 124 Cutaneous melanoma driver cytoband gains and losses
Annotated cytobands are melanoma driver regions determined by a GISTIC analysis of TCGA data.[1] Blue squares indicate whether there was loss or gain of at least one copy of the cytoband relative to the mean ploidy of all samples.

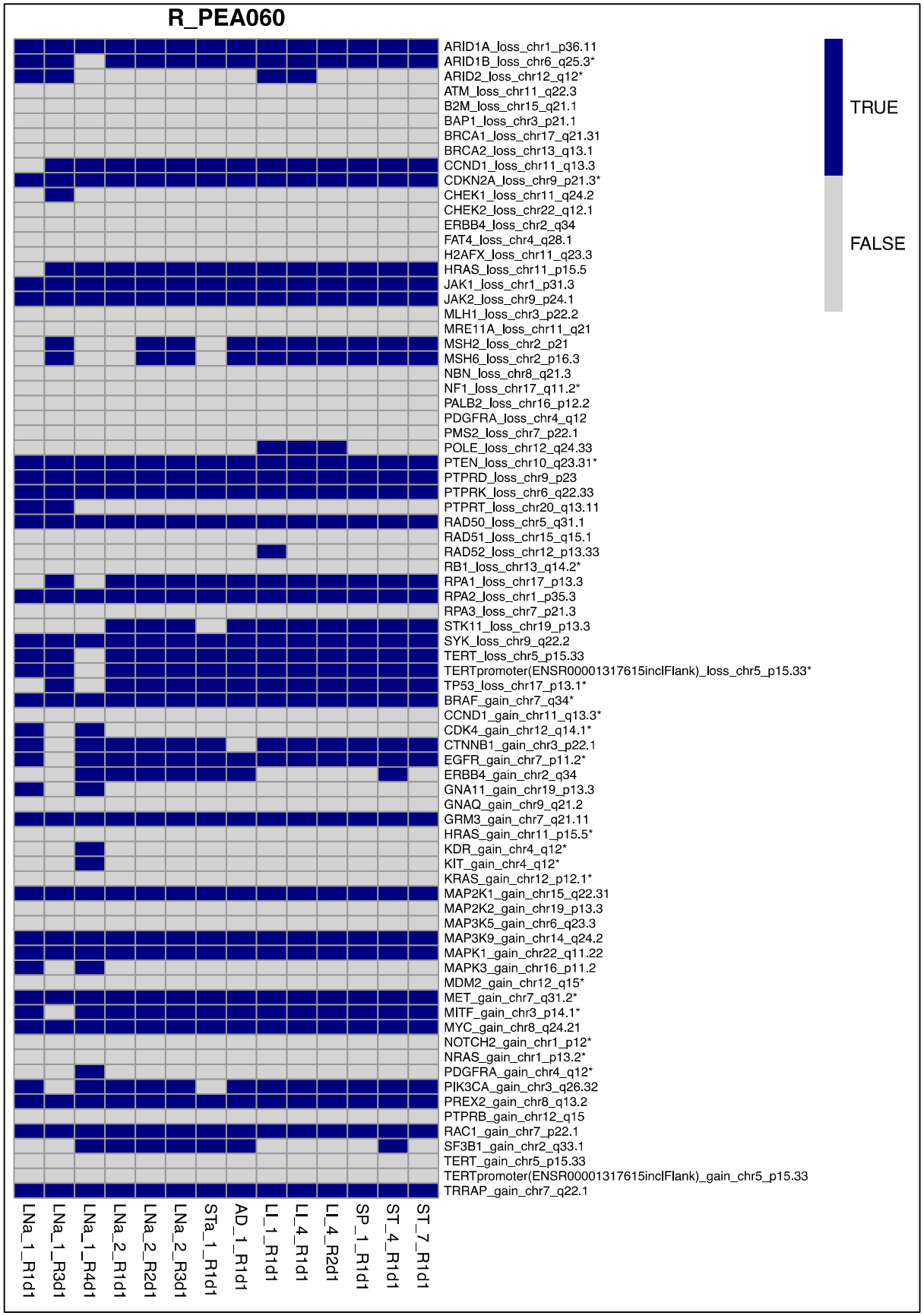

Figure 125 Driver gene gains and losses

Genes with an asterisk (*) are noted driver genes in the TCGA and Hayward data sets.[1,3] Blue squares indicate whether there was loss or gain of at least one copy of the gene relative to the mean ploidy of all samples.

Genomic mechanisms of treatment resistance

PEA060 received only one line of systemic therapy – two cycles of ipi+nivo- to which his disease appeared refractory. There are three putative genomic mechanisms of ICI resistance. First, loss of *PTEN* function has been associated with resistance to PD-1 blockade in preclinical melanoma models, with evidence of reduced T cell infiltration and increased levels of immunosuppressive cytokines.[4] Second, copy number loss of both *JAK1 & JAK2* (without corresponding mutations) may have downregulated the JAK/STAT pathway if there was haploinsufficiency (as already discussed in other cases), or if the other allele was methylated. The contribution of these alterations to ICI resistance is speculative, and transcriptomic profiling will potentially corroborate changes in the relevant pathways. Third, the high WGII score in PEA060 is suggestive of chromosomal instability, associated with immune evasion through chronic activation and subversion of the cGAS-STING pathway.[5]

Case summary

PEA060 provides an example of an aggressive melanoma with a high tumour mutational burden, which was refractory to combination checkpoint blockade. The presence of two rounds of clonal WGD coupled with a high WGII score suggests that the (unknown) primary tumour may have been characterised by a punctuated evolutionary event. The primary to metastatic seeding pattern was likely monoclonal, with initial seeding of the right inguinal lymph nodes and further evolution of this clone occurring prior to distant spread. Consistent with this, the sampled distant metastases at the TH were all monoclonal in their composition and there was no inter-metastatic heterogeneity in SNVs. The SCNA profile looked relatively uniform across the TH metastases as well, supporting the clustering analysis.

The mechanisms behind primary treatment resistance to ipi+nivo are likely to have led to immune evasion, but warrant further validation.

There is a lack of concordance in this case between the estimated ploidy by computational methods (4.15) and by FISH (mode of 2). This highlights the challenges of determination of ploidy, as noted by others.[6] This may be due to the limitations of interphase FISH (see **Materials and Methods Section 2.10**), and is explored further in the chapter discussion. Although Chr 2 and Chr 15 (the centromeric probes used for FISH) did not demonstrate arm-level events in PEA060, the higher ploidy may have increased nuclear size, leading to greater

segmentation of nuclei and under-representation of true chromosomal number. In the first instance, repeating the FISH analysis would be prudent.

Despite the absence of a 'classic' melanoma driver gene amenable to targeted therapy, other clonal mutations may represent potential drug targets. Mutations in *MAP2K4* are noted most frequently in breast cancer, and may confer sensitivity to MEK inhibition.[7] *SMARCA4* encodes the catalytic ATPase subunit of SWI/SNF pathway (SWItch/Sucrose Non-Fermentable) chromatin remodelling complexes and is frequently mutated in cancer.[2] In NSCLC, *SMARCA4* deficient tumours may be susceptible to CDK4/6 inhibition.[8] Deciphering druggable targets in *BRAF* wild-type melanomas remains an area of clinical need.

References for PEA060

1. Cancer Genome Atlas N: Genomic Classification of Cutaneous Melanoma. *Cell* 161: 1681–96, 2015.
2. Tate JG, Bamford S, Jubb HC, et al. COSMIC: the Catalogue Of Somatic Mutations In Cancer. *Nucleic Acids Res* 47: D941–D947, 2019.
3. Hayward NK, Wilmott JS, Waddell N, et al. Whole-genome landscapes of major melanoma subtypes. *Nature* 545: 175–180, 2017.
4. Peng W, Chen JQ, Liu C, et al. Loss of PTEN Promotes Resistance to T Cell-Mediated Immunotherapy. *Cancer Discov* 6: 202–16, 2016.
5. Bakhoum SF, Cantley LC: The Multifaceted Role of Chromosomal Instability in Cancer and Its Microenvironment. *Cell* 174: 1347–1360, 2018.
6. Dentro SC, Leshchiner I, Haase K, et al. Characterizing genetic intra-tumor heterogeneity across 2,658 human cancer genomes. *Cell* 184: 2239–2254 e39, 2021.
7. Xue Z, Vis DJ, Bruna A, et al. MAP3K1 and MAP2K4 mutations are associated with sensitivity to MEK inhibitors in multiple cancer models. *Cell Res* 28: 719–729, 2018.
8. Xue Y, Meehan B, Fu Z, et al. SMARCA4 loss is synthetic lethal with CDK4/6 inhibition in non-small cell lung cancer. *Nat Commun* 10: 557, 2019.

3.4 Discussion

3.4.1 Cohort overview

In this section I have presented detailed case studies of a cohort of 14 patients with metastatic melanoma who underwent research THs, focusing on hypothesised trajectories of metastatic seeding and evaluating metastatic heterogeneity. Clinically, this was a poor prognostic cohort, characterised by low rates of response to both targeted and immune checkpoint therapies (only 3/14 responding to ICIs and 3/4 cases with *BRAF V600E* mutations to MAPK inhibition), the presence of brain metastases (9/14) and a relatively short median overall survival from diagnosis and treatment of Stage IV disease (cohort median 15.4 months, versus 25 months for dab+tram,[32] 37.6 months for nivolumab monotherapy[33] and >60 months for ipi+nivo combination therapy).[34]

Due to the access afforded by the TH, a median of 36 metastatic regions were sampled per case, with 137 samples overall successfully profiled using WES for this analysis. Paired primary tumour samples were successfully profiled in 6/14 cases. The median TMB for both the sun-exposed cutaneous/MUP cases (13.26 SNVs/Mb) as well as the acral/mucosal/ perianal cases (2.5 SNVs/Mb) was consistent with that reported in the literature (16.8 mutations/Mb and 2.1 mutations/Mb respectively).[29,35] As expected, in most cases, the majority of mutations were clonal, consistent with other melanoma cohorts, and reflecting the fact that UV-induced mutations are accumulated prior to subclonal diversification.[26,36] In 3/14 cases I observed a higher proportion of subclonal mutations. In two of these cases (PEA012 and PEA038) mutational signatures highlight the role of cytotoxic chemotherapy in driving subclonal mutagenesis, fuelling the appearance of parallel events in putative oncogenic driver genes and genes involved in resistance mechanisms. In PEA026 subclonal clusters showed evidence of signatures consistent with homologous recombination deficiency and APOBEC enzyme- induced DNA alterations.

3.4.2 Tissue quality control

PMIs in the PEACE study are much longer than in other published research autopsy cases, with 12/14 undertaken after 24 hours, and 7/14 undertaken after 48 hours. In other studies most post-mortems are noted to be performed within 24 hours[2,3,37,38] or 48 hours,[4] or described as ‘rapid’ or ‘warm’[1] implying they are performed very soon after death.

Macroscopic tumour sampling guided by a histopathologist at the TH demonstrated reassuring accuracy, with >80% of samples containing more than 50% tumour. There were very few autolysed tumour samples (3%), suggesting this is not a major challenge in the analysis of PM tumour tissue.

Undertaking a TH more than 48 hours from death does not appear to compromise nucleic acid integrity as assessed by the DIN or RIN, as compared to THs performed under 48 hours. The tumour DNA quality was high overall (86% with DIN scores >6), also evidenced by successful WES from the vast majority of TH samples (100% in 8/14 cases, >85% in 4/14). The RNA quality was more variable however according to RIN values (only 12% having a RIN >6). There was no clear relationship between PMI and DNA & RNA quality metrics in this cohort, consistent with the literature.[8]

The relatively low RIN scores does not preclude the utility of RNA samples for sequencing. Samples with RINs of 2.7 have demonstrated robust hybridisation.[13] In the breast cancer PM study by De Mattos-Aruda et al.,[1] samples with RIN >2 were successfully profiled using RNAseq and immune deconvolution tools. In other work based in rats, mRNA of suitable quality for RT-PCR was extracted even after 96 hours; however, degradation over time was noted.[39] The RIN score itself may not be the best measure of RNA quality for this purpose, and bioinformatic quality control analyses such as mRIN and 3' mapping that are focused on messenger RNA integrity (rather than ribosomal RNA like RIN scores) will be explored in future for this cohort.[40,41]

There are other potential limitations in the quality metrics and interpretation of samples from the TH. This quality control analysis based on DIN/RIN scores and their relationship to the PMI does not take into account other variables such as the time from TH to extraction, nor the time from DNA extraction to sequencing (that is, the stability of nucleic acids stored at -80°C). Whether samples taken at post-mortem represent the true physiological state before death (for example in the tumour microenvironment) remains a question that is challenging to answer.[42] A biopsy of an accessible site shortly before death for direct comparison with a sample from the same site at TH would help clarify this.

3.4.3 High ploidy and subclonal variation

Fluorescent in situ hybridisation (FISH) was undertaken on at least two samples for each patient in this cohort as an orthogonal approach to validation of bioinformatics-derived

ploidy. This decision was based on an initial analysis suggesting higher rates of ploidy evident in our late-stage treated metastases relative to public datasets.[27] A pragmatic approach was taken to centromeric probe selection to enable use of the same two probes across all 14 cases (see **Materials and Methods Section 2.10**). While SCNA heterogeneity in melanoma has been demonstrated using FISH both within primary tumours and between primary and metastatic sites,[43] the extent of heterogeneity in ploidy that we initially demonstrated had not been previously described at the time of this analysis. Although most of the 14 cases had a modal ploidy range between 2n and 4n, consistent with other studies,[23,27,44] PEA005, PEA016 and PEA023 all appeared to have subpopulations of cells with ploidy >4n (up to 11n in PEA023). The cell to cell variation seen in these cases is suggestive of CIN.

In 8/14 cases the FISH-estimated ploidy (using a corrected mode value) was concordant with the bioinformatic estimates. In PEA004 FISH was able to capture the difference in the WGD-sample versus a non-WGD sample. In 6/14 cases, however, there was a notable discrepancy in at least one sample per case with regards to the FISH – and bioinformatic-estimated ploidy. In three cases the discrepant ploidy was underestimated by FISH (PEA023, PEA060 and PEA036). In PEA060, for example, the FISH-estimated mode ploidy was 2 (range 2–4 and range 2n3) for both samples; whereas bioinformatics estimates were 4.22 and 4.14. In two cases (PEA080 and PEA020) only one sample was inaccurate and ploidy was overestimated by one integer value (for example, in PEA020, FISH-estimated mode ploidy was 3 versus 2.46 as the bioinformatic estimate). In PEA005 one sample overestimated ploidy by FISH (Mode 4, range 4–6; bioinformatic estimate 2.61) and the other was underestimated by FISH (Mode 3, range 2–4; bioinformatics estimate 4.06).

In two cases (PEA017 and PEA023) I was able to evaluate both primary and metastatic samples by FISH. In both cases, a greater range of ploidy was evident in the metastases as compared to the primary tumours. This may reflect selection of more aneuploid populations that seed metastatic sites. Bakhoum and colleagues[45] found metastases to be more aneuploid than primary tumours on their analysis of other published studies, with CIN noted to be a feature driving metastatic competence in breast cancer in particular. In addition, SCNAs (suggestive of CIN) were noted to be enriched in metastases as compared with primary tumours in a large study of renal cell cancer.[46]

The strengths of this analysis include the number of nuclei scored per sample (207 on average) and the strong inter-rater reliability. There are several limitations to the data

interpretation; however, some of which are inherent to interphase FISH (as mentioned above in **Section 3.1.2** and in **Materials and Methods Section 2.10**). The absence of a melanoma-specific cell marker makes it harder to be confident in the cell selection for probe enumeration, although high purity tumour samples help mitigate this. Also, chromosome loss (versus loss as an artefact of nuclear segmentation) is not able to be determined. Additional measures may be useful in improving the approach: first, bespoke-selected probes for each case with an additional 1–2 probes, both centromeric and gene or cytoband-specific, may improve the accuracy of estimated ploidy. Second, an automated approach may be useful to reduce inconsistencies in manual probe enumeration. Third, a more refined approach to correction of values with adjustment for nuclear size based on total estimated ploidy may be helpful. Optimisation of the protocol for archival FFPE tissue is also needed. Utilisation of a thinner slide for hybridisation and undertaking manual review at the microscope for enumeration (rather than use of 'stacked' automated images) could be explored.

Validation of the cell-to-cell variation in ploidy noted in this analysis is being undertaken with whole genome single-cell sequencing of matched samples from this cohort.

3.4.4 Evolution of melanoma metastases

In this cohort, evidence of a polyclonal mode of metastatic seeding from the primary tumour (that is, that more than one clone from the primary tumour seeded metastases) was seen in the majority of cases (10/14; Table 15), highlighting the genetic divergence that may occur in metastatic melanoma. At least one region of the primary tumour was profiled in four of these 10 cases. In PEA016 and PEA017 there was evidence of two primary tumour clones each associated with a different metastatic site. In the other two cases with primary tumour sampling (PEA004, PEA036) and in the six cases without primary tumour sampling (PEA005, PEA012, PEA020, PEA025, PEA026 and PEA038) the polyclonal seeding pattern was inferred from the phylogenetic trees. While polyclonal seeding from the primary tumour to metastatic sites has been previously described in cutaneous melanoma in a case series of eight patients[25] and a single post-mortem melanoma case study,[4] the number of cases and extent of visceral metastatic sampling across this cohort is much greater. Monoclonal seeding (that is, only one primary tumour clone responsible for seeding metastases) was apparent in 4/14 cases (PEA009, PEA023, PEA060 and PEA080). No melanoma subtype demonstrated a predilection for any particular seeding pattern, although the small numbers limit the ability to generalise this observation.

Table 15 Summary of seeding patterns across the cohort of 14 patients
Based on the most likely seeding scenario.

	Monoclonal prim-met seeding	Polyclonal prim-met seeding
Monoclonal metastases *(ie CCFs of clusters are ≤15% of clonal cluster)*	PEA009 PEA023* PEA080*	PEA017* PEA026
Polyclonal metastases present *(ie CCFs of clusters are >15% of clonal cluster, OR clusters are present in an individual metastasis from exclusive branches of the phylogenetic tree)*	PEA060	PEA004*^{P} PEA036*^{P} PEA016* PEA005 PEA012^{P} PEA020 PEA025^{P} PEA038^{P}

Sun-exposed cutaneous/Melanoma Unknown Primary (MUP)
Acral/perianal melanoma
Mucosal melanoma
*primary tumour available
^{P}polyclonal metastases containing exclusive clusters

In five cases (PEA004, PEA012, PEA025, PEA036 and PEA038) there were polyclonal metastatic regions where clones containing exclusive clusters (that is, from separate branches of the phylogenetic tree) were found in a single region. Explanations for this situation include: 1) clonal mixing from intermetastatic seeding (where clones from metastatic sites may seed other metastases); 2) >1 primary tumour clone co-seeding a metastatic region; or 3) that the seeding clone originated in the primary tumour but was not detected due to sampling limitations. Intermetastatic seeding was hypothesised to account for these events in three cases (PEA004, PEA012 and PEA038). In PEA012 and PEA038, the exclusive clusters contained evidence of a temozolomide-induced signature, consistent with the clones being exposed to chemotherapy. In PEA004 the late emergence of this polyclonal metastatic site favours intermetastatic seeding. In PEA025 and PEA036 it is not possible to discern the mechanism behind this event. These were all cases in which there was evidence of polyclonal seeding from the primary tumour to metastatic sites. Intermetastatic seeding contributes to tumour heterogeneity in an unpredictable manner and has been described in melanoma,[4,25,44] prostate cancer[2] and breast cancer.[47] In their series of 10 prostate cancer patients sampled at autopsy, Gundem et al, concluded that metastasis-to-metastasis seeding was the most likely mechanism based on their inability to detect these clones in deep targeted sequencing of primary tumours.[2] In our cohort, for the cases with profiled primary tumours (PEA004 and PEA036), it may be possible to adopt this approach.

Looking at the phylogenetic trees, a number of additional evolutionary observations can be made. The phylogenetic trees for the four monoclonal seeding cases had no branching (PEA023, PEA060 and PEA080) or very little branching (PEA009), consistent with a linear pattern of primary-metastatic evolution where the fittest clone appears to have seeded distant metastatic sites and very limited metastatic divergence is noted. On the other hand, the 10 polyclonal seeding cases varied in their extent of branching and in the size of subclonal clusters, indicative of a spectrum of genomic divergence between metastatic sites (noting that genomic distance was not formally measured).

Within the cohort 9/14 patients had brain metastases but sampling at TH was only possible in 7/9 for practical reasons. From the perspective of clonal evolution, across these seven cases there are two groups: first, those in which a separate clone seeds the brain (for example, PEA012, PEA017 and PEA020); and second, those in which there was no clear distinction between clones seeding the brain and extracranial sites (PEA009, PEA025, PEA026). In the case of PEA005, which is more difficult to categorise, the similarity between the SCNA profiles of the brain metastases does hint towards a clonal origin distinct from the lung metastases.

Of particular interest is the case of PEA017, where the clone seeding the brain demonstrated a distinct clinical behaviour to other sites of disease. Where the asymptomatic, solitary brain lesion remained stable during BRAF/MEK targeted therapy, the intrathoracic sites responded completely, but then relapsed with florid disease. However, the brain lesion did not progress. The brain-seeding clone was distinct in its lineage from the thoracic sites of disease and was not characterised by WGD. This example of subclonally distinct, clinically relevant behaviour across metastatic sites challenges the argument that only clonal driver mutations are of relevance in molecular profiling.[48,49]

In PEA025 there were two distinct clones both seeding the brain, a phenomenon observed in the melanoma post-mortem case by Rabbie and colleagues.[4] One of the brain regions also appeared polyclonal in PEA025, containing two exclusive clusters of mutations, suggesting multiple waves of seeding, potentially temporally separate, and/or cross-metastasis seeding in the brain. Further profiling integrating gene expression and immunohistochemistry will be informative to correlate whether genomic heterogeneity underlies any phenotypic heterogeneity in metabolic pathways and the immune microenvironment, because work to date suggests these may be organ specific.[4,50]

Another point of interest in this cohort is evidence of whole genome doubling (WGD) occurring as a subclonal event. The rate of WGD in melanoma is reported as ~30–40%[27,44,51] and it was described as a clonal event in the one study with multi-region sampling of metastases.[44] In this cohort, 9/14 cases have evidence of WGD. In 4/14 cases (PEA016, PEA023, PEA036 and PEA060) all samples (including primary tumour regions in PEA016, PEA023 and PEA036) appeared to have undergone WGD, suggesting it is an early, clonal event in these cases. In the case of PEA016 and PEA060 some samples have undergone >1 round of WGD. Whole genome doubling appeared to be a subclonal event in 5/14 cases (PEA004, PEA005, PEA017, PEA026 and PEA038), suggesting it occurred later, and possibly under the selective pressure of treatment. There was no evidence of its occurrence in the primary tumour in PEA004 and PEA017; however, it may have been missed due to the complexity of subclonal copy number reconstruction (PEA004 – homogenised primary tumour sample) or limited sampling (PEA017). Parallel WGD events were noted in PEA005, PEA026 and PEA038, suggesting selection of these clones in late-stage disease – an example of convergent evolution. WGD-clones may have been selected due to their greater tolerance of copy number events favouring tumour growth, providing a clue that CIN may be a feature of late-stage disease. In PEA017, as discussed earlier, the clinical behaviour of the WGD metastases differed from the non-WGD metastasis, but this same pattern was not overt in the other cases.

A punctuated evolutionary event – where large-scale copy number events favourable to tumour growth occur – may have occurred in the primary tumour in three cases. PEA016, PEA023 and PEA060 were all characterised by clonal WGD (two rounds in the case of PEA023) and a high WGII score suggestive of multiple SCNAs. PEA023 and PEA060 followed a monoclonal seeding pattern as would fit a clonal sweep of the primary tumour by a fit, aggressive clone. PEA016 demonstrated a polyclonal pattern of metastatic seeding (two clones evident), but with limited branching of the phylogenetic tree, consistent with limited genomic divergence. The clinical course was very aggressive in PEA016 and PEA060, with only three and 12 months between first diagnosis and death respectively. In PEA023 overall survival was longer however (23 months from diagnosis of Stage IV disease).

An understanding of the metastatic process in melanoma has the potential to inform the design of future trials with regards to the timing of therapy, of particular importance for (neo)adjuvant therapy which is given to prevent clinical disease recurrence. Patient PEA004

was the only patient to receive adjuvant treatment in this cohort. While no firm conclusions can be drawn about the timing of metastatic spread, the clone characterising the resected Stage III lymph nodes was also seen at distant metastatic site and there was a second, independent clone that also seeded distant metastatic sites. These observations suggest that occult metastatic dissemination was widespread at the time of the ilioinguinal lymph node dissection and also that metastatic spread was independent of this site. Characterising circulating tumour clones prior to (neo)adjuvant treatment, which may potentially be facilitated by liquid biopsy, will be an important step in personalising (neo)adjuvant treatment strategies.

The majority of samples profiled as part of this cohort analysis are metastases that have been subjected to >1 lines of treatment, collected at a late stage in the course of disease. As such, these samples have been subject to clonal evolution through treatment, known to cause 'genomic contraction' in responding melanoma samples,[52,53] with evidence of immune-editing also demonstrated in colorectal[54] and breast cancer.[1] The sampling of metastases at TH implies they have not completely responded to treatment, and are more likely to be treatment-refractory. Treated metastases are more likely to harbour driver mutations relative to untreated metastases.[55,56] It is also possible that their copy number profile may be different to those of treatment naïve samples (such as those which were highlighted based on analysis of the TCGA and Hayward landscape profiled cohorts),[27,29] especially if progressive CIN and late WGD are associated with advanced disease. While these factors may have impacted the conclusions drawn from this study, they are unlikely to have had a major impact on the hypothesised evolutionary trajectories considering the large numbers of mutations involved in clustering analysis for cutaneous and melanomas of unknown primary in particular.

Putative genomic mechanisms of treatment resistance were examined in each case. Three cases harboured clonal mutations that may have impacted response to ICI therapy through impaired antigen presentation (*B2M*) and immune exclusion (*CTNNB1)*. Two cases had evidence of a *B2M* mutation with somatic copy number loss at 15q21: PEA016 in which the mutation was clonal, and mapped to a functional domain and may have contributed to primary resistance; and PEA026 in which it was subclonal and mapped outside a functional domain making its relevance less clear. In PEA036 there was a clonal *CTNNB1* mutation that may have conferred resistance to pembrolizumab. In six cases (PEA009, PEA017, PEA025, PEA023, PEA026, PEA038) there was somatic copy number loss of *JAK1* and/or *JAK2*, but

without an associated mutation in the corresponding allele. Although haploinsufficiency of *JAK2* is suggested by DECIPHER,[57] the hypothesis that interferon gamma pathway disruption resulted as a consequence of this requires further exploration, especially in the >2N cases where more than one wild-type allele may remain. Methylation of the wild-type alleles is another plausible explanation.

In terms of genomic mechanisms of resistance to BRAF/MEK targeted therapy, acquisition of mutations in MAPK pathway genes known to confer resistance occurred in three cases. In PEA012 different *NRAS* mutations (*Q61H* and *G13R*) were evident at different metastatic sites, providing an example of convergent evolution, similar to the case in which Juric and colleagues described multiple *PTEN* mutations in a breast cancer patient who progressed on treatment with a PI3K inhibitor.[58] In PEA026 there was an acquired *NRAS Q61R* mutation in a site that developed acquired resistance to dabrafenib and trametinib. In PEA017, an acquired *MAP2K1* mutation was evident in the thoracic sites of disease that progressed on dabrafenib and trametinib. In other cases with a *BRAF V600* mutation treated with BRAF/MEK inhibitors for at least two months (PEA005 and PEA025), no genomic mechanisms of treatment resistance were identified and resistance may have been mediated by transcriptomic or epigenetic alterations.

The cases in this cohort were treated with multiple sequential targeted and immune therapies, and this poses a challenge in terms of disentangling mechanisms of resistance, especially given known interactions between treatments (for example, BRAF inhibitors and the immune tumour microenvironment (iTME)). The iTME of tumours resistant to MAPK inhibitors is not favourable for the generation of an anti-tumour immune response.[59] On the contrary, an inflamed microenvironment appears predictive of response to MAPK inhibitors[60,61] and in theory could be facilitated by checkpoint blockade prior. Importantly, sequencing does appear to impact clinical efficacy in some retrospective studies with upfront checkpoint inhibition favoured for improved survival.[62] Further analysis of the transcriptome via RNAseq in these cases is likely to be informative in deconvolution of the iTME and signalling pathways, coupled with immunohistochemistry analysis (especially for immune exclusion which may be difficult to infer from RNAseq alone).

Two cases in this cohort highlight the discrepancy between traditional measures of progression on or after treatment (that is, growth of existing lesions and/or development of new lesions on imaging) and the potential clinical benefit from ICI treatment. In patients

PEA009 and PEA020 there was a 17 and 15 month latency respectively between the development of brain metastases (after progression following single agent anti-PD-1) and death. In both cases the brain metastases were treated (with WBRT in PEA009 and resection followed by SRS in the case of PEA020). Patient PEA009 did not receive further systemic therapy and PEA020 only had one cycle of dab+tram before ceasing 12 months prior to death. Further analysis may shed more light on whether particularly immunogenic tumour-associated neoantigens were present in these cases, resulting in an enhanced immune response.

Despite the opportunity for widespread sampling of sites of disease at TH, in some cases practical constraints mean it is not possible to access certain metastases, including the brain and skeletal sites. Other limitations of this approach include a bias in sampling favouring active, treatment resistant tumours.

While a strength of this study includes the successful profiling of primary tumours in 6/11 cases with a known primary, it also highlights how challenging it can be to obtain primary archival melanoma samples (unable to be sourced for three cases: PEA009, PEA025 and PEA026) and work with small amounts of material (purity insufficient for downstream analyses in two cases: PEA005 and PEA038). Furthermore, in taking a more conservative approach to mutation-calling in samples derived from archival FFPE tissue, where no de novo mutations were called due to concerns re artefact, we likely under-estimate the heterogeneity in SNVs in primary tumours. Evidence of ITH in SCNAs despite similarity in SNVs also highlights the limitations of a clustering analysis based solely on SNVs.

Validation of the phylogenetic tree construction would make the evolutionary inferences more robust. The presence of subclonal WGD complicates the interpretation of CCF values as it leads to populations of cells with different ploidy, rendering deconvolution from bulk sequencing extremely challenging. Programs such as CITUP (Clonality Inference in multiple Tumour samples Using Phylogeny[63] which aid in subclonal population clarification, or an orthogonal approach using the 'Poly G' method[64] which leverages somatic variants in hypermutable DNA regions to define clonal relationships, will be important next steps for this project.

Profiling of the other metastases (that is, those not subjected to WES) with the targeted melanoma panel, as well as transcriptomic and immune microenvironment analysis matched

to the samples thus far analysed using WES is planned for this study. Evaluation of neoantigens and HLA heterozygosity will also be undertaken. These additional analyses will provide a more comprehensive perspective on potential mechanisms of treatment resistance.

References for Section 3 (excluding individual case studies)

1. De Mattos-Arruda L, Sammut SJ, Ross EM, et al. The Genomic and Immune Landscapes of Lethal Metastatic Breast Cancer. *Cell* Rep 27: 2690–2708 e10, 2019.
2. Gundem G, Van Loo P, Kremeyer B, et al. The evolutionary history of lethal metastatic prostate cancer. *Nature* 520: 353–357, 2015.
3. Makohon-Moore AP, Zhang M, Reiter JG, et al. Limited heterogeneity of known driver gene mutations among the metastases of individual patients with pancreatic cancer. *Nat Genet* 49: 358–366, 2017.
4. Rabbie R, Ansari-Pour N, Cast O, et al. Multi-site clonality analysis uncovers pervasive heterogeneity across melanoma metastases. *Nat Commun* 11: 4306, 2020.
5. Bauer M: RNA in forensic science. Forensic Sci Int Genet 1: 69–74, 2007.
6. Chen L, Liu P, Evans TC, Jr., et al. DNA damage is a pervasive cause of sequencing errors, directly confounding variant identification. *Science* 355: 752–756, 2017.
7. Costello M, Pugh TJ, Fennell TJ, et al. Discovery and characterization of artifactual mutations in deep coverage targeted capture sequencing data due to oxidative DNA damage during sample preparation. *Nucleic Acids* Res 41: e67, 2013.
8. Fan J, Khanin R, Sakamoto H, et al. Quantification of nucleic acid quality in postmortem tissues from a cancer research autopsy program. *Oncotarget* 7: 66906–66921, 2016.
9. Hansen J, Lesnikova I, Funder AM, et al. DNA and RNA analysis of blood and muscle from bodies with variable postmortem intervals. *Forensic Sci Med Pathol* 10: 322–8, 2014.
10. Kong N, Ng W, Cai L, et al. Integrating the DNA Integrity Number (DIN) to Assess Genomic DNA (gDNA) Quality Control Using the Agilent 2200 TapeStation System, Agilent Technologies, Inc., 2014, 2016, 2016.
11. Schroeder A, Mueller O, Stocker S, et al. The RIN: an RNA integrity number for assigning integrity values to RNA measurements. *BMC Mol Biol* 7: 3, 2006.
12. Ferreira PG, Munoz-Aguirre M, Reverter F, et al. The effects of death and post-mortem cold ischemia on human tissue transcriptomes. *Nat Commun* 9: 490, 2018.
13. Gupta S, Halushka MK, Hilton GM, et al. Postmortem cardiac tissue maintains gene expression profile even after late harvesting. *BMC Genomics* 13: 26, 2012.
14. Zhu Y, Wang L, Yin Y, et al. Systematic analysis of gene expression patterns associated with postmortem interval in human tissues. *Sci Rep* 7: 5435, 2017.
15. Gallego Romero I, Pai AA, Tung J, et al. RNA-seq: impact of RNA degradation on transcript quantification. *BMC Biol* 12: 42, 2014.
16. van der Linden A, Blokker BM, Kap M, et al. Post-mortem tissue biopsies obtained at minimally invasive autopsy: an RNA-quality analysis. *PLoS One* 9: e115675, 2014.
17. Carithers LJ, Ardlie K, Barcus M, et al. A Novel Approach to High-Quality Postmortem Tissue Procurement: The GTEx Project. *Biopreserv Biobank* 13: 311–9, 2015.

18. Walker DG, Whetzel AM, Serrano G, et al. Characterization of RNA isolated from eighteen different human tissues: results from a rapid human autopsy program. *Cell Tissue Bank* 17: 361–75, 2016.
19. North J, Vemula S, Bastian BC: Chromosomal Copy Number Analysis in Melanoma Diagnostics, in Marincola MTaFM (ed): *Molecular Diagnostics for Melanoma: Methods and Protocols*. New York, Springer Science+Business Media, 2014.
20. Roylance R, Endesfelder D, Gorman P, et al. Relationship of extreme chromosomal instability with long-term survival in a retrospective analysis of primary breast cancer. *Cancer Epidemiol Biomarkers Prev* 20: 2183–94, 2011.
21. Lingle WL, Barrett SL, Negron VC, et al. Centrosome amplification drives chromosomal instability in breast tumor development. *Proc Natl Acad Sci* USA 99: 1978–83, 2002.
22. Farabegoli F, Santini D, Ceccarelli C, et al. Clone heterogeneity in diploid and aneuploid breast carcinomas as detected by FISH. Cytometry 46: 50–6, 2001.
23. Priestley P, Baber J, Lolkema MP, et al. Pan-cancer whole-genome analyses of metastatic solid tumours. *Nature* 575: 210–216, 2019.
24. Shain AH, Bagger MM, Yu R, et al. The genetic evolution of metastatic uveal melanoma. *Nat Genet* 51: 1123–1130, 2019.
25. Sanborn JZ, Chung J, Purdom E, et al. Phylogenetic analyses of melanoma reveal complex patterns of metastatic dissemination. *Proc Natl Acad Sci* U S A 112: 10995–1000, 2015.
26. Stefan C. Dentro IL, Kerstin Haase, Maxime Tarabichi, Jeff Wintersinger, Amit G. Deshwar, Kaixian Yu, Yulia Rubanova, Geoff Macintyre, Jonas Demeulemeester, Ignacio Vázquez-García, Kortine Kleinheinz, Dimitri G. Livitz, Salem Malikic, Nilgun Donmez, Subhajit Sengupta, Pavana Anur, Clemency Jolly, Marek Cmero, Daniel Rosebrock, Steven Schumacher, Yu Fan, Matthew Fittall, Ruben M. Drews, Xiaotong Yao, Juhee Lee, Matthias Schlesner, Hongtu Zhu, David J. Adams, Gad Getz, Paul C. Boutros, Marcin Imielinski, Rameen Beroukhim, S. Cenk Sahinalp, Yuan Ji, Martin Peifer, Inigo Martincorena, Florian Markowetz, Ville Mustonen, Ke Yuan, Moritz Gerstung, Paul T. Spellman, Wenyi Wang, Quaid D. Morris, David C. Wedge, Peter Van Loo, on behalf of the PCAWG Evolution and Heterogeneity Working Groupthe PCAWG consortium., the PCAWG consortium: Characterizing genetic intra-tumor heterogeneity across 2,658 human cancer genomes. *bioRxiv* 312041, 2020.
27. Hayward NK, Wilmott JS, Waddell N, et al. Whole-genome landscapes of major melanoma subtypes. *Nature* 545: 175–180, 2017.
28. Carter SL, Cibulskis K, Helman E, et al. Absolute quantification of somatic DNA alterations in human cancer. *Nat Biotechnol* 30: 413–21, 2012.
29. Cancer Genome Atlas N: Genomic Classification of Cutaneous Melanoma. *Cell* 161: 1681–96, 2015.
30. Curtin JA, Fridlyand J, Kageshita T, et al. Distinct sets of genetic alterations in melanoma. *N Engl J Med* 353: 2135–47, 2005.
31. Endesfelder D, McGranahan N, Birkbak NJ, et al. A breast cancer meta-analysis of two expression measures of chromosomal instability reveals a relationship with younger age at diagnosis and high risk histopathological variables. *Oncotarget* 2: 529–37, 2011.
32. Long GV, Stroyakovskiy D, Gogas H, et al. Dabrafenib and trametinib versus dabrafenib and placebo for Val600 BRAF-mutant melanoma: a multicentre, double-blind, phase 3 randomised controlled trial. *Lancet* 386: 444–51, 2015.

33. Wolchok JD, Chiarion-Sileni V, Gonzalez R, et al. Overall Survival with Combined Nivolumab and Ipilimumab in Advanced Melanoma. *N Engl J Med* 377: 1345–1356, 2017.
34. Larkin J, Chiarion-Sileni V, Gonzalez R, et al. Five-Year Survival with Combined Nivolumab and Ipilimumab in Advanced Melanoma. *N Engl J Med* 381: 1535–1546, 2019.
35. Newell F, Wilmott JS, Johansson PA, et al. Whole-genome sequencing of acral melanoma reveals genomic complexity and diversity. *Nat Commun* 11: 5259, 2020.
36. McGranahan N, Swanton C: Clonal Heterogeneity and Tumor Evolution: Past, Present, and the Future. *Cell* 168: 613–628, 2017.
37. Yachida S, Jones S, Bozic I, et al. Distant metastasis occurs late during the genetic evolution of pancreatic cancer. *Nature* 467: 1114–7, 2010.
38. Savas P, Teo ZL, Lefevre C, et al. The Subclonal Architecture of Metastatic Breast Cancer: Results from a Prospective Community-Based Rapid Autopsy Program 'CASCADE'. *PLoS Med* 13: e1002204, 2016.
39. Bauer M, Polzin S, Patzelt D: Quantification of RNA degradation by semi-quantitative duplex and competitive RT-PCR: a possible indicator of the age of bloodstains? *Forensic Sci Int* 138: 94–103, 2003.
40. Feng H, Zhang X, Zhang C: mRIN for direct assessment of genome-wide and gene-specific mRNA integrity from large-scale RNA-sequencing data. *Nat Commun* 6: 7816, 2015.
41. Sigurgeirsson B, Emanuelsson O, Lundeberg J: Sequencing degraded RNA addressed by 3' tag counting. *PLoS One* 9: e91851, 2014.
42. Pozhitkov AE, Neme R, Domazet-Loso T, et al. Tracing the dynamics of gene transcripts after organismal death. Open Biol 7, 2017.
43. Uguen A, Uguen M, Talagas M, et al. Fluorescence in situ hybridization testing of chromosomes 6, 8, 9 and 11 in melanocytic tumors is difficult to automate and reveals tumor heterogeneity in melanomas. *Oncol Lett* 12: 2734–2741, 2016.
44. Birkeland E, Zhang S, Poduval D, et al. Patterns of genomic evolution in advanced melanoma. *Nat Commun* 9: 2665, 2018.
45. Bakhoum SF, Ngo B, Laughney AM, et al. Chromosomal instability drives metastasis through a cytosolic DNA response. *Nature* 553: 467–472, 2018.
46. Turajlic S, Xu H, Litchfield K, et al. Tracking Cancer Evolution Reveals Constrained Routes to Metastases: TRACERx Renal. *Cell* 173: 581–594 e12, 2018.
47. Brown D, Smeets D, Szekely B, et al. Phylogenetic analysis of metastatic progression in breast cancer using somatic mutations and copy number aberrations. *Nat Commun* 8: 14944, 2017.
48. Reiter JG, Baretti M, Gerold JM, et al. An analysis of genetic heterogeneity in untreated cancers. *Nat Rev Cancer* 19: 639–650, 2019.
49. Reiter JG, Makohon-Moore AP, Gerold JM, et al. Minimal functional driver gene heterogeneity among untreated metastases. *Science* 361: 1033–1037, 2018.
50. Fischer GM, Jalali A, Kircher DA, et al. Molecular Profiling Reveals Unique Immune and Metabolic Features of Melanoma Brain Metastases. *Cancer Discov* 9: 628–645, 2019.
51. Bielski CM, Zehir A, Penson AV, et al. Genome doubling shapes the evolution and prognosis of advanced cancers. *Nat Genet* 50: 1189–1195, 2018.
52. Riaz N, Havel JJ, Makarov V, et al. Tumor and Microenvironment Evolution during Immunotherapy with Nivolumab. *Cell* 171: 934–949 e16, 2017.

53. Davidson G, Coassolo S, Kieny A, et al. Dynamic Evolution of Clonal Composition and Neoantigen Landscape in Recurrent Metastatic Melanoma with a Rare Combination of Driver Mutations. *J Invest Dermatol* 139: 1769–1778 e2, 2019.
54. Angelova M, Mlecnik B, Vasaturo A, et al. Evolution of Metastases in Space and Time under Immune Selection. *Cell* 175: 751–765 e16, 2018.
55. Hu Z, Ding J, Ma Z, et al. Quantitative evidence for early metastatic seeding in colorectal cancer. *Nat Genet* 51: 1113–1122, 2019.
56. Hu Z, Li Z, Ma Z, et al. Multi-cancer analysis of clonality and the timing of systemic spread in paired primary tumors and metastases. *Nat Genet* 52: 701–708, 2020.
57. Firth HV, Richards SM, Bevan AP, et al. DECIPHER: Database of Chromosomal Imbalance and Phenotype in Humans Using Ensembl Resources. *Am J Hum Genet* 84: 524–33, 2009.
58. Juric D, Castel P, Griffith M, et al. Convergent loss of PTEN leads to clinical resistance to a PI(3)Kalpha inhibitor. *Nature* 518: 240–4, 2015.
59. Hugo W, Shi H, Sun L, et al. Non-genomic and Immune Evolution of Melanoma Acquiring MAPKi Resistance. *Cell* 162: 1271–85, 2015.
60. Yan Y, Wongchenko MJ, Robert C, et al. Genomic Features of Exceptional Response in Vemurafenib +/- Cobimetinib-treated Patients with BRAF (V600)-mutated Metastatic Melanoma. *Clin Cancer Res* 25: 3239–3246, 2019.
61. Dummer R, Brase JC, Garrett J, et al. Adjuvant dabrafenib plus trametinib versus placebo in patients with resected, BRAF(V600)-mutant, stage III melanoma (COMBI-AD): exploratory biomarker analyses from a randomised, phase 3 trial. *Lancet Oncol* 21: 358–372, 2020.
62. Mason R, Dearden HC, Nguyen B, et al. Combined ipilimumab and nivolumab first-line and after BRAF-targeted therapy in advanced melanoma. *Pigment Cell Melanoma Res*, 2019.
63. Malikic S, McPherson AW, Donmez N, et al. Clonality inference in multiple tumor samples using phylogeny. *Bioinformatics* 31: 1349–56, 2015.
64. Naxerova K, Reiter JG, Brachtel E, et al. Origins of lymphatic and distant metastases in human colorectal cancer. *Science* 357: 55–60, 2017.

Section 4 Representative tumour profiling through homogenisation of residual tumour tissue

Contents

Tables

Figures

4.1 Introduction

At present, clinical decision making often relies on molecular information derived from a single sample (for example, fresh or FFPE biopsy of a primary or metastatic tumour or cut slides). This information guides treatment and prognosis in many tumour types, for example, HER2 expression in breast cancer or PD-L1 status in lung cancer. Work by our group has shown that in a pan-cancer TCGA cohort (n = 1666) of samples obtained in research setting, an average of 1.5% of the actual primary tumour mass is sampled (across all TNM stages), decreasing to 0.3% for Stage IV tumours (n = 188).[1] While a single biopsy may be 'sufficient for precision medicine'[2] this is in reference to the presence of single targetable driver genes that are clonal, and therefore reliably identified with a single biopsy. The field is moving beyond single driver-gene presence/absence in predicting responses to, for example, immune checkpoint therapy where clonality of all mutations that contribute to Tumour Mutational Burden (including passenger mutations) is important.[3,4] Treatment resistance variants are also frequently subclonal, for example, *PIK3CA* mutations in breast cancer[5] and *KRAS* mutations in colorectal cancer.[6]

As discussed in the main **Introduction Section 1.3.2 Representative sequencing through tumour homogenisation**, in collaboration with a team from Roche Tissue Diagnostics (RTD), we developed a protocol through which formalin-fixed tumour tissue that has not been paraffin-embedded is blended – 'homogenised' – to a liquid form, enabling DNA to be extracted from an aliquot of the homogenates and molecualry profiled. We refer to this approach as 'representative sequencing' (Rep-seq).

Pilot work to date in a case of clear cell renal cancer demonstrated that this approach leads to increased sensitivity to detect all mutations relative to a single spatially fixed sample. It is highly reproducible when multiple biological replicates are tested (separate aliquots of the homogenates) (Figure 126a), and can accurately infer clonal and subclonal architecture of the tumour (Figure 126b).[1] In particular, the ability to reliably distinguish between clonal and subclonal mutations in a single sequenced sample makes this approach very efficient from a time and economic perspective.

a)

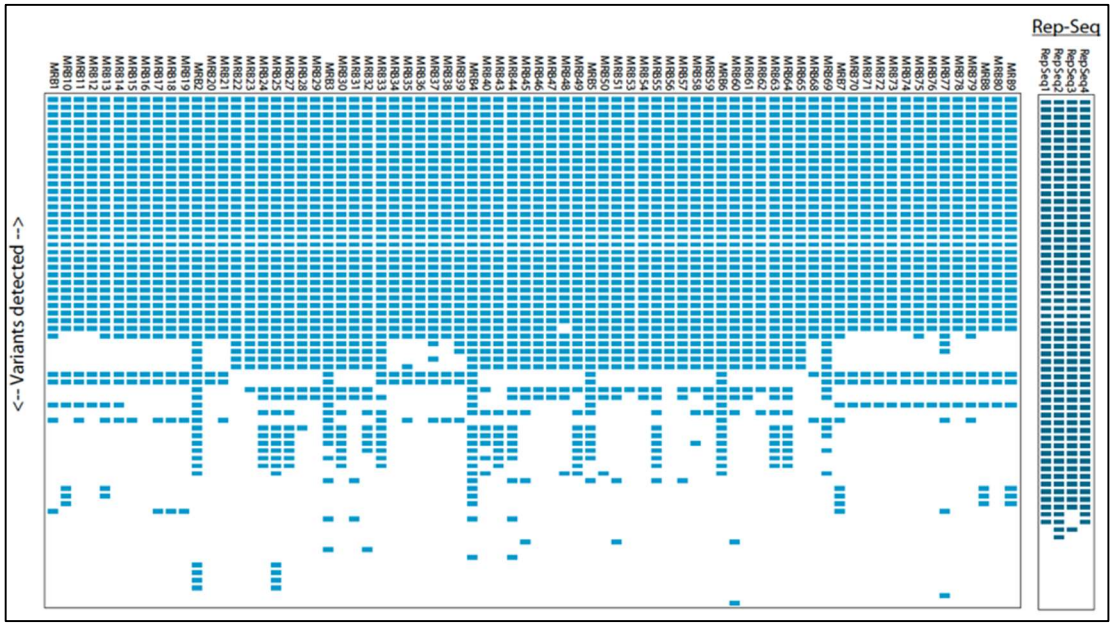

b)

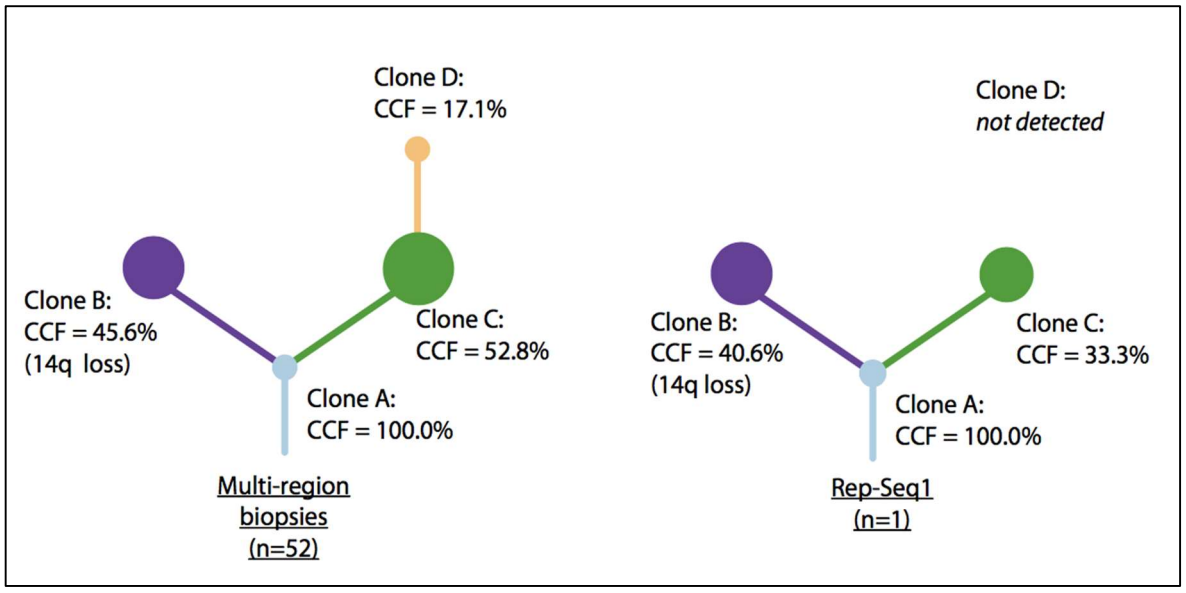

Figure 126 a) A heatmap of variants detected from multi-region sampling in comparison with variants detected on Req-Seq samples; b) clonality of variants

a) Variants detected in 68 sampled regions of a primary clear cell renal cell carcinoma and 11 regions from its locoregional lymph nodes are represented in the heatmap on the left. After diagnostic specimens were cut for routine paraffin embedding, the remaining tumour was homogenised. Variants detected from the homogenate fluid are represented in the heat-map on the right; four biological replicates were drawn. All samples were sequenced to 12,000× depth with a targeted custom panel.

b) phylogenetic trees for this case derived from multi-region biopsies (left) and RepSeq homogenate (right). Figure reproduced from Litchfield et al.[1]

Given the potential of this approach to: 1) overcome bias associated with single biopsies without expensive multi-region sequencing; 2) confidently differentiate clonal from subclonal mutations; and 3) reveal clinically relevant information (for example, subclonal treatment

resistance variants), further evaluation across different tumour types in a larger study was justified. In planning for this, I also sought to evaluate the volume of tumour tissue that is submitted for routine molecular profiling in clinical practice.

4.2 Aims

3. Determine the volume of tumour tissue that is routinely profiled in clinical practice at the Royal Marsden NHS Foundation Trust (Royal Marsden).
4. Explore the utility of homogenisation of residual formalin-fixed surgical tumour tissue in the assessment of tumour heterogeneity.
    - Develop a protocol for a feasibility study to: 1) evaluate the number of cases of leftover tumour tissue after surgery and routine pathology sampling across a number of tumour types; and 2) pilot the homogenisation process (n = 500 homogenised cases over a two-year period).
    - Implement the protocol at the Royal Marsden (through Cancer Clinical Research committee and Regional Ethics Committee submissions).
    - Undertake an informal interim analysis of the percentage of cases with residual tumour tissue after six months to guide the focus of translational work.
5. Evaluate the potential benefits of molecular profiling of the homogenate versus standard of care profiling.

4.3 Protocol development methodology

4.3.1 Service evaluation at the Royal Marsden Hospital

A service evaluation was designed to collect information from the molecular pathology service used by the Royal Marsden Hospital (RMH) (SE725, 2018) on the volume of tumour routinely profiled for diagnostic analyses. This was limited to colorectal cancers (looking for *KRAS/BRAF/NRAS/PIK3CA & TP53* mutations), melanomas (*BRAF & NRAS)* and sarcomas (RT-PCR for gene fusions depending on histological subtype) because these are the only streams funded for routine profiling in the NHS where surgery is routinely undertaken at the Royal Marsden. For melanomas, because primary tumour excisions are rarely undertaken at the Royal Marsden, this was limited to lymph node dissections.

Current practice in the molecular pathology department at the Royal Marsden in 2016–2018 was to extract DNA for diagnostic molecular tests from three 10 micron slides, cut from diagnostic FFPE tissue blocks (from surgery or from biopsy specimens). These are macro-dissected to enable DNA extraction from tumour rich regions.

Eligibility criteria

Any patient who had undergone surgery to remove a primary colorectal tumour, a primary sarcoma or melanoma lymph node dissection at the Royal Marsden and had this tumour sample molecularly profiled in our Molecular Pathology Department.

a) Inclusion criteria:

1) Surgery for tumour removal at the Royal Marsden with an available histopathology report for:
   a. primary colorectal tumours
   b. primary sarcomas
   c. melanoma lymph node dissections.
2) molecular profiling undertaken at the Royal Marsden
3) at least two macroscopic tumour dimensions noted on the histopathology report
4) available information on the number & thickness of slides used for molecular profiling.

b) Exclusion criteria:

1) surgery not performed at the Royal Marsden
2) inadequate information re size of macroscopic tumour on the histopathology report.

Acquisition of profiled case lists

Lists of colorectal, sarcoma and melanoma tumours profiled from 1 January 2016 to April 2018 were obtained from the Molecular Pathology Department and then cross-checked against the inclusion/exclusion criteria. The goal was to obtain n = 100 cases (minimum of n = 20 per tumour type) for a representative view.

Calculation of tumour volume

One dimension was treated as width (W) and the other as length (L) and tumour volume (T_V) was estimated using the following formula:

$$T\_V = (W^2 \times L) / 2$$

This was taken from the literature as the most accurate tumour volume measurement approach when only two dimensions are available.[13]

A copy of the submitted Service Evaluation is attached in **Appendix C**.

4.3.2 Translational study protocol development, amendments and logistics

4.3.2.1 Protocol development for feasibility study

Although the standard operating procedure for the homogenisation of leftover surgical tumour tissue had already been developed and piloted by Roche Tissue Diagnostics (RTD), the design of a translational study protocol that could be accommodated within the constraints of a busy histopathology department at the Royal Marsden required close collaboration with key personnel.

In the first part of the implementation exercise I sought advice from the department manager and the advanced practitioners (APs) in anatomical dissection as to which cancer types typically have surgically resected tumours which are not entirely embedded in paraffin for diagnostic purposes. For example, prostate, bladder and oesophageal cancers tend not to have residual tumour tissue available because all of the specimen is usually embedded and primary cutaneous melanomas are nearly always entirely embedded due their small size. Primary breast, renal, tubo-ovarian, colorectal, pancreatic, gastric cancers, and sarcomas and melanoma lymph node resections were concluded to be the cases that were most likely to have leftover tissue for homogenisation.

Direct patient consent was able to be waived for the study because samples were suitable for homogenisation under the umbrella of the 'tissues for research' consent. When patients are consented to cancer surgery at RMH they are all approached about giving their consent to donating samples of surgical tissue deemed excess to diagnostic needs. Under this consent, tumour and normal samples may be used for a range of downstream analyses, including molecular profiling and clinical data pertinent to the samples used may be collected. Because this is a standard, Trust-wide approach, we were able to waive the need for study-specific consent with a protocol that was approved for operation under the conditions of the tissues for research consent.

The protocol for *Homogenisation of Leftover Surgical Tissue: a Feasibility Study* (HoLST-F – see Appendix D) contains two key research components: 1) an audit of the percentage of suitable cases across eight key tumour types; and 2) pilot processing of homogenates from cases with tissues for research consent and leftover tumour tissue across any tumour type. Because the purpose of this study was to inform the design of a larger trial where homogenisation may be evaluated as a diagnostic tool, a feasibility design and endpoint were selected.[7] The primary endpoint was the evaluation of the percentage of cases with leftover

tumour tissue across primary breast, renal, tubo-ovarian, colorectal, pancreatic, gastric cancers, sarcomas and melanoma Stage III lymph node dissections. A feasibility threshold of 15% was selected as the minimum requirement for each tumour type to be taken forward for further development of this approach.

The original hypotheses, aims, objectives and endpoints are detailed below (in italics). These were updated in an amendment in 2019 (discussed in **Section 4.3.2.3** below):

Hypotheses

- Homogenisation of excess tumour tissue:
    - is feasible to perform on a significant number of leftover surgical samples across multiple tumour types
    - provides tissue of suitable quality for molecular analyses.

Aims

- Identify the proportion of primary tumour cases with leftover surgical tissue that may be amenable to homogenisation across multiple tumour types.
- Evaluate the process of homogenisation in multiple tumour types.
- Explore the differences in molecular profiling between a single diagnostic tumour sample and the homogenised sample.
- Explore immune cell infiltration in the homogenised samples.

Primary objective

- Evaluate the proportion of cases involving resection of the primary tumour, or in the case of melanoma involving a lymph node dissection, with leftover formalin-fixed tumour tissue >1 g (that is, tissue not embedded in paraffin for diagnostic purposes) across the following tumour types:
    - breast
    - colorectal
    - pancreatic
    - gastric
    - renal
    - ovarian
    - sarcoma
    - melanoma (lymph node dissections).

Feasibility threshold: if >15% of cases per tumour type have leftover surgical tissue, then further investigation into homogenisation is deemed feasible.

Secondary objectives

- Establish the amount of time required for dissection of the leftover formalin-fixed surgical tissue.

- Establish standard blending times required for adequate homogenisation of each tissue type.
- Compare the results of molecular analyses between the diagnostic and homogenised specimens, across the following primary tumour types:
    - breast
    - colorectal
    - pancreatic
    - gastric
    - renal
    - ovarian
    - sarcoma
    - melanoma (lymph node dissections).

Exploratory objectives

- Evaluate the immune cell infiltration of the homogenised tumour sample with flow cytometry.
- Evaluate the homogenised 'tumour-adjacent tissue' samples and compare this profile with that of the homogenised tumour and homogenised normal samples.

Primary endpoint

- The percentage of cases involving resection of the primary tumour, or, in the case of melanoma involving a lymph node dissection, with leftover formalin-fixed tumour tissue >1 g (that is, tissue not embedded in paraffin for diagnostic purposes that would otherwise be discarded) across the following tumour types:
    - breast
    - colorectal
    - pancreatic
    - gastric
    - renal
    - ovarian
    - sarcoma
    - melanoma (lymph node dissections).

Feasibility threshold: if ≥15% of cases per tumour type have leftover surgical tissue, then further investigation into homogenisation is deemed feasible.

Secondary endpoints

- Median time (in minutes) required from the start of dissection of the leftover surgical tissue into tumour, tumour-adjacent and normal tissue until its completion.
- Median time (in minutes) required for the actual homogenisation of each tissue type from the start until the stop of 'blending'.
- Difference in molecular profile (for example, number of gene mutations and copy number alterations, cancer cell fraction, tumour mutational burden) between the diagnostic block and the homogenised sample, as measured by next generation

sequencing techniques (NGS) across the following primary tumour types (analyses including but not limited to):

- breast (for example, ER, PR and Her2 amplification)
- colorectal (for example, KRAS, NRAS and BRAF mutations)
- pancreatic (for example, KRAS, EGFR)
- gastric (for example, KRAS, Her2)
- renal (for example, VHL)
- ovarian (for example, BRCA1 and BRCA2)
- sarcoma (for example, KIT, PDGFR, various translocations)
- melanoma (for example, lymph node dissections; BRAF, NRAS, KIT).

Exploratory endpoints

- Quantification of infiltrating immune cells (for example, CD8 positive lymphocytes) and expression of immune checkpoints (for example, PD-L1) in the homogenised tumour sample using flow cytometry.
- Compare the differences in the molecular and cellular profile of the homogenised 'tumour-adjacent tissue' sample with those of the homogenised 'tumour' and 'normal' samples (for example, compare gene mutations, immune cell infiltration).

With an aim to homogenise five cases per week, three aliquots per case (tumour, adjacent to tumour and normal), 15 × 50 mL Falcon tubes would be generated per case and require storage at 4° Celsius. Due to the constraints of storage at the Royal Marsden, the capacity for the study to be accommodated was discussed with the BioBank manager – a key approval process for feasibility of opening at the site.

In collaboration with the Statistics team I designed, developed and tested a MACRO database to capture the clinical and workflow information generated by the study.

Upon institutional and regional ethics committee and HRA approval, the study was registered with the National Clinical Trials database (NCT03832062).

4.3.2.2 Study logistics framework

The imposition of a new workflow to generate homogenised samples undertaken in the Trust histopathology department required a strategic approach to logistics. For example, we needed to identify and separate containers containing leftover tumour, as well consistently label the homogenised samples (that is, tumour, adjacent to tumour and normal tissues). With resource constraints limiting our ability to undertake some aspects of the study at the Royal Marsden (for example, cutting slides from diagnostic blocks), some of this workflow was undertaken at the Francis Crick Institute. I created a set of guidance documents in consultation with key team members to ensure we had documented processes to optimise the workflow and

minimise chance of sample error; numerous updates were made over time (see Appendix E and F). These covered the following areas:

1. identification of samples for homogenisation
2. sample labelling
3. transfer of samples to BioBank area
4. transfer of samples from Biobank to Roche Tissue Diagnostics (formerly known as Ventana) and the Francis Crick Institute
5. transfer of diagnostic blocks and slides
6. equipment restocking
7. equipment checks and faults
8. homogenate waste disposal
9. contacts for the study
10. Marken Depot materials list
11. homogenisation process guidance.

In November 2018, the Trust made a decision to suspend their automatic tissues for research consent process, therefore jeopardising our ability to homogenise any samples. I discussed this with the Biobank team and discovered that a precedent for a phone consent process had been set by the Genomics England (GEL) project. We adapted this phone consent approach for patients who were deemed to have leftover tumour tissue. A set of HoLST-F study phone consent procedures was devised and implemented (see Appendix G) and myself and subsequently a dedicated clinical fellow within the Skin & Renal Unit undertook this process. This enabled us to continue to have ethically approved access to leftover tissue for homogenisation and had proved particularly useful in the more recent times in the COVID-19 pandemic.

4.3.2.3 Protocol amendment

Four months after the study had commenced, I drafted a major protocol amendment and submitted this for ethics and governance approval in May 2019. The key changes proposed were:

1. **Amendment of the wording of the primary endpoint**. We had originally included the '1 g' as a nominal figure to indicate macroscopic tumour presence and it had not been

feasible to document a weight for every sample with leftover tumour tissue;, hence we disclosed that this is macroscopically visible tumour estimated by a histopathologist to weigh >1 g. The 1 g tumour criteria remained for samples being homogenised.

1. **Amending the collaboration with the Francis Crick Institute, to undertake translational work with homogenised samples**. This enabled more efficient translational work to be undertaken and greater control over the timelines for this output.

2. **Spectrum of analyses on homogenised samples**. We added additional details to the nature of analyses that may be undertaken on homogenised samples, including immune cell sequencing and proteomic analyses. To facilitate this, some of the sequencing analysis was allowed to be undertaken by Roche Sequencing Solutions, in an anonymised manner.

3. **Access to FFPE blocks for primary tumours where metastases are homogenised**. To enable meaningful comparative analysis, we requested to cut slides from the FFPE primary tumour blocks in cases where a non-primary tumour sample was homogenised.

4. **Additional storage facility**. To help with storage space, we requested to store samples at a paid-for, external, commercial facility. Wording was added to note that relevant approvals and agreements needed to be in place prior to sending samples.

5. **Creation of an FFPE block from homogenised tissue**. This enabled immunohistochemical analyses to be compared with those from the FFPE diagnostic blocks.

6. **Collection of second tumour-adjacent region where feasible**. Transcriptomic analyses of 'normal adjacent to tumour' regions have been described (for example, Aran et al. Nature Comm, 2017) and in order to obtain a comparable tissue source for homogenisation we wished to homogenise an additional adjacent region where possible.

7. **Elective sectioning and multi-region sampling of some tumours prior to homogenisation**. In some cases we planned to section the tumour and homogenise parts separately. Photos of the residual tumour specimens would be taken for documentation purposes. In other cases we would take multi-region biopsies of the residual, leftover tumour sample prior to homogenising with the intention to sequence these separately.

8. **Interim analysis**. In order to help prioritise translational work, we wished to conduct an interim analysis of the primary endpoint after six months of the study (data collection for this aspect commenced in December 2018).

9. **Consideration of addition of other sites for tissue acquisition**. We had discussions with the Royal Brompton Hospital regarding the provision of some lung tumour samples. They had a biobank with an equivalent of the 'tissues for research' consent we used at the Royal Marsden.

The amendments were officially approved by HREC/HRA in September 2019. Appendix D contains the most up-to-date version of the HoLST-F study protocol (version 2.0, September 2019).

4.4 Results

4.4.1 RMH audit of sampled tumour volume

Of the samples from 2016–2018 submitted for molecular profiling, n = 231 were melanoma, n = 922 were colorectal and n = 232 were sarcoma. Given a lack of tumours meeting the specific inclusion criteria, the stage of the resected tumour was widened to include resected metastases (as opposed to only primary tumours or lymph node dissections).

After 204/231 profiled melanoma cases were reviewed, 26 met eligibility criteria. Of 166/922 profiled cases for colorectal cancer, 25 met the criteria and of 232/329 reviewed for sarcoma, n = 25 met the criteria. The most common reasons for samples not meeting eligibility criteria included a lack of two documented macroscopic tumour dimensions, or a biopsy of a lesion being submitted for profiling (rather than a resected lesion).

With a median tumour volume of 21.3 cm^3, the median tumour proportion sampled across the three tumour types was 0.0005% (see Figure 127). This varied according to tumour type, with sarcomas having the lowest median proportion sampled (<0.0001%), mainly due to their larger median size (>100 cm^3).

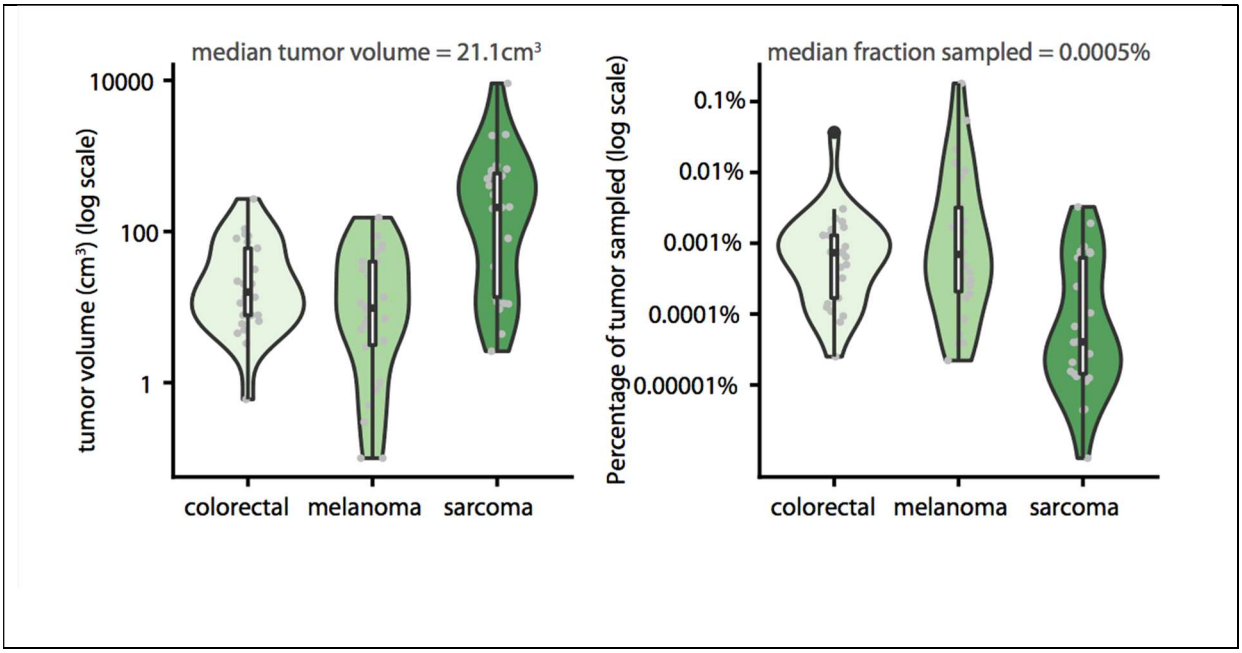

Figure 127 Tumour volume and sampling fraction from colorectal, melanoma and sarcoma cases profiled at the Royal Marsden
Left: violin plot showing the tumour volume modelled across colorectal, melanoma and sarcoma tumours from which molecular profiling was undertaken; right: violin plots representing the percentage of tumour sampled. Figure from Litchfield et al[1] (with data I supplied from audit).

4.4.2 Interim analysis of homogenised cases and study primary endpoint

From September 2018 until end of July 2019 (that is, 11 months into the study), 100 cases were homogenised (Figure 128), representing only 43% of the number predicted.

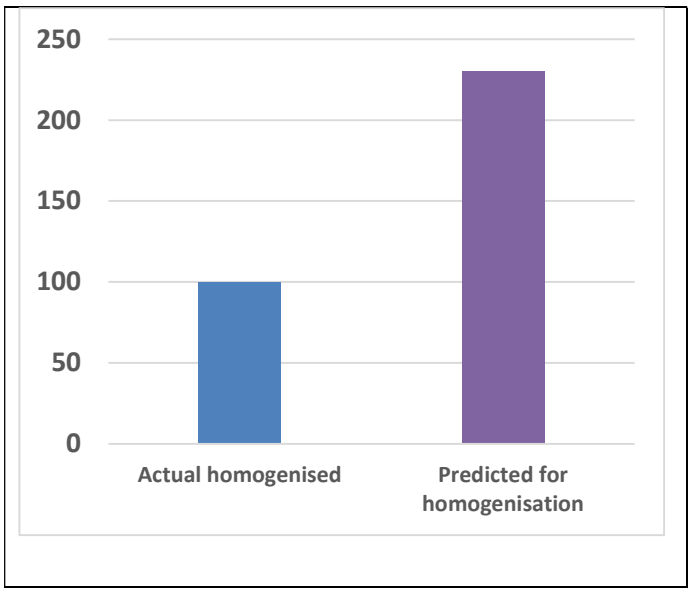

Figure 128 Number of cases homogenised (blue) versus number predicted (yellow) at beginning of the study

A breakdown of tumour types, and primary versus non-primary tumours is summarised in Table 16 and Figure 129. For this analysis, melanoma locoregional lymph node dissections (in cases naïve to systemic therapy) were counted as primary tumours, given their inclusion in the primary endpoint. Breast, sarcoma and melanoma tumours were the most frequently homogenised, with a predominance of primary tumours in breast and sarcoma cases. Sarcoma, breast, renal and tubo-ovarian cases had more primary tumour resections. Interestingly of the small number of colorectal cases homogenised, the majority were not primary tumours. Although uterine/endometrial cancers do not form part of the group of tumours flagged for the primary endpoint feasibility analysis, it was noted that five primary tumour cases were homogenised, a greater number than gastric, colorectal and treatment-naïve melanoma lymph node dissections.

Table 16 Breakdown of homogenised cases by tumour type and primary or other lesion (for example, lymph node, metastasis, local recurrence)

Tumour type	Primary	Other	Total
Breast	24	6	30
Renal	9	1	10
Tubo-ovarian	5	3	8
Melanoma	4*	10	14
Gastric	1	0	1
Colorectal	1	5	6
Pancreatic	0	0	0
Sarcoma	18	2	20
Uterine/Endometrial	5	0	5
Other	1	5	6
			100

* *Treatment-naïve lymph node dissections (LND).*

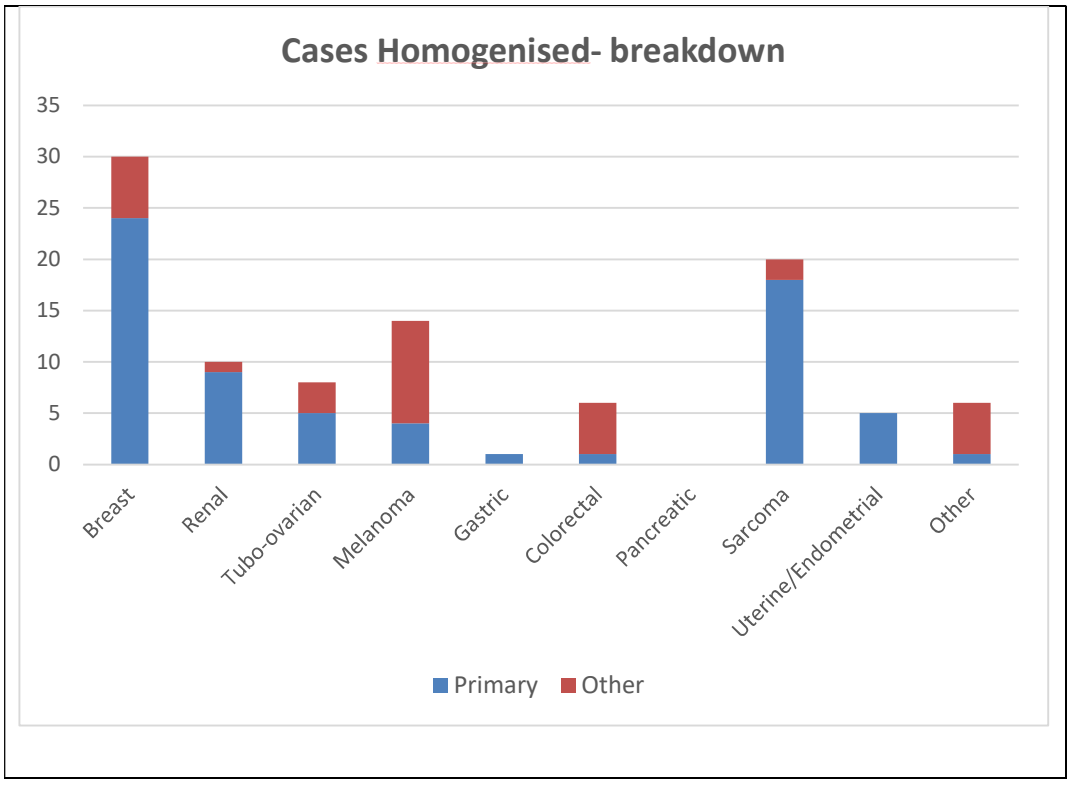

Figure 129 Proportions of primary vs other tumours homogenised according to tumour streams

In order to help the prioritisation and direction of translational analyses, an informal interim analysis of the primary endpoint data captured from December 2018 until end of June 2019

(that is, over seven months) was conducted. The absolute numbers of primary tumour surgeries conducted at the Royal Marsden were analysed for breast, renal, tubo-ovarian, gastric, colorectal and pancreatic cancers, as well as primary sarcomas and melanoma lymph node dissections were determined from lists provided by the Informatics department (see Appendix D – HoLST-F protocol, page 18) – see Figure 130. The number of primary breast cancer resections exceeded all others (n = 322), followed by sarcomas (n = 130). The remaining tumour types had less than n = 40 resections per year.

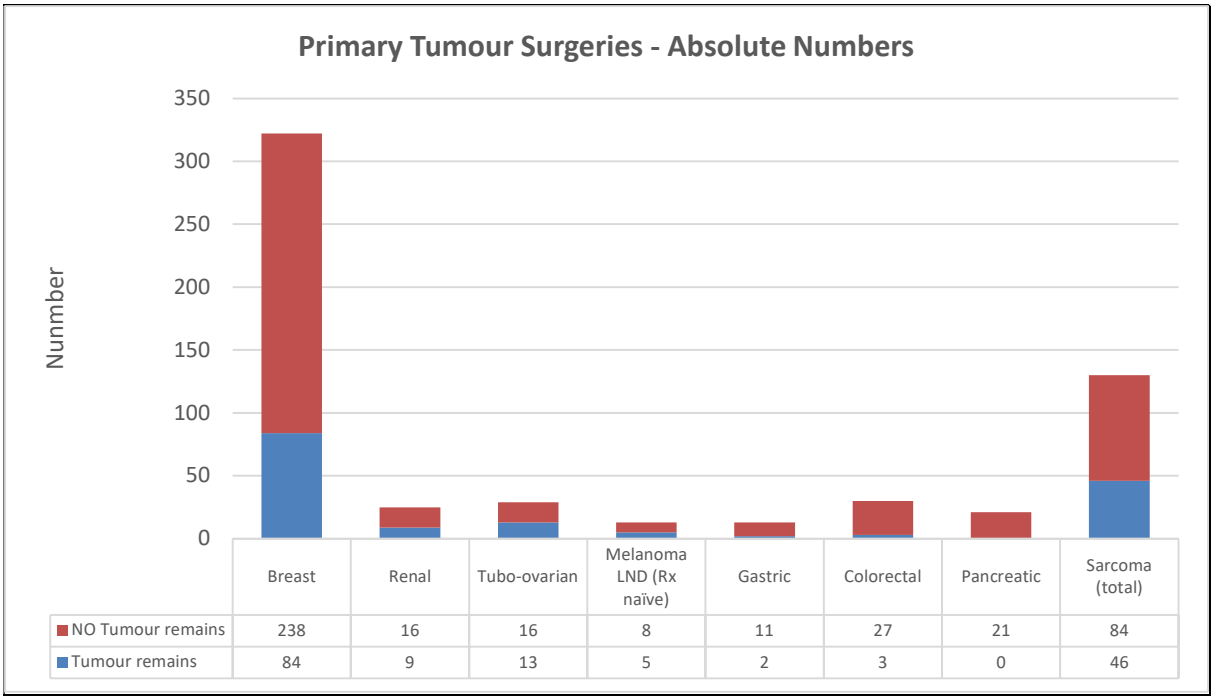

Figure 130 Absolute numbers of primary tumour surgeries

The proportion of these surgical cases with ≥1 g tumour remaining (as estimated and documented by the histopathologists at the time of cut-up; see Appendix D – HoLST-F protocol) is shown in Figure 131. At this interim analysis, tubo-ovarian, melanoma lymph node dissections, renal, sarcoma, breast and gastric cancers met the pre-specified 15% feasibility endpoint, at or above which it was deemed useful to pursue these tumour streams in a larger study. No cases with remaining tumour were identified for pancreatic surgery, and only a very low proportion in colorectal resections (10%). The absolute numbers of cases with leftover surgical tumour tissue (Figure 130) were highest in breast (n = 84), sarcoma (n = 46) and tubo-ovarian (n = 13) cancers.

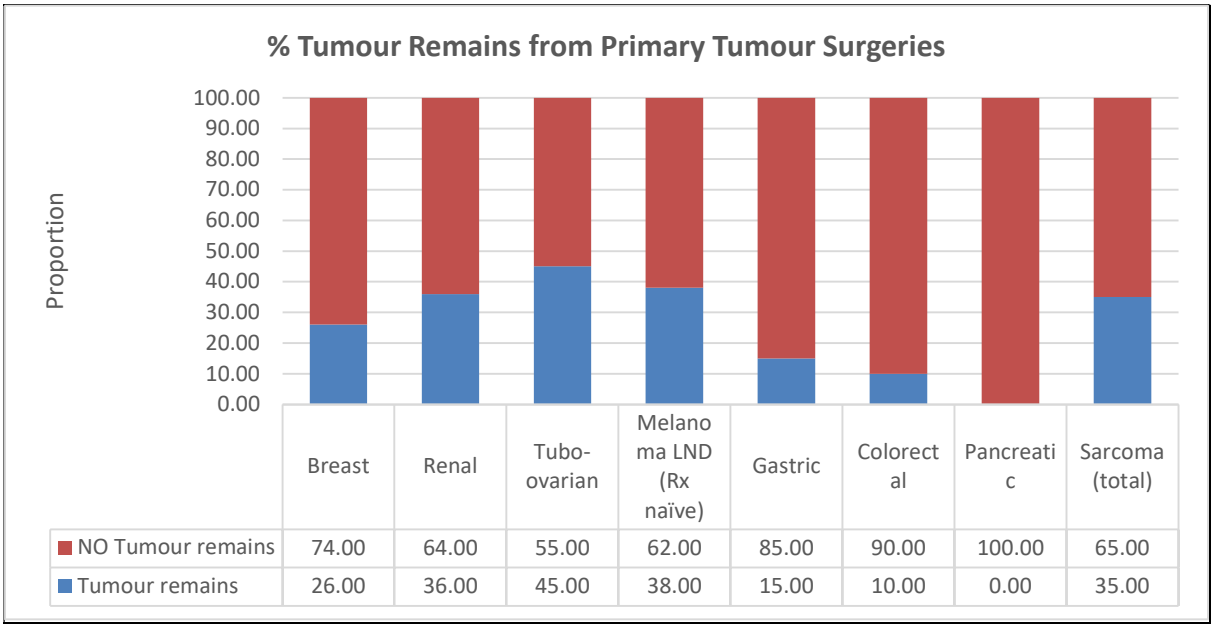

Figure 131 Proportion of cases with remaining tumour from primary tumour surgeries

Close review of these cases revealed some discrepancies which were further investigated. Given that renal cell cancers tend to be relatively large (for example, T2 being >7 cm versus T2 in breast cancer being 2–5 cm) the relatively low proportion of primary renal cancer surgeries with leftover, non-embedded tissue (that is, 36%) raised the question of whether these were all being identified on the tumour remains list. In fact, of the nine primary renal cell carcinomas homogenised, two cases were not captured as having 'tumour remains' by the histopathologists; rather, they were flagged through another translational protocol (renal TRACERx). Although these two cases were staged as pT1a (that is, ≤4 cm); whereas all the others identified as having tumour remaining were pT3, another four of the 25 renal primary tumour resections that were not flagged as having 'tumour remains' were also pT3.

Colorectal cases were also analysed in detail. Of the 30 primary tumour resections, only three were noted to have leftover tumour tissue. Of these, n = 22 were rectal or rectosigmoid cancers and n = 18 underwent neoadjuvant chemo-radiotherapy, which may have reduced tumour volume. Of the eight colon or sigmoid tumours, n = 3 underwent neoadjuvant chemotherapy, which again may have reduced tumour. Of the three flagged by the histopathologists as having remaining tumour tissue, two were from exenterative surgeries, suggesting large volumes of disease. Despite knowing the preference of one of the GI histopathologists for embedding entire surgical specimens, on review of the 30 primary tumour histopathology reports, remaining 'tissue' (a non-specific term) was documented on

17. Therefore it seems unlikely that all cases with leftover surgical tumour tissue were captured.

These two examples highlighted an imperfect capture of primary endpoint data on the interim review. To probe this further, discussions with individual tumour stream histopathologists were undertaken to discuss the analysis and whether it aligned with their expectations and whether they felt they were consistently and accurately capturing this information. Some of the feedback from histopathologists included the following:

- Missing capture of ~50% renal cancers; the pathologist had not been considering inclusion of private patients for the '>1 g tumour remains' capture.
- Missing capture of tubo-ovarian cases (given only 30% captured as 'tumour remains' versus an estimated 75%).
- Results in colorectal cancer thought to be consistent with expectations.
- Breast histopathologist thought 26% with leftover tumour tissue was an overestimate, thought this figure would be ~15% due to Royal Marsden demographics (early presentations with smaller tumours) and use of neoadjuvant chemotherapy.
- Suggestion that staff assisting them (for example, advanced practitioners) should take ownership over prompting the question of whether tumour tissue remains and documenting this.

This feedback suggested that an education-based intervention regarding the importance of capturing this information accurately could be implemented, targeted to pathologists and the advanced practitioners assisting in the dissection.

4.4.3 Molecular profile of homogenate

A pilot cohort of 12 homogenised cases was submitted for whole exome sequencing (WES). Samples included DNA extracted directly from the crude homogenate as well as DNA from flow-cytometry sorted (all) cells and flow-cytometry sorted *tumour* cells, both derived from the crude homogenate. Given the large volume of tumour homogenised, incorporating stromal material and non-tumour cells (for example, immune cell populations) enriching for cells and in particular tumour cells was performed with the aim to improve tumour sample purity. Library preparation was done with the NEBNext Ultra II DNA Library Prep Kit for Illumina (undertaken by the Roche Tissue Diagnostics Team) and sequencing on the NovaSeq 6000 Platform (performed by Genewiz, a commercial sequencing provider). The coverage across samples for each of these cases is listed in Table 17. The cohort median coverage for samples derived from the homogenate was 105×.

Table 17 Whole exome sequencing (WES) de-duplicated coverage and duplication rates for the 12 pilot homogenisation cases and their paired FFPE

Case	Clinical	DeDup coverage* - trial samples	Dup rate* - trial samples	DeDup coverage* - FFPE samples	Dup rate* - FFPE samples
HF012	atypical lipomatous tumour (?benign)	85	66	na	na
HF013	ossifying fibromyxoid tumour (?benign)	123	33	na	na
HF017	breast (T2)	102	43	na	na
HF018	ovarian (FIGO 1A)	99	44	na	na
HF019	melanoma (metastasis)	46	54	na	na
HF023	tubo-ovarian (low grade serous; Stage III; neoadj chemo)	98	41	na	na
HF025	GIST	124	43	na	na
HF028	Renal (pT3)	141	27	130	32
HF034	Renal (pT3)	134	30	164	29
HF039	breast (lobular; T4; multiple neo-adj Rx)	107	43	na	na
HF044	breast (lobular; T3)	103	33	na	na
HF048	melanoma (metastasis)	118	34	na	na
*Median values	**Cohort median**	**105**			

*'*median' is derived from the three samples submitted for each case. 'na' indicates sample not available/not sequenced.*

Two renal cell carcinoma cases had matched DNA samples extracted from their diagnostic FFPE blocks submitted for WES at the same time (HF028 and HF034; see Table 17). The de-duplicated coverage was similar for the FFPE-derived vs homogenate-derived samples, as was the duplication rate.

I undertook a preliminary review of the numbers of variants (nsSNVs and indels) and driver mutations across the paired WES samples in HF028 and HF034 (see Table 18 and Table 19). In both cases, the flow-sorted *tumour* sample had a higher number of variants than the crude homogenate and flow-sorted *all*-cell sample, as would be expected given the enrichment for cells and removal of stroma and debris. In HF028 the greatest number of variants was seen in the flow-sorted tumour sample (82 in total), whereas in HF034 the greatest number of variants was noted in FFPE block 2 (105 variants compared with 71 in the flow-sorted tumour sample), suggestive of higher tumour content.

Table 18 Total variant numbers (nsSNVs & indels) across samples in HF028 and HF034 (primary renal cell carcinomas)

Case	Crude Homogenate	Flow-sorted all cells	Flow-sorted tumour cells	FFPE block 1	FFPE block 2	FFPE block 3
HF028						
No. nsSNVs	na	47	59	57	43	54
No. Fsindels	na	14	23	18	11	14
TOTAL	**-**	**61**	**82**	**75**	**54**	**68**
HF034						
No. nsSNVs	30	60	67	70	81	70
No. Fsindels	7	11	11	19	24*	7
TOTAL	**37**	**71**	**78**	**89**	**105**	**77**
NB: using GL cutoff </= 1%; VAF >/=5% for SNVs; indels VAF >/=5% p</= 0.01; no manual IGV review undertaken						
na= not available (failed sequencing)						
*no P value						

No. = number; nsSNVs= non-synonymous single nucleotide variants; Fsindels= frameshift indels.

Table 19 Driver mutation variant allele frequencies (VAFs) across samples in HF028 and HF034 (primary renal cell carcinomas)

Case	Crude Homogenate	Flow-sorted all cells	Flow-sorted tumour cells	FFPE block 1	FFPE block 2	FFPE block 3
HF028						
VHL p.R126L	na	30	41.5	20.4	10.4	27
BAP1 p.G194A	na	6.3	9.4	18.8	0	31
BAP1 p.Y173C	na	4.4	10.1	0	0	0
SETD2 p.S430fsdel	na	2.3	2.1	31.6	0	28.7
HF034						
VHL p.Q132fsdel	4.8	17.6	14.3	25	30.6	10.7
PBRM1 p.K1106fsdel	12.3	18.7	14.1	31.4	44.7	12.5
MTOR p.S2215F	8.8	15.9	15.5	27.1	41.3	11.4
SETD2 p.C1520G	8.5	17.1	13	25.6	34.3	16.4
NB: using GL cutoff </= 1%; VAF >/=5% for SNVs; indels VAF >/=5% p</= 0.01; no manual IGV review undertaken						
na= not available (failed sequencing)						

All numbers represent percentage (%) frequency.

The putative driver mutations identified in HF028 included a missense mutation in *VHL* and two missense mutations in *BAP1,* as well as a *SETD2* frameshift deletion (Table 19). Although the DNA extracted from the crude homogenate failed sequencing, the flow-sorted samples derived from the homogenate both contained all putative drivers; whereas profiling failed to detect at least one driver variant each of the three regions profiled from the diagnostic FFPE blocks. The VAF of the *VHL* variant was 41.5% in the flow-sorted tumour sample compared with a VAF of 30% in the *all*-cell flow-sorted sample and 10–27% across the FFPE blocks. In contrast, the VAF was only 9–10% for both *BAP1* variants in the flow-

sorted tumour sample, but for *BAP1 p.G194A* the VAF in the two of three FFPE blocks where it was detected was higher (19–31%). The VAF of the *SETD2* deletion was also only 2% in the flow-sorted tumour sample and higher in the two FFPE blocks were it was detected (29–32%). The varying VAFs are difficult to reconcile and may reflect differences in clonality and tumour purity; however, in principle in this case the flow-sorted samples from the homogenate have detected a wider variety of variants than would have been derived from one FFPE sample.

In HF034, putative driver missense mutations were noted in *MTOR* and *SETD2*, and frameshift deletions in *VHL* and *PBRM1* (Table 19), and these were present across all samples. The VAFs differed across each sample (for example *VHL* variant was 14% in the flow-sorted tumour cell sample and 31% (the highest) in FFPE block 2, the latter being the sample with the greatest number of total variants in this case (which is likely to reflect the highest purity).

4.5 Discussion

There is a gap between progress in our understanding of heterogeneity as a biomarker in the context of research studies and what is being translated into clinical practice. The costs of genomic sequencing, although declining with the advent of next generation technology are high and a multi-region sampling approach (mandated by frequent spatial separation of distinct genetic clones in solid tumours) is too inefficient as well as too expensive to be feasible in routine care. Homogenisation and profiling of larger volumes of tumour instead helps overcome some of these challenges. While an additional workflow is required, the materials are not costly and a more representative sample of the whole is created, more akin to a blood draw in haematological malignancies. While liquid biopsy seems like an obvious alternative to capture ITH, it is not widely applicable. A reliable capture of tumour cell free DNA is challenging and varies with the volume and nature of tumour. The Repseq approach is compelling because it focuses on profiling of available tumour tissue. The volume created by the homogenisation approach optimises the use of 'precious' tissues, reducing potential for at least DNA exhaustion. This is an issue being increasingly identified by pathologists, because patients' samples are required for treatment decision making and access to clinical trials.[8]

The analysis of tumour volume sampled for sequencing in routine clinical care revealed only a very small proportion of tumour sampled for colorectal, melanoma and sarcoma tumours

(median 0.0005%). This was considerably less than the average value derived from analysis of TCGA research samples (1.5% across all stages, 0.3% for Stage IV samples),[1] which was still surprisingly low. The inclusion of a large proportion of sarcomas which tend to be larger tumours may have affected this, although both the melanoma and colorectal groups had median sampling proportions (<0.001%). While this may be representative for detection of targetable clonal driver mutations, considered by some groups to be the only clinically relevant genomic information,[2,9] with our increasing understanding of use and application of genomic information it will be insufficient for future progress.

The interim analysis of the HoLST-F study provided useful insights. First, fewer cases were able to be homogenised than predicted, with a large contributor being the interruption of the tissue for research consent, an obstacle that was logistical in nature. Fortunately we were able to navigate a solution to this with the introduction of phone consents. Second, the numbers of primary tumour surgeries highlight breast & sarcoma as dominant tumour types with leftover surgical tumour tissue at the Royal Marsden. This finding is likely to be institution dependent, particularly because sarcoma is a subspecialty interest and a general hospital may have a larger number of colorectal cases which do not require specialist cancer service expertise.

With regards to the primary endpoint, most tumour types met the ≥15% feasibility threshold, with the exception of pancreatic (0%) and colorectal (10%). The frequency for breast (n = 84) and sarcoma (n = 46) was highest in absolute numbers, but the proportion of tubo-ovarian (45%), melanoma lymph node dissection (38%) and renal (36%) cases also suggest that the evaluation of homogenisation in a more definitive study should involve all these tumour types. Inclusion of uterine/endometrial cancer may be useful to consider in future as well, given that five primary tumour cases were homogenised (despite not being included in the primary endpoint tumour type cohort). Molecular markers are becoming increasingly important in the selection of treatment in uterine/endometrial cancer, including identification of microsatellite instability and mutations in p. 53.[10,11]

The interim analysis uncovered issues with the quality of primary endpoint data, especially with regards to the accuracy of documentation of cases with remaining macroscopic tumour tissue (estimated to be >1 g). This prompted an intervention in the form of an educational campaign amongst the histopathologists and APs, with a view to improving data quality for the latter part of the study.

There is a bias in practice at the Royal Marsden where the gastrointestinal pathologists embed most of the colorectal tumours entirely in paraffin, a practice which may vary by department. The referrals for surgery at the Royal Marsden are also skewed to a more complex population and routine operations (such as a hemicolectomy for bowel cancer) and tend to be undertaken in a general cancer unit. Therefore, we did not anticipate a large number of colorectal cases, and the future exclusion of this tumour type should not be done based our analysis, especially because colorectal cancer is one of the four most prevalent cancer types, along with breast, lung and prostate.[12] Because lung surgeries are not performed at the Royal Marsden, lung tumour tissue was not incorporated in the original study protocol.

The preliminary data from paired sequencing of homogenate-derived and diagnostic FFPE blocks in two renal cancer cases reveals :1) the feasibility of sequencing from these samples; and 2) the potential for this strategy to capture tumour heterogeneity. The HF028 case in particular demonstrates a sampling bias in the FFPE-derived samples with regards to driver variants; however, these are all captured in the two samples derived from the homogenate. However, the VAF values differed widely between the samples. In the HF034 case there is no suggestion of any advantage in variant number or indeed VAF in the homogenised samples, with both favoured in the FFPE specimens. The flow-cytometry sorted samples appear to have higher VAFs and more variants detected relative to the crude homogenate sample in HF034, suggesting the benefit of an enrichment strategy, yet their lower VAF values reflected lower purity than in the FFPE samples. A greater number of cases warrant analysis before any firm conclusions can be drawn.

There are several limitations to the homogenisation / representative sequencing approach to tumour profiling, both within the constraints of the HoLST-F study, as mentioned, and in general. One key issue is that the ‘best’ (that is, tumour rich, not necrotic) tumour regions are usually embedded in paraffin for diagnostic purposes. This may result in a lesser quality of leftover tissue destined for homogenisation. Also, depending on the tumour size and the proportion embedded in paraffin, the volume of leftover tumour tissue will vary greatly across patients and between tumour types. Homogenisation of tumour may therefore only be achievable in a proportion of patients, and therefore is unlikely to become routine for all. Much more work is needed to understand the potential clinical benefits of this strategy, and looking at many more cases with paired sequencing within the HoLST-F study will be an important starting point. From a resource perspective, there were many challenges in

developing and implementing this pan-cancer feasibility study in a busy department, with multiple workstreams and reliance on biobank storage space. Physical and practical constraints will need to be considered alongside clinical potential; however, the workflow has now become established at the Royal Marsden within a busy unit, highlighting how this is possible.

Despite the limitations discussed, there is vast potential to utilise tumour homogenates beyond bulk genomic sequencing. The ability to sort the crude homogenates into single cells means that single cell profiling can be undertaken, providing an extra level of resolution for tumour heterogeneity. In addition, flow-assisted cell sorting may enable interrogation of aspects of the tumour immune microenvironment. Transcriptomic biomarkers may also be feasible to explore. The HoLST-F study samples will provide a suite of translational works that can inform how we can best utilise this information.

References for Section 4

1. Litchfield K, Stanislaw S, Spain L, et al. Representative Sequencing: Unbiased Sampling of Solid Tumor Tissue. *Cell Rep* 31: 107550, 2020.
2. Reiter JG, Baretti M, Gerold JM, et al. An analysis of genetic heterogeneity in untreated cancers. *Nat Rev Cancer* 19: 639–650, 2019.
3. McGranahan N, Furness AJ, Rosenthal R, et al. Clonal neoantigens elicit T cell immunoreactivity and sensitivity to immune checkpoint blockade. *Science* 351: 1463–9, 2016.
4. Wolf Y, Bartok O, Patkar S, et al. UVB-Induced Tumor Heterogeneity Diminishes Immune Response in Melanoma. *Cell* 179: 219–235 e21, 2019.
5. Juric D, Castel P, Griffith M, et al. Convergent loss of PTEN leads to clinical resistance to a PI(3)Kalpha inhibitor. *Nature* 518: 240–4, 2015.
6. Misale S, Di Nicolantonio F, Sartore-Bianchi A, et al. Resistance to anti-EGFR therapy in colorectal cancer: from heterogeneity to convergent evolution. *Cancer Discov* 4: 1269–80, 2014.
7. Research NNIfH: NIHR Research for Patient Benefit (RfPB) Programme: Guidance on Applying for Feasibility Studies, 2017, pp. 1–5.
8. McCall S, Dry S: Precision Pathology as Part of Precision Medicine: Are We Optimizing Patients' Interests in Prioritizing Use of Limited Tissue Samples? *Journal of Clinical Oncology: Precision Oncology*, 2019.
9. Reiter JG, Makohon-Moore AP, Gerold JM, et al. Minimal functional driver gene heterogeneity among untreated metastases. *Science* 361: 1033–1037, 2018.
10. Talhouk A, McAlpine JN: New classification of endometrial cancers: the development and potential applications of genomic-based classification in research and clinical care. Gynecol Oncol Res Pract 3: 14, 2016.
11. Le DT, Uram JN, Wang H, et al. PD-1 Blockade in Tumors with Mismatch-Repair Deficiency. N Engl J Med 372: 2509–20, 2015.
12. Sung H, Ferlay J, Siegel RL, et al. Global cancer statistics 2020: GLOBOCAN estimates of incidence and mortality worldwide for 36 cancers in 185 countries. CA Cancer J Clin, 2021.

13. Faustino-Rocha A, Oliveira PA, Pinho-Oliveira J, et al. Estimation of rat mammary tumor volume using caliper and ultrasonography measurements. Lab Anim (NY) 42: 217–24, 2013.

Section 5 Conclusion

The understanding of evolution and heterogeneity in cancer is increasingly relevant in this era of personalised medicine. While studies in this field are hypothesis-generating at present, they may inform the structure of future clinical trials and help the field move away from single biomarkers, which ineffectively predict tumour behaviour. In cutaneous melanoma in particular, which is dominated by a large burden of clonal mutations, single biopsy studies are challenged in their ability to discern subclones that may be of clinical importance.[1] Although hotspot driver mutations remain an important predictor of response to targeted therapies (for example, the presence of a *BRAF V600* mutation in melanoma or *EGFR* mutation in non-small cell lung cancer), greater heterogeneity in therapeutic targets, such as HER2 expression in breast cancer, has recently been shown to be associated with a lower response to Her2-directed therapy.[2]

Predictive biomarkers to immune checkpoint therapy would ideally include an assessment of clonal and subclonal neoantigen burden. The accuracy of predictive gene expression markers is also undermined by tumour immune microenvironment heterogeneity.[3] More representative sampling to improve the accuracy of disease profiling is therefore required to improve patient outcomes and minimise both physical and financial toxicity associated with anti-cancer therapy.

In this thesis I explore two novel approaches to the analysis of metastatic heterogeneity and clonal evolution. The work outlined in **Section 3** analyses a cohort of 14 patients with cutaneous, acral, mucosal and unknown primary melanoma who have undergone comprehensive metastatic profiling at a research post-mortem, paired with primary tumour analysis in six cases. While the PMIs for this cohort varied from one to six days, the quality of tumour DNA overall did not appear to vary with PMI, and 90% of samples submitted for WES were successfully profiled. Analysis of the phylogenetic trees across these 14 heavily treated cases confirms that a polyclonal mode of seeding from the primary tumour to metastatic sites was most common. In one case, the clinical behaviour of genomically distinct metastases differed markedly during treatment. In five cases there were metastatic regions characterised by the presence of exclusive clones, reflecting multiple seeding events.

While the analysis of putative mechanisms of treatment resistance was limited to genomic factors, intermetastatic heterogeneity was evident, with convergence on the MAPK pathway

characterised by multiple *NRAS* mutations in a patient treated with two rounds of BRAF/MEK inhibitors. WGD was more commonly noted as a subclonal, rather than clonal, event. In conjunction with cell-to-cell variation in (aneu)ploidy evident using FISH, this suggests that CIN is an active process in late-stage melanoma refractory to treatment. This is consistent with observations of 'dysregulation of genomic integrity' in a recently published cohort of seven melanoma patients profiled at autopsy.[4]

The implications of this genomic diversity evident in late-stage melanoma are twofold: the first is that single-sampling does not adequately reflect the status of disseminated disease in most cases and the second is that a one-size-fits-all treatment approach will not optimally control disease. While widespread metastatic tissue sampling is not feasible *in vivo*, other approaches to understanding diversity using liquid biopsy, repeat tissue biopsy and targeted imaging may assist in identifying different clones that are present and ones that emerge. Larger cohorts, in particular, with paired primary multi-region tumour sampling, will be required to help decipher features of the 'lethal clones' that metastasise, and whether this is determined or stochastic. For example, clones in the primary tumour with features such as a high WGII and clonal WGD reflecting punctuated events may be more prone to metastatic dissemination.

The work outlined in **Section 4** explores the feasibility of tumour homogenisation, designing and implementing a translational study (HoLST-F) based within the histopathology department of the Royal Marsden NHS Foundation Trust. An interim analysis of this study reveals that this approach looks most promising in primary breast, renal and tubo-ovarian cancers, as well as sarcomas and melanoma lymph node dissections because >15% of surgical resections from these tumour types have leftover tissue that could be homogenised. Consistent with the pilot work that has been done in this space,[5] a preliminary evaluation comparing samples derived from the homogenate to samples derived from FFPE tissue slides reveals the potential for a greater representation of variants. Homogenisation of tumour tissue may be conducted in real time, with results that could potentially direct patient care; for example, in uncovering treatment resistant subclones, or discerning clonal and subclonal mutation (and possibly neoantigen) burden. The scope of translational analyses conducted on homogenate-derived samples could potentially be broadened, including single cell analysis of tumour and immune cell populations.

Post-mortem sampling and homogenisation are feasible approaches to the understanding of subclonal genomic tumour dynamics, important in the assessment of heterogeneity and evolution. These methods warrant ongoing investigation with the ultimate aims of guiding more personalised anti-cancer treatment, optimising its timing, and improving patients' survival.

References for Conclusion

1. Dentro SC, Leshchiner I, Haase K, et al. Characterizing genetic intra-tumor heterogeneity across 2,658 human cancer genomes. *Cell* 184: 2239–2254 e39, 2021.
2. Metzger Filho O, Viale G, Stein S, et al: Impact of HER2 heterogeneity on treatment response of early-stage HER2-positive breast cancer: phase II neoadjuvant clinical trial of T-DM1 combined with pertuzumab. *Cancer Discov*, 2021.
3. Rosenthal R, Cadieux EL, Salgado R, et al. Neoantigen-directed immune escape in lung cancer evolution. *Nature* 567: 479–485, 2019.
4. Vergara IA, Mintoff CP, Sandhu S, et al. Evolution of late-stage metastatic melanoma is dominated by aneuploidy and whole genome doubling. *Nat Commun* 12: 1434, 2021.
5. Litchfield K, Stanislaw S, Spain L, et al. Representative Sequencing: Unbiased Sampling of Solid Tumor Tissue. *Cell Rep* 31: 107550, 2020.

Appendix A: Bioinformatic methods

Appendix A: Bioinformatic methods

Compiled by Desiree Schnidrig, Project Bioinformatician

Contents

1.1 SNV, and INDEL calling from multi-region whole exome sequencing (WES)

Paired-end reads (2 × 100bp) in FastQ format sequenced by Hiseq or NextSeq were aligned to the reference human genome (build hg19), using the Burrows-Wheeler Aligner (BWA) version 0.7.15. with seed recurrences (-c flag) set to 10,000.[1] Intermediate processing of Sam/Bam files was performed using Samtools version 1.3.1 and deduplication was performed using Picard 1.81 (http://broadinstitute.github.io/picard/). Single nucleotide variant (SNV) calling was performed using Mutect v1.1.7 and small-scale insertion/deletions (INDELs) were called running VarScan v2.4.1 in somatic mode with a minimum variant frequency (–in-var-freq) of 0.005, a tumour purity estimate (–tumour-purity) of 0.75, and then validated using Scalpel version 0.5.3 (scalpel-discovery in –somatic mode) (intersection between two callers taken) (2–4). SNVs called by Mutect were further filtered using the following criteria:

1. variants falling outside the targeted capture range (±50bp padding) or into mitochondrial chromosome, haplotype chromosome, HLA genes or any intergenic region were not considered
2. presence of both forward and reverse strand reads supporting the variant
3. >5 reads supporting the variant in at least one fresh-frozen tumour region of a patient
4. variants were required to have a VAF of 0.2 in at least one fresh-frozen tumour region
5. sequencing depth needed to be ≥20 and ≤3000 across all fresh-frozen tumour regions.

Mutations called in formalin-fixed and paraffin-embedded (FFPE) samples were restricted to variants which passed this additional filtering in fresh-frozen samples. Dinucleotide substitutions (DNV) were identified when two adjacent SNVs were called and their VAFs

were consistently balanced (based on proportion test P≥0.05). In such cases the start and stop positions were corrected to represent a DNV, and frequency related values were recalculated to represent the mean of the SNVs. Variants were annotated using Annovar.[5] Individual tumour biopsy regions were judged to have failed quality control and excluded from analysis based on the following criteria: 1) sequencing coverage depth below 100X; 2) low tumour purity, such that copy number calling failed.

1.2 SNP calling

Single nucleotide polymorphisms (SNPs), were called in the germline sample using Platypus version 0.8.1 with default parameters apart from –genIndels = 0 and –minMapQual = 40, and calls were restricted to the targeted capture range (±50bp padding). Tumour regions were genotyped based on the variants identified in the germline (parameters set to -minPosterior = 0 –getVariantsFromBAMs = 0). SNPs with a minimum coverage of 50× in the germline and the tumour sample were used for allele-specific copy number segmentation.

1.3 Copy number analysis

CNVkit version 0.7.3 was used with default parameters on paired tumour-normal sequencing data.[6] Outliers of the derived log2 ratio (logR) calls from CNVkit were detected and modified using median absolute deviation Winsorisation before case-specific joint segmentation of fresh-frozen samples to identify genomic segments of constant logR.[7] Formalin-fixed and paraffin-embedded (FFPE) samples were segmented separately, leveraging the segment information from the fresh-frozen samples. Copy number alterations were then called as losses or gains relative to overall sample wide estimated ploidy. Arm-level gains and losses were called if ≥50% of the arm were gained or lost. Driver cytoband copy number was identified by overlapping the called somatic copy number segments with putative driver copy number regions previously identified by GISTIC2 analysis of TCGA melanoma data.[8] The average proportion of the genome with aberrant copy number, weighted on each of the 22 autosomal chromosomes, was estimated as the weighted genome instability index (wGII). Allele-specific segmentation was performed using the paired PSCBS method after removal of single-locus outliers (R package PSCBS version 0.61.0).[9]

1.4 Purity and ploidy estimate

Tumour sample purity, average ploidy and absolute allelic copy number per segment were estimated using ABSOLUTE v1.2 in allelic mode.[10] In line with recommended best practice

all ABSOLUTE solutions were reviewed by three bioinformaticians, with solutions selected based on the majority vote.

1.5 Subclonal deconstruction

In order to estimate whether mutations were clonal or subclonal, and the clonal structure of each tumour, a modified version of PyClone was used. For each mutation, two values were calculated, obsCCF and phyloCCF. obsCCF corresponds to the observed cancer cell fraction (CCF) of each mutation. Conversely, phyloCCF corresponds to the phylogenetic CCF of a mutation. To clarify the difference between these two values, consider a mutation present in every cancer cell within a tumour. A subclonal copy number event in one tumour region may lead to loss of this mutation in a subset of cancer cells. While the obsCCF of this mutation is therefore below 1, from a phylogenetic perspective, the mutation can be considered 'clonal' because it occurred on the trunk of the tumour's phylogenetic tree, and as such, the phyloCCF may be 1.

To calculate the obsCCF of each mutation, local copy number (obtained from ABSOLUTE), tumour purity (also obtained from ABSOLUTE), and variant allele frequency were integrated. In brief, for a given mutation we first calculated the observed mutation copy number, n_{mut}, describing the fraction of tumour cells carrying a given mutation multiplied by the number of chromosomal copies at that locus using the following formula:

$$n_{mut} = VAF\frac{1}{p}[p\ CN_t + CN_n\ (1-p)]$$

where VAF corresponds to the variant allele frequency at the mutated base, and p, CN_t, CN_n are respectively the tumour purity, the tumour locus specific copy number, and the normal locus specific copy number (CN_n was assumed to be 2 for autosomal chromosomes). We then calculated the expected mutation copy number, n_{chr}, using the VAF and assigning a mutation to one of the possible local copy numbers states using maximum likelihood. In this case only the integer copy numbers were considered.

All mutations were then clustered using the PyClone Dirichlet process clustering.[11] PyClone version 0.13.1 was used for two cases (PEA036, PEA038 due to the exceptionally high tumour mutational burden (TMB) in these cases), while the remaining cases were analysed with PyClone version 0.12.3. For each mutation, the observed variant count was used and reference count was set, such that the VAF was equal to half the pre-clustering CCF. Given

that copy number and purity had already been corrected, we set the major allele copy numbers to 2 and minor allele copy numbers to 0 and purity to 0.5; allowing clustering to simply group clonal and subclonal mutations based on their pre-clustering CCF estimates. We ran PyClone with 10,000 iterations and a burn-in of 1000, and default parameters, with the exception of –var_prior set to 'BB' and –ref_prior set to 'normal'.

To determine the phyloCCF of each mutation, a similar procedure to that described above was implemented, with the exception that mutations were corrected for subclonal copy number events. Specifically, if the observed variant allele frequency was significantly different from that expected ($P<0.01$, using prop.test in R) given a clonal mutation, we determined whether a subclonal copy number event could result in a non-significant ($P>0.01$) difference between observed and expected VAFs. The pre-clustering CCF for each mutation was then calculated by dividing n_{mut} by n_{chr}. Subclonal copy number events were estimated using the raw values from Absolute output. Finally, to ensure potentially unreliable VAFs of indels did not lead to separate mutation clusters, each estimated indel CCF was multiplied by a region specific correction factor. Assuming the majority of ubiquitous mutations, present in all regions, are clonal, the region specific correction factor was calculated by dividing the median mutation CCF of ubiquitous mutations by the median indel CCF of ubiquitous indels.

1.6 Identification of subclonal mutations driven by copy number loss

Mutations were investigated in order to identify those whose absence, or low CCF values, may be driven by copy number loss events. For each tumour we identified any SNV residing in genomic segments of copy number heterogeneity across tumour regions, with minor and major copy number aberrations considered separately. For each chromosome, we grouped mutations into non-contiguous genomic segments with consistent copy number states within tumour regions and within SNV clusters defined above. To restrict our analysis to mutations lost in at least one tumour region, we determined the median CCF value of each SNV group, and only considered SNV groups where the median CCF value was ≤ 0.25 in at least one tumour region. We then evaluated whether copy number loss coincided with lower CCF levels using a one-sided Wilcoxon test or, if more than two copy number states were present across tumour regions, a one-sided Cochrane Armitage trend test.

To ensure the lower CCF value was driven by copy number and not tumour region, we also implemented a regression analysis, including both copy number and region in the model. If over 85% of mutations within a given Pyclone cluster were determined to be driven by copy

number, then the entire cluster was classified as copy number driven. Finally, to avoid overestimating copy number driven losses of mutations, only losses occurring in ≤75% of tumour regions were considered. In addition, comparisons were made between the results of each mutations obsCCF and phyloCCF. Given that the only difference between the calculation of the two is that obsCCF does not correct for subclonal copy number events, mutations which appear clonal by phyloCCF but subclonal by obsCFF may reflect copy number driven heterogeneity. To avoid overestimating copy number driven heterogeneity only mutations with a VAF of at least 1% were considered potentially to reside on a subclonal copy number and thereby considered as potentially driven by subclonal copy number loss.

1.7 Phylogenetic tree construction

To ensure accurate tree construction, mutation clusters were first filtered to ensure no violation of evolutionary principles. In brief, two principles were considered. First, the pigeonhole principle, which states that two mutation clusters cannot be considered independent and on separate branches of an evolutionary tree if the sum of the cancer cell prevalence values of the two clusters exceeds 100% within a single tumour region. Second, a descendent clone must exhibit a smaller cellular prevalence than its ancestor within each and every tumour region, referred to as the 'crossing rule'. Using these principles it can be determined whether particular mutation clusters conflict with each other and cannot be fitted to the same evolutionary tree. For instance, if the cellular prevalence of mutation Cluster 1 in tumour Region 1 is 80% and mean cellular prevalence of mutation Cluster 2 in tumour Region 1 is 60%, then, by the pigeonhole principle, Cluster 2 must be a descendent of Cluster 1. However, if, in a different tumour region, the cellular prevalence of Cluster 2 is greater than Cluster 1, it can be said that Cluster 1 and 2 conflict due to 'crossing rule'.

To ensure accurate tree construction, only clusters with at least five mutations were included. For the majority of tumours, all subsequent clusters were used to manually construct a phylogenetic tree. However, for a subset of tumours evolutionary conflicts were identified, and a small number of mutation clusters were therefore removed. In total, 65/177 mutation clusters were removed, 23 of these containing less than five mutations. This removed 528 mutations from a total 22,148 mutations, representing 2.4% of all clustered mutations.

1.8 Mutational signature analysis

Mutational signatures were estimated using the deconstructSigs package in R.[12] Subclone specific mutational signature analysis was restricted to subclones with at least 50 mutations.

References for Appendix A

1. Li H, Durbin R. Fast and accurate short read alignment with Burrows-Wheeler transform. *Bioinformatics*, 25(14), 1754–60, 2009.
2. Cibulskis K, Lawrence MS, Carter SL, Sivachenko A, Jaffe D, Sougnez C, et al. Sensitive detection of somatic point mutations in impure and heterogeneous cancer samples. *Nat Biotechnol*, 31(3), 213–9, 2013.
3. Fang H, Bergmann EA, Arora K, Vacic V, Zody MC, Iossifov I, et al. Indel variant analysis of short-read sequencing data with Scalpel. *Nat Protoc* (online). Nov 17, 11, 2529, 2016. http://dx.doi.org/10.1038/nprot.2016.150
4. Koboldt DC, Chen K, Wylie T, Larson DE, McLellan MD, Mardis ER, et al. VarScan: Variant detection in massively parallel sequencing of individual and pooled samples. *Bioinformatics*, 25(17), 2283–5, 2009.
5. Wang K, Li M, Hakonarson H. ANNOVAR: Functional annotation of genetic variants from high-throughput sequencing data. *Nucleic Acids Res*, 38(16), 1–7, 2010.
6. Talevich E, Shain AH, Botton T, Bastian BC. CNVkit: Genome-Wide Copy Number Detection and Visualization from Targeted DNA Sequencing. *PLoS Comput Biol*, 12(4), 1–18, 2016.
7. Nilsen G, Liestøl K, Loo P Van, Moen Vollan HK, Eide MB, Rueda OM, et al. Copynumber: Efficient algorithms for single- and multi-track copy number segmentation. *BMC Genomics*, 13(1), 2012.
8. Broad Institute TCGA Genome Data Analysis Center (2016): SNP6 Copy number analysis (GISTIC2). Broad Institute of MIT and Harvard. 2016.
9. Olshen AB, Bengtsson H, Neuvial P, Spellman PT, Olshen RA, Seshan VE. Parent-specific copy number in paired tumor-normal studies using circular binary segmentation. *Bioinformatics*, 27(15), 2038–46, 2011.
10. Carter SL, Cibulskis K, Helman E, McKenna A, Shen H, Zack T, et al. Absolute quantification of somatic DNA alterations in human cancer. *Nat Biotechnol* (online). 30(5), 413–21, 2012. http://dx.doi.org/10.1038/nbt.2203
11. Roth A, Khattra J, Yap D, Wan A, Laks E, Biele J, et al. PyClone: Statistical inference of clonal population structure in cancer. *Nat Methods*, 11(4), 396–8, 2014.
12. Rosenthal R, McGranahan N, Herrero J, Taylor BS, Swanton C. deconstructSigs: Delineating mutational processes in single tumors distinguishes DNA repair deficiencies and patterns of carcinoma evolution. *Genome Biol* (online). 17(1), 1–11, 2016. http://dx.doi.org/10.1186/s13059-016-0893-4

Appendix B: FISH tissue harvest sample list with H&E tumour purity and viability assessment

Appendix B: FISH tissue harvest sample list with H&E tumour purity and viability assessment

Case	Lab code	Sample Identifier	Metastatic site	Tumour purity (H&E)	Tumour viability (H&E)	Comments
R_PEA004	M16	LN_1_R1	Lymph node	e	e	
R_PEA004	M20	ST_2_R2	Soft tissue	e	c	
R_PEA005	M17	LU_1_R1	lung	e	d	
R_PEA005	M7	BR_7_R1	brain	e	e	
R_PEA009	M2	ST_1_R1	soft tissue	e	d	
R_PEA009	M1	ST_1_R2	soft tissue	e	d	
R_PEA012	M42	LI_10_R1	liver	e	d	
R_PEA012	M20	ST_4_R5	soft tissue	e	d	
R_PEA016	M5	LI_3_R2	liver	e	d	
R_PEA016	M4	LI_3_R1	liver	e	d	
R_PEA017	M40	DI_2_R3	diaphragm	e	e	*FAILED PROCESSING*
R_PEA017	M15	LN_2_R1	lymph node	e	e	
R_PEA020	M2	BR_1_R2	soft tissue	e	b	*FAILED PROCESSING*
R_PEA020	M26	ON_1_R1	optic nerve nodule	e	e	
R_PEA023	M17	LI_3_R1	liver	d	d	
R_PEA023	M21	LN_1_R1	lymph node	c	e	
R_PEA025	M1	SC_1_R1	soft tissue	e	c	
R_PEA025	M16	PC_1_R1	cardiac	e	e	
R_PEA026	M5	AD_1_R1	adrenal	e	d	
R_PEA026	M18	LN_2_R1	lymph node	e	e	
R_PEA036	M69	PE_1_R1	soft tissue	d	d	
R_PEA036	M54	LI_18_R1	liver	e	c	
R_PEA038	M26	LI_8_R1	liver	c	d	
R_PEA038	M11	LN_1_R3	lymph node	e	c	
R_PEA060	M13	AD_1_R1	adrenal	e	d	
R_PEA060	M19	LI_4_R1	liver	d	c	
R_PEA080	M1	LN_1_R1	lymph node	e	d	
R_PEA080	M14	LN_6_R2	lymph node	e	d	

Tumour content and Tumour viability as assessed on review of haematoxylin & eosin (H&E) stained slides of each sample

Key:	***Key:***
c=25-50%	c=50% viable
d=50-75%	d=mostly viable
e=75-100%	e=near 100% viable

Appendix C: Service evaluation for RMH cohort –Tumour Volume in Molecular Profiling

The ROYAL MARSDEN

R&D_TEM-34

Service Evaluation Proposal Form

- Service Evaluations are now administered through Research and Development (R&D)
- **Statistician involvement is MANDATORY** and Forms MUST be accompanied by either scanned versions with signatures **in section 2** or emails from both the statistician and Unit Head of Department approving the proposal before submission **before Clinical Review can be arranged**
- If a patient or public questionnaire is included, the Form, Questionnaire and a Patient Information Sheet must be forwarded to the Patient and Public Involvement (PPI) Lead for review. A Patient Information Sheet Template can be found on the Intranet in Clinical R&D\All Documents\Service Evaluation.
- Please complete this form as a 'Word' document and return a copy by e-mail attachment to 'Service Evaluation' (Service.Evaluation@rmh.nhs.uk)
- Data collection MUST NOT commence until WRITTEN approval from the CCR (Committee for Clinical Review) Reviewer has been given to the project, by Research and Development
- Refer to the guidance document on the Clinical Research & Development (R&D) site on the trust intranet for full guidance on the submission process, including design of Clinical Report Forms (data collection tools) and spreadsheets.
- Please send all queries to Service.Evaluation@rmh.nhs.uk

Thank you

Shaded boxes are for Statistics office use only.

Service Evaluation Title: Tumour volume evaluation in molecular profiling				
Is this required for an M Sc?		No	**If Yes, date M.Sc report required**	
Other Sites involved: No		**If Yes,** UK / International / Both	**Data collection:** Retrospective	
Applicant* Divn / Directorate				
Applicant *	**Name:**	Lavinia Spain		**Contact No: 07557983066**
	Designation:	Clinical Fellow		**Unit/ Dept: Skin & Renal**

Email address of Applicant:	Lavinia.Spain@rmh.nhs.uk		
Planned Start Date:	ASAP	**Date final report anticipated:**	MANDATORY: July 2018
Does the proposer plan to leave the RM before the expected report date?	No	If Yes, please state handover arrangements for project completion:	
Co- Investigator(s) (List all)	Samra Turajlic, Jennifer Thomas, Lisa Thompson		
Data Manager (Name)	Lavinia Spain/ Jennifer Thomas		
Is a questionnaire involved?	No	Is this a patient or staff questionnaire?	N/A
'Other' questionnaire please specify			
Name of Patient and Public Involvement (PPI) reviewer if patient questionnaire:	N/A		
Does SE have cost implications?	No	If Yes, state here how these will be met**:**	

Section 2.

Statistical support provided by (Name of statistician)	This will be undertaken at the Francis Crick by one of the Bioinformaticians	
****** I approve the above methodology **(Signed) Statistician**	(please send an email demonstrating agreement from statistician to service.evaluation.rmh.nhs.uk if unable to sign electronically)	Date:
∮ **Period for data retention**	Related to trial / research? No	

Approval By Head of Unit / Dept

This applicant has agreed to complete this service evaluation and to report the results back to the CCR in a timely fashion. If the proposer leaves the Royal Marsden before completing and reporting the project results back to the CCR, the handover arrangements detailed on page 1 of this form (or if un-anticipated, subsequently separately notified to Service.Evaluation@rmh.nhs.uk) will apply, and I confirm my agreement to these handover arrangements.		
Head of Unit / Dept Name: Block Capitals	MARTIN GORE	Date:
Head of Unit/Dept Signature:		
Note: ** All countersignatures MUST be obtained either electronically or in handwriting *before* submission and a fully countersigned copy submitted to the Service.Evaluation@rmh.nhs.uk in electronic format.		

Applicant Declaration and signature	I confirm that I have completed the following actions **prior to submitting this proposal to the Committee for Clinical Research (CCR) for clinical review** : i) obtained the involvement of a named trust/ICR statistician, who has reviewed and approved the proposal ii) sought and obtained approval for this evaluation from the clinical audit lead for my Unit / Department or Sutton & Merton Community Services, who has seen and signed a copy of this proposal iii) sought and obtained approval for this evaluation from my Head of Department who has seen and signed a copy of this proposal iv) have made/ will make arrangements that if I leave the Royal Marsden before this SE project is reported, the project (including all data), will be handed over to a suitable staff member (agreed by my Head of Department) to complete and report back to the Committee for Clinical Research. v) I have read the trust Service Evaluation Policy and the trust Confidentiality and the Data Protection Act Policy and will abide by the requirements therein.		
*** Applicant Declaration and signature**	Please see declaration and SIGN and DATE this form, after the Clinical Audit Lead and Head of Department. (*See* the end of the form, below).		
Signed (Applicant)		Date:	

**Note: The applicant is the person who is primarily responsible for the project design, data collection and reporting of the completed project.*

ϕ ***Note: Freedom of Information Act 2000 – Retention of Service evaluation data***

Data should be retained for *5 years* after the results and action plan have been agreed with the relevant Unit/ Department and reported to CCR and to IGRM.
However, If the SE data are related to ongoing research eg following extraction from a research data set – the SE data should be retained for the same period of time as the related research data set or for five years, whichever is the longer.

The following template can be used as a starting point for service evaluations. Text in blue has been written as a guide to completing the template – all the blue text should be replaced with your own text as appropriate to your study. The completed protocol should act as a blueprint or 'recipe book' to conducting your evaluation: that is, a reasonably well-informed person should be able to use the protocol (and only the protocol) as a set of instructions which are comprehensive enough to enable them to carry out the study from start to finish.

NOTE : All Sections of the following pages are MANDATORY for completion

LAY SUMMARY

When a cancer (malignant tumour) is removed at surgery there are several diagnostic tests that are performed. These include looking at its structure to determine the type of tumour as well as checking for certain genes within the tumour that may guide treatment decisions.

Tumours vary in size and we know that cells within the same tumour have differences in their genetic code (genes). Only a very small amount of the tumour from only one section is used for testing the genetic profile. This may not be representative of the rest of the tumour

and therefore alterations in significant genes may be missed. The larger the tumour, the greater the heterogeneity within it.

As part of two existing studies at the Royal Marsden– Renal and Melanoma TRACERx (CCR3723 and CCR3569 respectively) – we are evaluating a novel process called homogenisation. This involves blending relatively large volumes of tumour tissue that is leftover from surgery (ie tumour tissue that is not paraffin-embedded and kept in the histopathology department for diagnostic purposes) and then using DNA derived from this mixture to perform genetic testing. In theory this should provide a more comprehensive genetic profile of the tumour, overcoming some of the issues associated with utilising only a small sample from a single region.

We would like to evaluate the discrepancy in the volume of tumour used for genetic testing versus the volume that is not tested in 100 cases, across colorectal, sarcoma and melanoma tumours. This information will contribute to our pilot study on homogenisation within the Renal and Melanoma TRACERx protocols.

Background Information
This SE has been initiated by the Skin and Renal Unit to contribute to a pilot project being undertaken under the auspices of the TRACERx protocols, as detailed above.

Current practice within the molecular pathology department at the Royal Marsden Hospital is to extract DNA for diagnostic molecular tests (for example BRAF testing in melanoma) from three 10 micron slides, cut from diagnostic FFPE blocks. These are macrodissected for tumour rich regions. Molecular profiling is routinely performed on colorectal tumours (looking for *KRAS/BRAF/NRAS/PIK3CA* & *TP53*), melanomas (*BRAF & NRAS)* and sarcomas (RT-PCR for gene fusions depending on histological subtype). As such, we plan to target these tumour types for our assessment.

We hope to systematically demonstrate the discrepancy in the amount of tumour that is profiled versus that which is not profiled.

SE Aims
To look at the proportion of a tumour specimen on which molecular profiling is undertaken.

SE Objectives: Primary Objective

To calculate the volume of tumour that undergoes molecular profiling.

Secondary objective
N/A
SE design
This is a retrospective, observational study.

Eligibility for inclusion in the SE

Any patient who has undergone surgery to remove a primary colorectal tumour, a primary sarcoma or melanoma lymph node dissection at the Royal Marsden Hospital and has had this tumour molecularly profiled in our Molecular Pathology Department.

a) Inclusion criteria

1) Surgery for tumour removal at the Royal Marsden Hospital with an available histopathology report for:
    a. Primary colorectal tumours

b.Primary sarcomas
c.Melanoma lymph node dissections

2)Molecular profiling undertaken at the Royal Marsden
3)At least 2 macroscopic tumour dimensions on the histopathology report
4)Available information on the number & thickness of slides used for molecular profiling

b) Exclusion criteria

1)Surgery not performed at the Royal Marsden Hospital
2)Inadequate information re size of macroscopic tumour on the histopathology report.

Planned methodology

We will obtain a list from our Molecular Pathology Department of colorectal, sarcoma and melanoma tumours they have profiled in the last 12 months and then cross-check inclusion/exclusion criteria with histopathology reports. If we cannot obtain N=100 cases (minimum of N=20 per tumour type) then we will source retrospective data (eg from preceding 24 months) to reach our target.

Data Collection between (dates)	April 2018-June 2018
Data source(s) to be used	Molecular Pathology lists

Statistical considerations

Endpoints

The percentage of the whole tumour that undergoes molecular profiling.

Analysis methods

The whole tumour volume will be calculated from the dimensions provided on the histopathology report. Where 3 dimensions are available, results will be reported as mm3 or cm3 and where only 2 dimensions are available, results will reported as mm2 or cm2. The volume of tissue used for profiling will also be calculated from the number and thickness of the slides used (reported as um3) and the results will be described as a percentage.

Sample size

We are seeking to record information for N=100 cases (minimum of N=20 for each tumour type).

Study organisation

Patients will be identified through lists obtained from the molecular pathology department. This information will then be cross-checked with the electronic medical record to ensure that the patient meets the criteria detailed above.

Study organisation: Who does what

Dr Lavinia Spain will liaise with the molecular pathology department for a list of cases and then oversee the data collection that will be performed by Dr Jennifer Thomas.

Data storage and data handling

Data will be entered on to an excel spreadsheet (see attached- 1st tab) kept on the Royal Marsden's shared F drive, under the 'Research Fellow' folder. A unique identifier will be allocated to each case. Once the information for N=100 cases has been collected, an anonymised copy of this spreadsheet (see attached – 2nd tab) will be shared with one of the Bioinformaticians in Dr Turajlic's TRACERx team at the Francis Crick Institute.

References

APPENDIX: ADD LIST OF DATA ITEMS FOR COLLECTION

See spreadsheet attached (2 tabs)

Appendix D: HoLST-F protocol – version 2.0, September 2019

NHS
Health Research Authority

The ROYAL MARSDEN
Life demands excellence

Homogenization of Leftover Surgical Tissue across multiple cancer types: a Feasibility Study (HoLST-F)

Short Title:	HoLST-F
Chief Investigator:	Samra Turajlic
Co-investigators:	Lavinia Spain
	Glenn Noel-Storr
	Ashley Gilchrist
	Vanessa Primus
	James Larkin
	Zayd Tippu
	Lewis Au
	Scott Shepherd
RM Collaborators:	David Cunningham
	Nick Turner
	Robin Jones
	Susanna Banerjee
	Sanjay Popat
	Andrew Wotherspoon

	Ayoma Attygalle Steve Hazell Ashutosh Nerurkar Monica Terlizzo Khin Thway
External Collaborator:	Nelson Alexander (Ventana (Roche))
Bioinformatics :	Kevin Litchfield (Francis Crick)
Statistician:	Bernice Asare
Trial Manager:	Lyra Del Rosario
Sponsor:	The Royal Marsden NHS Foundation Trust Fulham Road, London SW3 6JJ
Site and collaborating laboratories addresses:	The Royal Marsden NHS Foundation Trust Fulham Road, London SW3 6JJ The Francis Crick Institute 1 Midland Road London NW1 1AT Ventana Medical Systems, Inc. *A member of the Roche Group* 1910 E. Innovation Park Drive Tuscon, Arizona 85755
Version number & date:	Version 2.0, 18th Sep 2019

Protocol Synopsis

Title	Homogenization of Leftover Surgical Tissue across multiple cancer types: a Feasibility Study (HoLST-F)
Sponsor	The Royal Marsden NHS Foundation Trust
Funding	Ventana Medical Systems
Number of sites	1
Rationale	Intratumour heterogeneity is well recognized in multiple cancer types and ultimately leads to therapeutic resistance. It also limits the ability of small samples to represent the whole tumour, having implications for diagnosis, molecular analysis and understanding of the tumour immune microenvironment. By blending- 'homogenizing'- leftover tumour tissue in excess of that required for diagnosistic purposes, one may create a more representative sample for analysis.
Study Design	Feasibility study
Primary objective	To evaluate how many surgical cases have left over tumour tissue amenable to homogenization
Secondary objectives	Evaluate the results of analyses on homogenized tissue versus diagnostic tissue as well as aspects of the homogenization process
Number of subjects	Aim to homogenize 500 samples over a 24 month period
Subject selection criteria	Patients who undergo cancer surgery and have leftover tumour tissue, including the subset who have signed consent for Tissues for Research
Duration of study	24 months
Primary endpoint	• The percentage of cases involving resection of the primary tumour, or in the case of melanoma involving a lymph node dissection, with leftover formalin-fixed tumour tissue estimated to weigh >1gm (ie tissue not embedded in paraffin for diagnostic purposes) across the following tumour types: o Breast o Colorectal o Pancreatic o Gastric o Renal o Ovarian o Sarcoma o Melanoma (lymph node dissections)
Secondary endpoints	• Median time (in minutes) required for dissection of the leftover surgical tissue into tumour, tumour-adjacent and normal tissue • Median time (in minutes) required for the blending (actual homogenization) of each tissue type • Difference in molecular profile (eg number of gene mutations and copy number alterations, cancer cell fraction, tumour mutational burden) between the diagnostic block and the homogenized sample, as measured by next generation sequencing techniques (NGS) across

	the following primary tumour types (analyses including but not limited to): o Breast (eg ER, PR and Her2 amplification) o Colorectal (eg KRAS, NRAS and BRAF mutations) o Pancreatic (eg KRAS, EGFR) o Gastric (eg KRAS, Her2) o Renal (eg VHL) o Ovarian (eg BRCA1 and BRCA2) o Sarcoma (eg KIT, PDGFR, various translocations) o Melanoma (lymph node dissections; eg BRAF, NRAS, KIT)
Safety evaluations	Serious incidents related to the homogenization process will be noted. No adverse events will be reported as there is no patient contact and only material that would usually be destroyed will be used, therefore this should have no impact on clinical care.
Statistics	Descriptive statistics will be used to report on the primary and some secondary endpoints. Sequencing and flow cytometry data will be analysed separately.

Contents

1. Background

Within a single tumour, be it primary or secondary, both genetic and phenotypic variation are observed. This so-called 'intratumour heterogeneity' (ITH) is recognized in multiple cancer types[1-5] and is largely driven by genomic instability[6]. This limits the ability of a single sample of tumour to be representative of the whole. ITH is recognised as an important driver of tumour progression, drug resistance and treatment failure in solid tumours[7]. This has important implications for diagnosis and also for biomarkers guiding treatment decisions and prognosis.

Ventana Medical Systems (Ventana; a subsidiary of Roche) have developed technology that enables formalin-fixed tumour tissue (ie before it becomes paraffin-embedded) to be blended, or 'homogenized'. With this method, a more representative sample than is otherwise provided by a limited number of biopsies may be sent for molecular (eg genetic sequencing for mutations) and cellular (eg flow cytometry for cell markers) analysis. In a pilot study conducted as part of the Renal and Melanoma TRACERx protocols (CCR3723 & CCR3569 respectively; unpublished data) surgical waste from three cases of renal cell carcinoma and two cases of melanoma were processed in this manner (see Figure 1, below). DNA was successfully isolated from the homogenized samples and subjected to library capture and sequencing. Analysis of the sequencing data revealed robust mutational calling (compared with fresh frozen tissue collected at the time of surgery) and specifically a more robust determination of the cancer cell fraction (that is the percentage of cancer cells in the tumour that harbour the particular variant), avoiding the risk of clonal illusion that is associated with single biopsy molecular assessments.

Figure 1: Kidney cancer pilot homogenization case. A) dimensions of a primary kidney tumour that underwent homogeniation; B) biopsies were taken at multiple sites within the tumour; C) an additional number of mutations were identified in the homogenized sample (in green) compared to those identified by multiregion sampling (blue, red and black).

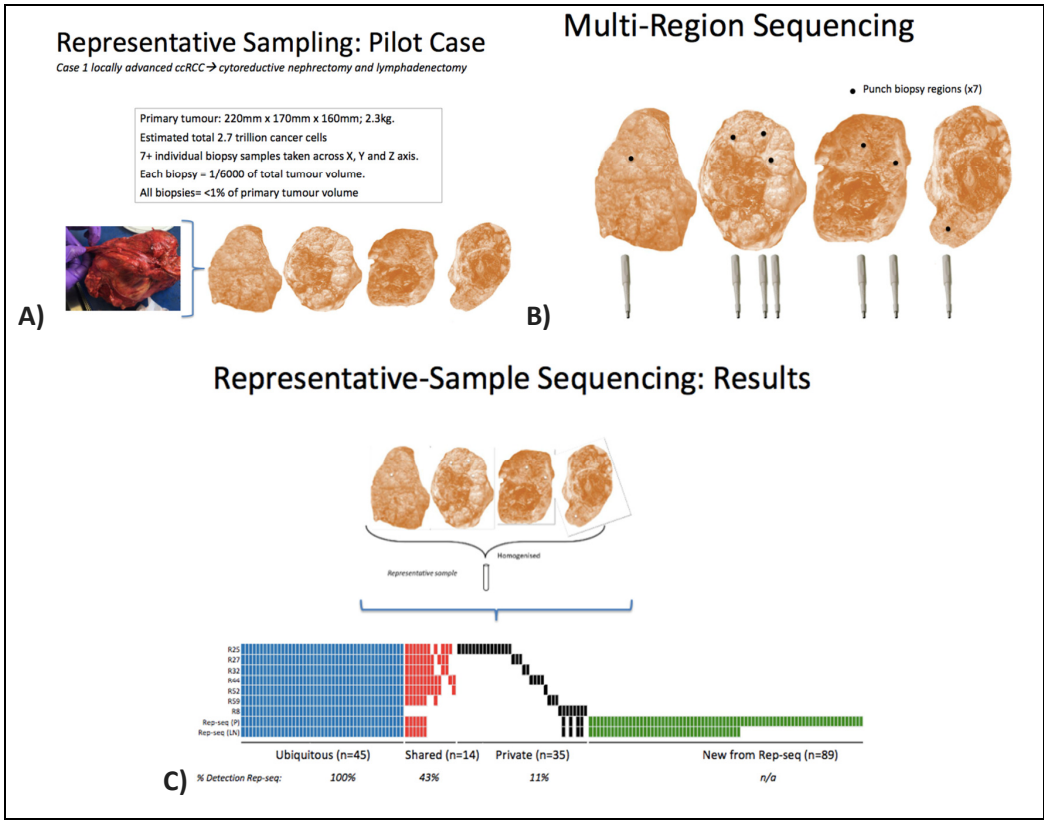

Additionally, analysing single cells from solid tumours have the potential to enable quantification of specific cell types, and to increase the sensitivity of detection of rare mutations within tumour sub-clones. This approach has been used to demonstrate tumour evolution in breast cancer[8]. Single-cell heterogeneity has also been described in rectal cancer[9]. Ventana has developed methods to further disassociate the crude homogenate (ie the blended tumour tissue) into single cells, utilizing mechanical and biochemical processes. Single cells from representative samples can serve as the input material for flow cytometry analyses of immune and tumour biomarkers for cancer therapy (eg T-lymphocyte cell surface markers to determine tumour infiltrating lymphocytes (TILs), PD-L1 expression). Increasingly TILs are recognised as prognostic and predictive biomarkers across several tumour types[10-12].

The theoretical benefit of the homogenization approach is supported in studies demonstrating the clinical limitations of intratumour heterogeneity in various assays.

For example, reports in prostate cancer strongly suggest that more thorough sampling of standard pathology samples yields more accurate information related to prognosis[13,14]. More specifically, in Cyll et al, the authors were able to link aneuploidy to shorter time to recurrence only when they improved their sampling methodology[14]. In comparing different PD-L1 assays in melanoma samples it was found that geographic heterogeneity of the tumour accounted for most of the variance between these[15]. The ability to understand a greater spectrum of mutations within a tumour may also enable identification of mechanisms of primary resistance to proposed therapies, influencing clinical decision-making.

Patients with large primary tumours are the ones least-served by a diagnostic approach reliant on a single or limited number of biopsies. The relationship between a larger primary tumour and a worse prognosis is documented across multiple tumour types[16-21] and one explanation for this is likely to be the greater heterogeneity within a larger tumour volume. The ability to homogenize residual tissue in these cases and provide a representative sample may be particularly useful.

The tissue adjacent to macroscopic tumour (tumour-adjacent tissue) differs from normal tissue in a number of ways. There may be microscopic tumour cells present rendering a macroscopically clear margin positive (ie an R1 resection), molecular alterations[22] as well as stromal changes[23]. A recent study[24] has shown that protein expression across multiple tumour types is abnormal even beyond 1cm from the tumour margin. The authors characterized a set of 18 genes specifically activated in this zone, many of which contribute to an inflammatory response conducive to tumour spread. Immune cell infiltration of this tumour-adjacent region is not characterized. As such, the opportunity to analyse this area may yield novel insights into factors that both facilitate and inhibit metastatic spread.

2. Rationale

Patients undergoing cancer surgery have a sample of tumour obtained for diagnostic and staging purposes that is formalin fixed after surgery and then paraffin-embedded. In some cases the entire tumour may be paraffin-embedded, for

example with small breast and colon primary tumours. However, leftover tissue from many surgical specimens (ie parts that are formalin-fixed but not paraffin-embedded) is thrown away when there is tissue in excess of diagnostic requirements. This is often the case in larger tumour types such as renal cell cancer, sarcoma and melanoma lymph node dissections, as well as in metastatic tumour resections. The proportion of cases with residual or leftover tumour tissue is unknown across most tumour types.

At the Royal Marsden, patients are provided the opportunity to give consent enabling access to excess surgical tissue for future research purposes. External sites may be considered for inclusion where a similar consent is available. This would be subject to a future protocol amendment and ethical approval. Furthermore in this protocol, this consent will be referred to as the 'generic tissue for research consent'. In these cases, a fresh sample of tissue is usually taken for biobanking, prior to formalin fixation. Whether homogenization of the leftover formalin-fixed surgical material is feasible in enough cases to be considered for further development of this process as part of routine care across primary breast, colorectal, gastric, pancreatic, ovarian, renal cancer and sarcoma, as well as melanoma lymph node dissections, will be explored. In cases where generic tissue for research consent has been provided, we plan to homogenize leftover tumour tissue across cancer types in both primary and metastatic settings. We will seek to compare the differences in molecular and cellular analysis of homogenized tumour tissue samples compared with information derived from slides cut from the diagnostic FFPE tumour blocks, as performed in routine care. We will also explore the profiling of tissue adjacent to the tumour where possible.

This study will be conducted in accordance with standard operating procedures, policies, local R&D management guidance, Good Clinical Practice including the UK Policy Framework for Health and Social Care Research and other applicable regulatory requirement(s) including but not limited to the Human Tissue Act 2004 and Human Tissue (Quality and Safety for Human Application) Regulations 2007.

3. Hypotheses

- Homogenization of excess tumour tissue:
    - Is feasible to perform on a significant number of leftover surgical samples across multiple tumour types
    - Provides tissue of suitable quality for molecular analyses

4. Aims

Our aims are to:

- Identify the proportion of primary tumour cases with leftover surgical tissue that may be amenable to homogenization across multiple tumour types
- Evaluate the process of homogenization in multiple tumour types
- Explore the differences in molecular profiling between a single diagnostic tumour sample and the homogenized sample
- Explore immune cell infiltration in the homogenized samples

5. Objectives

Primary Objective

- Evaluate the proportion of cases involving resection of the primary tumour, or in the case of melanoma involving a lymph node dissection, with macroscopically visible leftover formalin-fixed tumour tissue (ie tissue not embedded in paraffin for diagnostic purposes) across the following tumour types:
    - Breast
    - Colorectal
    - Pancreatic
    - Gastric
    - Renal
    - Ovarian
    - Sarcoma
    - Melanoma (lymph node dissections)

Feasibility threshold: if >15% of cases per tumour type have leftover surgical tissue then further investigation into homogenization is deemed feasible.

Secondary Objectives

- Establish the amount of time required for dissection of the leftover formalin-fixed surgical tissue
- Establish standard blending times required for adequate homogenization of each tissue type
- Compare the results of molecular analyses between the diagnostic and homogenized specimens, across the following primary tumour types:
    - Breast
    - Colorectal
    - Pancreatic
    - Gastric
    - Renal
    - Ovarian
    - Sarcoma
    - Melanoma (lymph node dissections)

Exploratory Objectives

- Evaluate the immune cell infiltration of the homogenized tumour sample with flow cytometry and immune cell sequencing
- Determine whether homogenized tissue is suitable for gene expression analysis
- Evaluate the homogenized 'tumour-adjacent tissue' samples and compare this profile with that of the homogenized tumour and homogenized normal samples

6. End Points

Primary Endpoint

- The percentage of cases involving resection of the primary tumour, or in the case of melanoma involving a lymph node dissection, with macroscopically visible leftover formalin-fixed tumour tissue estimated to weigh >1gm by a histopathologist (ie tissue not embedded in paraffin for diagnostic purposes that would otherwise be discarded) across the following tumour types:
    - Breast
    - Colorectal
    - Pancreatic
    - Gastric
    - Renal
    - Ovarian
    - Sarcoma
    - Melanoma (lymph node dissections)

Feasibility threshold: if ≥15% of cases per tumour type have leftover surgical tissue then further investigation into homogenization is deemed feasible.

Secondary Endpoints

- Median time (in minutes) required from the start of dissection of the leftover surgical tissue into tumour, tumour-adjacent and normal tissue until its completion
- Median time (in minutes) required for the actual homogenization of each tissue type from the start until the stop of 'blending'
- Difference in molecular profile (eg number of gene mutations and copy number alterations, cancer cell fraction, tumour mutational burden) between the diagnostic block and the homogenized sample, as measured by next generation sequencing techniques (NGS) across the following primary tumour types (analyses including but not limited to):
    - Breast (eg ER, PR and Her2 amplification)
    - Colorectal (eg KRAS, NRAS and BRAF mutations)
    - Pancreatic (eg KRAS, EGFR)

- Gastric (eg KRAS, Her2)
- Renal (eg VHL)
- Ovarian (eg BRCA1 and BRCA2)
- Sarcoma (eg KIT, PDGFR, various translocations)
- Melanoma (eg lymph node dissections; BRAF, NRAS, KIT)

Exploratory Endpoints

- Quantification of infiltrating immune cells (eg CD8 positive lymphocytes) and expression of immune checkpoints (eg PD-L1) in the homogenized tumour sample using flow cytometry
- Compare the clonal diversity of immune cells in different tissue samples by receptor sequencing
- Successful gene expression analysis of enriched cell populations or individual cells
- Compare the differences in the molecular and cellular profile of the homogenized 'tumour-adjacent tissue' and 'normal adjacent tumour' sample with those of the homogenized 'tumour' and 'normal' samples (eg compare gene mutations, immune cell infiltration)

7. Inclusion and Exclusion criteria

All patients with macroscopically visible leftover tissue from primary breast, colorectal, gastric, pancreatic, ovarian, renal cancer and sarcoma surgeries, as well as melanoma lymph node dissections, estimated by a histopathologist to contain >1gm of tumour, will be included in the feasibility assessment (primary endpoint).

The following criteria apply to eligibility for tumour samples to be homogenized:

Inclusion

1. >1gram leftover formalin-fixed tissue (ie that would be otherwise discarded by histopathology) from cancer surgery.
2. Generic tissue for research consent has been given by the patient.

3. Patient age ≥18 years old.
4. Minimum of 1 gram of residual tumour remaining in leftover surgical tissue
5. Minimum of 0.4 gram of normal tissue present.

Exclusion Criteria

1. Advanced Practitioner in histological dissection or equivalent deems tumour sample to be inadequate.
2. Leftover surgical tumour tissue greater than 20 kilograms.

8. Methodology

This is a non-interventional study designed to evaluate the feasibility of homogenization as a potential diagnostic tool that could improve clinical decision making. This includes an assessment of how many primary tumours across several tumour types actually have leftover surgical tumour tissue that would otherwise be discarded. Within this study we will also pilot the homogenization process across multiple tumour types to see whether this yields a sample of tissue suitable for molecular and cellular analysis. The average times required for homogenization of the various tumour types will also be calculated.

All patients who undergo their cancer care at the Royal Marsden are provided information on potential research that may be undertaken on tissue that is excess to diagnostic requirements. Information on 'Tissues for Research' consent is provided upon patient registration at the hospital, with the option of immediately providing consent at this time. Many other institutions have a similar procedure.

After cancer surgery, for many tumour types there is residual formalin-fixed tumour tissue that does not get embedded in paraffin blocks. Tissue studies (eg Genomics England (GeL) Pilot Study) typically sample fresh tissue, prior to formalin fixation, and therefore this study will not interfere with these. The tissue deemed excess to diagnostic requirements is kept in buckets in histopathology (labeled as either 'tumour' or 'tumour and normal' tissue). As per institution's local policy, usually

approximately 4 weeks after surgery, this leftover tissue is then incinerated. There may be a small or large residual amount, depending on the nature and size of the tumour. For example, many small breast and colorectal cancers are entirely paraffin-embedded and no tumour material will remain. In contrast, larger tumours such as sarcomas may have samples embedded in paraffin blocks, however the majority is subsequently discarded. This study plans to make use of this leftover tumour tissue (ie the component that would otherwise be deemed as waste and discarded) to trial the homogenization process in patients who have given 'Tissues for Research' consent.

Study plan

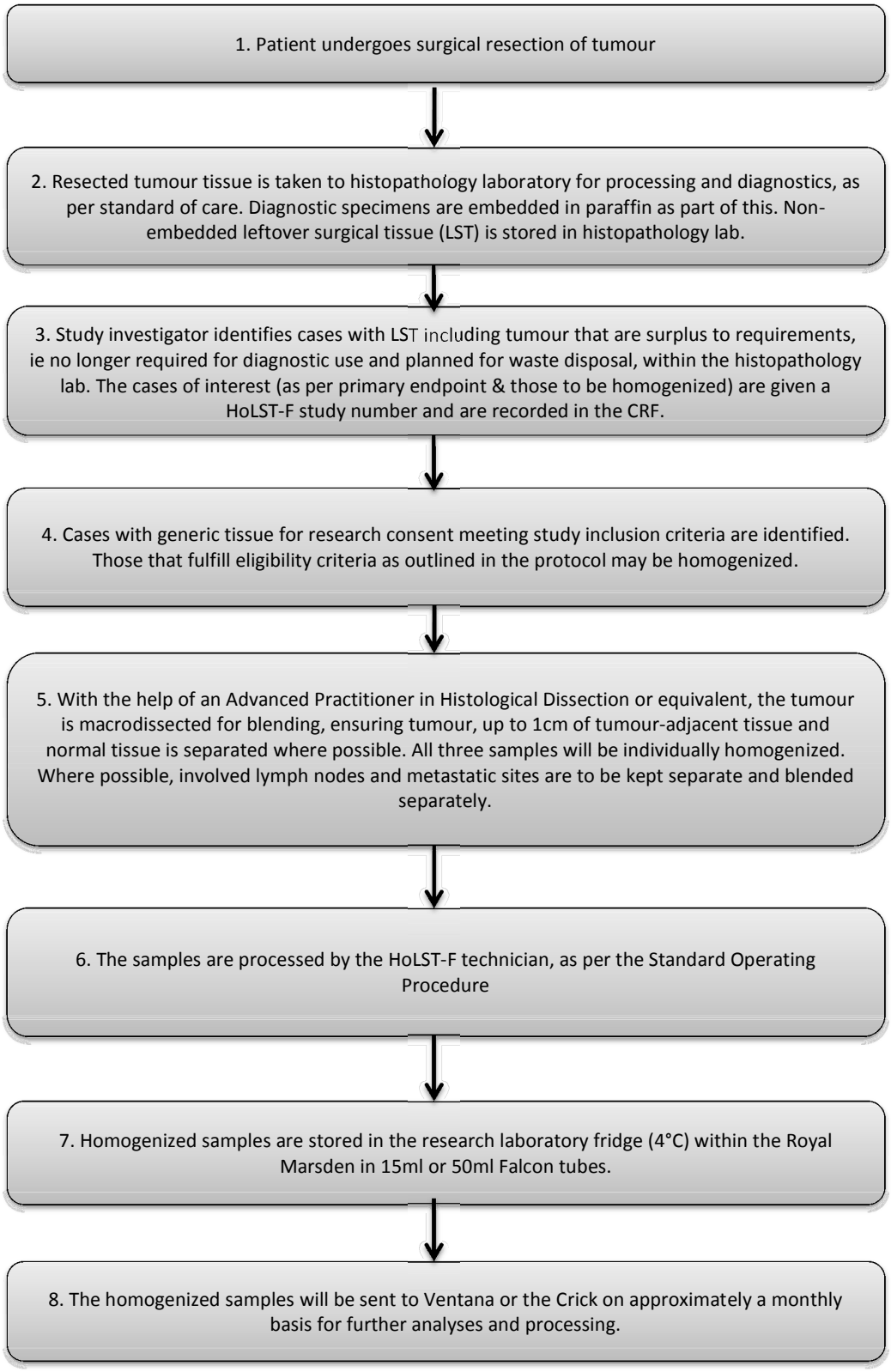
1. Patient undergoes surgical resection of tumour
2. Resected tumour tissue is taken to histopathology laboratory for processing and diagnostics, as per standard of care. Diagnostic specimens are embedded in paraffin as part of this. Non-embedded leftover surgical tissue (LST) is stored in histopathology lab.
3. Study investigator identifies cases with LST including tumour that are surplus to requirements, ie no longer required for diagnostic use and planned for waste disposal, within the histopathology lab. The cases of interest (as per primary endpoint & those to be homogenized) are given a HoLST-F study number and are recorded in the CRF.
4. Cases with generic tissue for research consent meeting study inclusion criteria are identified. Those that fulfill eligibility criteria as outlined in the protocol may be homogenized.
5. With the help of an Advanced Practitioner in Histological Dissection or equivalent, the tumour is macrodissected for blending, ensuring tumour, up to 1cm of tumour-adjacent tissue and normal tissue is separated where possible. All three samples will be individually homogenized. Where possible, involved lymph nodes and metastatic sites are to be kept separate and blended separately.
6. The samples are processed by the HoLST-F technician, as per the Standard Operating Procedure
7. Homogenized samples are stored in the research laboratory fridge (4°C) within the Royal Marsden in 15ml or 50ml Falcon tubes.
8. The homogenized samples will be sent to Ventana or the Crick on approximately a monthly basis for further analyses and processing.

In the case of tumours exceeding the capacity of a single blender (eg large sarcomas), the sample will be cut into multiple sections for blending. A single homogenate will then be created by mixing these individually blended sections. Elective sectioning may be performed in some large tumours, obtained at the Royal Marsden only, with individual sections homogenized separately. Photos may be taken of the residual tumour tissue in order to correctly document this process.

In selected cases planned for homogenization, multiregion sampling of the dissected tumour tissue will be performed. This would involve taking from 2 to 10 punch biopsies (1mm or 2mm; depending on the size of the residual tumour tissue) from which DNA and RNA would be purified for sequencing.
The proposed analyses on the homogenized samples include (but are not limited to):

- Molecular analyses:
    - Sequencing (including next generation sequencing whole exome and next generation sequencing panel techniques (bulk and single cell) for DNA, RNA and immune cell receptors)
    - Cytogenetics
    - Proteomics

  Cellular analyses (ie via flow cytometry):
    - Quantification of infiltrating immune cell subtypes (eg CD4, CD8 and FOXP3 T cells)
    - DNA ploidy analysis
    - PD-L1 expression

In all cases planned for homogenization, a minimum of 0.4 gram of normal tissue will be taken for the purpose of sequencing germline DNA (to act as a control compared to tumour).

For cases from the Royal Marsden Hospital only, where possible as per the Tissues for Research Consent, blood may be obtained from patients at the same time as routine blood tests. If this is possible to acquire in some cases (eg if the patient is due a routine follow-up appointment), the study team may phone the patient and

request this, referencing the Tissues for Research consent and not this specific protocol. Germline DNA would then be extracted from a buffy coat for sequencing.

In some cases, it may not be possible to acquire tumour-adjacent tissue and therefore analysis of this area may only occur in a subset of cases.

The diagnostic FFPE blocks (ie the tumour tissue that is embedded in paraffin and stored in histopathology) as well as the written histopathological and molecular reports will be accessed as a reference point. Where metastases are homogenized, access to the primary tumour FFPE blocks will also be requested. Slides will only be cut from the diagnostic FFPE blocks for cases where DNA from the homogenized sample has been deemed suitable for sequencing library preparation. In these cases, five 10µm unstained slides will be cut from representative blocks. These will be sent to Ventana for DNA (and where possible, RNA) extraction, in order to compare with the molecular analyses undertaken on DNA and RNA extracted from the homogenized sample. Five to ten 4µm slides will also be cut for immunohistochemical staining, eg for TILs and PD-L1 expression.

A sample of homogenized tissue may be embedded in paraffin and stored at Ventana.

9. Data Acquisition

Clinical information pertaining to the nature of surgery performed and its findings will be collected from the patient medical records. Relevant treatment information will also be noted.

The following information will be retrospectively obtained from the Informatics Team at the Royal Marsden and used to assist in calculating the primary endpoint:

- The number of patients who have had surgical procedures to remove primary tumours across the specified tumour types at the Fulham Road Royal Marsden location only (ie wide local excisions or mastectomies for

breast cancer, colectomy or anterior or abdominal-pelvic resections for colorectal cancer, Whipple's procedures for pancreatic cancer, gastrectomies for gastric cancer, oophorectomies (including debulking ovarian cancer surgery)

Due to the wide variation in sarcoma in terms of sites of disease, histology and surgical procedures, and the difficulty for Informatics in filtering this information, the total number of surgical cases will be cross-checked with the Sarcoma Unit Audit Database. This database is updated every 2 months by the Senior Sarcoma Surgical Registrar.

As mentioned, access to the diagnostic FFPE blocks will be made for comparative purposes as part of the study, as well as access to the relevant medical records.

10. Data Analysis

A fortnightly report of cases with leftover surgical tissue as well as those suitable for homogenization will be generated by the histopathology department at the Royal Marsden only. Clinical details will be recorded in a study database. Every 6 months the number of primary tumour surgeries for each cancer of interest (described above in *Data Acquisition)* will be sourced from the Informatics team and reviewed alongside the number of cases with leftover surgical tissue.

Final analysis of the data generated will occur after 500 cases have been homogenized, or the study has been running for 24 months, whichever occurs first.

11. Study Organisation

Responsibilities

The Chief Investigator will be responsible for the overall running of this study. A lead study Sub-investigator and Trial Manager will be the primary point of contact on a day-to-day basis. They will also be delegated individuals for overseeing completion of the study database.

A delegated senior histopathology manager will oversee the process of homogenization within the histopathology department. Advanced Practitioners in histological dissection or equivalent will be involved with leftover tumour tissue identification, processing and undertake a risk assessment prior to the commencement of this work. Along with the scientists undertaking the homogenization, they will be responsible for recording data on this aspect, as per the source data templates.

Statistical analysis of the primary and some of the secondary endpoints will be performed by the study statistician.

DNA and RNA extraction, molecular and cellular analyses, may be performed at Ventana or at the Francis Crick. Bioinformatic processing of raw sequencing data (DNA and RNA) and the comparison between the diagnostic and homogenized specimens may be undertaken by a bioinformatician in at the Francis Crick or Roche Sequencing Solutions (RSS) at Ventana.

The Francis Crick Institute will be an additional long-term storage facility for the homogenized samples. A paid-for commercial storage facility may be engaged for this purpose as required. Unstained slides from the diagnostic blocks will be cut at either at the Francis Crick or by a paid-for commercial provider and then returned to the Sponsor. Relevant contract agreements will be in place between the Sponsor, collaborating study laboratories and, as required, paid-for commercial service providers.

Study procedures

See Homogenization Standard Operating Procedure. Updates to this document may be done as required by the study team to optimize workflow and techniques. Updates will be version controlled and any new updates will result in a new version.

Adequate training for Advanced Practitioners in Histological Dissection, Biomedical Scientists and/or equivalents involved in the homogenization process will be provided by the Sponsor or Sponsor delegate. If there are any significant updates to the Homogenization Procedure, additional training will be arranged as necessary.

Start date definition

This study will open once ethical and all other relevant approvals have been obtained. This study opened in September 2018.

Study completion

Approximately 24 months from the start date or upon accrual of target number of samples. The study can also be deemed complete prior to the approximate duration upon discretion of the Chief Investigator and Sponsor.

12. Evaluation of outcomes

If greater than 15% of primary tumours within a tumour type (eg breast, colorectal) contain leftover surgical tumour tissue, then this tumour type would be appropriate for inclusion in a larger study of the homogenization process (eg for validation of this process).

Established bioinformatics pipelines (as detailed in section 14) will be used to evaluate the sequencing data and undertake the comparisons between the diagnostic block and homogenized tumour samples.

Translational work within this study will be contingent on the homogenized tumour tissue being of suitable quality.

13. Safety

As this study does not involve patient contact, adverse events will not be recorded.

Serious incidents (SI) are defined as: a) any occasion where routine clinical care is disrupted as a consequence of the study (eg delay in diagnosis, missing sample), b) where tumour is homogenized without consent, c) any laboratory accident. A record will be kept of all SIs (see Appendix A) in the Trial Master File and these will be logged and followed up through the relevant reporting systems as per institution practice.

14. Statistical considerations

Feasibility threshold

The low feasibility threshold of 15% was selected on the basis that this process may add meaningful information to patients' care, even if only possible in a minority of cases in a particular tumour type.

Sample size

The following table summarises the predicted number of primary tumour surgeries over a 24 month period (based on data for 2015-2017 sourced from the Royal Marsden Informatics team):

Tumour type	Number of predicted surgeries over 24 month period (to remove primary tumour)	Maximum width of 95% CI of proportion of cases with leftover tissue (assuming observed proportion is 50%)	Number of predicted cases with Tissues for Research Consent	Estimated number of cases per week available for homogenization
Ovarian	49	± 0.14	21	0-1
Melanoma LND	68	± 0.119	29	0-1
Breast	1092	± 0.03	595	5-6
Colorectal	141	± 0.083	51	0-1
Renal	66	± 0.121	37	0-1
Pancreatic	52	± 0.136	24	0-1
Gastric	63	± 0.123	31	0-1
Sarcoma	540	± 0.042	289	2-3

TOTAL	**2071**		**1077 (52%)**	**7-14**

Assuming that of the estimated 7-14 primary tumour samples per week with generic tissues for research consent, 5 have leftover surgical tissue, 500 cases may be potentially homogenized over 24 months. In the event that no suitable primary tumour samples are available, non-primary tumour samples may be homogenized. This meets the capacity within histopathology to dissect and homogenize approximately 5 cases per week.

Analysis of endpoints

The primary endpoint will be presented as a percentage for every tumour type alongside a 95% confidence interval. Where appropriate, the percentage of cases for the secondary endpoints will also be presented alongside 95% confidence intervals. Time required from 1) the start of the dissection of leftover tissue into its 3 components until this is completed and 2) the actual blending time (ie from start until the tumour homogenate reaches the desired consistency) for each type of tissue will be presented as mean, median and interquartile range (IQR).

An interim analysis of the primary endpoint will be undertaken after approximately 6 months of study start date, in order to inform planning of the translational work undertaken on the homogenized samples.

The molecular analysis secondary endpoint, in addition to the exploratory endpoints, will be analysed externally. Anonymised genomic sequencing data may be stored, processed and analysed either by the Bioinformatics team at the Francis Crick or by Roche Sequencing Solutions (RSS), in accordance with good clinical practice.

All bioinformatics analyses through the Francis Crick will be conducted utilising the following (or equivalent) tools. Paired-end reads (2x100bp) in FastQ format sequencing data will be aligned to the reference human genome (build b38), using the Burrows-Wheeler Aligner (BWA)[25]. Intermediate processing of Sam/Bam files will be performed using Samtools v1.3.1 and deduplication performed using Picard 1.81

(http://broadinstitute.github.io/picard/) [25]. Single Nucleotide Variant (SNV) calling will be performed using Mutect v1.1.7 and small scale insertion/deletions (INDELs) will be called running VarScan v2.4.1 and then validated using Scalpel v0.5.3 [26-28]. To estimate somatic copy number alterations, ASCAT and CNVkit v0.7.3 will be utilised [29]. Tumour sample purity, ploidy and absolute copy number per segment will be estimated using ABSOLUTE v1.0.6 [30]. The cancer cell fraction (CCF) of a mutation in a given sample will be calculated using the variant allele frequency (VAF) at the mutation base, tumour purity and the tumour locus specific copy number and the normal locus specific copy number. Mutation clustering will be performed using PyClone Dirichlet process clustering [31].

Data analysis by RSS will be undertaken using one of their in-house pipelines.

Flow cytometry will be performed and analysed at either Ventana or the Francis Crick, subject to the homogenized tissue being suitable for this. In theory, three technical replicates will be conducted, always starting with one million total cells. For TILs, gating will be placed on forward and side scatter where the immune cells can be detected as they are much smaller and more homogeneous in size than tumour cells. Positivity will be defined by using a negative control to set the negative fluorescent threshold. The presence or absence of TILs and PD-L1 on immunohistochemical staining of slides from the diagnostic FFPE blocks will serve as an indirect comparator for these markers.

15. Regulatory and Ethics Committee Approval

Independent Ethics Committee

This protocol has been reviewed by the Committee for Clinical Research at the Royal Marsden NHS Foundation Trust (CCR4838) and submitted for independent Research Ethics Committee (REC) approval (IRAS ID: 236131; REC ref: 18/NW/0391).

Patient information and consent

Only leftover tumour material from patients who have provided a generic tissue for research consent allowing the techniques described and collaboration with an external entity will be homogenized for this protocol. The nature of this consent covers the work proposed and is in accordance with the Human Tissue Act (2004).

Confidentiality

At the Royal Marsden, only the immediate research team will have access to patient identifying information, including identification of cases with leftover surgical tissue and access to the medical records for documentation of information related to these. In the case of samples from external sites being identified as suitable for homogenization, before transfer to the Sponsor, a request for a study number will be emailed to the Trial Manager who will then allocate study number for use to label the sample. No patient identifying information will be used to label the sample.

Subsequent to homogenization, all further samples will be labeled with a study number only. All samples leaving the Royal Marsden will be anonymised. An anonymised database of clinical information will be kept securely, in accordance with local data protection laws (see Storage of Tissue and Data below). Patient details will be anonymised in any published work from this study.

Regulatory requirements and GCP

This study will be undertaken in accordance with the principles of Good Clinical Practice (GCP).

Sponsor

The Royal Marsden NHS Foundation Trust is the sponsor of this study.

16. Storage of tissue and data

A secured, user-only access database of anonymised clinical information will be developed for the study. Information related to the homogenate process (eg start and stop times for tissue preparation, processing and actual homogenization) will be

captured on a paper case report form (CRF) by a delegated member of the research team and subsequently entered into the study database. These may be audited as required by any governing authority and the Sponsor. For cases where the photographs are taken to document the dissection process, these will be stored within a secured electronic drive.

Anonymised homogenized tissue samples will initially be stored at the Sponsor. They will be transferred directly to both Ventana and to the Francis Crick Institute (Cancer Evolution and Genome Instability Laboratory) on a monthly basis. The diagnostic FFPE blocks will be sent to the Francis Crick (or a paid-for commercial provider), and processed into unstained slides. All unstained slides are labeled with the study number only and will be stored at Ventana. All relevant agreements for sample transfer will be in place prior to study commencement. For future collaborating laboratories and paid-for commercial providers, approval from the Chief Investigator and the Sponsor will be obtained and relevant agreements will be in place prior to sample(s) being transferred.

The raw genomic sequencing data will be derived from DNA extracted from the anonymised samples (ie from the homogenized samples and the unstained slides cut from the diagnostic blocks). This information will be stored at both Ventana and the Francis Crick. Storage of the processed sequencing data will occur at the Francis Crick.

17. Financing, Indemnity and Insurance

The funding for this study will be provided by Ventana (Roche).

Insurance will be covered by the policy for Royal Marsden sponsored studies.

18. Publication policy

Data generated from this protocol may be presented at scientific meetings, or submitted for publication in a peer-reviewed journal. All co-investigators and

collaborators will have authorship rights. All patient information will be anonymised in any data presentation or paper.

19. Abbreviations

ITH	Intratumour heterogeneity
R&D	Research and Development
IHC	Immunohistochemistry
FFPE	Formalin fixed paraffin embedded
DNA	Deoxyribosenucleic acid
RNA	Ribose nucleic acid
PD-L1	Programmed-Death Ligand 1
SOP	Standard Operating Procedure
SI	Serious Incident
IQR	Interquartile Range
GCP	Good Clinical Practice
MTA	Material Transfer Agreeement
LST	Leftover surgical tissue
NGS	Next Generation Sequencing
CRF	Case report form
RSS	Roche Sequencing Solutions

20. References

1. Gerlinger M, Rowan AJ, Horswell S, et al: Intratumor heterogeneity and branched evolution revealed by multiregion sequencing. N Engl J Med 366:883-892, 2012
2. Torres L, Ribeiro FR, Pandis N, et al: Intratumor genomic heterogeneity in breast cancer with clonal divergence between primary carcinomas and lymph node metastases. Breast Cancer Res Treat 102:143-55, 2007
3. Szerlip NJ, Pedraza A, Chakravarty D, et al: Intratumoral heterogeneity of receptor tyrosine kinases EGFR and PDGFRA amplification in glioblastoma defines subpopulations with distinct growth factor response. Proc Natl Acad Sci U S A 109:3041-6, 2012
4. Campbell PJ, Pleasance ED, Stephens PJ, et al: Subclonal phylogenetic structures in cancer revealed by ultra-deep sequencing. Proc Natl Acad Sci U S A 105:13081-6, 2008
5. Andor N, Graham TA, Jansen M, et al: Pan-cancer analysis of the extent and consequences of intratumor heterogeneity. Nat Med 22:105-13, 2016
6. Burrell RA, McGranahan N, Bartek J, et al: The causes and consequences of genetic heterogeneity in cancer evolution. Nature 501:338-45, 2013
7. Fisher R, Pusztai L, Swanton C: Cancer heterogeneity: implications for targeted therapeutics. Br J Cancer 108:479-85, 2013
8. Navin N, Kendall J, Troge J, et al: Tumour evolution inferred by single-cell sequencing. Nature 472:90-4, 2011
9. Liu M, Liu Y, Di J, et al: Multi-region and single-cell sequencing reveal variable genomic heterogeneity in rectal cancer. BMC Cancer 17:787, 2017
10. Gibney GT, Weiner LM, Atkins MB: Predictive biomarkers for checkpoint inhibitor-based immunotherapy. Lancet Oncol 17:e542-e551, 2016
11. Hendry S, Salgado R, Gevaert T, et al: Assessing Tumor-Infiltrating Lymphocytes in Solid Tumors: A Practical Review for Pathologists and Proposal for a Standardized Method from the International Immuno-Oncology Biomarkers Working Group: Part 2: TILs in Melanoma, Gastrointestinal Tract Carcinomas, Non-Small Cell Lung Carcinoma and Mesothelioma, Endometrial and Ovarian Carcinomas, Squamous Cell Carcinoma of the Head and Neck, Genitourinary Carcinomas, and Primary Brain Tumors. Adv Anat Pathol 24:311-335, 2017
12. Hendry S, Salgado R, Gevaert T, et al: Assessing Tumor-infiltrating Lymphocytes in Solid Tumors: A Practical Review for Pathologists and Proposal for a Standardized Method From the International Immunooncology Biomarkers Working Group: Part 1: Assessing the Host Immune Response, TILs in Invasive Breast Carcinoma and Ductal Carcinoma In Situ, Metastatic Tumor Deposits and Areas for Further Research. Adv Anat Pathol 24:235-251, 2017
13. Haffner MC, Mosbruger T, Esopi DM, et al: Tracking the clonal origin of lethal prostate cancer. J Clin Invest 123:4918-22, 2013
14. Cyll K, Ersvaer E, Vlatkovic L, et al: Tumour heterogeneity poses a significant challenge to cancer biomarker research. Br J Cancer 117:367-375, 2017

15. Sunshine JC, Nguyen PL, Kaunitz GJ, et al: PD-L1 Expression in Melanoma: A Quantitative Immunohistochemical Antibody Comparison. Clin Cancer Res 23:4938-4944, 2017
16. Bilimoria MM, Holtz DJ, Mirza NQ, et al: Tumor volume as a prognostic factor for sarcomatosis. Cancer 94:2441-6, 2002
17. Jiang N, Deng JY, Ding XW, et al: Tumor volume as a prognostic factor was superior to the seventh edition of the pT classification in resectable gastric cancer. Eur J Surg Oncol 41:315-22, 2015
18. Kornprat P, Pollheimer MJ, Lindtner RA, et al: Value of tumor size as a prognostic variable in colorectal cancer: a critical reappraisal. Am J Clin Oncol 34:43-9, 2011
19. Lee JW, Cho A, Lee JH, et al: The role of metabolic tumor volume and total lesion glycolysis on (1)(8)F-FDG PET/CT in the prognosis of epithelial ovarian cancer. Eur J Nucl Med Mol Imaging 41:1898-906, 2014
20. Narod SA: Tumour size predicts long-term survival among women with lymph node-positive breast cancer. Curr Oncol 19:249-53, 2012
21. Singer S, Baldini EH, Demetri GD, et al: Synovial sarcoma: prognostic significance of tumor size, margin of resection, and mitotic activity for survival. J Clin Oncol 14:1201-8, 1996
22. Heaphy CM, Bisoffi M, Fordyce CA, et al: Telomere DNA content and allelic imbalance demonstrate field cancerization in histologically normal tissue adjacent to breast tumors. Int J Cancer 119:108-16, 2006
23. Trujillo KA, Hines WC, Vargas KM, et al: Breast field cancerization: isolation and comparison of telomerase-expressing cells in tumor and tumor adjacent, histologically normal breast tissue. Mol Cancer Res 9:1209-21, 2011
24. Aran D, Camarda R, Odegaard J, et al: Comprehensive analysis of normal adjacent to tumor transcriptomes. Nat Commun 8:1077, 2017
25. Li H, Durbin R: Fast and accurate short read alignment with Burrows-Wheeler transform. Bioinformatics 25:1754-1760, 2009
26. Cibulskis K, Lawrence MS, Carter SL, et al: Sensitive detection of somatic point mutations in impure and heterogeneous cancer samples. Nat Biotechnol 31:213-9, 2013
27. Fang H, Bergmann EA, Arora K, et al: Indel variant analysis of short-read sequencing data with Scalpel. Nature Protocols 11:2529-2548, 2016
28. Koboldt DC, Chen K, Wylie T, et al: VarScan: variant detection in massively parallel sequencing of individual and pooled samples. Bioinformatics 25:2283-2285, 2009
29. Talevich E, Shain AH, Botton T, et al: CNVkit: Genome-Wide Copy Number Detection and Visualization from Targeted DNA Sequencing. Plos Computational Biology 12, 2016
30. Carter SL, Cibulskis K, Helman E, et al: Absolute quantification of somatic DNA alterations in human cancer. Nat Biotechnol 30:413-21, 2012
31. Roth A, Khattra J, Yap D, et al: PyClone: statistical inference of clonal population structure in cancer. Nat Methods 11:396-8, 2014

20. Appendices

A) Serious incident report form

Appendix A – Serious Incident Report Form

Date:…….

Personnel involved:……

Description of

incident:……

……

……

……

……

……

……

……

……

Action

taken:……

……

……

……

……

……

……

……

……

Outcomes:……

……

……

……

……

……

……

Follow-up required:……

……

……

……

……

……

……

Appendix E: Guidance documents – version 5.0, July 2019

HoLST-F List of Guidance Documents for Study Processes

1. Identification of samples for homogenisation
2. Sample labelling
3. Transfer of samples to BioBank area
4. Transfer of samples from Biobank to Ventana & Francis Crick
5. Transfer of diagnostic blocks and slides
6. Equipment re-stocking
7. Equipment checks and faults
8. Homogenate waste disposal
9. Contacts for the study
10. Marken Depot Materials List

1. **Identification of samples for homogenisation**

- Every 2 weeks a list of the cases with leftover tumour tissue will be supplied to one of the clinical study investigators by the team in histopathology
- The list will be reviewed and *all cases with leftover tissue that are relevant to the primary endpoint* (i.e. breast, colorectal, gastric, pancreatic, renal, ovarian, sarcoma primary tumours and melanoma lymph node dissections) *will be assigned a unique HoLST-F identifier by the trial co-ordinator* (e.g. HF001, HF002).
- Relevant clinical details from these cases (e.g. nature of surgery, diagnostic information from the histology report) will be entered into the MACRO study database by a Clinical Investigator or a Clinical Trial Administrator (CTA).
- Leftover samples for whom Tissues for Research Consent was obtained will be identified as suitable for homogenisation. In addition, any cases for homogenisation that are outside the primary endpoint cohort (e.g. additional tumour types, metastatic resections) may be selected for homogenisation. Cases to be put forward ($\geq$5 per week, prioritising those pertinent to the primary endpoint or any paired metastasis to a previously homogenised case) will be selected by the Clinical Investigator.
- The signed Tissues for Research Consent form will be checked both by the clinical study investigator and a CTA (in the electronic medical record) to ensure this is appropriately completed prior to cases being deemed suitable for homogenisation.
- This annotated list will then be sent back to the team in histopathology, who will then confirm on the spreadsheet: 1) that >1gm of remaining tumour is present in cases flagged for the primary endpoint; 2) which cases go on to be homogenised
- If there are any cases who have an 'HF' number assigned, but are subsequently excluded (eg if <1gm tumour present or no tissue actually remains for homogenisation), then the reason will be noted on the spreadsheet and this number *will not* be reassigned.

2. Sample labelling SOP

- Once a leftover tumour tissue sample is identified as suitable for homogenisation by one of the study investigators, it will be labelled with its assigned HoLST-F number (eg HF005; as per Guidance Note 1 above).
- The unique HoLST-F identifier will be written on the leftover tissue bucket by one of the Advanced Practitioners in Anatomical Dissection or the Biomedical Scientist (BMS)
- All further tubes and equipment related to the sample will only be labelled with the unique HoLST-F identifier from this point (e.g. falcon tubes)
- Homogenised tumour samples will be given the letters 'Tu', e.g. HF001-Tu. Usually there will be 4 aliquots – 2 for Ventana, 2 for the Crick.
- Homogenised tumour-adjacent samples will be given the letters 'Ad', e.g. HF001-Ad. In some circumstances there may be 2 adjacent sections – one directly next to the tumour macroscopic margin and the other >2cm from the tumour macroscopic margin. Usually there will be 2 aliquots – 1 for Ventana, 1 for the Crick
- Homogenised normal samples will be given the letters 'No', e.g. HF001-No. Usually there will be 2 aliquots – 1 for Ventana, 1 for the Crick.

- In the case of a single tumour that is segmented, letters will be used to denote the sections:
    - HF001-Tu1a, Tu1b etc
- In the case of multiple discrete tumour deposits for a particular case:
    - HF001-Tu1 and Tu2 etc, with corresponding Ad1, Ad2 etc will be annotated
    - These may be from different anatomical sites or from the same anatomical site (eg several discrete tumour deposits from a resected section of bowel) – these sites should be noted on the sample labels for entry into FreezerPro

- In histopathology, buckets for homogenisation will be labelled using pre-printed labels provided by the BSC team. The Falcon tubes containing the homogenate liquid will also be labelled (with the study number as the only unique identifier). For example below:

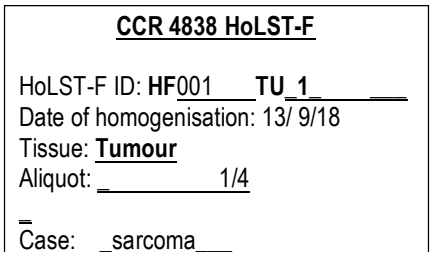

- Label colours for study specimens and homogenates will be as follows:
    - Charing Cross (leftover tumour tissue) Labels - Pink
    - Bucket Labels – White
    - Normal Tissue Labels – White
    - Adjacent Tissue – Blue
    - Tumour Tissue – Yellow
    - Tumour Remains – Orange

3. Transfer of samples to Biobank area

- Once the samples have been homogenised, the BMS will notify one of the Skin & Renal unit Bio specimen collectors (BSCs) by phone (1692/1698/1565) & email (see Contacts List below).
- Samples will be temporarily placed in the fridge (at 4 degree Celsius) within the histopathology department. A template email will be provided by the BSC team; this will be used for all correspondences regarding movement of samples from Histology to Freezer room.
- The BSC will collect the samples from histopathology using an insulated polystyrene box and transfer them to the Biobank fridge or freezer.
- The BSC will be responsible for logging the samples into Freezer-Pro

4. Transfer of samples from Biobank area to Ventana & The Francis Crick

- Every 2-4 weeks one of the Skin & Renal team BSCs will organise a shipment to send homogenised samples from the Royal Marsden to Ventana Medical Systems, Tuscon

Arizona. A mirrored batch of samples will be sent to the Francis Crick, c/o Andrew Rowan (i.e. up to 50ml from each area of each homogenised case).

- Sample boxes will be packaged in a plastic outer bag and refrigerated in appropriately labelled Category B and UN3373 shipping boxes. To maintain sample temperature ice packs should be placed within the insulated box.
- A hardcopy of the shipping list alongside the airway bill and commercial invoice must also be sent with samples. The sample list will be obtained straight from the Freezer pro database and exported into Excel. Instructions of how to complete this can be found in the Freezer-Pro SOP.
- Courier booking should be made at least a day in advance and this should be placed via MARKEN. A copy of the airway bill must be kept on site and airway bill and courier reference number must be tracked on Freezer-Pro.
- A printed list of samples for transfer will be emailed in advance to Lisa Gallegos, lead Scientist at Ventana (see Contact List below) and Andrew Rowan (lead Scientist at TCT Lab in the Crick), as well as printed and sent with the samples

5. Transfer of diagnostic blocks and slides

- Once the purified DNA from homogenised samples has been analysed for quality (ie parameters which will ensure successful sequencing), Ventana will communicate to both the Clinical Investigator and the Biological Specimen Co-ordinator at the Royal Marsden which samples (e.g. HF005) have passed the following thresholds:
    - $\geq$ 1ug of gDNA (using a Qubit or nanodrop measurement) – this is a scalable metric, for example if a 100ul aliquot contains $\geq$10ng of DNA this will be sufficient
    - 90% of the DNA is larger than 120bp (using a bioanalyser instrument)
- As per the study protocol, the diagnostic FFPE blocks for these cases will be requested for the cutting of slides. The block from which slides were cut for Diagnostic Molecular Pathology analysis (where relevant) should be flagged.
- The clinical Fellow for the study will review the pathology reports of the cases and flag which blocks contain tumour/are most representative – aim for minimum of 2 blocks per case to have slides cut
- The number of blocks with tumour available will determine how many may have slides cut from them:

    2 tumour blocks available - only cut one block
    3-6 tumour blocks available - cut 2 blocks
    >6 blocks – cut 3 blocks
    $\geq$10 blocks – cut 5 blocks
- The BMS working on the study may cut the slides in histopathology, or if there is no capacity, they will be transferred to the Francis Crick to be cut in Experimental Histopathology. The Clinical Fellow responsible at the Crick will request (in this order):
    - 1x 4um unstained on charged slide (ie for H&E)
    - 5x 10um unstained on uncharged slide (ie for DNA extraction)
    - 5 x 4um unstained on charged slide (ie for IHC)
- The blocks will then be returned to the Royal Marsden if sent to the Crick
- The cut slides will either be sent directly to Ventana from the Crick, or returned to the Royal Marsden first, accompanied by a manifest with the following information:

- Block number (to reference back to histopathology report)
- Anatomical site corresponding to block
- HoLST ID
- Slide number (eg 1/4)

  Labelling of the actual slide must contain the following information:

  1.CCR4838

  2.HF number

  3.An individual slide identifying number that corresponds to the manifest detailed above
- ***Slides need to be shipped to Ventana within 2 weeks of being cut to optimise their quality for DNA extraction and storage for IHC***

6. Equipment re-stocking

- Every month the equipment list will be reviewed and items that require restocking will be identified by the responsible person (*see sample below)*
- The required items will be ordered from the Marken Depot. No more than one order will be placed per week.
- Lisa Gallegos will be responsible for checking inventory at the Marken Depot on a monthly basis and re-stocking the depot with supplies as needed.
- The Trial study co-ordinator will be cc'd in to all correspondence regarding orders to centralise information

Refer to table at end of document – Materials List at Marken Depot

7. **Equipment Checks and Faults**

- Any equipment specific to the study (e.g. blenders) will be checked by the Royal Marsden Clinical Engineering Team prior to use.
- Upon any fault, they will be *replaced*, rather than repaired
- Commercial (consumer-use) blender bases will be used for a maximum of 3 months. A log of blenders will be kept by the study co-ordinator.

8. Homogenate Waste Disposal

- Waste generated from excess tumour homogenate will be disposed of in rigid yellow bins (medicinally contaminated/for incineration). For large volumes of excess homogenate, secondary containment is required.

9. Contacts for the study

Name	Role	Number/email
Lavinia Spain	Clinical Investigator - Lead	Ph: 07557983066 lavinia.spain@rmh.nhs.uk
Zayd Tippu	Clinical Investigator	Zayd.tippu@rmh.nhs.uk x1986
Lewis Au	Clinical Investigator	lewis.rmh@rmh.nhs.uk
Samra Turajlic	Chief Investigator	Samra.turajlic@crick.ac.uk
Ashley Gilchrist	Advanced Practitioner Anatomical Dissection	ashley.gilchrist@rmh.nhs.uk
Vanessa Primus	Advanced Practitioner Anatomical Dissection	Vanessa.Primus@rmh.nhs.uk
Somya Agrawal	Biomedical Scientist	somya.agrawal@rmh.nhs.uk
Lee Gumble	Biomedical Scientist and database manager	Lee.Gumble@rmh.nhs.uk
Glenn Noel-Storr	Manager, Histopathology	Glenn.noel-storr@rmh.nhs.uk
Nahid Shaikh	Biomedical Specimen Co-ordinator	Nahid.shaikh@rmh.nhs.uk
Aida Murra	Biomedical Specimen Co-ordinator	Aida.murra@rmh.nhs.uk
Justine Kortweg	Biomedical Specimen Co-ordinator	Justine.Korteweg@rmh.nhs.uk
Dilruba Kabir	Clinical Trial Co-ordinator	Dilruba.kabir@rmh.nhs.uk
Hamid Ahmod	Clinical Trial Administrator	Hamid.ahmod@rmh.nhs.uk
Kim Edmonds	Research Nurse	Kim.edmonds@rmh.nhs.uk
Lisa Gallegos	Ventana – Lead Scientist	Lisa.gallegos@roche.com +1 (858) 692-2188
Nelson Alexander	Ventana – Lead Investigator	Nelson.alexander@roche.com
Andrew Rowan	Principal Laboratory Research Scientist Translational Cancer Therapeutics Laboratory	Andrew.rowan@crick.ac.uk c/o CEGI Laboratory 1 Midland Road NW1 1AT

	Francis Crick Institute	

Suppliers

Name	**Item**	**Contact person & details**
Marken	Blender supply depot	Kim Rossall <Kim.Rossall@marken.com> +1 (310) 908-5844
VWR	Consumables	https://www.vwr.com/

Materials list at Marken Depot

Item	Cat. No.	Details	Unit	link
VWR Weighing boats (square, standard, disposable)	10803-148	100mL	Pack of 500	https://us.vwr.com/store/product/16773457/vwr-disposable-square-weighing-boats
	10803-170	250mL	Pack of 500	
50 ml conical Tubes	89039-660	50mL	Case of 500	https://us.vwr.com/store/product/4675770/vwr-high-performance-centrifuge-tubes-with-flat-or-plug-caps-polypropylene
Cardboard Storage Boxes, Globe Scientific	10147-816	16 tube capacity	Case of 38	https://us.vwr.com/store/product/13025862/cardboard-storage-boxes-globe-scientific
disposable forceps	SKU: 8485	13 cm	pack of 100	https://www.medisave.co.uk/instrapac-plastic-forceps-blue-13cm.html
MACS C tubes	130-093-237	25 tubes	pack of 25	https://www.miltenyibiotec.com/US-en/products/macs-sample-preparation/tissue-dissociators-and-tubes/c-tubes/gentlemacs-c-tubes.html#25-tubes-sterile-single-packed
Ninja 72oz blender	507KKU770	72 oz	Case of 4	
Total Crushing 6 balde Assembly	311KKU	blade for 72 oz	Case of 16	
16oz Nutri Ninja Cups & Lids	XWP002CS	16 oz	Case of 8	
Single Serve Blade Assembly	307KKU	blade for 16 oz	Case of 48	

Appendix F: Homogenisation process document – version 3, September 2018

Homogenisation Process Guidance

Following the official case sign-off by the pathology department, the residual leftover surgical tissue (LST) stored in formalin will be dissected by a pathology assistant or surgical pathologist to isolate 3 regions (where possible): the remaining tumor tissue, tissue adjacent to the tumour and distant normal tissue (preferably >5 cm from tumor, if possible; see Figure 1). Each region will be weighed separately.

Figure 1: Macrodissection areas for homogenisation

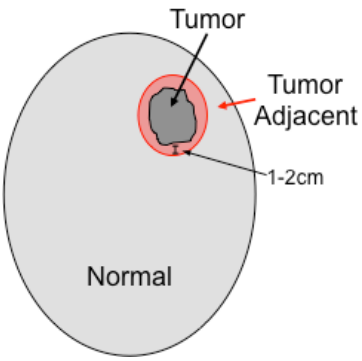

Some distant normal tissue will also be dissected to serve as a germline control.

The dissected tumor, adjacent and distant normal tissue samples are incubated in phosphate buffered saline (PBS) overnight in separate containers to remove residual formalin.

Materials required for blending (the day following macrodissection):

- Cutting board
- Scalpel
- Stir plate and stir bar
- Beaker for preparing PBS
- Graduated cylinders for measuring water and PBS + 0.09% azide
- PBS tablets (VWR cat #97062-732; each tablet makes 100 ml PBS)
- 5% solution of sodium azide
- ddH2O
- Blender containers
- Blender base

- Tissue to be homogenized
- Scale
- Labeled 50 ml tubes
- Plastic Pasteur pipettes (50 ml, 10 ml)
- Electronic pipetteman
- Timer
- Pen/log book

Before you begin:

Prepare homogenization area, if desired, by lining the work bench with absorbent material. Prepare labeled 50 ml conical tubes for each tissue sample (up to two for larger tumor samples). Wear standard PPE. Wear double gloves, if desired, to minimize contact with homogenized tissue. Use eye protection with side shields.

Steps

1. Weigh tissue samples on an electronic scale and record the weight. If necessary, use a scalpel to cut tissue to fit into disposable blender container. Place tissues into appropriate blender container.
    a. 150 grams or less: 16 oz container
    b. 150 grams to 1000 grams: 2L container
    c. 1000 grams+: see note below.

2. Calculate volume of PBS (using guidelines in Step 3) and prepare it.
    a. For every 100 ml of water, add 1 tablet PBS (VWR cat #97062-732); stir to dissolve

3. Add PBS to the blender container and close container. Record volume of PBS added.
    a. 50 grams or less: add up to 100 ml volume
        i. e.g. to 1 gram tissue, add 99 ml PBS
        ii. e.g. to 10 grams tissue, add 90 ml PBS
        iii. e.g. to 50 grams tissue, add 50 ml PBS.
    b. 50 grams to 1000 grams: add equal volume of PBS and tissue
        i. e.g. to 51 grams tissue, add 51 ml PBS
        ii. e.g. to 700 grams tissue, add 700 ml PBS
    c. samples larger than 1000 grams: see note below.

4. Place container on blender base. Blender will not function if container is not "clicked" properly into place. Blend for 30 s to 1 min; record time.
    a. 16 oz container: hold down pulse button for required amount of time.
    b. 2 L container: press 3; stop after required amount of time.

    ***Note – homogenization times are generally no longer than 30 s, but in some instances the blending time will be determined empirically. A log of blending times will be kept for each tumor sample. The solid tissue fragments must be sufficiently blended to create a liquid sample capable of being aspirated by a 10ml serological pipette.

5. Add 1 ml of sodium azide to each labeled 50 ml conical sample tube, up to four tubes per tumor. Transfer homogenized sample to labeled 50 ml conical tubes containing 1 ml 5% sodium azide. Pour sample directly into tubes if sufficiently dilute, or use a 10-50 ml pipette. If sample in excess of 200 ml is generated, dispose of excess sample in appropriate waste receptacle.
    a. Sodium azide is toxic; take care to handle minimally with gloved hands.

6. Each blender container is for single use only, except for samples larger than 1000 grams. Following homogenization and tissue transfer, dispose of blender in appropriate waste receptacle.

***Note - for samples greater than 1000 g, use the following protocol:

a. Separate the sample into sections weighing 1000 g or smaller
b. Process the first section at a 1:1 ratio of tissue (g) to PBS using the 2L blender container.
c. Take an aliquot of blended tissue equal to 1/10th of the starting weight of the tissue section.
    i. e.g. take a 100 ml aliquot from the blend of a 1000 g sample.
    ii. e.g. take a 50 ml aliquot from the blend of a 500 g sample.
d. Add the aliquot of blended tissue to a second 16 oz or 2 L MIXING blender container, as appropriate. The 16oz blender container will hold a maximum of 400 ml.
e. Pour off the remaining blended tissue from the first blender into a waste container.

f. To the first blender container, add the second tissue section and an equal volume of PBS.
g. Repeat steps b-e to blend and sub-sample the second tissue section, adding the aliquot of blended tissue to the same MIXING blender container.
h. Blend and sub-sample any additional tissue sections, each time adding an aliquot to the same MIXING blender container.
i. Once the last tissue section has been sub-sampled, place the second MIXING blender containing all of the aliquots on the blender base. Blend for 30s to homogenize the aliquots and create a final homogenized representative sample.
j. Transfer the final homogenized representative sample to 50 ml conical tubes containing 1 ml of 5% sodium azide for storage. Store four 50 ml conical tubes of the final homogenate (200 ml total).

The conical tubes will be stored at 4ºC in the Biobank refrigerators at the Royal Marsden Hospital, prior to being shipped to Ventana. Samples with sufficient volumes may be aliquoted into five 1ml cryogenic vials and stored at -80°C for long-term sample archiving.

Appendix G: Phone consent process documents

CCR4838 HoLST-F RSM Tissue for Research Consent process

1. **List of patients to consent will be generated by RSM Research Fellow**
   - Check patient intention to consent on the EPR cover sheet and/or if a consent is available.
   - If 'NO' is recorded on the EPR cover sheet – please do not approach for consent

   NOTE: The list of patients mentioned above is generated by RM Histopathology which lists the patients that have had surgery and had excess tissue available to use for this study.

2. **Approach and consent patients**
   - Telephone consent: please refer the Renal and Melanoma guidance for remote consenting (saved in F:\Backup\GoreM\1 - T R I A L S\6 Admin - Research\9. SOPs and Guidance Notes\Guidance Notes)

3. **Once the initial phone call has been conducted, the consenting individual :**
   a. Annotate the call on EPR case notes section using the template below:

Annotation header: Tissue for Research Consent Call

Annotation text: <Patient name> was contacted on <date of call> in order to discuss their interest regarding the Tissue for Research Consent. <Patient name> expressed interest in consenting and therefore will be sent a consent pack in the post containing a cover letter, Using and storing tissue samples for research in the future patient information leaflet version PI-0280-09, Tissue for Research consent form version 12, dated 30-Apr-2019 and a return envelope. A follow-up phone-call to confirm consent is scheduled on <date of next phone call>.

   b. Update the patient log (saved in F:\Backup\GoreM\1 - T R I A L S\2 Melanoma\CCR4838- HoLST-F\2. Trial Documents\2.2 Informed Consent Form\2.2.3 TFR consent log)
   c. Print the patient specific consent via EPR
   d. Notify the relevant TC/CTA and forward them the patient specific consent

4. **Send Consent pack to patient**
   - To be sent by TC/CTA

5. **Once the signed consent is received, the individual who conducted the consent is to:**
   i. Ensure that the patient has made a choice as evidenced by ticking once of the boxes.
   ii. Check that the patient has printed their name, signed and dated the consent form
   iii. Consenting individual to sign and date the consent form using the current date
   iv. Consenting individual to write the following note at the bottom of the consent form, initial and sign: *NOTE: This patient is consented via telephone consent.*

6. **Consenting individual to scan the consent and upload a copy on the consent tab of the EPR.** Please note that consents uploaded elsewhere are invalid.

7. **Consenting individual to annotate consent in the case notes section of the EPR using the unit template:**

Annotation header: Tissue for Research Consent Confirmation

Annotation text: <Patient name> was given the *patient information sheet and leaflet for Tissue for Research* on <insert date PIS was given>. They have had time to read the *Using and storing tissue samples for research in the future patient information leaflet version PI-0280-09* and *Tissue for Research consent form version 12, dated 30-Apr-2019*. The patient signed <date of consent> and I have countersigned it <today's date>. <He/ she> also had time to ask questions and <none were raised/ I answered those that were raised (please give details of the answers provided)>.

Consenting individual to change the EPR cover sheet to indicate intention or consent

- Patient Consent Register Maintenance (HIS Command ConsentR)

Current	Action
BLANK	If patient consents, please change to YES.
BLANK	If patient does not consent and has verbally confirmed no intention to consent, please change to NO.
YES	Patient has indicated intention to consent during registration. If the patient consented, please do not change.

NOTE: You cannot change YES or NO to BLANK

8. The original countersigned consent form to be destroyed as per Biobank process